The geologic and tectonic evolution of the Pan-African/Mozambique Belt in East Africa

Thesis

THE GEOLOGIC AND TECTONIC EVOLUTION OF THE PAN-AFRICAN / MOZAMBIQUE BELT IN EAST AFRICA

A Thesis presented for the Degree of Doctor of Philosophy

by

Seife Michael Berhe
B.Sc., Addis Ababa University, 1973
M.Sc., Leicester University, 1981

Department of Earth Sciences
The Open University

February 1988

EX12

HIGHER DEGREES OFFICE

LIBRARY AUTHORISATION FORM

STUDENT: S. M. BERHE SERIAL NO: M7021/64

DEGREE:

TITLE OF THESIS: THE GEOLOGIC AND TECTONIC EVOLUTION OF THE PAN-AFRICAN / MOZAMBIQUE BELT.

I confirm that I am willing that my thesis be made available to readers and maybe photocopied, subject to the discretion of the Librarian.

SIGNED: DATE: 5/2/88

ABSTRACT

The presence of ophiolite complexes in NE and E Africa has been documented using Landsat, field and geochemical studies. This has led to the recognition of five ophiolite belts. These ophiolite belts represent sutures marking the position of island arcs and could be traced to Saudi Arabia on a pre-Red Sea drift reconstruction. Most of the ophiolites are dismembered, their mode of occurrence varies widely resulting in different structural relationships. The Yubdo complex in Western Ethiopia is formed of harzburgite which grades into dunites and pyroxenitic units, a cumulate sequence of ultramafic and gabbroic rocks and sheeted dykes. The Baragoi complex in Kenya is formed of tectonised ultramafics with dunite and chromite pods, a cumulate sequence of ultramafic and gabbroic units and a dyke unit. Trace element data of the Baragoi complex shows a transitional MORB to IAT affinity, and the presence of boninites suggest a supra- subduction setting, while data from the Adola- Moyale belt (S Ethiopia- NE Kenya) indicate an island-arc and MORB geochemistry, which developed in a back-arc setting. The chromites of Baragoi and Moyale have high Cr_2O_3 which follow an ophiolitic trend.

Major and trace element data for granitoids from W Ethiopia, S Ethiopia- NE Kenya and central Kenya indicate three geochemically distinct granitoid groups: volcanic arc granitoids, crustal melt granitoids and within-plate granitoids. Calc-alkaline rocks predominate in W Ethiopia, whereas the proportion of crustal melts appear to increase going further south in S Ethiopia/ NE Kenya and central Kenya. Diorites form about 10 percent of Precambrian outcrop in NE Sudan, while further south diorites are almost insignificant. Only in NE Sudan, W Ethiopia and Saudi Arabia do diorites feature prominently. However the lack of extensive calc-alkaline volcanic rocks, could simply reflect relatively narrow oceans and insufficient subduction of oceanic crust to produce large quantities of calc-alkaline melts, while the increase in the proportion of crustal melt granitoids in the southern part of the Mozambique belt indicates crustal thickening due to continent-continent collision.

This study shows that the major lineaments identified in the Horn of Africa trend 010 ± 10°, 055-065° and 145-165°. The 010 ± 10° and 145-165° trending lineaments form conjugate sets, while a later deformation episode reactivated 145-165° (NW-SE) trending lineaments and caused

055-065° (NE-SW) lineaments. Two deformation mechanisms most likely controlled the growth of the major fault zones. Structural and metamorphic evidence suggests that crustal shortening was severe in S Sudan, Kenya and SE Ethiopia as compared to Saudi Arabia, NE Sudan and N and W Ethiopia due to oblique collision from the southeast causing stacking of crustal blocks along NW trending faults.

Regional geologic, tectonic and geochemical studies suggest rifting c.1200 Ma which subsequently led to the development of intraoceanic arcs and associated marginal basins in the north and narrow basins within the sialic basement gneisses further south in Kenya and Tanzania. This was followed by continent- continent collision which led to accretion of island arcs by mild collision from the northeast in Saudi Arabia and NE Sudan and severe crustal shortening in S Sudan, Kenya and SE Ethiopia as compared to Saudi Arabia, NE Sudan and N and W Ethiopia due to oblique collision from the southeast.

Acknowlegements

I wish to express my thanks to the following organisations, institutions and individuals who have assisted in this work. I would especially like to thank my supervisor Professor Robert Shackleton for initiating the project and stimulating my awareness of the challenges involved in this study and also for offering guidance and suggesting improvements to earlier drafts of this thesis. I am indebted for support and encouragement given to me by fellow members of the Open University NE Africa reasearch group; namely Professor I. Gass, Alison Ries and Robert Price. Alison for helping me to get started with this project. Robert Price for constant support throughout my study and for allowing me to use his unpublished geochemical data . The World University Service (WUS) for providing a reasearch studentship and the Open University for subsequent funding and travel grants to attend several conferences. I would like to thank the staff of the World University, especially Sarah Buxton and Sarah Locke , their consistent support is gratefully acknowleged. In addition I would like to thank Steve Drury, Dave Rothery and Gavin Hunt for their support in the Remote Sensing study. Dave Rothery was instrumental for acquiring Landsat CCT by swapping from different organisations. Buying this data would have been impossible with my limited funds. I would like to thank the staff of Nigel Press Associates especially Nigel Press and Will Duncan who provided Landsat imagery either free and some others at cost price. Robert Price, Steve Drury, Dave Rothery, Nigel Harris, Frank McDermott, Nick Rogers and Bram Murton read parts of the thesis and made very useful comments which improved the text greatly. Drs. Pearce and Kostopoulos are thanked for help in geochemistry of ophiolites and for their hospitality in Newcastle Upon Tyne. Chris Hawkesworth and Pete Van Calstren are thanked for discussion on isotope geochemistry on various occassions and Gareth Davies for geochronological work on the Baragoi samples.

In Ethiopia and Kenya field work would not have been possible without logistical support from the Ethiopian Institute of Geological Surveys, Addis Abeba and Department of Mines and Geology, Nairobi, Kenya. The Geology Department of the University of Nairobi provided camping equipment and made available a temporary office for my use during my stay there. I would like to thank Drs.

Nyambok and Tole of the Department of Geology at the University of Nairobi who were instrumental in providing logistical support and friendly advice. Particular thanks are due to Mengesha Teffera, Alemu Shifferaw of the Ethiopian Institute of Geological Surveys and Drs. Hackman, Roger Key and Tim Charlesly of the Mines and Geology Department (on technical aid from the British Geological Survey) who gave field support and afforded me generous amounts of their time. Many thanks to Albert Gizuli who assisted me in carrying out fieldwork.

Permission to work in Kenya came from the Office of the President and is gratefully acknowledged. The people of Baragoi, Moyale (Kenya) and Geba, Yubdo and many other villages in Ethiopia for allowing us to set up field camps in their villages. The United Touring company for allowing me concessionary fees for hiring a vehicle used in the field, in particular Mr. D. Howarth and Mr. Zul Danje.

At the Open University the technical staff are thanked for skilful aid to many analytical problems. In particular John Watson for patiently putting up with persistent requests to have my samples run; Andy Tindle for showing me how to run the microprobe, and introducing me to the Mac-life saver. Nick Rogers for help with the INAA analyses and Phil Potts for advice on analytical problems. Ian Chaplin and the thin section laboratory staff for excellent and swift production of thin sections and John Taylor and Helen Boxall for cartographic advice. John Taylor for drawing the most important figures in this thesis. John Holbrook for help in travel grants.

This thesis has been produced using the Macintosh. Patience and helpful advice have been shown by the User Support Group in ACS at the Open University. Computing assistance from Andy Tindle, Dave Wright, Dave Peate and Steve Roberts is appreciated.

I also thank the following for help and advice Bram Murton, for ophiolites, Nigel Harris for metamorphic petrology, Cherry Lewis for granites, Steve Roberts for chromites, Kirsten Fraser, Mathew Willis and especially Frank McDermott for everything I know about granite geochemistry. Dr. A. Warden for encouragement and discussion about the Pan-African on various occassions. Ammanuel Gebray for help in crushing rocks. My appreciation to Nick Brough, Fiona McGibbon, Sian May, Sarah Everett and Mathew Watkinson for the last push to get the thesis out of the way by colouring maps and helping in zeroxing. Carol Whale and my wife are thanked for typing the thesis.

My wife, my parents and my uncle Abeselom Yehdego deserve the final mention, for without their encouragement and continual emotional and financial support this work would not have been completed.

The proposals put in this thesis are based on this work together with numerous investigations carried out by the Geological Surveys of Sudan , Ethiopia, Kenya, Somalia and Tanzania and the French Bureau des Recherches Geologiquees et Minieres in Mozambique and Madagascar which have been of crucial help for this reconstruction .

Dedicated in memory of Temesgen Haile and Bill Morton

CONTENTS

Dedicated in memory of Temesgen Haile and Bill Morton

List of Tables

List of Plates

List of Figures

Chapter 3

Chapter 4

Chapter 5

Chapter 6

CHAPTER 1

1.1 REGIONAL GEOLOGY OF NE AND E AFRICA

1.1.1 The Arabian- Nubian Shield

The Arabian-Nubian shield extends from Saudi Arabia and Egypt in the north to Ethiopia and Sudan in the south (Figure 1.1). The Arabian-Nubian shield consists of late Proterozoic ophiolites, island-arc volcanics with associated sedimentary rocks intruded by syn-to post-tectonic calc-alkaline batholiths and plutons. Post dating all of these are a series of anorogenic alkaline complexes.

Various models have been proposed to account for the evolution of the Arabian-Nubian shield basement complex (Table 1.1). The occurrence of ophiolites and their association with calc-alkaline volcanic rocks of island-arc affinity has led several authors to conclude that the continental crust in this area developed through a process of horizontal crustal accretion between about 1000 to 650 Ma (Bakor *et al*, 1976; Greenwood *et al.*,1980; Gass, 1977; 1981) whereas others favour repeated rifting of an Archaean to mid-Proterozoic craton involving the formation and closure of small ocean basins (Kroner,1979b; Stern, 1979; Kemp *et al.*, 1980; Delfour, 1980).

Several authors believe that ophiolites mark sutures, however the direction of subduction at the suture zones is controversial (Garson and Shalaby,1976; Greenwood *et al*,1976; Gass, 1981). Subduction zones are suggested to have dipped towards the west in western Ethiopia (Kazmin *et al.*, 1979a, 1979b), because there are calc-alkaline batholiths west of the ophiolitic suture, while in Sekerr (western Kenya) subduction was suggested to be easterly (Vearncombe, 1983b) based on the fact that the thrust slices dip to the east.

The Pan-African Orogeny (Kennedy,1964) is a tectono-thermal event supposedley dated c. 550-650 Ma, but these are now known to be cooling ages. The range of this thermal event is now controversial. Recent workers (Kroner, 1979b; Gass, 1981, 1982; Delfour, 1981) have proposed that the term Pan-African should be expanded to include the period from 1100 to 500 Ma. However since there are other belts, with different sequences and similar time spans across Africa which were affected by this thermotectonic event, various authors (Almond,1983; Warden and Horkel,1984;

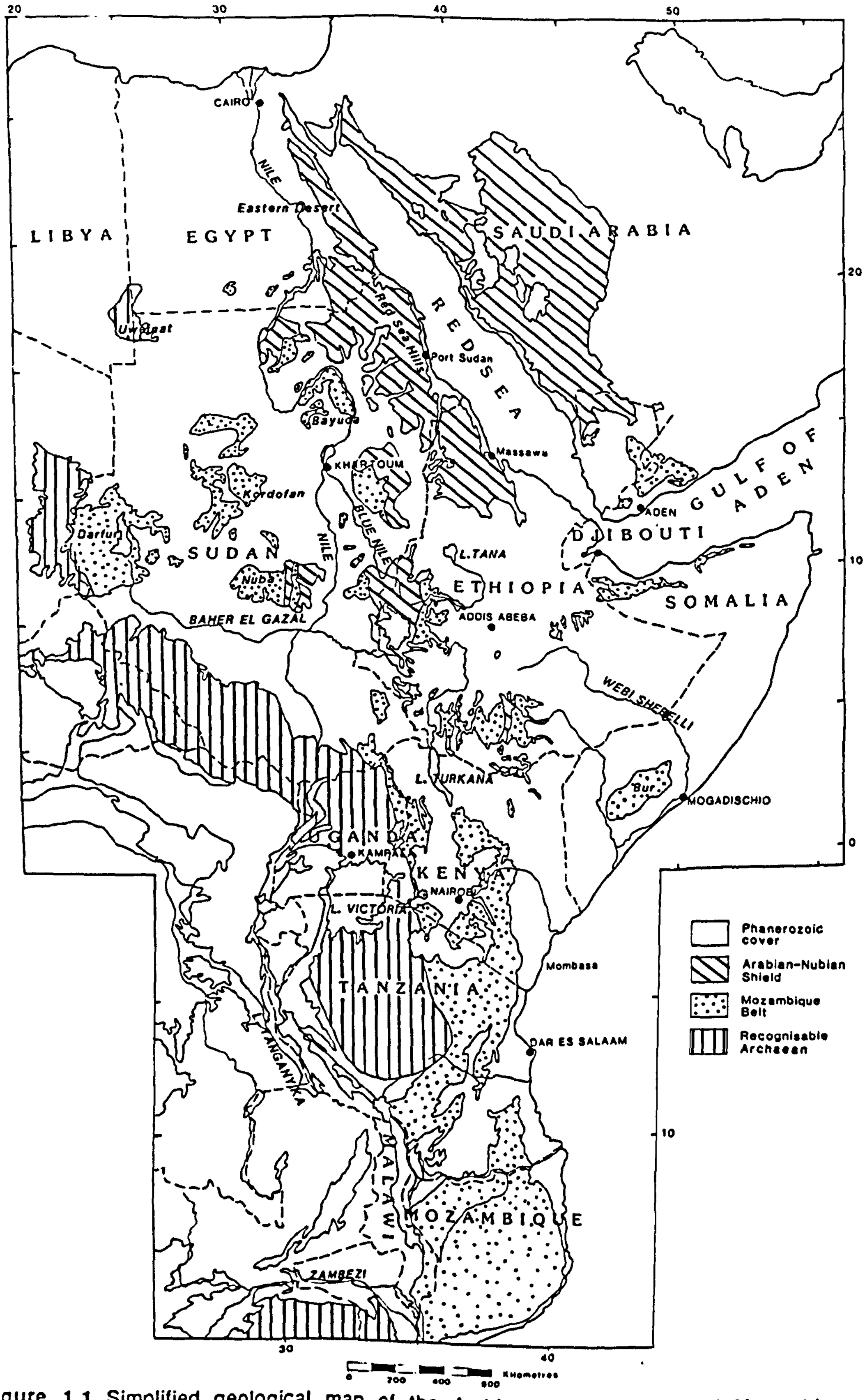

Figure 1.1 Simplified geological map of the Arabian-Nubian Shield and Mozambique Belt.

Price,1984) argue that the Pan-African episode should be restricted to the original defintion of orogeny which is c. 500-600 Ma (Kennedy, 1964). In this study the term Pan-African is extended to include 1100 to 500 Ma, however the c. 500 Ma orogeny is considered as the cooling ages related to the Pan-African episode of metamorphism and deformation. The term Pan-African/Mozambique belt is used because since at least 1100 Ma both belts have experienced a similar tectonic history.

The age of ophiolites and the suturing events is not known. There is no direct evidence of Archaean crust in the NE and E African region, except the Jebel Uweinat region (Libya), but a significant intermediate group of model ages of 1900 - 1600 Ma have been found (Harris *et al.*, 1984) in the Wadi Mubarak and Wadi Nugrus, (Eastern Desert of Egypt), in the Bayuda desert (Sudan) and the Sekerr area (Kenya) indicating a contribution from a pre - Pan-African crust.

The recognition of older (i.e. pre Pan-African 1000 Ma) crustal components in Arabia either as discrete rocks or through Pb- isotope systematics (Stacey and Stoesser, 1983; Calvez *et al.*,1983; Claesson *et al*, 1984) has revived interest in models that rely on repeated rifting of an Archaean to mid-Proterozoic craton.

Table 1.1 Origin and relationship of the Pan African- Mozambique Belt.

Orogenic Belt	Rock Assemblage Reference		Age(Rb-Sr)	Origin
Arabo-Nubian Shield (Pan African Belt)	Ophiolites,island-arc volcanics associated with sedimentary rocks intruded by syn to post tectonic calc-alkaline batholiths & anorogenic alkaline complexes.	1000-650 Ma	Accreted island arcs developed in an intra-oceanic island-arc environment.	Bakor *et al.*(1976) Greenwood *et al*(1980) Gass (1977,1981) Duyverman (1981)
	"	"	Repeated rifting of an Archaean to mid-Proterozoic craton.	Kroner(1979b) Stern (1979) Kemp *et al.* (1980) Delfour (1980)
Mozambique Belt	Gneisses & migmatites and granulites with infolded schists, marbles, amphibolites intruded by various granitoids.	>1000 Ma	Orogenic belt, uplifted and eroded.	Holmes (1951)
		c.500 Ma	Disruption of existing craton and its partial regeneration into a mobile zone.	Kennedy (1964)

650-600 Ma	older basement to geosyncline (650-600 Ma) considered as early phase of deformation and metamorphism. 500 Ma considered as age of uplift).	Cahen and Snelling (1966)
	orogenic belt; reworked remnants of older cycles.	Clifford (1968)
680-580 Ma	(Katangan episode of deformation and metamorphism.)	"
580-500 Ma	Damaran episode.	"
	Basement reactivation resulting from crustal thickening during Himalayan type convergence.	Burke and Dewey (1972).
>1400 Ma	Remobilised Archaean rocks.	Kazmin (1971, 1975) Kazmin *et al*. (1978)
	Older ensialic belt.	Clifford (1970) Hepworth (1979).
	Mozambique belt evolved from an ensialic mobile belt into a circum Pacific type.	Kroner (1979a, 1979b)
	Ophiolites continue into the Mozambique belt, but the Pan African and the Mozambique belt could be of different ages.	Shackleton (1979)
	The Mozambique belt is an extension of the Arabo-Nubian Shield but only of a higher metamorphic grade.	Vearncombe (1983b)
	Both belts are different, but developed in structural and metamorphic continuity during the Pan - African event.	Almond (1983)
Late Proterozoic to Archaean assemblage.	Mozambique belt evolved as a result of plate tectonic processes .The belt is marked by ophiolite sutures, and represents the result of successive collisions.	Shackleton (1986)

1.1.2 Mozambique Belt

The Mozambique belt was first defined by Holmes (1951) to describe a N-S trending belt extending from Mozambique to Kenya (Figure 1.1) of high grade gneisses and migmatites, with infolded schists, marbles, and amphibolites intruded by granites. Holmes (1951) made it clear that the Mozambique belt incorporated within it an old basement, as well as metasedimentary cover rocks, and is characterized by ages of 400-700 Ma (Cahen, 1961).

The relationship between the Arabian-Nubian shield and the Mozambique belt of East Africa is still not clear. This is because no one has as yet done a traverse across the boundary. All studies so far undertaken have tended to be in specific areas. Some workers have claimed that, at its northern end, the Mozambique belt interfingers with the Arabian-Nubian volcanic arc (Vail, 1976; Kazmin *et al*, 1978) and may form the local basement (Hepworth, 1979; Delfour, 1980). In Tanzania and Mozambique this belt has been regarded as ensialic and composed of reworked Archaean rocks (Johnson, 1968; Hepworth, 1979) (Table 1.1).

The proposal that ophiolite belts marking possible sutures can be traced as far as the Mozambique belt in Kenya (Shackleton, 1979) is supported by other work (Kazmin, 1976; DeWit and Chewaka, 1981; Vearncombe, 1983b).

However there are profound differences between the Arabian-Nubian shield island-arc assemblages which are modestly deformed and metamorphosed in the greenschist facies, and the Mozambique Belt high grade metasediments and granitoids which have experienced polyphase episodes of deformation and metamorphism (see Table 1.1). These have been attributed to difference in depth of erosion (Vearncombe, 1983b) or difference in age, the Mozambique belt being considered as older than the Arabo-Nubian shield (Clifford, 1970; Hepworth,1979; Shackleton,1979; 1986). The Mozambique Belt could be as old as 1850-2000 Ma in the Usagaran belt of Tanzania (Wendt *et al.*, 1972; Gabert and Wendt,1972). In the central part of Kenya (Ries *et al.*, in press; Shibata and Suwa,1979; Suwa *et al.*,1979) and in SE Tanzania (Wendt *et al.*, 1972; Cahen *et al.*, 1984), Pan- African ages (< 1000 Ma) prevail. These younger ages were considered the result of overprinting by the Pan-African thermo-tectonic event occurring at around 600-450 Ma (Kennedy, 1964). However because the relationship between the Arabian-Nubian Shield and

Mozambique Belt is still not clear, no definite conclusion can be drawn. In this study attempts will be made to rationalise all the available evidence to put further constraints on the evolution of the Mozambique belt.

1.2 THE RECOGNITION OF OCEANIC LITHOSPHERE IN HIGHLY DEFORMED TERRAIN

Ophiolites refer to a distinictive assemblage of mafic and ultramafic rocks. In a completely developed ophiolite the rock types occur in the following bottom to top sequence: an ultramafic (mantle) complex, consisting of harzburgite, lherzolite, and dunite usually with a metamorphic tectonite fabric, a gabbroic complex, containing cumulus peridotites, pyroxenites, a mafic sheeted dyke complex, overlain by pillow lavas. This sequence is generally overlain by chert, limestone and shale interbeds (Penrose, 1972).

The lowermost of the above-named units is, in the framework of the oceanic lithosphere model, assumed to be a fragment of the uppermost mantle and is commonly termed the mantle sequence (Allen, 1975), a term that will forthwith be used here, while the cumulates are comprised of a thick unit of gabbros and peridotites exhibiting phase layering, planar orientation and intercumulus growth.The base of the cumulate sequence is a sharp contact whose structures in the underlying mantle sequence are truncated. In other ophiolite complexes this contact has been termed "petrological Moho" (Gass and Smewing, 1973), where it is envisaged that crustal magmatic rocks are underlain by rocks of the mantle sequence that are believed to be the solid residue from partial melting.

It is now generally accepted that ophiolite complexes are slices of former oceanic crust formed at a constructive ridge axis by sea-floor spreading (Coleman, 1977; Gass, 1982). Ophiolite assemblages in the Pan-African/Mozambique orogenic belt are usually incomplete, dismembered or metamorphosed in the upper amphibolite facies. This makes it difficult to ascertain their original structure, original mineral assemblages and tectonic setting. Hence one of the methods adopted was to map on a regional scale to see if the scattered mafic-ultramafic complexes in an area could be

pieced together to establish the ophiolite pseudo-stratigraphy, but this would be incomplete without geochemical study which would help to characterise its tectonic setting. In highly dismembered and metamorphosed terrains the only suitable trace elements that could be used are the HFS elements Z, Y and Ti. Microprobe analysis of chromitites can also be effective in discriminating the ophiolitic identity of highly altered and dismembered ultramafic bodies.

In the absence of geochemical data, the field relations, palinspastic reconstruction of the various mafic-ultramafic rocks, and investigating whether the mafic-ultramafic complexes lie along a particular linear belt that leads to a well studied area can be used with a fair degree of certainity. Such an approach was adopted in this study.

1.3 OBJECTIVES AND AIMS OF THE PRESENT STUDY

The Open University has carried out research in East Africa for a number of years, and my work follows on from Price (Price, 1984) who studied three mafic-ultramafic complexes in NE Africa. The research was initially started to study the extent of ophiolite belts in NE Africa and to carry out geochemical and geochronological work on rocks collected from the Yubdo-Birbir belt of W. Ethiopia (Gore mapsheet) which was mapped with a colleague (Mengesha Teffera) between 1978-1979. However, this study was later extended to Kenya, and further field work was undertaken in 1984 in N, and NE Kenya and central Kenya. This study benefited greatly from unpublished maps, and reports from the Ethiopian, Sudanese, Kenyan, and Tanzanian Geological Surveys for which appropriate references are given. Landsat study was used as a base in a wide area in NE and E Africa and critical areas were selected to give a complete picture of the geology of the area. These studies were constrained by field studies carried out by the author as part of the Ethiopian Institute of Geological Survey work in N. Ethiopia between 1973-75, (Axum mapsheet) S. Ethiopia in 1975, (Adola area); SE Ethiopia between 1976-1978 (Berhe,1982), W Ethiopia between 1978-79. Most of the studied areas can be reached by four-wheel drive vehicles, however the rugged topography of Ethiopia necessitated mainly foot traverses with the help of donkeys or porters to carry equipment. Foot

traverses of more than two weeks were not uncommon.

The aim of the project is to test the island-arc accretion models of Gass (1977, 1981) and Greenwood *et al.* (1980) for NE and E Africa and to evaluate by Remote Sensing techniques whether the isolated and scattered ophiolitic complexes form linear belts (Shackleton, 1979). East Africa is a prime candidate for such techniques as there are large areas that have not been geologically mapped. Additionally the aim was to reconcile the relationship of the Pan-African and Mozambique Belt. Did these two belts evolve separately in time and space or have they both undergone a common structural evolution, and evolved coevally? To achieve this, greater emphasis was placed on identifying mafic-ultramafic complexes, and establishing whether they formed a convincing Penrose (1972) ophiolitic assemblage. The preservation and location of remnant allochthonous pieces of former oceanic or back-arc lithosphere in ophiolite belts are believed to represent the sites of ancient plate margins, in this case of accreted-arc terrains. It was hoped that the new understanding of the disposition and tectonic relationships of the mafic- ultramafic complexes would help constrain an evolutionary model for the Pan-African/Mozambique belt.

Three widely separated mafic-ultramafic complexes have been studied in detail for the first time, and a review is made of some of the better documented ophiolites (Price, 1984) mostly located in NE and E Africa and compared with those of Saudi Arabia. The Yubdo-Tulu-Dimtu belt (W. Ethiopia) was studied in the field, while the Baragoi (N. Kenya) and the Adola-Moyale belt (S. Ethiopia/NE Kenya) were also examined petrologically and geochemically to ascertain their ophiolitic character.

The relationship of the ophiolitic suites and the flanking high grade Mozambique gneisses are studied, including the degree of metamorphism and the presence of diagnostic mineral assemblages in order to determine the precursors of these rocks and their metamorphic grade. Granitoids associated with the Mozambique belt were studied for their geochemical affinity and tectonic setting. The geological study of these areas is backed by petrographic study involving several hundred thin sections, of which only a small fraction is presented. An extensive range of samples are only available from Kenya, while a large proportion of the samples from Ethiopia were retained by the Ethiopian Institute of Geological Surveys.

The geology of various key areas in NE Sudan, Ethiopia and Kenya are briefly reviewed. In most cases these are described here for the first time; in others existing data were used including those of Tanzania, Somalia and Madagascar which are re-evaluated and re-interpreted. These are then integrated with field data including major structures acquired from Landsat, and geochemical study to present a coherent dynamic model for the evolution of the Pan-African/Mozambique belt.

The lack of a standardised approach in stratigraphic nomenclature resulted in considerable stratigraphic confusion. These problems were compounded by a tendency to correlate little known sequences over unjustifiably large distances. The difficulties in stratigraphic correlation are addressed in this study.

1.4 PRESENTATION OF THIS STUDY

The present study is divided into seven chapters, the first being this introduction. The second chapter describes the geology and geochemistry of the Baragoi mafic-ultramafic complex of N. Kenya. The third chapter describes the geology and geochemistry of the Adola-Moyale Belt, S Ethiopia/NE Kenya. In this chapter the geochemical study of mafic rocks as well as granitoids from the same area has been undertaken. The fourth chapter describes the regional geology and structural evolution of W Ethiopia. The limited geochemical analyses are restricted to the Gore area of W Ethiopia, which includes granitoid rocks as well as mafic rocks from a marginal basin. Chapter five deals with basic principles and methods of remote sensing, the definition of lineaments, their origin and uses are discussed. It also deals with methods used in structural and lithologic interpretation using remote sensing data. In chapter six fracture analyses, and implications of major fractures is discussed. Finally chapter seven is mainly a discussion of data presented in the previous chapters and seeks to establish a working model for the Pan-African/Mozambique belt. Recommendations for future studies are incorporated. Analytical techniques and geochemical analyses are presented in the appendices. Geological maps are enclosed inside the rear cover.

CHAPTER 2

THE BARAGOI MAFIC-ULTRAMAFIC COMPLEX - N. KENYA

2.1 INTRODUCTION

The Baragoi mafic-ultramafic complex formally referred to as the Siambu Complex (Key, in press) is bounded by latitudes 1°20'N and 2°N and by longitudes 36°40'E and 37°E and lies about 500 kms NE of Nairobi. The area is readily accessible by a principal road from Nairobi that leads to Maralal and thence to Baragoi. The area around Baragoi forms undulating plains, to the west it flanks the Kenya rift, while to the east of Baragoi, there are the Ndoto Mountains. A fuller account of the climate and vegetation is given in Baker (1963). Baragoi is the only township in the area, and the area is populated by the Samburu and Turkana pastoralists.

The main aim of this study was two fold; - (i) to map a section across the mafic-ultramafic complex and to establish from the geological and geochemical data whether the complex is an ophiolite, and (ii) to attempt to identify the palaeotectonic environment and origin of the complex and that of its associated volcanics.

2.1.1 Previous work and general geology

The study area lies within the Baragoi 1:125,000 sheet (degree sheet 27, NE Quarter) which was mapped by Baker (1963). Further south Shackleton (1946) pioneered geological exploration in the Nanyuki-Maralal area (Central Kenya). Recently a British Geological Survey team made systematic mapping and exploration in Central and Northern Kenya, for which a preliminary report has been written (Charlesly *et al.*, 1984). In the summer of 1984 I visited as many mafic-ultramafic complexes as possible in the Baragoi area, and made a detailed traverse along the Baragoi River (section ABC) (Figure 2.1). The general geology of the area is shown on Figure 2.1, modified after Baker (1963).

The greater part of the Baragoi area is divided into two major tectonic domains:

(a) Baragoi Domain - this domain is cored by the Baragoi mafic-ultramafic complex and associated sediments. Lithologies include: (1) ultramafic complexes; (2) metagabbros; (3) amphibolites and

mafic gneisses which form over sixty percent of the area and have been subdivided into amphibolites, hornblende plagioclase gneisses and banded hornblende biotite plagioclase quartz gneisses; (4) basic dykes and sills; (5) metasediments (including marbles, quartzites, quartzofeldspathic gneisses, biotite gneisses, granitoid biotitic gneisses, and hornblende migmatites); (6) post-tectonic granites.

(b) Barsaloi domain - This domain is formed exclusively of metasediments. These include paragneisses, grey biotite gneisses, quartzofeldspathic gneisses; metapelitic and psammitic gneisses with marbles and graphitic gneisses. These rocks have been described as the Ol'Doinyo Ng'iro Gneisses (Charlesly *et al.*, 1984).

This research is not concerned with the study of these metasediments.

2.2 FIELD RELATIONS AND PETROGRAPHY

2.2.1 Ultramafic rocks

Introduction

The ultramafic rocks form elongate bodies and sometimes narrow lenses over a wide area extending from the Nachola ultramafic complex southwards to the Siambu ultramafic, while other lenses pass around the Morilem syncline and continue northwards past Barenyiro complex, Koitokol and extending up to Keleshwa valley area (Figure 2.1). To the southwest there are large irregular elongate bodies in the Kangura area. Most of the ultramafic bodies have been altered to serpentinites and talc-tremolite actinolite rocks forming soft unfoliated bodies coloured in shades of yellow brown to brown and greenish brown.

Originally the ultramafic sequence was represented dominantly by dunite and wehrlite. Although extensively serpentinised, the ultramafic sequence retains a pervasive, high temperature deformation fabric that is readily identifiable in the field. However the tectonic fabric may be obscured where strong weathering and shearing has affected joint surfaces. The foliation is occasionally enhanced by serpentinisation which exploits the anisotropy of the host ultramafic rock.

GEOLOGICAL MAP OF THE BARAGOI AREA

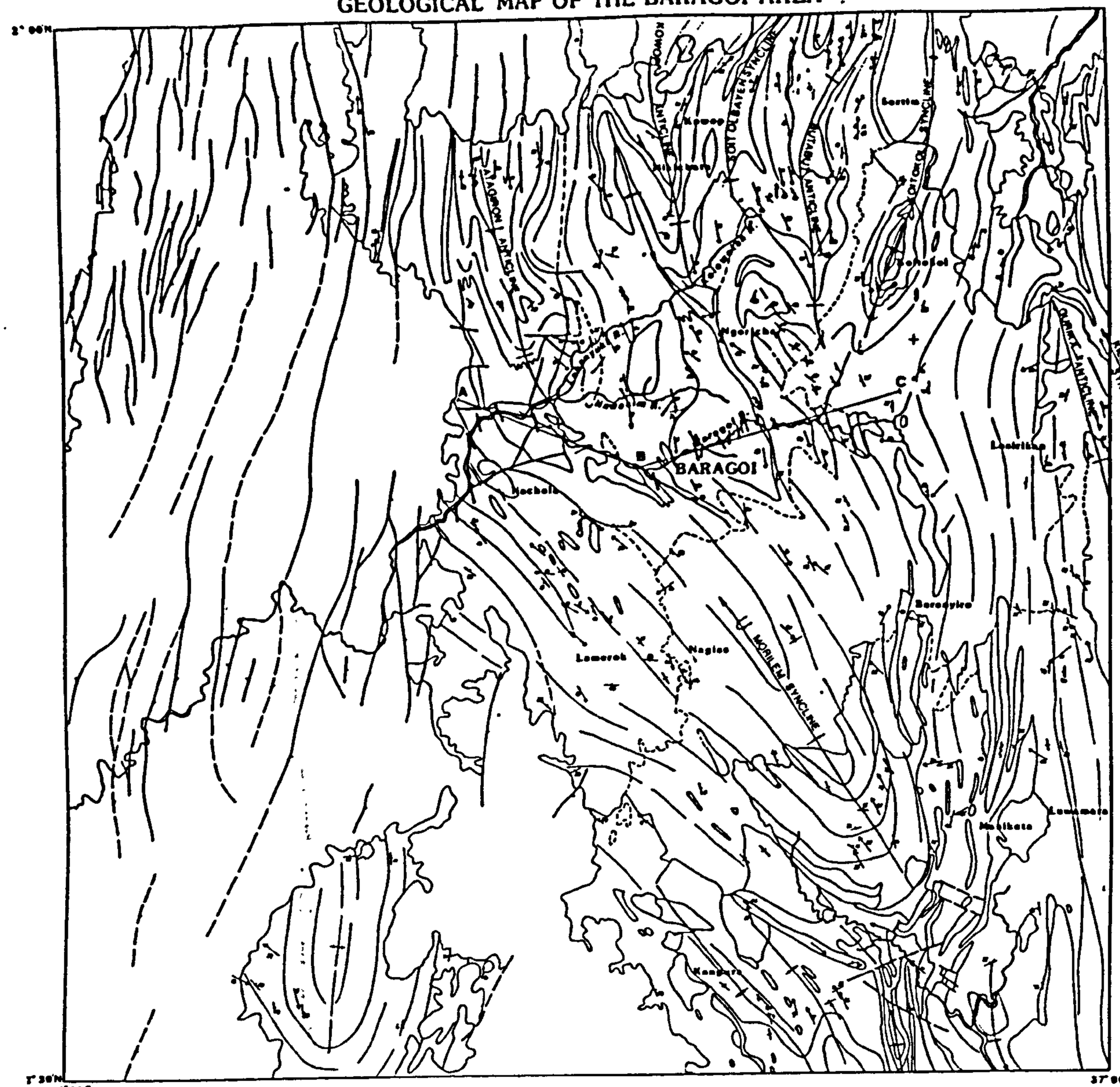

Legend

- Foliation dip and strike, measured
- Foliation, not measured
- Foliation, vertical
- Foliation, horizontal
- Lineation, trend and plunge
- Fold axis, synclinal
- Fold axis, anticlinal
- Overturned anticline
- Overturned syncline
- Shear zones
- Generalised strike trends
- Faults, observed
- Faults, inferred-approximate
- Lithological contact
- Dykes

Alluvium	QUATERNARY	
Tertiary volcanics	MIOCENE	
Biotite granite	LUWAMARA GRANITE	PRECAMBRIAN
Biotite migmatite		
Hornblende migmatite	SIAMBU COMPLEX	
Amphibolite		
Garnetiferous hornblende gneiss		
Hornblende plagioclase gneiss		
Hornblende biotite plagioclase gneiss		
Biotite gneiss		
Marble		
Ultramafic serpentinite		
Metagabbro		
Quartzo feldspathic gneiss	OL DOINYO NGIRO GNEISSES	
Graphitic gneiss		
Biotite gneiss		
Muscovite biotite gneiss		

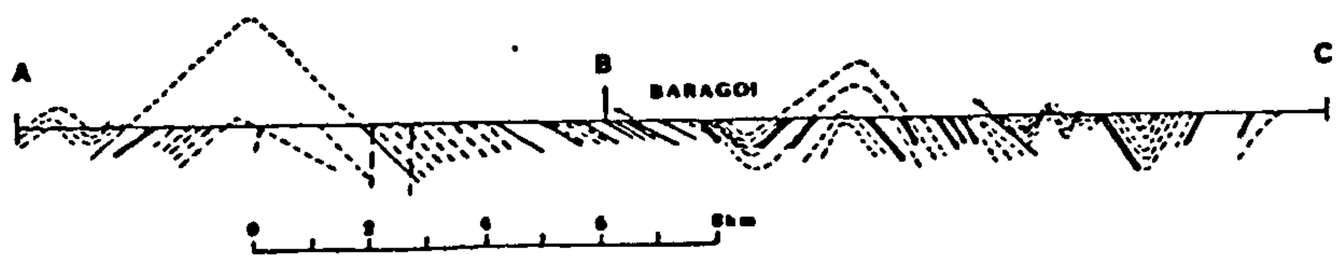

The ultramafic lenses have been folded and as a result the foliation plane strikes NW to NNW and NS to NNE and dips between 20-40° to the NE and SW.

The serpentinite bodies such as Kangura, Morilem and Keleshwa are traversed by numerous thin magnesite veins and contain rare amphibolite lenses; talc is common as a minor constituent. Several vertically foliated amphibolites cross the summit of most of the ultramafic bodies. These amphibolites appear to be dykes and sills. Of all the ultramafic bodies visited Keleshwa, Nachola, Koitokol, Barenyiro and Kangura have been studied in detail. A detailed description of each complex is included here.

2.2.1.1 Keleshwa Ultramafic Complex

The main part of the Keleshwa ultramafic body is a serpentinite approximately 1.3 km in length and 0.6 km wide that is cut by many narrow magnesite veins. The serpentinite is lens-shaped, fine to medium grained and variable in colour from grey white to yellow brown. It forms a prominent hill, in marked contrast to the surrounding savannaha grasslands, it forms a barren landscape. Large stellate tremolite aggregates occur within actinolite rocks associated with anthophyllite asbestos. The northerly ultramafic body consists of serpentine with many magnesite veins. The dunite is cut by a few amphibolite dykes. These dykes which have chilled against and recrystallised the adjoining serpentine body are of gabbroic and doleritic composition. A number of thrusts are observed, which show well developed slickensides and mylonitisation. A major thrust has cut the ultramafic body and the thrust plane is itself folded along N-S trending axes and plunge to the south.

Several specimens of ultramafics have been petrographically studied. The ultramafics are subdivided into two groups according to their mineralogy: the mantle dunite and cumulate dunites, wehrlites and gabbros.

Partially serpentinised mantle dunites contain up to 75% relict olivine, and while some have scattered grains of altered magnetite, forming not more than 5% of groundmass, others have chrome spinel as an accessory mineral. Thin sections studied show advanced stages of serpentinisation. The main mineral assemblage is antigorite plus chromite with accessory talc. A partly serpentinised rock (Plate 2.1) shows rare relict olivines in a largely serpentinised matrix with

chrome spinel forming not more than 5%. This is a cumulate dunite.

The other set of samples are dominantly anthophyllite forming around 70% of rock, replacing orthopyroxenes (enstatite) which forms 15% of groundmass as well as titanomagnetite 5% and rare crystals of rutile. In some sections olivine is observed, while in others it has been serpentinised. In thin section the metagabbros are dominantly actinolites, forming over 50% of groundmass, which replace pyroxene and is associated with small radiating tremolite needles. Plagioclase of bytownitic composition (An_{50-60}) forms 40% of the groundmass and shows a cumulate texture. Scattered aggregates of epidote are to be observed. One metagabbroic unit is observed to be a layered pyroxene plagioclase gabbro. Quartz is rarely found as a secondary mineral.

2.2.1.2 Nachola Ultramafic Complex

The Nachola complex is a lens-shaped ultramafic body 2.5 km in length and 1.1 km wide. The complex is made up of a series of serpentinites, tremolite-anthophyllite rocks which in places are altered to talc. The serpentinites are found associated with smaller gabbroic bodies. The tremolite-anthophyllites commonly contain lenses of chlorite schists, which were produced by shearing along northwesterly trending faults. The complex trends N50°W with steep dips to the southwest.

The Nachola ultramafics are dominantly cumulate wehrlites. In thin section the main mineral is actinolite forming 50% of the rock replacing clinopyroxenes. Relict olivines and rare orthopyroxenes are also present with aggregates of epidote, with accessory sphene and calcite. The opaques are largely magnetites.

The metagabbros are largely formed of tremolite-actinolites which replace clinopyroxenes. Primary plagioclase forms 45% of the groundmass. In some sections the plagioclase has been replaced by quartz and amphibole.

2.2.1.3 The Barenyiro Complex

The complex is made up of a succession of dunites (usually serpentinised) with few amphibolitic dykes. The serpentinites are cut by thin ultramafic dykes and sills which show reaction rims along contacts with the serpentine body. A detailed section was measured across the complex (Figure 2.2).

The Barenyiro ultramafics contain rare relict olivine crystals which are largely surrounded by serpentinite, and actinolites replacing pyroxenes. Titanomagnetite forms 10% of the section. In some sections chlorite is abundant. Few calcite veinlets are observed cutting the ultramafic body. In section SB59 (Plate 2.2) tremolite-anthophyllite forms more than 70% of rock, with rare corundum grains as an accessory mineral.

2.2.1.4 Kangura Ultramafic Complex

Kangura is an elongate body more than 3 kms long and up to 1 km wide. It is formed of massive greenish brown serpentine locally associated with carbonates, talc schists, and tremolite-actinolite rocks and chromite lenses. It is also frequently cut by magnesite veins. The southern part of the complex contains several chromite lenses. The Kangura chromite deposits of the Baragoi area were first described by Baker (1963). The chromites are lens or pod shaped bodies, and are invariably parallel to the long dimensions of the dunite body (Plate 2.3). They are generally boudinaged producing a podiform effect and are sheared at their margins. The chromite bodies are generally massive with more than 95% chromite (<51% according to Baker,1963). Outside the pods chromite grains are disseminated, showing evidence of banding. The massive chromites display a variety of textures mainly related to deformation processes. Cataclastic textures are developed in some sections due to shearing. The grains in the massive chromitites are large (up to 5 mm) interlocking and subhedral to anhedral. Disseminated chromites are sometimes observed in the dunites which is characterised by an abundance of talc veins. The host rock is a serpentinised dunite body with many magnesite veins.

Three chromite lenses have been sampled in detail. One is about 14.2 m long and 1.7 m wide, but narrows down to 0.5 m. It strikes N20°E with steep dips to the SE, although dip angles are

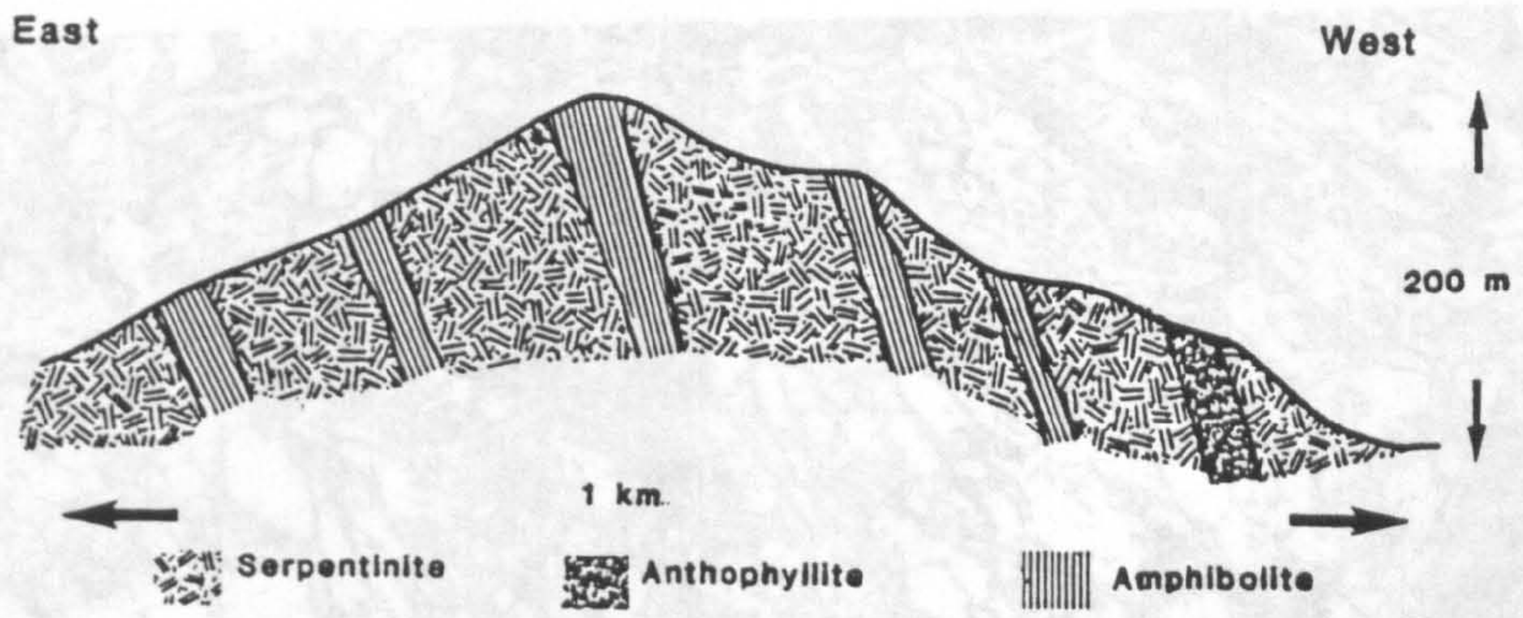

Figure 2.2 Schematic section of the Barenyiro mafic-ultramafic complex.

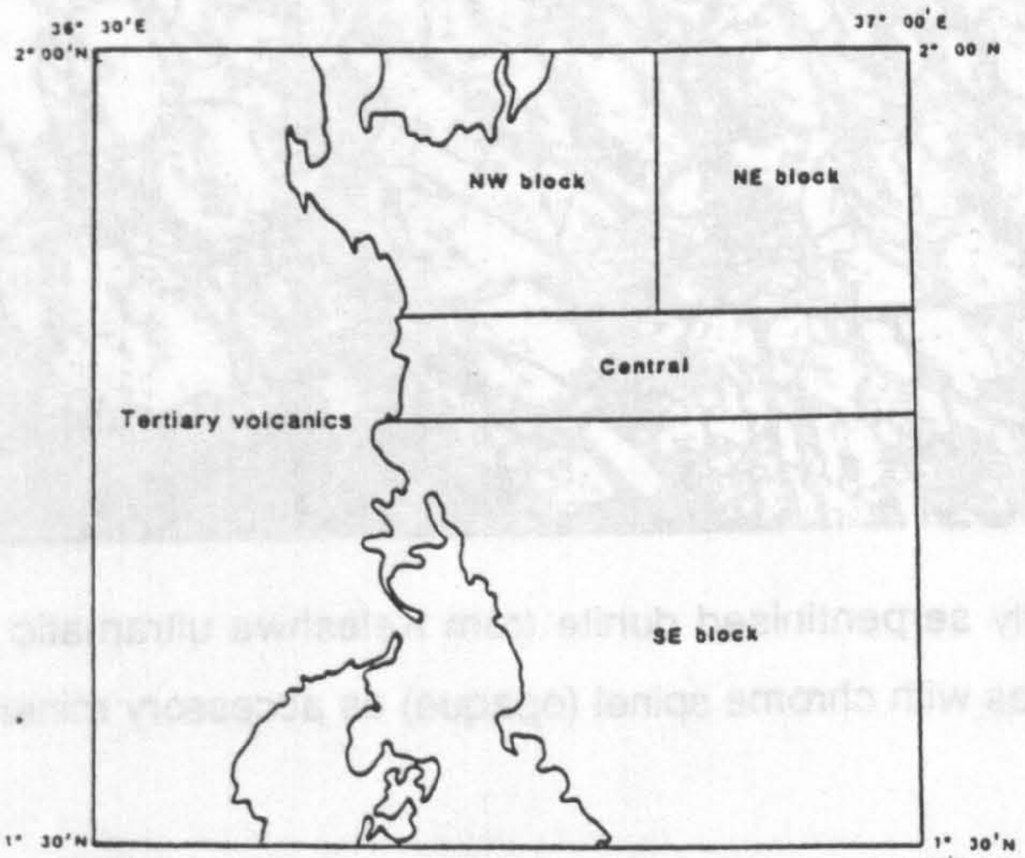

Figure 2.3 The Baragoi area showing subdivision of tectonic blocks.

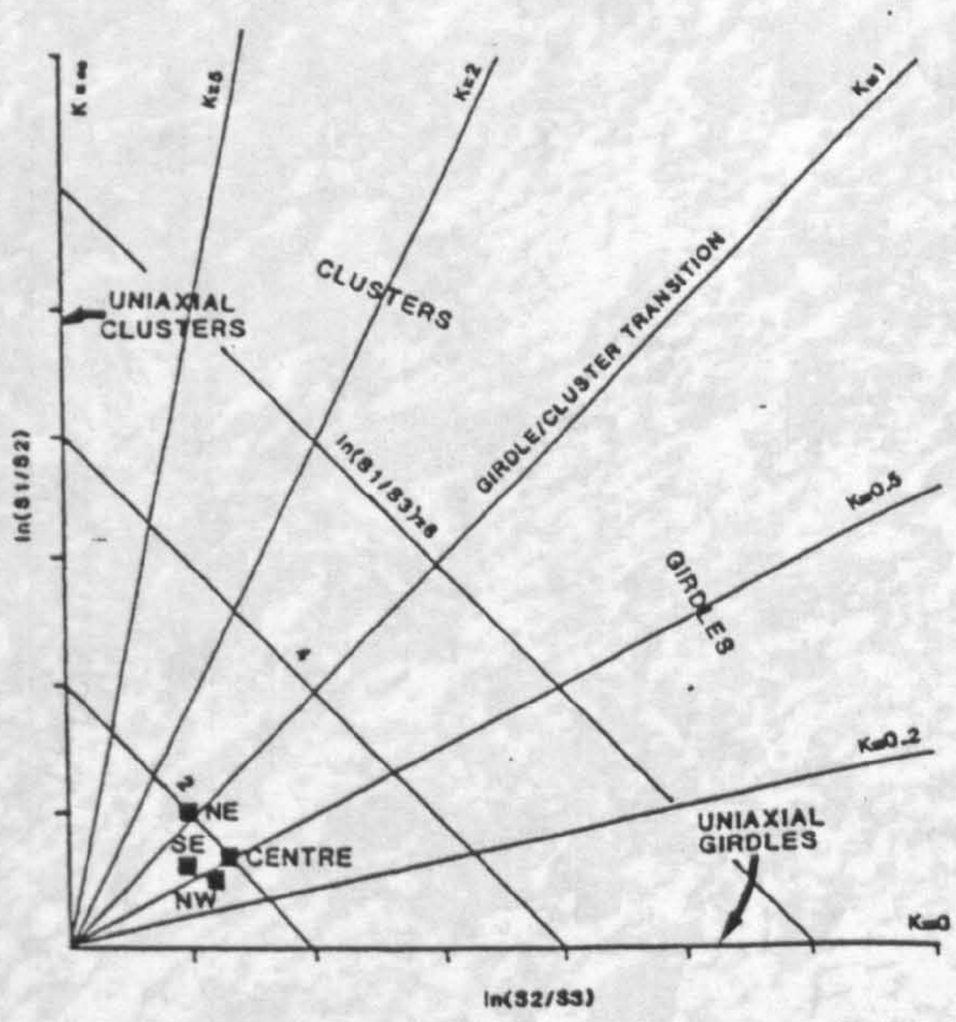

Figure 2.4 Fabric shape and strength plotted using eigen vectors S1, S2 and S3, where K=ln(S1/S2)/ln(S2/S3) varies with the strength of distribution cluster and the value C= ln(S1/S3) varies proportionally with the strength of any preferred fabric orientation (after Woodcock,1977).

Plate 2.1 Partially serpentinised dunite from Keleshwa ultramafic complex (SB15B). Uniformly sized relict olivines with chrome spinel (opaque) as accessory mineral. Cross nicols. Field of view 3.47.

Plate 2.2 Fibrous tremolite-anthophyllite which form the bulk of the rock (sample SB59). The opaques are titanomagnetite, while the bluish crystals are corundum. Barenyiro ultramafic complex. Field of view 3.47.

Plate 2.3 A massive chromite lens within a serpentinised dunite body. The lens is 11m long and its width ranges from 1.3m to 0.5m.

Plate2.4 Koitokol gabbro. Megacryst of plagioclase partially enclosed by epidotes (upper right). The rock is set in a finer matrix of interlocking grains of hornblende (greenish and yellow brown) (SB96A). Field of view 3.47.

variable (Plate 2.3). The second chromite lens trends N60°W and is 5 m long and 1.5 m wide, and tapers rapidly to 0.35 m. The third lens trends N60°W and is 11.2 m long and its width varies from 1.3 to 0.9 m.

The petrology and geochemistry of the Kangura ultramafics and chromites are discussed later in greater detail.

2.2.2 Metagabbros

Gabbros have been sampled from three separate intrusive bodies: the Baragoi, the Headstream gabbro (found east of Baragoi village) and the Koitokol hill. Gabbroic rocks are well developed in the Baragoi town area, and form a large proportion of the Nachola, and Koitokol mafic-ultramafic complexes (Figure 2.1). The largest gabbroic body is found in the Baragoi river east and west of the road crossing (1° 47' N, 36° 48' E) extending eastwards up to Nderentei. The gabbros are cut by a swarm of dykes; both the host rock and the dykes have been folded together with fold axes trending N30-40°W. The Baragoi metagabbros can be subdivided into two groups as they range in composition from typical gabbro to gabbro-diorites (Group II) and anorthositic gabbro (Group I). Following the Baragoi river upstream the gabbros become gneissose, and elsewhere are laminated with feldspathic and hornblende laminae. The gabbros have autoliths due to incorporation of their chilled margins.

The gabbros in the Koitokol hill are layered but become massive up the sequence. The Koitokol gabbros are generally coarse grained and contain hornblende crystals up to 1 cm long, and megacrysts of plagioclase (An_{80-90}), which forms 50-70% of the rock, are set in a finer matrix consisting of sodic plagioclase and microcline and/or quartz; with interlocking grains of hornblende associated with sphene, biotite, and small grains of epidote (Plate 2.4). Rarely the gabbros are anorthositic. To the southwest of Lokongori (Figure 2.1) strongly foliated gabbros occur which have broken hornblende crystals, and streaks of fine grained hornblende and biotite. The plagioclase is generally granular in these rocks.

South of Nderentei (Figure 2.1) gabbroic augen gneisses are observed which are characterized by the occurrence of porphyroblastic microcline in replacement of quartz and

plagioclase set in a fine matrix of plagioclase, biotite, hornblende, apatite and sphene with minor epidote.

2.2.3 Amphibolites

Amphibolites are widespread in the Baragoi area. They usually occur as narrow lenses associated with the hornblende plagioclase gneisses, hornblende plagioclase biotite quartz gneisses and occassionally associated with the Nachola and Barenyiro mafic-ultramafic complex. The thickness of the amphibolites ranges from a few metres to 250 metres in the Nikichata area and the largest irregular lens like body between Barenyiro and Nderentei is about 400 m thick. In the Masiketa area they form 200-400 m wide parallel amphibolite bodies trending N-S. The amphibolites are generally dark greenish grey in colour, coarse-grained and crudely foliated. In highly deformed areas the amphibolites are resistant to plastic deformation and granitization. No relict igneous textures have been observed but the presence of orthopyroxene and hornblende strongly suggests that they are metamorphosed basic igneous rocks.

In the Koitokol Hill area, the amphibolites overlie the ultramafic rocks and in places massive bands of ultramafics have been thrust into the amphibolites. Relict E-W microfolds plunge to the east.

The Nikichata amphibolites trend N10°E dipping 28°NW. There are microfolds with fold axes trending parallel to the strike of foliation. The amphibolites show evidence of shearing and have been plastically deformed and boudinaged on a regional scale (Plate 2.5). They are cut by quartz veins, both concordant to, and cutting across the foliation. Few of the veins have been boudinaged. In thin section the Nikichata amphibolites are dominantly composed of hornblende (>50%) that is sometimes porphyroblastic, with pale green orthopyroxenes partly replaced by hornblende. The matrix is formed of a mosaic of orthopyroxenes and hornblende, with quartz forming 5-10% of the rock, and rare feldspar, biotite, and epidote (Plate 2.6).

The amphibolite between Barenyiro and Nderentei has either abundant hornblende or actinolite. The hornblendes are generally porphyroblastic crystals reaching up to 1.5 cm in length, partially replacing orthopyroxenes. The matrix contains aggregates of hornblende, epidote and

Plate 2.5 Sheared and deformed amphibolites. The microfolds (D_1) are E-W trending and plunge to the east. Nikichata area.

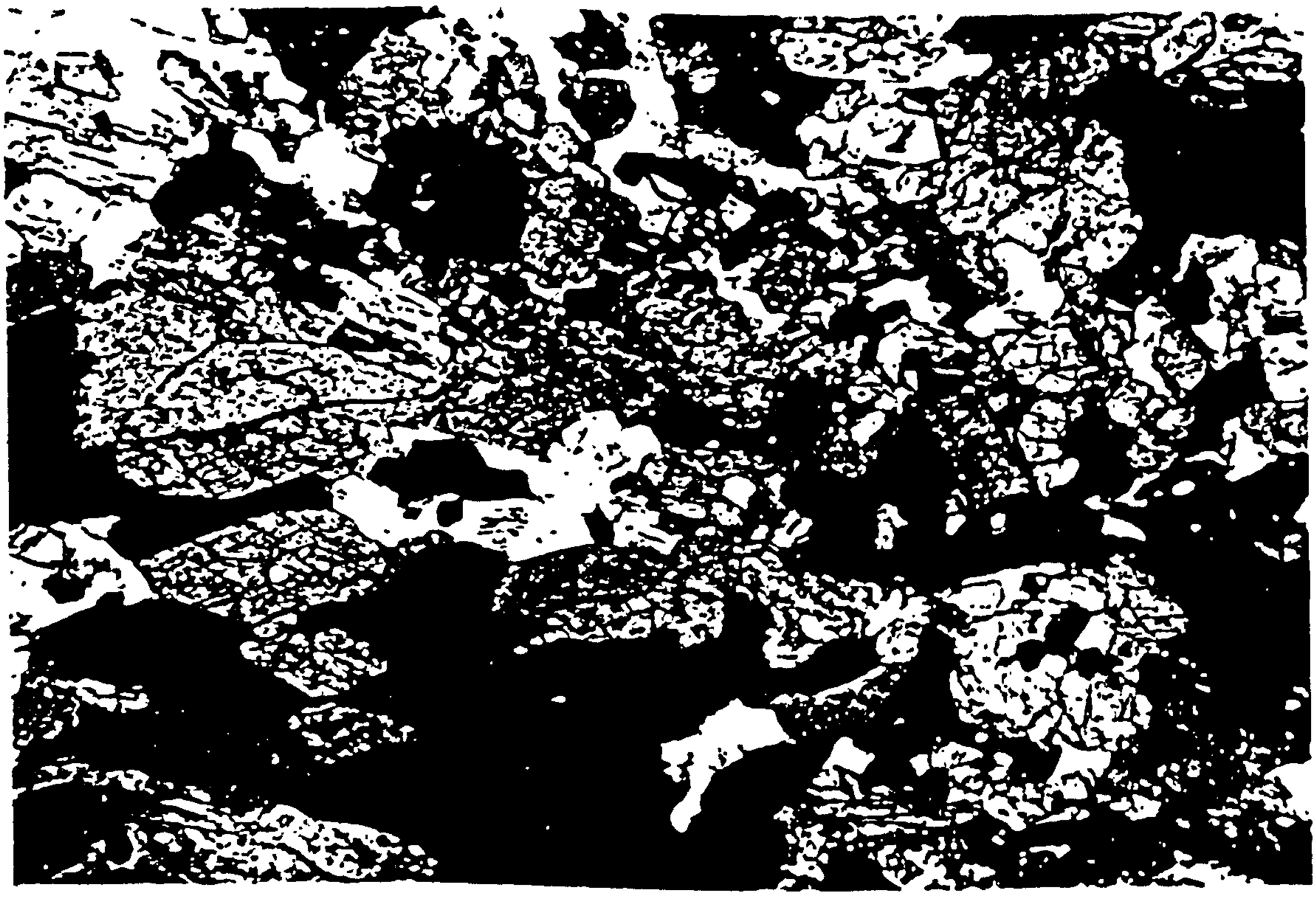

Plate 2.6 This section is mostly composed of hornblende (dark green and pale brown) partially replacing orthopyroxenes (pale green). Nikichata amphibolites (sample SB18A). Field of view 3.47.

quartz. Sphene occurs as an accessory mineral and rarely with ore grains. The amphibolites are interpreted as a series of metamorphosed lavas.

2.2.4 Hornblende plagioclase gneisses

The Hornblende plagioclase gneisses are the most widespread rocks in the Baragoi area. In the Baragoi, Nawakim, Lebanyuki, and Kolowotan rivers, the hornblende plagioclase gneisses occur together with amphibolite lenses and hornblende biotite plagioclase gneisses. 2 kms west of Baragoi town, the hornblende plagioclase gneisses have been cut by lenses of gabbro-diorite.

The commonest hornblende plagioclase gneisses are mesotype to melanocratic, coarse grained, in places, migmatitised and cut by numerous pegmatite veins. Fine grained varieties are usually fissile, while the coarse grained varieties are banded with streaks of granular feldspar. Occasionally epidote is observed in hand specimens.

The hornblende plagioclase gneisses overlie the hornblende biotite gneisses at a shallow angle, 3 kms north of Nachola, whereas 6 kms west of Baragoi town the hornblende plagioclase gneisses underlie the biotite gneisses with a steep thrusted contact. The hornblende plagioclase gneisses are folded with fold axes trending N40°W, usually plunging to the SE. However in places relict E-W isoclinal folds have been observed.

In thin section the hornblende plagioclase gneisses show poikloblastic textures, with hornblendes enclosing granular aggregates of plagioclase. Sometimes the hornblendes have been uralitized. Plagioclase occurs as anhedral aggregates, often in lenses. It is commonly twinned and ranges in composition from An_{30} to An_{45}. It commonly contains inclusions of zoisite. Rare minor relict orthopyroxenes (as in section SB19A), are usually partly replaced by green amphibole. Microcline is equally rare and forms 5% of the rock (Plate 2.7). Epidote occurs as clusters in plagioclase or at the margins of the hornblende crystals. Quartz appears in most sections as either isolated granular quartz grains, or as small clusters of small grains associated with plagioclase. Biotite, forming 5% of the rock, is observed to cut earlier hornblende. Baker (1963) suggests that the appearance of biotite is due to feldspathisation and shearing. Sphene is a common accessory mineral sometimes, accompanied by apatite. Calcite and magnetite were observed in two sections.

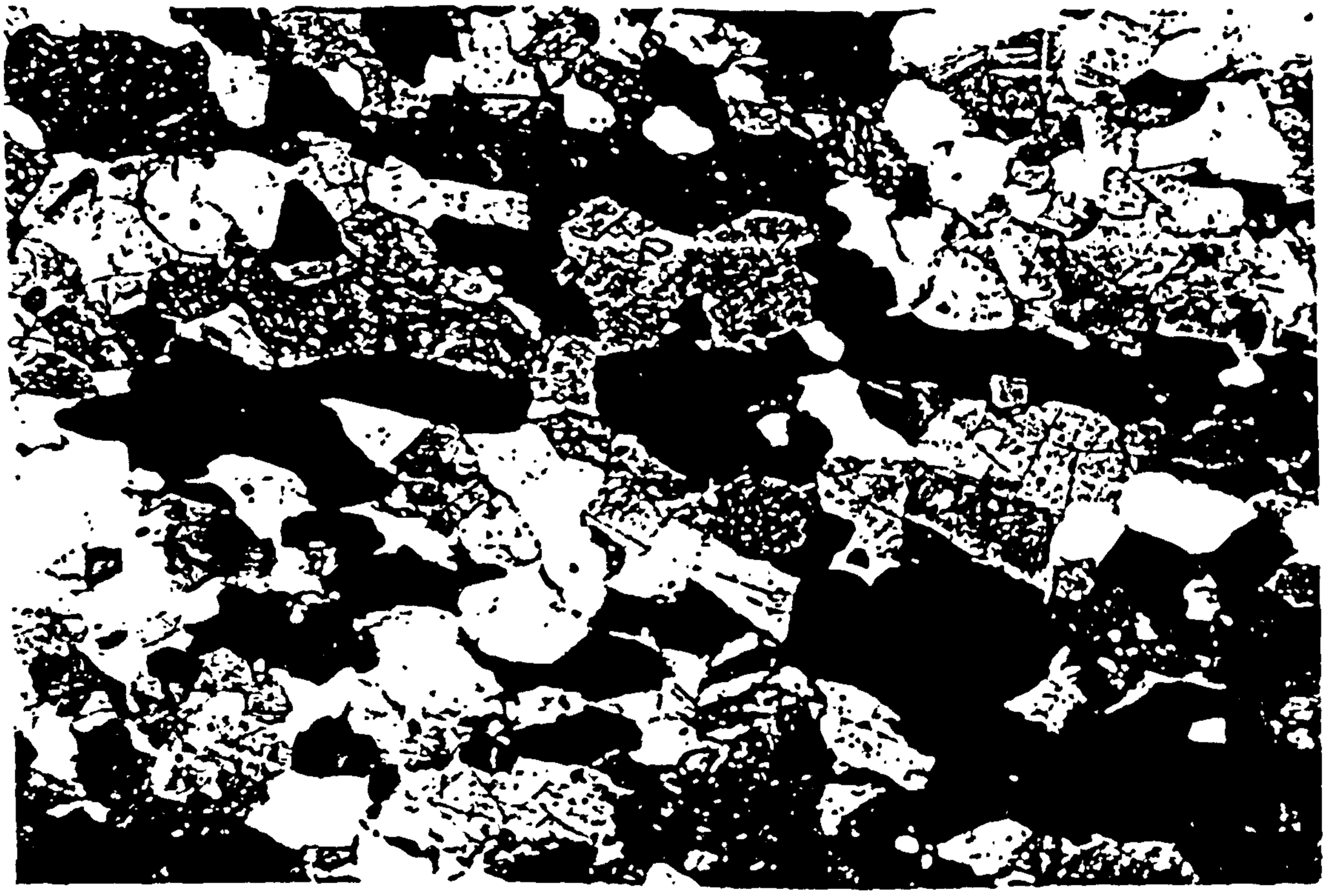

Plate 2.7 Hornblende plagioclase gneisses. Parallel orientation of hornblende (pale to dark brown) in a predominantly plagioclase-quartz matrix (SB19A). Baragoi area. Field of view 3.47.

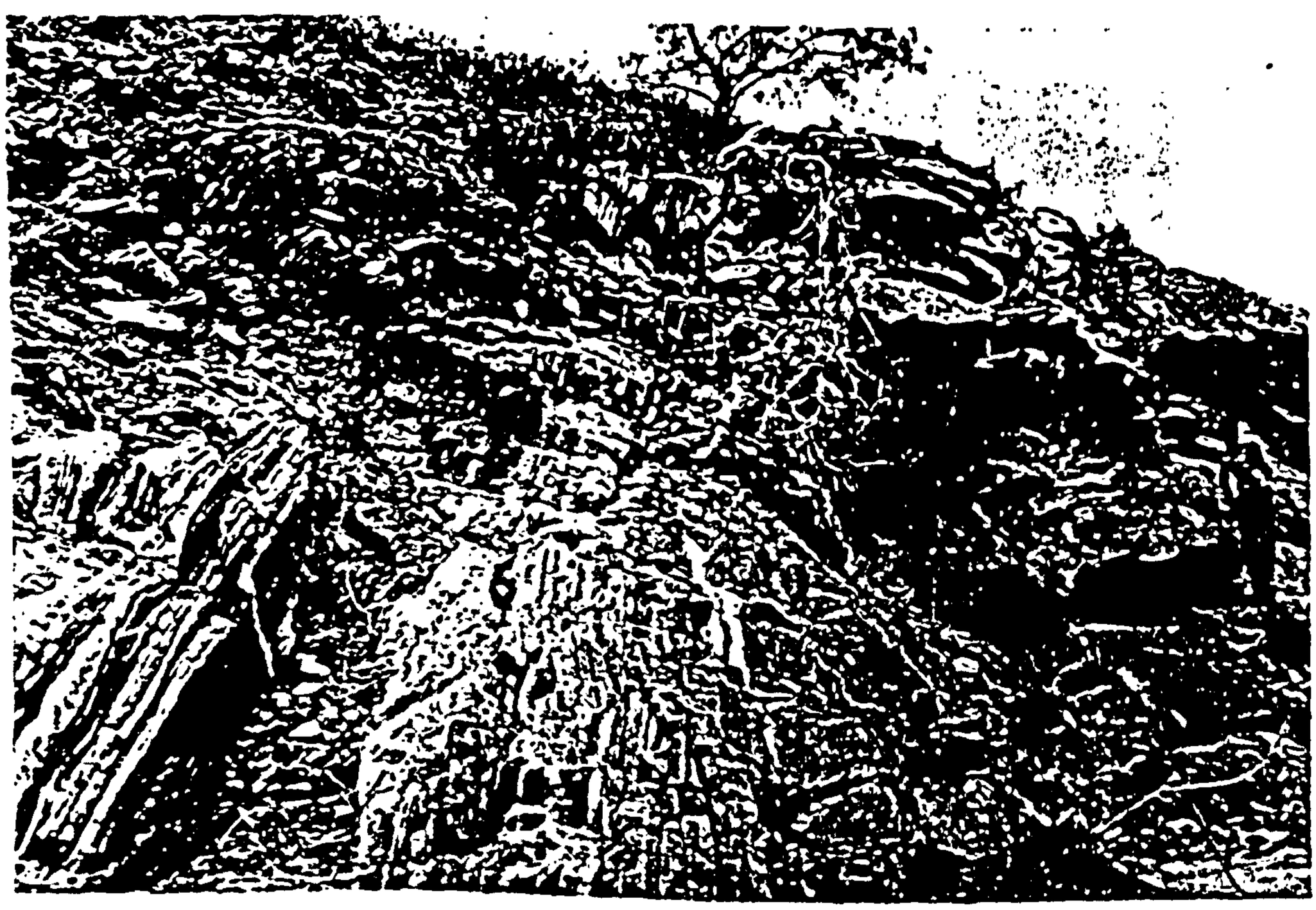

Plate 2.8 Well foliated hornblende plagioclase gneisses (right side) laminated with quartzofeldspathic hornblende biotite plagioclase quartz gneisses. Masiketa area.

Although these igneous rocks are gneissose, the dominance of hornblende, plagioclase and the presence of relict pyroxene suggests that they are metamorphosed basic lavas.

2.2.5 Hornblende, biotite, plagioclase quartz gneisses

These rocks comprise a succession of regularly banded fissile fine to coarse grained hornblende biotite plagioclase gneisses. In hand specimen they are light coloured, friable and laminated with granular feldspathic lenses alternating with hornblende and biotite rich layers (Plate 2.8). They usually occur interfolded with the hornblende plagioclase gneisses or they have a thrusted or a gradational contact.

In the Nachola area they generally form homogeneous light coloured coarse quartzofeldspathic rocks. They range from migmatitic to gneissic in texture. Southwest of Nachola the rocks form migmatitic hornblende gneisses, and they are traversed by stringers, veins and lenses of pegmatite which grade locally into aplites. In this area the formation is cut by basic sills associated with basic lavas. The basic lavas preserve structures that look like pillows (Plate 2.9). The pillow structures are c.20-25cm long. In the Baragoi area this unit contains rounded pebbles or clasts of hornblende gneisses indicating their partly sedimentary origin. These rocks could be volcanoclastics.

The hornblende biotite plagioclase quartz gneisses are widely developed between Kangura and Masiketa areas. Six miles west of Masiketa village the hornblende biotite plagioclase gneisses are interbanded with the hornblende plagioclase gneisses and amphibolite lenses of not more than 100 m thickness. Lenses of marble are sometimes found intercalated within the sequence. Increasing felspathisation leads to the development of mesotype and leucocratic gneisses often with sieved porphyroblastic hornblende augen gneisses.

In thin section they contain porphyroblastic hornblende crystals and inequigranular quartz grains with strain shadows, set in a granular matrix of anhedral quartz and oligoclase grains. Small biotite grains are intimately intergrown with hornblende. Minor constituents are epidote and titanomagnetite crystals, while sphene as a rare accessory. Some of the more mafic horizons show dominantly granular aggregates of hornblende forming up to 40% of rock, partially enclosing plagioclase An_{70-80} surrounded by an interlocking matrix of feldspar grains with a small amount of

Plate 2.9 Deformed pillow lavas. Baragoi area.

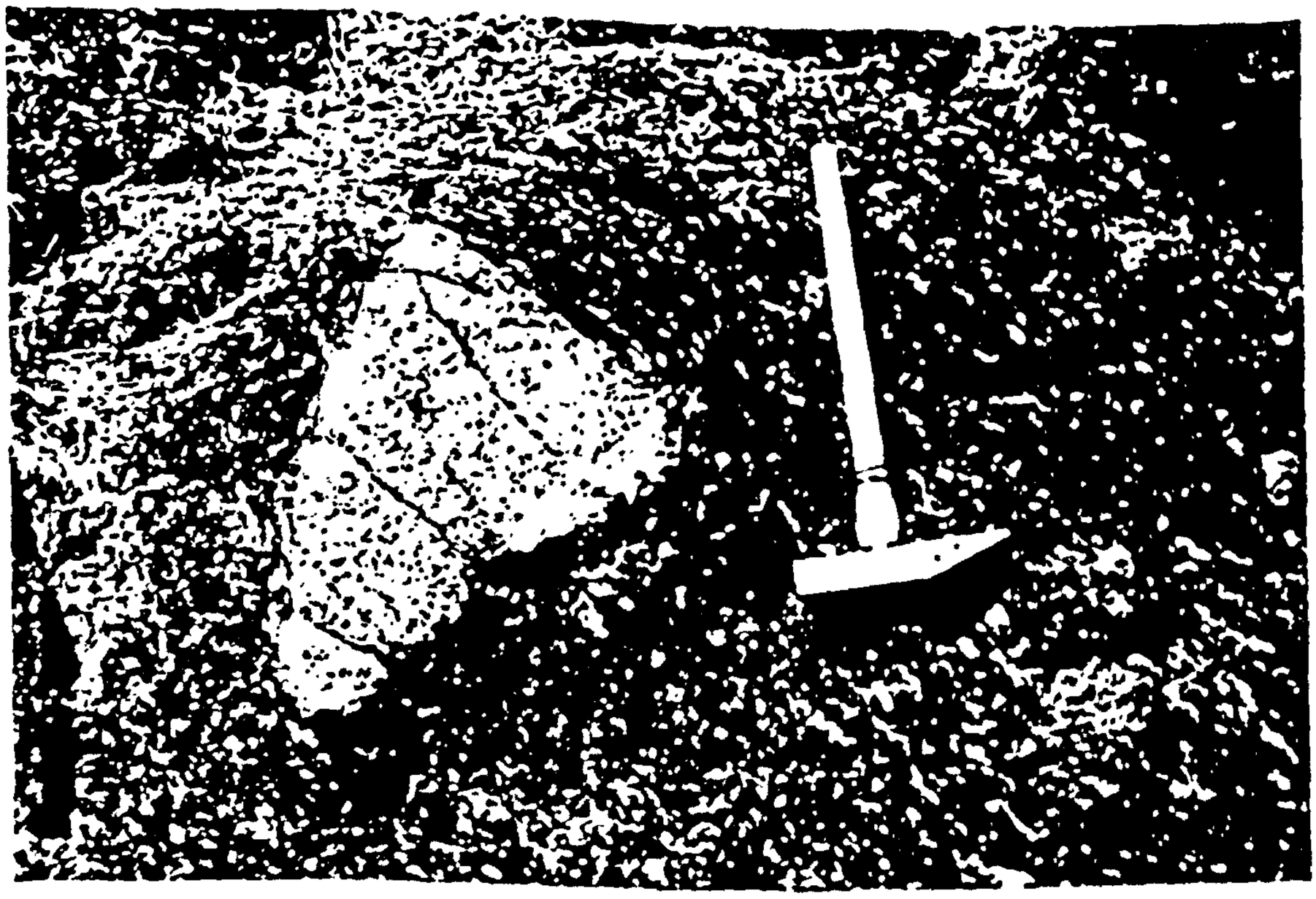

Plate 2.10 A gabbroic block engulfed by amphibolitised lava. Evidence of chilling can be observed surrounding the gabbro.

quartz and epidote.

2.2.6 Dykes and sills

2.2.6.1 Basic dykes and sills

Dykes are common in the Baragoi area, cutting the metagabbros, the hornblende plagioclase gneisses, the granitoid gneisses and occasionally cutting ultramafic bodies such as Nachola and Barenyiro. The dykes are usually not more than 2 m thick. Some of the intrusives are concordant with foliation while others are discordant which implies that one set of intrusives pre-date the foliation and others post-date it. Some of the earliest dykes in the Baragoi area cutting the metagabbros have been refolded together with the gabbros. The pre-tectonic dykes usually trend to the northwest.

Dykes occur in four areas: (a) those that cut the metagabbros in the Baragoi town area; (b) those cutting the metagabbros 8 km NE of Baragoi town; (c) those cutting hornblende biotite granitoid gneisses SW and NE of Nachola, and (d) those cutting Barenyiro and Nachola ultramafics. The dyke units are described in detail:

(a) the dykes cutting the gabbros are not more than 0.5 m thick. These dykes are folded together with the gabbros. They have been weathered so much that it was difficult to get representative fresh samples. Some of the dykes are feldspar-rich in hand specimen.

(b) 8 km NE of Baragoi, a series of basic dykes half a metre each cut the metagabbros. In places the deformation was so severe that the dykes were stretched and boudinaged. The majority of these dykes have bifurcated upwards, and have engulfed blocks of gabbro (Plate 2.10). The basic dykes are generally garnetiferous.

(c) The granitoid gneisses along the Nawakim river have been cut by numerous basic sills. Going south of Nachola, along Baragoi river, a series of dykes 0.5 m wide are observed cutting the granitoid gneisses. In this area there are volumetrically few basic sills as compared to dykes. Since the granitoid gneisses have been proved to be younger than the gabbros, the later dykes must have been emplaced after the formation of the granitoid gneisses.

(d) The Barenyiro ultramafic complex is cut by five fine grained amphibolitic dykes. The dykes are 2 to 5 m thick. The ultramafic body is recrystallized along the contacts of the amphibolites.

The dykes in the Baragoi area show alignment of hornblende interspersed with bands of feldspar hornblende crystals. The hornblende usually form 40-50% of groundmass and usually envelope plagioclase megacrysts which form 20-30% of groundmass. They contain small rare biotite laths, with minor epidote, and infrequently sphene as accessory minerals.

2.2.6.2 Felsic dykes

There are distinctive flaggy leucocratic intermediate dykes and sills which cut hornblende gneisses and gabbros. They are exposed in the Kolowotan, Lebanyuki, Lamerok and Baragoi rivers. They are usually between 0.5-2 m wide and have usually experienced similar deformation histories to the country rocks. They are foliated, mesocratic medium grained rocks, with biotite flakes up to a maximum of 2 cm in diameter. The best examples are in the Baragoi river, north of Baragoi town, (1° 48' 10" N, 36° 49' 13" E), in Nawakim 3.5 km northeast of Baragoi town and in the Baragoi river approximately 4.5 kms southwest of Nachola. They appear to be older than the granitic, aplitic and pegmatitic intrusives as they were never observed cutting them.

In thin section (SB114 and SB116) hornblendes are oriented at random, in an equigranular fine-grained matrix that consists of interlocking intermediate plagioclase grains, microcline and often irregular quartz grains. The plagioclase is untwinned and contains small inclusions of hornblende, biotite and minute rods of zoisite. Sphene is usually plentiful in association with hornblende. The felsic dykes may be classified as hornblende diorites.

2.2.6.3 Pegmatites

Pegmatites occur as concordant and cross-cutting sheets and veins varying from a few centimetres to 30 metres wide, and a kilometre long; they are found throughout the area. The pegmatites are characterised by their sheet like form with parallel walls and sharp contacts and a marked coarseness of grain. The smaller pegmatites are frequently deformed, and it seems that they are syntectonic, while the larger pegmatites are rarely deformed, cut earlier structures, and hence are thought to be late to post-tectonic. The small pegmatite veins are frequently slip-folded or have experienced shearing.

In the Nawakim river there is a swarm of post-tectonic pegmatites cutting the biotite hornblende gneisses. Individual dykes are usually 10-20 cm thick.

2.2.7 Biotite gneisses

Biotite gneisses are found in the core of the Kowop anticline, and form the nose of Butabut anticline. In addition they are found as thin localised bands usually associated with hornblende gneisses or granitoid gneisses. The biotite gneisses are dark, well foliated, frequently flaggy and are medium grained.

A typical rock specimen from Ngoriche area (SB5) is medium to fine grained, well foliated with quartzofeldspathic lenses and has dominant biotite. Feldspars consist of irregular oligoclase and small interstitial microcline grains. The microcline has replaced quartz and plagioclase. Myrmekitic texture is well developed . Biotite is ubiquitous with less muscovite, epidote and rare garnet. Biotite gneisses with notable amounts of garnet are rare, and usually occur associated with granitised hornblende gneisses.

A sample from Kowop Mountain shows a dominance of inequigranular quartz grains, with elongated aggregates of garnet. Biotite occurs as irregular flakes between quartz and plagioclase grains and is also intergrown with rare muscovite flakes.

2.2.8 Granitoid gneisses

The most important outcrops are in the Kowop, at Butabut, in Lebanyki river, and east of Lesirikan. These rocks form ridges and isolated hills, whereas the Kowop granitoid gneiss forms a stratiform body. The granitoid gneiss 4 kms SW of Ngoriche hill is mantled by hornblende plagioclase gneisses, and hence could be a mantled granitic gneiss dome. The granitoid gneisses are poorly foliated and outcrop as massive rounded boulders. The granitoid gneisses are generally buff to yellowish brown in colour and are granular in texture and contain isolated biotite flakes. In thin section the rocks are texturally inequigranular and xenomorphic. The gneisses are composed dominantly of microcline, and oligoclase with minor quartz, biotite and iron oxides. Microcline is observed replacing plagioclase and quartz.

and quartz.

2.2.9 Granites

The Sartim and Luwamara granites are the two most important intrusive bodies.

2.2.9.1 Sartim granite

The Sartim granite is an elongate body, 2.5 kms wide by 9.5 km long. A narrow zone of migmatites occurs along its margin. At the southwestern side it is composed of interbanded gneissic granite and hornblende biotite gneisses. Going towards the centre a granitic body intruding the gneissic host rock, becomes more prominent. Close to the centre it is composed of homogeneous gneissic biotite granite. Elsewhere there are very light coloured microgranites showing intrusive relationship with the gneissic granites. At the southern extremity of the granitic body the gneissic granites contain inclusions of amphibolite and hornblende plagioclase gneisses. The occurrence of xenoliths in the western side of the granite body suggests that the central part is definitely intrusive.

Feldspar forms about 50% of rock. Oligoclase (An_{20}) occurs as xenomorphic aggregates. Microcline and myrmekites occur as small intergranular crystals. Irregular grains of quartz up to 3 mm in diameter are characteristic. Biotite forms either as clusters or along grain boundaries. Sphene is a common accessory mineral.

2.2.9.2 Luwamara granite

This is a 2.5 km by 3.5 km long granitic body, which forms a distinctive hill with two summits. The granite is a moderately homogeneous body, containing only a few small quartz veins and pegmatites. It is well foliated, with augen texture frequently developed, and variations in texture occur which are due to differing degrees of deformation. The central part of the granitic body has a foliation trending NNW with steep deep, oblique to that of the surrounding hornblende plagioclase gneisses, while the marginal parts of the mass have an ill defined foliation parallel to the margins. Apophyses of the granite penetrate the hornblende plagioclase gneisses along its western margin indicating its intrusive origin. In hand specimen the augen are porphyroblastic feldspars with granular plagioclase

matrix and subordinate quartz and biotite.

In thin section, SB82A, there are porphyroblastic microcline, in a matrix of xenomorphic-granular plagioclase with subordinate quartz. Biotite forms 5% of the rock and occurs as large crystals. Hornblende occurs rarely, but muscovite is observed in section SB82A.

2.2.10 Summary

The most common ultramafic rock type is dunite and forms about 80% of the ultramafic outcrop. Small podiform chromite lenses are found in a dunite body of the Kangura area. Since in most complete ophiolite sections chromite bodies occur mainly towards the top part of the mantle sequence, and within the lower cumulates it is suggested that there is little residual mantle in the Baragoi complex. The wehrlitic rocks may represent thrust slices of the ultramafic unit or form an ultramafic cumulate unit within the gabbro pile as in Nachola ultramafic complex.

Dyke swarms are found cutting the gabbro, and the dykes are considered to be feeders of the overlying basic gneisses and amphibolites. However the nature of the dyke-lava boundary is not clearly established. Pillows have not been found except possibly in one locality. However petrographic evidence suggests that the Hornblende plagioclase gneisses and the Amphibolites are of igneous origin and hence they have been interpreted as metamorphosed lavas. Typical ophiolitic assemblage as defined by Penrose (1972) is present in the Baragoi area, however since the complex has been complexly imbricated and has suffered an upper amphibolite facies metamorphism, geochemical constraints are required to establish its ophiolitic identity.

2.3 STRUCTURE

Introduction

The intention of the present study was not to make a thorough analysis of the structure of the Baragoi mafic-ultramafic complex, however foliation was recorded during routine mapping, and along two detailed traverses across the complex. The lineation was found to be particularly difficult to define and where measured was mostly intersection of bedding and cleavage. Close observation of

foliation was used to determine whether its attitude could be related to the folding of the Morilem syncline (Baker, 1963).

For ease of structural interpretation the area has been subdivided into four blocks (Figure 2.3). All acquired foliation and lineation data, and including Bakers' data (1963) were plotted on equal area, lower hemisphere projection. To aid comparison between data sets of varying size (Starkey, 1977) the projections have been contoured using the STATIS programme developed by N.G. Woodcock on the Cambridge University Main Frame IBM-370 computer. The programme also analyses the distribution and fabric shape of the data using the eigen-vector method of Watson (1965 and 1966). Normalised eigen-values S_1, S_2, S_3 define three eigen-vectors, V_1, V_2 and V_3 which approximate the Fisher Mean (Fisher, 1953), an intermediate value and the pole to the best fit great circle respectively.

Woodcock (1977) developed K and C parameters to quantify the shape and strength of fabric distributions by making two axis, logarithmic comparisons of normalised eigen-values. Figure 2.4 illustrates such a two-axis covariation, where the value K = ln (S1/S2)/ln(S2/S3) varies inversely with the strength of cluster in a distribution and the value C = ln (S1/S3) varies proportionally with the strength of any preferred orientation fabric.

2.3.1 Data for area sub-divisions

2.3.1.1 Northwestern block

A total of thirty-six foliation data points are plotted on a contoured equal area net (Figure 2.5a). The foliation planes measured in this block show a well ordered distribution, (C = 2.09, K = 0.53), with a mean foliation attitude of 72/313 and a best fit girdle pole at 14/169.

Twenty-seven lineation data plotted on a contoured equal area net (Figure 2.5a) show a cluster (C = 1.96, K = 1.70), with a mean trend of 0/344. The clustering in two separate areas means that the lineation has been folded along a 9/74 axis plunging NNW and SSE.

2.3.1.2 Northeastern block

A total of forty-six foliation data points were plotted (Figure 2.5b). The foliation planes measured are intermediate between a cluster and a girdle (C = 2.08, K = 0.93), with a mean foliation attitude 82/278, and a best fit pole to girdle 2/175.

Lineation plot based on twenty-seven points show a cluster (C = 2.60, K = 2.36), with a mean trend 3/172. The lineation plunges gently to the N and to the south. This is approximately parallel to fold axes.

2.3.1.3 Baragoi Centre

A total of seventy-three foliation data plotted (Figure 2.5c) show a girdle (C = 1.98, K = 0.58), with a mean attitude of 35/350 and a pole to best fit girdle 14/159. Although it forms a girdle three separate clusters are observed.

Lineation plot based on nineteen points show a well ordered girdle, (C = 1.98, K = 0.64) with a mean lineation trend of 20/155.

2.3.1.4 Southeastern block

The foliation planes measured in this area show a girdle (C = 2.39, K = 0.72) (Figure 2.5d), with a mean foliation attitude 67/123, and the pole to best fit girdle is 22/323. The scatter of data from an idealised great circle is due to localised structural variations.

20 lineation data points plotted between a cluster and girdle (C = 2.39, K = 1.09) and with a mean lineation trend of 27/317.

In the NW and NE blocks the lineations plunge gently to the SSE while south of Baragoi town, the lineations plunge to the NNW. There are anomalous lineations plunging SW and W in the eastern quadrant (Lesirikan area). This is due to the intersection of the original foliation S_1 and the penetrative slip-planes S_2.

Plots of individual folds show a moderate degree of monoclinic symmetry, and the fold axes could be determined (Figure 2.5). The fold axis varies through an angle approximately 50° in the horizontal and vertical planes, and there is gentle undulation and curvature of the local fold axes.

NW Block – Foliation

NW Block – Lineation

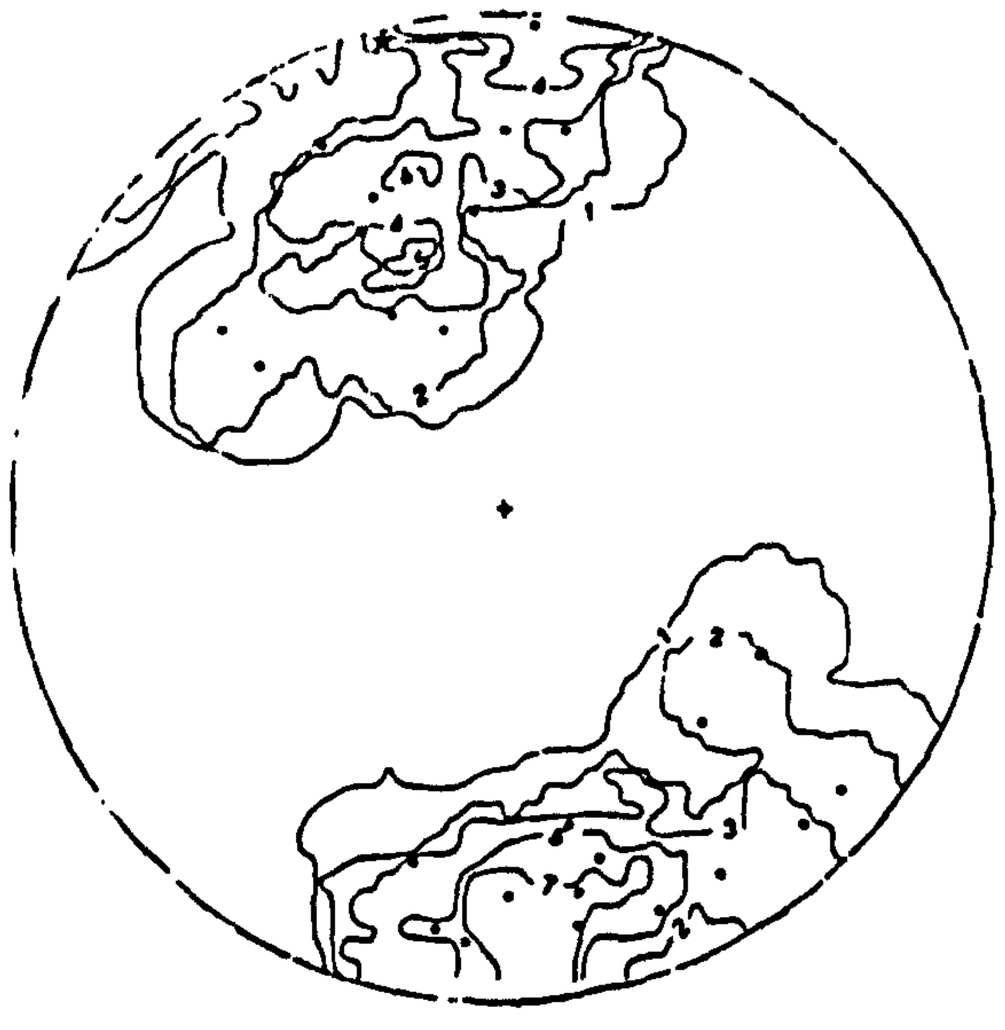

A

NE Block – Lineation

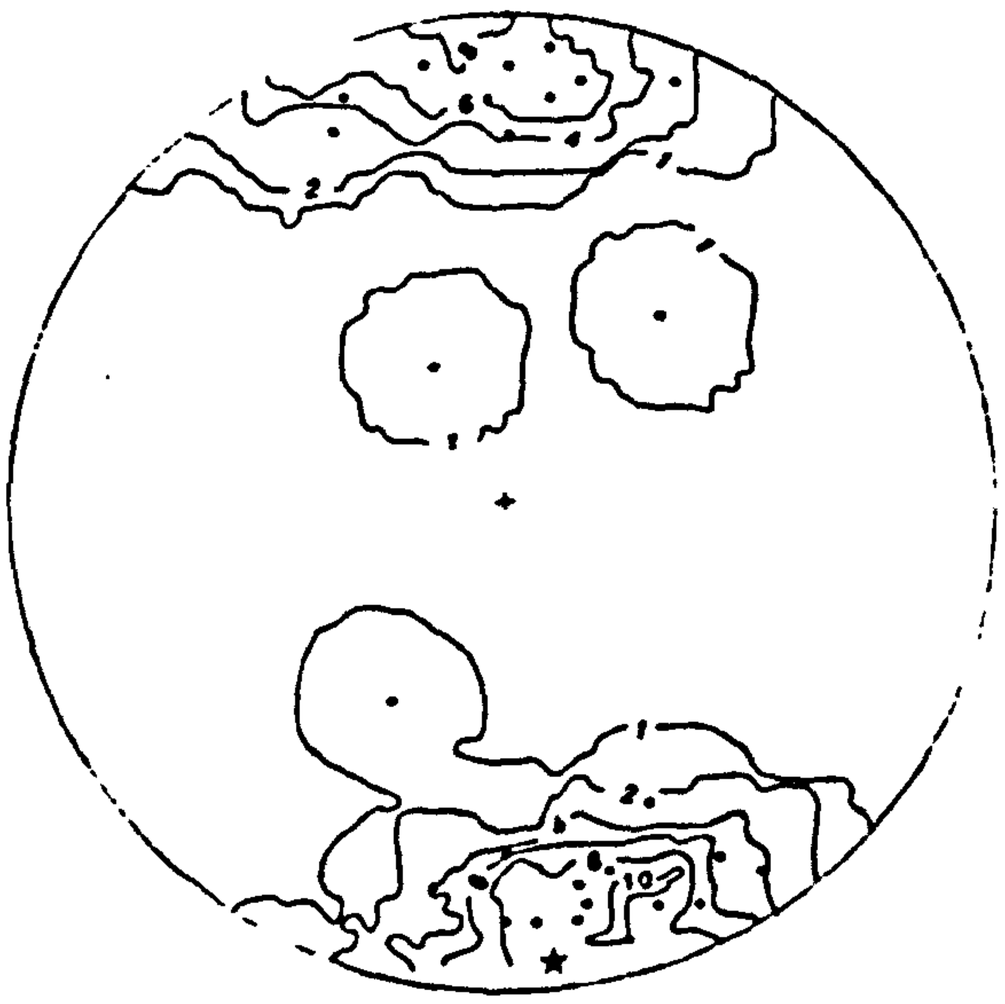

NE Block – Foliation

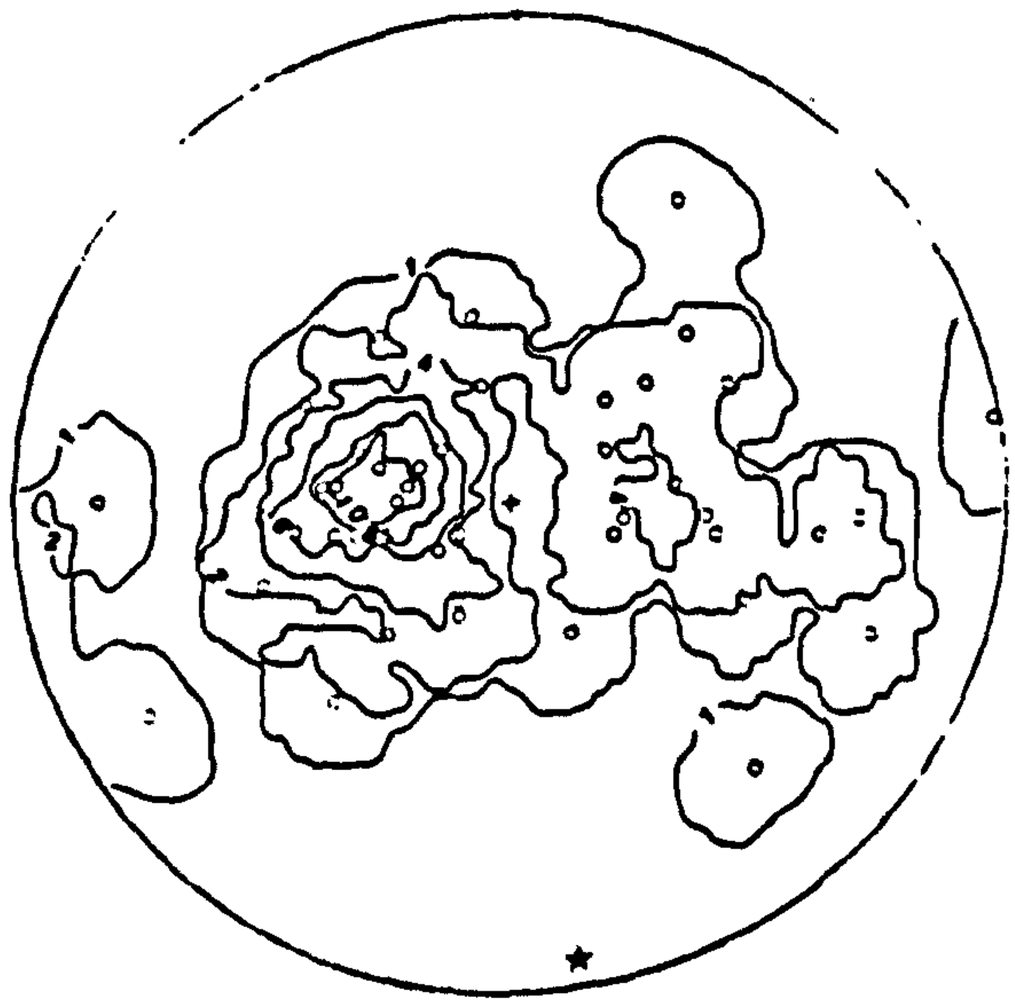

B

Figure 2.5 Lambert equal area plots of foliation and lineation data of the Baragoi area. The pole to the great circle girdle is shown by a star. The contours are hand drawn. a) NW block, b) NE block.

Centre Block – Foliation

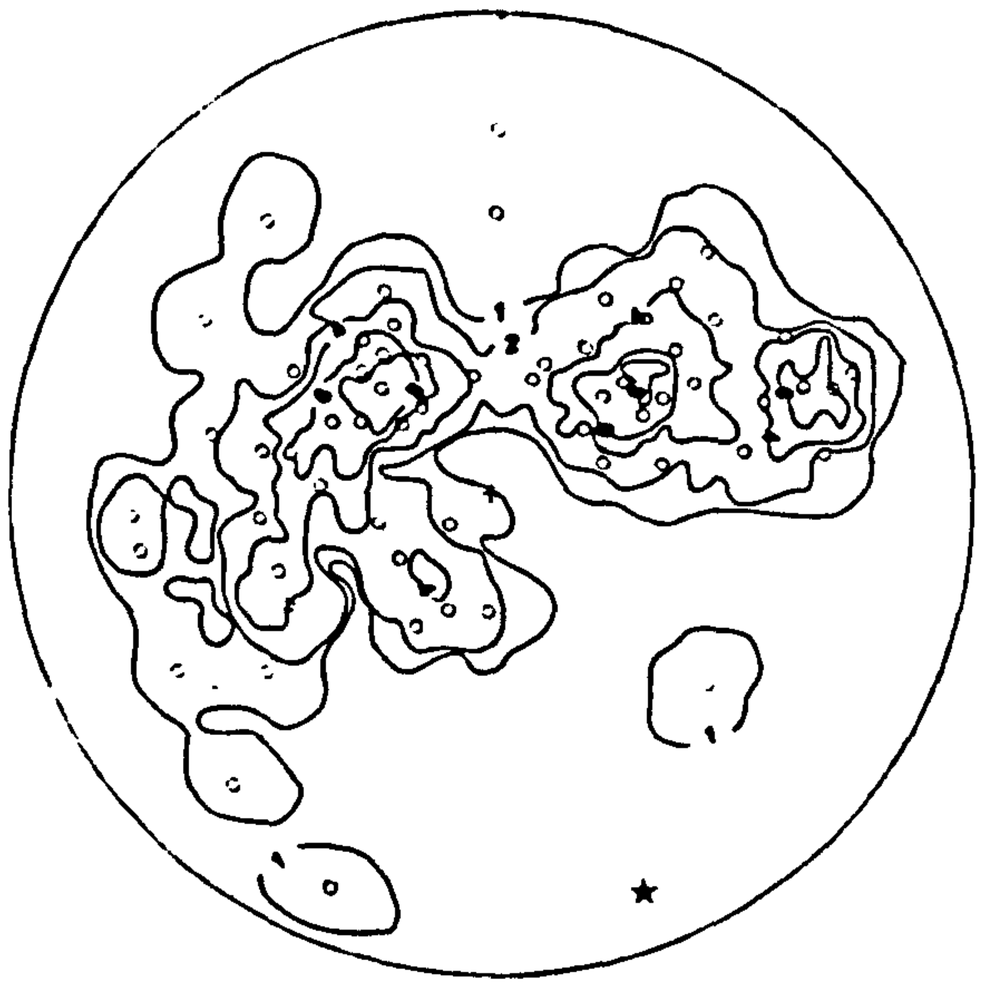

Centre Block – Lineation

C

SE Block – Foliation

SE Block – Lineation

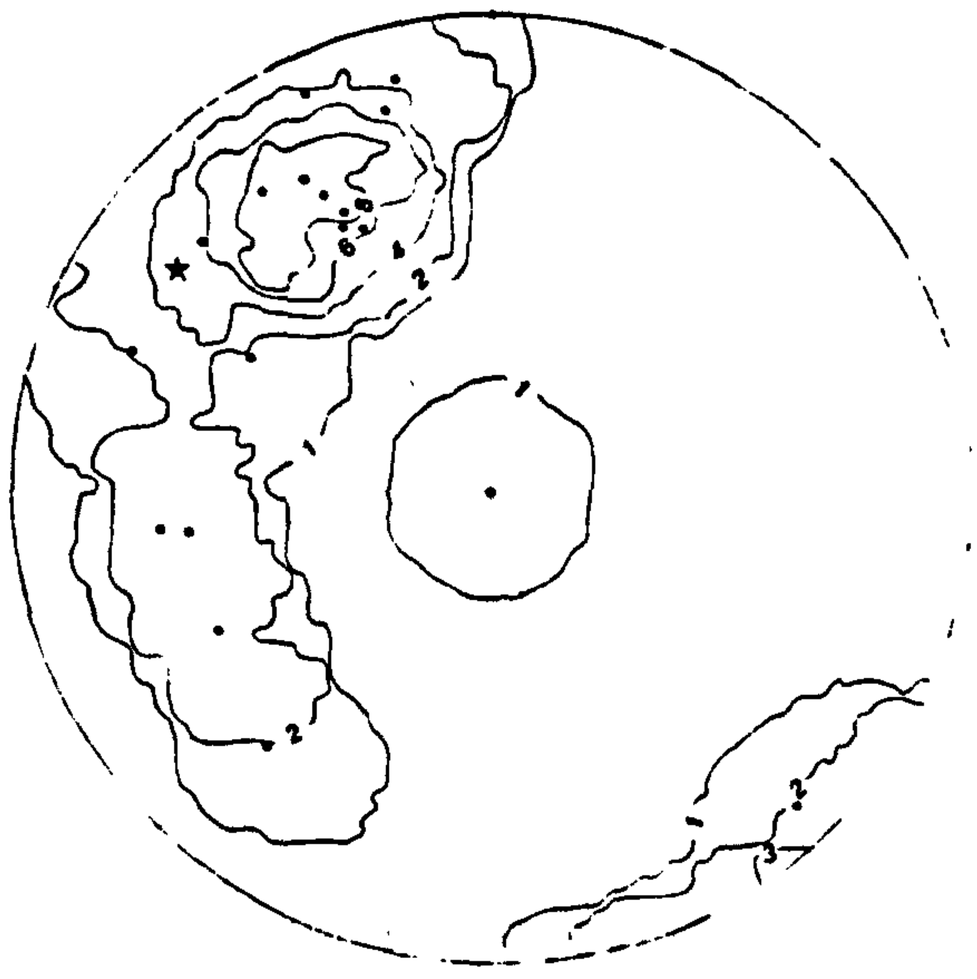

D

Figure 2.5 Lambert equal area plots of foliation and lineation data of the Baragoi area. The pole to the great circle girdle is shown by a star. The contours are hand drawn. c) Centre block, d) SE block.

The structural data referring to the SE block of the Morilem syncline shows only moderate degrees of structural homogeneity in that area. It is observed that the fold axis is co-axial with the maximum number of lineations observed. The scatter of data from an idealized great circle of projection is due to localised structural variations such as the swell of foliation in the Luwamara granitic area (Baker, 1963; Figure 2.5d). Structural complications also arise wherever slip has taken place on surfaces oblique to the principal foliation trend. Such slip-planes have caused slip-folding about axes differing from the local fold-axis.

In the northern part of the Baragoi area (NW and NE blocks) the strike of the foliations and trends of the lineations gradually rotate from a NW-SE foliation strike and lineation trend at the southern end, to a NNW foliation strike and lineation trend. North and south of Lesirikan there is an area of more intense deformation, where the foliation has a constant N-S trend. In the areas of less intense deformation the constantly trending N-S foliation is still present but an earlier foliation is also preserved in some areas. The only evidence from the field that one foliation is earlier than the other, is based on the relative orientations of the foliations. With an increase in the intensity of deformation which produces the N-S strike of the foliation, the earlier NW-SE trending foliation is progressively rotated by shearing from its original orientation towards the later N-S direction. Where the N-S foliation strike is only very weakly developed, the earlier foliation poles form a dispersed cluster pattern as in Figure 2.5c.

In areas where the N-S striking foliation is strongly developed, the earlier foliation trend has been destroyed by a total rotation into the later trend and also by extensive recrystallisation of the mineral phases with regrowth in the later foliation direction. A single-cluster foliation pole pattern is developed in these areas.

2.3.2 Macrofolds

Three major episodes of deformation have been identified in the structural evolution of the Baragoi area. An early stage involved deformation immediately following formation of the complex. This episode (D_1) is referred to as the Samburu phase (Charlesly *et al.*, 1984), and these early structures are preserved east and west of a zone 35-40 km trending north-south through the centre of the

Samburu block. This episode of deformation generated recumbent to isoclinal folds, with fold axes trending approximately east-west. It has been suggested that the stress regime that was responsible for the E-W structures resulted in the emplacment of the Baragoi mafic-ultramafic complex from the north or northeast (Charlesly *et al.*, 1984).

Table 2.1 Deformation events in the Baragoi Area

Tectonic Episode		Structural Trend	Phases of Deformation
Barsaloi	D_3	N-S	One
Baragoi	D_2	NW-SE	One
Samburu	D_1	E-W	Polyphase

The second deformation (D_2) is a large-scale folding event which produced upright to overturned folds plunging 20-30° to the northwest. This tectonic episode that produced the NW trending Morilem Syncline (Baker, 1963) has been named the Baragoi phase (Charlesly *et al.*, 1984). Generally the principal foliation (S_1) of the area parallels the bedding of the metasedimentary rocks. However, a second foliation (S_2) has been found transverse to the regional foliation trend. The axial planes of the Morilem fold system are either vertical or dip steeply toward the WSW or W.

The third deformation event (D_3) caused refolding of the Morilem syncline into a series of NNW trending folds plunging 170°SSE. D_3 cleavage can locally be seen crenulating a D_2 cleavage. D_3 cleavage and fold axial plane strike to the NNW. At the southern tip of the Atagirion, and Kowop anticline complex structures are observed, transposition of foliation and slip folds are ubiquitous.

The Baragoi mafic-ultramafic rocks give way to rocks of high grade metasedimentary and granitic gneisses along a N-S zone of shearing, faulting and interfolding. Earlier structures are almost entirely obliterated in Lesirikan area (east of Baragoi town), where the succeeding Barsaloi phase generated upright horizontal or gently plunging folds trending north to northeast. The small folds east of Kangura and the Gurika and Keleshwa northeast of Lesirikan are products of this episode of

deformation. In this area deformation was hetereogeneous: zones of high strain are foliated with mineral lineation in the 'M' turn over zones; penetrative fracture cleavage developed in zones of low strain (Charlesly *et al.*, 1984). Upper to middle amphibolite facies metamorphism was sustained during all these episodes of deformation.

In this area one can observe a progressive reorientation of the fold axis from NNW to N-S during the Barsaloian episode of deformation. Later episodes of folding and shearing have been observed in localised areas. Charlesly *et al.* (1984) have unravelled more than five episodes of deformation in Central Kenya.

2.3.3 Microfolds

There are plenty of microfolds in the Baragoi area and these have been used to decipher the tectonic history of the area. The microfolds have been subdivided into two types (Baker, 1963); flexural-slip folds and slip folds. The flexural-slip folds are characterised by simple cylindrical patterns and by the presence of only one foliation, and have corrugated limbs yielding a strong lineation. These lineations are parallel to the axes of folds in all scales.

The slip folds are dominantly confined to areas of migmatisation. The wavelength of these folds do not exceed 1 m. The folding of the lithological layers (S_1) is acute to the axial plane of the folds, while schistosity (S_2) is parallel to the axial planes of the folds. This type of fold could be the result of shearing. In areas where slip folding is prevalent bedding and foliation are parallel over considerable distances, and that S_1 and S_2 can only be differentiated locally. In migmatitic areas isoclinal folds are observed with closely compressed subparallel limbs and squeezed out cores. This is a consequence of shear which results in the elongation of the limbs of the folds and gives rise to a second foliation (S_2) in the nose of the folds.

Most of the flexural-slip and slip folding examples are observed in the northwest and southeast of Baragoi as well as in Lebanyuki river. Most of the microfolds are observed to be concordant to the regional foliation trend, however, in places a later tectonic episode has caused minor folds along the flanks of major folds which are of different orientation.

East of Baragoi town the hornblende plagioclase gneisses are observed trending N10-30°W

dipping 65°NE. However, open folds are observed at the flanks which are not more than 2 m wide and whose fold axis trend N40°E and plunges to the NE. This shows that two phases of folding is clearly observed; an earlier one which trends to the NW, which is being refolded into a NE axis.

In Nawakim River (1° 49' 20" N, 36° 43' 41" E) biotite hornblende gneisses and hornblende plagioclase gneisses are observed interfolded together. These have been cut by a 10 cm wide aplitic dyke and were subsequently refolded together along a N50°E axis with shallow dips to the southeast (Plate 2.11).

2.3.4 Shear zones and thrusts

Numerous shears and thrusts have been observed in the Baragoi region. In the Keleshwa area (NE block) there is a major thrust which show strong developed striae (Plate 2.12). The direction of striae being from N to S. The thrust plane is itself folded with fold axis trending N-S and plunging to the south. However all along the Baragoi river a series of thrusts are observed with slices overthrust upon each other in a northwesterly direction. In Opoipa river near Baragoi town a succession of gabbro- amphibolites and hornblende biotite gneisses are repeated by thrusting and folding. The direction of movement has not been ascertained because of a lack of convincing striae direction. A melange zone occurs in the core of the Keleshwa syncline, where graphitic schists, marble lenses and fragments are found as tectonic inclusions in the contorted and broken graphitic schists. This could be due to a major shear zone that passes through the Lesirikan area. This is an area where the ophiolitic rocks give way to rocks of higher grade metasediments. It is the product of the Barsaloian episode of deformation (D_3) which is a lot younger than the S to SE directed thrusts of the Keleshwa area.

Related to the thrusts are a series of NE trending shear zones, generally trending 10-20°NE, which have sinistrally displaced lithologic units. 5 kms west of Baragoi the Hornblende plagioclase gneisses have been sinistrally offset by half a metre. The sinistral shears are almost perpendicular to the thrust planes, which may suggest that they acted as transcurrent faults to accommodate severe shortening in the Northern Baragoi area (NW and NE blocks) where there are a series of tightly folded anticlines and synclines.

Plate 2.11 Two stages of deformation. Hornblende biotite quartz plagioclase gneisses (light colour) and the hornblende plagioclase gneisses are interfolded together. Subsequently intruded by aplitic dyke and the whole sequence is refolded. Baragoi river.

- Plate 2.12 A thrust plane in a serpentinised dunite body. Keleshwa complex.

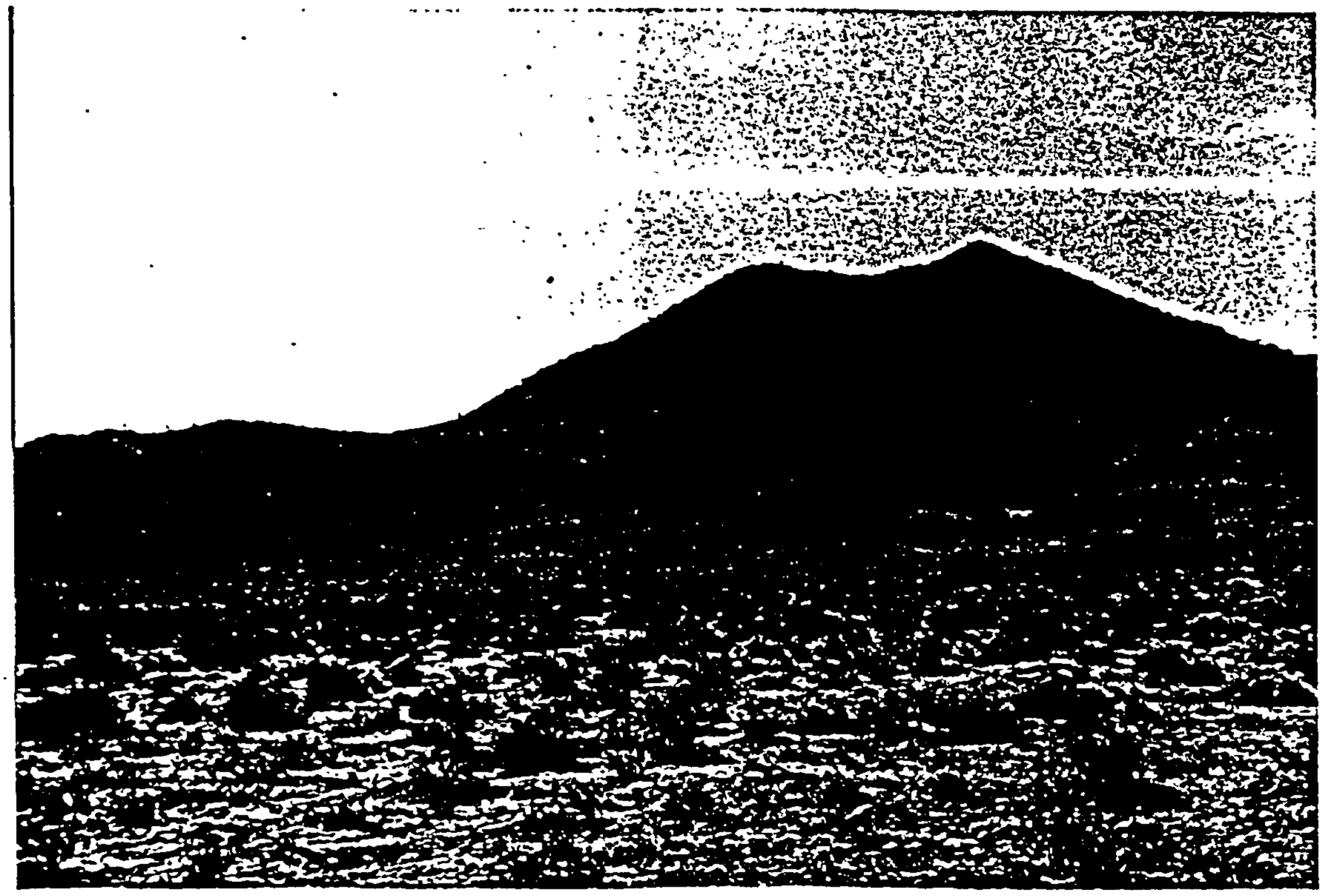

Plate 2.13 An inward dipping synform forming a repeated thrust sequence of ultramafics, gabbros and amphibolites.

The Koitokol Hill is a boat-like inward plunging synform. Detailed observation shows that there is a repeated sequence of ultramafics, gabbros and amphibolites which have been emplaced as two separate thrust sheets (Plate 2.13). These were probably emplaced during obduction of the ophiolitic sequence.

2.4 METAMORPHISM

Critical to the determination of metamorphic grade is not only the presence or absence of certain minerals in the rock, but also its composition. However, in the absence of original relict mineralogy, mineral assemblages and index minerals were used to determine the P-T conditions of the Baragoi mafic-ultramafic rocks.

The rarity of unaltered relics of olivine or pyroxene-bearing igneous rocks suggests that mineral transformation is complete in this area. The absence of sillimanite and rarity of pyroxenes also suggests that temperatures were moderate. Sillimanite has not been recognised in Baragoi area, however further south Shackleton (1946) mentions that sillimanite is the characteristic mineral in the pelitic gneisses, whereas kyanite is absent.

The formation of zoisite from calcic plagioclase, actinolite from hornblende and the formation of chlorite-magnetite schists are retrogressive effects which took place during the period of declining temperature. Typical mineral assemblages of the various rocks in the Baragoi area are shown in Table 2.2. Talc is common as a minor constituent in larger altered ultramafic bodies, and is seen as irregular bodies in tremolite-anthophyllite rocks. The serpentinites are generally found associated with talc schists and actinolite rocks. Evans and Trammsdorf (1970) have observed that the first appearance of the association forsterite and talc occurs somewhat above the beginning of medium grade metamorphism marked by the formation of staurolite in metapelitic rocks. At higher temperatures the expected sequence of reactions is the formation of anthophyllite and talc or forsterite followed by the formation of enstatite and forsterite. Since anthophyllite and talc or forsterite reaction takes place around 650°C (Evans and Trammsdorf, 1970) it can safely be inferred that this level of temperatures were reached in the Baragoi rocks (Figure 2.6).

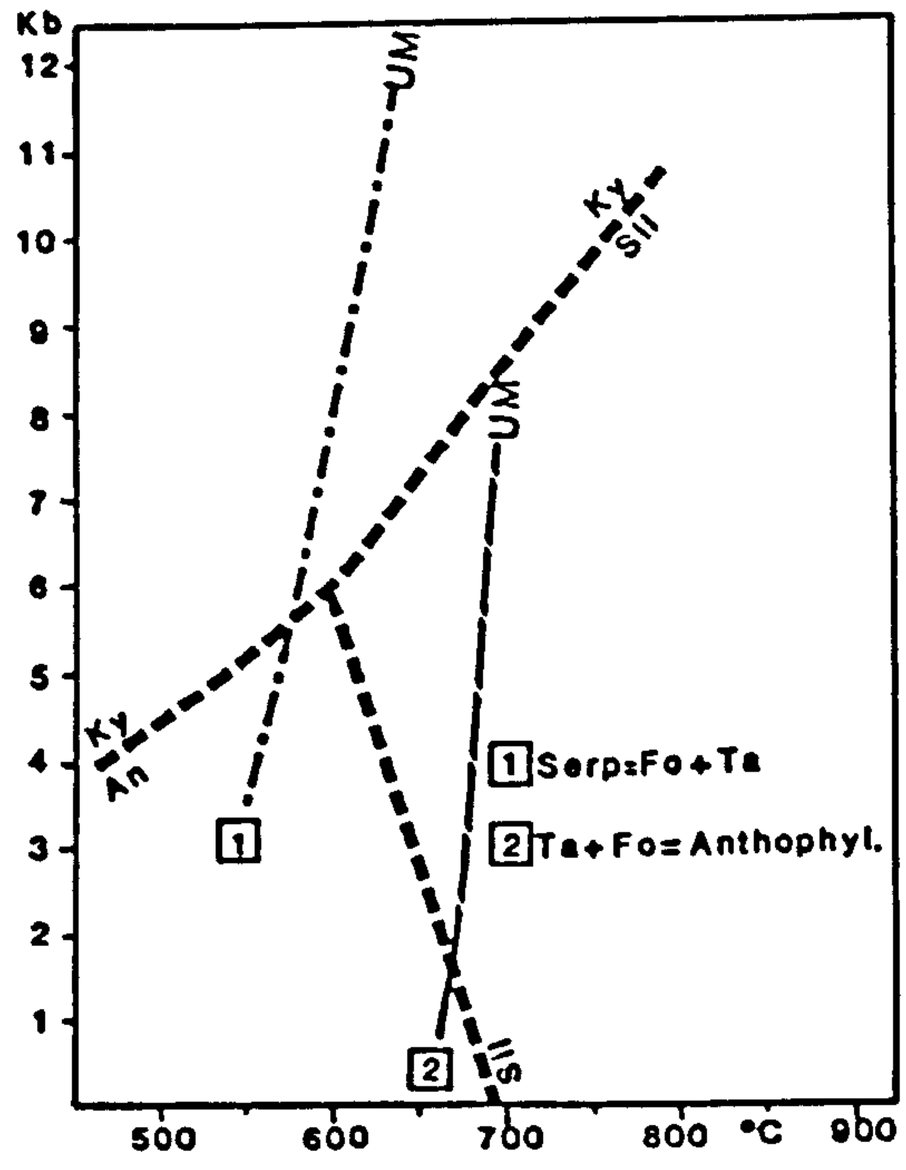

Figure 2.6 Pressure-temperature grid for regional metamorphism of ultramafic rocks. Reaction curves from Winkler (1976). Mineral abbreviations : Ky=kyanite, An= andalusite, Sil= sillimanite, UM= ultramafic, Serp= serpentine, Fo= forsterite, Ta= talc and anthophyl= anthophyllite.

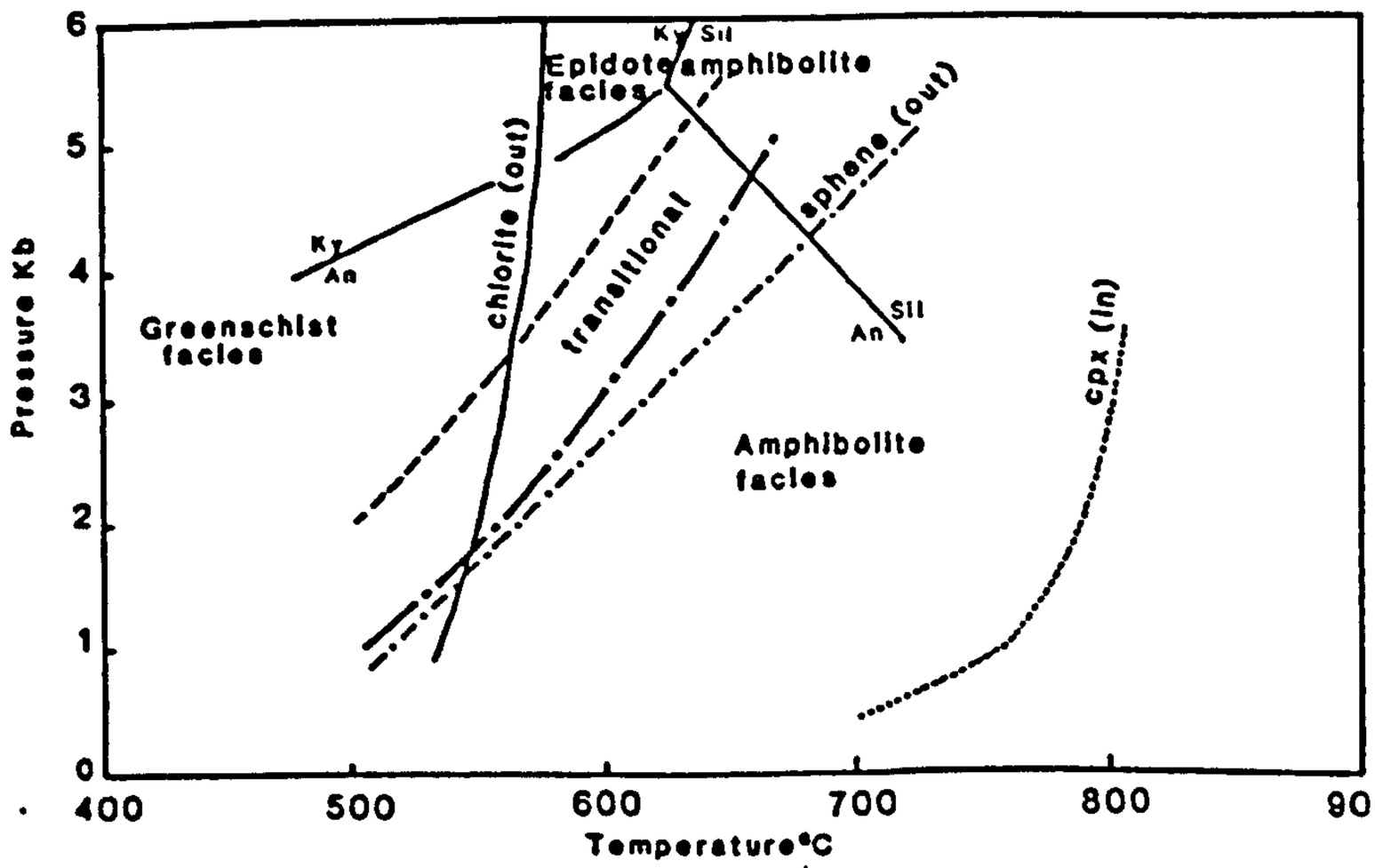

Figure 2.7 Pressure-temperature grid for regional metamorphism of amphibolites. Reaction curves from Liou et al (1974), Spear (1981). Mineral abbreviations: Ky= kyanite, An= andalusite and Sil= sillimanite.

Similarly the presence of antigorite in serpentinites suggests that temperatures up to 550°C (Evans *et al.*, 1976) have been reached in the area, while the presence of anthophyllite suggests that pressures of <5kb have been attained, because anthophyllite is not stable above 5 kb (Chernosky, 1976).

Since amphibolites and basic gneisses form a large part of the Baragoi area, their mineral assemblages could be used to determine the pressure and temperature conditions of metamorphism as proposed by Laird and Albee (1981) for greenschist facies assemblage: actinolite + chlorite + epidote + albite + quartz ± muscovite/biotite ± calcite, and in the amphibolite facies: hornblende + andesine + ilmenite + quartz (Moody *et al.*, 1983). Based on the mineral assemblages of amphibolites in the Baragoi area (Table 2.2) it is suggested that they plot in the epidote amphibolite facies (Figure 2.7). The greenschist-amphibolite boundary is characterised by actinolite or actinolitic hornblende, chlorite's disappearance marking the end of transition and plagioclase change from albite to oligoclase, to andesine in amphibolite facies (Lion *et al.*, 1974; Moody *et al.*, 1983). Increasing Al, Ti and Na content of the amphibole until in the amphibolite facies it forms hornblende.

There is no direct evidence to connect the metamorphism with any granite mass, as no granitic intrusions of batholitic dimensions have been found as yet. There is no significant variations in the grade of metamorphism in the area, even in the proximity of intrusive bodies. Upper amphibolite facies metamorphism has been maintained throughout. Deformation in the area has been severe because, migmatisation with intense unsystematic deformations have been observed. However, hydrostatic pressure does not seem to have been exceptionally high, as dense eclogitic facies rocks have not been discovered in the Baragoi mafic rocks. Shackleton (1946) suggests that high temperatures and penetrating fluids were the essential factors in the metamorphic processes, whereas shearing stress and hydrostatic pressure were considered to be of less importance.

Table 2.2 Typical mineral assemblages of the Baragoi rocks

Rock type	Mineral assemblages
Ultramafic (talc tremolite schists)	Tremolite/anthophyllite ± talc ± chlorite ± carbonate ± chromite
Serpentinite	Antigorite ± chrysotile ± carbonate (accessory)± talc ± magnetite
Amphibolite	Hornblende ± pyroxene ± epidote ± actinolite ± sphene (accessory) ± magnetite
Hornblende plagioclase gneisses	Hornblende + plagioclase (An_{43}-An_{30}) ± epidote (rare) ± quartz ± garnet ± biotite ± pyroxene (rare) ± magnetite
Granitoid gneisses	Microcline + oligoclase + quartz + biotite ± garnet ± iron oxide
Luwamara granite	Microcline + plagioclase (An_{20}) + quartz ± biotite ± green hornblende ± sphene

2.5 GEOCHEMISTRY

2.5.1 Introduction

The purpose of the geochemical analyses was to establish the detailed geochemical characteristics of the rock types of the Baragoi mafic-ultramafic rocks, and to identify rock associations which could be compared with published works in order to define whether the complex is ophiolitic, to define the environment of eruption of the volcanic rocks, and establish its tectonic setting. All standard geochemical techniques are discussed in Appendix A; and all geochemical results are tabulated in Appendix B.

2.5.2 Elemental mobility

It is necessary to test whether elements have been mobile during possible alteration events. Previous studies (Cann, 1971; Hart, 1973; Coish, 1977) provide evidence that some elements tend to be mobilised during alteration. These studies found that major elements are the most susceptible to modification during low grade metamorphism and submarine alteration and are therefore considered to be of limited use in determining magma trends in volcanic rocks (Jakes and Gill, 1970;

Pearce *et al.*, 1977; Garcia, 1978).

A test to show which elements have been mobilised is to plot each against a known immobile element eg. Zr (Coish, 1977). Regular co-variation implies little redistribution whereas a scatter would indicate mobilisation. The majority of the major elements have poor correlations with Zr, especially SiO_2, Na_2O, K_2O, CaO and MgO. Examination of Figure 2.8 shows that TiO_2, P_2O_5, Y and Nb show regular co-variation with Zr and it is suggested that they are relatively immobile. Al_2O_3, Fe_2O_3, and MnO show coherent correlation and it can be suggested that this may reflect limited mobility. For the trace elements poor correlation is shown by Ba, Sr and Ni against Zr. Cr at first glance seems to show scatter, however the variations reflect rock types, or are related to modal phenocryst phases.

2.5.3 Ultramafics

Major element data of ultramafic rocks are presented in Appendix B. All samples analysed from the Keleshwa and Barenyiro are rich in MgO and low in Al_2O_3, TiO_2 and CaO. The high LOI is attributed to high degrees of serpentinisation. All the dunites are very magnesian and rich in Cr and Ni reflecting the original high modal abundance of olivine and chromite. Those from the mantle sequence are lower in TiO_2 (compare SB15C a mantle dunite with SB61 a cumulate dunite). Where CaO and Al_2O_3 abundances are higher they reflect the occurrence of relict pyroxene, these rocks are serpentinised wehrlites. Chemical data suggest that the dunite pods are part of an ophiolite mantle sequence. A Cr_2O_3-Ni O plot is used to separate the cumulate from the mantle sequence (Figure 2.9).

In order to check whether the mantle sequence ultramafics are characteristic of SSZ ophiolites or MORB ophiolites a Cr-TiO_2 plot was attempted. Although the data set is small they all plot in the SSZ ophiolitic field of Pearce *et al.* (1984b) (Figure 2.10).

2.5.3.1 Chemistry of Kangura Chromites, Baragoi

Nine probe sections were analysed with a total of forty-six analyses (Appendix B). In any one sample a minimum of six grains were analysed including one core and rim pair. However those analyses

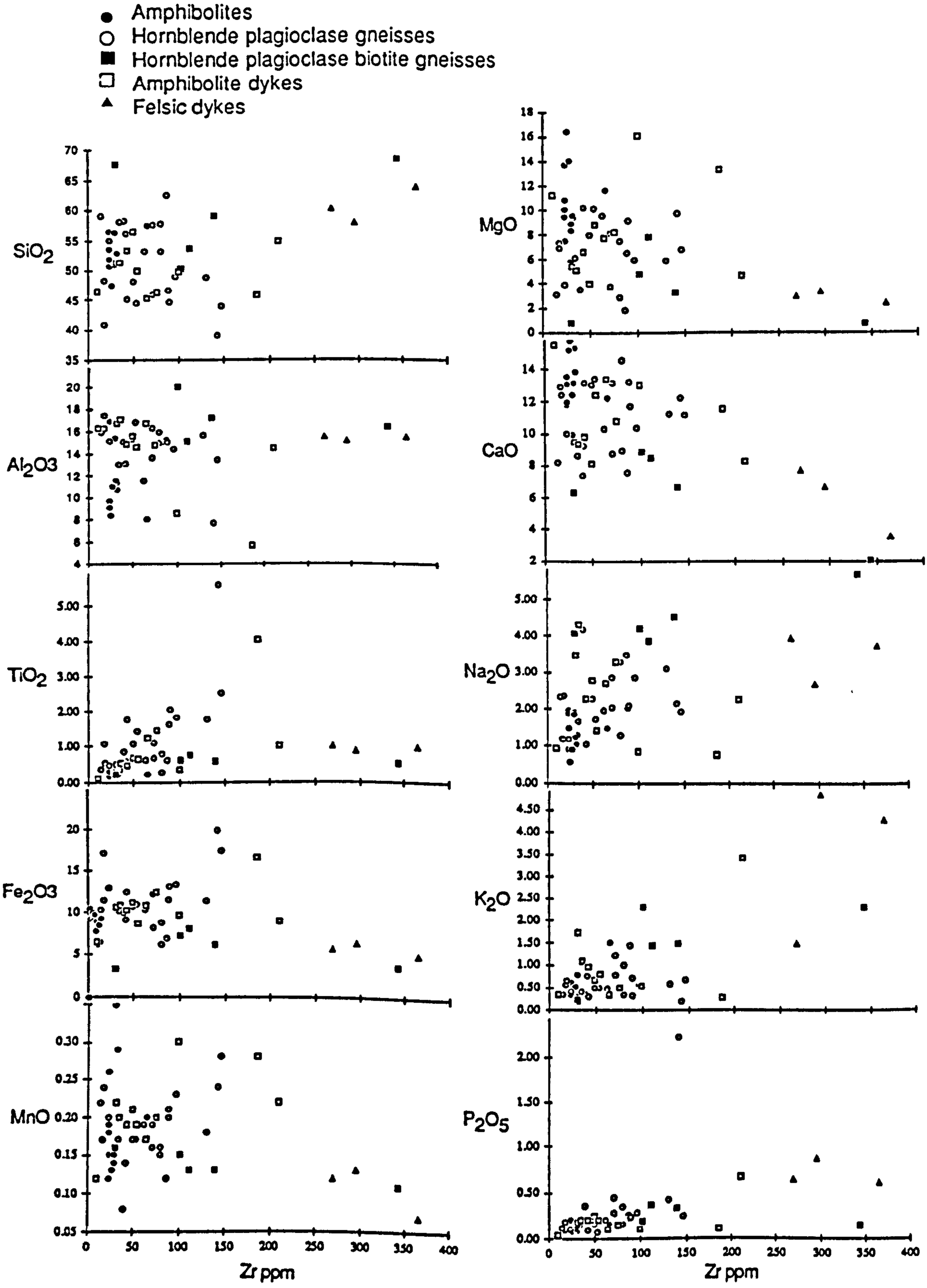

Figure 2.8 (a) Major element composition of the Baragoi basic gneisses, amphibolites and dykes plotted against an immobile element; Zr. A good co-variation implies little mobility, whilst a scatter suggests mobility.

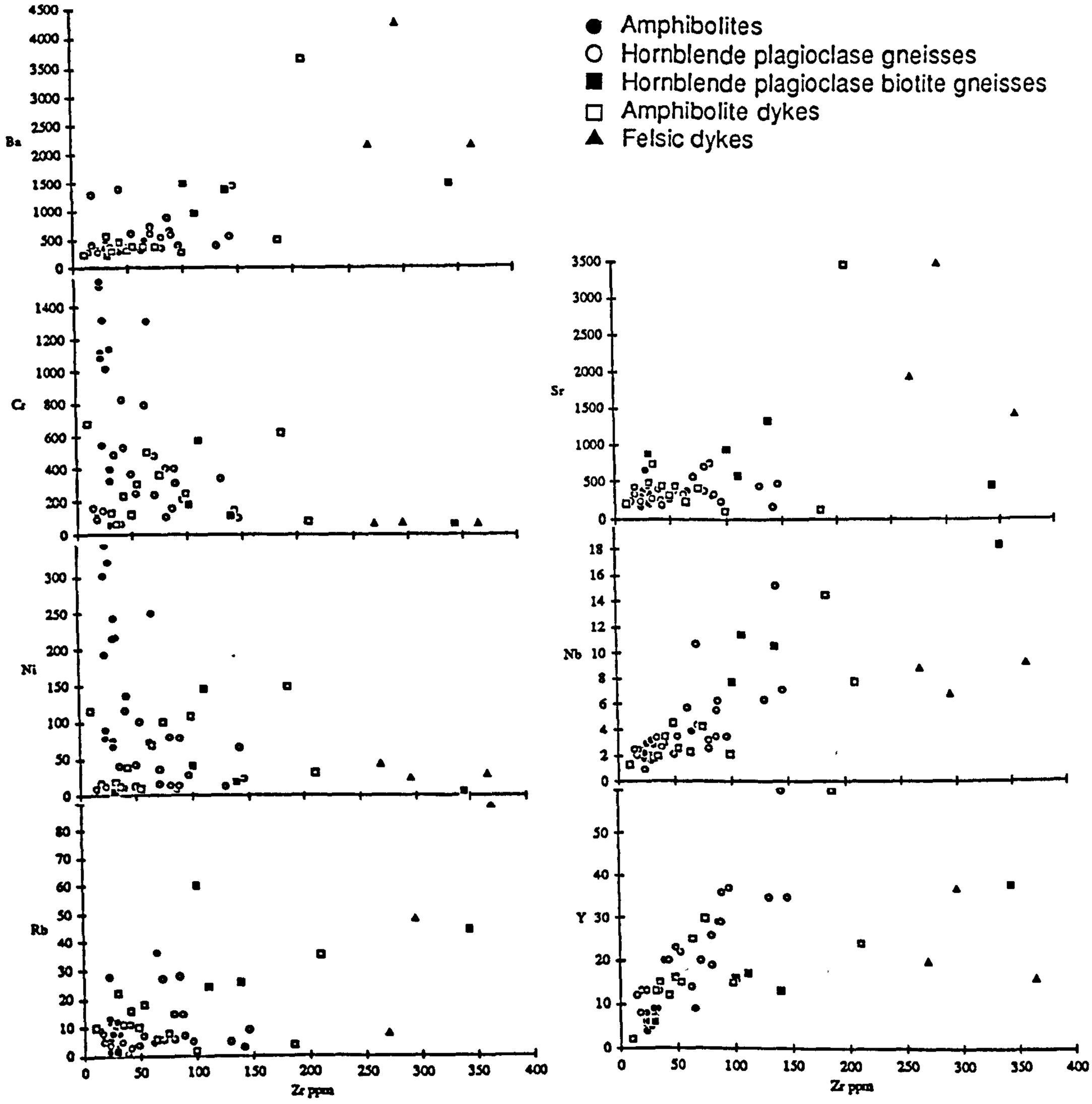

Figure 2.8 (b) Trace element composition of the Baragoi basic gneisses, amphibolites and dykes plotted against an immobile element; Zr. A good co-variation implies little mobility, whilst a scatter suggests mobility.

which had totals lower than 98.5 or higher than 101 were discarded. Sampling was undertaken along and across strike of every deposit in order to see whether there is any chemical variation. The results of this study shows that there are minor variations in TiO_2, Fe_2O_3, Mn and Cr. The rims of the chromite grains usually have higher Fe and Cr and lower Al and Mg than the cores; features already observed by previous workers on other deposits (Golding and Baylis, 1968; Beeson and Jackson, 1969; Engin and Aucott, 1971). No detectable zoning was found in single chromite grains from chromitites, the compositional differences being related to alteration.

The Kangura chromites were plotted in the spinel prism projection of Stevens (1944) and Irvine (1965). Spinels from the dunites in the mantle show a restricted range in Cr/Cr+Al from 0.8 to 0.83 while $Mg/Mg+Fe^{+2}$ values range from 0.5 to 0.7; and $Fe^{+3}/Cr+Al+Fe^{++}$ range from 0.02 to 0.15 (Figure 2.11) On this figure there is a fairly consistent Cr/Cr+Al while $Mg/Mg+Fe^{+2}$ shows limited variation.

In the $Fe^{+++}/Cr+Al+Fe^{+3}$ vs Mg/Mg+Fe plot (Figure 2.11) there is a large variation in the $Fe^{+3}Cr+Al+Fe$ values in each sample and as compared with the other samples. It is suggested that this could be due to alteration, the Al values being changed due to metamorphism and hydrothermal alteration. The fact that Mn is also variable could mean that this variation may not necessarily be only due to alteration, there could be minor grain to grain variations due to fractionation.

The data plot in the Alpine field of Irvine (1965). This is corroborated by the fact that spinels are rich in alumina and very low in Ti as compared to those from stratifrom complexes (Figure 2.12) and hence are similar to chromite from ophiolite complexes (Allen, 1975; Menzies, 1975; Brown, 1982). Using the Fe^{+2}/Mg vs TiO_2 plot (Figure 2.13) the Kangura chromites plot within the podiform field of Dickey (1975).

2.5.4 Cumulate Geochemistry

There is a group of rocks from Koitokol and Nachola area where CaO and Al_2O_3 abundances are higher indicating the occurrence of pyroxene. Since this group of rocks is highly altered their origin is only inferred from their geochemistry. In the NiO vs Cr_2O_3 discriminant diagram they plot in the cumulate field (Figure 2.9). The Nachola cpx cumulate trend is dominated by olivine and pyroxene

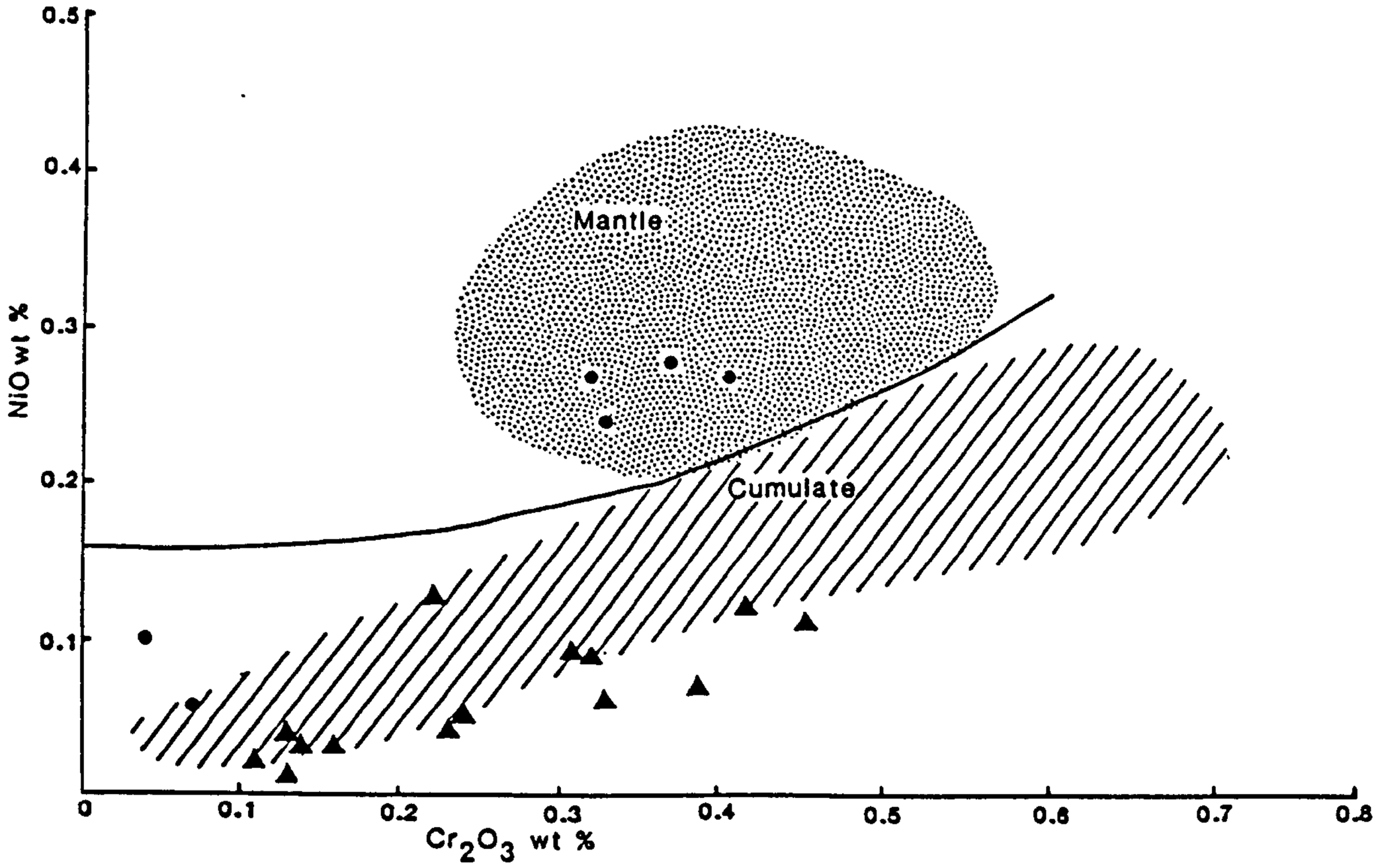

Figure 2.9 NiO- Cr_2O_3 plot for the Baragoi ultramafic rocks. Shaded areas of the Bay of Islands mantle and cumulate sequences (Malpas,1978). Dividing line taken from Irvine and Findlay (1972). Symbols: black dots represent dunites from the Baragoi area, while triangles are Nachola cpx cumulates.

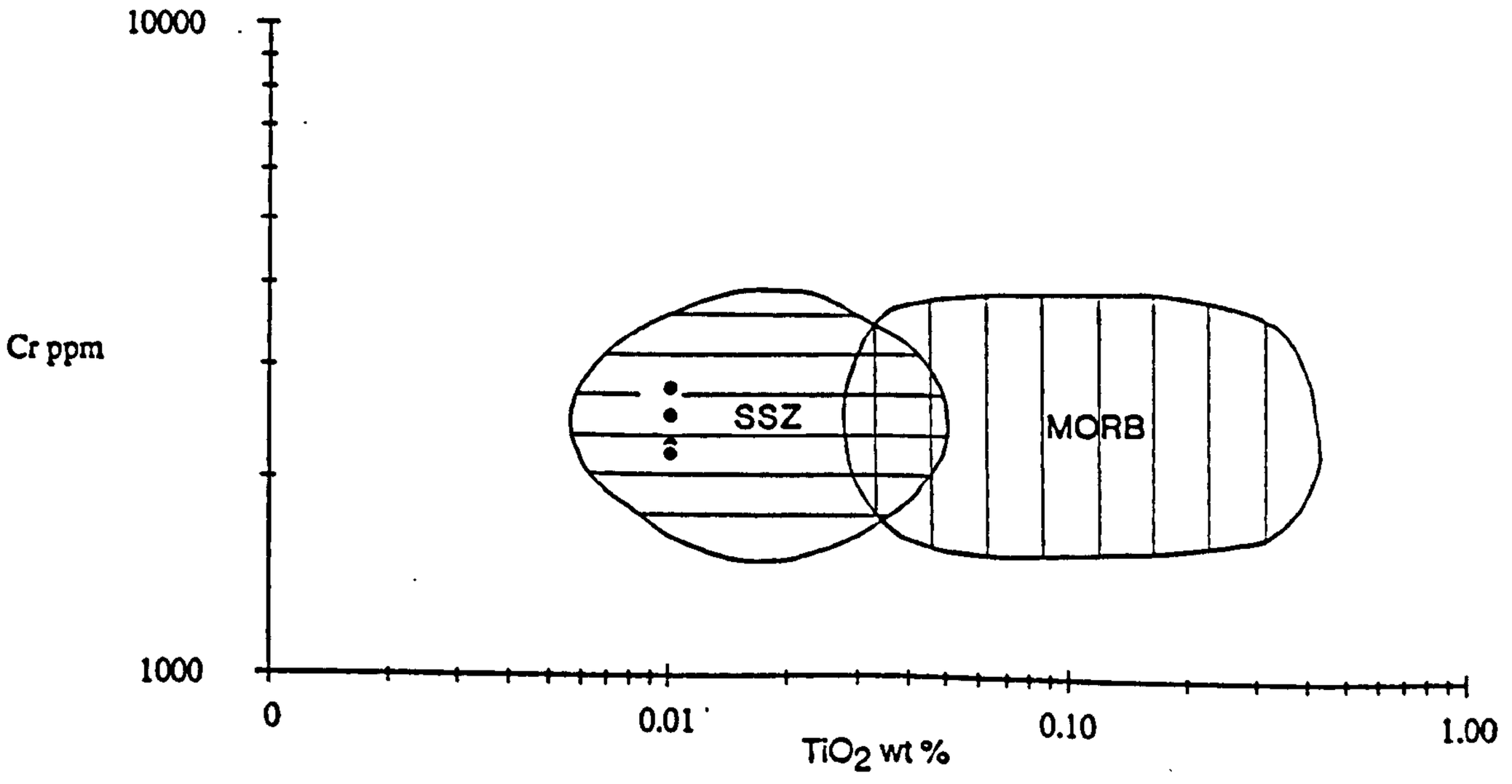

Figure 2.10 Cr-TiO_2 plot for tectonised ultramafic rocks from the Baragoi area. The 'SSZ' ophiolite mantle residue generally carries less TiO_2than that of the 'MORB' ophiolites (shaded fields taken from Pearce et al, 1984a).

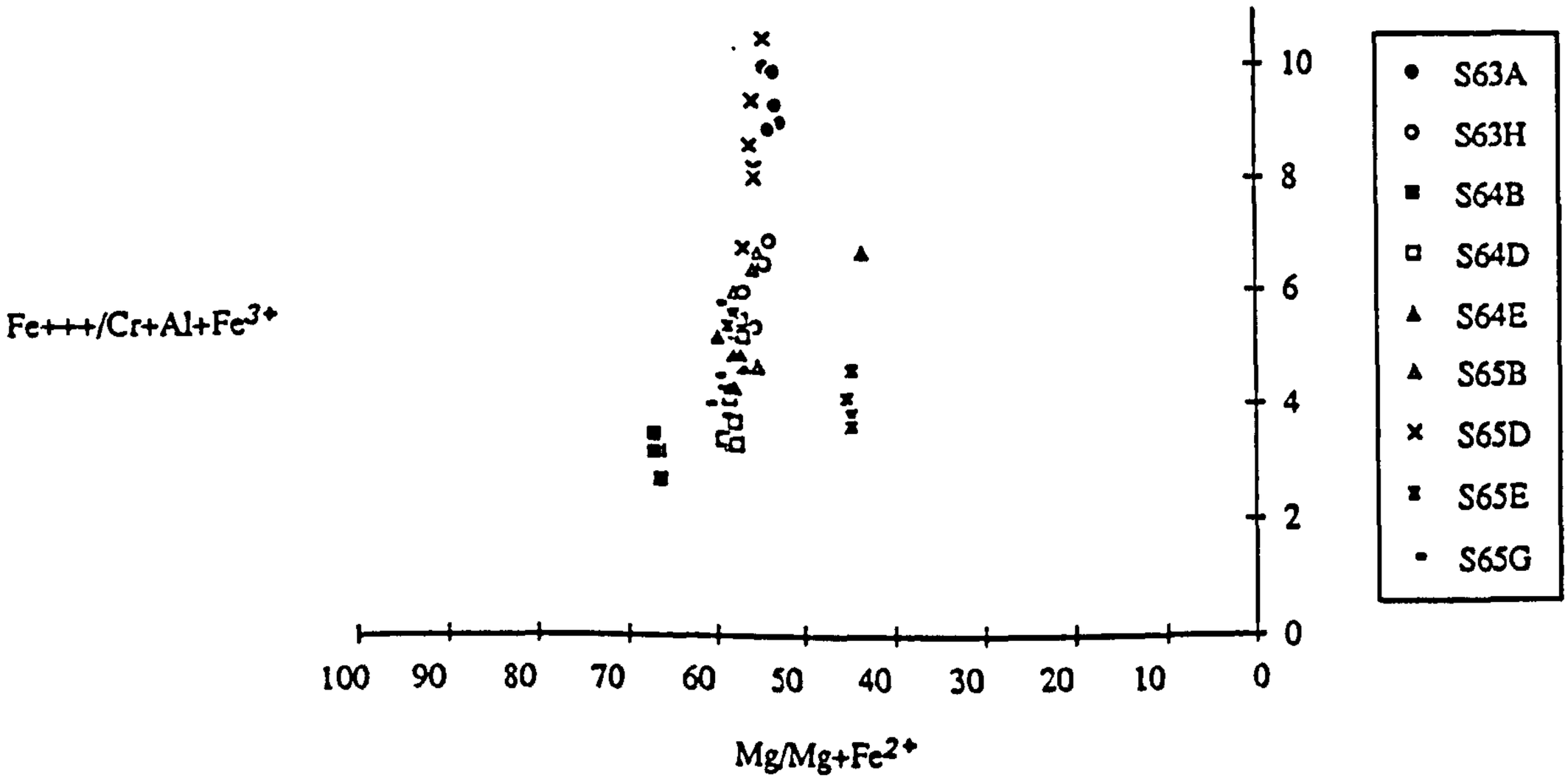

Figure 2.11 Chromite compositions $Mg/Mg+Fe^{2+}$ - $Fe^{3+}/ Cr+Al+Fe^{3+}$. This plot shows wide variations in $Mg/Mg+Fe^{3+}$ in the separate lenses, while there is large variation in the $Fe^{3+}=/Cr+Al+Fe^{3+}$ values in each specimen as compared with the other samples.

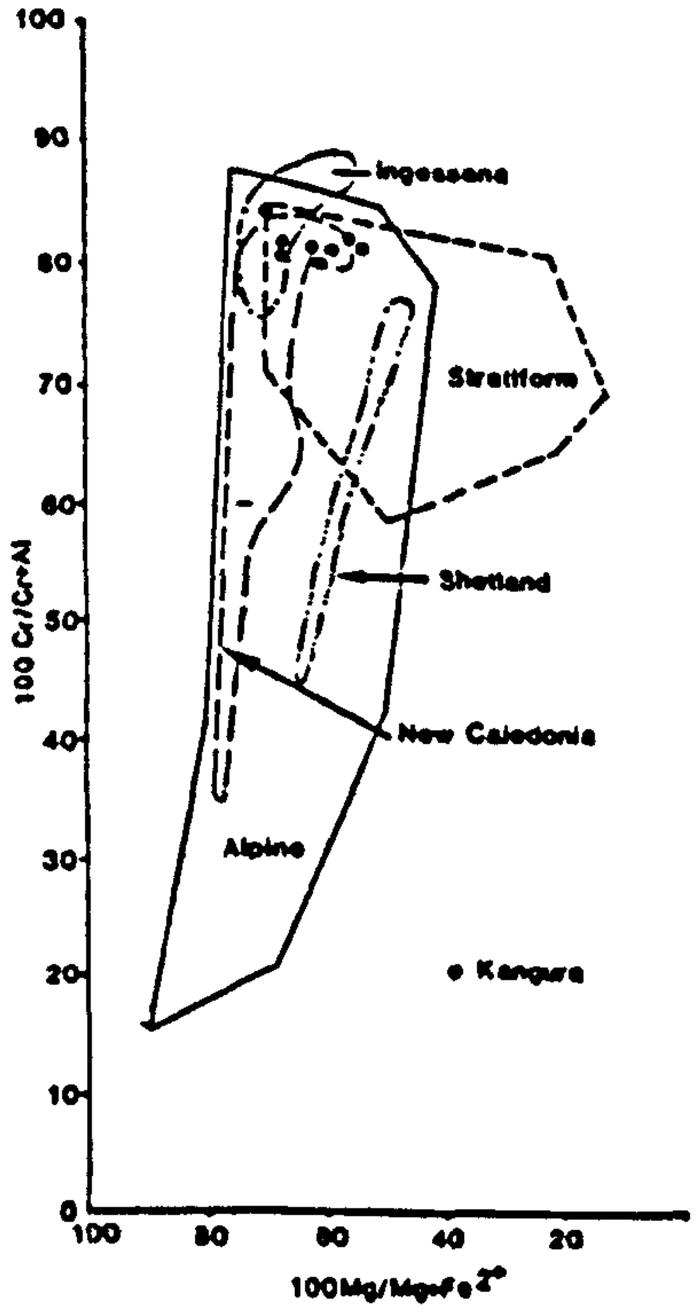

Figure 2.12 $Mg/Mg+Fe^{2+}$ - Cr/Cr+Al plot for the Kangura chromites together with comparative data for massive chromitites from other ophiolite complexes. The Kangura chromites plot at the top end of Shetland (Pritchard,1982) and New Caledonia (Rodgers, 1979), while it is enriched in $Mg/Mg+Fe^{2+}$ as compared to that of Ingessana (Price,1984). Alpine and stratiform fields are taken from Irvine and Findlay (1972).

fractionation. The cpx cumulates (wehrlites?) of Koitokol are more primitive than the Nachola cpx cumulates (Figure 2.14a) because they have higher Ni. The Koitokal cumulates have lower Al_2O_3/TiO_2 ratios than the Nachola and Baragoi cumulates (Figure 2.14b).

2.5.4.1 Metagabbros

Major Elements

The metagabbros have been sampled from three separate intrusives based on field work: the Baragoi, the Koitokol and the Baragoi Headstream gabbros. However the Baragoi gabbro which have been sampled from one gabbroic body are geochemically split into two and this division of the gabbros is best defined by TiO_2 content. In the Al_2O_3 vs TiO_2 (Figure 2.14b) it can be shown that the chemical evolution is most consistent with plagioclase and clinopyroxene fractionation. The Baragoi (I) and the Koitokol gabbros are distinguished by a trend of decreasing Al_2O_3, with increasing TiO_2 (Figure 2.14b). This reflects the importance of plagioclase as a fractionating phase, which is consistent with the high abundance of plagioclase in these rocks. The TiO_2-Ni plot suggests that olivine is also involved.

The low abundance of P_2O_5 (0.1-1.05%), TiO_2 (0.22-1.58%), Y (4-21 ppm) and lack of a strong Fe (3-9.68 ppm) enrichment suggests that they are similar to other ophiolite gabbros (Coleman, 1977). Sample SB2 is exceptional as it shows high K_2O, Zr and Y, which could probably be because it contains significantly high SiO_2 (c. 57%) which is a result of late metamorphism.

The evolutionary trends of the respective gabbro suites suggests their separate genetic identities as shown in Figures 2.14a and 2.14b. The Baragoi gabbros lie on an evolution trend dominated by ol-pyroxene fractionation and can be related to the cpx cumulates. The distinctive trend for the Baragoi Headstream gabbro reflects the importance of plagioclase accumulation which is consistent with the high abundance of plagioclase in the rocks.

There is a wide variation of TiO_2 values ranging from 0.2 to 2%. This variation cannot simply be explained by fractionation, because that would require fractionation as high as 90%, hence a complex fractionation melting episode could be envisaged or they could be different gabbros. In particular the Baragoi (Group II) gabbros could be a result of separate event, as it has elevated TiO_2

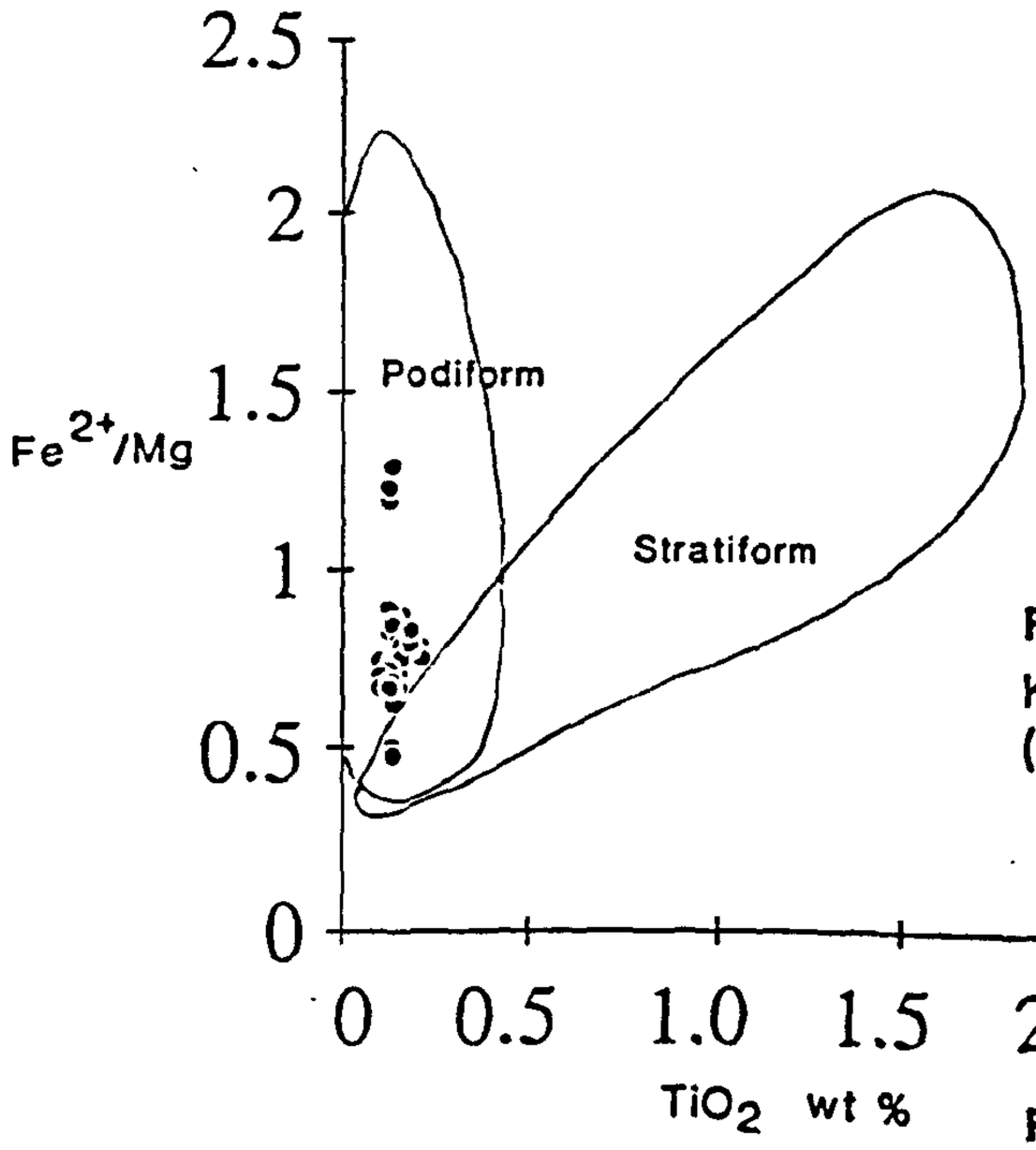

Figure 2.13 TiO_2-Fe^{2+}/Mg plot for the Kangura chromites. Fields taken from Dickey (1975).

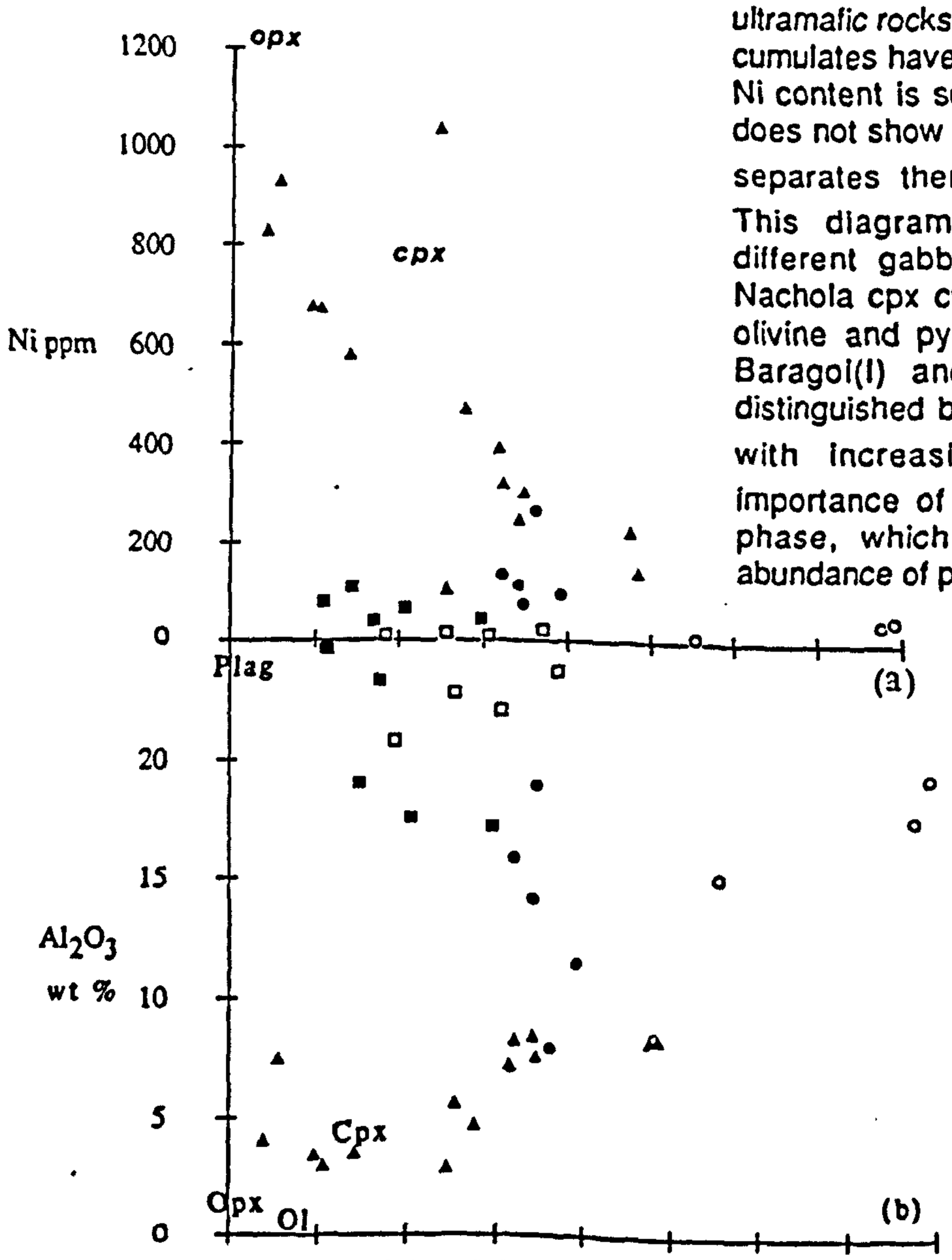

Figure 2.14 (a) Variation of TiO_2-Ni for ultramafic rocks of the Baragoi complex. The cpx cumulates have a wide range of Ni content. The Ni content is so similar for the gabbros that it does not show Ni fractionation; TiO_2 effectively separates them.(b)Variation of TiO_2-Al_2O_3. This diagram differentiates between the different gabbros and cpx cumulates. The Nachola cpx cumulate trend is dominated by olivine and pyroxene fractionation, while the Baragoi(I) and the Koitokol gabbros are distinguished by a trend of decreasing Al_2O_3, with increasing TiO_2. This reflects the importance of plagioclase as a fractionating phase, which is consistent with the high abundance of plagioclase in these rocks.

(1.11-1.58 %) as compared to the rest.

Trace elements and REE data

Both Zr and Y are high field strength elements that are relatively immobile during alteration and metamorphism, and are extremely incompatible during fractionation. As a result Zr/Y remains almost constant during fractionation and partial melting processes (with absence of garnet) and as long as no phase with Zr and Y partitioning is involved. Hence Zr vs Y plot (Figure 2.15a) were attempted for the gabbro suites. It is found that the Koitokol and Baragoi gabbros (Group I) align along the N-type MORB line (ie. Zr/Y = 3, Pearce, 1980), but Group II Baragoi gabbros and the Baragoi Headstream gabbros vary (ie. Zr/Y > 3). However all the gabbro suites plot in the low Ti class of ophiolite gabbro of Serri (1981) (Figure 2.15b).

REE patterns for the two gabbroic suites (Figure 2.16a) show positive Eu anomalies indicating plagioclase accumulation, which is also reflected in high Sr values. The Koitokol gabbros have lower REE contents than the Baragoi gabbros, and show similar REE profiles suggesting possible similar sources which could be related with different degrees of partial melting but the geochemical patterns are slightly different. The Ce/Yb_N values of Baragoi Gabbro II (SB3) is 4.4 while that of Koitokol is 3.84.

The geochemical pattern of the Baragoi gabbro (Figure 2.16b) show LIL enrichment, however the Koitokol gabbro shows a loss in Th and Ta, and has low values of K, Zr, Hf, Ti, Y and Yb.

2.5.5 Basic igneous rocks

Lavas

Four major mafic rock formations were established in the field:

(a) the amphibolites

(b) hornblende plagioclase gneisses

(c) garnetiferous hornblende plagioclase gneisses

(d) hornblende biotite plagioclase gneisses

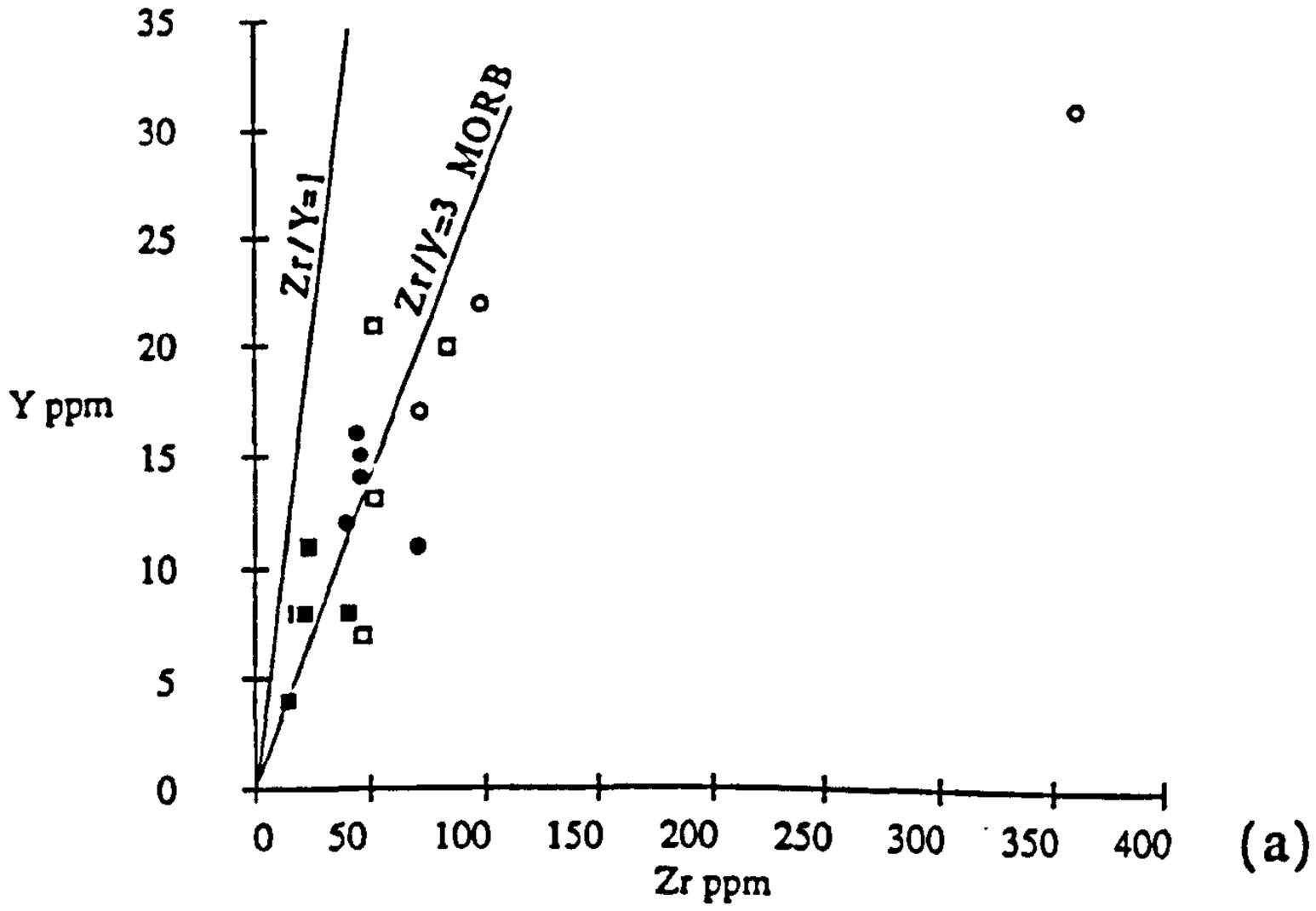

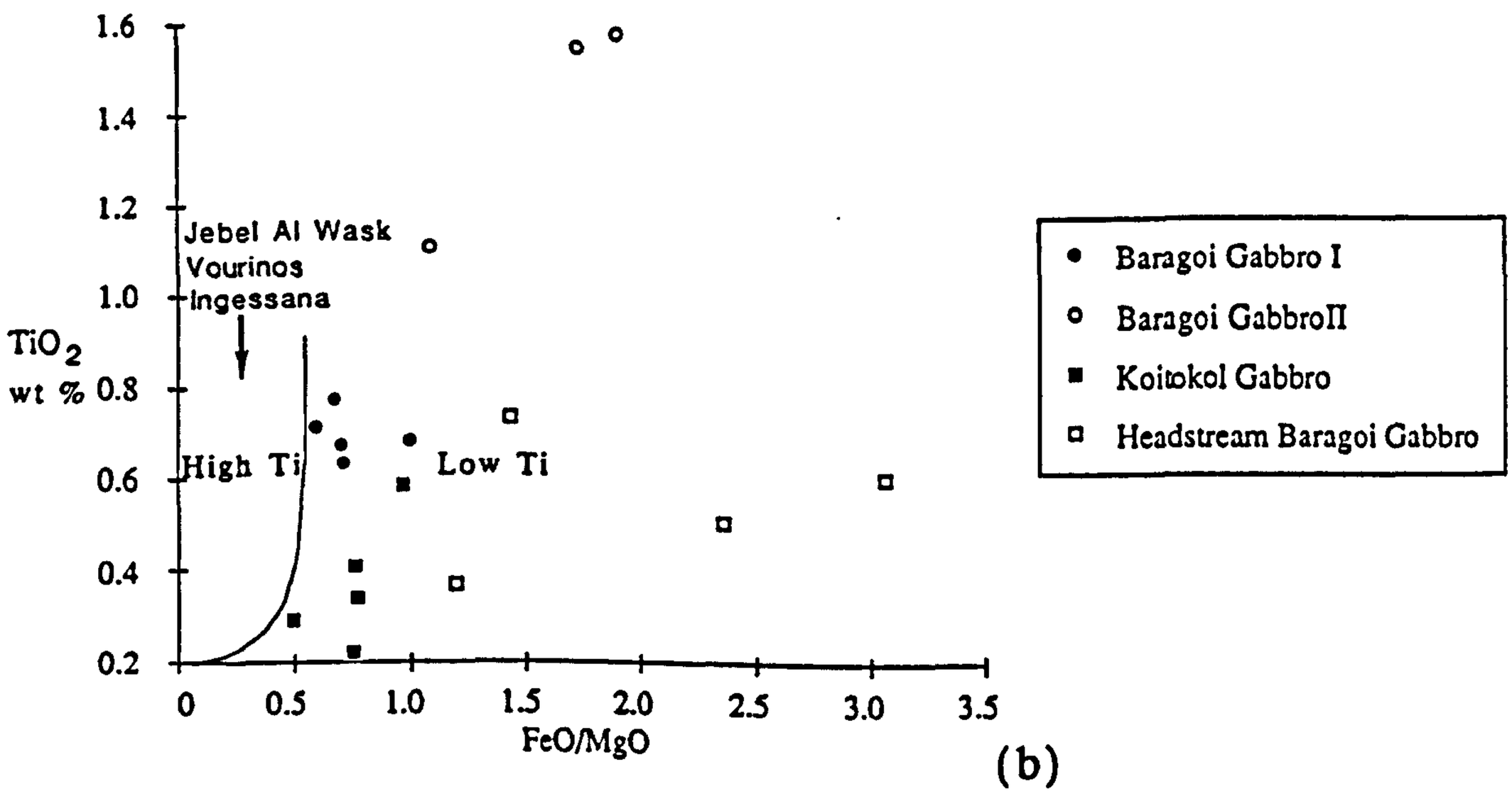

Figure 2.15 (a) Zr-Y plot. Both Zr and Y are high field strength element(HFSE) that are immobile during alteration and moderate grades of metamorphism and are incompatible during basaltic fractionation. As a result Zr/Y remains constant during fractionation and partial melting. In this diagram the Koitokol and Baragoi (Group I) gabbros align along the N-type MORB line (I.e Zr/Y=3, Pearce,1980), while the Baragoi (Group II) and the Bargoi Headstream gabbros vary (I.e Zr/Y >3). **(b)** FeO/MgO-TiO_2 plot for Baragoi and Koitokol gabbros. The data set show a depletion in TiO_2 relative to other ophiolite complexes. Dividing line between high and low Ti gabbros taken from Serri (1981).

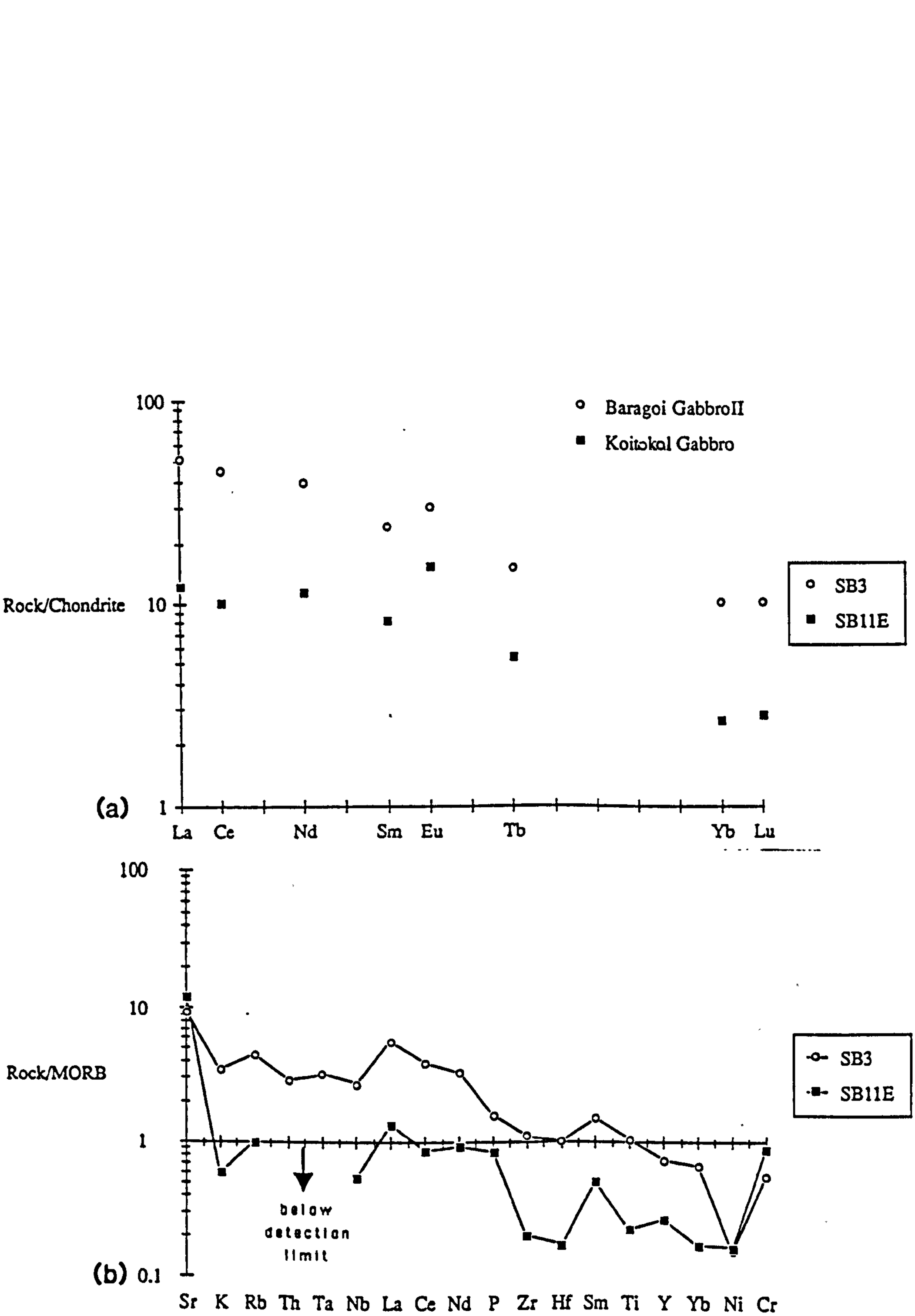

Figure 2.16 (a) Rare earth element patterns for the Baragoi and Koitokol gabbros.
(b) Geochemical pattern diagrams for the Baragoi and Koitokol gabbros.

Dykes

The dykes are also subdivided into two based on their petrology: (i) amphibolite dykes and (ii) felsic dykes. The majority of the dykes are parallel to S_2 foliation, while a few that cut the pre-existing structure are thought to be younger in age.

However, geochemical study has shown that the lavas and dykes could be subdivided into three. It has also been observed that dykes cutting the same host rocks have diverse chemistry, and the hornblende plagioclase gneisses which have been grouped as one rock formation contained at least two chemically distinct lavas. In the Baragoi area they are subdivided into island arc tholeiites and andesites and in the Masiketa area they also incorporate minor amounts of boninitic lavas.

2.5.5.1 Characterisation of rock types using ESCORT System

The Baragoi mafic-ultramafic complex as has been described in the previous section has suffered upper amphibolite facies metamorphism. Hence it was difficult to separate the rocks in terms of phenocryst assemblage as hardly any relict minerals are preserved. The geochemical data of fifty mafic rocks were analysed using an ESCORT program developed by Pearce (1987). The ESCORT (Expert System for Characterisation of Rock Types) System enables geochemical evidence to be integrated with geological, petrological and mineralogical evidence in identifying the eruptive setting of ancient volcanic rocks. Pearce's approach involves to making detailed tectonic subdivision on the basis that the probabilistic treatment used does not require perfect discrimination of the different groups: any overlaps being assigned probabilities. The tectonomagmatic environments of the Baragoi mafic rocks discriminated using ESCORT are listed, with abbreviations used in Table 2.3.

Based on this classification it was possible to subdivide the lavas and dykes into ocean ridge (OR) basalts; volcanic arc (VA) basalts; andesites and dacites; collision zone (CZ) basalt and Continental Flood basalts (CFB). Since the ESCORT program chemically differentiates rock types into three major groups as basalts, intermediate, and evolved it was essential to subdivide each group of rocks based on their chemistry to show their geological affinity. This classification helped to regroup the samples making it easier to carry out further major and trace element analysis.

Table 2.3 Geochemical classification of the Baragoi mafic rocks using ESCORT program

Sample Number	Locality	Rock Name	Magma Type	RockType	Chemical Affinity
SB17	Nikichata	Amphibolite	O-VA	Intermediate	Boninitic
SB18A	Nikichata	Amphibolite	O-VA	Intermediate	Boninitic
SB18B	Nikichata	Amphibolite	O-VA	Intermediate	Boninitic
SB20	Nikichata	Amphibolite	O-VA	Intermediate	Boninitic
SB21	Nikichata	Amphibolite	O-VA	Intermediate	Boninitic
SB23A	Nikichata	Amphibolite	O-VA	Intermediate	Boninitic
SB23B	Nikichata	Amphibolite	O-VA	Intermediate	Boninitic
SB42	Kisima	Amphibolite	O-VA	Intermediate	Boninitic
SB43	Kisima	Amphibolite	O-VA	Intermediate	Boninitic
SB44	Kisima	Amphibolite	O-VA	Intermediate	Boninitic
SB81	Masiketa	Amphibolite	O-VA 53%	Intermediate	Boninitic
SB84	Masiketa	Amphibolite	O-VA 92%	Intermediate	Boninitic
SB86	Masiketa	Amphibolite	O-VA90%	Basalt	Arc tholeiite to Boninite
SB87	Keleshwa	Amphibolite	O-VA 93%	Intermediate	Boninite
SB88	Keleshwa	Amphibolite	- VA 97%	Intermediate	Boninite to Arc tholeiite
SB121	Baragoi	Hornblende plag gneisses	O-VA 92%	Basalt	Arc tholeiite
SB127	Baragoi	Hornblende plag gneisses	C-VA 54% N-CF 39%	Basalt	Arc tholeiite
SB118	Baragoi	Hornblende plag gneisses	N-CF 50% C-VA 48%	Basalt	Arc tholeiite
SB19A	Baragoi	Hornblende plag gneisses	C-VA 88%	Intermediate	Arc tholeiite (Andesite)
SB19B	Baragoi	Hornblende plag gneisses	C-VA 86%	Basalt	Arc tholeiite (Andesite)
SB119	Baragoi	Hornblende plag gneisses	O-VA 86%	Basalt	Arc tholeiite (primitive andesite)
SB120	Baragoi	Hornblende plag gneisses	O-VA 70%	Intermediate	Arc basalt
SB130	Nawakim	Hornblende plag gneisses	VA 91%	Basalt	Arc andesite
SB133	Nawakim	Hornblende plag gneisses	O-VA 90%	Basalt	Arc basalt
SB77B	Masiketa	Hornblende plag gneisses	O-VA	Intermediate	Calc-alkaline (Dacite)
SB78	Masiketa	Hornblende plag gneisses	C-VA 99%	Basalt	Arc basalt
SB79	Masiketa	Hornblende plag gneisses	O-VA 91%	Intermediate	Andesite
SB69	Kangura	Hornblende plag gneisses	C-VA 94%	Intermediate	Calc-alkaline Silicic andesite
SB76A	Masiketa	Hornblende biotite gneisses	VA 50% CF 30%	Basalt	Calc-alkaline (Andesite)

SB76B	Masiketa	Hornblende biotite gneisses	VA 90%	Intermediate	Calc-alkali basalt
SB75	Masiketa	Amphibolite	VA 97%	Basalt	Arc basalt
SB112	Nachola	Hornblend plag gneisses	I-OR 54% N-CF 38%	Basalt	MORB
SB136	Nachola	Hornblend plag gneisses	I-OR 69% O-VA 30%	Basalt	MORB
SB1	Baragoi	Garnetiferous hornblend gneiss	O-VA 93%	Intermediate	Andesite
SB49	Baragoi	Garnetiferous hornblend gneiss	O-VA 73% O-VA 20%	Basalt	Andesite
SB40	Baragoi	Garnetiferous hornblend gneiss	I-OR 73% N-OR 21%	Basalt	MORB
SB4A	Baragoi	Amphibolite dyke	CZ	Intermediate 87% Basalt 13%	Arc andesite
SB100	Baragoi	Amphibolite dyke	C-VA 45% N-CF 54%	Basalt	Arc basalt to Continental Flood Basalt
SB102	Baragoi	Amphibolite dyke	C-VA 62% B-CF 35%	Intermediate	Arc basalt
SB110A	Baragoi	Amphibolite dyke	O-VA 92%	Basalt	Arc basalt
SB110B	Baragoi	Amphibolite dyke	O-VA 90%	Basalt	Arc basalt
SB111	Baragoi	Amphibolite dyke	O-VA93%	Basalt 60% Intermediate 40%	Arc basalt
SB135	Baragoi	Amphibolite dyke	O-VA93%	Basalt	Arc basalt
SB53	Barenyiro	Amphibolite dyke	I-OR 37% N-OR 20%	Basalt	MORB
SB56	Barenyiro	Amphibolite dyke	I-OR 37% N-OR 20%	Basalt	MORB
SB62	Barenyiro	Amphibolite dyke	C-VA 67% O-VA 24%	Basalt	Andesite
SB117	Barenyiro	Amphibolite	N-CF 90%	Basalt	Continental Flood Basalt (Magnetite Accummulation)
SB125	Headstream Baragoi	Amphibolite lava	N-CF 85%	Basalt	Arc tholeiite
SB129	Headstream Baragoi	Amphibolite	VA 32% N-CF 43%	Basalt	Arc tholeiite

2.5.6 Major element geochemistry of basic gneisses and amphibolites.

2.5.6.1 Basic gneisses (lavas)

The AFM diagram (Figure 2.17) shows an alkali enrichment trend for the basic gneisses (lavas) and amphibolite dykes. Using the dividing line between calc-alkali and tholeiitic suites of Irvine and Baragar (1971) and the calc-alkaline ("Cascades") trend line of Carmichael *et al.* (1974) it is evident that almost all samples have tholeiitic affinities. The Hornblende biotite plagioclase gneisses fall outside this field since they show calc-alkaline affinities. However, as has already been shown in Section 2.5.2, misclassification can arise in AFM diagrams because of mobility of major elements, especially the alkalies. Hence the triangular diagrams are only a rough guide.

The mafic rocks have been subdivided into three major groups as defined by Al_2O_3 and Ni against TiO_2 content (Figures 2.18a and 2.18b) (Coish *et al.*, 1982). The Hornblende plagioclase gneisses have high Al_2O_3 (11.5-17.5 %) and low Ni abundances (10-100 ppm) while TiO_2 content is (0.38-0.64 %) for Group I lavas and (0.7-1.83 %) for Group II lavas. Ni content for Group I and II lavas and dykes have a similar wide range. The wide range in Ni content probably reflects fractionation of mafic phases but since the variations in TiO_2 are large within each group, these variations cannot be accounted by simple fractionation processes.

In order to see if these subdivisions are consistent and could be picked by other major element discriminant diagrams, further plots were made. On a Al_2O_3/TiO_2-TiO_2 (Figure 2.19) (Sun and Nesbit, 1978) the lavas could still be divided into three, lavas with less < 0.5% TiO_2 plot in the boninite field while lavas ranging between 0.5-0.75% are island arc volcanics and TiO_2values >0.75% plot in the MORB field.

2.5.6.2 Amphibolites

The amphibolites have low TiO_2 (0.2 - 0.35 wt%) are low in Al_2O_3 (8-17%), and have high nickel abundances (60 - 350 ppm) (see Figures 2.21 and 2.22). The amphibolites form a flat evolution trend with TiO_2 effectively buffered with respect to Al_2O_3, indicating approximately equal proportions of clinopyroxene and plagioclase fractionation. In summary the major elements show a narrow and primitive compositional range.

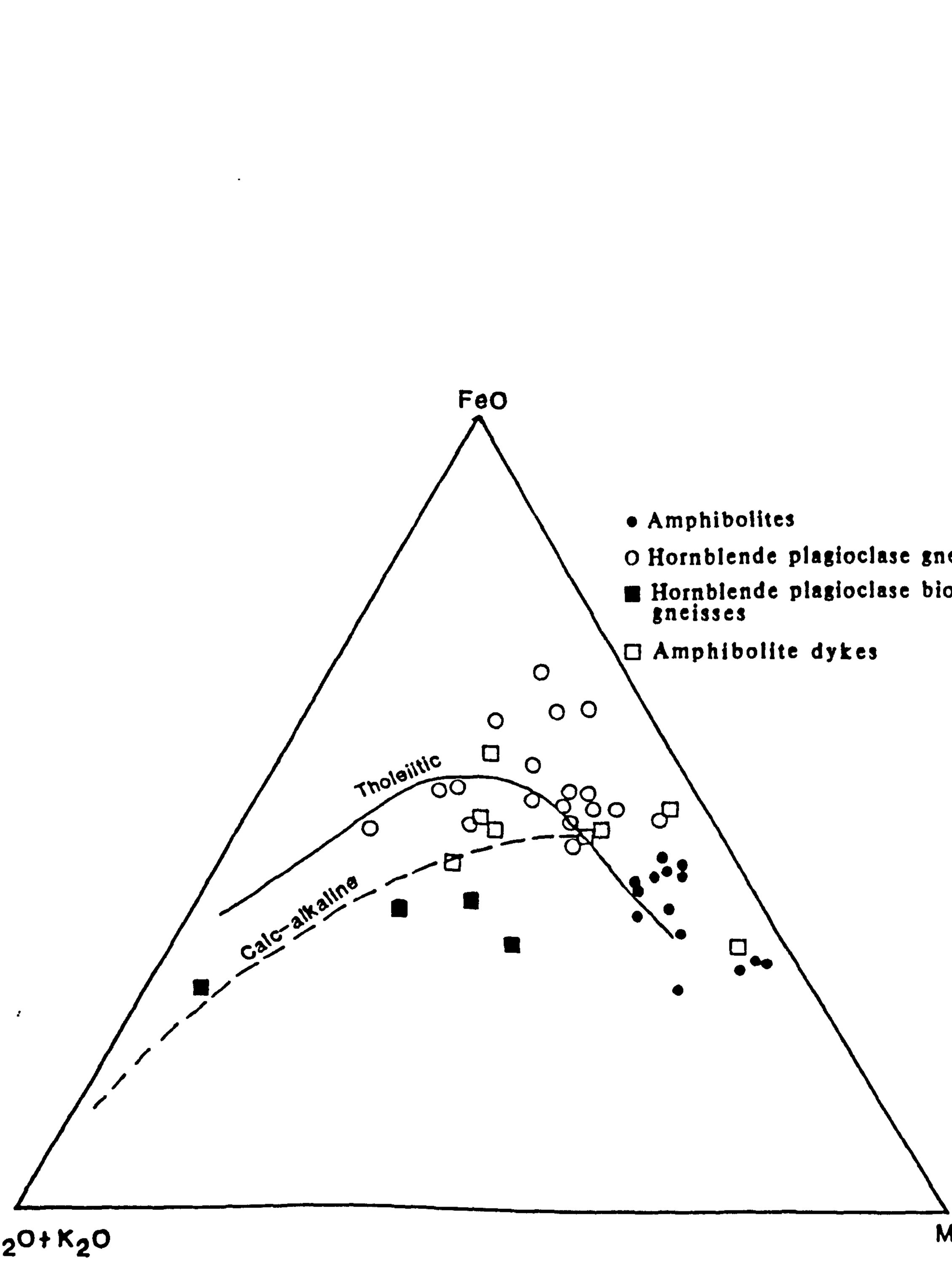

Figure 2.17 AFM diagram for the Baragoi basic gneisses, amphibolites and dykes. Dividing line for tholeiitic suites from Irvine and Baragar (1971). The dashed calc-alkaline ('Cascades') trend from Carmichael et al(1974).

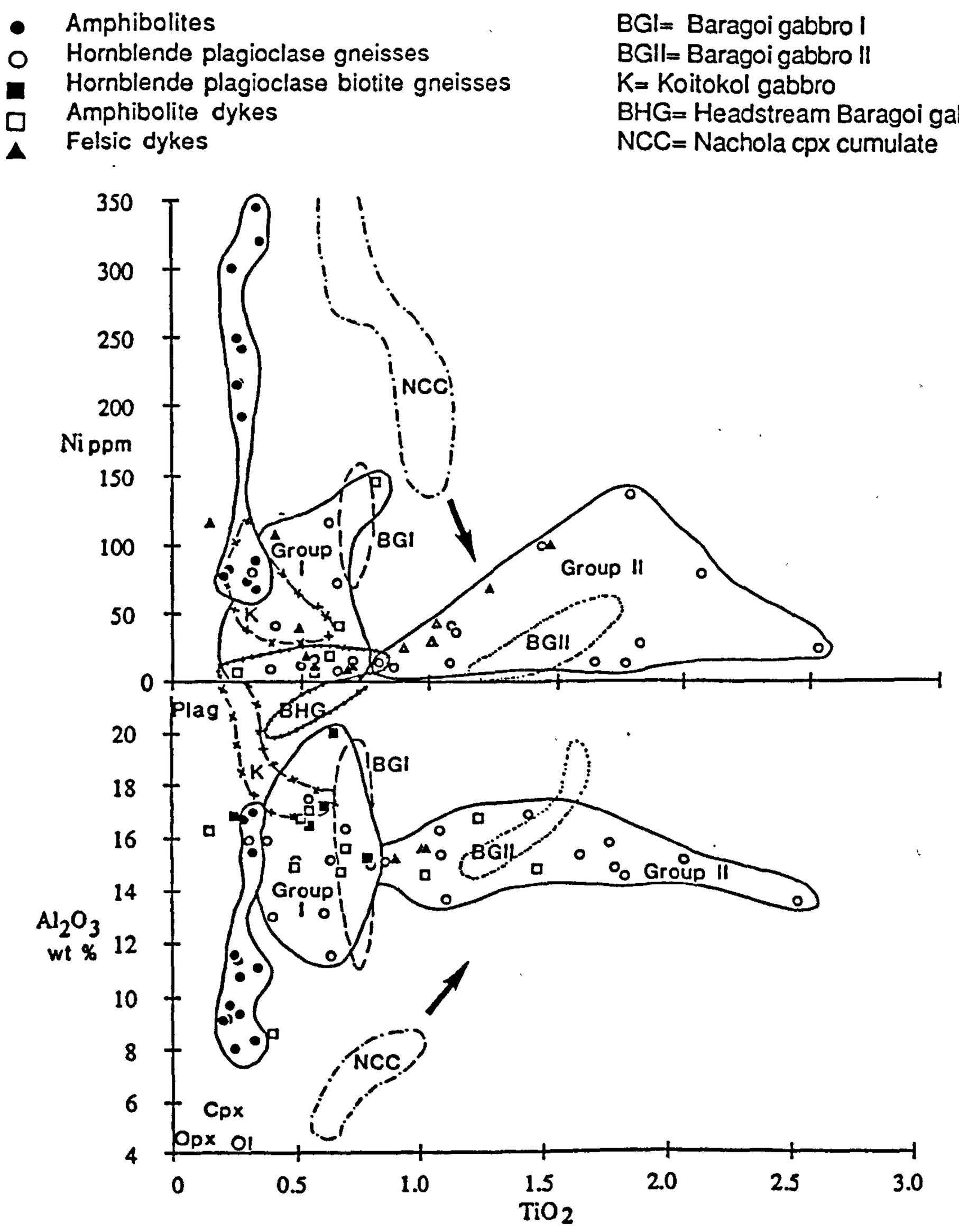

Figure 2.18 (a) Variation of TiO_2-Ni for the Baragoi basic gneisses, amphibolites and dykes. The rocks are effectively split into three groups. The hornblende plagioclase gneisses were grouped petrographically as one group, however they have been geochemically split into two groups. Ni content for Group I and II lavas and dykes have a similar wide range. The wide range in Ni content probably reflects fractionation of mafic phases. **(b)** Variation of TiO_2-Al_2O_3 for the Baragoi basic gneisses, amphibolites and dykes. The amphibolites form a vertical evolution trend with TiO_2 effectively buffered with respect to Al_2O_3, indicating approximately equal proportions of clinopyroxene and plagioclase fractionation. Comparative data of the gabbros and cumulates are outlined. Cpx cumulates are related to the Baragoi gabbros (II) by fractionation. The Baragoi gabbros show major similarities with the basic gneisses, amphibolites and dykes.

In the AFM diagram (Figure 2.17) they show calc-alkaline to tholeiitic affinity. In Figure 2.19 the amphibolites plot in the boninite field. They have low TiO_2 and Al_2O_3/TiO_2 ratios upto 57. In contrast high Ti ophiolitic basalts have either chondritic (20 and 17, respectively) or lower ratios (Sun and Nesbitt, 1978).

Although the amphibolites look like boninites in their major and trace element chemistry, they tend to have slightly elevated P_2O_5 as compared to boninites from the Marianas (Dietrich *et al.*, 1978; Crawford *et al.*, 1981) and Cyprus (Cameron *et al.*, 1983; Murton, 1986). Various possibilities are that it could be contamination, or could be a primary feature. The fact that P_2O_5 is consistently high in all the samples indicates that it is not contamination. If there are high concentrations of HREE it would imply that garnet melted in the source, however, REE data for one amphibolite sample indicates the contrary (Figure 2.24). It is suggested that the amphibolites have been selectively enriched by phosphorus. This enrichment process will be discussed in the petrogenesis section.

2.5.7 Trace elements

Introduction

The above section established a tholeiitic magma affinity for the Hornblende plagioclase gneisses and the amphibolite dykes. Major element data indicate that the mafic rocks could be subdivided into boninites, island arc volcanics and MORB. However the AFM diagrams have been found unsuitable for quantitative discussions (Miyashiro, 1974). In section 2.5.2 it was shown that a number of elements have been mobilised by secondary processes. The high field strength elements Ti, Y, Zr, Nb, Cr and Ni appear to be relatively immobile. The discussion will concentrate on these immobile elements, and the rare earth elements, which behave like the high field strength elements (Saunders *et al.*, 1980).

In the following section a detailed geochemical interpretation of the various basic gneisses and amphibolites dykes is attempted.

2.5.7.1 Amphibolites

On a Ti-Zr diagram (Figure 2.20) the data show that the amphibolites are very depleted plotting below to the left of the island arc volcanics field of Pearce and Cann (1973). They also plot outside the discriminant fields on a Zr/Y-Zr diagram (Figure 2.21). Zr/Y ratios (3.2-7.2) are high as compared to boninites of Cyprus (average Zr/Y value is c.2) (Murton, 1986). This could be due to retention of Y by residual phases in the source, or it could be that the Y values are so low (5-9 ppm) that analytical errors could shift the results 1-2 ppm either way making large variations in the Zr/Y ratios.

The most informative trace element co-variation diagam that shows evolution trends in the Hornblende plagioclase gneisses and amphibolites is Ti/Cr v Ni (Figure 2.22). Since both Cr and Ni are compatible during basaltic fractionation they decrease, while Ti is incompatible, and increases until magnetite supersaturation and precipitation. Hence Ti/Cr should also increase during fractionation. In detail the amphibolites form a dispersed trend away from very primitive Ni values (c. 300 ppm). The evolution trend has a gradient that is between the vectors for olivine and pyroxene fractionation. Further indication to a boninitic affinity is shown as the data plots in the boninite field of Beccaluva *et al.* (1983) (Figure 2.22).

The chemistry of an amphibolite has been plotted on a geochemical pattern diagram (Figure 2.23a) normalised against the average MORB values of Pearce (1980). The amphibolite (boninitic affinity) are richer in Ni, Cr while they are poorer in HFSE (Y, Hf, Zr, Nb), TiO_2 and REE than MORB. This is consistent with derivation from a depleted mantle source. This lava has a positive P_2O_5 peak and negative Ta.

REE data are presented in Appendix B and plotted on a chondrite normalised diagram (Figure 2.24a). The amphibolite have lower REE abundances and Yb/Sm when compared to N-type MORB but are LREE enriched. Similarly it has lower La/Yb (2.9) (Figure 2.24a) as compared to the Hornblende plagioclase gneisses (island arc tholeiites), which ranges from 4 to 6.2 (Figure 2.24b) indicating their relative LREE enrichment. The REE pattern is similar to boninites from Marianas and Bonin Islands (Hickey and Frey,1982).

The Baragoi amphibolites lie outside the majority of basalt discriminant fields. Instead, the extremely low abundances of incompatible elements (Zr, Y, Nb, TiO_2) and moderately high MgO of

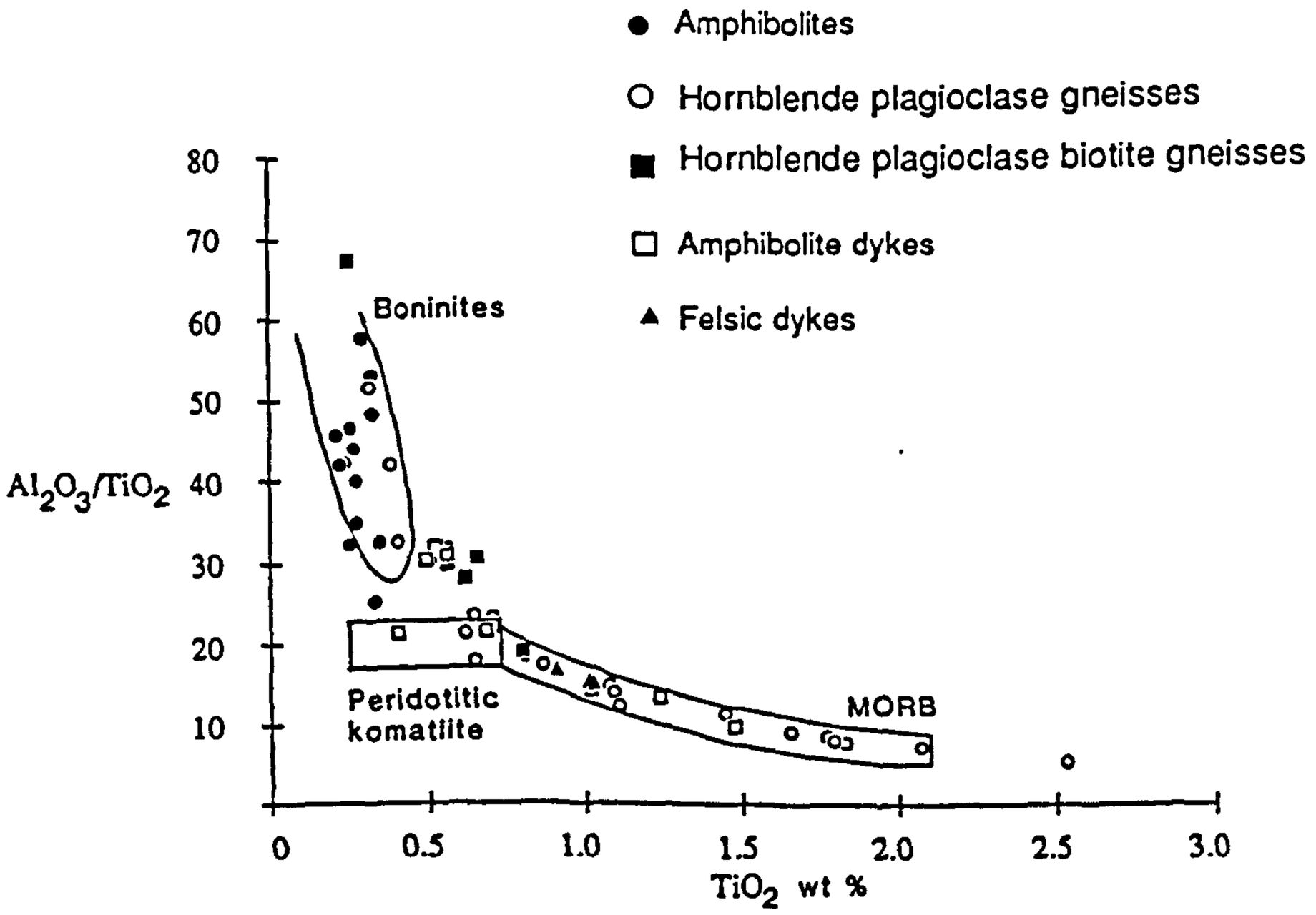

Figure 2.19 Al_2O_3/TiO_2-TiO_2 plot for the Baragoi basic gneisses, amphibolites and dykes. Fields taken from Sun and Nesbitt (1978).

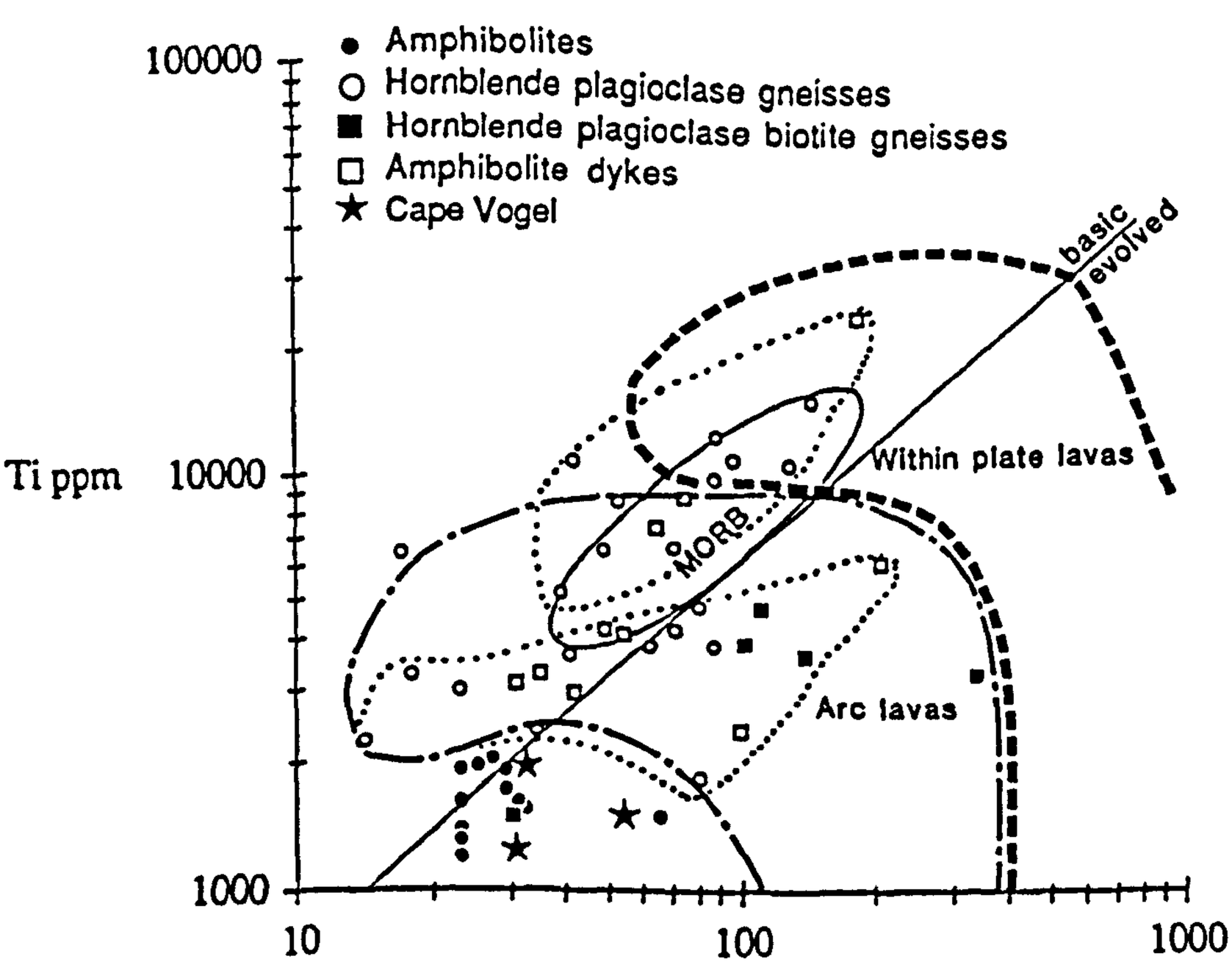

Figure 2.20 Ti-Zr co-variation diagram for the Baragoi gneisses, amphibolites and dykes. Fields taken from Pearce (1980). Comparative data sources for boninites of Cape Vogel (Hickey and Frey,1982).

the amphibolites are similar to 'boninites' from Cape Vogel, (Dalwitz *et al.*, 1966; Dalwitz, 1968; Jenner, 1981) the Mariana trench wall (Dietrich *et al.*, 1978; Sharaskin and Dobretsou, 1979; Hawkins *et al.*, 1979) and Mariana fore-arc region, DSDP site 458 (Meijer, 1980; Meijer *et al.*, 1981). Table 2.4 gives the average composition of the Baragoi amphibolites compared to a number of 'boninitic' compositions published by Hickey and Frey (1982), and Murton (1986). Although the major elements of the Baragoi area are unreliable, approximate comparison can be made.

Table 2.4 Baragoi amphibolites compared to representative boninite compositions.

	Bonin Islands Japan	Cape Vogel Papua New Guinea	WLFC lavas Cyprus	Baragoi amphibolites Kenya
Wt %				
SiO_2	58.46	56.80	52.50	52.88
TiO_2	0.10	0.33	0.22	0.26
Al_2O_3	13.37	11.9	15.8	11.41
FeO^*	8.27	7.10	7.60	9.26
MnO	0.12	0.16	0.15	0.29
MgO	9.36	12.60	12.12	9.46
CaO	8.11	7.89	10.82	13.85
Na_2O	1.59	1.05	0.44	1.28
K_2O	0.70	0.41	0.52	0.32
P_2O_5	–	–	0.03	0.13
ppm				
Sr	97	339	163	217
Rb	12	8	10	10
Th	–	–	0.28	0.35
Ta	–	–	0.4	–
La	1.27	1.47	1.35	3.49
Ce	2.57	3.51	2.85	5.76
Nd	1.65	2.09	2.85	–
Zr	25	29	15	32
Hf	0.69	0.58	0.41	0.76
Sm	0.43	0.60	0.40	1.03
Y	5	7	8	9
Yb	0.59	0.81	1.09	1.15
Ni	140	154	266	217
Cr	538	715	848	1153
Tb	0.10	0.14	0.19	0.28
Lu	0.10	0.13	0.20	0.18

Boninte data for Bonin Islands and Cape Vogel (Hickey and Frey,1982); Cyprus (Murton,1986).

2.5.7.2 Hornblende plagioclase gneisses

On a Ti-Zr diagram (Figure 2.20) the Hornblende plagioclase gneisses are subdivided into two: Group I plot in the island arc field and Group II lavas plot in the MORB field. Although the Hornblende plagioclase gneisses were not subdivided in the field they form two different units geochemically.

Group I lavas have Ti/Zr ratio of 51-70, while Group II lavas have Ti/Zr ratio of 76-120. Although the range of Ti/Zr of Group II lavas are wide the MORB values of 110 (Sun and Nesbitt, 1978) are found in the middle.

In Ti/Cr vs Ni (Figure 2.22) the Hornblende plagioclase gneisses are split into MORB/IAT fields, however, few samples that originally plotted in the MORB field have been classified into the IAT field. By comparing the gradient of the lava evolution trend to the various phase extraction vectors, the petrogenesis of the lavas could be determined. Although one can observe a dispersed trend, the evolution has a gradient that is between the vectors of olivine and pyroxene fractionation.

Geochemical patterns for Group I lavas of the Hornblende plagioclase gneisses shown (Figure 2.23b) compare favourably with oceanic calc-alkaline basalts (Pearce, 1982) and Sol Hamed lavas (Price, 1984). There is selective enrichment of Sr-Ba due to hydrothermal processes and/or mobilisation of aqueous fluids driven off a subducted slab into the overlying mantle (Ringwood, 1974; Hawkesworth *et al.*, 1977). The remaining elements show various levels of depletion producing an irregular pattern. These patterns are typical transition between MORB and IAT. SB130 has higher Cr values than SB121 indicating a more primitive composition. Nb shows a depletion characteristic of arc magmatism.

REE data is plotted for the same samples (Figure 2.24b) normalised to chondrite values. The lavas show LREE enriched pattern and a slightly depleted HREE, whilst the trace elements discriminant diagrams point to volcanic arc affinity. REE and geochemical pattern diagram suggest a transitional MORB to IAT. These transitional type lavas, showing moderate enrichment can be associated with the initial stages of back-arc spreading (Tarney *et al.*, 1981).

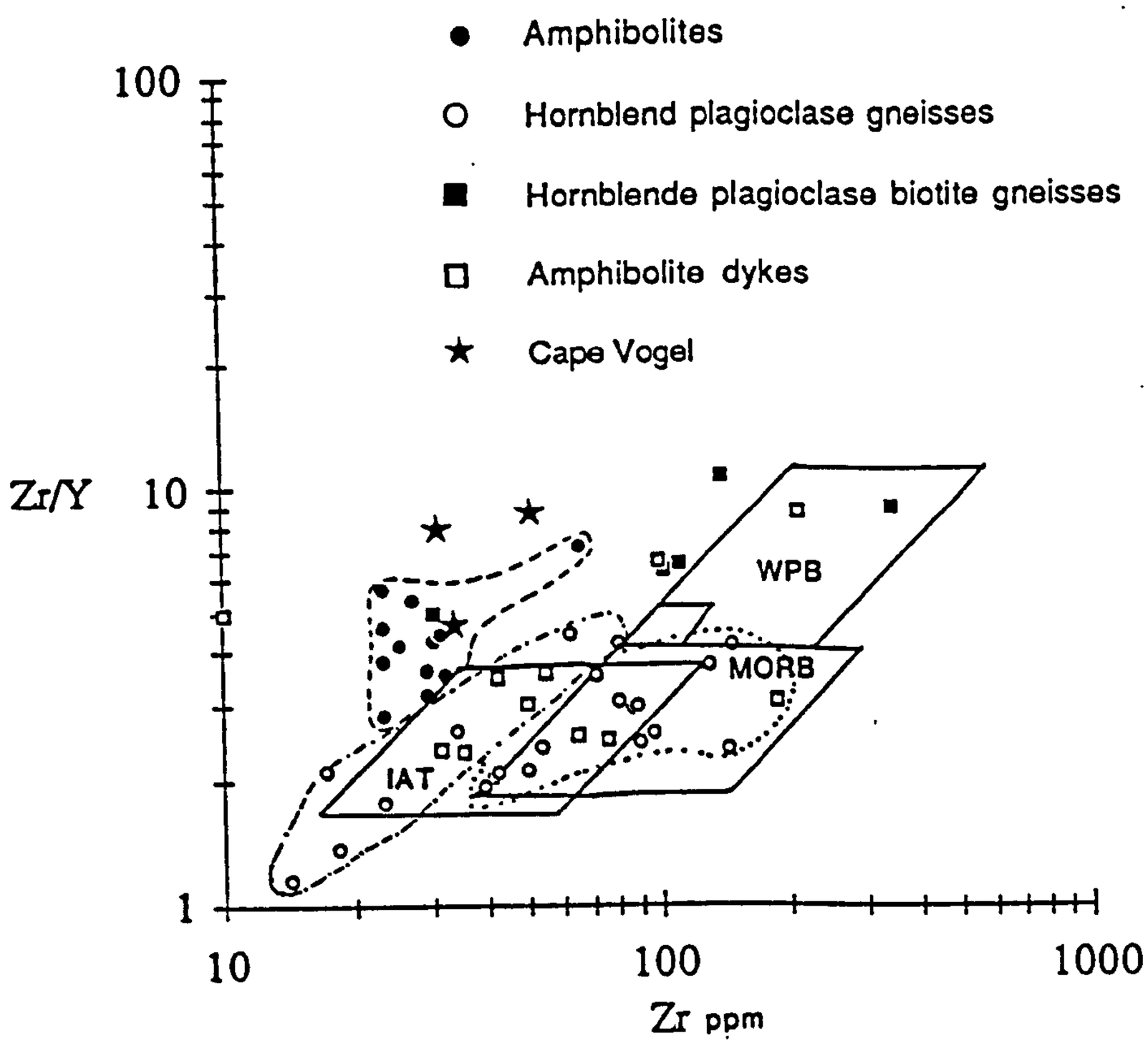

Figure 2.21 Zr/Y-Zr discriminant diagram for the Baragoi basic gneisses, amphibolites and dykes. Fields taken from Pearce and Norry (1979).

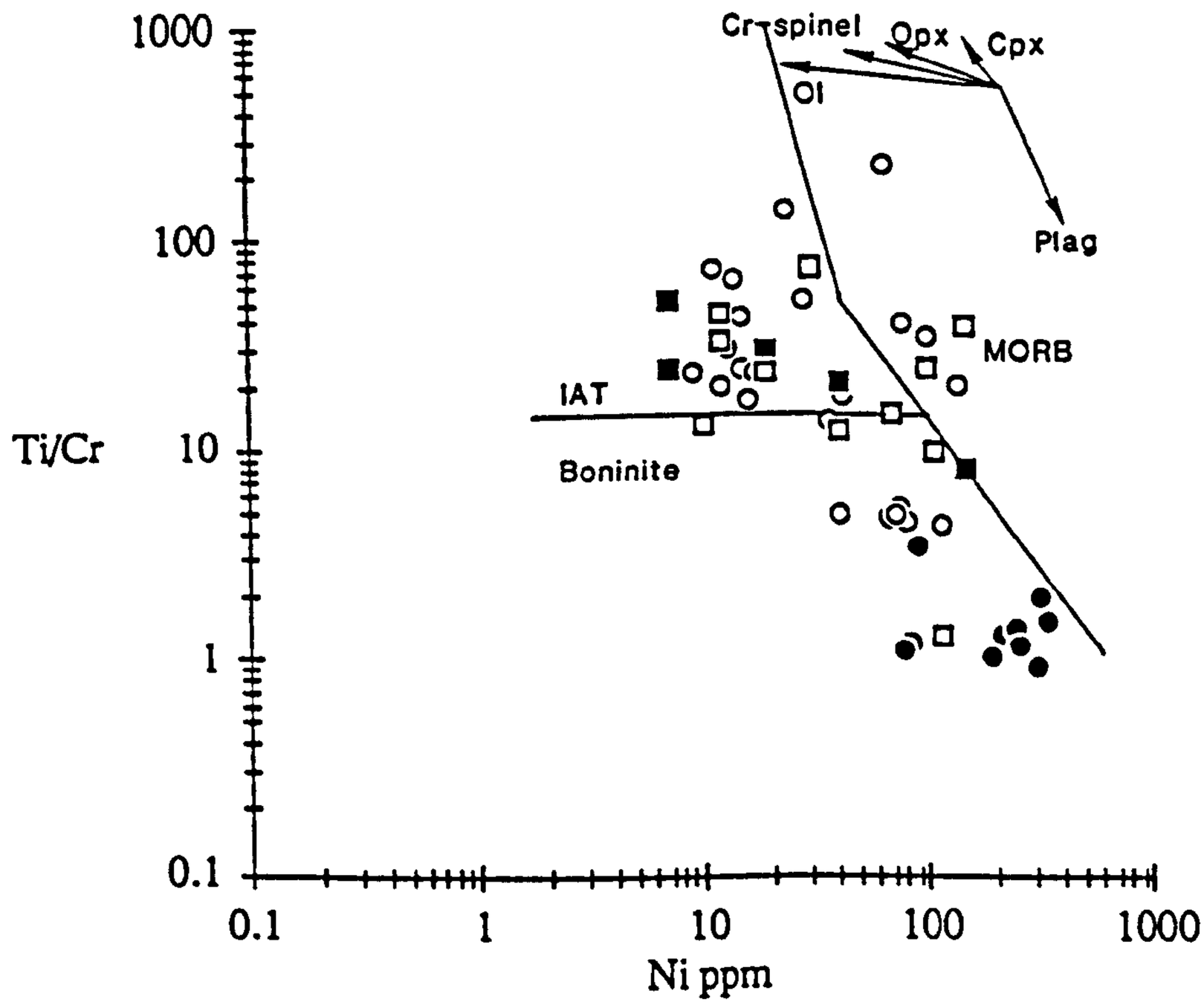

Figure 2.22 Ti/Cr-Ni diagram showing distribution of Baragoi basic gneisses, amphibolites and dykes analysed. Boninite field taken from Beccaluva et al (1983).

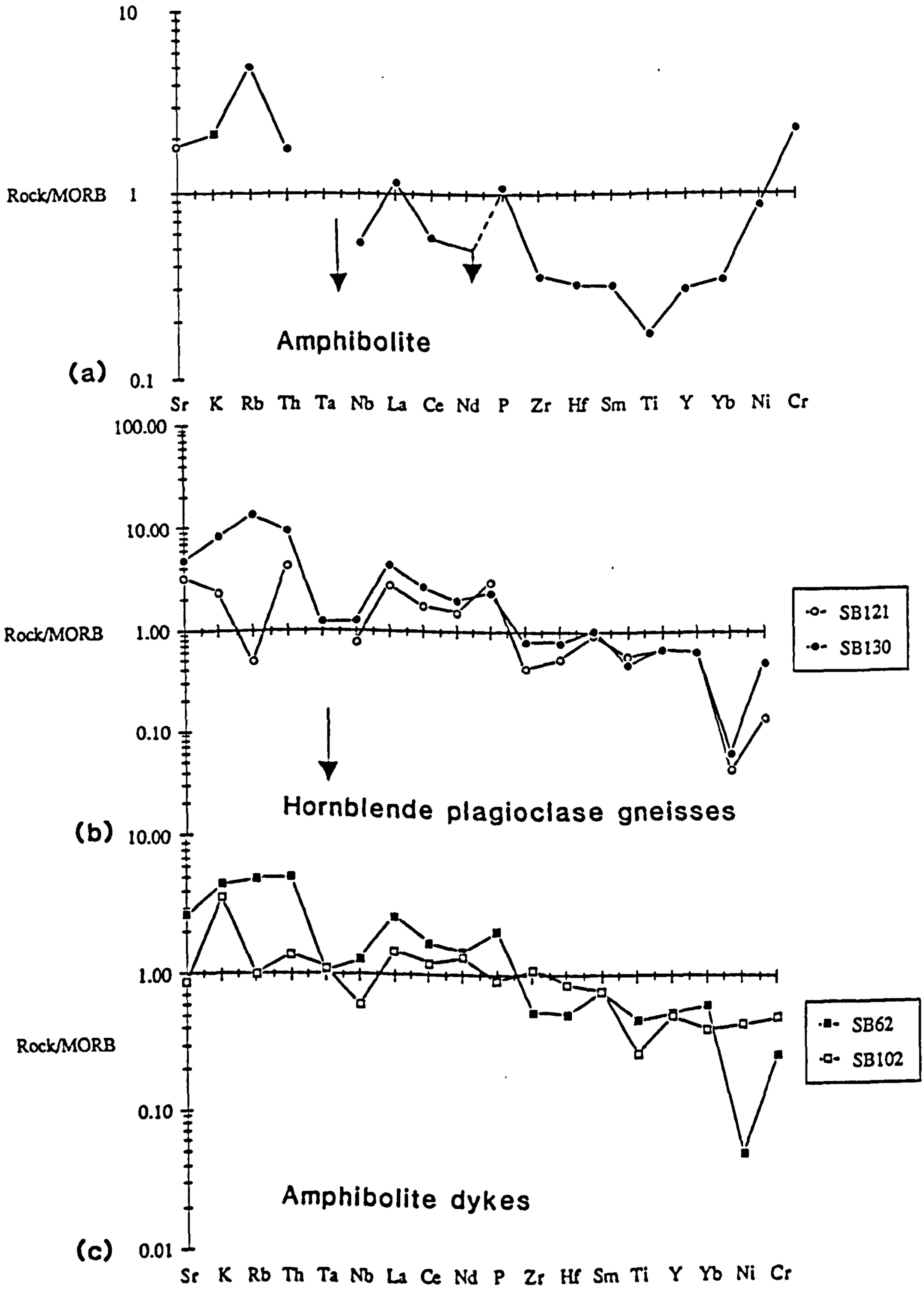

Figure 2.23 (a) Geochemical pattern diagram for the Nikichata amphibolites. **(b)** Geochemical pattern diagram for the Hornblende plagioclase gneisses. **(c)** Geochemical pattern diagram for the Baragoi dykes. Normalising values taken from Pearce (1980).

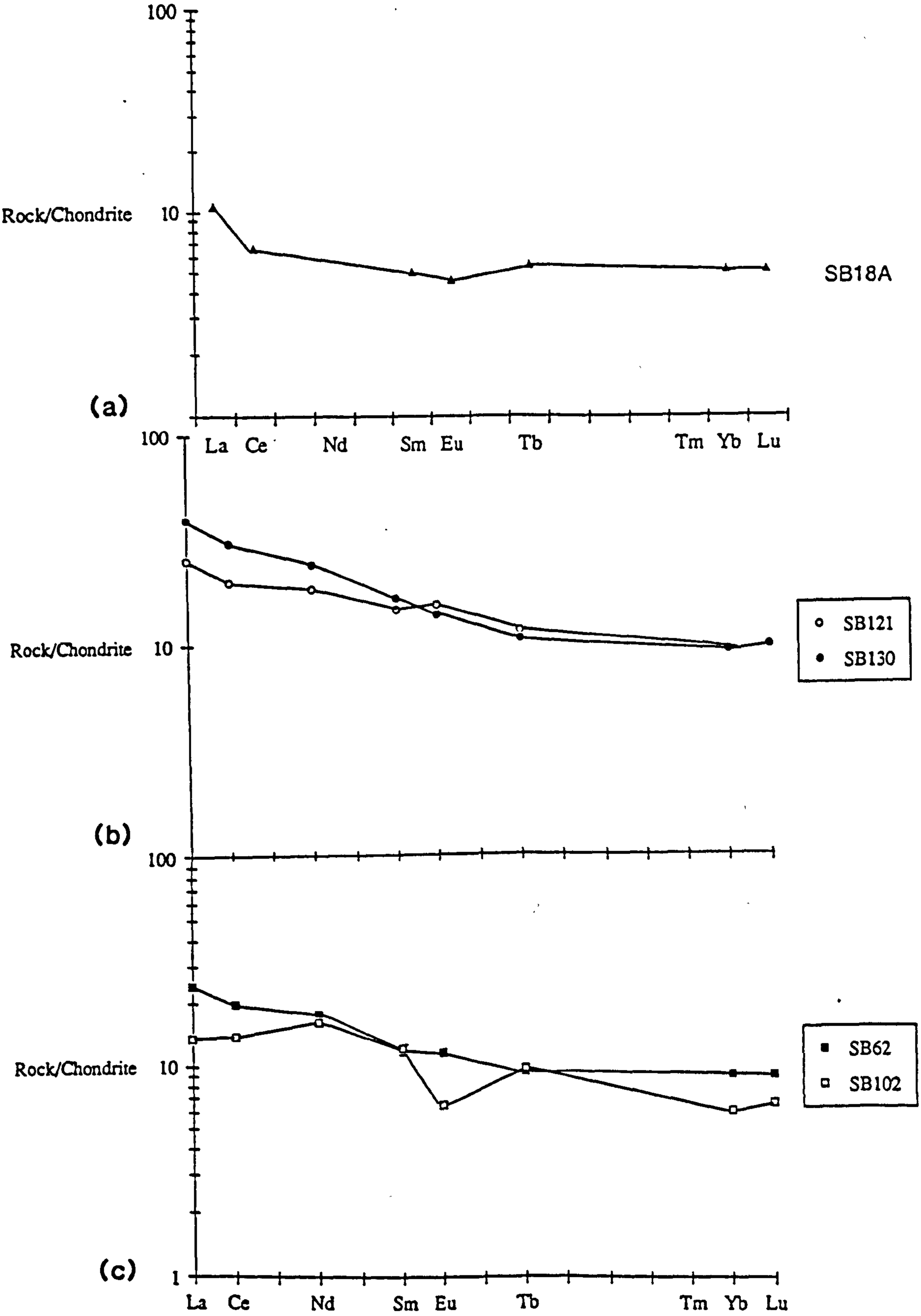

Figure 2.24 (a) Chondrite normalised REE diagram for Nikichata amphibolites. **(b)** Chondrite normalised REE diagram for the Hornblende plagioclase gneisses. **(c)** Chondrite normalised REE diagram for the Baragoi dykes.

2.5.7.3 Dykes

The dykes of the Baragoi area are subdivided into amphibolite and felsic dykes. On a Ti-Zr co-variation diagram (Figure 2.20) most of the dykes except for SB4a and SB102 plot within the basic field. They also plot in the overlap of MORB and arc lava fields, and show a good trend towards increasing Ti and Zr values.

Before trying to discriminate between the MORB and volcanic arc fields it is necessary to remove any basalts that have within-plate charcteristics. A Zr/Y vs Zr diagram (Figure 2.21) achieves this discrimination (Pearce and Norry, 1979) and partly discriminates MORB and IAT. Note that nearly all the samples plotting in the evolved fields in the Ti-Zr diagram plot in the within-plate field in the Zr/Y against Zr discriminant diagram. Two dykes plot in the within-plate field (Figure 2.21), SB4A which has been classified as continent collision related basalts by ESCORT system (Table 2.3) is enriched in Sr, Ba and Th; while SB100 has high Fe-Ti and V suggesting magnetite precipitation. This partial separation is accounted for by higher mean Zr values in MORB lavas. In the Ti/Cr vs Ni covariation diagram the dykes show close relationship with the lavas (Figure 2.22).

Geochemical patterns are shown for the Baragoi dykes (Figure 2.23c), unfortunately both are from Group I dykes. These patterns are similar to the volcanic arc basalts (Pearce, 1980). Like all island arc tholeiites, Sr, K, Rb, Ba and Th are selectively enriched, in addition Ce, P and Sm show variable degrees of enrichment. In contrast Ta, Nb, Zr, Hf, Ti, Y and Yb are moderately depleted when compared to typical tholeiite MORB. SB62 dyke is highly enriched in LILE relative to sample SB102. Pearce (1982) suggests that the elements Sr, K, Rb, Ba, Th, Ce, P and Sm may be derived in part from a subduction zone whereas Ta, Nb, Hf, Zr, T, Y and Yb are mantle derived.

The REE patterns (Figure 2.24c) are sub-parallel with Ce_N/Yb_N ratio ranging from 2.1 to 2.3. Sample SB102 shows a distinct negative Eu anomaly consistent with plagioclase fractionation. The REE distributions of these dykes are very similar to those in the Sarmiento marginal basin ophiolite complex in Southern Chile (Saunders *et al.*, 1979).

2.5.7.4 Hornblende biotite plagioclase gneisses

Hornblende biotite plagioclase gneisses are the least sampled in the Baragoi area. The chemical analysis is based on five samples. In the AFM diagram (Figure 2.17) these rocks show calc-alkaline affinities. These rocks are clearly enriched in alkalies, and show less Fe enrichment than the other arc lavas. They are enriched in the incompatible elements (K, Rb, Ba, Sr, Zr, Nb, Th) compared with the Hornblende plagioclase gneisses, but are lower in V (see Appendix B).

SB69 and SB76B are silicic andesites that have come from the same source or melting episode, but SB76B is a primitive andesite with high Zr (101 ppm), Y(16 ppm), Nb (7.7 ppm) and Ba (1492 ppm) and also has high Cr (188 ppm) and Ni (41 ppm). In order to produce rocks rich in incompatible elements you need low degrees of partial melting or a rich source, however Cr and Ni should remain in the residue. But in this case the Cr and Ni values are still high which means that there may have been crustal contamination.

On a Ti-Zr diagram (Figure 2.20) they plot (4 out of 5) within the evolved island arc field. In the Zr/Y vs Zr diagram (Figure 2.21) the samples plot outside the discriminant fields, this is because Zr is highly enriched, and hence this diagram is not useful for their discrimination.

2.5.8 Comparison of the gabbros, cumulates, amphibolites, hornblende plagioclase gneisses and dykes

The gabbros form a distinct group because they have a higher Al_2O_3/TiO_2 compared to the ultramafics. The cpx cumulates can only be related to the Group II Baragoi gabbros by fractionation. The other three gabbroic suites show different fractionation trends, hence have separate evolutionary history (Figures 2.18a and 2.18b).

Comparison between the Gabbroic suites and the lavas show major similarities:

(i) the Koitokal gabbros and the amphibolites (boninites), lie along the same trend indicating that the Koitokal gabbro could be due to plagiocalse accumulation (Figures 2.18a and 2.18b).

(ii) the Group I Baragoi gabbros, coincide with the respective fractionation trends of the Group I lavas (basic gneisses) supporting their being cogenetic.

(iii) Group II Baragoi gabbros are cogenetic with Group II lavas (basic gneisses and amphibolites)

and dykes, as they overlap in both Figures 2.18a and 2.18b.

2.6 PETROGENESIS

Major, trace and REE element studies indicate magma types which range from boninites to tholeiites and calc-alkaline affinities for the studied area. Modern analogues of these volcanics are situated near destructive plate margins above subduction zones (Pearce, 1982) in an island arc setting.

In order to explain the geochemical characteristics of the Baragoi Amphibolites and Hornblende plagioclase gneisses and to assess the potential of depleted mantle melts to fractionate to the observed arc type Baragoi mafic magmas require a possible source composition. However, in this area, harzburgites or leherzolites have not been found that could be used as a source composition or mantle residue. Ophiolite complexes that have formed in a supra-subduction setting have harzburgite as a mantle residue following extraction of picritic liquids (Browning, 1982). Although residual mantle does not occur at Baragoi the similarities with other supra -subduction zone ophiolites suggests that it existed but has not been preserved during emplacement of the ophiolite. For any modelling a geochemical study of a harzburgite residue is essential to model the original mantle sources. It is suggested that arbitrary choice of starting source or magma compositions results in major discrepancies that would make the modelling too hypothetical. Therefore, detailed modelling has not been attempted. However, by petrogenetic modeling of the geochemical variations observed in the Cr-Y diagram it is possible to place constraints on the genesis of the Baragoi complex. Y and Cr do not appear to be significantly affected by the processes that cause heterogeneities in the upper mantle. The diagram is also suitable for modelling fractional crystallisation as Cr acts as an index of fractionation producing a sub-vertical trend parallel to the Cr axis (Figure 2.25a and 2.25b). Projecting the trend of the Baragoi lavas and dykes shows that the melting curve is intersected in three places. Pathway C represents the setting for typical MORB lavas and from its intersection with the melting curve the primary magma was derived by about 15% partial melting of a mantle source.

Projecting pathway B back to the melting curve suggests that the Hornblende plagioclase

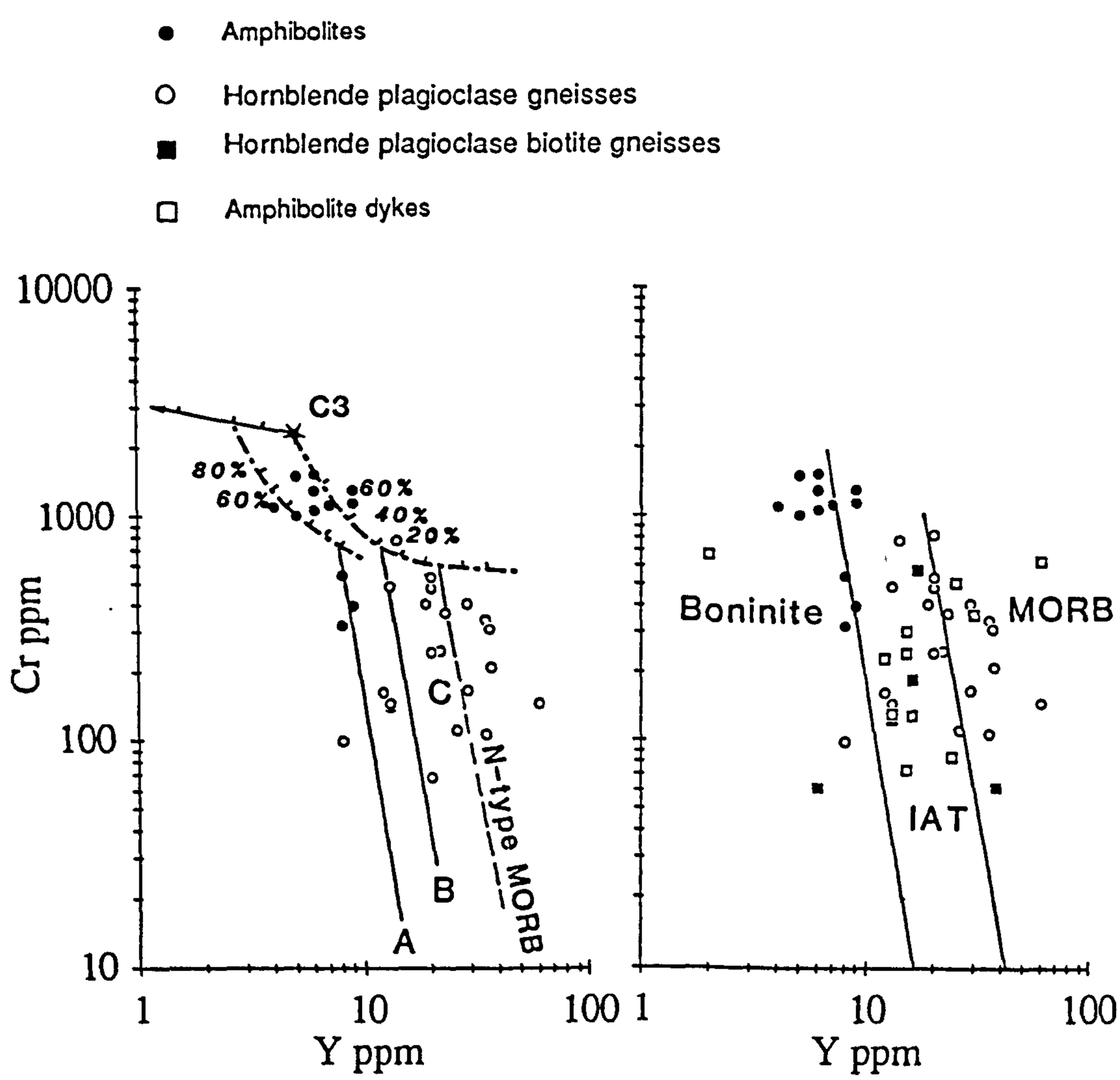

Figure 2.25 (a) Cr-Y co-variation diagram in which incremental batch melt proportions are modelled. The position of N-type MORB and C3 chondrite are given for reference. Melt curves are based on those of Pearce *et al* (1984a). The Hornblende plagioclase gneisses were derived by about 15% partial melting of a mantle source. Pathway A represents the pathway for the amphibolites of boninitic affinity. Pathway B is typical for SSZ ophiolites of island-arc affinities. Pathway C represents the setting for typical MORB lavas.

(b) Cr-Y co-varition diagram discriminates between parental liquid compositions and genetically unrelated suites. Since Cr is compatible and Y incompatible in basaltic magmatic processes, different parental liquids will start from and evolve along fractionation paths that are approximately vertical and parallel (Pearce,1980). The Hornblende plagioclase gneisses and the dykes plot in the MORB and IAT field, while the Amphibolite plot in the boninite field. The boninte field taken from Kostopoulos and Pearce (in prep).

gneisses (Group I lavas) and dykes require about 35% partial melt (Figure 2.25a) implying exceptionally hot, thermal conditions in the source region. This anomalous condition has been used by Menzies and Allen (1974); Pearce (1982); Duncan and Green (1980) and Pearce *et al.* (1984b) to argue in favour of incremental melting in the genesis of similarly depleted magmas.

Pathway A represents the pathway for the amphibolites (boninitic lavas). The projection of the composition back to the partial melting curve would require a minimum melt of >60%. This higher level of partial melt is geologically unrealistic and Pearce *et al.* (1984b) proposed that the source of these magmas was not the convecting upper mantle, but overlying sub-oceanic lithosphere, which had lost a basaltic component, and hence they favour incremental melting in the genesis of similarly depleted magmas.

2.7 GRANITOID GEOCHEMISTRY

Introduction

Major and trace element data are presented for the Luwamara, and Sartim granites of the Baragoi area, and the Ol'Doinyo Wassin granodiorites and Sabatchi granitic gneisses which are found about 140 kilometers south of Baragoi (Figure 2.26). The Ol'Doinyo Wassin granodiorites and Sabatchi gneisses have been included in this chapter although they are not related to the Baragoi mafic - ultramafic rocks. This geochemical study is mainly aimed at fingerprinting the genesis and tectonic setting of the granitoids which would elucidate the overall tectonic evolution of the belt, and to identify the geochemical variations of granitoids from west to east across the Pan-African/ Mozambique belt.

Jenning (1967) described a sequence of biotite and hornblende biotite gneisses in Sabatchi Hills, which are 15 miles NE of Archers Post, Central Kenya (Jennings, op. cit) and considered them to be of semi-pelitic origin. In thin section they could be described as biotite and hornblende biotite granitic gneisses, and at least the biotite hornblende granitic gneiss may have been of igneous origin (Table 2.6). The British Geological Survey team (R. Key pers. comm.) describe the gneisses of Sabatchi Hills as migmatites that are thrust into a biotite gneiss complex. Both units were sampled in

order to observe their geochemical affinity and for geochronological purposes as the migmatites are considered to be the oldest rocks in the area.

Similarly a major granodioritic pluton has been mapped north of Sabatchi, (R. Key, pers. comm.) in the Serolevi area which was originally mapped by Rix (1973). This is of major significance because it is the first time that such a major pluton was described in the Late Precambian of Kenya.

2.7.2 Classification Scheme

Petrographic description are given for representative samples from each of the granitoids (Table 2.5).

Table 2.5 Typical mineral assemblages of the Baragoi , Ol'Doinyo Wassin and Sabatchi granitoid rocks

Rock type	Mineral assemblages
Luwamara granite	Microcline + plagioclase (An_{20}) + quartz ± biotite ± green hornblende ± sphene
Sartim granite	K. feldspar 40 % + plagioclase (albite) 15 % + microcline 2% + quartz 15-20 % + biotite 20 % ± chlorite ±sphene± rutile
Ol'Doinyo Wassin granodiorite	Plagioclase(albite) 50 %+ quartz 15 % + biotite 10% + hornblende ± muscovite 1% ± magnetite ± apatite
Sabatchi granitoid gneiss (I)	Plagioclase (An_{36}) 40 % + microcline 15 % + quartz 15 %+ biotite 10 % + hornblende 10 % + magnetite ± sphene± allanite.
Sabatchi granitoid gneiss (II)	Plagioclase 35 % + quartz 20 % + biotite 15% + homblende 10 % + microcline 5 % ± myrmekite ± magnetite ± epidote ± muscovite ± chlorite ± sphene ± allanite

The granitoids have also been classified according to the Streickeisen classification scheme (Streickeisen, 1975) based on Norm program developed by Nigel Harris for recalculation of major element analysis into mineral phases. Misclassification can arise using this approach because the presence of pegmatoid veins can shift the chemical composition into a different field as is the case with one of the Ol'Doinyo Wassin granodiorites (Figure 2.27) which has higher SiO_2 content. The Ol'Doinyo Wassin granodiorites are characterised by quartz, K-feldspar, plagioclase (usually albite), biotite, minor amount of muscovite, and haematite. The Sabatchi granitic gneisses (I) are

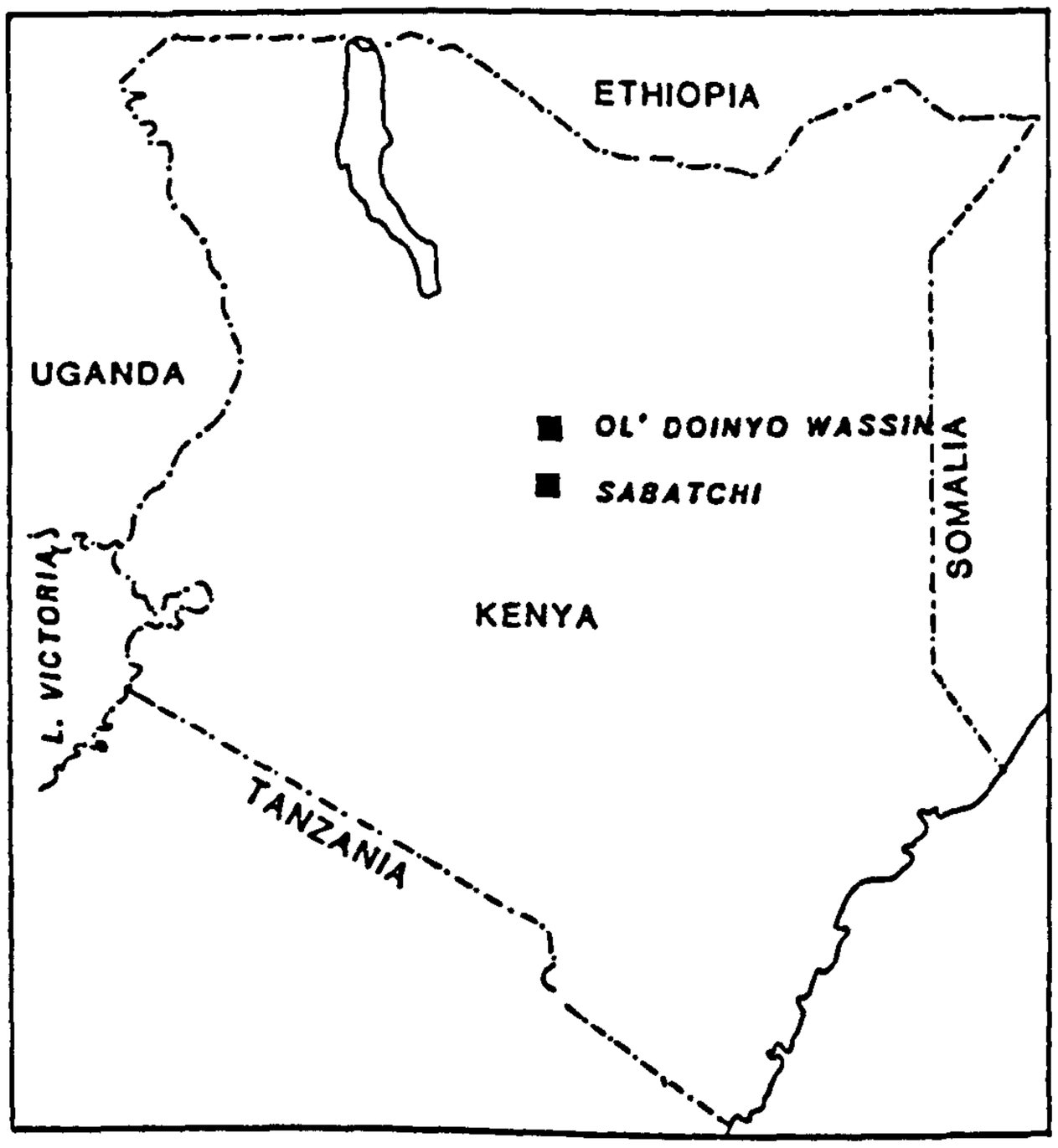

Figure 2.26 Location map of the Ol' Doinyo Wassin granodiorites and Sabatchi gneisses.

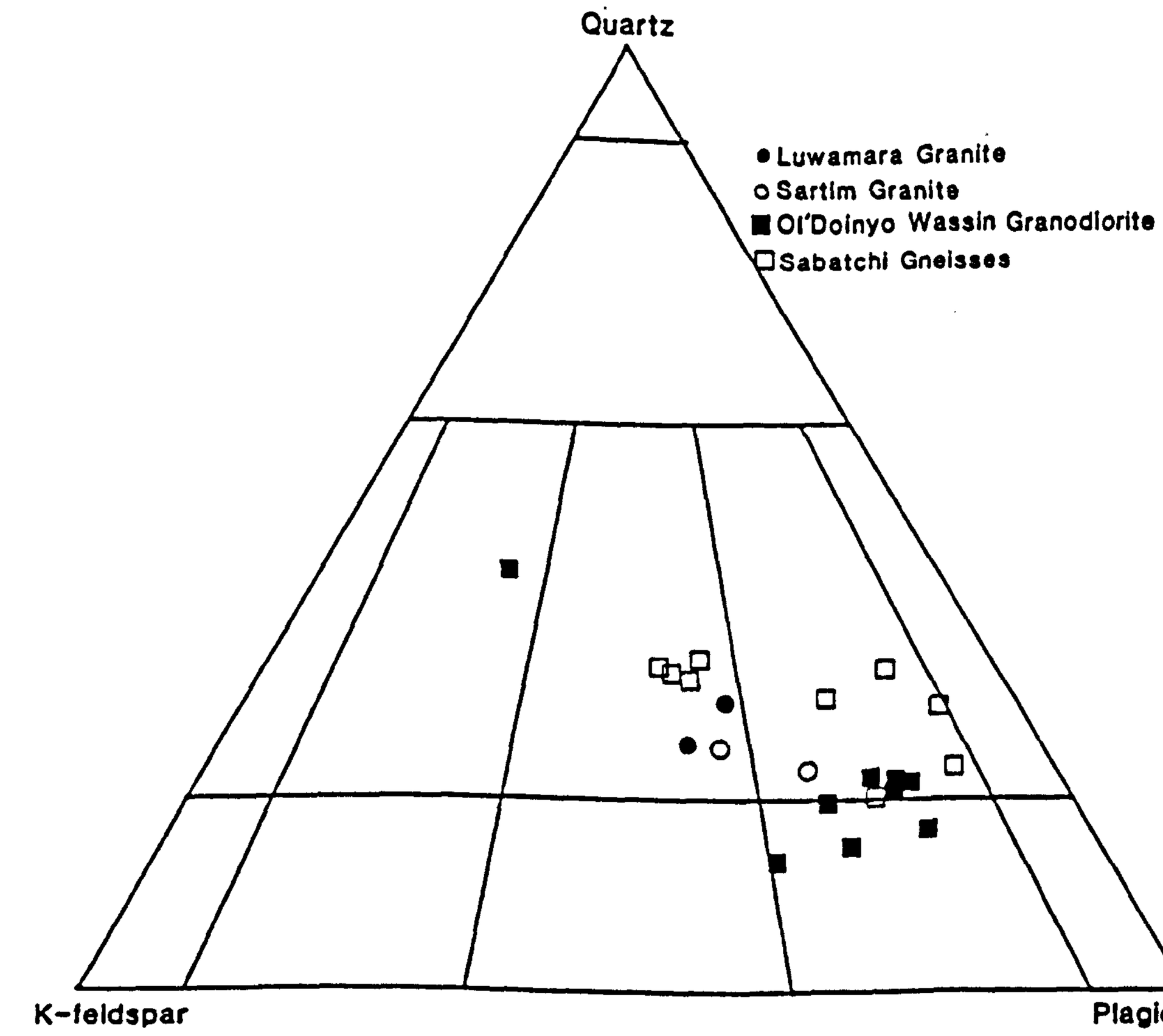

Figure 2.27 Streckeisen diagram showing representative samples from the granitoids of central Kenya. Modal analyses are based on Norm program developed by Nigel Harris for recalculation of major element analysis into minor phases.

characterized by quartz, plagioclase (albite), hornblende, pyroxene, and haematite, while the Sabatchi gneisses (II) have higher content of K-feldspar and biotite, and muscovite is sometimes present. The Sabatchi gneisses (I) could be metamorphosed granodiorite. Model analyses are given in Appendix B.

2.7.3 Major Elements

Figure 2.28 show a plot of the Shand Index (Shand, 1951) against the HFS elements Nb + Y (Pearce *et al.*, 1984a). It is observed that the Luwamara, Sartim and Ol'Doinyo Wassin granitoids plot in the peraluminous field, while Sabatchi (I) gneisses (SA11 and SA 12) plot in the calc-alkaline field, and the Sabatchi (II) gneisses plot in the peraluminous and calc-akaline field. The Ol'Doinyo Wassin granodiorites have anomalous Sr (>900 ppm) except for SA3 (209 ppm) and Rb is compatible. The high Sr is probably due to melting of feldspathic source.

2.7.4 Trace elements

In the Rb/Zr -$Si0_2$ plot (Figure 2.29) all the grantoids plot within the Group III granite field of Harris *et al.* (1986) which includes post-collision and calc-alkaline intrusions, however these are similar to pre-collision and volcanic arc granites.

To constrain this further trace element patterns and REE data of representative suites are required unfortunately REE data is only available of the Ol'Doinyo Wassin granodiorites. The trace element abundances of Ol'Doinyo Wassin have been normalised to the trace elements of an ocean ridge granite (ORG) (Pearce *et al.*,1984a) and is illustrated in Figure 2.30. The granodiorites have elevated K_20, Rb and Ba, but have relatively low Th,Ta, Nb, Ce, Hf, Zr, Sm, Y, and Yb are exceptionally low. Hf and Zr have relatively higher values as compared to their adjacent elements. The higher K, Rb, and Ba and the low HFS elements indicates a volcanic arc affinity. The elevated Ba could be explained by higher feldspathic content of the rock. The melting of a feldspathic source can also explain the increase of Sr, and the dilution of HFS elements.

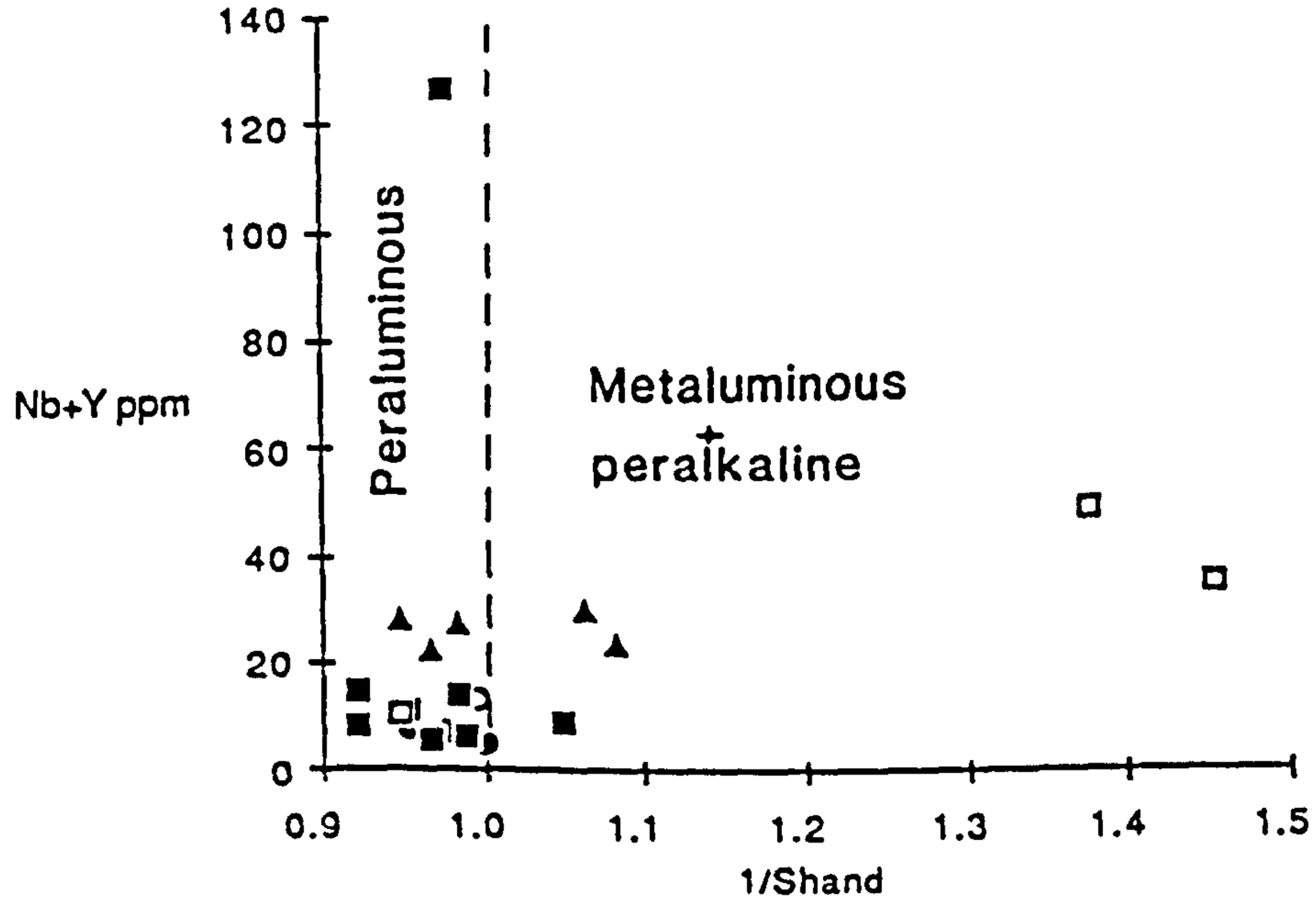

Figure 2.28 Plot of 1/Shand Index (CNK/A) vs the high field strength (HFS) elements Nb+Y for central Kenya granitoids.

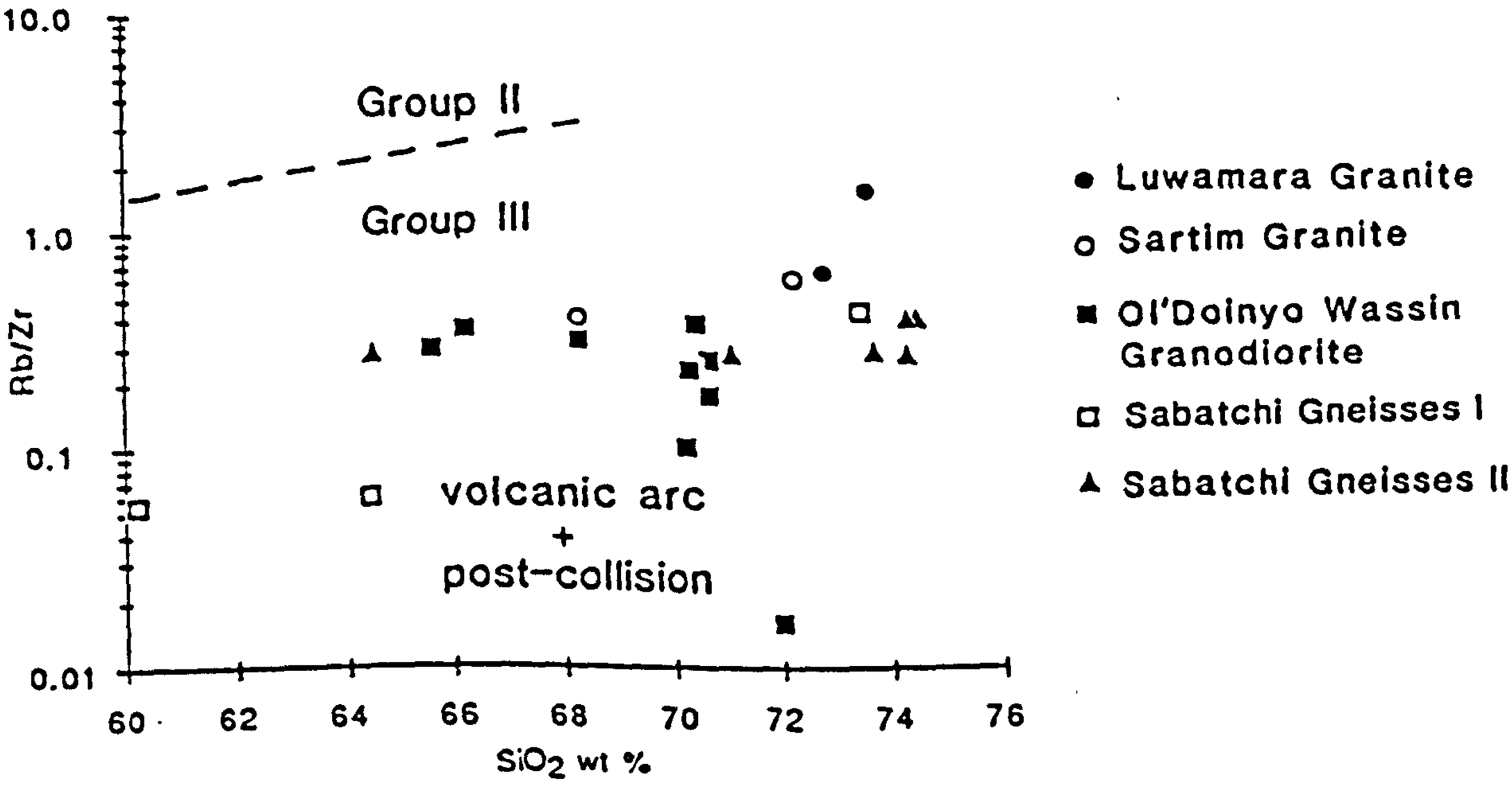

Figure 2.29 Rb/Zr vs SiO2. The central Kenyan granitoids plot in the Group III volcanic arc and post-collision granite field of Harris et al (1986).

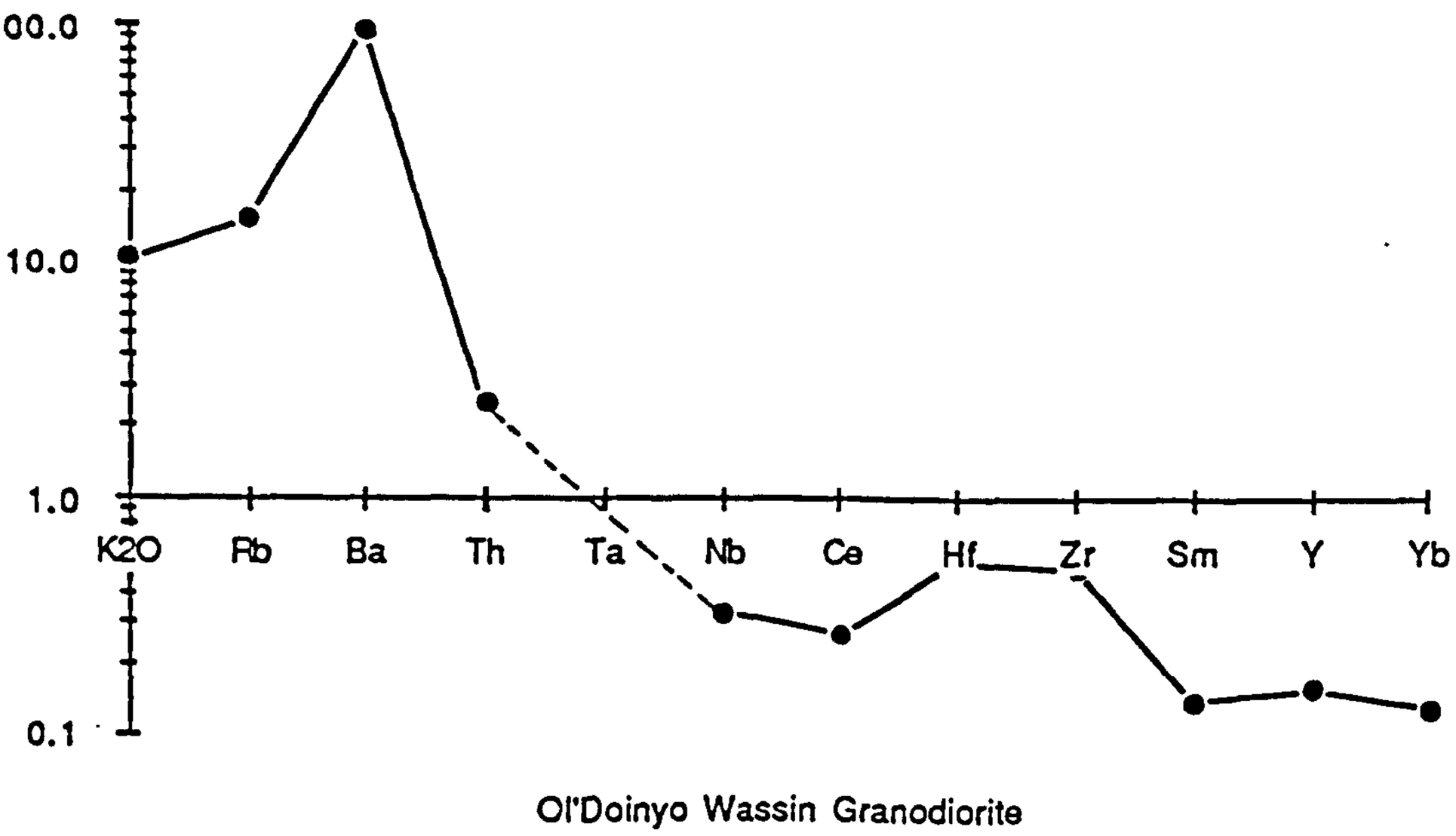

Figure 2.30 Geochemical pattern diagrams for the Ol'Doinyo Wassin granodiorite.

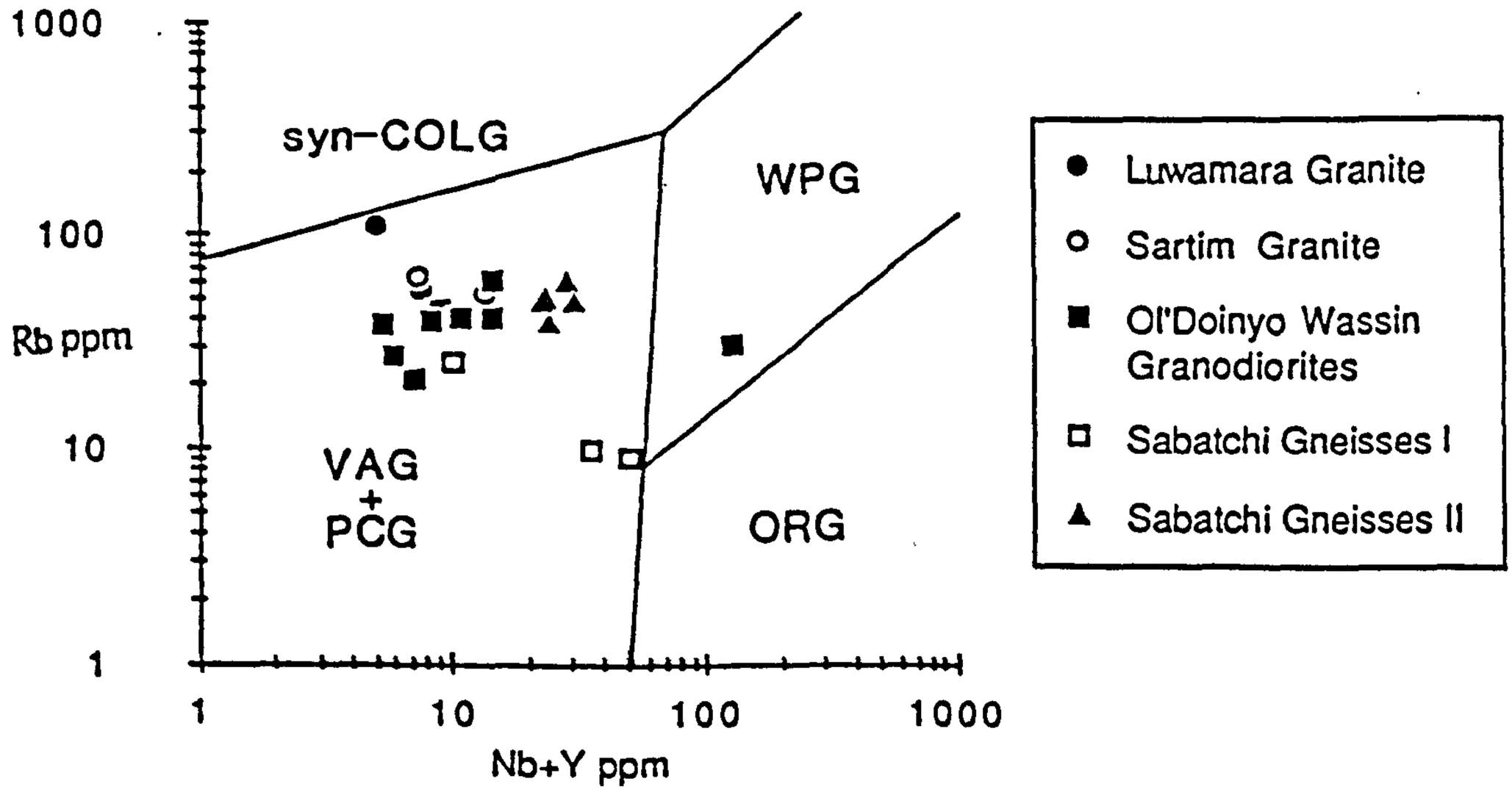

Figure 2.31 Rb vs (Nb+Y) granite discriminant diagram (after Pearce et al,1984b) for the central Kenyan granitoids. Syn-collision (syn-COLG), volcanic arc (VA), within plate (WP), ocean ridge granite (ORG).

2.7.4.1 Discriminant Diagrams

Pearce *et al.* (1984a) and Harris *et al.* (1986) have established a granite classification scheme which assigns granites to four major tectonic settings. The Rb - Nb +Y plot (Pearce *et al.*,1984a) was prepared to show the tectonic setting of the granitoids. Almost all the granitoids plot in the volcanic arc/post-collision field, except the Luwamara granite (SB 82 B) which plots close to the syn-collision field, while one sample SA3 of the Ol'Doinyo Wassin granodiorite plots in the oceanic ridge granite field (Figure 2.31). The sample that plots in the ORG field has been described to contain high Zr value, which has contributed to the increase in the Nb and Y values, hence shifting it to the ORG field. The Luwamara granite has elevated Rb, and probably could be a syn- collision granite related to the emplacement of the Baragoi ophiolite while the Ol'Doinyo Wassin granodiorite plot in the volcanic arc field.

2.8 TECTONIC EVOLUTION

The preceding discussion indicates that the Baragoi mafic-ultramafic complex is an allochthonous piece of late Proterozoic oceanic crust. The units characteristic of a Penrose ophiolite are present but are dismembered and in no way stratigraphically coherent. It contains lavas of both boninitic, island arc and MORB affinities and is also characterized by a strongly depleted mantle sequence containing podiform chromite deposits which are similar to the Supra Subduction Zone (SSZ) ophiolites (Pearce *et al.*,1984b).

The trace element discriminant diagrams of a major portion of the Hornblende plagioclase gneisses point to volcanic arc affinity while REE and geochemical patterns suggest a transitional MORB to IAT affinity. These transitional type lavas, showing moderate enrichment can be associated with the intial stages of back-arc spreading (Tarney *et al.*, 1981). The presence of Hornblende biotite plagioclase gneisses with calc-alkaline affinities suggests a tectonic setting transitional between volcanic arc and within-plate. This requires a multiple series of events in the source or a mixing of two magmas from different sources. Few plot in the within-plate field and the ESCORT system of

classification of volcanic rocks has shown that few rocks could probably be interpreted as Normal continental flood basalts. This means that the minor volcanic rocks are not related to the ophiolitic suite, but were products of a later rifting episode. This requires further work.

Three major episodes of deformation have been identified in the structural evolution of the Baragoi area. An early stage involved deformation immediately following formation of the complex. This episode (D_1) is referred to as the Samburu phase (Charlesly *et al.*, 1984). This episode of deformation generated recumbent to isoclinal folds, with fold axes trending approximately east-west. It has been suggested that the stress regime that was responsible for the E-W structures resulted in the emplacment of the Baragoi mafic-ultramafic complex from the north or northeast (Charlesly *et al.*, 1984).

The second deformation (D_2) is a large-scale folding event which produced upright to overturned folds plunging 20-30° to the northwest. This tectonic episode that produced the NW trending Morilem Syncline (Baker, 1963) has been named the Baragoi phase (Charlesly *et al.*, 1984). Generally the principal foliation (S_1) of the area parallels the bedding of the metasedimentary rocks. However, a second foliation (S_2) has been found transverse to the regional foliation trend. The axial planes of the Morilem fold system are either vertical or dip steeply toward the WSW or W. The third deformation event (D_3) caused refolding of the Morilem syncline into a series of NNW trending folds plunging 170°SSE. D_3 cleavage can locally be seen crenulating a D_2 cleavage. D_3 cleavage and fold axial plane strike to the NNW.

In the northern part of the Baragoi area (NW and NE blocks) the strike of the foliations and trends of the lineations gradually rotate from a NW-SE foliation strike and lineation trend at the southern end, to a NNW foliation strike and lineation trend. North and south of the Lesirikan there is an area of more intense deformation, where the foliation has a constant N-S trend. With an increase in the intensity of deformation which produces the N-S strike of the foliation, the earlier NW-SE trending foliation is progressively rotated by shearing from its original orientation towards the later N-S direction. Where the N-S foliation strike is only very weakly developed, the earlier foliation poles form a dispersed cluster pattern as in Figure 2.5c. In areas where the N-S striking foliation is strongly developed, the earlier foliation trend has been destroyed by a total rotation into the later trend and

also by extensive recrystallisation of the mineral phases with regrowth in the later foliation direction. A single-cluster foliation pole pattern is developed in these areas.

Related to the emplacement of the ophiolites are thrusts and numerous shears. In the Keleshwa area (NE block) there is a major thrust which show strong developed striae. The direction of striae being from N to S. The thrust plane is itself folded with fold axis trending N-S (Plate 2.14) and plunging to the south. However all along the Baragoi river a series of thrusts are observed with slices overthrust upon each other in a northwesterly direction. In Opoipa river near Baragoi town a succession of gabbro-amphibolites and hornblende biotite gneisses are repeated by thrusting and folding. The direction of movement has not been ascertained because of a lack of convincing striae direction. This is the product of the Barsaloian episode of deformation (D_3) which is a lot younger than the S to SE directed thrusts of the Keleshwa area.

There are a series of 10-20°NE trending shear zones, which have sinistrally displaced lithologic units. The sinistral shears are almost perpendicular to the thrust planes, which may suggest that they acted as transcurrent faults to accommodate severe shortening in the Northern Baragoi area (NW and NE blocks) where there are a series of tightly folded anticlines and synclines.

The rarity of unaltered relics of olivine or pyroxene-bearing igneous rocks suggests that mineral transformation is complete in this area. The typical mineral assemblages of ultramafic rocks in the Baragoi area are serpentinites generally found associated with talc schists, actinolite rocks and tremolite -anthophyllites. Since anthophyllite and talc or forsterite reaction takes place around 650°C (Evans and Trammsdorf, 1970) it can safely be inferred that this level of temperatures were reached in the Baragoi rocks. Similarly the presence of antigorite in serpentinites suggests that temperatures up to 550°C (Evans *et al.*, 1976) have been reached in the area, while the presence of anthophyllite suggests that pressures of <5kb have been attained, because anthophyllite is not stable above 5 kb (Chernosky, 1976). Based on the mineral assemblages of amphibolites in the Baragoi area (Table 2.2) it is suggested that they plot in the epidote amphibolite facies (Figure 2.7).

Since the Baragoi ophiolitic complex has a wide range in composition of magma types it is important to synthesise this in a tectonic model. It has been suggested that the unusually low TiO_2, high MgO and SiO_2 and slightly concave shaped REE patterns of the amphibolites are chemically

similar to boninites. Such low TiO_2 contents (< 0.3%) are not found in modern ocean ridge basalts. Hence Serri (1981); Meijer, (1980) and Crawford *et al.* (1981) suggested that the very low TiO_2 basalts (boninites) in the Marianas which are usually associated with tholeiitic island arc volcanics (Meijer, 1980) are found either in a fore-arc setting (Meijer, 1980; Crawford, *et al.*, 1981) or along the arc-ward trench wall (Dietrich *et al.*, 1978; Hawkins *et al.*, 1979). Crawford *et al.* (1981) envisaged the lateral splitting of an island arc system into two.

However In the Baragoi area the amphibolites which have been geochemically designated as boninites, occur as narrow bands and lenses or thrust slices within the Hornblende plagioclase gneisses (this group forms undifferentiated volcanic arc and MORB lavas) and occasionally occur cutting ultramafic rocks. The geochemistry of the ultramafics and chromites suggests a SSZ setting. Hence it is proposed that the first significant volcanic episode is a spreading event, which is followed by suduction, hydration and melting of suboceanic lithosphere which gives rise to boninites and depleted IAT in a fore-arc setting as suggested by Pearce *et al.* (1984b).

With closure of the ocean basin these materials became thrust southeastwards. Granites formed at depth during the arc building were melted to form the Sartim granites. During the final stages of closure with attendant regional metamorphism the thrusting produced a thickened crust and the evolution of Luwamara syn-collision granitoids.

CHAPTER 3

THE GEOLOGY AND GEOCHEMISTRY OF THE ADOLA - MOYALE BELT, S. ETHIOPIA/ NE KENYA

3.1 INTRODUCTION

The term Adola-Moyale Belt is applied, in a broad sense, to include three parallel zones of mafic-ultramafic rocks, the Adola and the Kenticha belts and the mafic-ultramafic assemblages of the Negelle area, southern Ethiopia (Figure 3.1 and 3.2). The Adola-Moyale belt extends in a north-south direction for about 350 kms. The Moyale mafic-ultramafic rocks occur south of the well documented Adola mafic-ultramafics of southern Ethiopia (Kazmin, 1976). East of Moyale the Mash Hills gabbros and metabasites are aligned with the Negelle mafic-ultramafic complex of southeastern Ethiopia. All three zones are entirely fault bounded.

3.1.1 Location and Access

The Adola area lies in southern Ethiopia, while Moyale lies in NE Kenya. The Adola area is approximately 500 km south of Addis Ababa and is reached by a tarmac road as far as Moyale. This same road from Moyale-Kenya changes into an all weather gravel road and leads to Nairobi, Kenya (Figure 3.1). The Moyale area is approximately 700 km NE of Nairobi.

3.1.2 Previous work

A major portion of the Adola-Moyale Belt (c. 60%) has not been systematically mapped. Early works were restricted to the Adola Goldfields (Jelenc, 1966; Ministry of Mines unpublished reports). Some of the ultramafic bodies have also been explored for nickel (UNDP, 1972; Clark, 1978; Arthena, unpublished reports).

A study was carried out by a joint United Nations-Ethiopian Mineral Survey team in an area covering 55,734 sq. km. (UNDP, 1972) but the geological maps were mostly based on photo-interpretation and limited fieldwork, and hence were inaccurate.

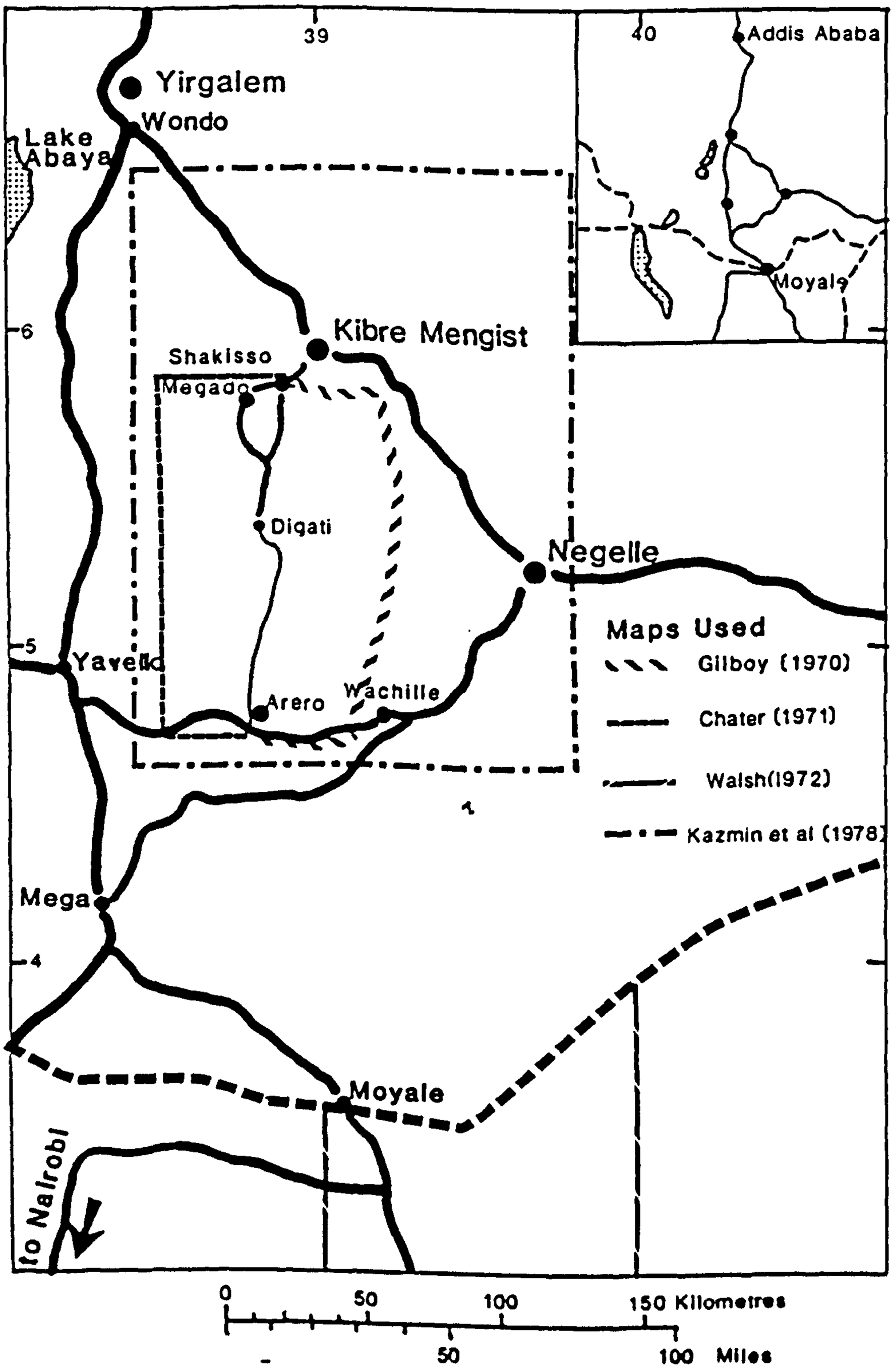

Figure 3.1 Locality diagram of the study area.

The first systematic studies of the Adola area were carried out by Gilboy (1970) and Chater (1971). Further work by Kazmin (1971, 1975, 1976) and Kazmin *et al.* (1978) have greatly contributed to the understanding of the geology of the area. Warden (1981) and Warden and Horkel (1984) were the first to attempt a geological synthesis of the NE Mozambique Belt of Kenya, Ethiopia and Somalia and more recently the Ethiopian Institute of Geological Surveys has published a series of geological maps.

Geological reconnaissance of Northern Kenya was carried out by Parkinson (1920), and Walsh (1972) systematically mapped the Moyale area. With the exception of studies by Gilboy (1970) and Chater (1971) these works were field based, with little or no geochemical and geochronological data.

This study is based on fieldwork carried out in the Adola area in 1975, in NE Kenya in the summer of 1984, aided by numerous published and unpublished maps and reports. The geochemical study is based on rocks collected by the author supplemented from a powder collection of Gilboy (1970). The main aim was to establish from the geological and geochemical data whether the Adola and Moyale mafic-ultramafic complexes are ophiolites and to establish whether they lie along the same suture. In addition to identify the origin and palaeotectonic environment of the ophiolitic and granitoid rocks, which would help to establish a geotectonic model for the area.

3.2 LITHOLOGIC AND PETROGRAPHIC DESCRIPTION OF THE ADOLA AREA ROCK UNITS, SOUTH ETHIOPIA

3.2.1 Introduction

Gilboy (1970); Chater (1971) and Kazmin (1971, 1975) suggested three major stratigraphic divisions for the Southern Ethiopian region, namely the Lower, Middle and the Upper Complexes based on lithology, structural relationships and grades of metamorphism. The arrangement of these subdivisions is consistent with an overall decrease in metamorphic grade from the Lower to the Upper Group. The Lower Complex comprises various high grade gneisses and migmatites with relics of older structures represented by isoclinal recumbent folds. In contrast, the Middle Complex is represented by psammitic and pelitic sediments with subordinate marbles, calc-silicates and

amphibole schists. The Upper Complex consists of the Adola ophiolite Group and the Mormora Group, which commonly retain sedimentary features (Kazmin, 1976; Kazmin *et al.*, 1978).

Gilboy (1970) and Chater (1971) consider the contact between the Lower and the Middle Group to be gradational, with no apparent break in sedimentation of the two groups, however the variability of the sediments of the Middle Group compared with the monotonous regularity of those of the Lower Group was interpreted by Gilboy (1970) as a marked change in depositional environment. Gilboy (1970) suggested an orogenic event between the deposition of rocks forming the Lower and Middle Groups and those of the Upper Group, because the Upper Group possess only one planar fabric, while the Lower and the Middle Group have developed two planar fabrics. He also indicated that they are separated by a strip of metamorphosed ultramafics which crop out as an extensive shear, while the extensive development of amphibolites in the Upper Group indicated that they are a separate group. However Chater (1971) regarded them as conformable on the basis that the amphibolites are interbanded with the gneisses of the Middle Group which define its upper limit.

Gilboy (1970) and Chater (1971) considered the mafic-ultramafic rocks in the Adola as intrusive bodies, which occur within the paragneisses of the Lower, Middle and Upper Group. However Chater (1971) suggested that some ultramafic bodies in the Upper Group may represent extrusive rocks, because the amphibolite he described contain pillow structures. Kazmin (1975) and Kazmin *et al.* (1978) suggested a major unconformity between the Lower and the Middle Complexes while the presence of sheared ultrabasic material along the contact indicated that it is a thrust (Kazmin *et al.*, 1978). Warden and Horkel (1984) revised the stratigraphy and suggest that there are temporal and lateral overlaps and transitions between the Middle and Upper Complexes (Table 3.1).

The classification suggested in this work (Table 3.2) is broadly similar to that of Warden and Horkel (1984), although the three fold classification of the gneisses into Upper, Middle and Lower complexes is avoided, and the relative position of the Wadera and Yavello gneisses are changed. The Alghe and Awata gneisses (which are equivalent to the Lower Complex) are considered to be the oldest units in the area, in contrast to Kazmin (1972) who suggested that the Konso gneisses were older. The Konso gneisses are not discussed further as they lie outside the area of interest. The Wadera and Yavello gneisses of the Middle Complex are regarded as the same unit (Warden and

Horkel, 1984), because the Wadera Group and the Yavello gneisses constitute a cover rock sequence which is less strongly deformed and metamorphosed than the underlying gneisses. The Wadera Group is restricted to a fault bounded area which is 50 km across and hence evolved separately but contemporaneously with the Yavello gneisses. The Upper Group are in thrusted contact with the underlying Wadera Group and because of their different rock assemblages are treated separately.

Table 3.1 Lithostragraphic Table for the Basement of Southern Ethlopia

	Gilboy (1970); Chater (1971)	Kazmin (1975); Kazmin *et al.* (1978)	Warden and Horkel (1984)
Upper Complex	Metamorphosed conglomerate and arkosic Grit; phyllites; marble	Mormora Group metasediments	Mormora Group
	Mafic-ultramafic rocks	Adola Group Ophiolites	Adola Group
Middle Complex	Quartzofeldspathic gneisses		Burji Gneiss
	Muscovite-biotite gneiss and Schists	Wadera Group	Wadera Group/ YavelloGneiss
Lower Complex		Metamorphic Granitoids	
	Biotite hornblende Gneiss	Yavello Gneiss	
		Awata Gneiss	Awata Gneiss
	Biotite Gneiss	Alghe Gneiss	AlgheGneiss

Table 3.2 Suggested Stratigraphic Succession for Southern Ethiopia

		Post-Tectonic Granites (515 m.y.-480 m.y)
Mormora Group	Adola Group (ophiolites)	Syntectonic Granites (ca. 680 m.y)
Wadera Group		
Yavello Gneiss		
Awata Gneiss		
Alghe Gneiss		

3.2.2 Alghe Gneiss

These rocks occur west of Neghelli and east of Awata Valley (Figure 3.2). The Alghe gneiss which is considered to be the oldest unit (Warden and Horkel, 1984), consists of a rather monotonous sequence of grey biotite-amphibolite gneisses with amphibolite bands. It is extensively migmatised with both gradational and sharp contacts with granodioritic and trondjemitic gneiss commonly coring the folds (Plate 3.1). Although upper amphibolite metamorphism and migmatisation render identification of the original rock types difficult, Warden (1981) suggests that they could consist mainly of metamorphosed greywackes and impure calcareous rocks represented by amphibolite. Ortho-amphibolite and orthogneiss are also present. These rocks are characterised by mineral assemblages such as oligoclase/andesine- quartz - microcline - hornblende - biotite ± almandine ± perthite with accessory sphene and apatite. This mineral assemblage indicates metamorphism in the mid-amphibolite facies. The Alghe gneiss preserves relics of east-west trending isoclinal recumbent folds (m. scale) and is strongly folded about north to northwest trending fold axes related to the main Mozambique deformations. These structures are locally refolded by east-trending folds.

Geological Map of the Adola-Moyale Belt

39°E 40°E 7°N 6°N 5°N 4°N 3°N

Lake Abaya
Road
Adola
Kibre Mengist
R. Mormora
Megasa
Kajimiti
Kenticha
R. Kenticha
R. Genale
Negelle
Road
Yavello
Gedolosa
R. Dawa
ETHIOPIA
KENYA
Moyale
Dubel
Buna
Marsabit

A B B' C

0 25 50 75 100km

Legend

- Foliation dip and strike, not measured
- Fold axis, synclinal
- • • , anticlinal
- Thrusts
- Generalized strike trends
- Faults, observed
- • • , inferred-approximate
- Lithological contact

I ADOLA ZONE
II KENTICHA ZONE
III NEGELLE ZONE

Alluvium	QUARTERNARY	
Tertiary Volcanics	OLIGOCENE MIOCENE	
Limestones, Sandstones	MESOZOIC	
Post Tectonic Granitoids	PRECAMBRIAN	
Syntectonic Granitoids		
Kajimiti Beds	Mormora Group	
Mormora Metasediments		
Amphibolites	Adola Group	
Ultrabasics		
Marble		
Wadera Group		
Yavello Group		
Awata Gneiss		
Alghe Gneiss		

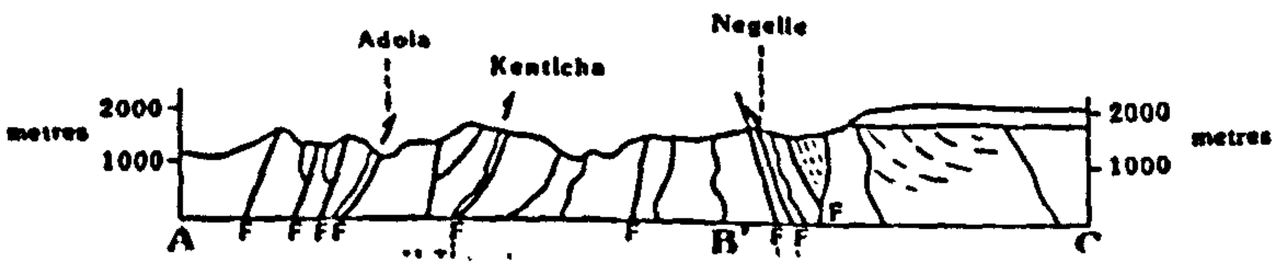

3.2.3 Awata Gneiss

The Awata gneiss tectonically overlie the Alghe gneisses (Figure 3.2). It shows considerable lithological variation, but consists mainly of mafic gneisses with pelitic and psammitic units, (a sequence of greywacke, impure calcareous rocks, pelite, quartzite and meta-arkose). The quartzofeldspathic layers within the sequence commonly merge into granitic paragneisses along strike. Tectonised lenses of talc-tremolite schist within the mafic gneisses represent a disrupted ultramafic unit. The Awata gneisses are metamorphosed in upper amphibolite facies. Characteristic mineral assemblages are listed in Table 3.4. These gneisses were strongly folded about NNE trending fold axes during the main Mozambique episode of deformation (c. 600 Ma).

3.2.4 Yavello Gneiss

This gneiss is restricted to the western part of the Adola Belt (Figure 3.2). The Yavello gneiss typically consists of a flaggy, regularly layered (cm scale) sequence of granoblastic quartzo-feldspathic psammites with minor intercalations of biotite schist and amphibolite. Rapid transitions are evident in the Yavello gneiss along strike from psammite through migmatite to granitic gneiss. It is less intensely deformed than the other units in the Lower Complex and displays a more open style of folding about north trending axes with dips in the range 15-50° (average 30°).

The Yavello metasedimentary gneiss typically consists of microcline-quartz-biotite ± hornblende ± perthite ± oligoclase ± opaques. The presence of biotite, hornblende and oligoclase suggests metamorphism in the amphibolite facies.

The Yavello gneisses are lithostratigraphyically equivalent to the Wadera Group and are considered to represent a clastic sequence of arkoses and impure sandstones with minor intercalations of mudstone and impure calcareous sediments probably deposited in intracontinental basins (Warden, 1981).

3.2.5 Wadera Group

The Wadera group is divided into a lower unit of meta-arkoses and quartzites with subordinate intercalations of marble, metacalcareous rocks and amphibolites, and a thinner upper unit consisting of quartzofeldspathic rocks, interlayered with biotite and quartz-muscovite schist rarely containing amphibole. The Wadera forms the Middle Complex of Kazmin (1971, 1975) and is thought to rest conformably on the Lower Complex. However, Warden and Horkel (1984) argued that the contact relationships with the underlying gneisses are obscured by intense migmatisation and shearing and hence are difficult to demonstrate. The Wadera metasediments are thought to have been deposited in shallow basins or rifts (Kazmin, 1971; Warden and Horkel, 1984), because the Wadera Group are restricted to a fault bounded area 50 km across. (Figure 3.2).

The Wadera Group shows a range of sedimentary structures, such as cross bedding and ripple marks. In addition, they show a granular fabric preserved throughout much of the sequence which may reflect good sorting in the original sediment. Locally, subordinate layers of amphibolite and biotite hornblende schist are interbedded with the psammites and become increasingly abundant in the north of the belt suggesting a primary lithological transition.

Like the Yavello gneiss, the Wadera psammites merge laterally and vertically into granitic gneiss, often through migmatitic transitional zones with abundant quartzofeldspathic veins (Plate 3.2). This anatectic transition is particularly marked at the base of the unit and in the vicinity of shear zones, for example near the eastern contact where it is probably overthrust by the Alghe gneiss (Warden, 1981). Within the basal gneiss unit are bands and lenses of talc-tremolite and talc schist up to 300 m wide which were considered to represent an ophiolitic suture (Kazmin, 1976; Warden and Horkel, 1984). The Wadera rocks are folded on northerly trending axes, and generally the gneissic layering dips 30-50° to the west. Folding is tight to isoclinal in the vicinity of major faults, which are associated with zones of mylonite up to 0.5 km wide, while complex flow folding is developed in the associated granitic gneisses.

Microcline is the dominant feldspar and forms up to 65% of the rock, although in some thin sections plagioclase is dominant. The assemblage microcline - quartz - biotite - magnetite ± muscovite with accessory zircon, sphene, apatite, tourmaline and rutile is characteristic of the Lower

Plate 3.1 Strongly migmatitised hornblende gneiss with stretched and boudinaged layers. Alghe Gneisses.

Plate 3.2 Granitic gneiss with interlayerd amphibolite and pegmatite bands. Wadera Gneisses. Awata river junction.

Wadera psammites. The presence of string perthite in some samples indicates the continuation of deformation after metamorphism (Gilboy, 1970).

3.2.6 The Adola Group

The Adola belt extends in a north-south direction for about 150 km, swinging to almost due west in the south (Figure 3.2). The zone is bordered on both sides by gneisses of the Lower Complex (Kazmin, 1972). The westerly dipping eastern contact of the zone is marked by a discontinuous belt of altered ultrabasics (Figure 3.2). The presence of strongly sheared ultramafic rocks suggests that it is a thrust. The detailed internal structure of the ultramafic-amphibolite belts is unclear but going westwards the following general sequence is evident: ultramafic rocks - metagabbro - metabasalt (Adola Group) and associated sediments (Mormora Group). The ultramafics are mostly altered to talc, talc-serpentine and talc-tremolite schists and occur as belts, some of which extend for about 100 km. These belts include lenses of massive serpentinites. Chlorite and magnetite-chlorite schists are closely found associated with these talc schists and serpentinites (Kazmin, 1976).

In the Adola belt large masses of amphibolites predominate. The amphibolites are dark greenish - grey in colour, varying from fine to coarse grained and ranging from massive to foliated and schistose varieties. Chater (1971) pointed out that the lower part of the amphibolites are gneissose, while the upper parts are weakly foliated, with pillow structures, and intercalations of graphitic phyllites. He also noted that ultramafic rocks occur in the lower part of the amphibolitic succession which occur usually in fault separated blocks or as long strips. The amphibolites are cut by young gabbroic and dioritic intrusive bodies. Meta-sandstones, biotite pelitic schists, graphite schists and graphitic and ferruginous quartzites, occur as intercalations in the metabasic rocks. Cross-bedding have been observed within the arkosic sandstone of the Adola belt.

The ultramafic lenses have a core of silicified serpentinite, with some subordinate peridotite which contains pyroxene pseudomorphs, and pyroxenite showing a relict cumulate fabric (Warden, 1974). Small lenses of chromite occur locally. The ultramafic lenses sometimes are zoned comprising an inner zone of talcose serpentinite which passes outwards through talc-tremolite schist and anthophyllite schist, to an outer rim of magnetite-chlorite schist. These reaction zones are up to

200 m thick, though some are occasionally absent. Magnesite is developed locally in the ultramafic rocks, and in some localities, for example the Bul-Bul basin, (Figure 3.2), they are extensively altered to talc. The mafic - ultramafic rocks contain mineral assemblages typical of greenschist facies, irrespective of the higher grades of metamorphism of the surrounding rocks, which indicates that the gneisses are considerably older than the Adola rocks.

3.2.7 Mormora Group

The Mormora metasediments consist of chloritic phyllites, graphitic pelitic schist, carbonaceous sandstone, quartzite and rare marble. They form bands or horizons from a few metres to 500-600 m thick (Kazmin, 1972). South of Mormora river the metasediments intercalated with the upper part of the amphibolites of the Adola Group. The Kajimiti beds which consist of conglomerate, carbonaceous sandstone and biotite schist, are tentatively included in the Mormora Group and occur in a small area between Shakisso and Digati. The Kajimiti occur usually in fault bounded blocks or as long strips, so that their relation with the Adola remains obscure although near Kajimiti the layered part of the metasediments are younger than the amphibolites as they rest on the Adola Group with a marked unconformity (Kazmin, 1976).

3.2.8 Syntectonic Granitic Gneisses

Gneissose granite occurs as sheet-like bodies within the Alghe, Awata and Wadera Groups. An extensive gneissose granitic body was traced from the Awata river in the north to the Neghelli-Yavello road in the south (Gilboy, 1970). Gilboy (*op. cit.*) suggested an intrusive igneous origin for these gneisses because of their exceptional homogeneity and because they enclose large areas of Lower Group gneisses. Gradation along strike into banded biotite gneiss of the Lower Group is common and is well seen 11 km east of Gariboro. The eastern contact is gradational over a distance of up to about 20 metres, with bands of granitic gneiss alternating with biotite-muscovite schist. The western contact against talcose and actinolitic schists appears to be a thrust.

The gneissose granites are medium-grained and fairly well foliated. The foliation is defined by layers with differing biotite content and by segregated coarse-grained quartzofeldspathic bands. In

thin section the mineral assemblage is seen to be quartz - microcline - plagiocalse ± biotite ± hornblende ±muscovite. Sphene, zircon, apatite and opaques occur as accessories. Microcline is occasionally replaced by quartz and plagioclase and is often microperthitic and sericitized. Biotite forms over 10% of the rock while hornblende is occasionally present in very small amounts.

3.2.9 Post-Tectonic Granites

Post-tectonic granitic plutons crop out over an area of approximately 15,000 km^2. Regional metamorphism of the country rock is suggested by the lack of contact metamorphism and by the absence of chilled margins (Gilboy, 1970). The only effect of the intrusions on adjacent gneisses has been the formation of granitic veins, within the gneisses sub-parallel both to the margins of the intrusions and to the regional foliation. One of the major granite bodies is the Godoloka granite which appear to have pushed aside the surrounding gneisses. At the granite contacts a planar fabric is parallel with foliation trends of the gneisses.

The rocks are typically pink, medium to coarse-grained, equigranular granite lacking foliation except towards the pluton margins. In thin section they show quartz-microcline-plagioclase±biotite ±amphibole. Accessory minerals include magnetite, ilmenite, sphene, apatite, zircon, allanite, chlorite, sericite and calcite. Biotite forms 5-10%, while amphibole occurs in small amounts.

Rb-Sr age determinations were carried out by Gilboy (1970) and Chater (1971) on whole rock and mineral separates of post-tectonic granites. The Godoloka granite gave an age of 515±10 Ma with initial ratio of 0.7062±0.0091 (Gilboy, 1970), while a combined whole rock and plagioclase mineral separate of the Sawana Granite yielded an age of 480±50 Ma with an initial ratio of 0.708±0.001 (Chater,1971).

3.3 GEOLOGY OF THE MOYALE AREA, NE KENYA

3.3.1 Introduction

The metamorphic rocks of the Moyale area can be divided into two major groups: the ultramafic rocks and plagioclase amphibolites (which are equivalent to the Adola Group), and the metasedimentary gneisses and schists. The metamorphic rocks are intruded by syntectonic and post-tectonic granites (Figure 3.3). The ultramafic rocks are represented by serpentinites, talc schists, and amphibolitised ultramafics and have a thrusted contact with the plagiocalse amphibolites, while the contact relationship of the gneisses with the mafic-ultramafic rocks is not clear, because they are poorly exposed.

The area has been affected by two episodes of deformation. The first period of deformation (D_1) resulted in NE-SW trending folds, which were later refolded by NW trending folds (D_2). The area has been metamorphosed in the mid-amphibolite facies with metamorphic grade increasing eastwards during the D_2 event.

Since the area lacks continuous outcrops, the study was concentrated in localized areas of mafic-ultramafic rocks, and granites which form ridges and hills. The sparse outcrop makes a thorough study impossible and constrains interpretation.

3.3.2 Ultramafic rocks

3.3.2.1 Introduction

The ultramafic rocks are exposed west of Moyale town are about about 20 miles long and 5 miles across (Figure 3.3). The major ultramafic outcrop lies in the Debel area. Walsh (1972) divided the ultramafic rocks into three units; the amphibolitised ultramafic rocks, the serpentinised dunites and the talc schists. The amphibolitised ultramafics outcrop in Kara Duse and Iladu Hills area, while the serpentinites are well developed in the Debel area (Figure 3.3), and the talc schists occur south of Moyale town.

The ultramafic rocks which are well preserved in the core of a synform are layered and foliated. Layering and foliation planes are parallel and the strike is 330˚/60°NE.

GEOLOGICAL MAP OF THE MOYALE AREA

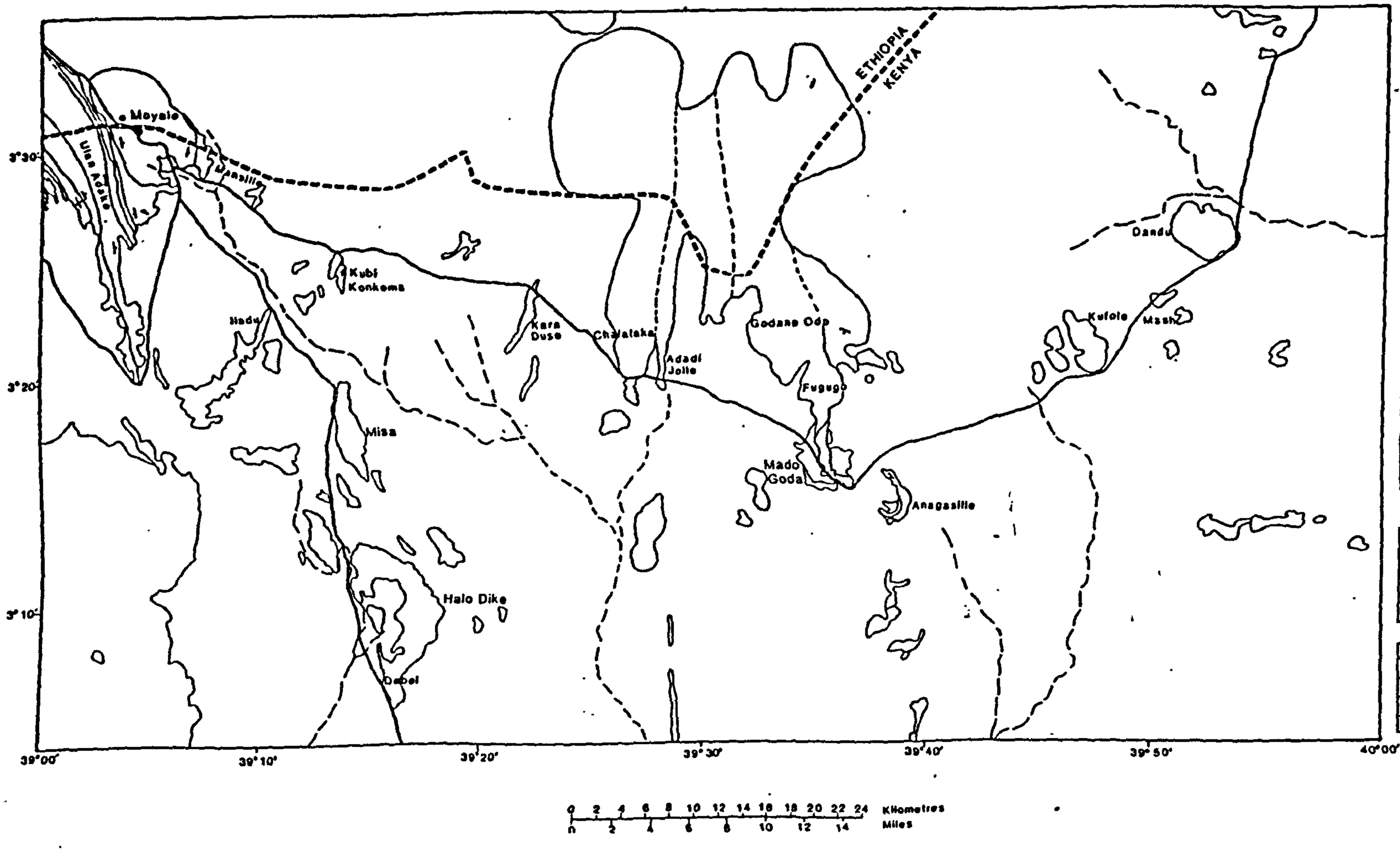

Legend

- Quaternary sediments
- Tertiary volcanics
- Post tectonic Granites
- Post tectonic Granodiorites
- Syntectonic Granitoid gneisses
- Quartzites
- Marble
- Graphitic gneisses
- Hornblende gneisses
- Biotite gneisses & migmatites
- Plagioclase amphibolites
- Gabbros/Metabasites
- Talc schists
- Amphibolitised ultramafics
- Serpentinites

PRECAMBRIAN

0 2 4 6 8 10 12 14 16 18 20 22 24 Kilometres
0 2 4 6 8 10 12 14 Miles

In the Halo Dike area a massive serpentinised body with disseminated chromite is observed. The foliation trends 070˚/dip 40°NW, in contrast to the regional foliation which is northwesterly.

3.3.2.2 Amphibolitic ultramafic rocks

The amphibolitic ultramafics south of Moyale form rounded hills dotting the plains. The Iladu Hills which are made up of massive layered ultramafic units are composed of two lithologies. The amphibolitised ultramafic rocks are medium to coarse grained and greenish-grey in colour. Two thin sections were studied; the Kara Duse ultramafic show, large grains of pale green actinolite which are partly altered to clinozoisite and relict plagioclase occurs in minor amounts with secondary calcite and quartz. This section shows a relict cumulate texture which suggests that the rock may have originally been a pyroxenite. In the Iladu area ultramafics (Plate 3.3) actinolite forms 40%, chlorite about 20%, while plagioclase (labradorite) forms about 10% and clinozoisite is also observed replacing plagioclase. Occasionally the actinolite rims are altered to greenish brown hornblende. Accessory minerals are serpentine, opaques and sphene. This rock has a cumulate texture and is suggested to be a mafic gabbro.

The amphibolite ultramafics, which are found associated with talc schists are medium-grained dark grey to green in colour and contain granular clinozoisite, pale green actinolite or tremolite-actinolite marginally altered to hornblende, with small amounts of quartz-calcite and Fe-oxides. It is clear from thin section study that the amphibolitised ultramafics represent gabbroic and pyroxenitic rocks.

3.3.2.3 Serpentinites

The serpentinites are rarely foliated and are fine grained, usually grey to green, but occasionally red to purplish in colour. In a few localities, such as the Debel Hills, there are patches of talcose rocks, and secondary magnesite, which is generally found marginal to large outcrops. Asbestos veins do not occur in these serpentinites, though asbestiform tremolite-actinolite occurs locally in small grains. Chromite occurs as lenses (10 cm to 60 cm wide) and disseminations throughout the serpentinite of the Debel area, but also occurs as float in a wide area .

Plate 3.3 Iladu ultramafic complex (SM 58). Relict cumulate texture is blurred by metamorphism. Actinolite (yellow green in colour) extensively replacing pyroxenite (dark brown). The other minerals present are plagioclase and chlorite. Field of view 3.47.

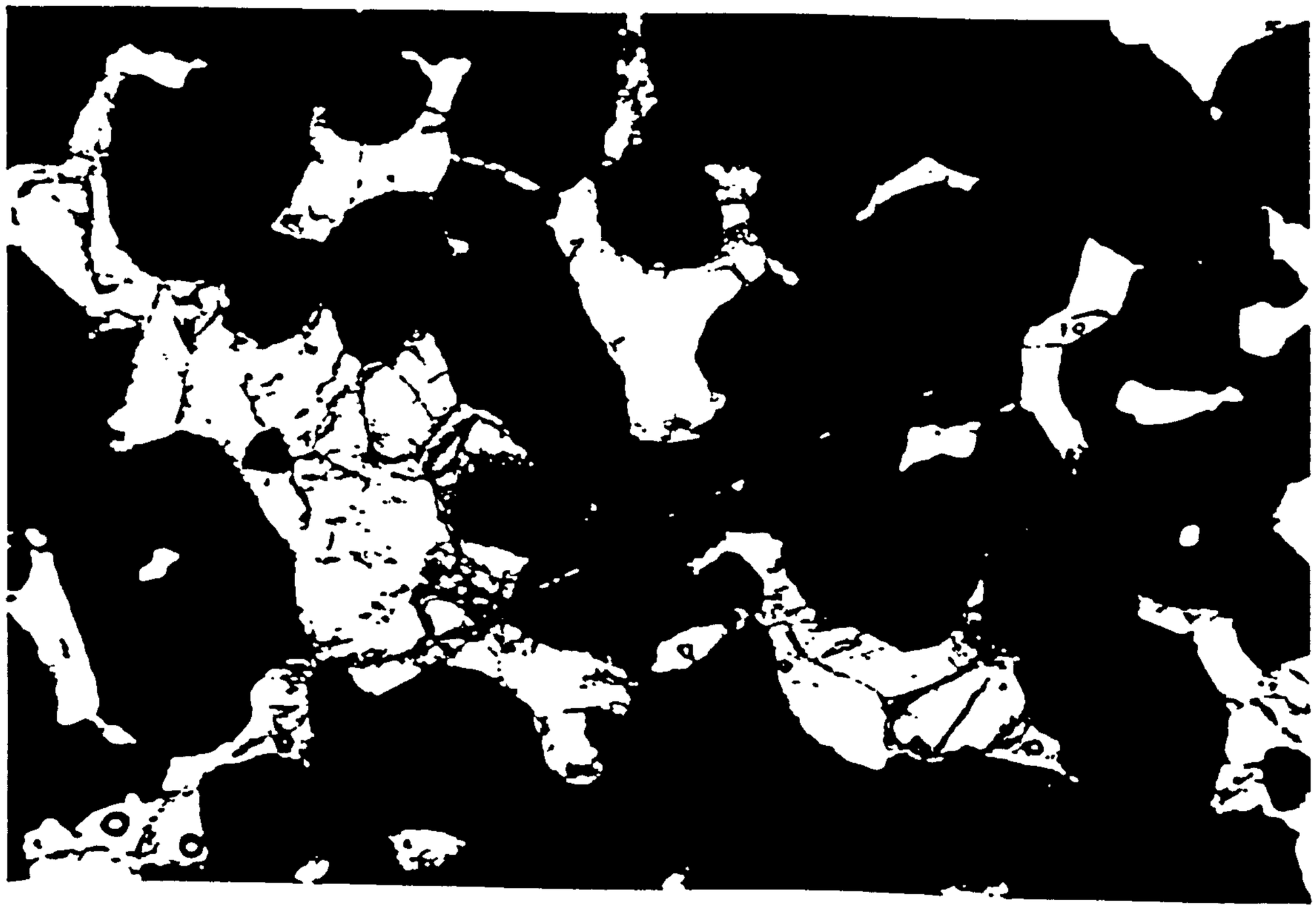

Plate 3.4 Chromite clinopyroxene (greenish in colour) cumulate. Debel area.

In thin section the serpentinites usually contain massive serporphite and fibrous antigorite. There are secondary opaques and calcite and relict grains of pyroxene are occasionally found.

3.3.2.4 *Moyale chromites*

Occurrences of chromite deposits were first reported by D.K. Hamilton (unpublished report, 1951) and were subsequently confirmed by Walsh (1972). Chromite deposits are found in serpentinite at Debel, Dudati and Rabali. The author visited the Debel area, which was suggested previously by Hamilton to be of economic significance. All the chromite finds in the area are observed as either lenses or surface float. The chromite lenses are aligned and trend between NE and NW . Most of the lenses are less than 0.5 m thick and generally are 10-15 cm wide and 1.5-5 m long. The chromite bodies can never be traced more than 2-3 m partly because they occur as restricted lenses and pods and also because of thick acacia vegetation and carbonate cover. Chromite float occur in an area 2 x 3 km. Two types of chromite deposits are observed:

Type 1 are massive chromitite deposits and type 2 deposits consist of layered chromitite with interstial minerals mostly clinopyroxenes. The layering in type 2 chromites may be due to tectonism because the grains are crushed and there is no evidence for size grading (Plate 3.4).

3.3.2.5 Talc schists

Talc schists outcrop south of Moyale town where they form a NW trending linear ridge about 100 m wide. They are usually coarse grained and grey to buff in colour. Occasionally enclaves of amphibolites occur. These rocks were not analysed in thin section but according to Walsh (1972) the mineral assemblages show a fibrous aggregate of talc which are stained by red-brown iron oxides, with minor amounts of Fe-oxides and calcite. The talc schists are sheared ultramafics along the contact with the plagioclase amphibolites and are thought to be a thrust.

3.3.2.6 Gabbros

The largest gabbroic outcrop studied is in the Mash Hills area (Figure 3.3) east of Moyale. These rocks are found associated with metadolerites. Although the gabbros form part of the metamorphic

sequence no planar fabric is observed. These rocks are aligned along strike with the mafic-ultramafic rocks of Negelle and are dark grey and medium to coarse grained. In thin section these gabbros contain laths of feldspar enclosing ferromagnesian minerals. The feldspars are usually twinned andesine - labradorite and are broken while the ferromagnesians are pale green augite and olivine. The augite is sometimes altered to hornblende and is associated with Fe-oxides. Minor epidote is present and metamorphic quartz is preserved. This rock is an isotropic gabbro.

3.3.3 Amphibolites

Amphibolites occur around Moyale and in the Mash Hills/Kufole area (Figure 3.3). In the Moyale area the exposure is good, while the Kufole/Mash Hills exposure is limited and discontinuous because of superficial cover.

3.3.3.1 Plagioclase amphibolites - Moyale Area

The plagioclase amphibolites are extensively developed east and west of Moyale town (Figure 3.3). They are approximately 2 km thick and form linear NNW trending ridges. The plagioclase amphibolites are found associated with the ultramafic rocks. The contact between the ultramafics and the plagioclase amphibolites is obscure however, as the plagioclase amphibolites have a linear contact and since in one locality they are separated by sheared talc schists and gabbro. It is therefore inferred to be a thrust. The plagioclase amphibolites in the vicinity of Moyale are clearly foliated and generally strike N-S to NNW-SSE. East of Moyale town the amphibolites dip 60°W, while they dip at 66°E on the west side of the town. Structural data indicate that there is a northward plunging syncline through Moyale.

The plagioclase amphibolites are coarse grained rocks associated with bedded amphibolitic lenses and occasionally are gneissose with quartzofeldspathic bands parallel to the foliation (Plate 3.6a). The amphibolites are cut by 5-10 m thick granodioritic and gabbroic lenses. East of Moyale they are interbedded with or in contact with metasediments.

In thin section three rock types were identified. In (Plate 3.6b) the dominant mineral assemblage is actinolite (c.50%), while plagioclase (oligoclase, 20%), mostly altered to clinozoisite,

Plate3.5 Mash Hills metadolerites (SM2A). Clinopyroxenes (show yellow interference colours) subophitically enclose plagioclases. Relict olivines (greenish) are altered at the margins. The other minerals present are epidote and magnetite. Field of view 3.47.

Plate 3.6a Plagioclase amphibolites interbedded with quartzofeldspathic bands. Oda river, Moyale.

chlorite (10%), epidote and relict clinopyroxene. This is a typical metadolerite and may have been a dyke. In section SM32 it is composed of veins of actinolite (30%), plagioclase (40%) and clinozoisite replacing plagioclase (15%). Texturally it is coarse and may have been a lava. In section SM96, hornblende is the dominant mineral c. 35%, plagioclase c.30% with secondary quartz (15%) and magnetite. This is a high grade metabasalt (Plate 3.7). Another section is dominantly made of plagioclase (40%) altered in places to sericite. It shows parallel alignment of biotite flakes (10%) and iron oxides (5%). Calcite forms 20% while rare allanite is observed. In conclusion the plagioclase amphibolites are made up of metamorphosed lavas, dykes, gabbroic lenses and amphibolitised volcanoclastics.

3.3.3.2 Metadolerites - Mash Hills area

The metadolerites of the Mash Hills are exposed in an area of 20 m by 5 m and have been exaggerated on the map for clarity. The mafic rocks of the Mash Hills area are dark grey, medium grained and are non-foliated.

In thin section (Plate 3.5) laths of andesine-labradorite (40%) enclose anhedral grains of augite (30%). The augite is occasionally altered to epidote, chlorite and hornblende. Olivine forms about 10% and Fe oxides occur as secondary minerals. Rarely apatite grains also occur.

3.3.4 Metasedimentary gneisses, schists and marbles

The metasedimentary gneisses include biotite gneisses, migmatites, hornblende gneisses, graphitic gneisses and quartzofeldspathic gneisses, while the schists include quartzites and marbles. The sparse outcrop of the gneisses compared with the granitoids makes a thorough study impossible and so they have been grouped together.

Quartzites form steep-sided prominent hills in Mado Goda area and in the southeastern part of the map area (Figure 3.3). In hand specimen they are white or pale grey with streaks of brownish-purple iron stains. The quartzites sometimes contain abundant sericite layers which produce a quartz-sericite schist and in the Mado Goda area are interbedded with crystalline limestone. The crystalline limestones are widely developed in the centre of the mapped area where they form steep

Plate 3.6b The section (SM29) shows plagioclase, actinolite (blue green and brown colours) and epidote. Plagioclase is mostly altered to clinozoisite. Field of view 3.47.

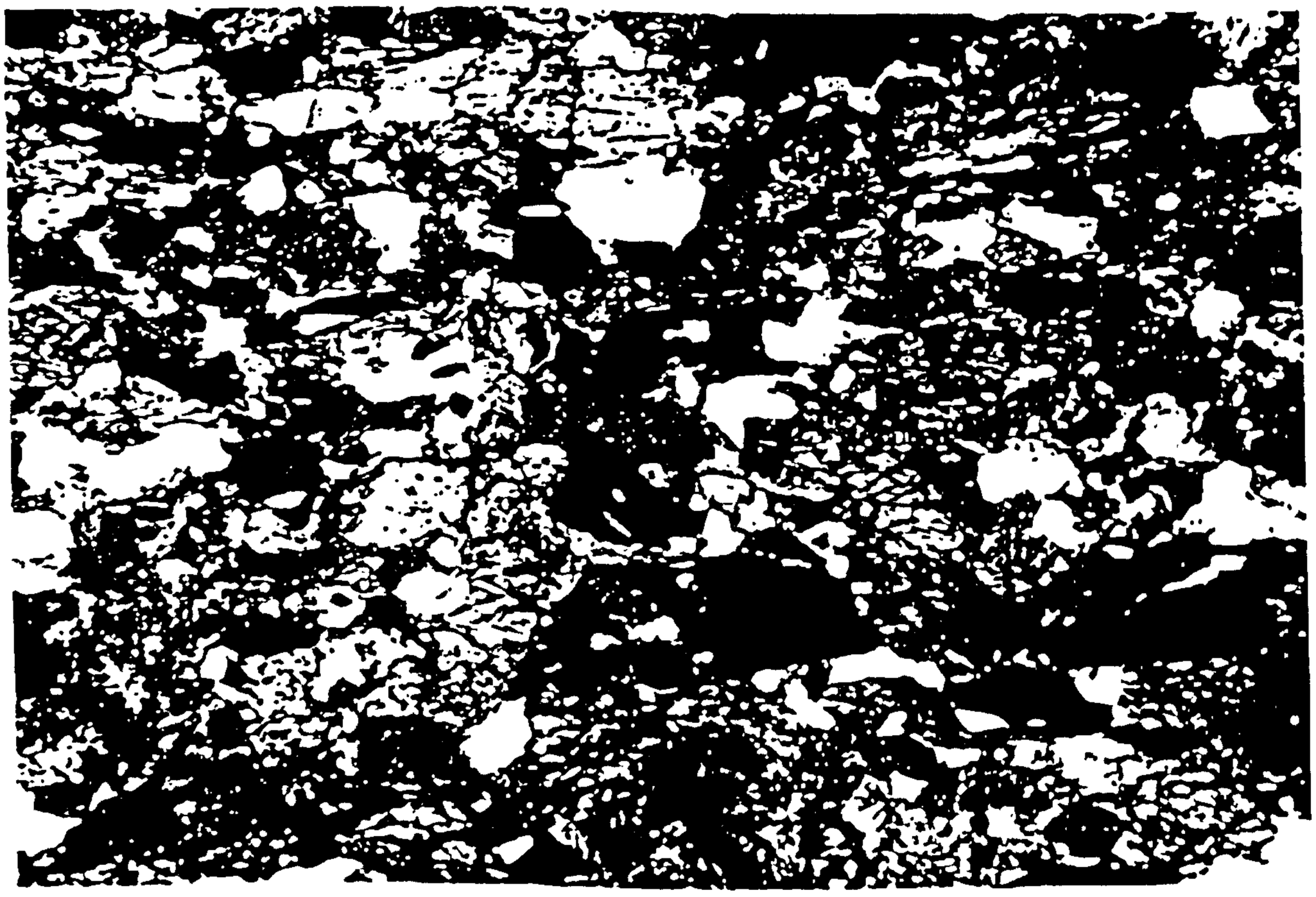

Plate 3.7 Moyale plagioclase amphibolites (SM96). Dominantly hornblende and plagioclase. Schistosity formed by parallel orientation of hornblende. Field of view 3.47.

ridges and flat platforms. The limestones are generally white to grey in colour and are coarse grained. Graphitic gneisses are the next most abundant metasediments and occur mainly southeast of Moyale. The gneisses are generally fine grained and are composed of quartz, feldspars and disseminated graphite which does not exceed about 3% of the rock.

Other widespread rocks are biotite gneisses and granitoid gneisses which occur in the form of rounded outcrops and as craggy tors respectively.

3.3.5 Syn-tectonic granitoid gneiss - Adadi Jolle

Granitoid gneisses form craggy hills dotted along the Ethio-Kenyan border. The Adadi Jolle granitic gneiss was examined in detail and forms a N-S trending linear ridge striking N-S. In this area the granitoid gneisses have a gradational contact with the granitoids of Fugugo.

The granitoid gneisses are medium to coarse grained, varying in colour from pale to dark grey. Sometimes the foliation is marked by alternating pink and grey layers with lenses of white quartz and mica flakes. In thin section all show abundant quartz (30%) and are sometimes myrmekitic. Plagioclase forms 40% of rock and is oligoclase to andesine in composition. Microcline (10%) mainly occurs as porpyroblasts. The predominant ferromagnesian mineral present is biotite (5%) which is occasionally chloritised. Epidote is a common alteration product of biotite and the feldspars. Sphene occurs in trace amounts. Other accessory minerals are muscovite, sericite and magnetite (Plate 3.8). All mafic minerals have moved along the plane of schistosity.

3.3.6 Post-tectonic granites

Post-tectonic granites are ubiquituous in the Moyale area. The Chalalaka, Godano Odo, Fugugo and Kufole granitic plutons were sampled. The largest of the granitoids are the Chalalaka and Godano Odo intrusives which are about 30 km long and about 9 km wide in the north tapering to about 5 km in the south. Fugugo and Kufole outcrop over a length of 6 km and a width of 3 km. All are generally coarse grained, with white or grey groundmass and pink or red porphyroblasts of feldspar.

The Fugugo granite shows a faint N-S trending tectonic fabric. In thin section (Plate 3.9) the porphyroblastic granites are dominantly formed of perthitic microcline (20%), quartz (10%), and

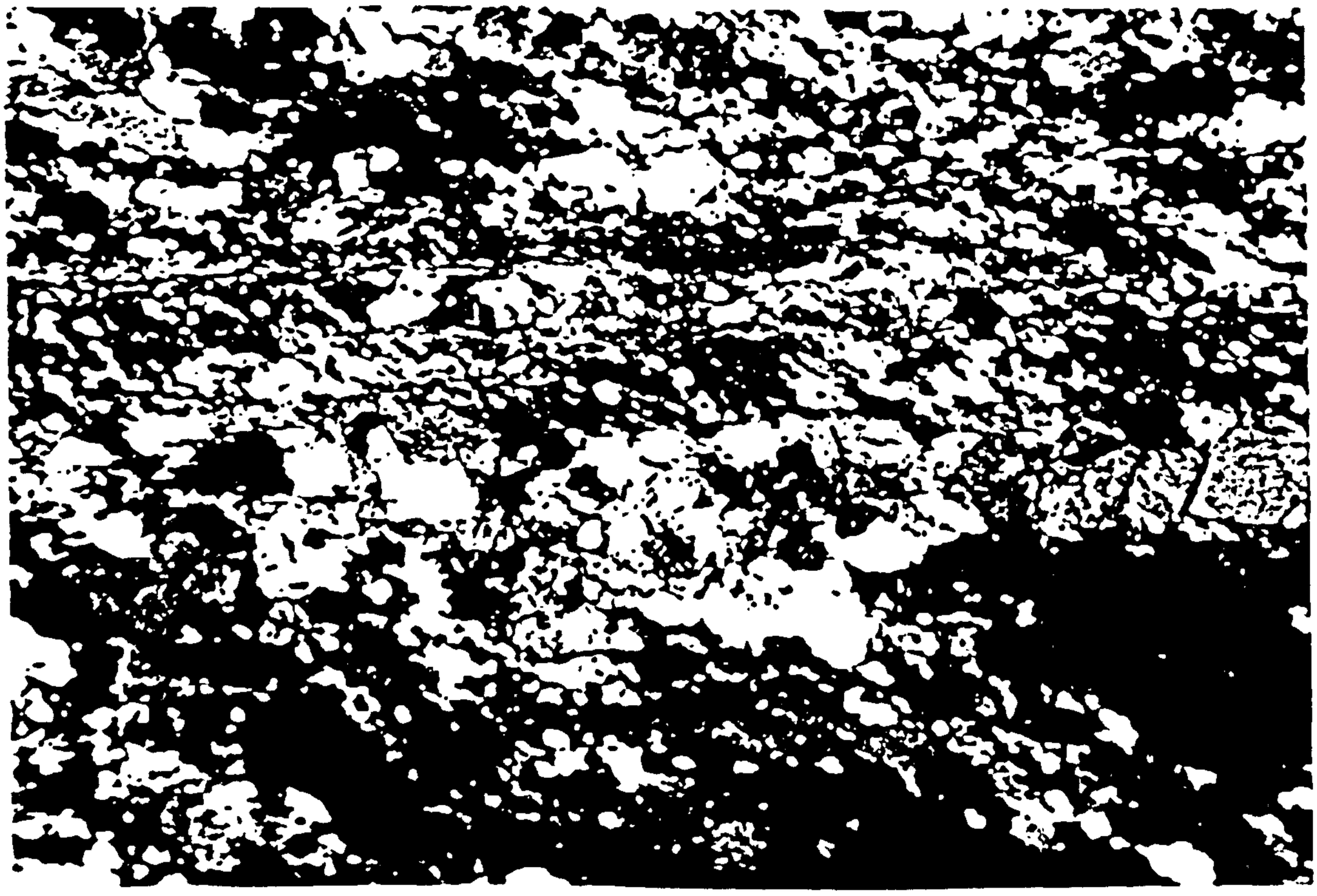

Plate 3.8 Adadi Jolle granitoid gneiss (SM41). Gneissose texture with elongate crystals of quartz and orthoclase due to intense deformation. Mica flakes are observed parallel to foliation. Field of view 3.47.

Plate 3.9 Fugugo granite. A granular mixture of quartz and feldspar with biotite (brown colour) enclosing epidote (pink). Most of the plagioclase crystals show some alteration and can be recognised by the presence of multiple twinning. Sphene (dark brown) shows sieve texture and magnetite (opaque). Sample (SM5). Field of view 3.47.

plagioclase (albite) forms 30% which is often sericitised. Biotite (10%) is partially chloritised and sometimes encloses epidote. Ilmenite is common, while sphene and apatite are observed as accessories. Sphene, epidote, allanite and zircon occur in small amounts.

The Kufole granites are porphyritic in texture. They are dominantly composed of quartz (20%), microcline (40%), albite (15%), biotite (3%), muscovite c.1% and magnetite. In some thin sections there is sericite due to alteration of K. feldspar. Zircon, sphene and allanite are observed as accessory minerals.

3.3.7 Moyale granodiorites

The granodiorites range from fine to coarse grained biotite granodiorites to diorites. The grandiorite is foliated around the margins, but is massive in the core. In places it is slightly migmatitised, with concordant quartzites. The grandiorites in the Gurumesa Valley (Figure 3.3) show mineral lineations trending 350°, plunging steeply 60° SE. Flow folding (slip folding) and shearing is observed locally (Plate 3.20). There are also quartz veinlets discordantly cutting the regional strike trend.

At the eastern side of the Moyale granodiorite the contact relationship with the amphibolites is obscure, but quartzitic units are observed along the boundary with tectonised talc schists and gabbro. Locally thick granodioritic units have a concordant intrusive relationship with the amphibolites.

The grandiorites contain quartz (20%), albite-oligoclase (40%) and biotite. Biotite exceeds 5%, and is greenish brown showing alteration to epidote, sericite and trace amounts of chlorite. The granodiorites also contain primary and secondary muscovite (Plate3.10). Sillimanite (fibrolite) and rare myrmekitic intergrowth is observed. Trace minerals observed include apatite, sphene and opaques. Pleochroic haloes around zircons are observed in biotite. No alkali feldspar was found in the Moyale granodiorites, and so they may be termed Trondhjemites.

Plate 3.10 A two mica granodiorite (SM13A). Dominantly plagioclases which are sericitised. Very rare myrmekitic intergrowth. At the right hand corner there are biotites (brownish colour) which enclose muscovite (blue interference colours). Moyale. Field of view 3.47.

3.4 STRUCTURE

A map has been prepared (Figure 3.4) showing the major structural and tectonic zones of S Ethiopia-NE Kenya, using bulk processed enlarged Landsat MSS images at a scale of 500:000. The structural interpretation of this region was constrained by geological studies carried out by Gilboy (1970), Chater (1971), Kazmin (1976), Kazmin *et al.* (1978), Walsh (1972) and field observations by the author.

The whole area has been subdivided into four tectonic zones:

(1) Zone 1 (western zone) is characterised by E-W trending folds. The rocks are shallowly inclined and show minor variations in strike. Shallow dome structures are common. The structure in this area could also reflect granite diapirism.

(2) Zone 2 (transition zone) is characterised with structural trends varying from N-S to E-W, with subvertical dips.

(3) Zone 3 (eastern zone) is characterised by major tight N-S trending folds. This episode of deformation is considered to be the major folding event (F_3 Chater,1971). The structural trend in the Negelle area swings from NE to SE and also shows some local variation in orientation.

(4) Zone 4 (southwestern zone) is characterised by major NW-SE trending structures, with local variations trending NE at the southeastern corner of the area.

Zones 3 and 4 preserve the same fabric but in zone 4 the zone 3 fabric was later refolded along shear zones.

It is suggested here that zone 1 represents the earliest episode of deformation with shallow dipping E-W trending folds (F_1 of Chater, 1971). This was refolded into north-south trending folds (F_2), (zone 2) so that there is a transition zone where there was a progressive reorientation of the fold axes from E-W to N-S during the F_3 episode of deformation. Zone 3 represents an area where E-W structures have been completely obliterated by north-south tectonism (F_2 of Gilboy, 1970; and F_3 Chater, 1971). Zone 4 reflects a major tectonic episode whereby all the four major tectonic zones have been sheared and refolded into a NW-SE trending domain. This sharp swing to the SE can be explained as a result of major NW-SE trending shear belts that became prominent further south.

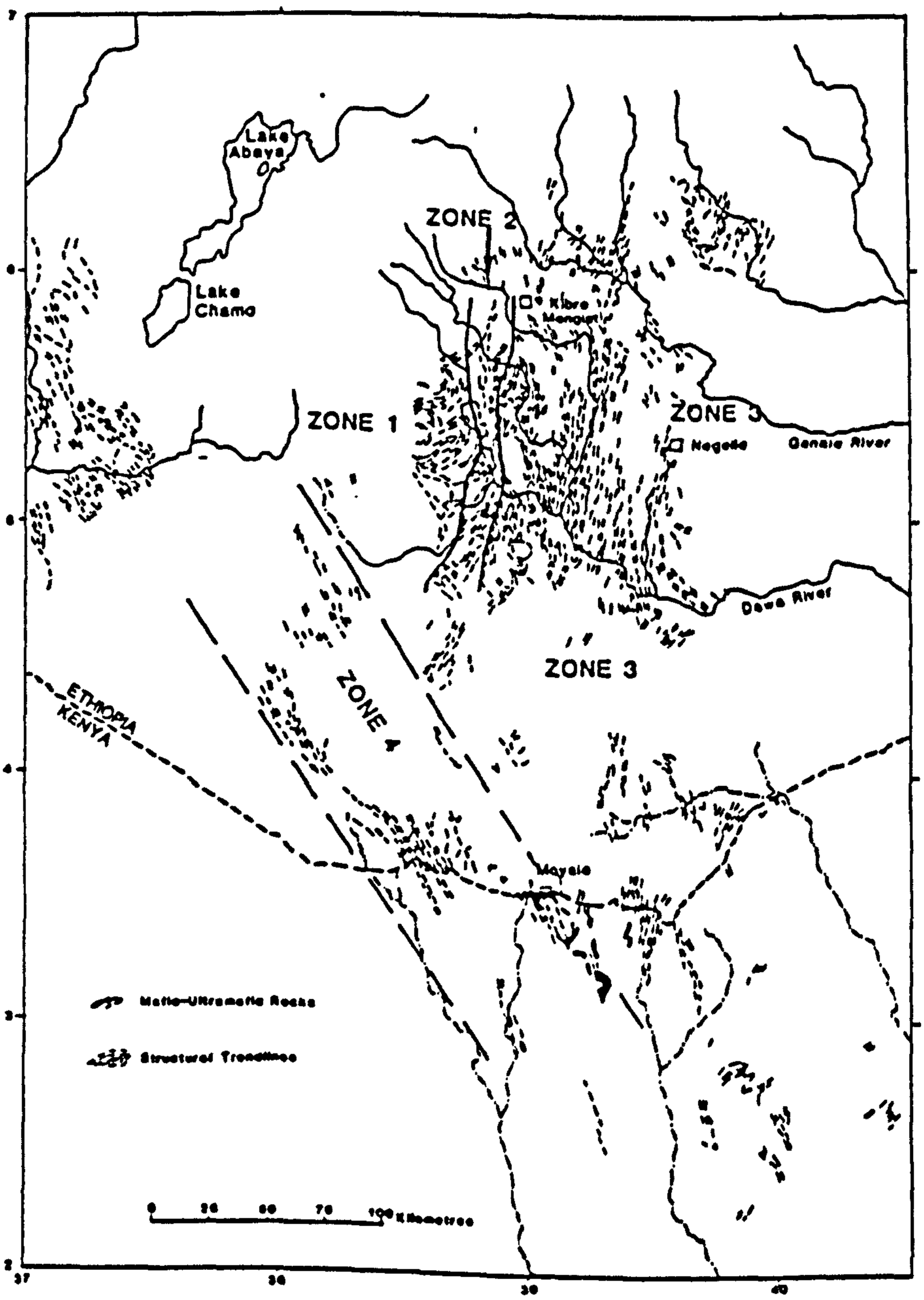

Figure 3.4 Major structural and tectonic zones of SE Ethiopia/NE Kenya. Based on Landsat interpretation.

Large transcurrent motion along the NW trending shear zones has caused bending of the regional foliation in the proximity of these zones (Berhe, 1986). Local variations within these zones are products of minor adjustments during the deformation process.

Four episodes of deformation which resulted in different planar fabrics and folds have been recognised in southern Ethiopia (Gilboy, 1970; Chater, 1971). A summary of the major episodes of deformation in southern Ethiopia is presented in Table 3.3.

Table 3.3 Major Episodes of Deformation

Episode of Deformation	Gilboy (1970)	Chater (1971)	Present Study
D_1	The development of foliation parallel to axial planes of recumbent isoclinal folds. E-W isoclinal folding in gneisses.	This caused the E-W trending gneissosity of the meta-sediments. They are mostly represented by planar fabrics (S_1). F_1 minor folds are rare and small and always isoclinal.	Represented by E-W trending open folds.
D_2	Open to isoclinal upright folds with a gentle or moderate northwesterly plunge, and late F_2 thrusts developed mainly on the flanks of the folds. Minor lineations developed parallel to the fold hinges.	Flat lying folds with approxi-mately E-W axis, refolded into E-W upright folds during F_2. Minor folds are usually tight to isoclinal. The strike varies from N-S to E-W.	E-W to N-S trending upright folds. Early stage development of thrusts.
D_3	Steeply isoclinal or upright open folds with east-west axial traces and subhorizontal axes. Restricted to the NW part of the area. Mineral lineations have a gentle to moderate W-NW or E-NE plunges.	The development of major N-S trending synclinorium with sub-vertical dips.	F_2 refolded into N-S trending fold structures, and associated minor structures. Thrusting is well developed at this stage. Eastward directed thrusts.
D_4	Major axial trace which trends NNW/SSE.	The formation of a series of large scale E-W trending upright folds. Restricted to the west of Megado.	This episode is charac-terised by major NW/SE trending structural trends and shear zones.

In this table one can observe that the classification F_1 to F_4 of Chater (1971) does not represent the same sequence of events as that of Gilboy (1970). In the new classification the four episodes of deformation are adopted and these are related to a progressive deformation and reorientation of folds in the whole area. Local deviations in structural trend have a tendency to develop at the boundaries between the different tectonic domains as deformation progresses.

The first episode (D_1) is represented by flat lying E-W trending open folds west of Digati, while in the east they form isoclinally recumbent folds which been have progressively refolded (D_2) into upright E-W or N-S trending folds. Thrusts were developed during the second stage of deformation which began separating the rocks into several tectonic (km scale) slabs. The third (D_3) episode of deformation caused major N-S trending folds and associated minor structures. The axial planes of the main regional folds are subvertical or dip steeply to the west. Tectonic slabs are overthrust in an easterly direction during D_3 (Figure 3.2). The fourth (D_4) episode is restricted in the Megado area, but further south major axial traces which trend NW/SE are observed.

The similarity in fold style between the Adola belt and flanking gneisses is taken as evidence that these units underwent the same folding event during the Mozambique deformational cycle (c. 600 Ma). Earlier structures in the gneisses have been destroyed during these events (Kazmin, 1972; Kazmin *et al.*, 1978). The rocks of the Adola belt are strongly folded by D_3, in some cases isoclinally, and are so dismembered marginally and internally by reverse and transcurrent faults that a coherent structural-lithostratigraphic sequence cannot be deciphered.

In the Moyale area two episodes of deformation are observed. F_1 folds are minor folds which trend N20E with shallow plunges to the southeast and are refolded by the dominant NW-SE (D_3) trending foliation. This deformation event has resulted in NW trending folds, exemplified by the Moyale and the Mado Goda synclines which plunge northwards. The mafic-ultramafics are preserved in the Moyale syncline, while crystalline limestones and quartzites form the core of the Mado Goda syncline. Walsh (1972) presented the structural data of the Moyale area and the wide scatter of poles to foliation planes suggests at least two episodes of deformation.

In summary, the Adola-Moyale belt experienced three major episodes of deformation. The sequence of events are D_1 which caused E-W trending folds, refolded by D_2 N-S folding episode

and then during D_3 refolding by NW-SE trending shear zones took place. This has been based on age relationships of different fold generations.

3.4.1 Major thrusts and shear zones

The rocks within the Adola-Moyale belt are so strongly tectonised and dislocated by strike slip faults that they have reactivated earlier reverse faults, which represent steepened thrusts. Few of the thrusts are considered to be reactivations of normal faults of earlier episodes of basement rifting, which have controlled the deposition of the Wadera Group metasediments. Gilboy (1970) identified two major shear zones in the Adola area. However, further work by Kazmin *et al.* (1978) and Landsat study has shown that at least six major N-S trending faults and others of less regional significance are present. Major faults are marked by belts of intensely crushed and sheared talc, talc-serpentinite and chlorite schists. Later D_2 folding with axial plane shears, probably related to the regional wrench faulting, are locally developed in the ultramafic schists of the Adola area.

The major thrust belts (100-180 km long) are described from west to east. The strike of foliation in the Adola Group is sometimes parallel with the gneisses, but often is discordant (UNDP, 1972). West of Digati the western margin of the Adola Group is a steeply dipping fault (Chater, 1971). The major thrust belts are the Burji and the Mormora (Figures 3.2 and 3.4) (Gilboy, 1970). These thrusts are marked by several elongated lenses of sheared and foliated ultramafic rocks and their trends are parallel to the F_2 fold limbs, although occassionally they cut across the axial planes of F_2 folds. These thrusts could be the sole of a nappe. The Burji shear belt has a 170 km long fault plane which dips 60-70° to the west (Chater, 1971). The Burji thrust belt has been deformed by E-W trending fold axes at its northern end. Although this shear zone had been active at an early stage of the D_2 episode of deformation, it is clear that they were still active during the D_3.

In the Kenticha zone (Figure 3.2) there are three or more tectonic slabs overthrust in an easterly direction (Kazmin, 1976; Kazmin *et al.*, 1978). These zones are characterised by several sheared lenses of ultramafics along the shear belt. Distorted bands and blocks of banded ferruginous quartzite occur in a talc-serpentinite matrix occur at the base of the Kenticha thrust belt. Further east in the Negelle area the mafic-ultramafic rocks (equivalent to the Adola Group) are

separated from the gneisses to the west by a sharp N-S contact - possibly a tectonic break - which has been partly obliterated by migmatite formation (Huntings, 1969). The migmatites are at least 20 km wide parallel to the contact and affect both gneisses of granitic and dioritic composition.

Further south along the Ethio-Kenyan border a Landsat study has shown that two major NW trending faults continue into Moyale and further south to the Debel area. These lineaments coincide with streams and the Moyale mafic-ultramafic complexes is also fault bounded. Southwest of Moyale northwest trending shear zones are developed and extensive mylonitisation has occurred which obliterated earlier structures (Figure 3.4). These shear zones play a prominent role in the regional tectonic evolution further south in Kenya. The major swing in the strike of the Adola belt southeastwards in the Moyale area reflects these NW trending shear zones.

3.5 METAMORPHISM

The Adola-Moyale belt can be subdivided into four zones based on metamorphic index minerals (Figure 3.5). These metamorphic zones partly overlap the structural zones that were established in section 3.4. Zone A is equivalent to tectonic Zone 1; Zone B is equivalent to tectonic Zone 2; while Zone C and D are equivalent to tectonic Zone 3. These classifications are based on the mineral assemblages of pelitic rocks studied by Gilboy (1970) and Chater (1971).

The characteristic minerals within the pelitic rocks in the west (Zone A) are garnet, staurolite, kyanite and muscovite. In zone B garnet, biotite, chlorite, quartz and rare cordierite, and eastwards in zone C staurolite, kyanite, garnet, biotite and muscovite, plagioclase An_{15-25}. In zone D the characteristic minerals are sillimanite, garnet, biotite and plagioclase (An_{15-25}) (Figure 3.5). The metamorphic P-T fields for the Adola-Moyale belt gneisses are presented in Figure 3.6.

The absence of staurolite and kyanite in zone B might reflect that this zone is of a lower grade than the adjoining zones, or the rocks do not have an appropriate bulk composition. However zones C and D may be compared. The presence of sillimanite in zone D reflects an increase in temperature eastwards, while its presence in the southeastern part of the Adola area and in the Moyale area suggests that the sillimanite isograd cut across the Adola-Moyale belt.

In the Moyale area the typical mineral assemblage of metasediments is plagioclase-biotite-microcline-quartz - hornblende-epidote. Muscovite is subordinate to biotite, while hornblende is seldom an important constituent and is usually replaced by biotite (Walsh, 1972). Kyanite was not found in the area, but rare fibrolitic sillimanite has been observed in the Moyale granodiorites (Table 3.2) and Parkinson (1920, p.27) has recorded sillimanite south of Moyale area. Hence the Moyale area are of similar grade to zone D of the Adola area (Figure 3.5).

The mafic-ultramafic rocks contain mineral assemblages typical of greenschist facies metamorphism although the surrounding metasediments have been exposed to higher grades of metamorphism. The Adola metabasites are a transition between greenschist facies (chlorite + quartz and actinolite) and the amphibolite facies (epidote/clinozoisite + An_{15-30} and hornblende).

The mineral assemblages of the Bul Bul mafic-ultramafic rocks (which are east of Negelle) (Huntings, 1969) indicate that they are metamorphosed in the quartz-albite-epidote-biotite subfacies of the greenschist regional metamorphism. This is similar to the mineral assemblages of the Adola Group (Table 3.4).

The ultramafic mineral assemblages in the Adola area are talc-tremolite-antigorite-chlorite and secondary carbonate (see Table 3.4). Although pelitic rocks may be used to establish pressure and temperature conditions of metamorphism, this can be further constrained by mineral assemblages of metamorphosed mafic igneous rocks (Liou *et al.*, 1974; Spear, 1980; 1981). The presence of epidote, hornblende and/ or actinolite suggests that it is in the epidote amphibolite facies (Figure 3.7).

The presence of antigorite in serpentinites suggest that temperatures up to 550°C were reached (Evans *et al.*, 1976; Winkler, 1976). The development of kyanite in the gneisses also shows that temperatures up to 600°C at about 6 kb may have been reached (Figure 3.6).

The rapid changes of metamorphic grade across strike, and the fact that the mafic-ultramafic rocks contain mineral assemblages typical of greenschist to mid-amphibolite facies when the adjoining rocks have been exposed to higher grades of metamorphism, poses a problem in interpretation. The evidence suggests that the sillimanite and kyanite metamorphism is earlier than the greenschist metamorphism of the ophiolites and the sediments associated with them.

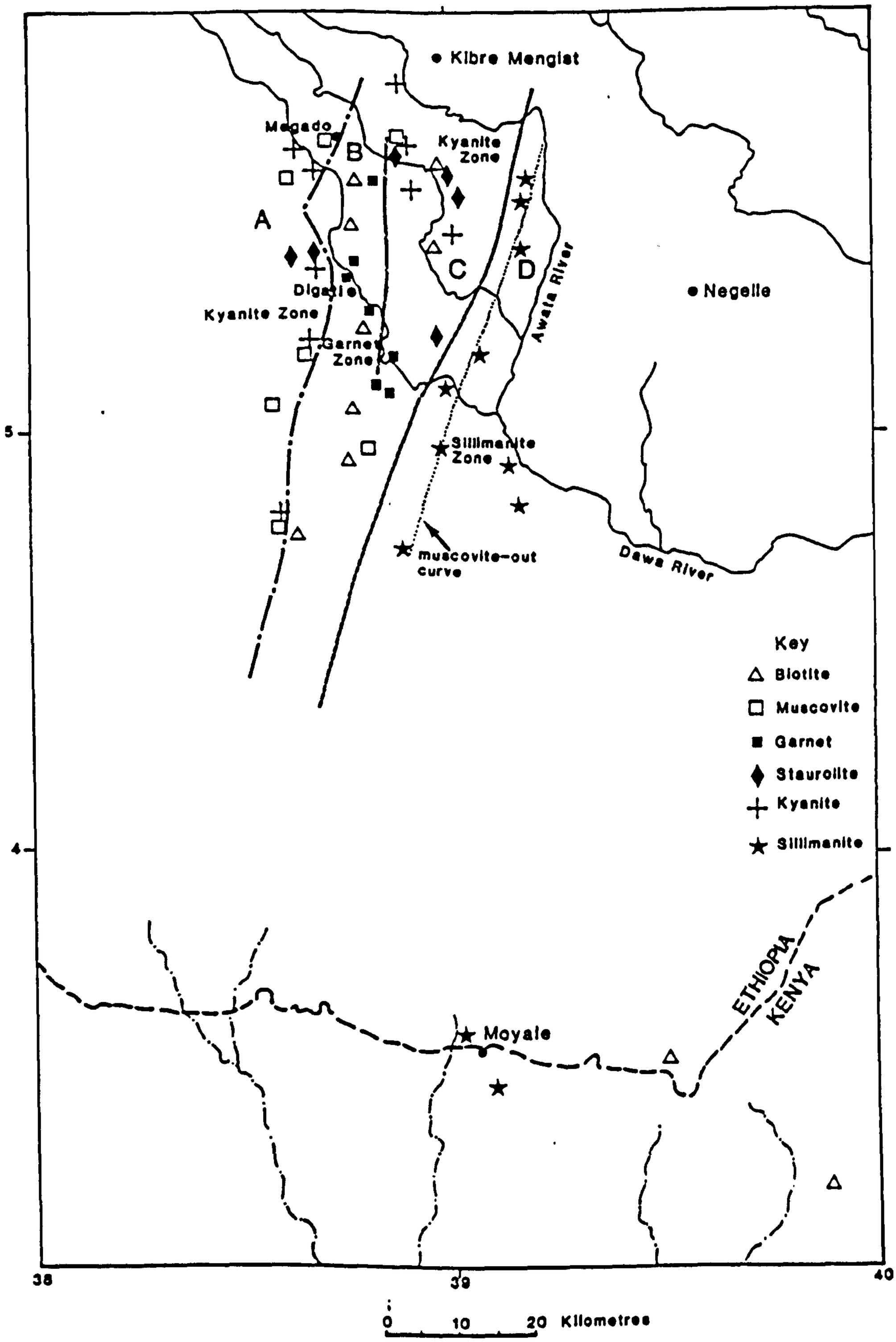

Figure 3.5 Distribution of metamorphic index minerals in the Adola-Moyale Belt. (Sources of data: Gilboy,1970; this study).

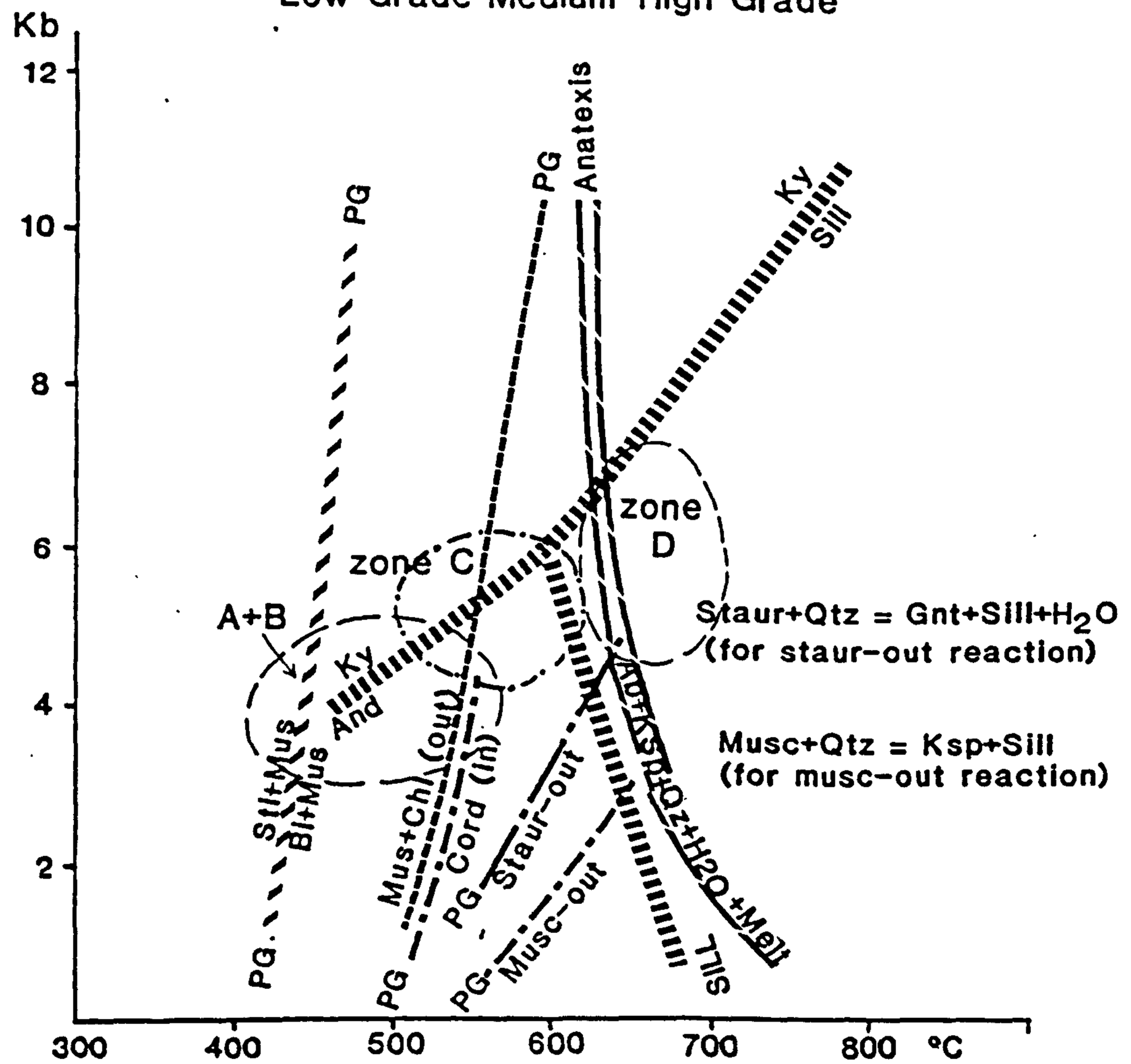

Figure 3.6 Metamorphic P-T fields of the Adola-Moyale Belt, SE Ethiopia/ NE Kenya. PG = pelite and graywacke. Reaction curves after Winkler (1976).

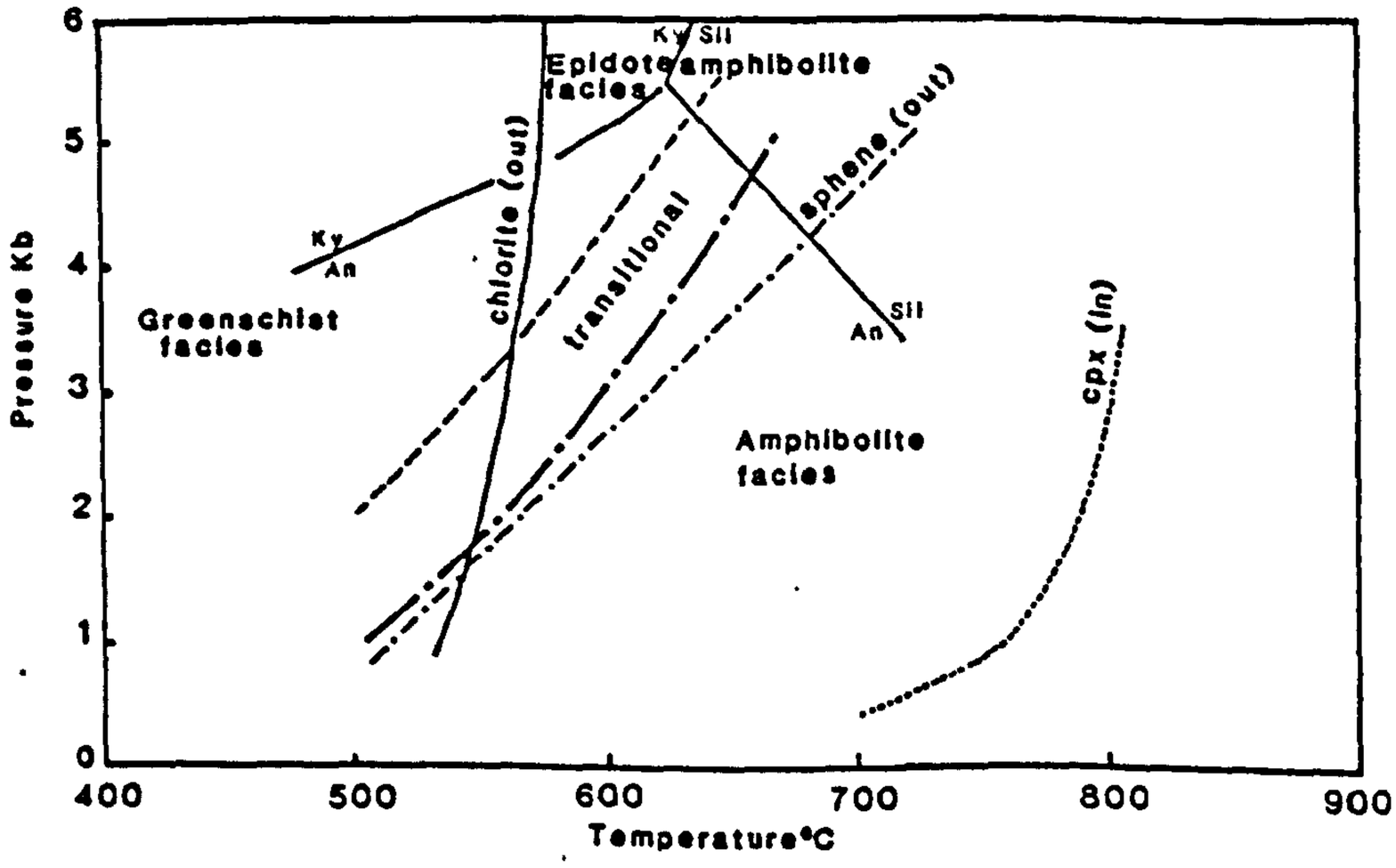

Figure 3.7 Pressure-temperature grid for regional metamorphism of amphibolites. Reaction curves from Liou et al (1974), Spear (1981). Mineral abbreviations: Ky= kyanite, An= andalusite and Sil= sillimanite.

Table 3.4 Typical mineral assemblages of the Adola-Moyale area

Rock Group	Rock Type	Mineral Assemblage
Awata and Alghe Gneisses (Lower Group)	Biotite Gneisses	Quartz+biotite+plagioclase (An_{15-25})± microcline (±sillimanite ±garnet±muscovite)
	Biotite Hornblende Gneiss	Quartz+plagiocalse+biotite+hornblende±microcline. Accessory minerals include magnetite, sphene, apatite, zircon.
Wadera Gneisses (Middle Group)	Quartzofeldspathic gneisses	Quartz+microcline±plagiocalse (An_{0-10}) (±biotite± muscovite ±sillimanite).
	Biotite Hornblende Gneisses	Quartz+plagiocalse+biotite+hornblende (±garnet± sillimanite± staurolite±muscovite±epidote±microcline). Accessory minerals include magnetite, pyrite, sphene, chlorite, zircon and tourmaline.
	Staurolite-garnet-biotite schists	Quartz+plagioclase+biotite(±staurolite ±muscovite ±kyanite). Accessory minerals include apatite, tourmaline, zircon, sphene and magnetite
Mafic-Ultramafic Rocks	Ultramafic (Adola area)	Antigorite+tremolite/actinolite + talc + chlorite ± carbonate with subordinate hornblende anthophyllite, spinel, phlogophite, chromite garnet. Orthopyroxene and olivine are rarely preserved.
	Ultramafic (Moyale area)	Actinolite+clinozoisite±diopside±hornblende. Accessory minerals are serpentine, Fe oxides and sphene.
	Serpentinite (Moyale area)	Serpophite+antigorite+chromite±pyroxene (relict)
	Amphibolite (Adola area)	Hornblende and/or actinolite+plagioclase±epidote ±calcite ±quartz.
	Amphibolite (Moyale area)	Actinolite±hornblende+oligoclase±clinozoisite.
Syntectonic Granites	Gneissose granites (Adola area)	Quartz+microcline+plagioclase±biotite±hornblende ±muscovite. Accessory minerals include magnetite, sphene, zircon and apatite.
	Granitoid gneisses (Moyale area)	Quartz+microcline+plagioclase (An_{10-20})+biotite±chlorite ±epidote. Accessory minerals include sphene, muscovite, sericite, apatite and Fe oxides

cont.....

	Godoloka granite (Adola area)	Quartz+microcline+plagioclase (An_{5-25})±biotite± amphibole. Magnetite, ilmenite, sphene, apatite, zircon, allanite, chlorite, sericite and calcite are the usual accessory minerals.
Post-tectonic Granites		
	Biotite granites (Moyale area)	Quartz+microcline+plagioclase+biotite+chlorite. Sphene, apatite, epidote, allanite and Fe oxides are the usual accessories
	Moyale granodiorite	Quartz+plagioclase (An_{5-20})±biotite±myrmekite± muscovite±fibrolite. Accessory minerals are sphene, apatite, zircon.

The sequence of metamorphism from west to east changes from mid-amphibolite (zone A), to greenschist-mid amphibolite facies (zone B), mid to upper - amphibolite facies (zone C), upper amphibolite facies (zone D). One plausible explanation is that the grades of metamorphism are directly related to the intensity of tectonism and lithology. The most intensely deformed zone (zone 3) has attained the highest grade of metamorphism, this is testified by the absence of muscovite. The presence of sillimanite and partial melting of quartzofeldspathic paragneisses which produced early granites suggests that temperatures over 600°C must have been reached. Anatexis in gneisses may take place at minimal temperatures of about 660°C at 3.5 kb and 615°C at 10 kb depending on H_2O availability (Winkler, 1976).

Gilboy, (1970) suggested that the Gariboro area suffered two episodes of metamorphism. The Lower and Middle Complexes (the Alghe and Awata Groups) have been considered to have been affected by two episodes of deformation, while the Upper Complex (the Adola Group) by one deformation episode. Chater (1971) argues that the Upper Group (Adola Group) have been affected by the initial tectonothermal event, because of the regional development of migmatites at low levels within the amphibolites, and the presence of cordierite in phyllites, however this could be due to contact metamorphism.

In the Megado region (Chater, 1971) gneisses underlie weakly metamorphosed sediments which still contain well preserved sedimentary structures. The weakly metamorphosed sediments are definitely younger than the gneisses.

The rapid changes in metamorphic grade in localised areas may result from major faults which involve considerable vertical and/or lateral displacement, and have juxtaposed blocks of contrasting metamorphic grades. Similar transitions in SW Ethiopia have been ascribed to a local increase in temperature in the vicinity of granite batholiths and nappes, (Davidson *et al.*, 1976). However the sillimanite and kyanite zones are regional extending from Ethiopia to S. Tanzania and are not related to local increase in temperature near granites (Shackleton, pers. comm.).

3.6 GEOCHEMISTRY OF MAFIC-ULTRAMAFIC ROCKS

3.6.1 Introduction

The purpose of this section is to geochemically characterise the rocks of the Moyale mafic-ultramafic complex and to define the tectonic setting of the volcanic rocks. For this purpose fourteen lavas were analysed for major and trace elements. Thirty-three chromite grains and twenty-two clinopyroxenes were probed from ultramafics. This study does not not cover the geochemistry of the Adola mafic-ultramafics.

Standard analytical techniques are discussed in Appendix A, and geochemical data are tabulated in Appendix B. Sample locality maps have been included (Figure 3.3).

3.6.2 Chromite Chemistry

A total of thirty-three microprobe analyses of chromite grains were made from five samples (see Appendix C for probe data). The compositional variations of Al, Cr and Fe^{+3} are shown in Figure 3.8. This shows that there is little enrichment of Fe^{+3}, relative to Cr and Al and less variation in total Fe, compared to stratiform deposits. However, Cr varies in composition compared with those of Kangura, Baragoi area which form a cluster. In the Baragoi chromites Fe^{+3} is low compared with Cr and Al values. The Baragoi chromite is restricted in extent, when compared to that of Al'Ays (Neary and Brown, 1979). The Kangura chromites plot separately from the Kapalagulu chromites of Tanzania (Almohandis, 1983) indicating their different origins.

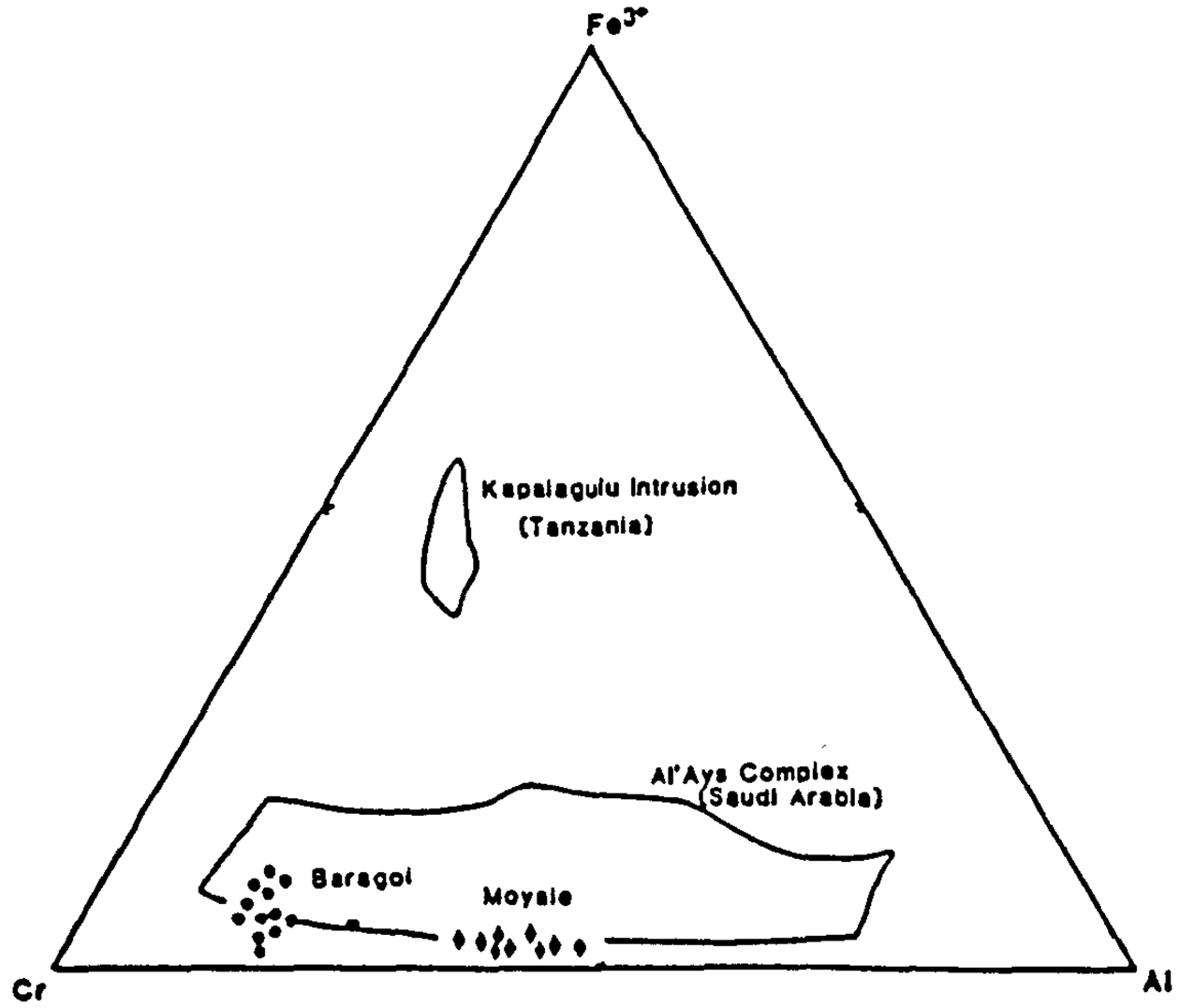

Figure 3.8 Compositional fields of Al, Cr and Fe^{3+} of the Moyale chromites as compared to the Kangura (Baragoi,Central Kenya) chromites; Al'Ays complex, Saudi Arabia (1979) and Kapalangulu intrusion, Tanzania (Almohandis, 1983).

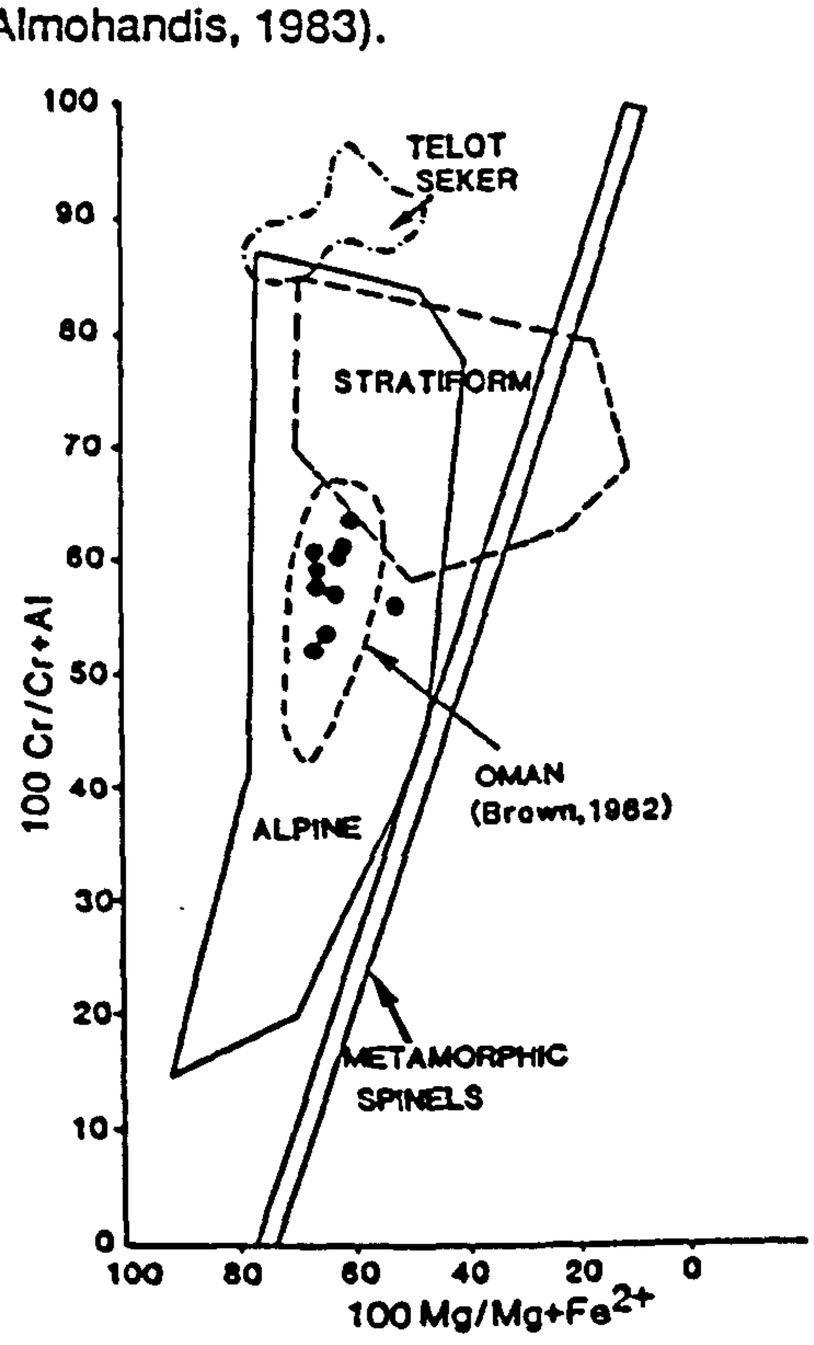

Figure 3.9 $Mg/Mg+Fe^{2+}$ - Cr/Cr+Al plot for the Moyale chromites. The Moyale chromites plot in the Oman chromitite field (Brown,1982). Comparative data from Telot,Sekerr NW Kenya (Price,1984). Alpine and stratiform fields are taken from Irvine and Findlay (1972).

The chromite in the Moyale ophiolitic sequence varies in composition from Cr/Cr+Al 0.52-0.63 Mg/Mg+Fe 0.53-0.674 (Figure 3.9) and Fe^{+3}/Cr+Al+Fe^{+3} 0.22-0.34 (Figure 3.10). The Cr/Cr+Al ratios have a small range suggesting that there is little chemical variation in the chromite pods. In the Fe^{+++}/Cr+Al+Fe^{+2} against Mg/Mg+Fe plot the chromites are high in Mg and Fe^{3+} (Figure 3.10).

The titanium content of chromite in mantle sequence chromitites and dunites is generally low (< 0.23%) (Figure 3.11). Manganese contents of chromite from mantle sequence chromitites vary between 0.32-0.56 Mn wt% and no zoning in chromite grains was detected.

The variation of Cr/Cr+Al vs. Mg/Mg+Fe^{+2} may be compared to those of Telot, NW Kenya and Oman (Figure 3.9). The Moyale chromitites have a restricted range, and plot in the Oman chromitite field (Brown, 1982) which is different from the Telot field (Price, 1984).

The data plot in the Alpine field of Irvine (1965) although using the Fe/Mg vs. TiO_2 plot of Dickey (1975) the results are unequivocal as there is an overlap in the Alpine and Stratiform Field (Figure 3.11). In the Fe^{+++}/Cr+Al+Fe^{+3} vs. Mg/Mg+Fe^{+2} the Moyale chromites show a restricted range indicating that there was no fractionation of the chromite pods (Figure 3.10).

3.6.3 Clinopyroxenes

Chromitites of the Moyale area contain interstitial clinopyroxenes and 22 analysed clinopyroxene show a restricted range of composition (Figure 3.12). Except for one analyses which plots in the endiopside field, the remainder are of diopsidic composition. The total compositional range of the clinopyroxenes are: (Mg/Mg+Fe+Ca) cpx or En is 0.48 to 0.61; (Fe/Mg+Fe+Ca) cpx or Fs ranges 0.0 to 0.036 while (Ca/Mg+Fe+Ca) cpx or Wo ranges from 0.48 to 0.50. The interstitial clinopyroxene in chromitite lies at the Mg-rich end of an Fe enrichment/Mg depletion trend. Clinopyroxene compositions are similar to those described from the Oman chromitites (Brown, 1982).

3.6.4 Discussion

Compositional variations of chrome spinels have been used by many researchers to constrain the petrogenesis of mafic-ultramafic rocks (eg. Irvine, 1965; Irvine,1967; Cameron, 1975; Dick and Bullen, 1984). Using spinel compositions Dick and Bullen (*op. cit.*) divided alpine-type peridotites

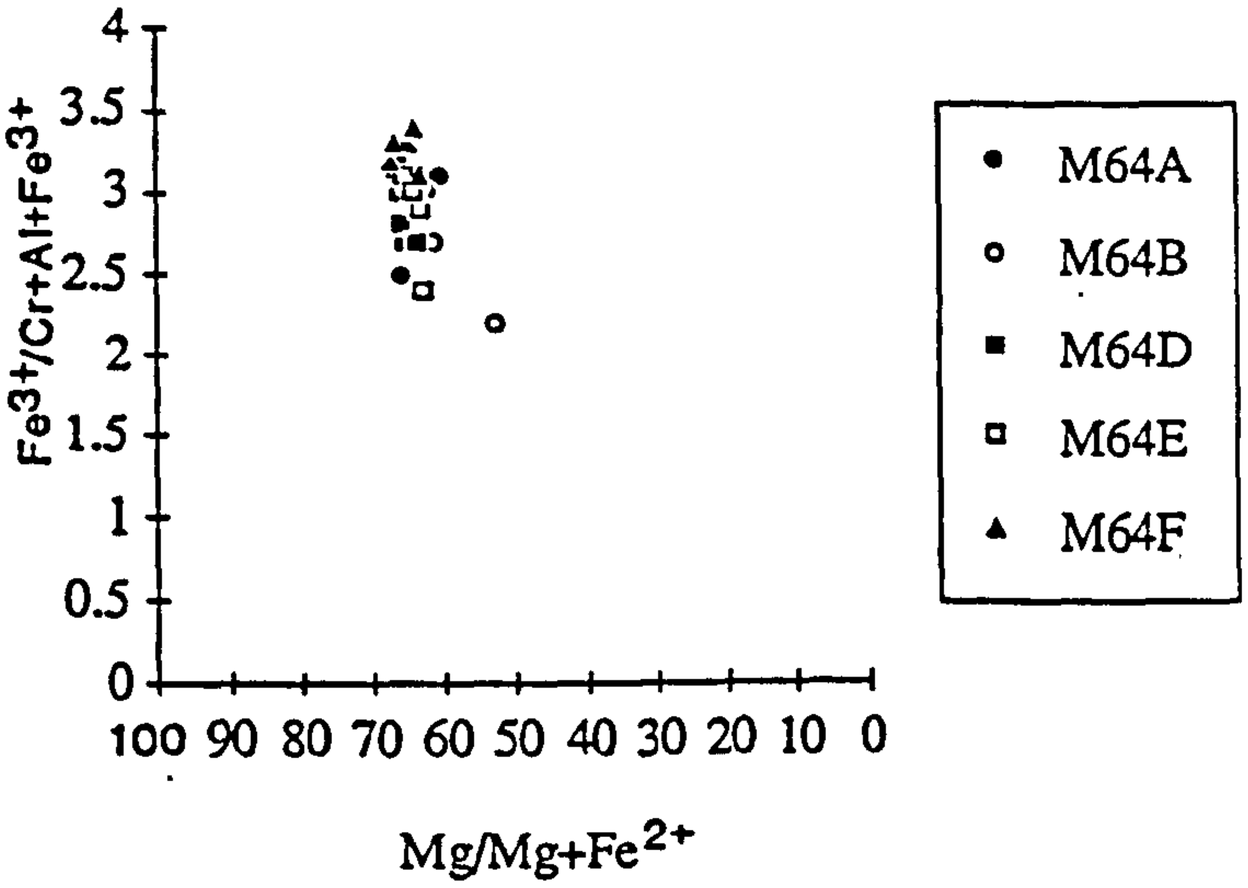

Figure 3.10 Chromite compositions $Mg/Mg+Fe^{2+}$ - $Fe^{3+}/ Cr+al+Fe^{3+}$. The Moyale data show no wide chemical variation in the various specimens.

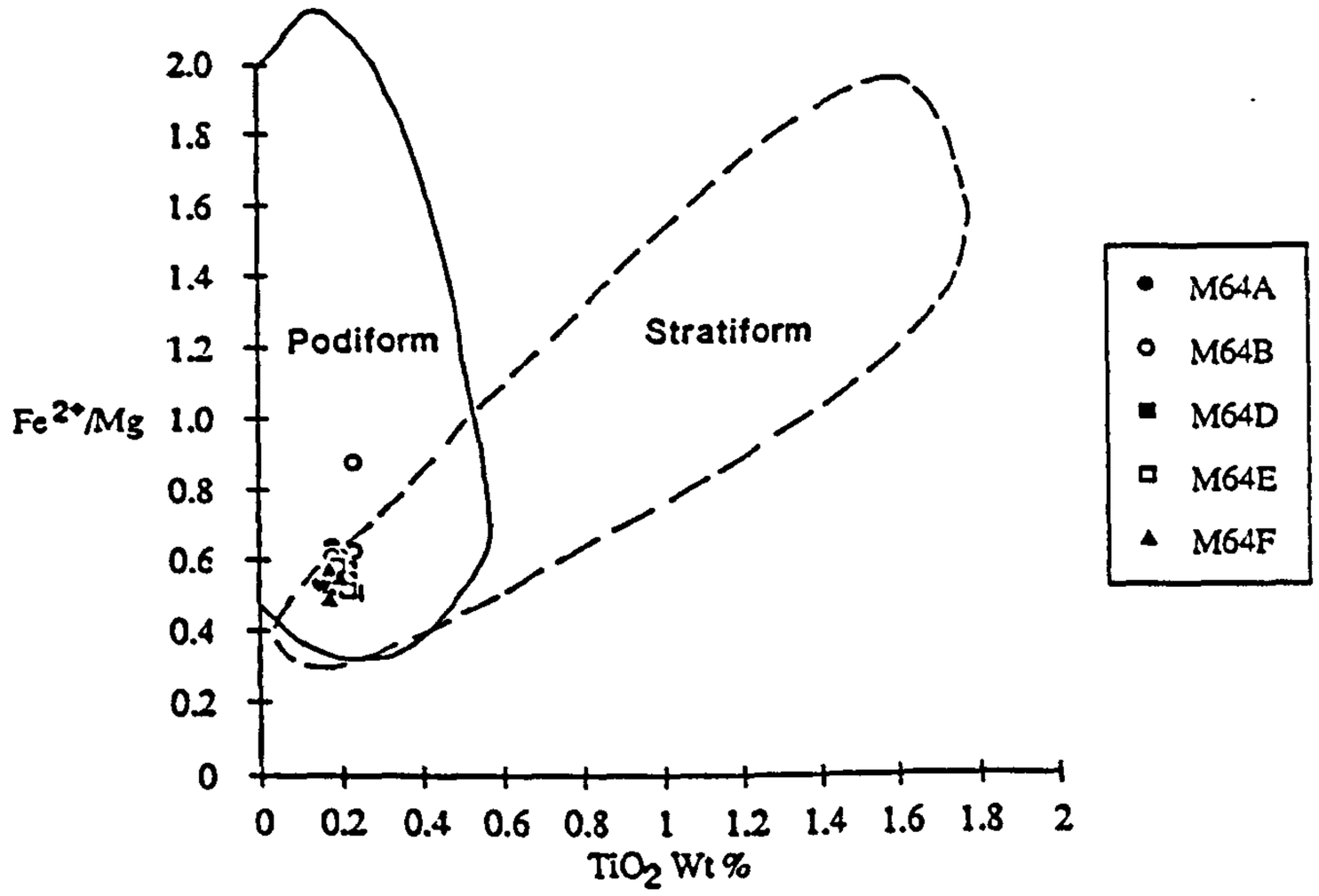

Figure3.11 TiO_2-Fe^{2+}/Mg plot for the Moyale chromites. Fields taken from Dickey (1975).

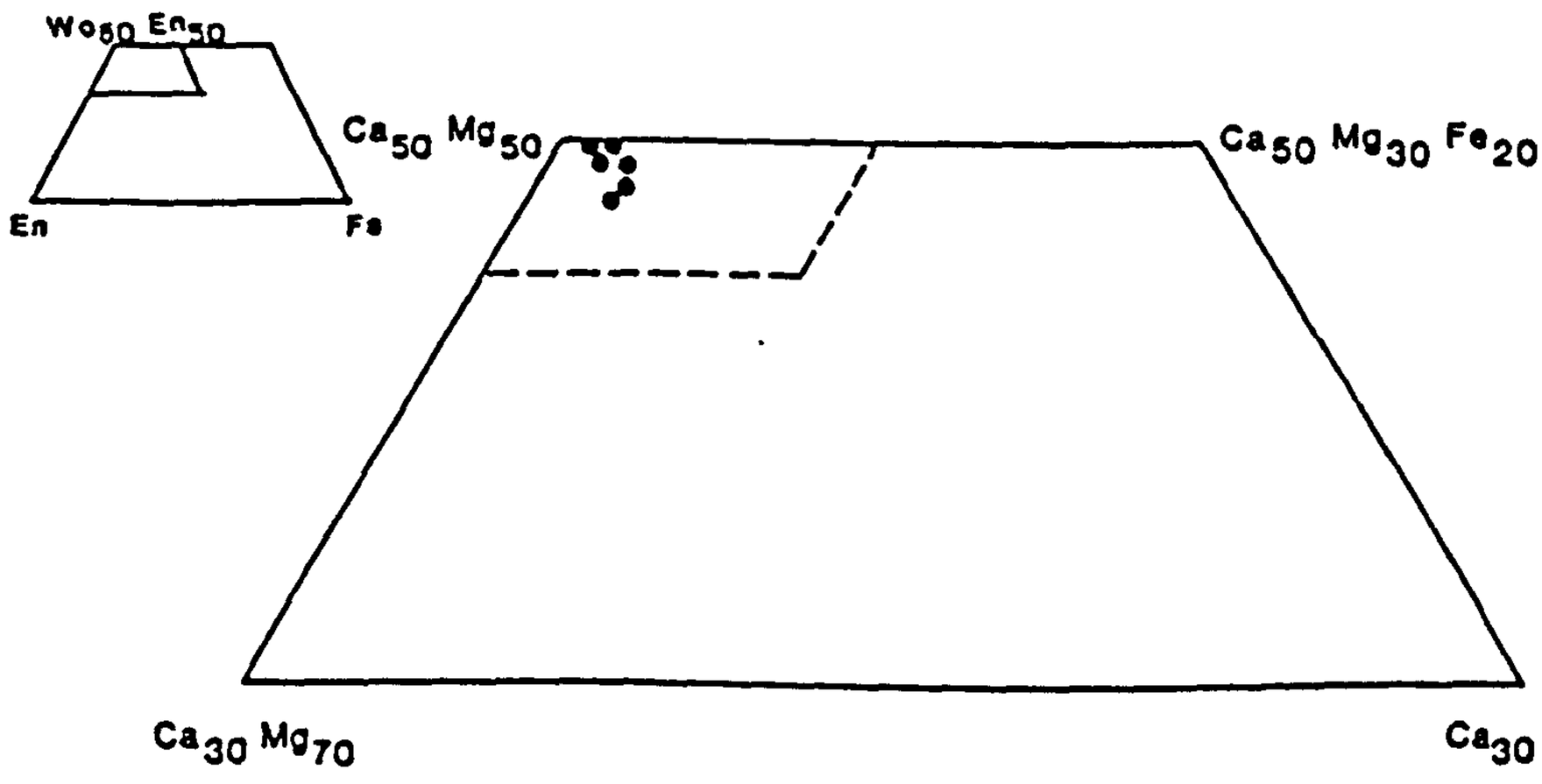

Figure 3.12 Clinopyroxenes from the Moyale chromitite sequence plotted on the pyroxene quadrilateral.

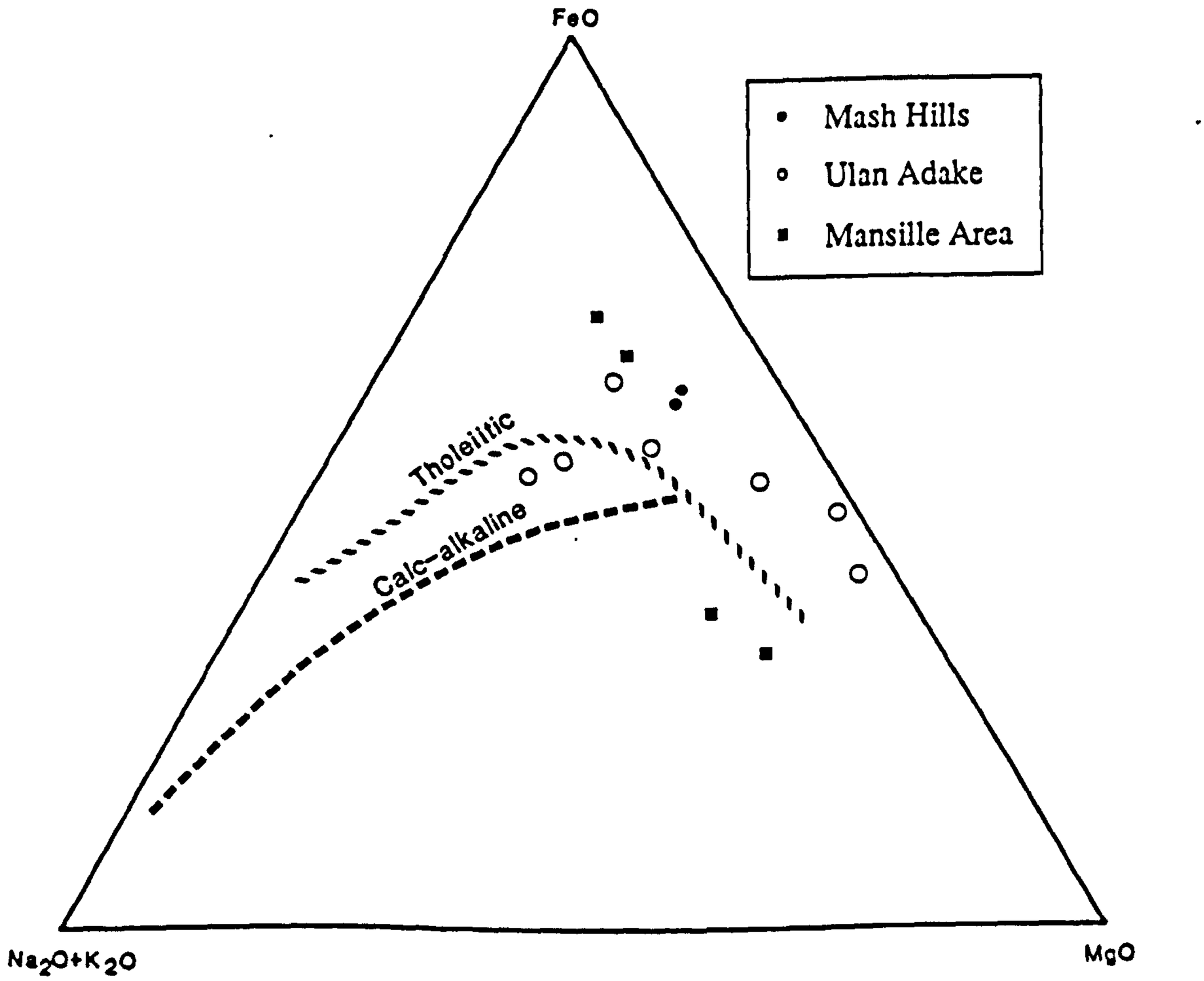

Figure 3.13 AFM diagram for the Moyale amphibolites. Dividing line for tholeiitic suites from Irvine and Baragar (1971). The dashed calc-alkaline ('Cascades') trend from Carmichael et al(1974).

into three types. Type I peridotites and associated volcanic rocks contain spinels with Cr # <0.60, Type III peridotites have Cr # >0.60 and Type II is a transitional group spanning the full range of spinel compositions of Types I and III peridotites. According to this classification the Kangura (Baragoi) chromites are Type III, which are analogues of arc - related volcanic rocks, (related to the earliest stages of arc formation in oceanic crust environments). The Moyale chromites (Debel area) could be classified as Type II because their composition falls between Cr # 0.64 and 0.53. This reflects a composite origin such as the formation of an island arc on ocean crust (Dick and Bullen, 1984), or form lithosphere formed at the earliest stages of arc or continental rifting.

3.7 PLAGIOCLASE AMPHIBOLITES

3.7.1 Introduction

The plagioclase amphibolites which are considered to be metamorphosed lavas and dykes occur in two areas, around Moyale and in the Mash Hills area, which is 80 kms east of Moyale. In the Moyale area samples were collected from two localities; the Ulan Adake and the Mansille areas (Figure 3.3).

3.7.2 Major Elements

The AFM diagram (Figure 3.13) shows that almost all samples show Fe enrichment during early fractionation indicative of tholeiitic affinities. However, as has already been discussed in section 2.5.2 misclassification can arise in AFM diagrams because of mobility of major elements, especially the alkalis.

The mafic rocks plot as one major group as defined by NiO and Al_2O_3 against TiO_2plots (Figures 3.14a and 3.14b). However, samples SM29 and SM30 plot separately in the Ni-TiO_2 plot. These are considered as mafic melts contaminated with crust. These rocks have high Cr (1300-1809 ppm) and Ni (373-559 ppm) and elevated Zr, Y and Ba (see Appendix B). The plagioclase amphibolites have low Al_2O_3 (8-15%) content and low Ni abundances (10-150 ppm) except for SM29 and SM30 which range from 373-560 ppm. The wide range in Ni content and significant TiO_2 variations probably reflect fractionation of mafic phases.

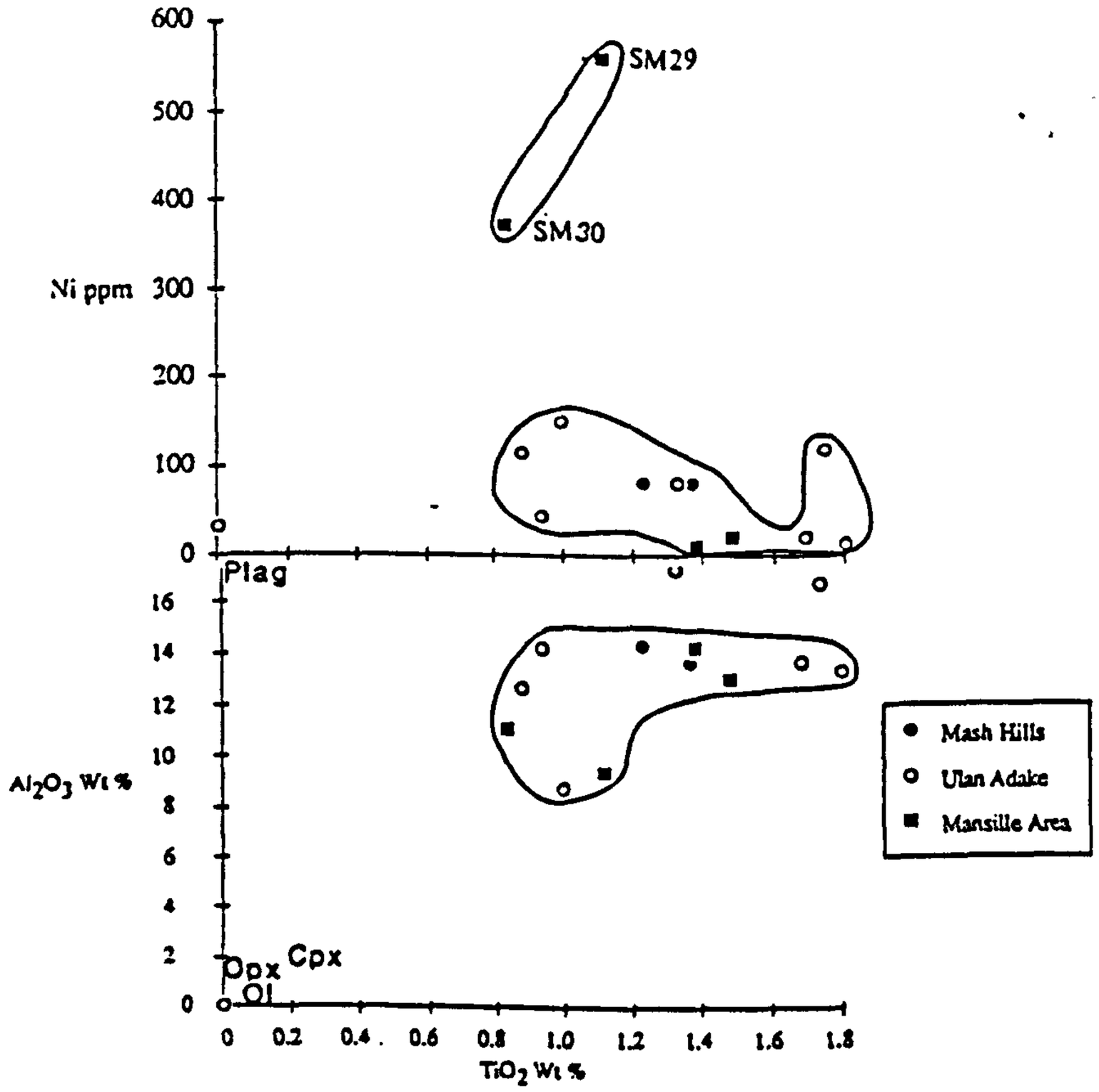

Figure 3.14 Variation of TiO_2 vs Ni and Al_2O_3 for the Moyale amphibolites. In both diagrams the mafic rocks plot as one major group. Samples SM29 and SM30 plot separately in the TiO_2 plot.

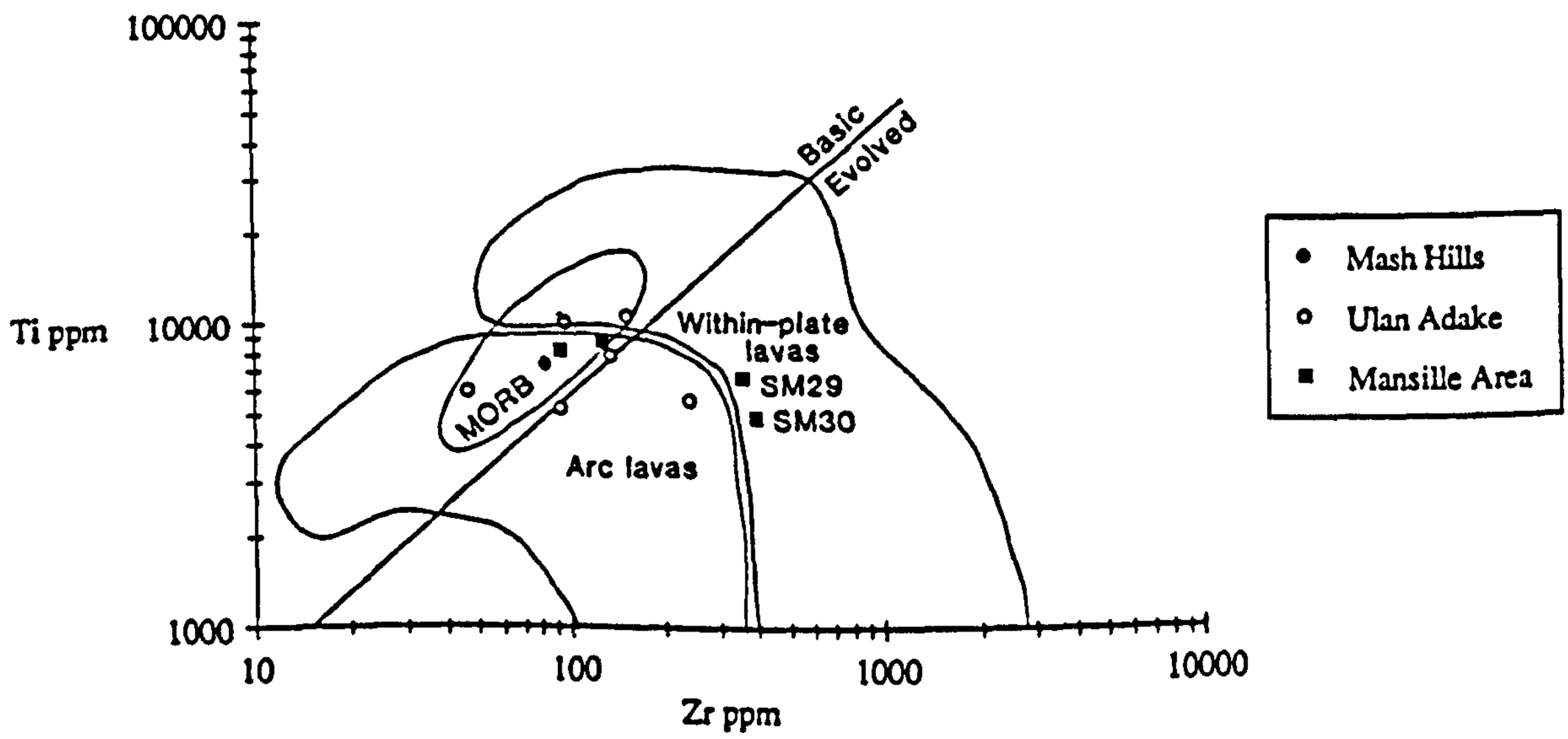

Figure3.15 Ti-Zr co-variation diagram for the Moyale amphibolites. Fields taken from Pearce(1980).

3.7.3 Trace Elements

Since major elements have been mobilised by secondary processes, the discussion will concentrate on high field strength elements Ti, Y, Zr, Nb, Cr and Ni which appear to be relatively immobile (Pearce, 1975).

On a Ti vs Zr diagram (Figure 3.15) the plagioclase amphibolites of Ulan Adake and Mash Hills area plot in the MORB/IAT field, but two samples (SM29 and SM30) from Mansille area plot in the within-plate field.

In the Ti-Zr-Y diagram (Figure 3.16) the lavas plot in the Ocean Floor Basalt field. Although this diagram does not distinguish between ocean floor and volcanic arc origin, it definetely rules out a within-plate setting for most of the Moyale lavas. However, two samples (SM 29 and SM30) from Mansille area show enrichment in Zr, hence plot away from the discriminant fields.

In a Zr/Y vs. Zr (Figure 3.17) discriminant diagram (Pearce and Norry, 1979) two lavas which have been classified as arc lavas in the Ti-Zr plot, plot in the within-plate field, while two samples (SM29 and SM 30) from the Mansille area plot outside the discriminant field. This separation is accounted for by higher mean Zr values in MORB lavas. The rest of the lavas plot in the MORB field.

Ti vs. Cr plot distinguishes between fractionation suites and reflects parental liquid compositions, and is useful in distinguishing ocean floor from island - arc basalts (Pearce, 1975). In this plot (Figure 3.18) the lavas plot dominantly in the MORB field, supporting the Ti-Zr plots.

The most informative trace element co-variation diagram that shows evolution trends in these lavas is Ti/Cr vs. Ni (Figure 3.19). Since both Cr and NI are compatible during basaltic fractionation their abundances decrease, while Ti is incompatible and increases until magnetite begins to crystallise. Hence Ti/Cr should also increase during fractionation. The evolution trend has a gradient that is between the vectors for olivine and pyroxene fractionation. In this diagram the Mash Hills lavas plot in the MORB field, while the Ulan Adake lavas plot in the MORB and IAT fields which is consistent with all the other discriminant diagrams. However, the Mansille plagiocalse amphibolites are spread in all the discriminant fields, because of variable Ti/Cr ratios which reflects variable Cr values.

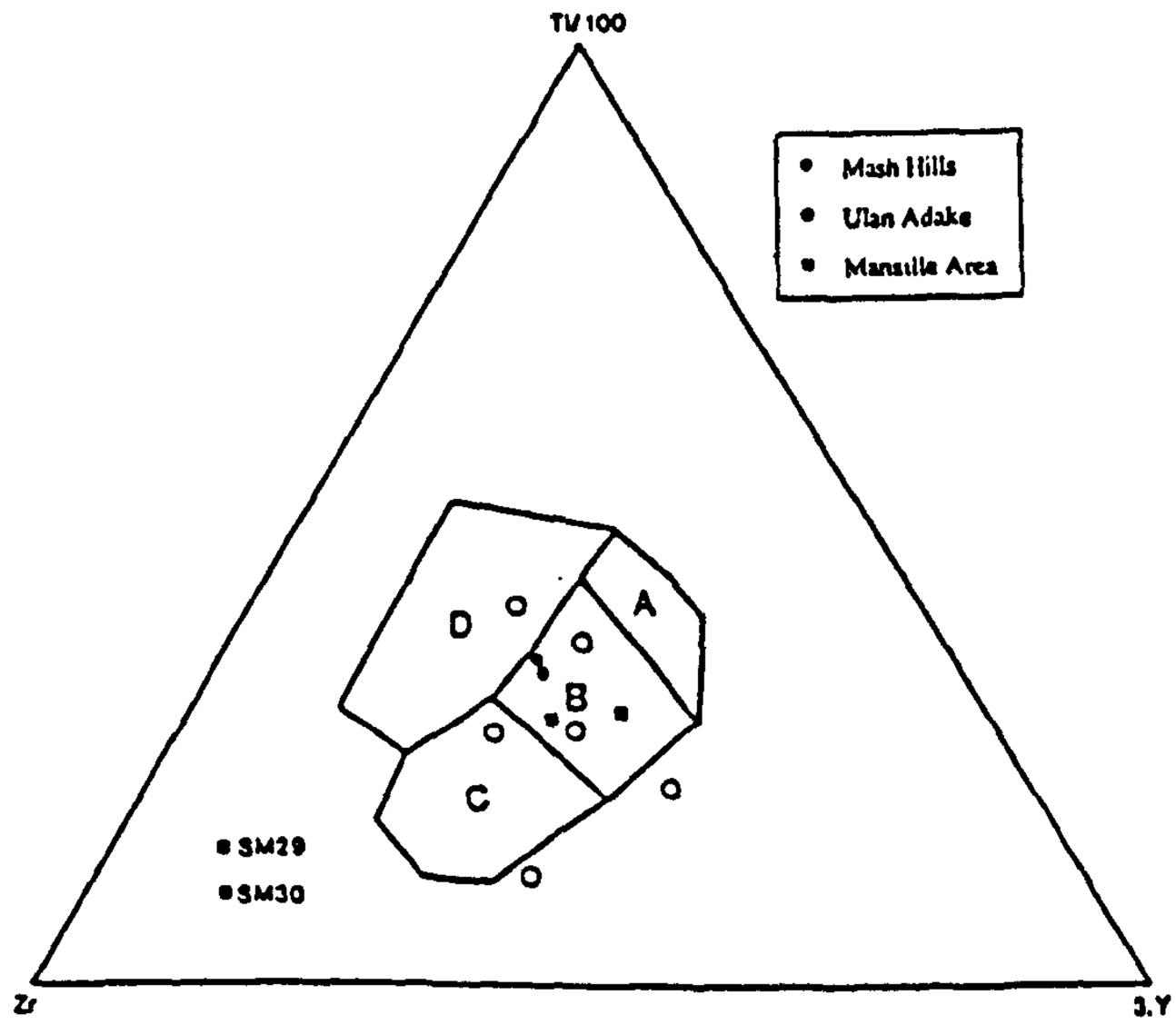

Figure 3.16 Ti-Zr-Y discriminant diagram (Pearce and Cann,1973) showing the distribution of the investigated Moyale amphibolites and dykes. SM29 and SM30 plot outside the discriminant fields. Within-plate basalts plot in field D, ocean floor basalts in field B, low potassium tholeiites in fields A and B, calc-alkali basalts in fields C and B.

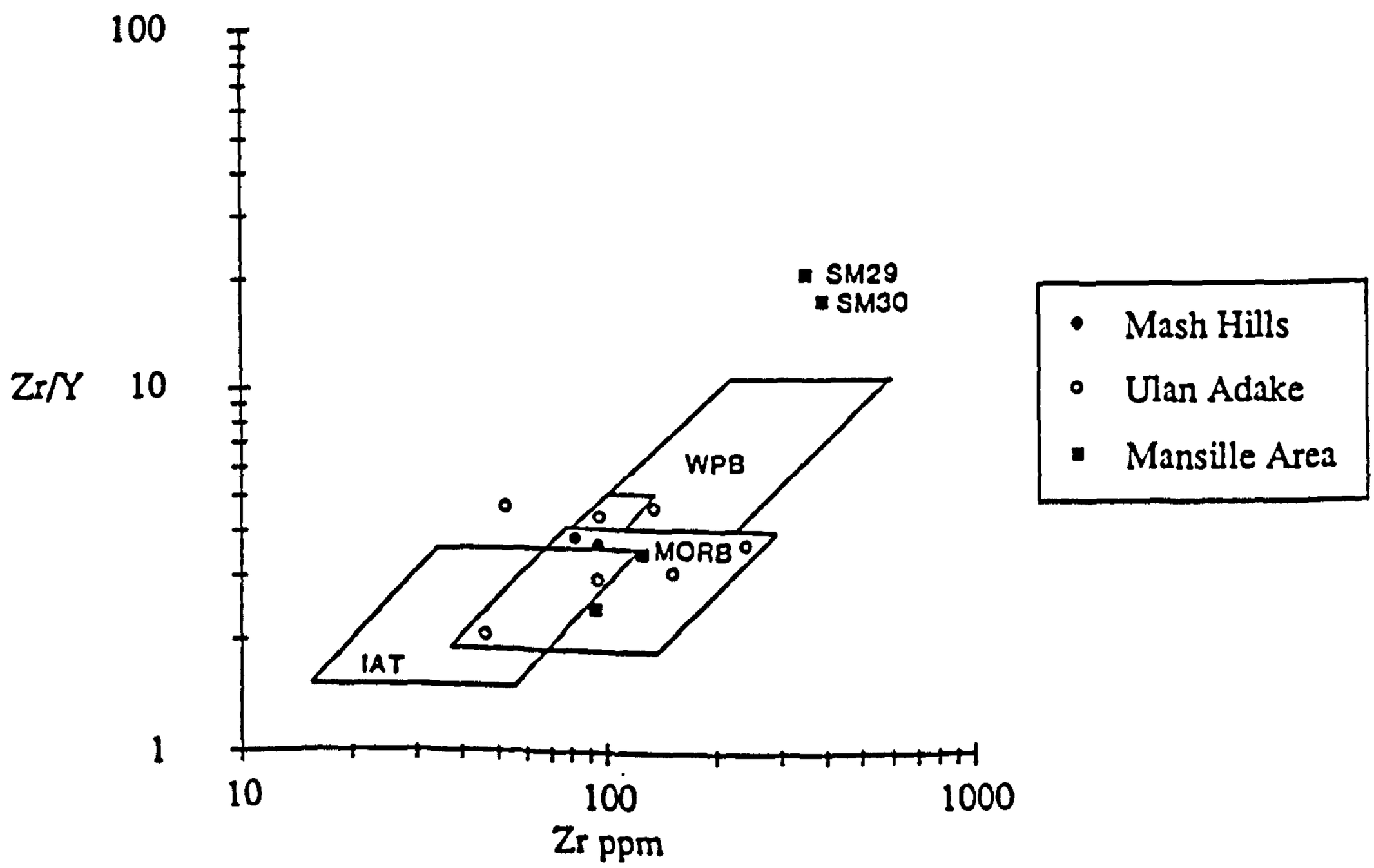

Figure 3.17 Zr/Y-Zr discriminant diagram for the Moyale amphibolites and dykes. SM29 and SM30 plot outside the discriminant fields. Fields taken from Pearce and Norry (1979).

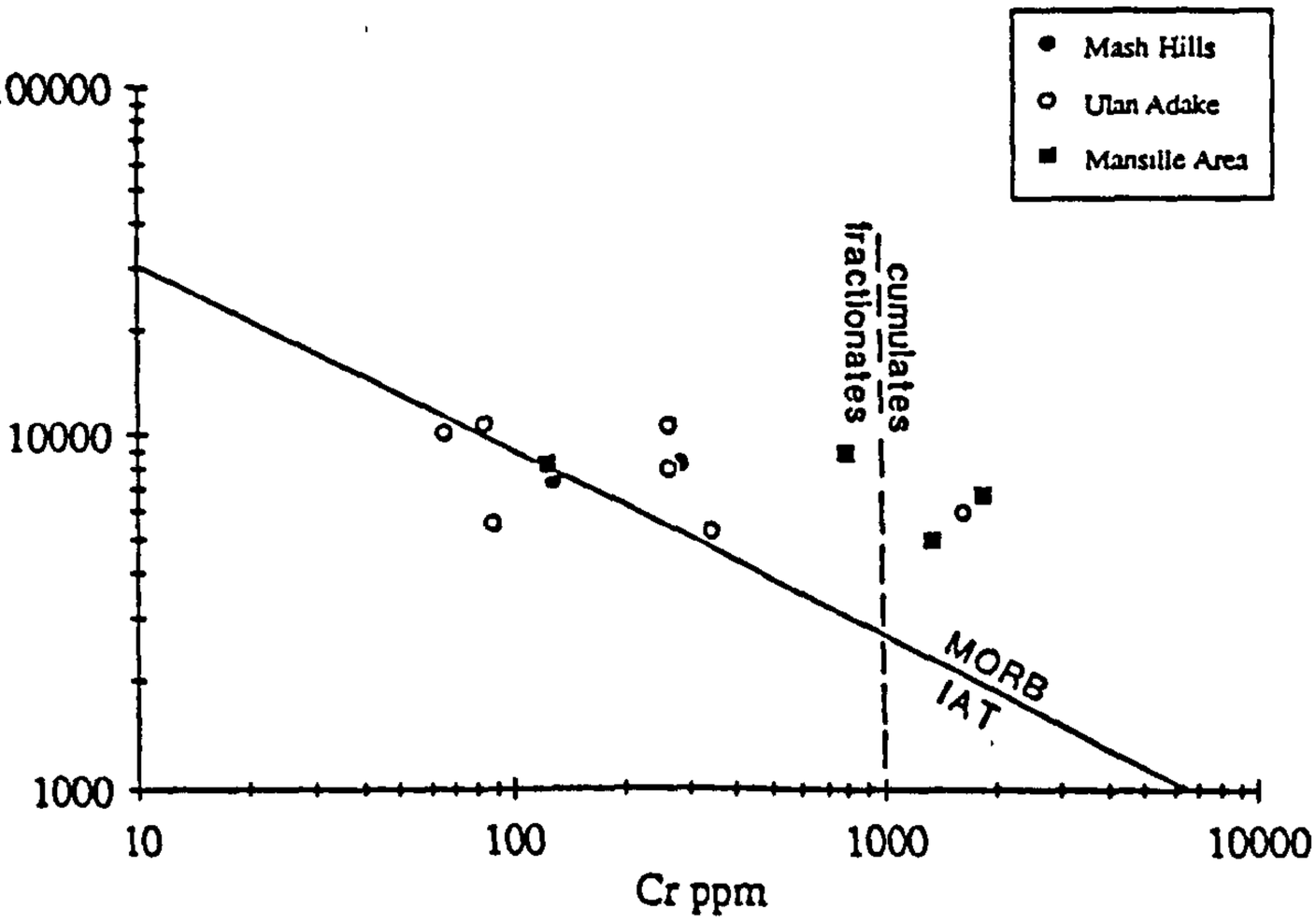

Figure 3.18 Ti-Cr diagram. This plot differentiates between fractionation suites and reflects parental liquid compositions and is useful in distinguishing ocean floor and island-arc basalts (Pearce,1975). All the lavas plot in the MORB field.

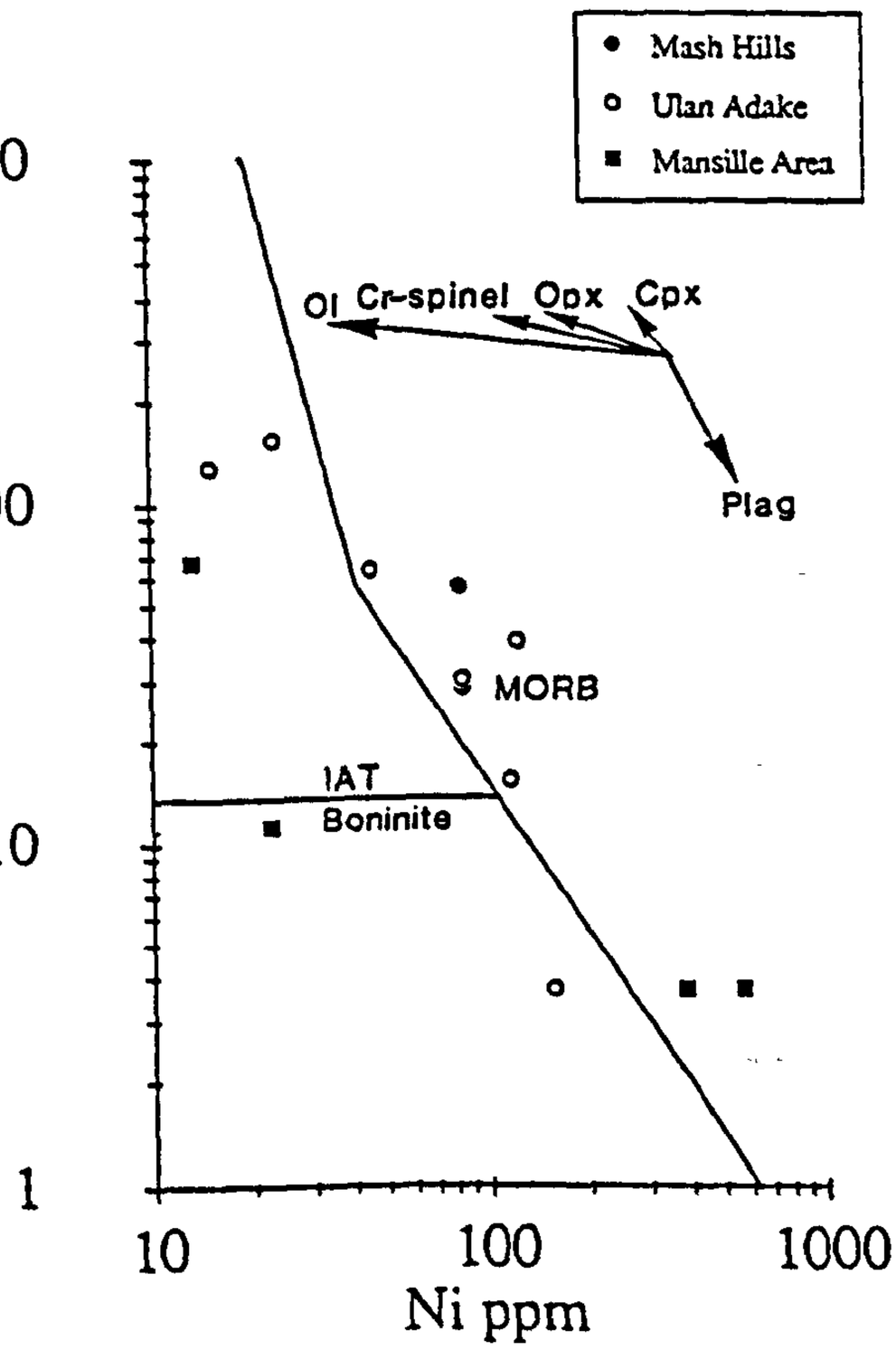

Figure 3.19 Ti/Cr-Ni diagram showing distribution ofMoyale amphibolites and dykes. Fields from Beccaluva et al (1983).

In summary it is concluded that the Moyale mafic rocks have subduction-related and MORB geochemistry. Hence it is suggested that this complex is a piece of oceanic lithosphere and forms part of an ophiolite.

3.8 GRANITOID GEOCHEMISTRY

3.8.1 Introduction

Six intrusive granitic bodies were studied geochemically from the Adola-Moyale belt, in order to observe variations in major and trace elements and to establish their tectonic setting. For this purpose thirty-eight granitoid samples were analysed. Major and trace element data are presented for a wide variety of Adola-Moyale granitoids (Appendix B). The granitoid suites studied from NE Kenya are the Kufole, Fugugo, Moyale and Adadi Jolle plutons, while the Gariboro and Godoloka granites have been studied from the Adola area, Southern Ethiopia. Although the localities of the granitoids in the Adola and the Moyale areas are separated by about 180 kms they lie along the same belt. An improved understanding of their genesis and tectonic setting would elucidate the overall tectonic evolution of the belt.

Each granitoid suite has been classified according to the Streckeisen classification scheme (Streckeisen,1975) using a Norm program (N.W. Harris, pers. comm.) for recalculation of major element analysis into mineral phases in granitic system (Figure 3.20a). The Kufole and Adadi Jolle granitoids fall in the granite field, while the Moyale granodiorites extend from the granodiorite to the granite field. The Fugugo which has low quartz content plots in the monzonite field. The Gariboro and the Godoloka granitoids of the Adola area lie in the granitic field (Figure 3.20b). Normative proportions of minerals are given in Appendix B.

In general the classification of granitoids is problematical and several classification schemes have been published (Peacock, 1931; Shand, 1951; Pearce *et al.*, 1984a; Harris *et al.*, 1986). The approach has been to combine several geochemical parameters to classify and establish the tectonic setting of the granitoids.

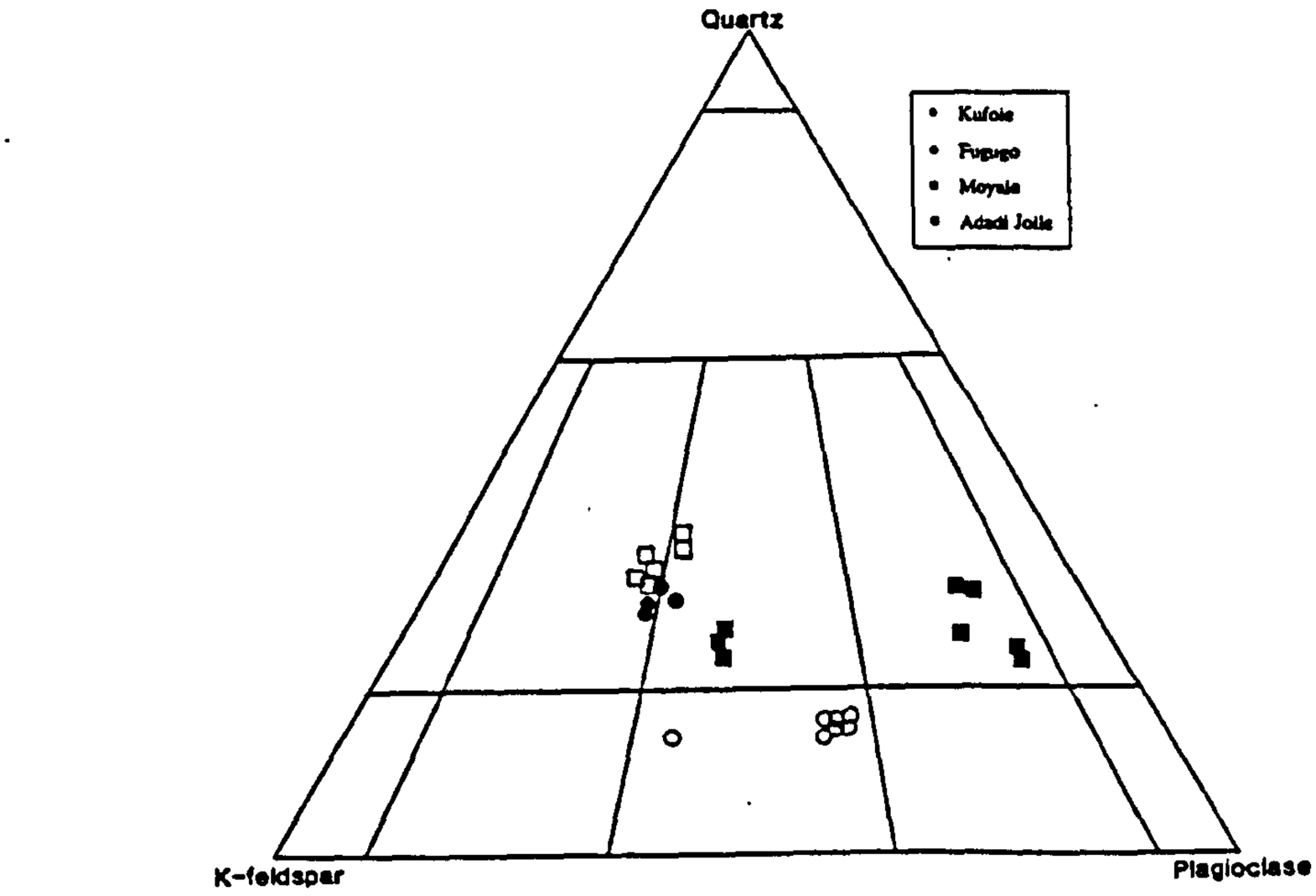

(a)

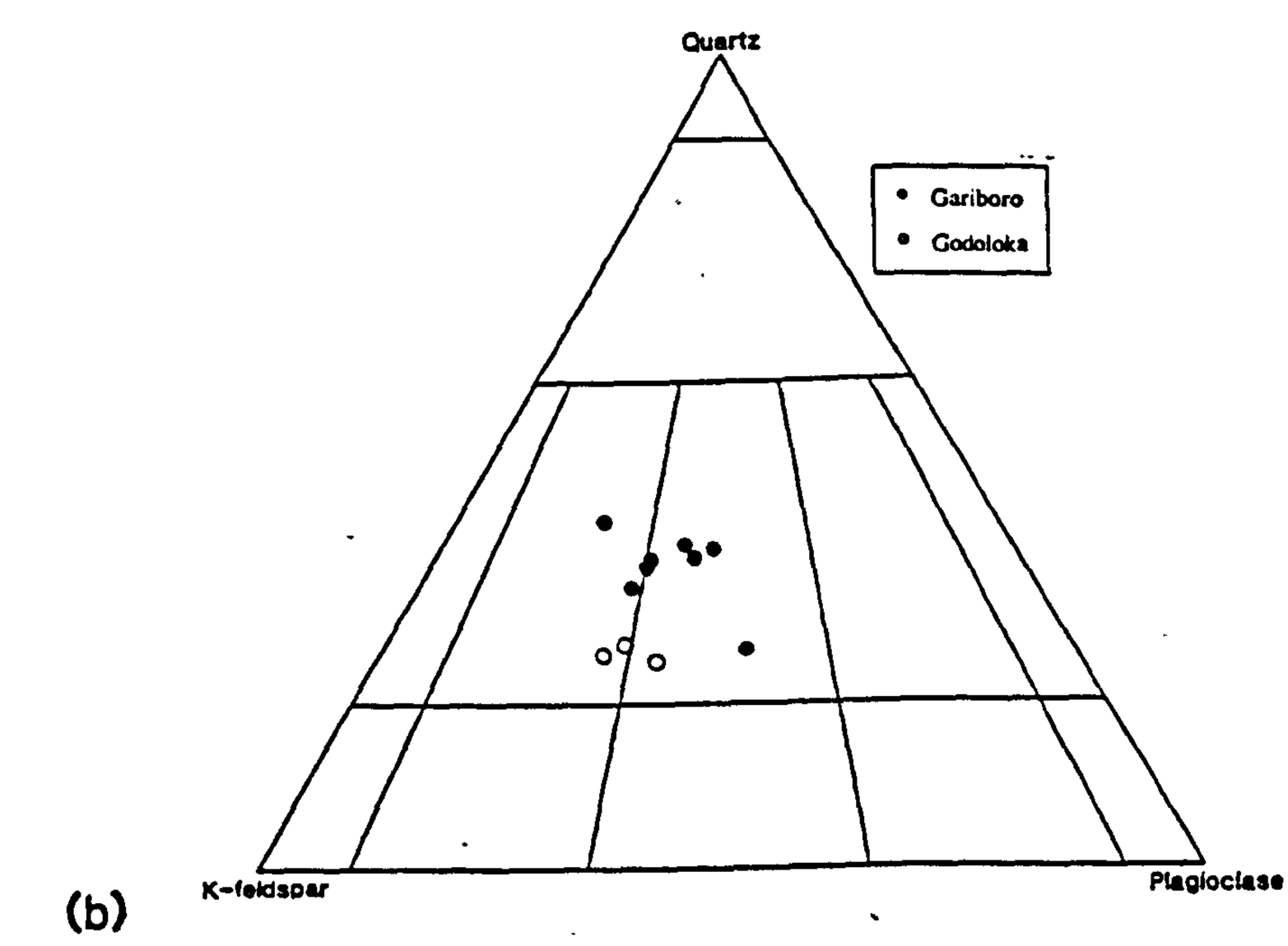

(b)

Figure 3.20 (a) Streckeisen diagram showing representative samples from the granitoids of NE Kenya. **(b)** Streckeisen diagram showing representative samples from the granitoids of the Adola area, S Ethiopia. Modal analyses are based on Norm program developed by Nigel Harris for recalculation of major element analysis into minor phases.

The Adola-Moyale belt granitoids are subdivided in the field into syntectonic and post-tectonic granites, while petrographically they form six distinct plutons. Two geochemically distinctive granitoid types have been identified in the Adola-Moyale belt. These are the volcanic arc and within-plate granitoids as defined by discriminant diagrams (Pearce *et al.*,1984a).

The degree of alumina saturation allows the classification of the granitoids (Shand, 1951; Chappell and White, 1974). The molecular ratio (% $Al_2O_3/CaO+Na_2O+K_2O$) is used to classify the granitic rocks into peraluminous, metaluminous and peralkaline granites (Shand, 1951).

Peraluminous granitoids - $Al_2O_3 > Na_2O + K_2O + CaO$

Metaluminous granitoids - $Na_2O + K_2O < Al_2O_3 < Na_2O + K_2O + CaO$

Peralkaline granites - $Al_2O_3 < Na_2O + K_2O$.

There is little consensus as to whether peraluminous grantoids require peraluminous source rocks. Miller (1985) argues that while most peraluminous granitoids are derived from continental crustal material, a sedimentary source is not necessarily required to generate peraluminous magmas and White *et al.* (1986) argue that only strongly peraluminous cordierite-bearing granitoids require a sedimentary source. Hence, the Adola-Moyale granites could not be classified as melts of peraluminous source as they are not strongly peraluminous, since they have A/(CNK) (% $Al_2O_3/CaO+Na_2O+K_2O$) ratios less than 1.1.

Variations in the molecular proportions of alumina, alkalies, and CaO have been plotted in a triangular diagram (Figures 3.21a and 3.21b). The Adadi Jolle granitic gneisses and the Kufole granites plot in the peraluminous field, while the Fugugo granites plot in the metaluminous field. The Moyale granodiorites plot on the boundary between metaluminous and peraluminous. Figures 3.22a and 3.22b are plots of the Shand Index (Shand, 1951) against the HFS elements Nb+Y (Pearce, *et al.*, 1984a). It is observed that Adadi Jolle and Kufole granitoids, and early gneissose granites are peraluminous, while Fugugo granites are metaluminous. The two granitic suites of the Adola area plot in the peraluminous field (Figure 3.21b), whereas in the Nb+Y vs Shand Index plot they are close to 1 (Figure 3.22b). Most of the granitoids except Fugugo plot within the peraluminous field.

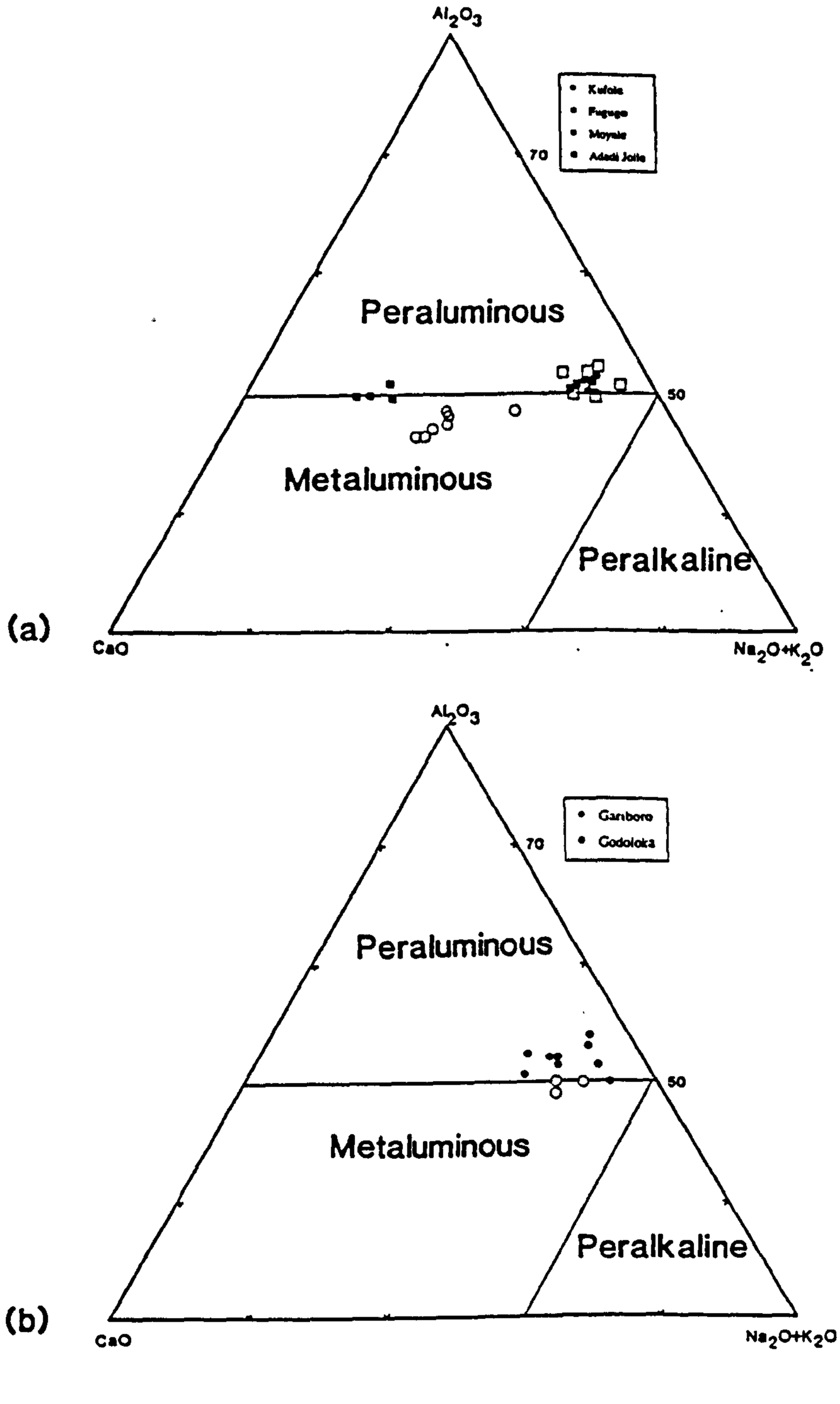

Figure 3.21 (a) Alumina/CaO/alkalis triangular diagram showing granitoids of the Moyale area., NE Kenya. Kufole, Moyale and Adadi Jolle plot in the peraluminous field, while Fugugo plots in the Metaluminous field. **(b)** Alumina/CaO/alkalis triangular diagram showing granitoids of the Adola area., S Ethiopia. The Gariboro granitoid gneisses plot in the peraluminous field, while the Godoloka plot in the metaluminous field.

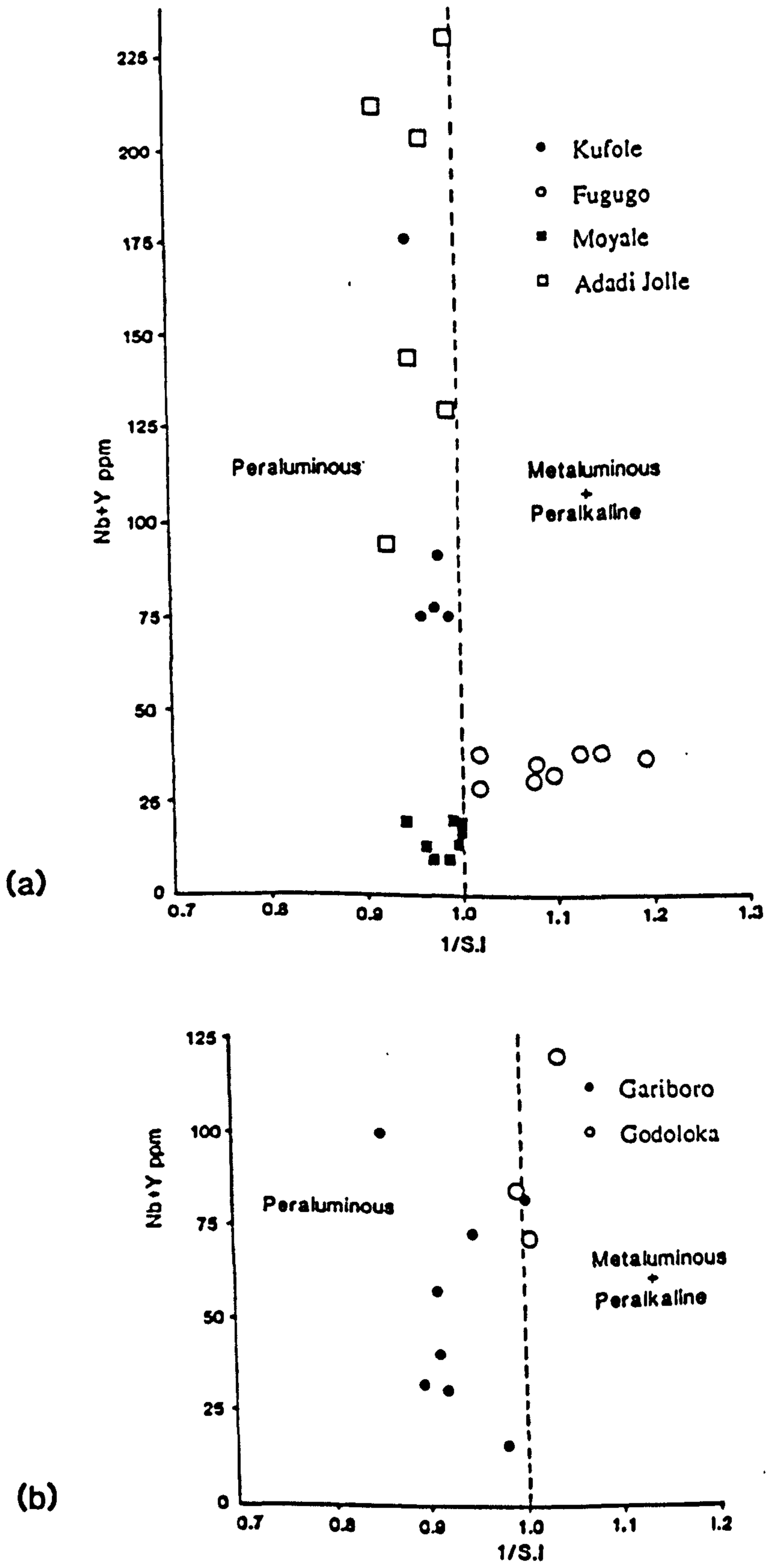

Figure 3.22 (a) Plot of 1/Shand Index (CNK/A) vs the high field strength (HFS) elements Nb+Y for NE Kenya granitoids. All the granitoids except Fugugo plot in the peraluminous field. **(b)** Plot of 1/Shand Index (CNK/A) vs the high field strength (HFS) elements Nb+Y for Adola belt granitoids. Gariboro plot in the peraluminous field, while the Godoloka granite is metaluminous.

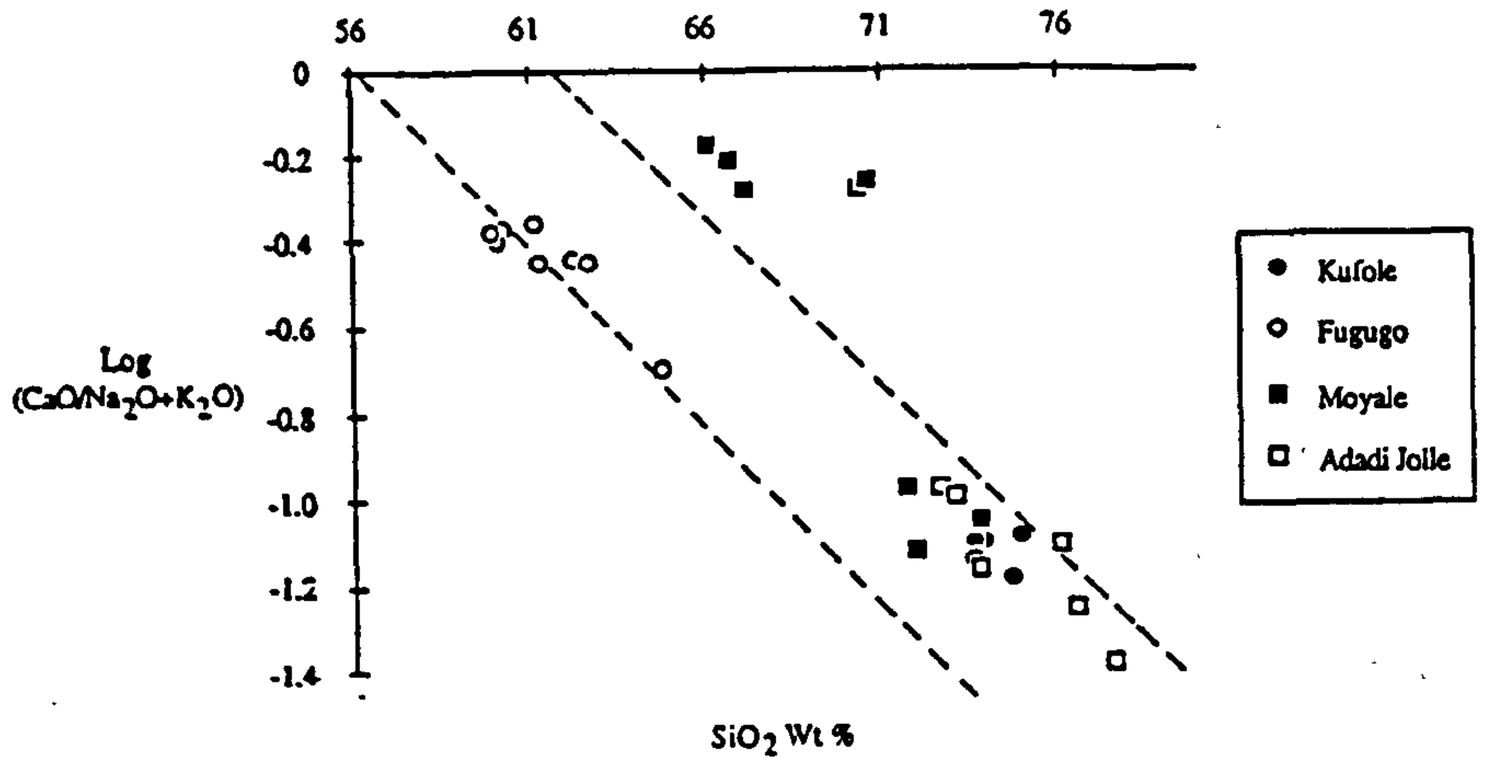

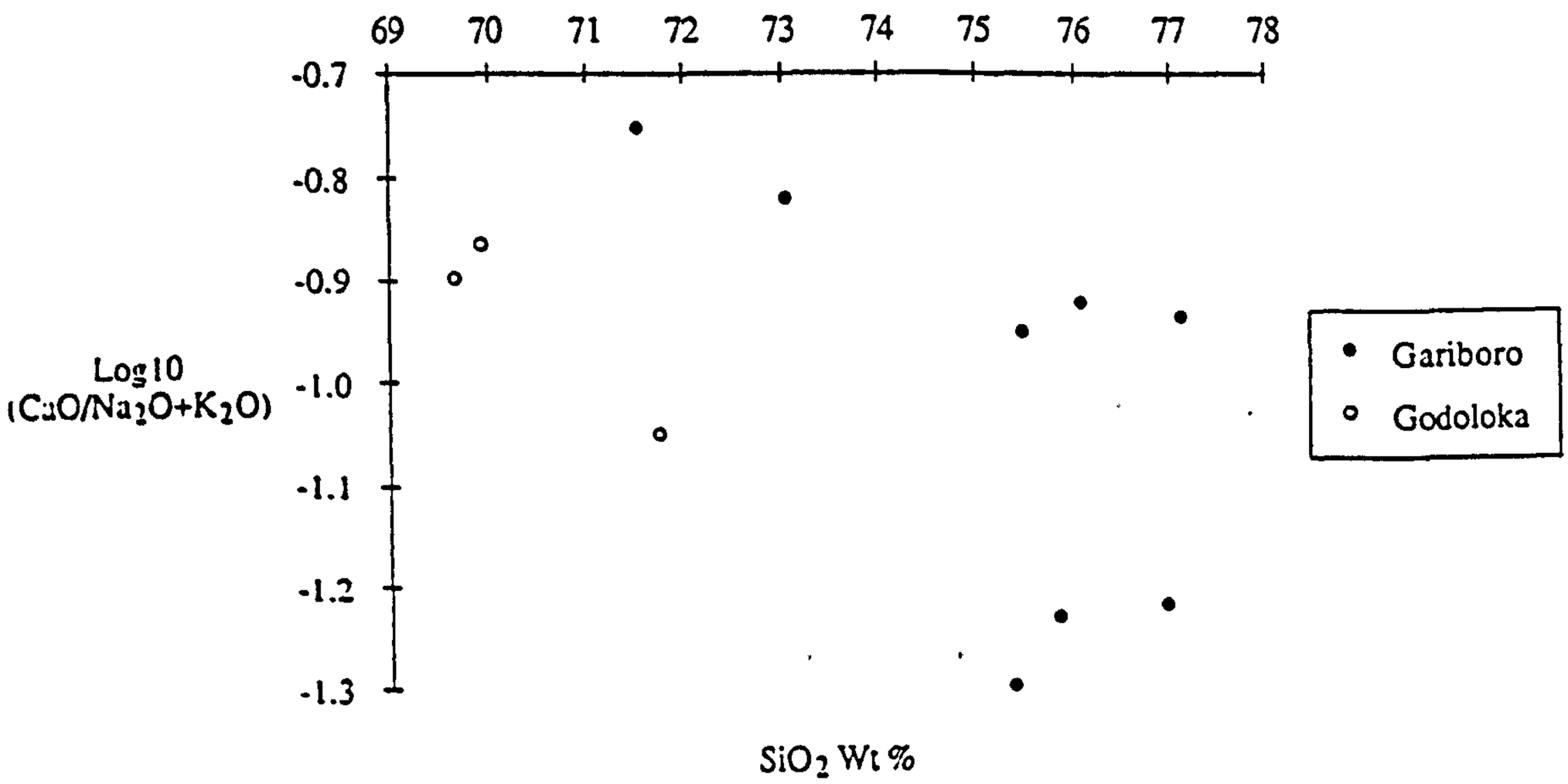

Figure 3.23 (a) Calcium oxide/alkalies vs silica diagram for NE Kenya granitoids. Calc-alkaline field after Brown(1979). Kufole, Moyale and Adadi Jolle granitoids plot in the calcic field (Peacock,1931) while Fugugo granitoids are calc-alkaline. **(b)** Calcium oxide/alkalies vs silica diagram for Adola belt granitoids. Calc-alkaline field after Brown(1979).

In the Peacock alkali-lime classification (Brown *et al.*, 1979) the Kufole, Moyale and Adadi Jolle granitoids plot in the calcic field, whereas the Fugugo granites plot in the calc-alkaline field (Figure 3.23a). The Gariboro granitoid gneiss and the Gariboro granites plot as calc-alkaline (Figure 3.23b).

3.8.2 Harker Variation Diagrams

Harker variation diagrams are presented for six granitoid suites. These diagrams suggest that major and trace elements in individual intrusives behave in a coherent manner and thus reflect igneous processes (Figure 3.24 and 3.25).

The SiO_2 values of the Kufole granites vary from 73.57 to 74.90 wt % and plots of SiO_2 against all major trace elements show a restricted composition. The Fugugo granitoids show a wide compositional range. SiO_2 values vary from 59.94 to 62.68 wt%. Plots of SiO_2 vs. all major and trace elements (Figure 3.24) show linear trends except plots against Na_2O and Zr. The Kufole granites are compositionally more 'evolved' than the Fugugo granites because they have higher SiO_2 and lower TiO_2, Fe_2O_3, MnO and MgO.

The Adadi Jolle granites have SiO_2 values ranging from 72.63 to 77.55 wt %. Plots of SiO_2 vs. TiO_2, Fe_2O_3, MgO, CaO, K_2O, P_2O_5, exhibit tightly defined linear trends. The Moyale granodiorites exhibit a wide SiO_2 range from 66.11 to 73.79 wt%. TiO_2, Al_2O_3, Fe_2O_3, MgO, CaO and P_2O_5 contents decrease as SiO_2 increases.

The Kufole granite is characterised by higher Rb and lower Sr, contents than the Fugugo granites. Ba, and Sr decrease with increasing SiO_2 in the Fugugo granites. The decrease of Ba and Sr reflects feldspar and biotite removal.

In the Adadi Jolle granitic gneiss Ba, Sr, Zr and Th decrease with increasing SiO_2, while Rb remains constant and Nb and Y are incompatible. The sharp decrease in Zr reflects zircon crystallization. Since this intrusion shows coherent trace element patterns it is selected for trace element modelling.

The Moyale granodiorites show a decrease in Sr with increase in SiO_2 suggesting that plagioclase removal was an important petrogenetic process, while Y, Zr and Nb remain constant. Ba, Rb and Nb are the only incompatible elements analysed.

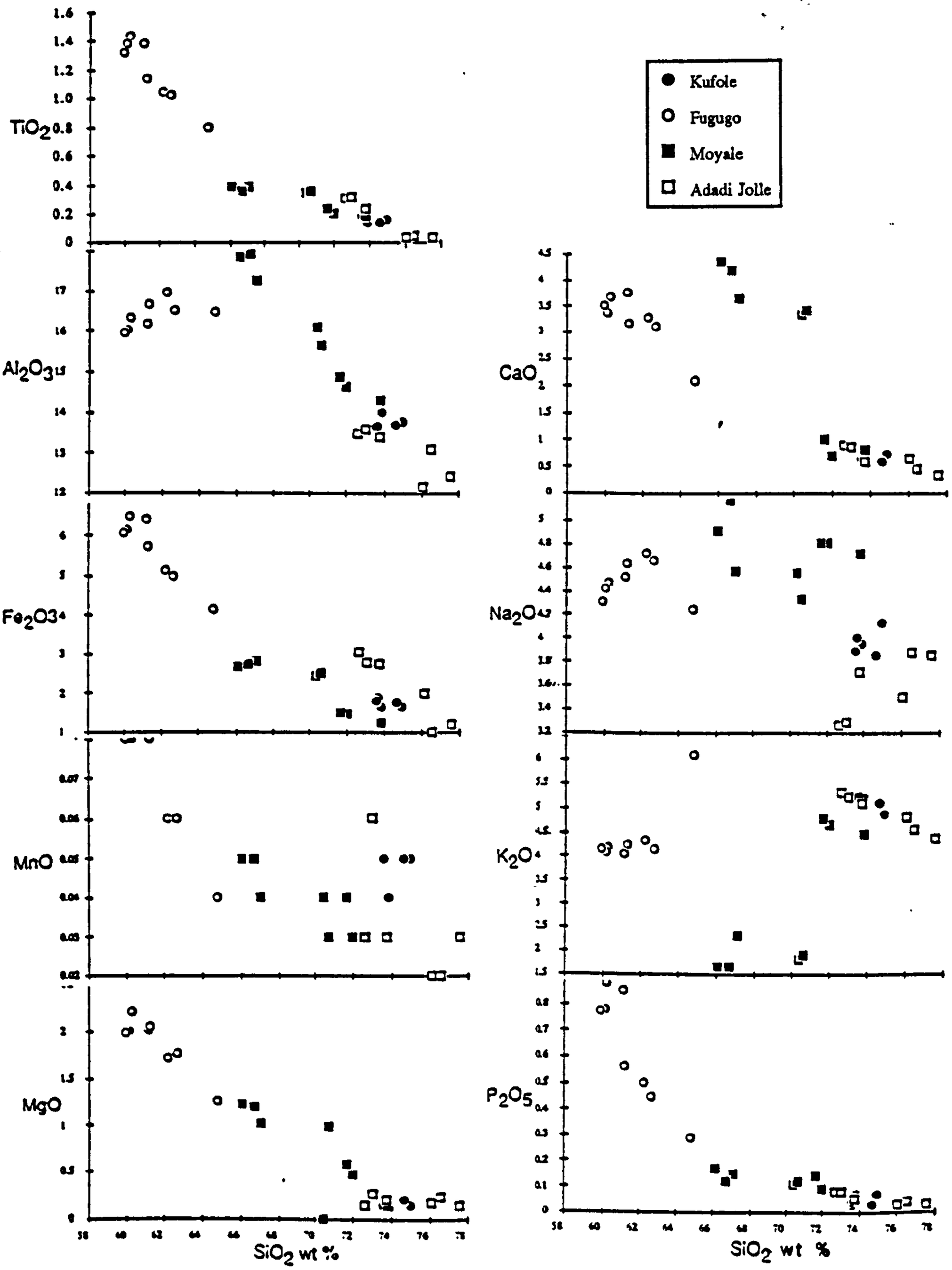

Figure 3.24 Harker variation diagrams for the NE Kenya granitoids.

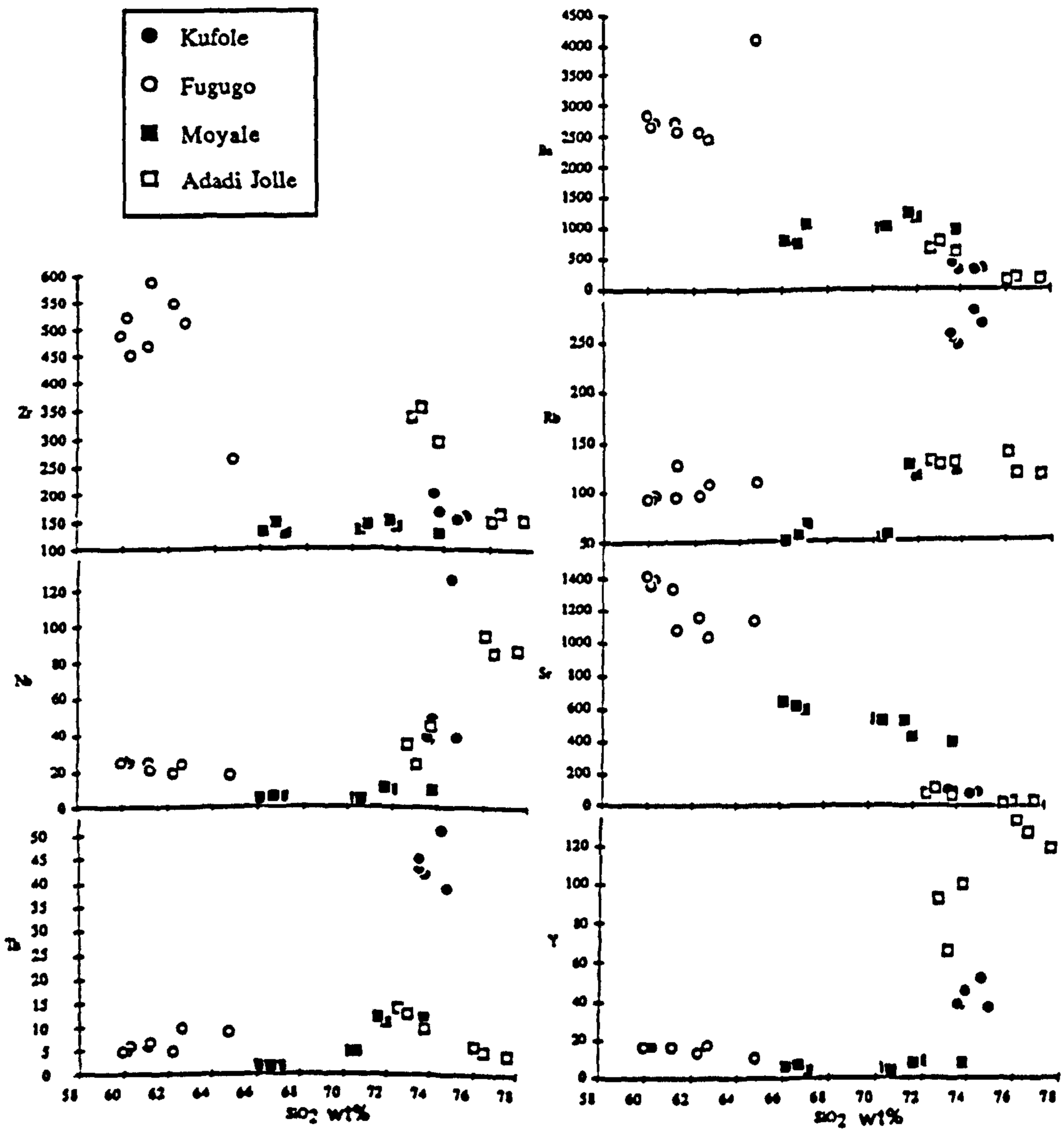

Figure 3.24 Harker variation diagrams for the NE Kenya granitoids.

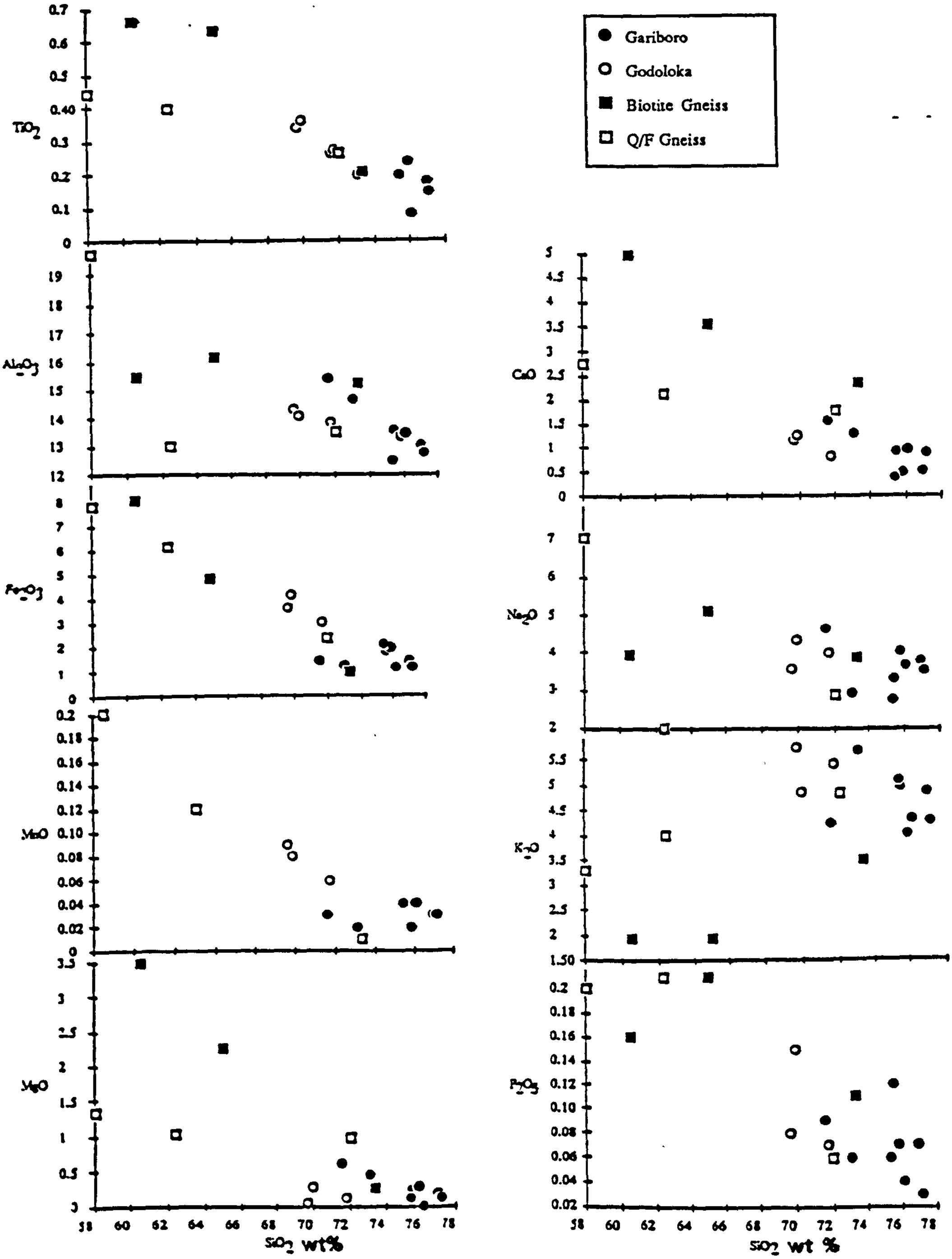

Figure 3.25 Harker variation diagrams for the S Ethiopia granitoids.

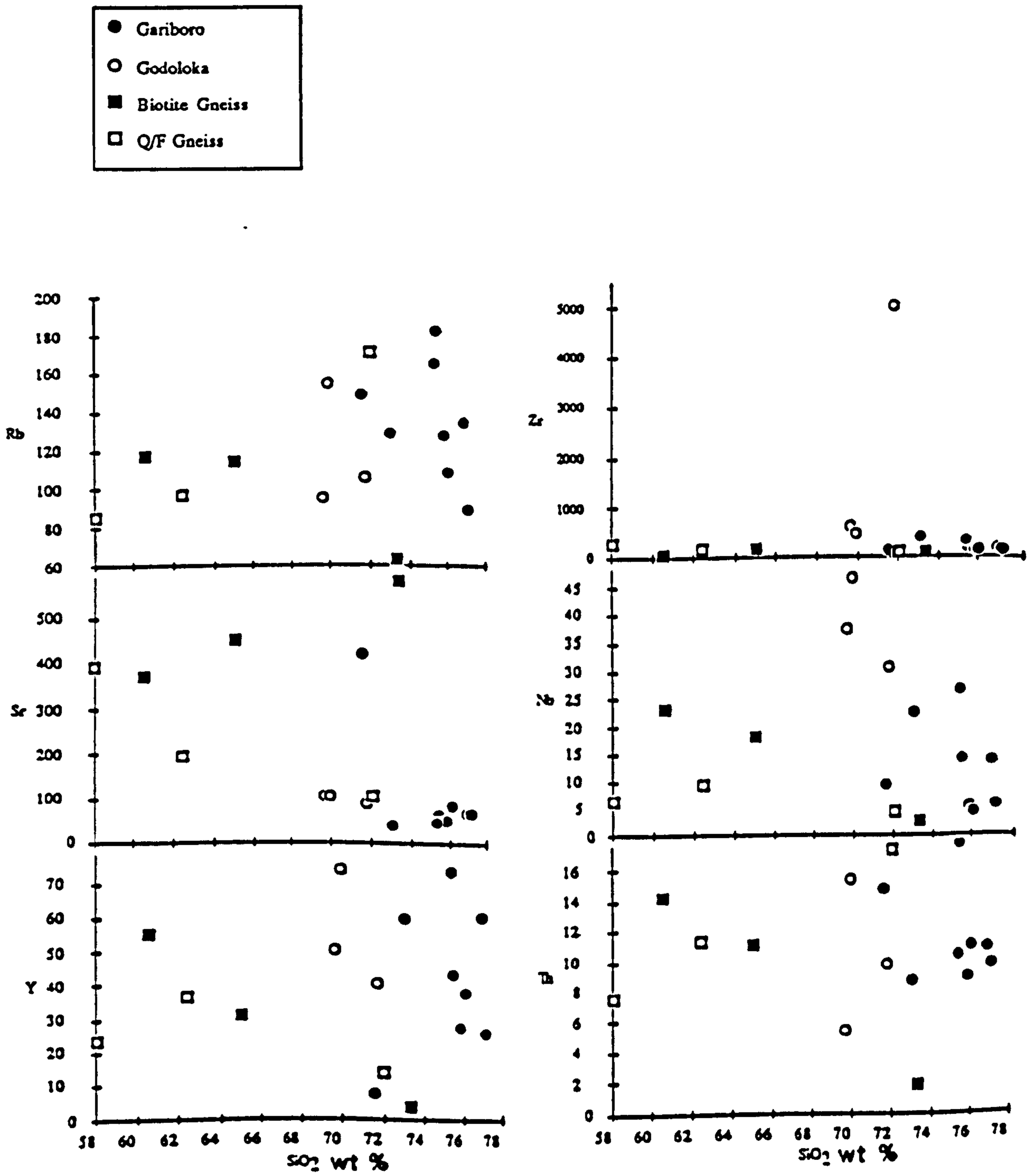

Figure 3.25 Harker variation diagrams for the S Ethiopia granitoids.

In the Adola area the Gariboro granitic gneisses exhibit SiO_2 values ranging from 71.52 to 76.94 Wt%. Al_2O_3, MgO, CaO and P_2O_5 decrease with increasing SiO_2 Wt%. The Godoloka granites are compositionally restricted, their SiO_2 values range from 69.66 to 71.74 Wt%. TiO_2, Al_2O_3, Fe_2O_3, MnO, CaO and P_2O_5 decrease with increasing SiO_2 content. Both the Godoloka and Gariboro granites do not show coherent trace element co-variation diagrams, possibly because of a restricted SiO_2 range. The granitic gneiss show a wide spread in Rb values, while Sr is quite low except for samples D10 and D6. Thus the Gariboro granitic gneiss can be split into two populations (see Figure 3.23b and 3.25). The Gariboro granitic gneisses are characterized by lower Nb than the Godoloka granites. However, both have similar Rb, Sr and Y values.

3.8.3 Characterising granites using trace elements

3.8.3.1 Introduction

Trace elements are powerful in characterising granitic sources, as has been demonstrated by Arth and Hanson (1975), Fourcadre and Allegre (1981), Pearce *et al.* (1984a) and Harris *et al.* (1986). However, granite petrogenesis is much more complex from that of basalt, because the observed trace element variations are affected less by the source composition but more by evolutionary petrogenetic processes such as crystal fractionation, volatile fluxing and stability of minor phases.

3.8.3.2 Trace elements

Rb-Sr plots are important in distinguishing the different granite types (Figure 3.27). In this plot Kufole granite has high Rb /Sr and the other samples have low Rb contents but are distinguished by their Sr values. In the Rb/Zr - SiO_2 plot (Figure 3.30), all the granites except the Kufole plot within the Group III granite field of Harris *et al.* (1986) which includes post-collision and subduction related intrusions. The Kufole granite plots in the Group II crustal granite field of Harris *et al.* (1986) (Figure 3.28).

Trace element distribution patterns for six representative suites are illustrated in a spider diagram (Figures 3.26a, 3.26b and 3.26c). The trace element abundances have been normalised to the trace element pattern of an ocean ridge granite (ORG), (Pearce *et al.*, 1984a).

Trace element distribution patterns of the Kufole granites and the Fugugo granites are

compared (Figure 3.26a). The Kufole granites have elevated K_2O, Rb, Th, Ta and Nb, but have low Hf, Zr, Sm, Y and Yb. The exceptionally high Rb, Ce and Sm values relative to their adjacent elements, implies that it is a crustal granite. The Kufole granite has a negative Ba anomaly, which is typical of crustally derived granites, however it could simply reflect K- feldspar fractional crystallization. The geochemical pattern is intermediate between a within-plate and a syn-collision granite of Pearce *et al.*, (1984a). The Fugugo granites are enriched of K, Rb, Ba, Ce and Sm which is characteristic of volcanic arc granites.

In Figure (3.26b) the trace element patterns of Moyale granodiorites and Adadi Jolle granites are compared. The Moyale granodiorites have lower K_2O and are low in high field strength elements (eg. Ta, Nb, Zr, Y), whereas the Adadi Jolle granitoids have elevated K_2O and HFS elements suggesting within-plate characteristics. The Moyale granodiorite plot (Figure 3.26b) shows it to be similar to subduction-related granites with enrichment in LIL elements. In general, the calc-alkaline Moyale granodiorites have lower HFS elements and HREE than the within-plate Adadi Jolle granite and crustally contaminated granites have high Rb/HFS ratios and negative Ba.

McDermott (1986) suggested the Nb/Rb against Rb/Sr plot to be effective in discriminating the various granitic types of the Damara orogen, Namibia. Nb/Rb ratios discriminates between within-plate granitoids (Nb/Rb > about 0.1) and crustal melt granitoids which have low Nb/Rb ratios (< about 0.1). In Figure (3.29) the Fugugo and Moyale granodiorites are characterized by low Rb/Sr ratios and plot in the calc-alkaline field as compared to the within-plate Adadi Jolle, Kufole and Godoloka granites. However, the Gariboro post-tectonic granites have low Nb/Rb ratios and hence plot within the crustal melt field similar to the Damara (McDermott, 1986). Although the Kufole granites show slightly high Nb/Rb ratios and plot in the within-plate field, they have been shown to have high K_2O, low Ba and are low in HFS elements, consistent with crustal contamination.

The trace element abundances of the Gariboro granitoid gneiss and Godoloka granites are compared (Figure 3.26c). The similarity of these plots indicate that they may be genetically related although, the trace element abundances of the Godoloka granites are lower than those of Gariboro.

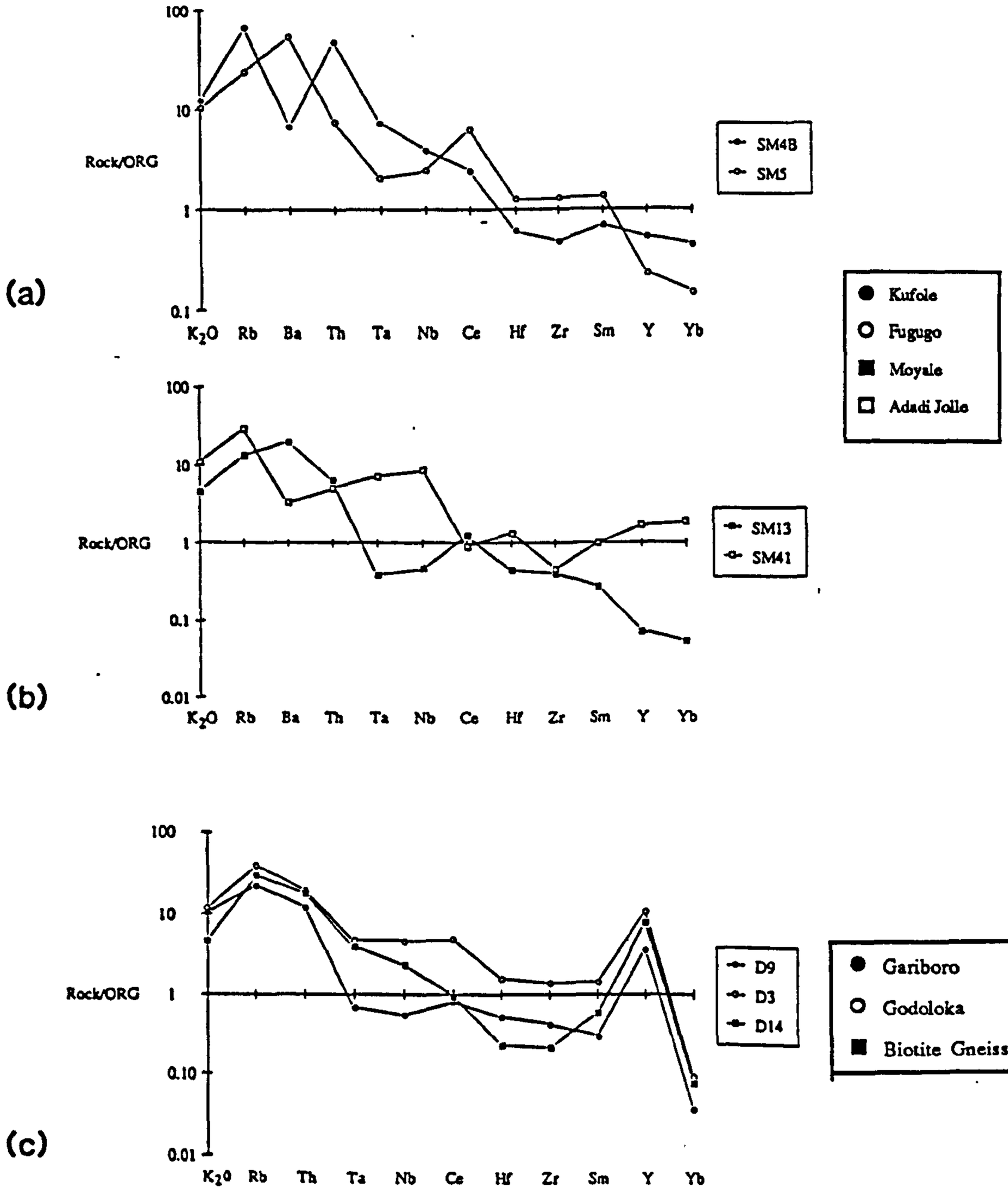

Figure 3.26 (a) Geochemical pattern diagrams for the Kufole and Fugugo granitoids. The Kufole granitoid is enriched in Rb, Th and the HFS elements Ta and Nb as well as REE's. The Fugugo has moderately elevated Rb, Ba and low high field strength elements. **(b)** Geochemical pattern diagrams for the Moyale and Adadi Jolle granitoids. Moyale has low HFS elements Ta, Nb, Zr and Y. Adadi Jolle is enriched in HFS elements Nb, Zr, Hf, Y as well as the REE's. **(c)** Geochemical pattern diagrams for the Gariboro and Godoloka granitoids. Gariboro has low HFS elements and low REE; Godoloka has high HFS, Ta, Nb, Zr, Y and high REE's. The biotite gneisses which were put for comparison show striking similarity in geochemical profile.

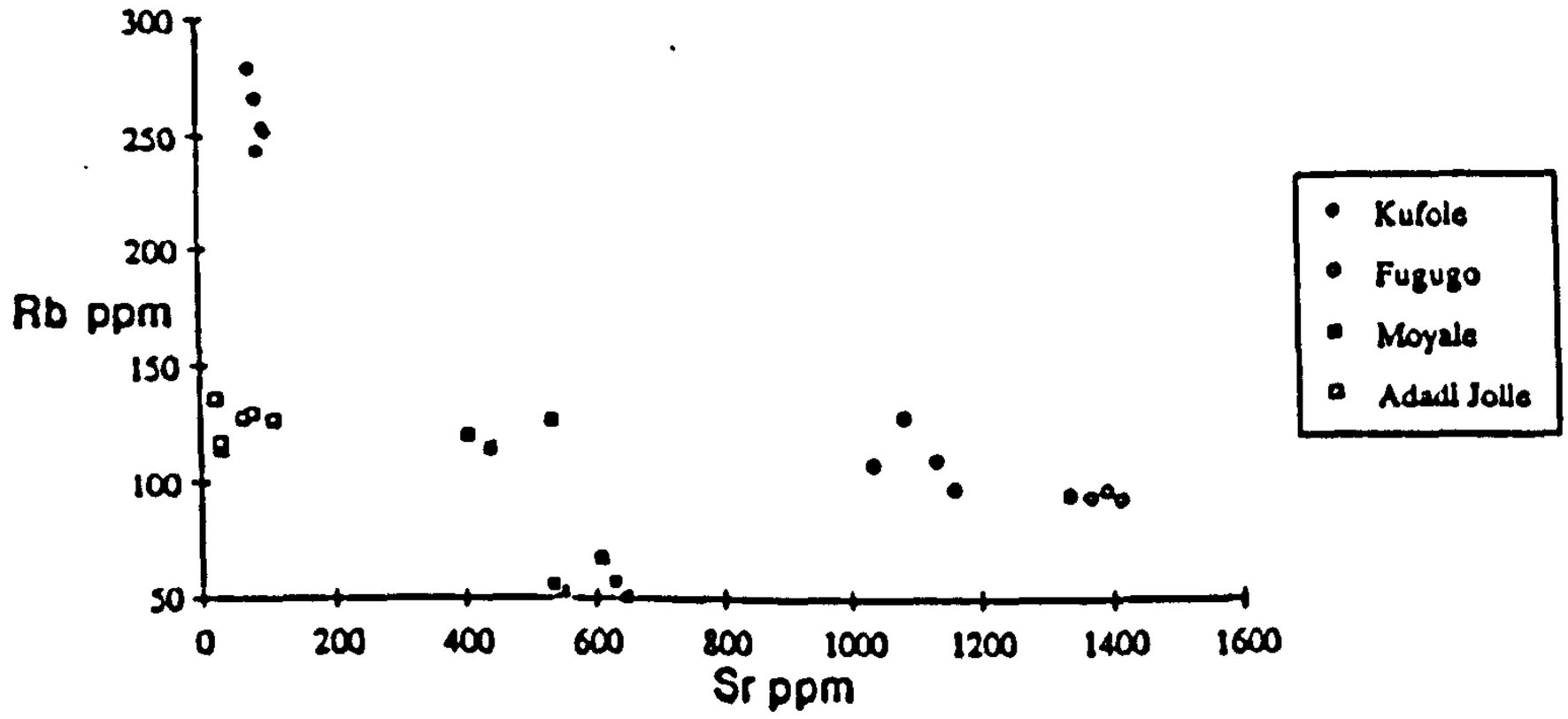

Figure 3.27 Rb-Sr plots for distinguishing the different granitoid types. The Kufole are highly enriched in Rb and Moyale granodiorites has the lowest Rb.

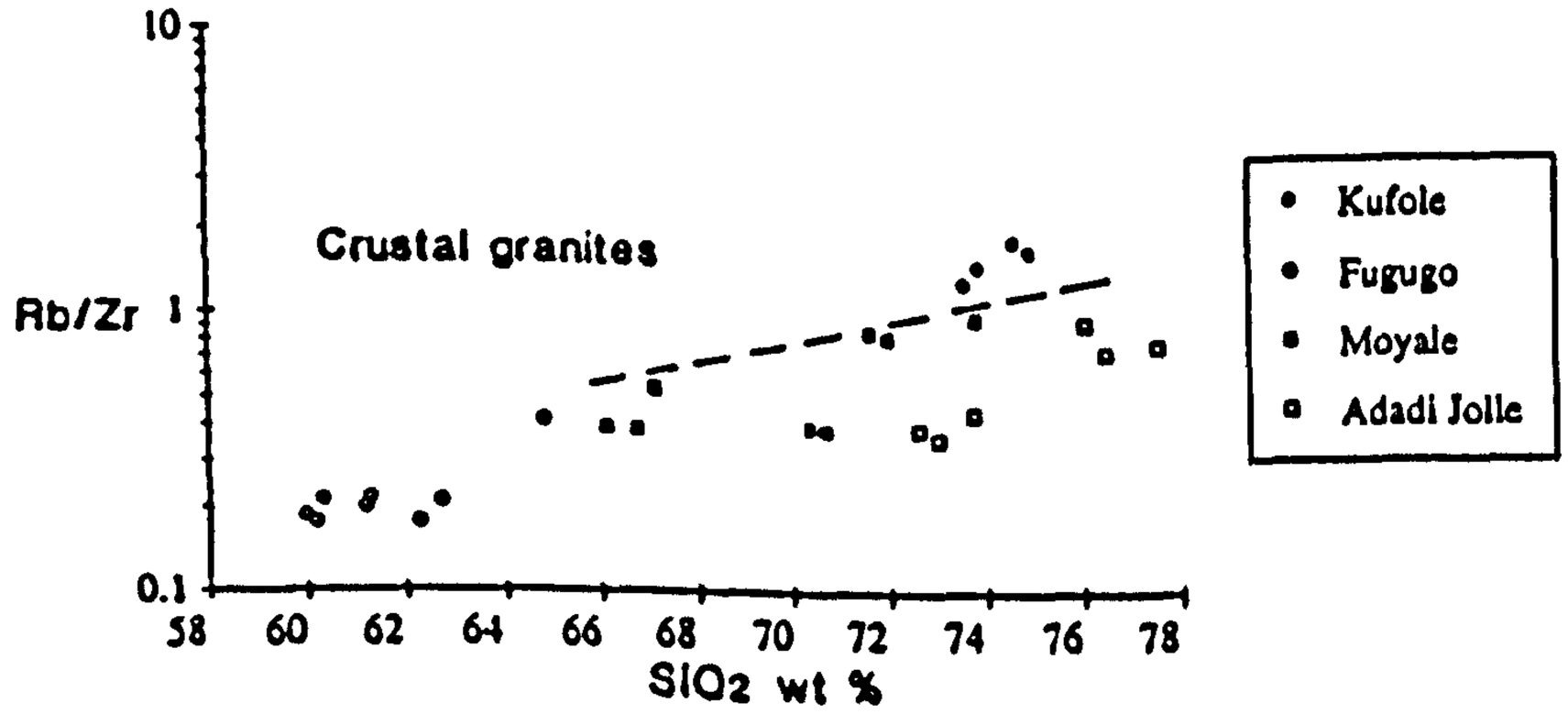

Figure 3.28 Rb/Zr vs SiO_2. The Kufole have high Rb/Zr ratios and hence plot in the Group II crustal granite field of Harris et al (1986).

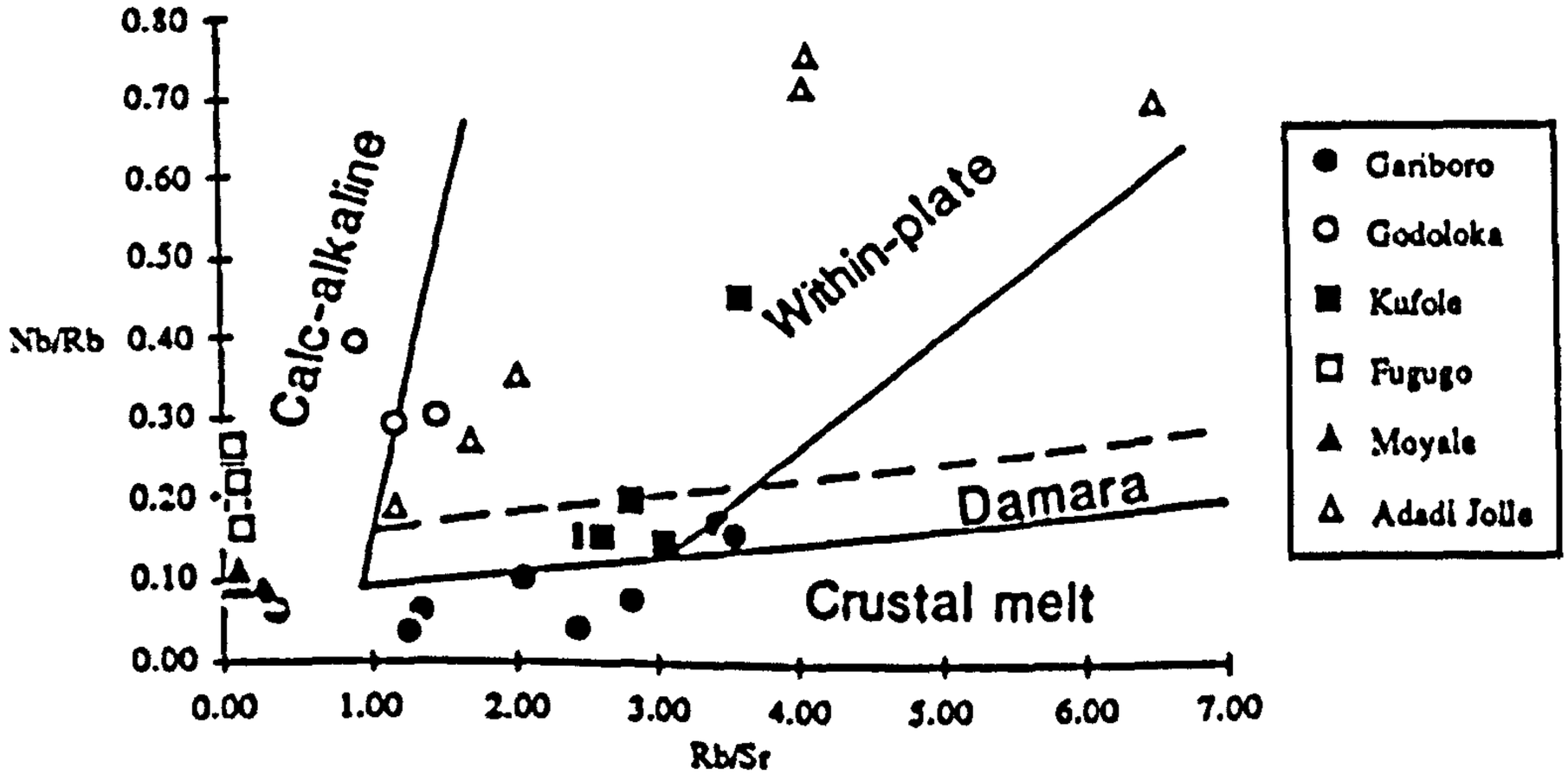

Figure 3.29 Nb/Rb vs Rb/Sr diagram for the Adola-Moyale belt granitoids. Within-plate granitoids have high Nb/Rb ratios, whereas crustal-melt granitoids have low Nb/Rb ratios. Crustal-melt granitoids have high Rb/Sr ratios, whereas calc-alkaline granitoids have low Rb/Sr ratios.

The high K_2O, and elevated HFS elements of the Godoloka granite indicate within-plate granites while the Gariboro has low HFS elements which is characteristic of volcanic arc rocks. Biotite gneisses from Southern Ethiopia were plotted for comparison and show striking similarity to the Gariboro and Godoloka granites. The profile of the Gariboro and Godoloka granitoids also suggests that they either had a similar source region or experienced the same style of crustal fractionation. The elevated Y values are typical for the three suites (Figure 3.26c) but the unusual high Y contents could be controlled by amphibole. In the field granitoid gneisses and the biotite gneisses are observed to have a gradational contact, while the Godoloka has intrusive relationship with the gneisses.

3.8.3.3 REE data

REE profiles for six representative samples are shown as chondrite-normalised diagrams (Figures 3.30a, 3.30b and 3.30c). In Figure (3.30a) the REE profiles of Kufole and Fugugo granites are shown. The Kufole granites show relatively flat REE profiles with a negative Eu anomaly. In contrast, the Fugugo granites are LREE enriched similar to calc-alkaline rocks. In Figure 3.30b the Moyale granodiorites and Adadi Jolle granites REE profiles are compared. The Moyale granodiorites show LREE enriched profiles, at lower abundances than for the Fugugo granites. The Adadi Jolle granites have flat REE profile and a very large negative Eu anomalies which are typical of within-plate granites.

REE profiles are plotted for Gariboro, Godoloka granites and gneisses of Southern Ethiopia (Figure 3.30c). The Gariboro and Godoloka granites have similar profiles characterized by a relatively flat REE profile and large negative Eu anomaly. These are characteristic of within-plate granites. Their REE patterns, except for Eu are very similar to those of metasediments they intrude (Figure 3.30c). Comparison of the relative REE abundances suggests that the Gariboro granitic gneiss (D3) may have been derived from the biotite gneisses (D14).

3.8.3.4 Discriminant Diagrams

Pearce *et al.* (1984a) and Harris *et al.* (1986) have established granite classification schemes which assign granites to four major tectonic settings. Pearce *et al.* (1984a) suggest that the post-collision

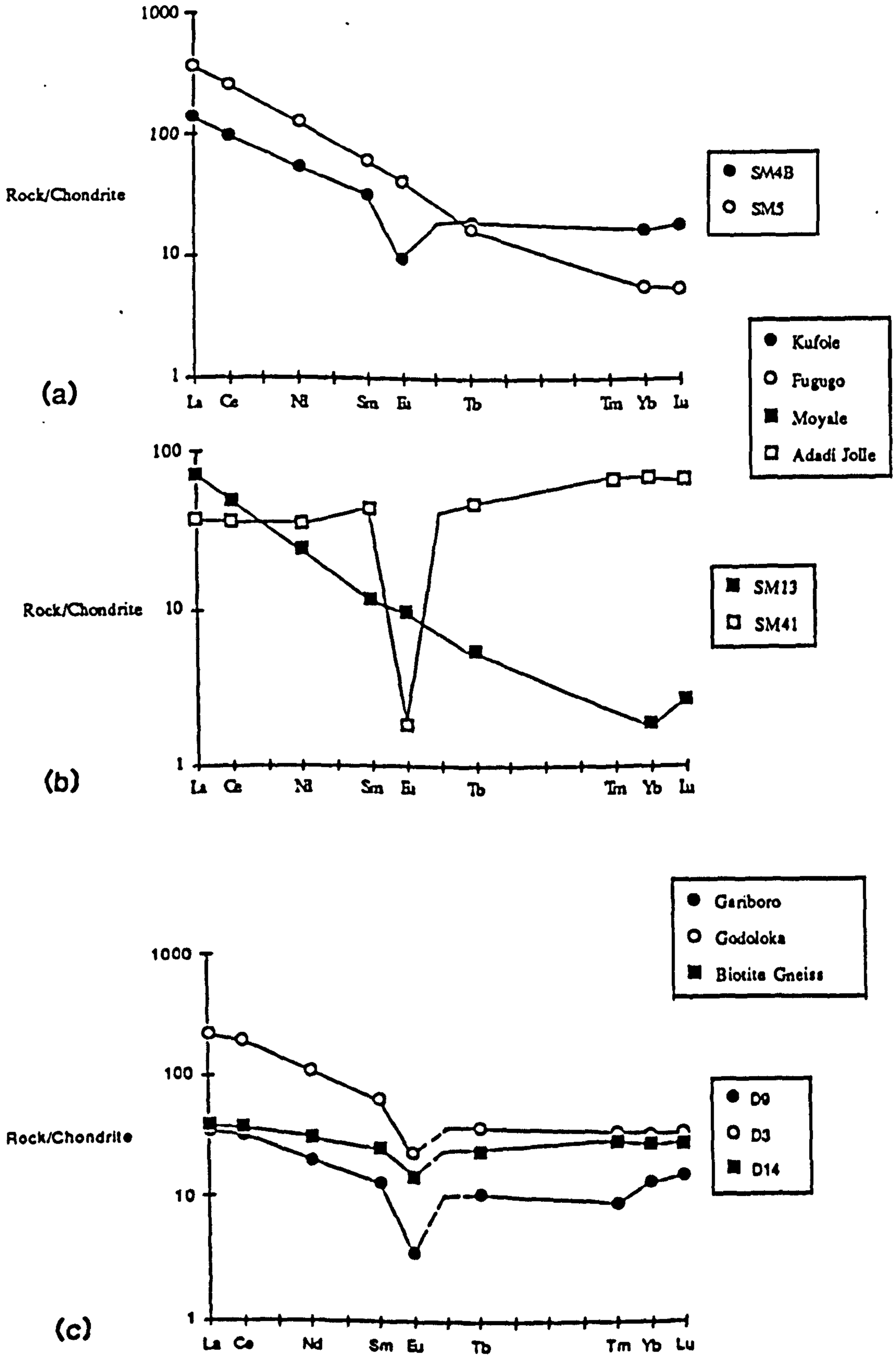

Figure 3.30 (a) Chondrite normalised REE diagram for Kufole and Fugugo granitoids. (b) Chondrite normalised REE diagram for Moyale and Adadi Jolle granitoids. (c) Chondrite normalised REE diagram for Gariboro, Godoloka granitoids and biotite gneisses.

granites are the most difficult, since their trace-element abundances depend on the nature and timing of collision events, lithospheric thickness and composition. Harris*et al.* (1986) suggested discriminant characteristics of collision-related granites and proposed a four fold classification. In this study all the discriminant diagrams were used to evaluate the tectonic settings in conjuction with geological constraints.

Two diagrams show the tectonic setting of granites in S Ethiopia (Figure 3.31a) and NE Kenya (Figure 3.31b). In Figure 3.31b the Fugugo and the Moyale granodiorites plot in the volcanic arc/post-collision field, while Kufole and Adadi Jolle granites plot in the within-plate field. The Fugugo granites have earlier been shown (Figure 3.30a) to have calc-alkaline affinities, albeit with slightly elevated Ce, Hf, Zr and Sm. Although, the Fugugo granites lie in the V.A.G field their Ta/Nb ratios are c. 0.059 so they plot in the late or post- collision field of Harris *et al.* (1986).

In Figure 3.31a the Gariboro granitic gneisses extend from a volcanic arc to within-plate field. This could reflect sampling of more than one suite or were generated in a 'transitional' environment at some distance from an active margin giving a within-plate characteristic. Nb+Y decrease with increasing SiO_2 ,which means that it is probably fractionating (due to some minor phases) towards the volcanic arc field. The Godoloka granites are restricted to the within-plate field.

3.8.3.5 Summary

In summary three geochemically distinct granitoid types have been established in the Adola-Moyale area. Kufole, Adadi Jolle, (NE Kenya) and Godoloka granites (S. Ethiopia) show within-plate characteristics, but the Kufole intrusion has exceptionally high Rb, Ce and Sm which implies that it is a crustal granite.

Moyale and Fugugo granitoids show calc-alkaline major element fractionation trends and volcanic arc trace element characteristics. Fugugo has relatively elevated K, Rb and Ba suggesting some crustal involvement. The calc-alkaline affinity shown by Moyale and Fugugo intrusions could reflect that they were closer to an active margin (see distribution of various granitoids in Figure 3.3), while the Kufole granite is the furthest from the postulated ophiolitic suture, or they could be pre-existing volcanic arc granites remobilised during the Pan-African. These granitoids are

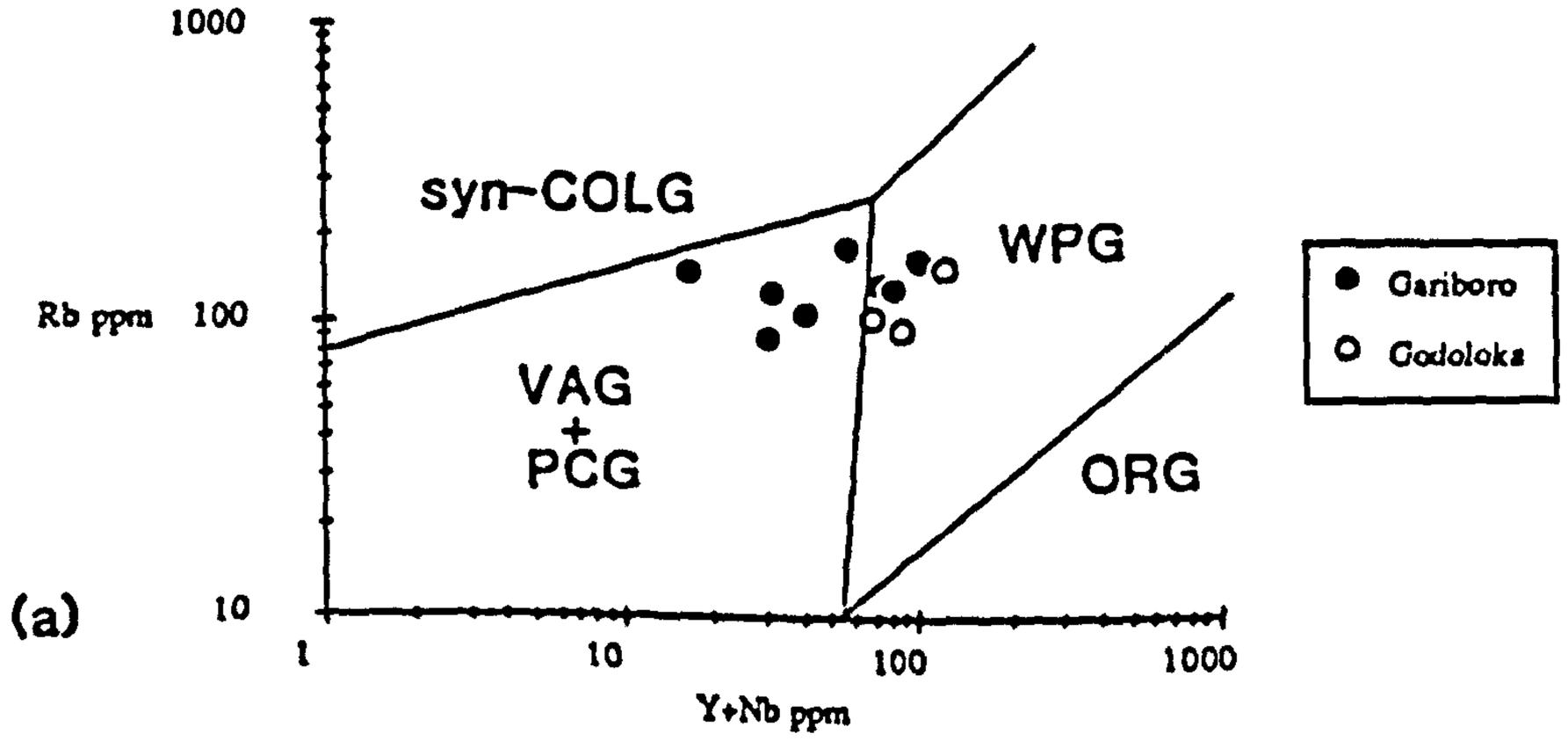

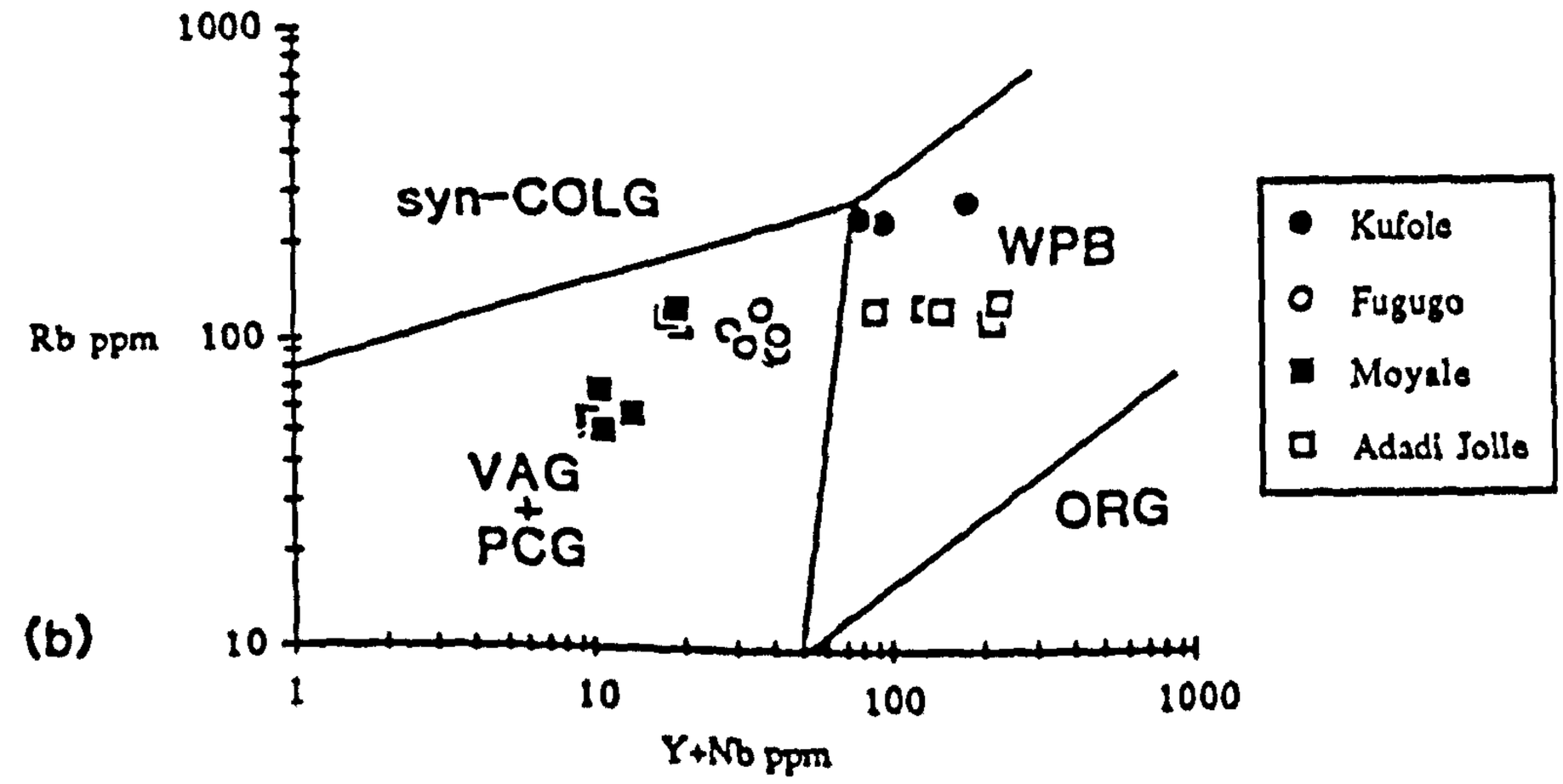

Figure 3.31 (a) Rb vs (Nb+Y) granite discriminant diagram (after Pearce et al,1984b) for the Adola belt granitoids. The Gariboro granitoid gneiss extend from a volcanic arc to within- plate field.
(b) Rb vs (Nb+Y) granite discriminant diagram (after Pearce et al,1984b) for the Moyale area granitoids.

equivalent to post-collision granites (Group III, of Harris *et al.*, 1986) which have formed from a LIL -enriched mantle wedge above subducted oceanic crust but have been modified by melts from the lower crust.

The Gariboro gneissose granite has high alkalies, Y, depleted HREE and low HFS elements. Although in the discriminant diagram the Gariboro gneisses extend from a volcanic arc to a within-plate field, they were probably generated in a transitional environement at some distance from an active margin giving a within-plate signature. Field evidence and elevated Rb values suggests that it could be genetically related to the biotite gneisses.

3.8.4 Trace Element Modelling

3.8.4.1 Introduction

Large ion lithophile (LIL) elements Ba, Rb and Sr have been used for petrogenetic modelling of granite systems (McCarthy and Hasty, 1976; Tindle and Pearce, 1981) and are useful because they are largely partitioned into major silicate phases in granitic systems. The LIL data are presented as logarithmic plots of Ba against Rb and Ba against Sr (Figures 3.32a and 3.32b). The objective is to define the main fractionation trends and to compute the mineral combinations that best fit the observed trends. The modelled variations are based on Rayleigh fractional crystallization using the equation:

$$C_1/C_0 = F(D_a-1)$$

where C_0 = conc. of element 'a' in the original melt

C_1 = conc. of element 'a' in the residual melt

F = weight fraction of melt remaining

D_a = bulk distribution coefficient for element 'a'

Fractionation vectors have been superimposed on the log-log plots of LIL elements. F values are shown at 0.1 intervals along each vector. The distribution coefficients used for trace element modelling are given in table 3.5.

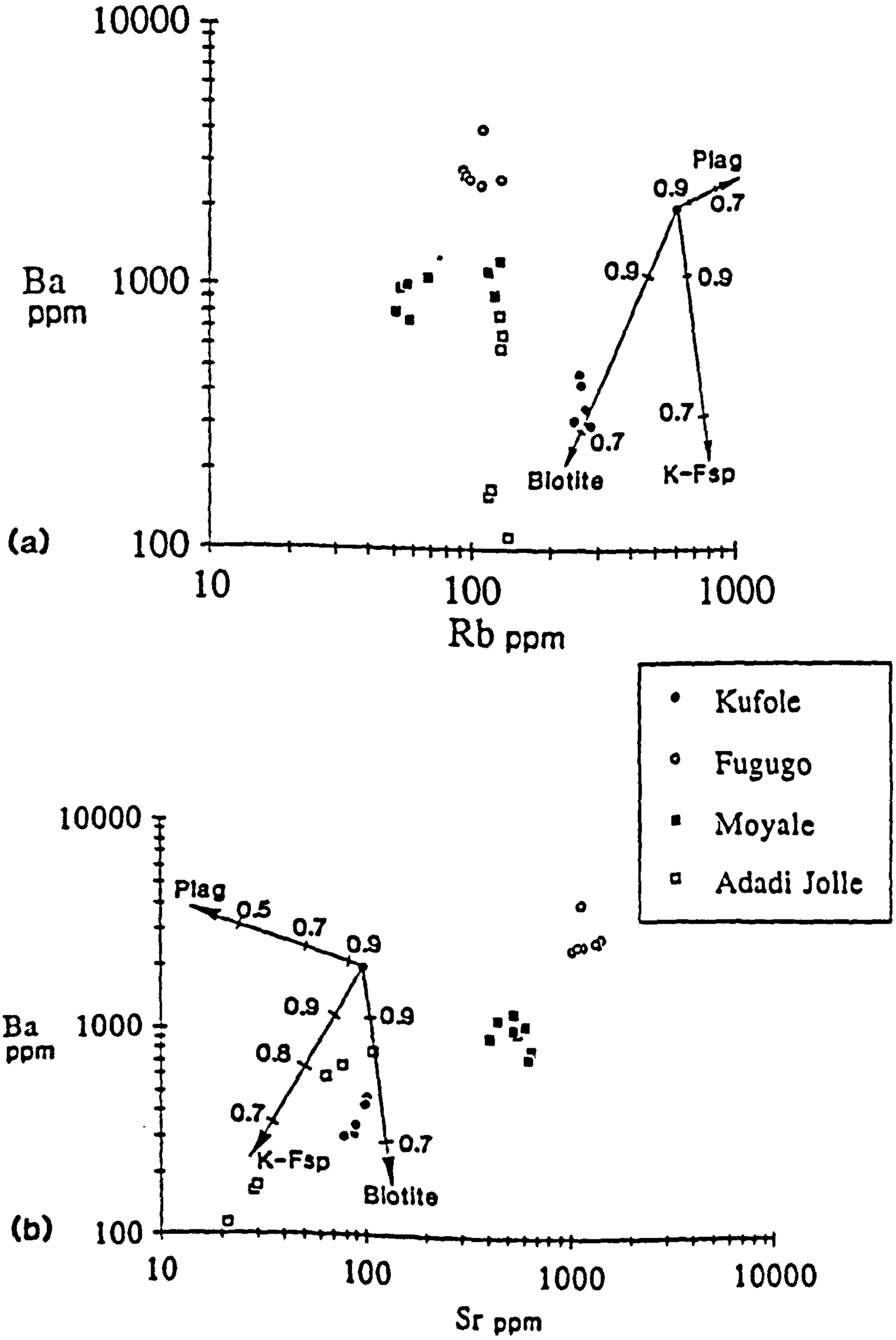

Figure 3.32 (a) Ba vs Rb log-log diagrams for the Kufole, Fugugo, Moyale and Adadi Jolle granitoids. **(b)** Ba vs Sr log-log diagrams for the Kufole, Fugugo, Moyale and Adadi Jolle granitoids.

Table 3.5 Distribution co-efficients in LIL modelling

	Plagioclase	K-feldspar	Biotite
Ba	0.36	6.12	6.36
Sr	2.94	3.87	0.12
Rb	0.05	0.34	3.26

(K_d *values after Arth and Hanson, 1975 and Hanson, 1978)

(* When a mineral is in chemical equilibrium with a liquid, elements are partitioned between the two phases according to their chemical activity in each. K_D is a constant known as the 'distribution' or 'partition coefficient' for the crystal-liquid equilibrium. For an element whose concentration is low in both application of Henry's Law leads to the relationship: Concentration in mineral/ Concentration in liquid).

The degree of fractional crystallization required to produce the observed variation in LIL elements may be calculated. The least and most evolved samples of a suite are selected on the basis of major and trace element data. These are assumed to represent the initial and final liquid respectively and are related by simple Rayleigh fractional crystallization. McDermott (1986) used the approach of Allegre *et al.* (1977) to estimate bulk distribution coefficients (K_D) for a range of trace elements based on hygromagmatophile element systematics (Treuil and Varet, 1973). Since most trace elements behave compatibly during fractional crystallization of granitic magmas, the most incompatible elements were used to calculate the D values of other trace elements.

The following equation derived from Rayleigh fractional crystallization by McDermott (1986) was used:

$$D^i = (\text{Log } C_l^i - \text{Log } C_{o\iota}^i / \text{Log } C_{o\iota}^H - \text{Log } C_l^H) + 1$$

where C_l^i is the concentration of the trace element in the final liquid

$C_{o\iota}^i$ is the concentration of trace element i in the original liquid

$C_{o\iota}^H$ in the concentration of incompatible element in the original liquid

C_l^H is the concentration of the most incompatible (hygromagmatophile element) in the final liquid

D^i is the bulk distribution coefficient for trace element I

3.8.4.2 Observed variations

Moyale granodiorites

In the Ba-Rb plot (Figures 3.32a) Rb increase with increase in Ba, while in the Ba-Sr plots (Figure 3.32b) Ba values decrease with decreasing Sr values. The observed variations in LIL elements suggest that plagioclase and some biotite could have controlled the fractionation trend. One sample behaves differently because it shows a decrease in Ba with increasing fractionation suggesting control by K-feldspar.

REE data for sample SM13 (Figure 3.30b), shows that there is slight negative Eu anomaly which coupled with increasing CaO with SiO_2 implies that plagioclase is fractionating (Figure 3.24).

The least evolved sample of the Moyale granodiorites is SM21 (with LIL element concentrations, Ba = 751 ppm, Sr = 628 ppm and Rb = 57 ppm), while the most evolved sample observed is SM16 (Ba - 1150 ppm, Sr = 438 ppm and Rb = 115 ppm). Table 3.6 shows the average bulk D values calculated for a range of trace elements using Rb and Th as 'hygromagmatophile' elements as shown in left hand column. Th was found to be the most incompatible trace element, hence the D values calculated are assumed to be the best available estimates. Sr is a highly compatible trace element, while Rb, Ba, Zr, Nb and Y are incompatible during fractional crystallization of the Moyale magma. The observed variation in all trace elements for which D values have been calculated (Table 3.6) may be accounted for by about 84% fractional crystallization. Taking Sr as an example and using equation derived from Allegre *et al.* (1977):

Using Equation $\text{Log } F = \text{Log } C_l^l - \text{Log } C_{o.l.}^l / D^l - 1$

$$\text{Log } F = \text{Log } 438 - \text{Log } 628 / 1.22 - 1$$

$$\text{Log } F = \frac{2.64 - 2.80}{0.22}$$

F = 0.19 ~ 81% fractional crystallization

Adadi Jolle Granitic Gneiss

Both Ba and Sr behave as compatible trace elements, while Rb abundances remains constant . In this suite Ba decreases rapidly while Sr decreases and Rb remain constant. The variations in LIL elements suggest that fractionation is controlled by alkali feldspar and there may be a small amount of biotite involved, but D_{Rb} remained <1. REE data (Figure 3.30b) shows a strong negative Eu anomaly consistent with feldspar fractionation. LIL element concentrations in the Adadi Jolle granite primary magma are assumed to be Ba = 784 ppm, Sr = 109 ppm and Rb = 127 ppm; which is based on the least evolved sample SM46, while the most evolved end member is assumed to be SM45 (Ba = 114 ppm, Sr = 21 ppm and Rb = 137 ppm). Table 3.7 shows the average bulk D values calculated using equation derived from fractional crystallization (McDermott, 1986) for a range of trace elements using Nb and Y as hygromagmatophile elements as shown in the left hand column. Nb was found to be the most incompatible trace element. Sr, Zr and Th were highly compatible trace elements while Rb is roughly constant and , Ba, Y and U were incompatible during fractional crystallization of the Adadi Jolle granitic magma. The observed variation in all trace elements for which D values have been calculated (Table 3.7) may be accounted for by about 76% fractional crystallization. Taking Sr as an example and using equation derived from Allegre *et al.* (1977).

Using Equation $\text{Log } F = \text{Log } C_l^l - \text{Log } C_{o.l.}^l / D^l - 1$

$$\text{Log } F = \frac{\text{Log } 21 - \text{Log } 109}{2.2 - 1} \text{ fractional crystallization}$$

$$\text{Log } F = \frac{1.3 - 2.04}{1.2}$$

F = 0.24 ~ 76% fractional crystallization

Table 3.6 Average D values calculated for Moyale Granodiorite Fractional Crystallization

	Rb	Sr	Ba	Zr	Nb	Y	Th	U
Th	0.60	1.22	0.76	0.99	0.72	0.87	-	-

Table 3.7 Average D values calculated for Adadi Jolle Granitic Gneiss Fractional Crystallization

	Rb	Sr	Ba	Zr	Nb	Y	Th	U
Nb	0.93	2.2	2.40	1.62	-	0.48	1.56	0.63

3.8.4.3 Summary

Fractional crystallization in the Adadi Jolle within-plate granitoids is dominated by K-feldspar which is reflected in high inferred bulk D values for Ba and Sr. The observed trace element variation can be accounted by about 76% fractional crystallization.

In contrast the fractional crystallization in the calc-alkaline Moyale granodiorites is controlled by plagioclase and some biotite. The degree of fractional crystallization required to produce the observed trace element variation is 81%.

3.9 DISCUSSION

The Adola-Moyale belt forms part of an orogenic belt which initially developed as an intracontinental rift system (Kazmin *et al.*, 1978) that progressively evolved into an ocean basin which subsequently closed forming a nappe pile which was thrusted from the west to east, overlying authochonous continental shelf deposits. Calc-alkaline rocks have not been recognised by any workers in the Adola belt (Gilboy,1970; Chater,1971; Kazmin,1976; Warden and Horkel,1984), whereas calc-alkaline volcanics have been found in the Moyale area (this study) but are volumetrically insignificant compared to W Ethiopia. Hence it is inferred that the tectonic setting of the Adola belt is similar to that of passive rift margins where rifting of the continental crust (Alghe gneisses or the

Lower Complex) was accompanied by basaltic activity and clastic sedimentation (Middle Complex) followed by seafloor spreading.

The characteristic features of a Penrose ophiolite are present as dismembered units in the Adola area. The general succession of the Adola Group is from ultramafics mostly altered to talc serpentinite and anthophyllite schists at the base to amphibolitic gabbros, amphibolites (basic lavas) which are overlain by metasediments. Trace element data indicate that the Adola-Moyale mafic rocks have an island arc and MORB geochemistry (see Section 3.6). The fact that we have crustally contaminated mafic melts suggests that the lithosphere formed at the earliest stages of arc or continental rifting.

The geochemistry of chromites from the Moyale ultramafics reflect a composite origin such as the formation of an island arc on ocean basin (Dick and Bullen, 1984), or from lithosphere formed at the earliest stages of arc or continental rifting.

The Adola-Moyale rocks outcrop as three major parallel mafic-ultramafic belts: the Adola, Kenticha and Negelle belts. Kazmin (1976) pointed out that the Adola and Kenticha zones have westerly-dipping thrust contacts and that the Kenticha zone consists of three or more tectonic scales overthrust in an easterly direction. He also suggested that they could represent a series of nappes overthrust into the margins of a continental block, subsequent refolding having steepened the contacts. The Negelle ophiolite are similarly underlain by a low angle thrust which represents a nappe derived from the west.

The western contact of the Adola belt is a thrusted contact, while at the eastern contact between the Adola Group and the gneisses there are several elongated lenses of sheared ultrabasic rocks which suggests a thrust zone. The predominantly westerly dip of thrust planes suggests that the ophiolite was obducted from the west. The relationship of thrusting to the three sets of folds suggests that folds formed in response to the changing stress pattern during the thrusting event rather as three distinct phases of folding.

The Adola-Moyale belt was subjected to deformation and metamorphism at three different times: the earliest was probably ca. 1030 Ma (Rb/Sr age of phyllites, Chater, 1971), the second episode of deformation c. 680-630 Ma (age of biotite gneisses and syntectonic granites) and the

third phase was c. 555-500 Ma (age of post-tectonic granites, Gilboy, 1970; Chater, 1971).

The metamorphic grade increases eastwards which partly overlap with increase in the intensity of deformation. The widespread development of cordierite porphyroblasts and anatexis suggests that a regional metamorphism of Abukuma type (Winkler, 1976) may have affected all the rocks of Megado area, S. Ethiopia (Chater, 1971). A second high pressure regional metamorphism, both accompanied and followed the second episode of tectonism (Gilboy, 1970). Temperatures up to 600°C at c. 6 kb, have been reached in the area.

One of the major problems is the age relationship of the Alghe and Awata gneisses (the Lower Complex) and the Awata and Yavello gneisses (Middle Complex) with the Adola ophiolitic sequence. In the absence of reliable ages it is difficult to separate rocks of different age and metamorphic grade between the gneisses west and east of the Adola-Moyale mafic-ultramafic complexes.

The Wadera gneisses (Middle Complex) are controlled by large Precambrian faults (Kazmin *et al.*,1978). This suggests that sedimentation was probably controlled by differential subsidence of older adjacent blocks (Alghe gneisses) during the rift phase. Chater (1971) suggested that the Middle Complex gneisses which have arkosic horizons indicated environments of rapid deposition and a granitic source area. Large quantities of arkoses are usually deposited in either a continental environment of intermountain basins or in a deltaic system on the continental shelf. Hence the presence of shelf sediments and arkosic rocks indicates the proximity of a continental platform on which these sediments were laid. However the biotite gneisses in the west are unlikely sources of the arkosic horizons so it is inferred that the continental platform has to be thought east of the Adola-Moyale mafic-ultramafic belt.

In summary three geochemically distinct granitoid rocks have been established in the Adola-Moyale area. Kufole, Adadi Jolle, (NE Kenya) and Godoloka granites (S. Ethiopia) show within-plate characteristics, but the Kufole intrusion has exceptionally high Rb, Ce and Sm which implies that it is a crustal granite. Trace element geochemistry of granitoid rocks suggests that a substantial crustal component is involved in their genesis. Even though we do not know the age of this component, it is possible that the sources are much older than the 680-515 Ma ages obtained by the Rb/Sr whole rock method. The slightly high initial Sr^{87}/Sr^{86} ratios (c. 0.7049-0.708) obtained

for some granitoids (Gilboy, 1970) suggests the existence of older rocks at depth. However, it is not clear whether the older rocks are restricted to east of the postulated Adola-Moyale suture or if they are present west of the suture. Age determinations of granitoids in NE Kenya and trace element geochemistry of granitoids west of the Adola-Moyale belt are required to further elucidate the tectonic evolution of this area.

CHAPTER 4

GEOLOGY AND GEOCHEMISTRY OF THE YUBDO - BIRBIR BELT, W. ETHIOPIA

4.1 INTRODUCTION

The Yubdo - Birbir belt covers an area of approximately 108,825 km^2 (Figure 4.1) more than half of which has not been geologically investigated. A large proportion of the area is covered by Late Proterozoic rocks which are dominantly formed of high grade gneisses and migmatites, mafic-ultramafic rocks, low grade metavolcanics and metasediments, all of which are intruded by syntectonic and post-tectonic granitoids.

In the absence of a complete coverage of geological maps it was necessary to identify the major lithostratigraphic sequence based on fieldwork carried out in the Yubdo area between 1978-79 with colleagues from the Ethiopian Institute of Geological Surveys (see Figure 4.2) and supported by Landsat study. Landsat study was most useful in the unmapped northern area.

The main aim of this study is to integrate all available field information, supported by petrographic work, and a limited amount of geochemical analyses of representative samples from the Yubdo area. However there was no systematic sampling of rocks in Western Ethiopia, and after the Landsat study was finalised it was not possible to go back to carry out further sampling, due to the political situation. It should be stressed that this is not intended to be a definitive study, but an attempt to indentfy the major tectonic and lithologic units in order to provide a framework for more detailed study in the future.

4.1.1 Location and Access

The study area (Figure 4.1) is located between latitude 8° 00' and 12° 00' and longitude 34° E to 36°30' E. The area is crossed by two major roads. The southern area can be reached from Addis Ababa via Jimma, while the northern part is reached by the Addis Ababa-Gimbi road, which continues to the Sudanese border (Figure 4.1). There is a network of small dry-weather roads around the

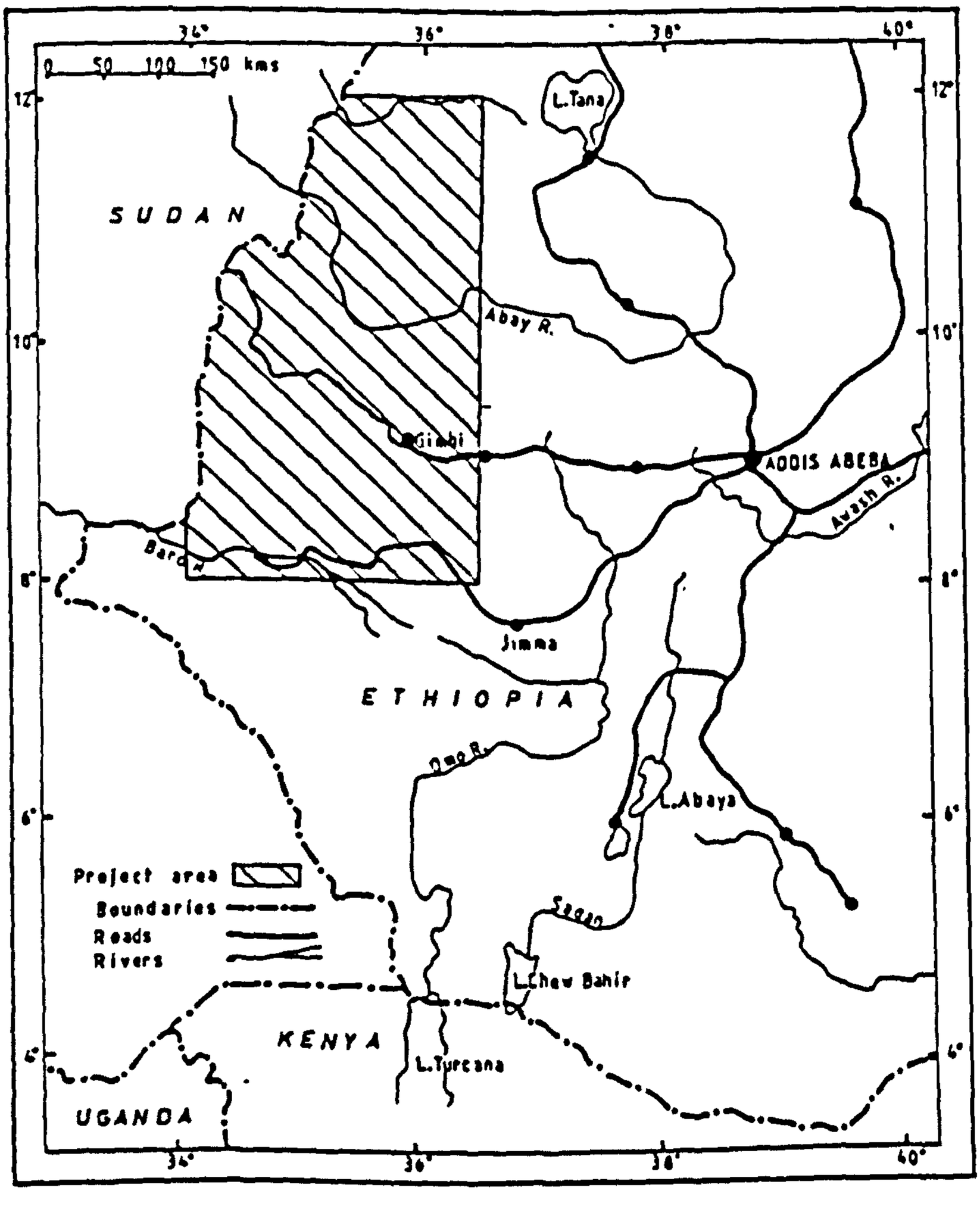

Figure 4.1 Location map of the study area.

Gimbi-Nejo and Yubdo areas.

Access to the north of the Blue Nile (Abbay River) is very difficult because tributaries of the Blue Nile form a series of gorges. In this area there is only one dry weather road that passes through Metekel to Guba. Fieldwork is generally obstructed from June to December because of the tall elephant grass, that is burnt to use the land for agricultural purposes. There are also air services to Gore, Gambela, Dembidelo, Nejo, Mendi, Asosa and Begi by Ethiopian Airlines.

4.1.2 Previous Work

Early Italian Colonial works were generally restricted to gold prospects. Two important papers were published in 1936, one by Muhlen (1936) which deals with the general geology of the Welega highlands and Dabus valley, the second by Muhlen and Hellmens (1936) which describes the petrology of the same area. The earliest geological maps were by Desio (1940) one of which covers the whole of Welega (1:2,000,000) and the other describes the western part of the province (1:500,000). These maps and colonial works are available in the British Museum Library and the Geological Science Library.

In 1967-71 a joint United Nations - Ethiopian Mineral Survey team undertook exploratory works in an area of 75,587 km^2 (UNDP,1972). Photogeological mapping for this project was contracted to Huntings Geology, and Geophysics Limited, and maps of 1:100,000 were prepared. The maps were unsatisfactory because of limited fieldwork and were inaccurate, resulting from photointerpretation of areas with thick lateritized cover. The 1967-71 survey undertook photogeological mapping, airborne geophysics of selected areas, and ground surveys including geologic, geochemical and geophysical prospecting.

More recently systematic mapping and exploration has started. Kazmin's works (1971, 1975) have contributed greatly to the understanding of the geology of the area. The Ethiopian Institute of Geological Surveys has started to publish a series of geological maps in recent years (Figure 4.2).

Some mineralised target areas recommended by the joint United Nations - Ethiopian survey were studied in detail by Soukhoroukov *et al.* (1980a; 1980b), DeWit and Aguma (1977), DeWit *et al.* (1978) and Kazmin (1978). DeWit and Chewaka (1981) were the first to give a preliminary account

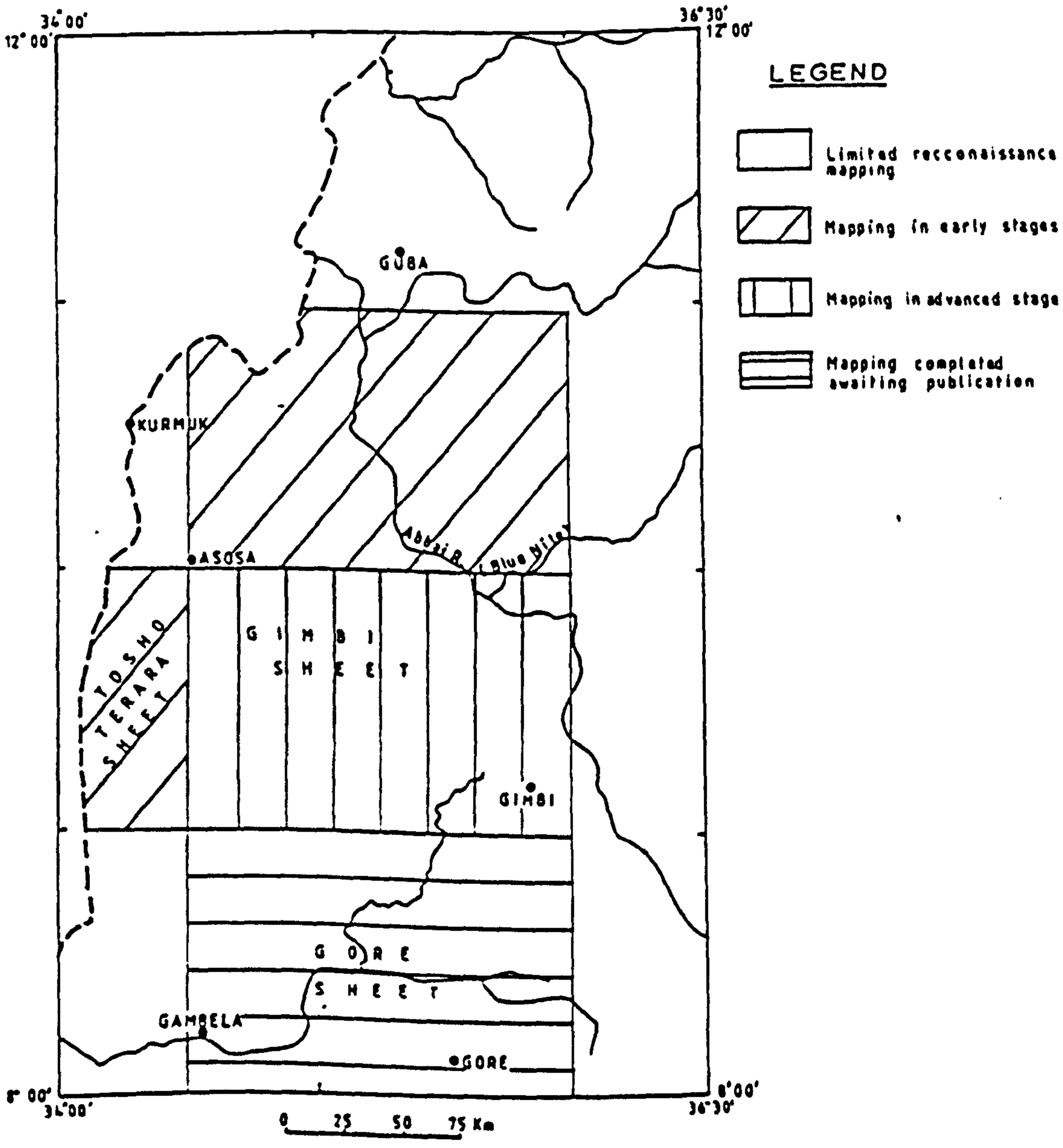

Figure 4.2 State of geological mapping for western Ethiopia.

of ore deposits of Ethiopia in terms of plate tectonics. More recently Kazmin *et al.* (1979a and 1979b) and Berhe (1981) have discussed the general outline of the basement structure and metallogeny of Western Ethiopia . Warden *et al* (1982) carried out geochemical analyses of a small suite of rocks of the Tulu Dimtu mafic-ultramafic complex, and suggested it to be ophiolitic. However these works were incomplete because of lack of detailed field, petrographic, and geochemical data, some of which are presented in this study.

4.2 LITHOLOGIC AND PETROGRAPHIC DESCRIPTION OF ROCK FORMATIONS

4.2.1 INTRODUCTION

The Precambrian rocks of Western Ethiopia have been subdivided into three major stratigraphic divisions by Kazmin *et al.* (1978). However further work (Kazmin *et al.*,1979a,1979b; Berhe, 1981) showed that the area could be subdivided into five major tectonic zones (Figure 4.3). From east to west these are: 1. eastern block of high grade gneisses (Geba Domain); 2. ophiolite belt (Yubdo Domain); 3. zone of dioritic-granodioritc batholiths and associated intermediate volcanics; 4. metavolcanic-metasedimentary belt (Birbir Domain) and 5. western block of high grade gneisses (Baro Domain). In this study the Baro Domain has been subdivided into the Gambela and Bonga tectonic belts. The Geba Domain consists of ortho- and paragneisses and granodiorites metamorphosed to the middle and upper amphibolite facies and the Yubdo domain consists primarily of mafic and ultramafic rocks. Eastwards there is a zone of dioritic-granodioritc batholiths and associated volcanics while the Birbir Domain consists of a variety meta-igneous rocks, schists and mylonites metamorphosed to lower amphibolite facies.The Baro Domain is similar in lithology and metamorphic grade to the Geba Domain. The boundaries between the domains are highly tectonised and have lost their original contact relationships.

The area was interpreted as representing a Mid-Upper Proterozoic oceanic basin between older continental blocks. Most of the magmatic and sedimentary rocks of the belt sandwiched between the eastern and western block of high grade gneisses were thought to be of island arc and back arc origin. It was earlier suggested (Kazmin *et al.*,1978) that the oceanic rifts narrowed to the

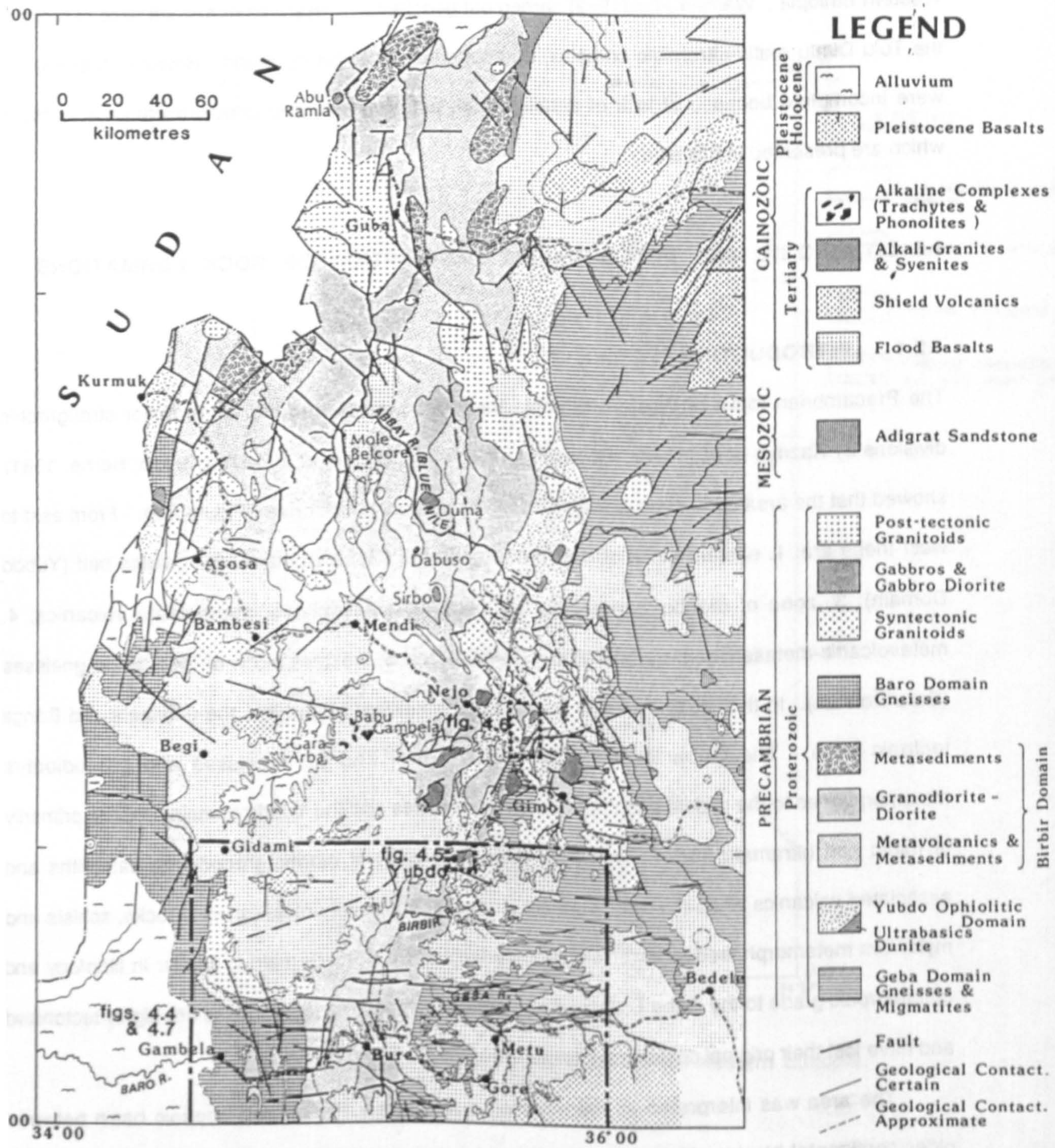
00
0 20 40 60
kilometres
N
Abu Ramla
Guba
SUDAN
Kurmuk
Mole Belcore
ABBAY R. (BLUE NILE)
Duma
Dabuso
Asosa
Sirbo
Bambesi
Mendi
Nejo
Babu Gambela
fig. 4.6
Begi
Cara Arba
Gimbi
Gidami
fig. 4.5
Yubdo
BIRBIR
Bedele
GEBA R.
figs. 4.4 & 4.7
Gambela
Bure
Metu
Gore
BARO R.
00
34°00
36°00
LEGEND
CAINOZOIC
Pleistocene Holocene
Alluvium
Pleistocene Basalts
Tertiary
Alkaline Complexes (Trachytes & Phonolites)
Alkali-Granites & Syenites
Shield Volcanics
Flood Basalts
MESOZOIC
Adigrat Sandstone
PRECAMBRIAN
Proterozoic
Post-tectonic Granitoids
Gabbros & Gabbro Diorite
Syntectonic Granitoids
Baro Domain Gneisses
Metasediments
Granodiorite - Diorite
Metavolcanics & Metasediments
Birbir Domain
Yubdo Ophiolitic Domain
Ultrabasics Dunite
Geba Domain Gneisses & Migmatites
Fault
Geological Contact. Certain
Geological Contact. Approximate

south, and continued as continental rifts, however DeWit and Chewaka (1981) and Kazmin *et al.* (1979a) reiterated that the oceanic structures continued further south to Kenya.

A geological map (Figure 4.3) is presented based on Ethiopian Institute of Geological Survey maps (Teffera and Berhe, in press), supplemented by Landsat work. Geological synthesis is based on this map, however emphasis is placed on the Gore mapsheet (Figures 4.4) where the author has good ground control.

The five tectonic domains which are subdivided based on differences in lithologic assemblages and structural style are described from east to west.

4.2.2 Geba Domain

The Geba Domain gneisses and migmatites are observed in a 70 km strip in the eastern part of the area (Figure 4.4). In the south they are exposed in the Geba and Dipa River Valleys (Figures 4.3 and 4.4) and can be traced further north to Didessa valley , Blue Nile area. The Geba Domain includes various gneisses and migmatites which are usually coarse grained, foliated, greyish in colour, and often banded due to injection of granitic material. Transitions from foliated and banded rocks to massive varieties are common. The Geba Domain has been intruded by a succession of foliated gabbro-diorites and tonalites.

The Geba Domain can be broadly subdivided into two units (Kazmin *et al.*, 1979a,1979b):- a) this unit consists of interlayered amphibole, and biotite-amphibole, sometimes garnetiferous, banded gneisses which grade into rather massive granodiorites and dioritic rocks. b) this unit shows distinctive compositional layering and, apart from dominant biotite and hornblende paragneisses and schists, contains intercalations of quartzofeldspathic rocks and quartzites.

In the Geba area (on the way to Supe) (Figure 4.4) there are lithologically distinctive banded garnetiferous gneisses. A similar unit is found west of Alga Guracho village. South of Geba bridge there are biotiite gneisses, with pegmatites that contain pyrite crystals. In a quarry in Gumero area there are porphyroblastic biotite gneisses, which are strongly migmatitised in places. The pink pegmatitic bands cut across the white feldspar bands and the amphibolites.

Along Dipa river near Wabeco village there are highly deformed porphyroblastic granitic

34°30
9°00
36°00
9°00
8°00
34°30
36°00
8°00

Yubdo
Gobera
Dipa R.
Wabeco R.
Nole Kaba
Gelel
Supa
Karo
Ijobo
Gibe R.
Gutete
Alga
Guracho
Mato
Gumero
Bure
Gambela
Bonga
Gore

Alluvial deposits
Tertiary volcanics
Post-tectonic granites

Proterozoic

Upper

Bero Domain
- Syntectonic granitoids
- Calc-silicate gneisses
- Biotite gneisses & paragneisses
- Granitoid & Biotite gneisses

Bonga

Birbir Domain
- Syntectonic tonalites & quartz diorites
- Syntectonic granodiorites
- Gabbro-pyroxenites, wehrlites
- Gabbros & amphibolites
- Metasedimentary schists
- Silicic schists
- Granodiorite-diorite batholith

Yubdo Domain
- Metasedimentary schists
- Syntectonic granodiorites
- Greenstones & metabasalts
- Gabbro-diorites & pyroxenites
- Ultramafics : dunites

Gebe Domain
- Quartzofeldspathic gneisses
- Paragneisses
- Mafic gneisses
- Granitoid & Biotite gneisses

Faults
Domain boudaries

A
B
2000
1500
1000
500
0
metres

Horizontal scale 1:250.000

gneisses, with biotite rich enclaves. East of Gimbi melanocratic amphibole gneisses and amphibolites occur within the granitic gneisses while south of Gimbi granodioritic amphibole gneisses and fine grained foliated biotite paragneisses crop out.

East of Yubdo area the paragneisses are represented by biotite and quartz muscovite schists and quartzites. Sometimes the rocks look gneissose, although the metamorphic grade is not as high as that of the Geba area. Over a broad area porphyroblastic augen gneisses are observed. Generally the Geba Domain is largely plutonic in origin, mainly granitic or granodioritic in composition with subordinate paragneisses and amphibolites. Migmatisation increases from Gimbi southwards into Geba area.

Thin section study shows that the majority of the gneisses and migmatites are of granodioritic origin. Typical sections show metamorphic segregation due to recrystallization. Relic igneous textures are preserved in some sections. The mineral assemblage is dominantly quartz, plagioclase, biotite, hornblende, with minor microcline or myrmekite, epidote, allanite, sphene, apatite, zircon, and iron oxides (Plate 4.1). Some sections are so sheared it is difficult to infer their origin.

4.2.3 The Yubdo Domain

Introduction

On the west the block of gneisses and migmatites is bounded by a narrow 10-15 km belt of ophiolitic rocks which was traced for about 300 kms (Figure 4.3). The ophiolitic belt pinches out north of Geba river and cannot be traced further to the south. Landsat study shows that this ophiolite belt extends much further to the north (Berhe,1981), and was subsequently also recognised to the south in the Omo River valley area, Southwestern Ethiopia (Davidson, 1983).

The Yubdo Mafic-Ultramafic Complex

Introduction

The Yubdo ultramafic complex (Figure 4.5) is about 10 km in length, some 30 km^2 in extent and centred approximately on 8° 56' N, and 35°28' E, I e. 50 km SW of Gimbi, from which it is accessible by secondary roads. The complex forms a group of NNE-SSW trending hills, the tops of which mark

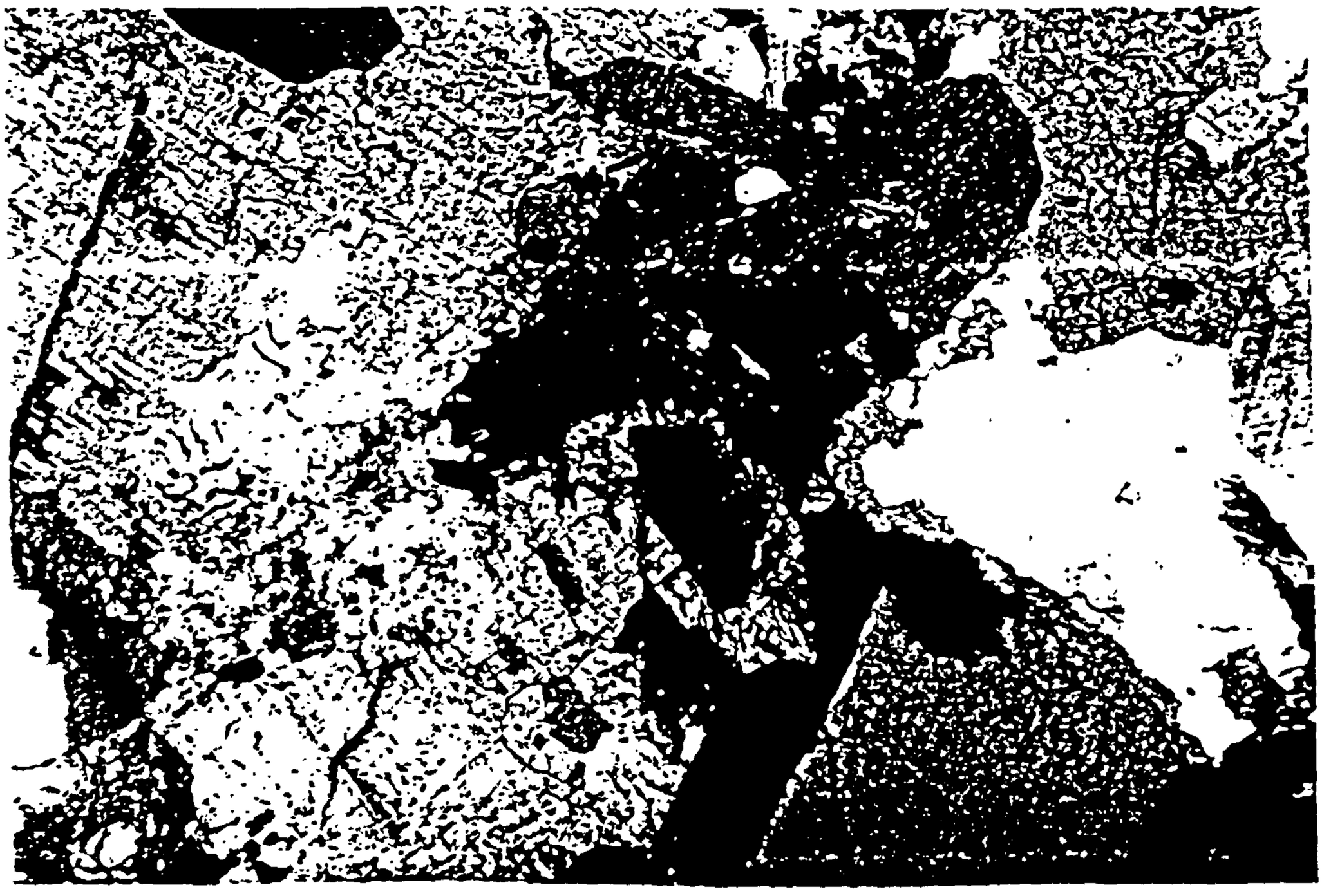

Plate 4.1 Geba hornblende granodioritic gneiss (SB317). It is granular in texture. The hornblende is pleochroic in shades of green and brown (four crystals in the centre). The epidote (yellow colour) encloses allanite. Micrographic intergrowth of quartz and alkali feldspar observed on the left hand side of the photomicrograph. Field of view 3.47.

Plate 4.2 Birbir granodiorite (SB 260). A foliated quartz-feldspar-biotite rich rock. Subparallel alignment of biotite flakesdefines fabric. Field of view 3.47.

the Welega peneplain. The hills are quite distinct from the surrounding terrain in morphology and sparsity of natural tree cover. Eluvial mining of platinum has left large scars on the flanks. Although the Yubdo ultramafic complex was explored for platinum for many years, it was not until after systematic mapping of the Gore mapsheet that they were recognised as Ophiolites (Kazmin *et al.*,1979a,1979b; Berhe,1981). Yubdo is the largest of the Welega ultramafic bodies and includes various rocks ranging in composition from diorite to partly serpentinized dunite,which is locally altered to the siliceous capping rock, birbirite. There is some development of talc and magnesitic vein material. Quartz veins and dyke rocks are also found.

Geology of the Yubdo Area

A large part of the Yubdo mafic-ultramafic complex is made up of a thick series of ultramafic rocks. They show rhythmic layering (cm scale) with peridotites at the base grading upward into feldspar rich gabbroic rocks with discontinuous dioritic rocks. Peridotites are found at the southernmost edge of the ultramafic complex. The peridotites grade into more dunitic and pyroxenitic units. As well as being interlayered with dunite, the peridotites are also cut by massive dunitic bodies. The peridotites are dark grey, fine to medium grained rocks, which are often porphyritic. They are usually coarser than the dunites and less affected by serpentinization. They consist largely of olivine and pyroxene, with accessory magnetite and chromite.

The dunite consists almost entirely of olivine, now more or less altered to serpentine minerals, sometimes the olivine is altered into magnesite. According to Augustithis (1965) the dunite also contains magnesite grains along the margins and cracks in olivine, chromite and sperrylite grains. Fresh outcrops can rarely be encountered along the Birbir river, and other minor rivers that cut the ultramafic complex. East of Yubdo village are found extensive talc-serpentinite units, which were probably peridotites.

A large homogeneous serpentinised dunite is the best exposed unit because of lack of vegetation. Serpentinisation is very extensive, usually more than 80% of outcrop. The dunite body is largely covered by eluvial lateritic cover called birbirite (Augustithis,1965) which is a brown or yellowish brown rock containing varieties of silica, chalcedony, quartz with hematite, limonite and


Birbir River
YUBDO
Birbir River
Tertiary Basalts
Birbirite
Granodiorite
Diorite
Quartzites & arenaceous metasediments
Metasedimentary schists
Metavolcanics: greenstones & metabasalts
Talc serpentinite schist
Pyroxenite &gabbro-diorites
Peridotite
Dunite
Granitic gneiss
Fault
0
2
4
Kilometres

residual chromite. Small dunite patches also occur within the peridotites. Most of the gabbro-diorites are thrust and outcrop mostly east of the ultramafic complex.

The uppermost part of the succession, consists of greenstones and metabasalts. Metavolcanics are found parallel to the main axis of the Yubdo ultramafics, east of Yubdo and extending further south along strike of the complex. In the Dipa River, south of Yubdo, a series of greenstone units cut the intrusive rocks and metasediments which are the only evidence of sheeted dykes. These dykes extend downward into the underlying gabbros. The mafic volcanic complex is not seen to be pillowed.

The mafic-ultramafic rocks are intruded by granodiorite-dioritic rocks. Granodioritic and dioritic rocks are exposed in the middle of the massif southeast and southwest of Yubdo town. Some small quartz veins possibly originating from these granitoids traverse the surrounding country rock. Most of the granodiorites are observed along the margins of the dunite bodies closely associated with the talcose rocks 4 km east of Yubdo.

The metasedimentary units (phyllites, graphitic schists, quartzites and conglomeratic schists) unconformably overlie the metavolcanics. In the Wabeco-Dipa river junction (Figure 4.4), the succession of interbedded units is talc-serpentinite schist at the base overlain by quartzites, cherty bands and graphite schist while north of Gobera village (south of Yubdo), a succession of phyllites, metadiorites and quartzitic metasediments with intercalations of greenstones were observed. This unit thins out in Golol river (Figure 4.4).

Due to difficulties in obtaining access to the collected samples, petrographic examination of the mafic-ultramafic rocks has not been possible.

Geology of the Tulu Dimtu Mafic-Ultramafic Complex

Tulu Dimtu is part of a predominantly mafic-ultramafic belt, trending northeast of Yubdo through eastern Welega (Figure 4.6). The Tulu Dimtu area consists of a metagabbro-serpentinised ultramafic complex, unconformably overlain by a sequence of metasediments and metavolcanics which were later intruded by large metadiorite-granodiorite bodies and quartz-plagioclase porphyries (DeWit and Aguma,1977; Kazmin, 1978).

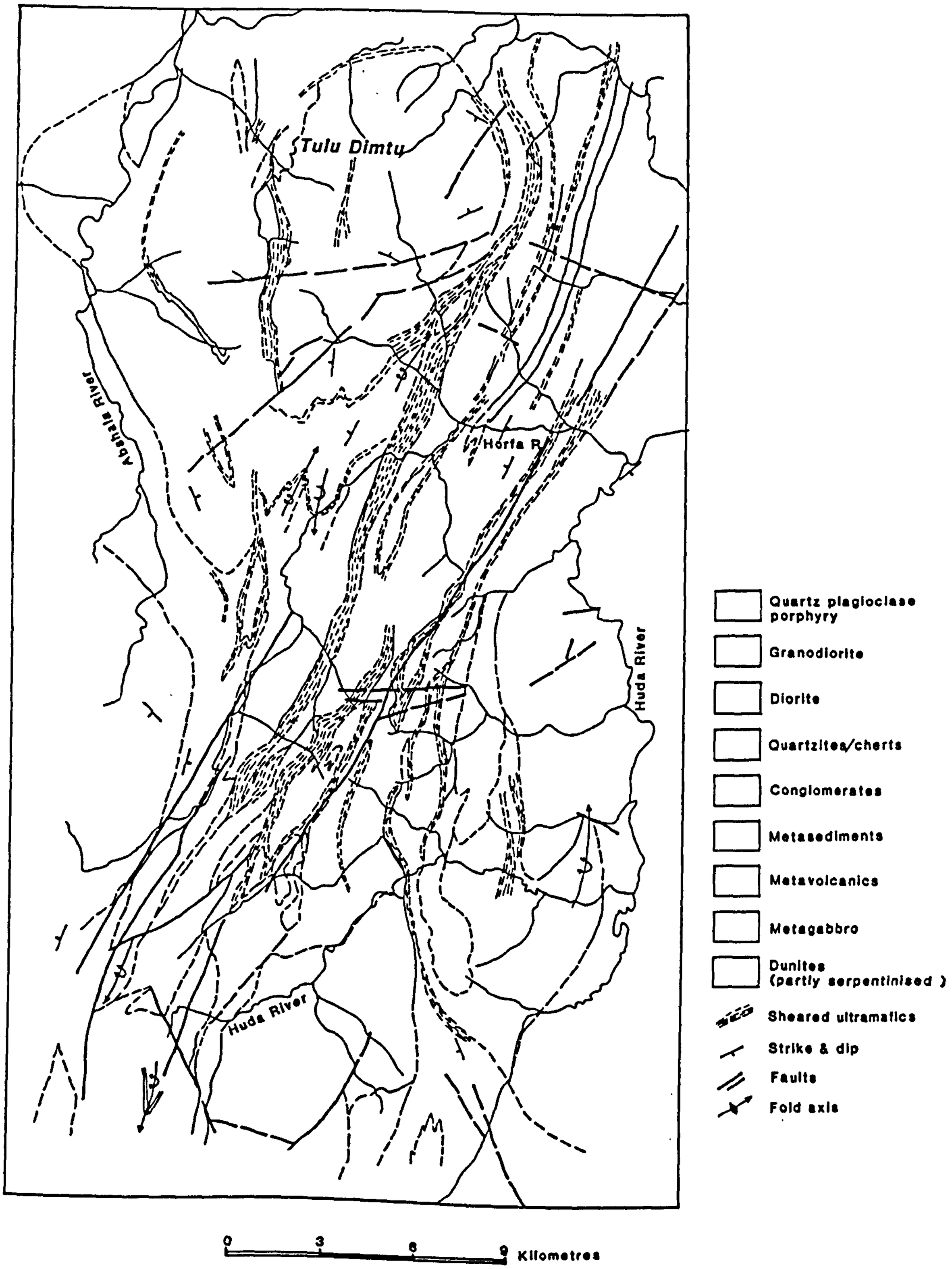
Tulu Dimtu
Abnabia River
Horta R.
Huda River
Huda River
Quartz plagioclase porphyry
Granodiorite
Diorite
Quartzites/cherts
Conglomerates
Metasediments
Metavolcanics
Metagabbro
Dunites (partly serpentinised)
Sheared ultramafics
Strike & dip
Faults
Fold axis
0
3
6
9
Kilometres

The mafic-ultramafic complex represents the oldest rocks exposed in the area, because there is an uncomformable relationship with the overlying metasediments and also a vast amount of coarse serpentine detritus was found by DeWit and Aguma (1977) in the overlying metasediments. The metasediments have been be divided into two units: a) pelitic and psammitic sediments and b) psammites, pelitic schists and associated acidic metavolcanics. The pelitic and psammitic sediments form a sequence of interbanded quartzites (metacherts) and black shales-slates and have been observed to overlie the serpentinite uncoformably southeast of Tulu Dimtu massif. The shale-quartzite succession are also interbanded with graphite schists, marble and conglomerates. This sequence of metasediments is the most widespread. The second group of meatsediments are an interbedded sequence of metasediments and metasilicic volcanics which occur west of Tulu Dimtu. These metasediments were considered to have been derived from a silicic volcanic-granitic-granodioritic terrain (DeWit and Aguma,1977). The metasediments include abundant metavolcanics of basic, intermediate, and acidic composition and numerous plutonic bodies ranging from dunite to granite.

Tulu Dimtu measures six by three kilometres and is almost entirely built of serpentinised dunite. Most of the ultramafics which are foliated and yellow green to greenish black in colour appear either as serpentine or talc-serpentine schists. The other ultramafic bodies are long, narrow and concordant with the structure of the surrounding metasediments. At least nine large ultramafic bodies were mapped in this area (DeWit and Aguma,1977; Kazmin,1978; this study) but there are smaller bodies not shown on the map (Figure 4.6). The characteristic feature of this belt is the development of numerous linear bodies of highly sheared ultramafic material. These bodies range from 10-100 m in length (Figure 4.6). The shear zones are delineated by elongated pods of chromite and magnetite. Shearing and serpentinisation appear to be most extensive along the contacts of the ultramafic bodies which formed during tectonic emplacement of the dunites or in the course of subsequent deformation (Kazmin,1978).

Various types of gabbroic rocks were mapped in the area. At least two generations of gabbroic rocks are associated with the Tulu Dimtu complex. One is strongly metamorphosed and probably coeval with the ultramafics, while the others comprise younger fresh gabbroic intrusives. They mostly

form elongate, sill like plutons intruding both ultramfics and the surrounding meatsediments. In the younger intrusives no layering or gradational contacts with ultramafics were observed. They could be late stage basic intrusives.

Amphibolites are widespread south of Tulu Dimtu, closely associated with the gabbros. They are usually dark, fine grained schistose rocks, which display rare gneissose banding. The ultramfic bodies are cut by mafic and ultramafic dykes. Dykes are well developed in the ultramafic body north of Huda river (in the southwestern part of the mapped area).

The mafic-ultramafic complex has been intruded by large diorite-granodiorite bodies. In the Abshala river area (Figure 4.6) DeWit and Aguma (1977) noted that the diorite contains numerous serpentinised xenoliths of dunite with concentric metamorphic zoning. It is apparent that the dunite body was engulfed by the diorite pluton.

Summary

The Tulu Dimtu mafic-ultramafic complex which lies along strike to the Yubdo complex forms part of an ophiolite belt which was traced for over 300 km northwards. The ultramafic rocks range from peridotites, serpentinised dunites, pyroxenites and cumulate gabbros. Serpentinite has been converted to anthophyllite schists. The dunites contain pods of chromite which seems to be charcteristic of ophiolites derived from marginal basins. However no significant magmatic segregations of chromite were noted.

Metabasalts are abundant in the uppermost part of the succession and are usually interbedded with metasediments. No pillow structures have been observed. Basic dykes occur within many of the ultramafic bodies, although no classical dyke swarm have been observed. Dyke swarms are a common feature of ophiolites however they are not necessarily universal.

Some high level granodiorites, quartz-plagioclase porphyries may represent the late stage acid differentiates similar to the plagiogranites of other ophiolites. The close relation that leucocratic rocks have to the gabbroic parts of ophiolites and their compositional gradation from tonalite to albite granites have convinced many workers that these leucocratic rocks represent the end product of differentiation within ophiolitic sequences (Coleman, 1977).

The metagabbro-serpentinised ultramafic complex are unconformably overlain by a squence of deepwater metasediments associated with ultramafic metvolcanics, volcanoclastics and shallow marine sediments. The presence of pelagic sediments (phyllites, graphitic schists and cherts) in the upper levels of the mafic-ultramafic sequence is further proof of having been formed in oceanic environments.

The features characteristic of an ophiolite are present as several thrust slices but are in no way coherent. No geochemical data is available for the Yubdo area, however geochemical study of the Tulu Dimtu (Warden *et al.*,1982) confirm the petrological and field evidence that the complex is an ophiolte suite of probable back-arc origin. Although their ophiolitic affinity has been ascertained a detailed geochemical study is mandatory in order to understand their genesis.

4.2.4 Diorite - Granodiorite batholith and associated volcanics

West of the ophiolite belt is a zone of large elongate bodies of diorite, granodiorite and tonalites. This zone pinches out to the south and widens to the north. In the northern part it is formed of four elongate massive granodioritic and dioritic bodies separated by roof pendants of volcano-sedimentary rocks. The volcano-sediments are composed of metavolcanics of andesitic and dacitic composition, various volcanoclastic rocks, phyllites, quartzites, and arkoses with intercalations of cherts, marbles, and ironstones. In the central part (in the Mendi - Nejo area) it is a homogeneous dioritic pluton while to the south the batholith is dominantly formed of highly deformed linear granodioritic plutons (Figure 4.4). The plutons are generally massive at the centre but are sheared at the margins, possibly caused during emplacement. Flanking the western edge of the granodiorites there is a continous north-south succession of muscovite-rich quartzites associated with paragneisses and amphibolites. This succession is clearly seen to be intruded by metadiorites along the western flank of the granodioritic batholith which is west of Gobera village (Figure 4.4) and extends further south east of Bure where the paragneisses are more schistose, and rich in biotite with few feldspathic bands.

The Birbir batholith show a wide range of mineral assemblages, from diorite to granodiorite and to more evolved biotite granites. Thin section study of the components of the Birbir batholith shows

that they are coarse grained often porphyroblastic rocks, and in some cases schistose. The mineral assemblages consist dominantly of plagioclase, anhedral quartz and subordinate alkali feldpars. In addition there are minor amounts of biotite, and/or hornblende with secondary muscovite (Plate 4.2) and epidote, and accessory apatite and sphene. Rarely pyroxene is preserved as in section SB 329, however it has mostly been recrystallized to amphibole.

4.2.5 The Birbir Domain

This is a belt of metavolcanic and metasedimentary rocks which are intruded by strongly deformed elongate bodies of granite and granodiorite (gneissose granites) and small intrusions of metadiorite. The Birbir domain which is separated from the Baro and Geba domains by shear zones widens to the north, and also swings northwestwards to the Asosa - Kurmurk area (Figure 4.3).

Geologic traverses along the Baro river carried out indicates that this belt can be subdivided into six major lithologic units: metasedimentary schists; psammitic and pelitic schists; silicic schists; gabbro-pyroxenites and dunites; greenstones, gabbros and amphibolites; and syntectonic granodiorites and orthogneisses (Mengesha and Berhe,in press).

A) In the Birbir domain the predominant rocks are the metasedimentary schists which are fine to medium grained, interbanded mafic and leucocratic biotite hornblende, and biotite schists, quartzites and cherts. The metasedimentary schists also consist of metavolcanoclastic rocks and metaturbidites. The clasts in the conglomeratic lenses are of volcanic and acidic composition varying from andesite to rhyolite. Quartz mica schists and metaconglomerates are also locally present, but have not been shown on the map. Marble is present as small lenses interbedded with the biotite and hornblende schists. The stratified metasedimentary schists have been decribed as mylonites by Moore *et al.* (1987).

B) Silicic schists and associated agglomerates occur west of Bure and along the western margins of this belt. They comprise of metaignimbrites with well preserved eutaxitic texture, associated with silicic agglomerates. Rhyolitic clasts up to several centimetres in diameter are observed. The silicic rocks are generally associated with pelitic, semi-pelitic, and psammitic schists.

West of Bure and extending northwards there is a belt of psammitic and pelitic schists. The

rocks are finely foliated. Quartz and microcline make up the bulk of the rocks, with minor green-brown biotite, muscovite is subordinate while magnetite is an accessory (Plate 4.3). Biotite defines the main period of metamorphism. In some sections quartz is dominant forming more than 60% indicating that the psammites were originally quartz arenites. 22 kms NW of Bure, there are pelitic schists which are found interlayered with greenstones and amphibolites. Section MT 115b shows a banded rock with biotite, epidote, and muscovite-rich layers. The biotites form poikiloblasts, which are intergrown with quartz, and minor alkali feldspar or plagioclase (Plate 4.4). Schistosity is observed wrapping around cordierite (Plate 4.4) which suggests that cordierite is earlier, than the last episode of metamorphism. Apatite and magnetite are the accessory minerals.

C) Gabbro-pyroxenite and dunites occur extensively in the Birbir area (see Figure 4.4). The dunites are generally serpentinised. Slivers of ultramafic chlorite and actinolite schists are also observed (northeast of Bonga) but are too small to be shown on the map. Ultramafic bodies have also been reported near Bambesi on the way to Asosa (UNDP, 1972). Birbirites outcrop 5 km north of Bambesi while talc rocks occur about 20 km south of Asosa (UNDP, 1972). The mafic-ultramafic assemblage in the Birbir belt widens northwards.

Three thin sections were studied, two of these form lenses within the metavolcanic-metasedimentary assemblege. MT 109(b) is composed dominantly of actinolite, with rare plagioclase, epidote and quartz (Plate 4.5). It has preserved relict cumulate fabric and so may be an intrusive rock. MT 211 shows cumulate texture and is composed of actinolite, plagioclase, with relict clinopyroxene preserved. Apatite and titanomagnetite are accessories. This is a metagabbro, and can be called cpx plagioclase cumulate. The third thin section contains olivine, plagioclase, secondary quartz, epidote, chlorite and spinel. It could be a poikilitic wehrlite.

D) Greenstones, gabbros and amphibolites are continously exposed striking N-S along the Baro river. They are usually associated with psammitic and pelitic schists, and basic and felsic dykes. In the middle of this succession there are thin bands of biotite and hornblende granitic gneisses. The greenstones vary from schistose to massive, with consistent vertical banding several centimeters to several meters across. Mafic and felsic dykes occur in the Birbir Domain sometimes constituting up to 50% of outcrop. Many of the dykes are mildly deformed suggesting that their

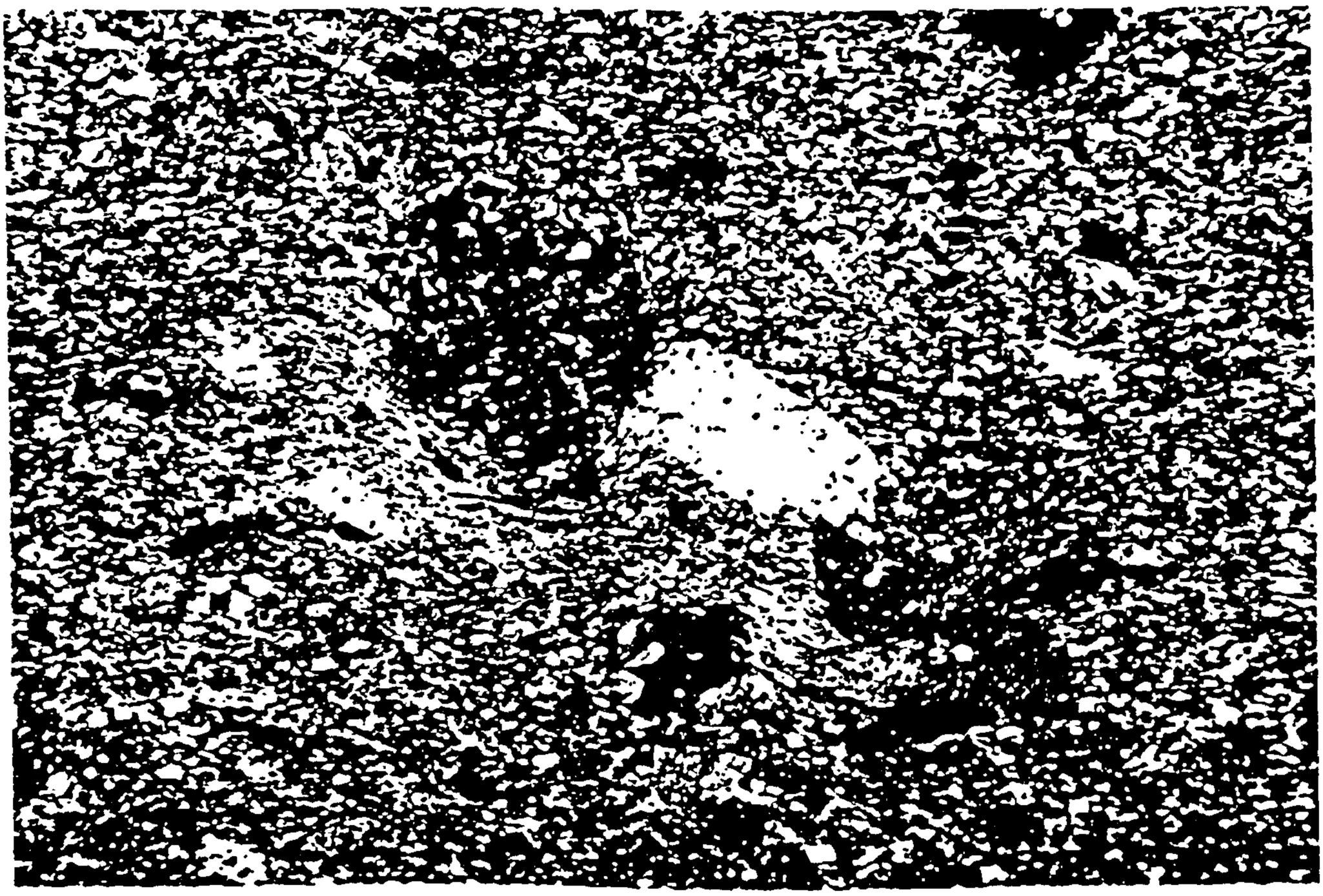

Plate 4.3 Simple schistosity in quartz biotite schist. Muscovite wrapping around biotite.Sample (MT434). Field of view 3.47.

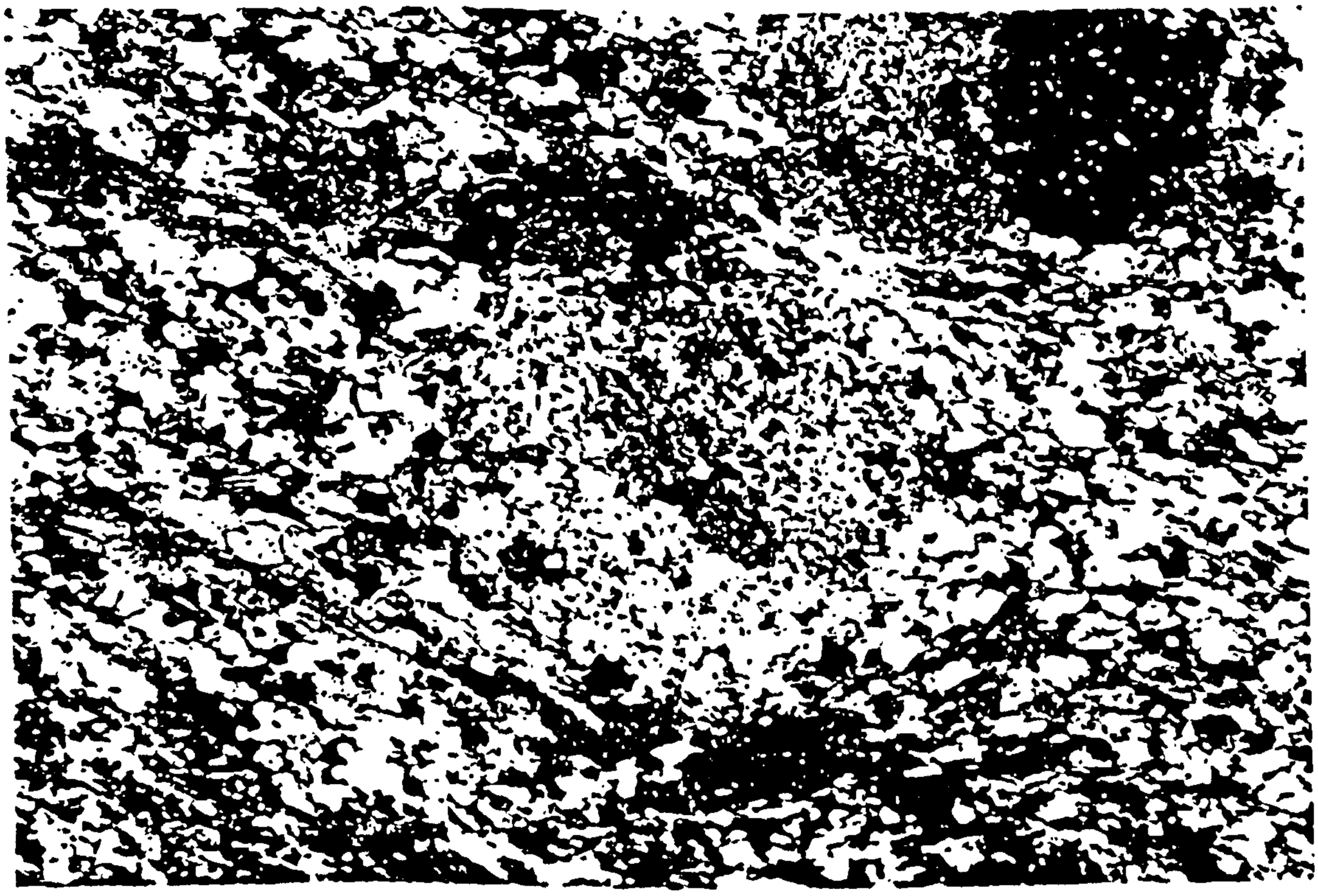

Plate 4.4 Birbir metapelitic schist (MT 109B). Schistosity wrapping around cordierite. Muscovite (yellow to pale brown) on the left hand side, while the biotites on the right hand side. Metamorphism (M_1) has been earlier than the last episode of deformation (D_1). Field of view 1.6.

intrusion was late relative to time of shearing, while the highly deformed dykes are pre-tectonic. Thin section study shows that the dominant minerals are actinolite and plagioclase, with minor tremolite, chlorite, and metamorphic quartz. In some sections (Plate 4.6) plagioclase, and hornblende are dominant, with garnet, biotite, and chlorite. Magnetite is an accessory mineral. The quartz is usually strained, while garnet shows a disequilibrium texture.

North of Bure a similar sequence of rocks is observed. Plagioclase, hornblende and quartz are abundant, with or without tremolite, epidote, rare biotite, and chlorite. Accessory minerals are apatite, sphene and magnetite.

Quartzofeldspathic gneisses occur separating greenstone belts in the Bure area. The gneisses are strongly foliated usually forming augen gneisses. These rocks are dominantly formed of quartz, plagioclase, with limited alkali feldspars, hornblende, biotite and epidote. Opaques are the only accessory minerals. The fact that these rocks have dominant quartz, suggests that they could be of sedimentary origin.

e) Throughout the area several granitic, granodioritic and/or quartz diorites crop out. The intrusive bodies in the east have a well developed planar fabric along the contacts while there is no evidence of any internal deformation. A few of the granitoids are gneissose throughout and evidently pre-tectonic. These intrusives will be discussed in a later section.

4.2.6 Baro Domain

This domain, which is exposed along the Sudan border, is made up of high grade granitic and biotite gneisses, with units of paragneisses and calc-silicate rocks. It extends from the Gambela area in the south to Guba village in the north (Figure 4.3). The Baro domain can be subdivided into two belts: the Gambela and the Bonga belts.

A) In the Gambela belt, the dominant rocks are granitoid gneisses, biotite gneisses, and numerous undifferentiated quartzo-feldspathic pegmatites. Southeast of Gambela the gneisses contain both early lenticular orthogneisses, deformed granite and granodiorite with fold axes trending north-south, and post-tectonic granitoids. The granitoid gneisses, which are the dominant rocks have biotite as their major mafic constituent. In thin section quartz and microcline are the

Plate 4.5 Birbir gabbro-pyroxenite. Relict cumulate texture preserved but blurred by metamorphism. Dominantly made of mottled actinolite, rare plagioclase, epidote and quartz. The actinolites enclose the plagioclases. Field of view 1.6.

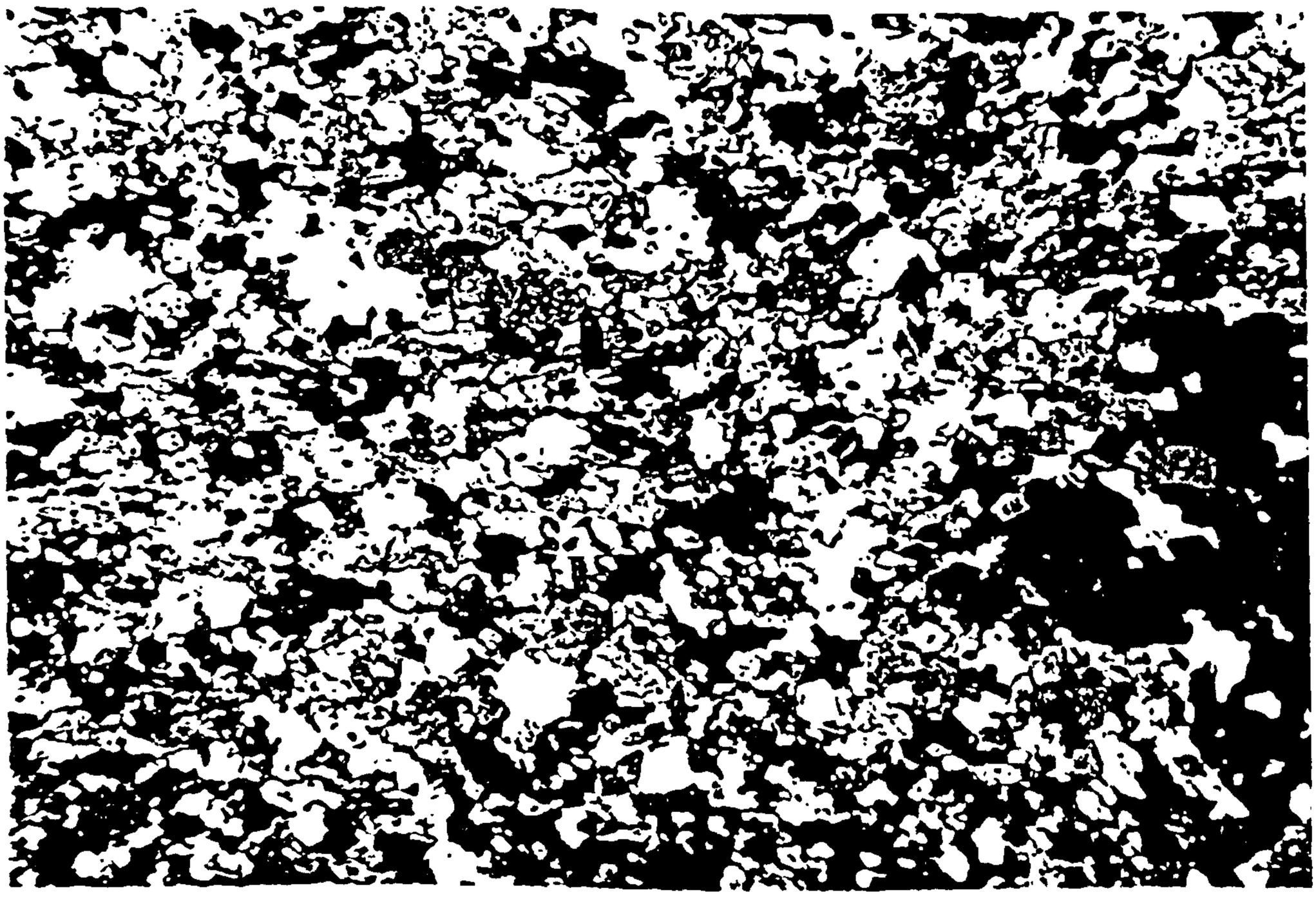

Plate 4.6 Garnetiferous amphibolite (MT107B). Fine grained aggregates of plagioclase, quartz and hornblende (pleochroic in green and brown shades). There is a garnet crystal (right hand side corner) with a disequilibrium texture. Field of view 3.47.

dominant minerals, with biotite and minor plagioclase. The accessory minerals are sphene, allanite, and apatite.

B) In the Bonga belt there are leucocratic gneisses, calc-silicate gneisses, and sillimanite garnet orthogneisses. The compositional characteristics and lack of uniformity of the garnet-amphibole gneiss, garnet-sillimanite gneiss and calc-silicate gneisses in the Bonga area indicate that they are primarily paragneisses. The calc-silicate gneisses have been observed to contain large pods (ca. 10 cm) of wollastonite (DeWit, 1977). Thin section analysis shows that one section (Plate 4.7) is composed of a mosaic of quartz and microcline, rimmed by and intergrown with epidote, plagioclase, and quartz. Garnets(grossular) commonly overgrow the gneissic banding. Light green diopside commonly envelopes hornblende. Accessories include sphene, zircon, apatite, allanite, calcite and magnetite. The mineral assemblage in section MT47 D (Plate 4.8) is dominantly quartz, microline and plagioclase with minor hornblende, epidote and calcite. The accessory minerals are sphene, zircon and allanite. Section MT47D shows a more igneous texture than MT 31C. These assemblage suggests high-grade thermal metamorphism superimposed on amphibolite facies metamorphism.

There are also fine grained leucocratic gneisses. These consist mainly of quartz, microcline, with minor plagioclase, and variable amount of muscovite and biotite.

Two kilometers west of Bonga there are melanocratic and mesocratic gneisses interbanded with the leucocratic gneisses, which form ridges. A thin section shows a quartz-plagioclase (An 25-30)-biotite assemblage. Large garnet grains occur as either augen, or overgrowing the gneissic banding. Sillimanite shows different habits. It occurs mostly as fibrolite, intergrown with biotite and sometimes occurs as radiating needles; at times it is feathery (Plate 4.9). The random sillimanite growth indicates that deformation had ceased before peak metamorphic conditions were reached. DeWit (1977) suggests that such textural patterns indicate fast growth. These rocks are of pelitic origin.

4.2.7 Syntectonic Granitoids

Syntectonic granitoids are widespread in W. Ethiopia. They occur west, south and north of Asosa , in the Baro river area, and north and east of the Nejo - Yubdo area within and parallel to the ophiolitic

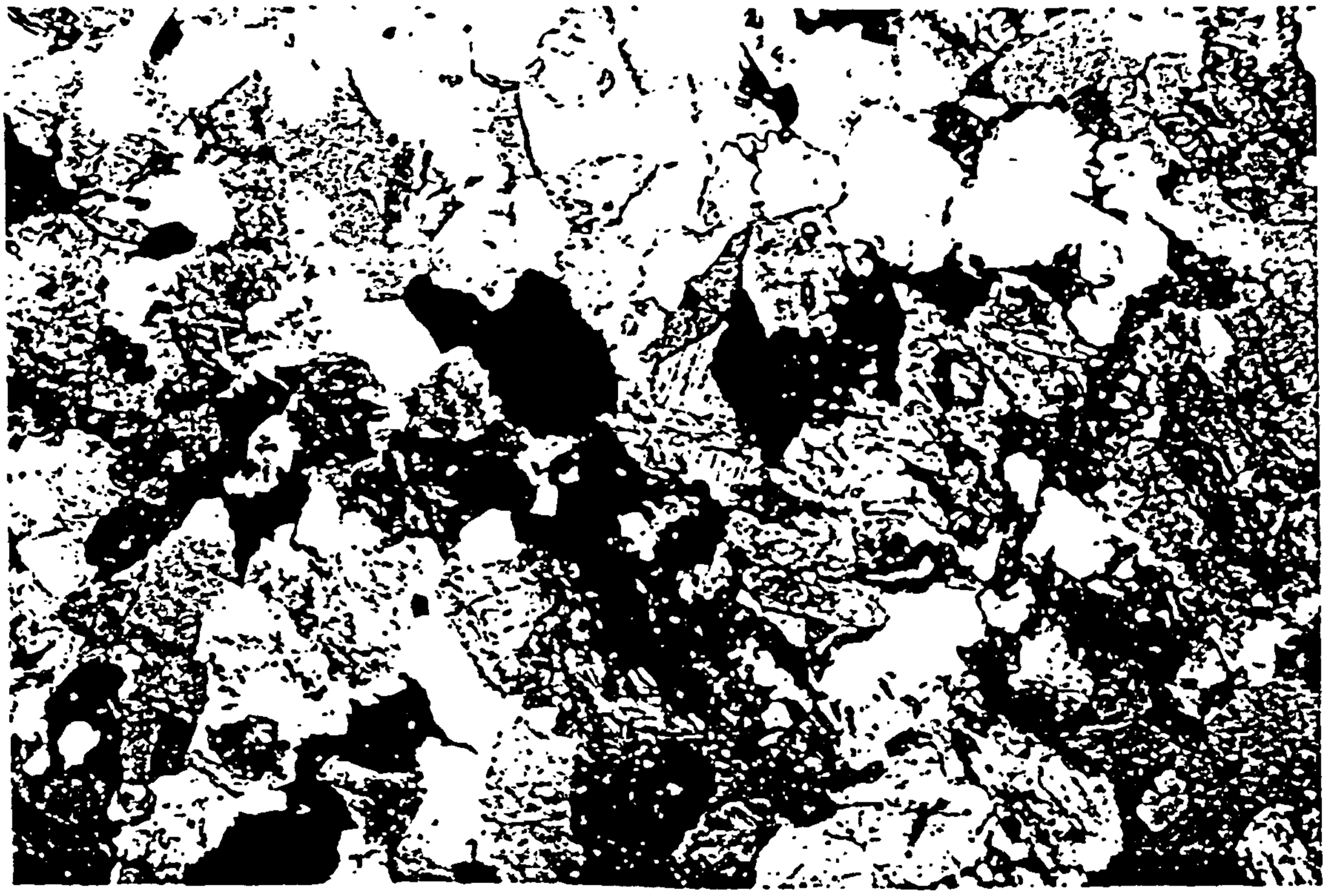

Plate 4.7 Baro calc-silicate gneiss (MT31C). Granular aggregates of quartz, plagioclase, and rare microcline surrounding hornblende (pleochroic in shades of green and brown) and epidote (yellow). In the center there are three crystals of calcite and two sphene crystals with their characteristic diamond shape. Field of view 3.47.

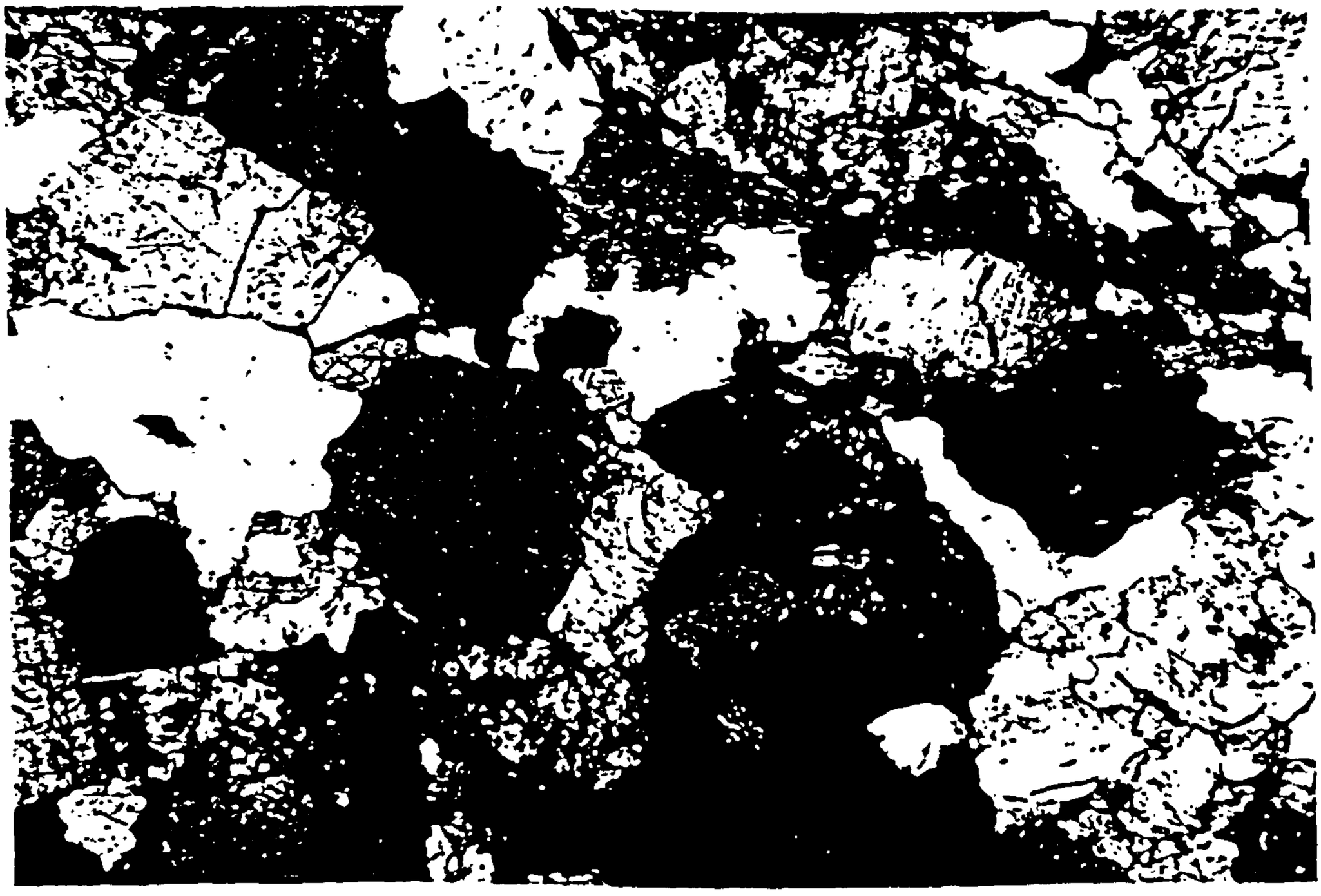

Plate 4.8 Hornblende granodiorite. Granular aggregates of quartz, twinned plagioclase, alkali feldspar, hornblende (shades of brown and green) and epidote (yellow). Sample No. MT47D. Field of view 3.47.

Plate 4.9 Bonga paragneisses (MT239). A quartz-plagioclase assemblage with augen garnets. Random growth of sillimanite (fibrolite) needles indicates that deformation has ceased before peak metamorphic conditions were reached. Field of view 3.47.

Plate 4.10 Biotite granite (GS205). The quartz, microcline (with characteristic cross-hatched twinning) and albite crystals (grey) which make up the bulk of the rock are anhedral and have slightly interdigitating boundaries. There are scarce elongate biotite crystals. Field of view 3.47.

suite (Figures 4.3 and 4.4). They generally form large massifs roughly concordant with the general strike. All the syntectonic granitoids are inhomogenously deformed and are mylonitised in varying degrees. Metagranodiorite includes some biotite metagranite. The metagranites are comprised mainly of magnetite bearing leucogranites to quartz-syenite sheets up to 2 km in width. Most of the eastern boundary of the Birbir Domain and the Bonga belt is occupied by granitoids.

The existence of thin folded granitoid bodies within the high grade gneisses has helped in elucidating the structural evolution of the area. The syntectonic granites are generally pink or yellowish-grey and are sometimes porphyritic. They are strongly foliated especially along the margins. A characteristic feature of these granites is the abundance of pegmatite and aplite veins. No thin sections of these granites were made.

4.2.8 Post- tectonic Granites

The post-tectonic granites show a wide areal distribution. They are massive, often porphyritic and are usually discordant to folded structures. Variation in composition and texture of the various granites suggest several phases of intrusion. There are several granitic bodies throughout the area (Figure 4.3). In many cases they have a well developed planar fabric along the edges, while they have not suffered any internal deformation. Two post-tectonic granites have been studied from the Gore area. In thin section they are composed of orthoclase, microcline, and quartz with minor plagioclases and biotite (Plate 4.10). Accessory minerals are apatite and magnetite. Sometimes they include granite porphyries.

4.2.9 Alkaline Intrusives

Three massive alkaline intrusives are so far known: Abu Ramla, Gangan and Tulu Kapi (UNDP, 1972). They are all post-tectonic and may belong to the last stages of a late Precambrian-Lower Palaeozoic magmatic cycle. They may be correlated with certain alkaline complexes of Eastern Sudan (Vail, 1978).

Abu Ramla and Gangan Mts. seem to be controlled by north - south lineaments. Abu Ramla, near the Sudanese border, is mostly syenite. The main rock types forming Gangan are alkali

granites, riebeckite granite, and leucocratic alkaline syenite (UNDP, 1972). Several thin veins of pegmatites containing beryl crystals, which are exposed to the north within the syntectonic granites. It is not clear whether these pegmatites are related to the alkaline complex or to the granites. Tulu Kapi alkaline rocks outcrop in the vicinity of Tulu Kapi village where they form two or three stock-like massifs. These rocks may be classified as alkaline quartz syenite.

4.2.10 Gabbroic Complexes

Three gabbroic complexes occur linearly with north-south arrangement in the Blue Nile Valley, northwest of Nejo. These are Duma, Dabuso and Sirba (UNDP, 1972). They show a concentric structure and are presumed to be formed by a number of arcuate dykes. Included with this group are the gabbro-diorites and gabbroic anorthosites which form part of, or flank the ophiolitic belt (Figure 4.3). The alkaline intrusives, and gabbroic complexes have not been studied during this work and will not be discussed further.

4.3 STRUCTURE

Introduction

The most conspicous tectonic trend in Western Ethiopia is north-south, with deviations to northeast and northwest. These trends are characteristic for the low grade rocks of the Upper Proterozoic Red Sea fold belt (Kazmin *et al.*, 1978). It is increasingly clear that what are usually assumed to be slight deviations are in fact the result of different tectonic episodes that have been co-axially folded.

In most of the map area (except the Geba Domain) bedding as well as lithologic contacts are parallel or nearly parallel to schistosity and are on average north-south trending except in intrafolial folds. In Birbir Domain foliation dips are mostly steep to vertical, while in the Baro and Geba Domains foliation is openly folded with shallow plunging axes. Stretching lineations strike parallel throughout the map area, plunging gently north or south.

Most of the tectonic domains in the Welega-Ilubabor area have thrust contacts. The Baro Domain high grade gneisses are thrust onto the Birbir volcano-sedimentary domain. The Birbir

Domain and the granodiorite-diorite batholith have a tectonic contact. In the eastern marginal part of the zone these rocks appear to be an upward continuation of the sedimentary succession of the ophiolite belt. Here the contact is most probably gradational. There is a common development of shear zones along the thrust planes, but striae have not been observed.

For ease of structural interpretation the area has been subdivided into five structural domains, and each zone will be discussed separately. All acquired foliation and bedding data of the Baro and Birbir Domains were plotted on equal area, lower hemisphere projection. To aid comparison between data sets of varying size (Starkey, 1977) the projections have been contoured using the STATIS program developed by N.G. Woodcock on the Cambridge University Main Frame IBM-370 computer. The program also analyses the distribution and fabric shape of the data using the eigen-vector method of Watson (1965,1966). Normalised eigen-values S_1, S_2, S_3 define three eigen-vectors, V_1, V_2 and V_3 which approximate the Fisher Mean (Fisher, 1953), an intermediate value and the pole to the best fit great circle respectively.

Woodcock (1977) developed K and C parameters to quantify the shape and strength of fabric distributions by making two axis, logarithmic comparisons of normalised eigen-values. Figure 2.4 illustrates such a two-axis covariation, where the value K = ln (S1/S2)/ln(S2/S3) varies inversely with the strength of cluster in a distribution and the value C = ln (S1/S3) varies proportionally with the strength of any preferred orientation fabric.

4.3.1 The Geba Domain

The structure in this area can be divided into two subareas: the strip that is nearer to the Granodiorite-diorite batholith and the Birbir Domain and those farther away. In the Nopa area (Figure 4.4) there are gentle isoclinal folds with E-W axes. The general strike of banding and foliation is E-W with deviations to WNW and ENE (Figure 4.7). A number of such folds each 20 to 25 kilometres long and 5 to 10 kilometres wide were mapped (Kazmin *et al.*,1979b). These are accompanied by small amplitude (metres and tens of metres) isoclinal folds of the same trend with sharply undulating axes. In general it appears that prior to the formation of north-south folds there existed an earlier isoclinally folded gneiss - migmatite complex dipping at 30° to 50° to the north. The E-W isoclinal

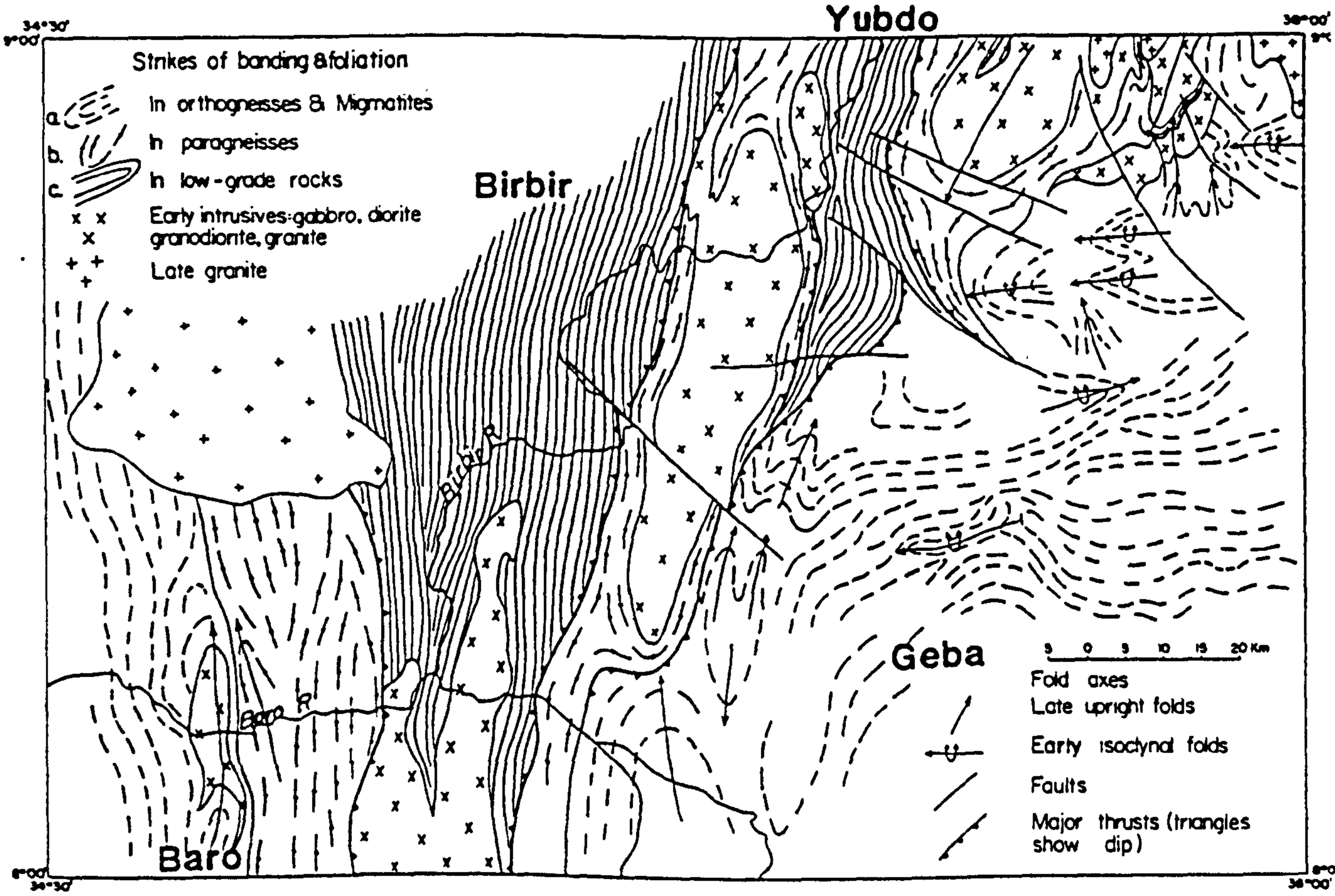

Figure 4.7 Structural sketchmap of the Gore region, W Ethiopia. Showing the five tectonic domains studied. Modified after Kazmin et al (1979a).

folds are generallly overturned to the south. In the Geba River gorge (east of Metu) the gneissic rocks are isoclinally folded with axial planes dipping to the east and axes plunging north. North of Gutete there is a series of gently undulating and upright folds, plunging 25° to the north. It forms part of an E-W structure. Going westwards (north of Nole Kaba) the folds trend northwestwards, and slowly reorient into N-S direction. The severity of deformation increases westwards, with banding and foliation strongly refolded into tight upright folds of general north-south strike.

North of Nopa the gneisses have experienced a series of kink type flexures. These kink bands seem to be spread in between the eastern region, and the margin of the gneissic block. In Karo area there are old northwest trending shear zones that have produced drag folds in the gneisses. The movement along the shear zones was dextral. West of Alga Guracho gneissic foliation is observed to be cut by pegmatitic and migmatitic bands. It is possible that gneissic foliation was developed before regional migmatisation.

Small scale isoclinal folds, and even microfolds are observed in the north-south folded gneissic complex. This is evidence of the older structure. Isoclinal folds usually have their axis parallel to foliation. Two stages of deformation are clearly observed, although further events could be envisaged.

4.3.2 Yubdo Domain

The rocks in the area have undergone a complex polyphase deformation and metamorphic history. The earliest deformational fabrics recognised are linear fabrics, which are confined to the serpentinised dunites predating serpentinisation and thus probably represent hot ductile deformation processes during the formation and/or emplacement of the dunite (DeWit and Aguma,1977). The mafic-ultramafic rocks additionally underwent extensive brittle deformation and serpentinisation prior to, and during, the serpentinisation period. There is extensive evidence for shear zones which have highly sheared the ultramafic material.

The Tulu Dimtu massif is bounded on all sides by well developed shear-zones and in some cases it is clear that sedimentary units and fold axes are obliquely cut by these zones (Figure 4.6). The characteristic feature of the high deformation Tulu Dimtu - Yubdo belt is the wide development

of linear bodies of highly sheared ultramafic material (Figure 4.6). These bodies range from 10 or 20 metres to 500 or 1000 metres in length. The belt can be described as consisting of numerous closely-spaced steep shear-zones. In the west the Tulu Dimtu belt is bordered by a large dioritic pluton with a highly deformed eastern contact: the eastern border of the shear belt has not yet been defined. In Tulu Dimtu the maximum deformation is concentrated in a narrow (4 to 5 kilometre) zone running from the highway between Tulu Kingi and Ghidano to the Sal river east of the Tulu Dimtu massif, which can be traced in the southwesterly direction for about 80 kilometres to Yubdo. This zone was regarded as a major tectonic suture by (Kazmin, 1978).

The Yubdo ultramafic complex is affected by faults trending N-S, E-W and NE-SW. The E-W and NW trending faults are characterised by severe cataclasis. Kazmin (1978) observed two sets of steep cleavages, northeasterly and northwesterly, with the development of crenulation at several points in the mapped area and in neighbouring regions of Welega. They indicate at least two stages of deformation. To the later stage belong northwesterly and latitudinal faults cutting and displacing northeasterly folds and shear-zones. Left-lateral displacement was noted along some northwesterly trending faults.The ophiolite contacts with the high grade rocks are all tectonic.

Most of the ophiolitic succession dips northwestwards to southwestwards (Berhe, 1981) and a series of thrusts are observed, which dip to the west. This suggests that the ophiolites were thrust to the east and formed a series of nappe sheets. A westerly subduction is confirmed by a westward increase of K_2O/K_2O+Na_2O in the magmatic arc suites of the Birbir Domain (Teklewold *et al.*,1987).

Ghidey W. Gabriel (1981) considered the Yubdo ultramafic body as an intrusion, because of the existence on the eastern side of the body of a strip of hornfelsic aureoles. But he also describes a major crushed cataclastic rock along a major fault scarp on the extreme NE side of the massif, which may be interpreted as a thrust.

The general structural interpretation suggested above implies that the ophiolitic rocks form a sheet-like body or bodies folded and faulted together with underlying and overlying metasediments. This is usually interpreted as a result of napping of ophiolitic rocks on to basinal sediments. In many cases the nappes are buried by later sediments and then folded together with them in the course of subsequent tectonic episodes. The subsequent deformation caused shearing and faulting of the

ophiolite complex.

4.3.3 Birbir Domain

The Birbir belt is affected by a complex fold-thrust structure. Major folds are expressed by a synclinorium which extends from the Birbir-Baro junction northwards to Geba area (UNDP, 1972). The structural trend changes from NE-SW in the Birbir basin to NW-SE in the Mendi-Nejo area. Further north the trend swings N-S in the Blue Nile - Asosa area. The regional trend of the granitoid batholith swings from northeast to northwest and again north-south to northeast in the Blue Nile area (Kazmin *et al.*, 1979a , 1979b). This belt was most probably produced by sinistral movement of a block of high grade gneisses and migmatites situated east of this area. This strike-slip movement occurred along the contact of the batholith, and the volcano- sedimentary rocks. The location of the volcano-sedimentary succession appears to be controlled by major lineaments (see Chapter 5).

In the Birbir domain a total of 69 foliation data points are plotted on a contoured equal area net (Figure 4.8a). The foliation planes measured are close to the girdle/cluster transition (c=2.4, K=0.86) with a mean foliation attitude 36/100 and a best fit pole to girdle 4/008. Although it forms a girdle two separate clusters are observed.

In the Birbir-Baro River area a single main cleavage, schistosity affects the low grade rocks whilst the granitic rocks show a gneissic fabric. Bedding, as well as lithologic contacts has a north-south trend and is parallel or subparallel to schistosity. In the Birbir Domain foliation dips are steep to vertical. In the Bure area, the schistosity generally has a northeasterly trend with steep dips to the west (Figures 4.8a and 4.8c). The schistosity is sometimes oblique to bedding and is parallel to the axial planes of the major folds. Crenulation cleavage related to the open folds is well developed east of Bure (DeWit, 1977) and the Asosa - Kurmuk area. Small open late folds are locally observed refolding F_1 folds. These are considered local adjustments to the regional deformation.

Birbir foliation data

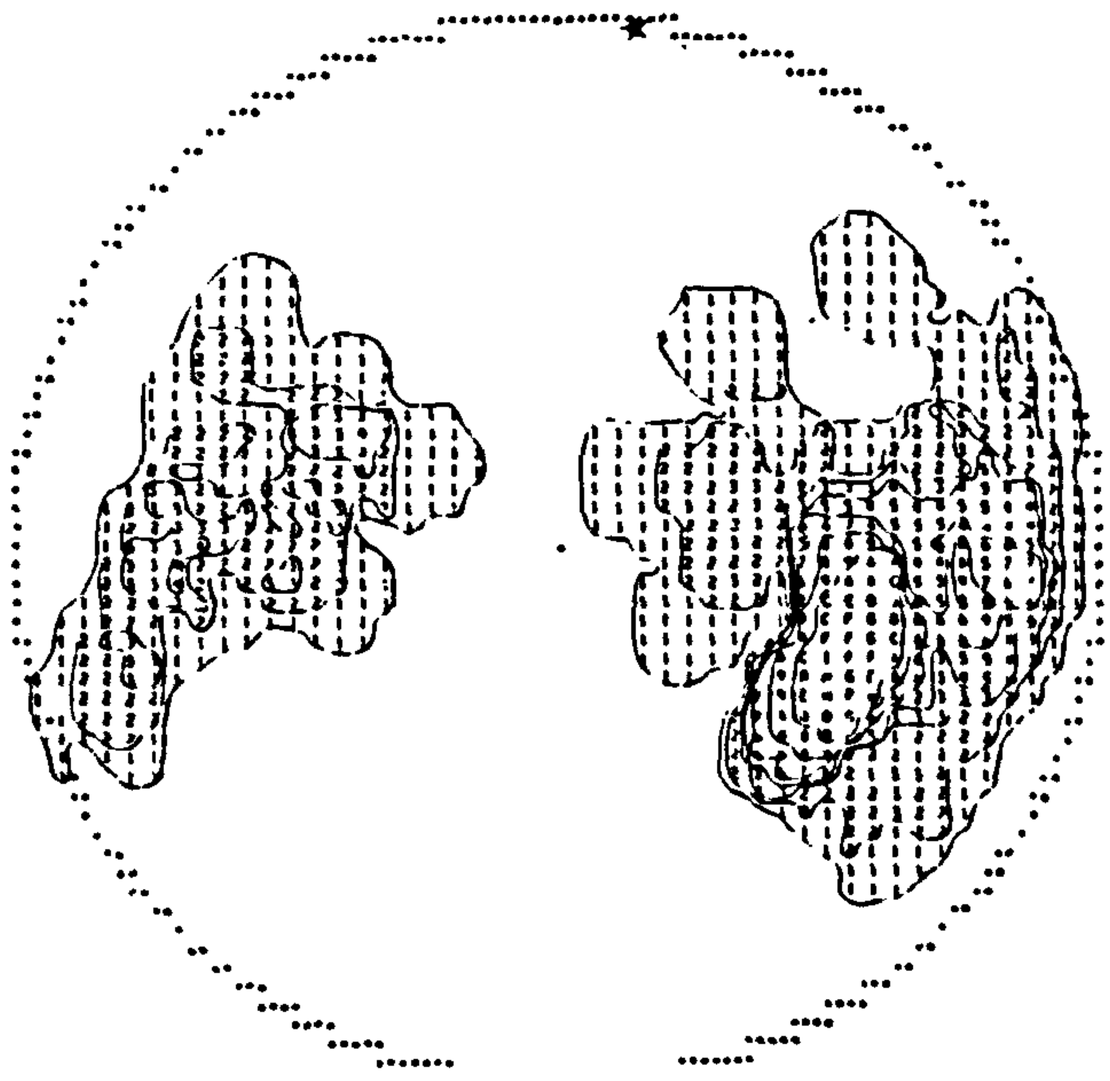

A

Bonga bedding/banding data

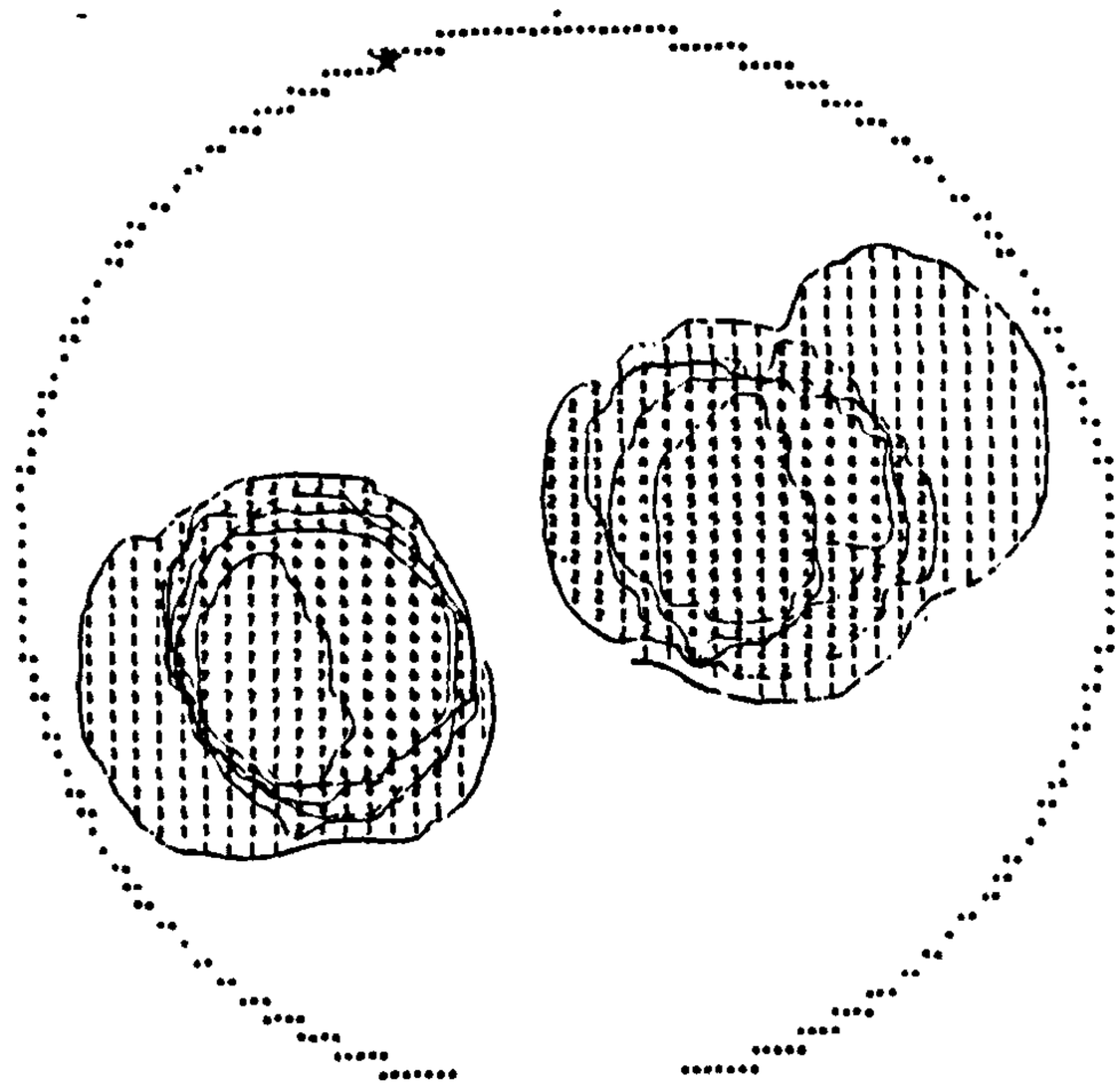

B

Birbir/Bonga data

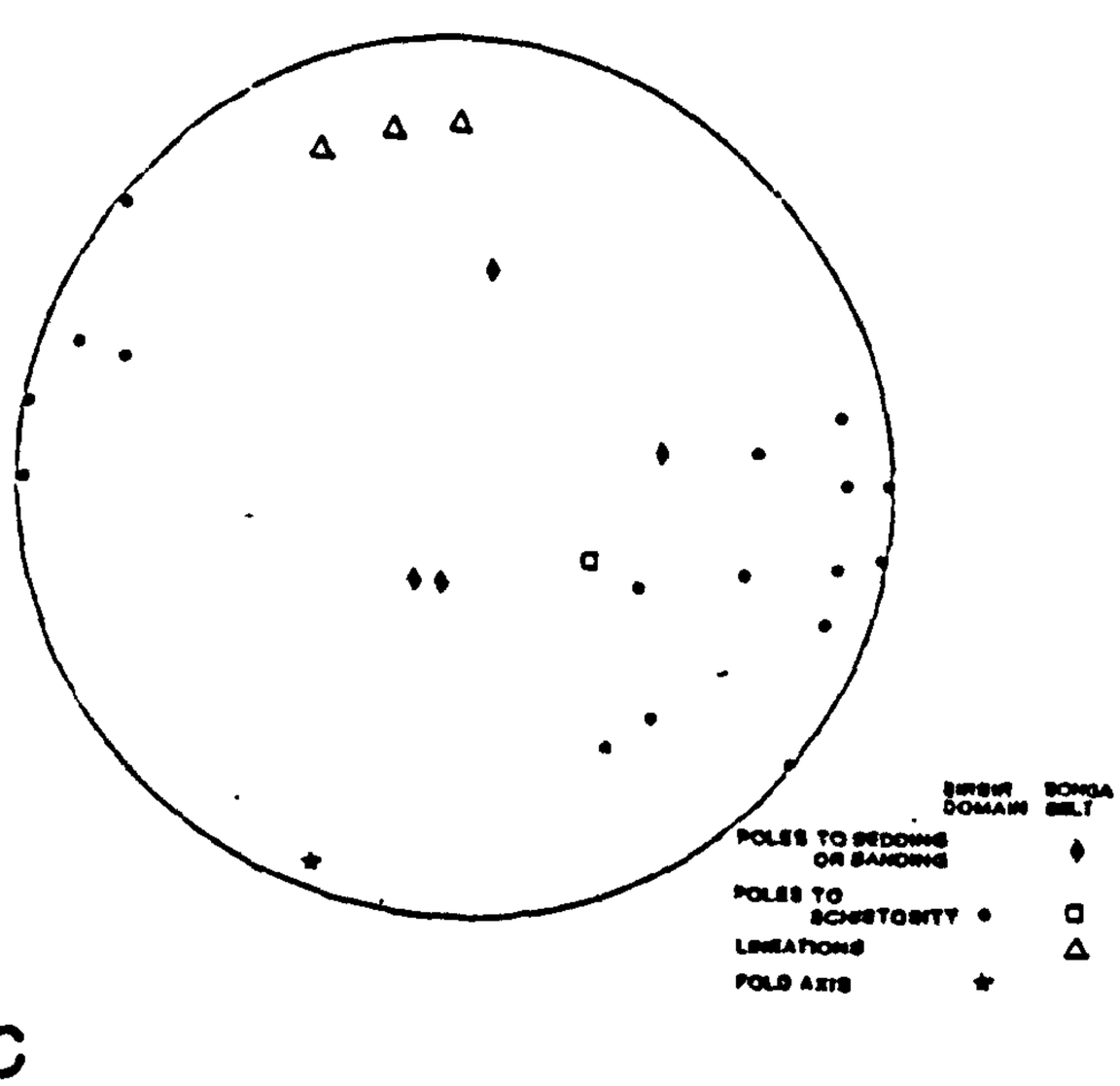

C

Figure 4.8 (a) Lambert equal area plots of foliation data of the Birbir area. The pole to the great circle girdle is shown by a star. The contours are hand drawn. (b) Lambert equal area plots of Bonga bedding and banding data. The pole to the great circle girdle is shown by a star. The contours are hand drawn. (c) Equal area lower hemisphere projection plots of the structural elements of the Baro-Birbir junction, SW Ethiopia. After DeWit (1977).

4.3.4 Baro Domain

The western most zone is made up of high grade gneisses bearing evidence of polyphase deformation. The margin of the Baro Domain gneisses shows tight north-south trending folds (Figure 4.8b) parallel to that in the Birbir Domain. The older gneissic banding was refolded along north-south axes, as indicated by the intersection of gneissic banding with later axial plane cleavage (Kazmin *et al.*,1979b). Along the northeastern margin of the Baro Domain a major foliation antiform which strikes NNW-SSE and plunges northwards dies out a few kilometres south of the Baro river (Moore *et al.*,1987).

Bonga belt

In Bonga the foliation is openly folded about moderately plunging axes. A total of thirteen bedding-banding data points from the Bonga belt were plotted on a contoured equal area net (Figure 4.8b). The bedding planes measured show a transition from a girdle to uniaxial girdle (C=5.02, K=0.13) with a mean foliation attitude 73/247 and a best fit to girdle 1/341 (Figure 4.8b). Although it forms a girdle two separate clusters are observed.

A pronounced north-south lineation and/or rodding with a low (20°) northerly dip (Figure 4.8c) defined by the metamorphic mineral grains and quartzo-feldspathic segregations marks this domain. It appears that this lineation is the result of two overprinted deformations.The earlier fabric in the rocks is manifested by a well developed gneissic banding. This banding may be of sedimentary origin as in the case of the calc-silicates, but has since been considerably altered by subsequent flattening. No folding related to this deformation was observed, but small tremolite/actinolite pods in the gneisses about halfway between Gambela and Bonga were probably derived through extensive boudinaging of larger pre-existing bodies (DeWit, 1977).

Large scale refolding of the gneissic banding is evident on both sides of Bonga village, but is best exposed in a series of ridges about 1 kilometre west of Bonga. Open folds, with wavelengths ranging from 100 metres to several kilometres and with near vertical axial planes, have an axial planar fabric. The latter varies from an anastomosing schistosity or fracture cleavage in the cores to a pronounced schistosity in the limbs where it clearly transposes the gneissic banding. Commonly

minor granitic pegmatites crosscutting the gneissic banding have been observed .

4.3.5 Summary

Two major episodes of deformation have been identified in the structural evolution of western Ethiopia. An early stage of deformation (D_1) generated isoclinal folds with fold axes trending approximately east-west and these structures are preserved and restricted to the Geba Domain. The second deformation (D_2) is a large scale folding event which produced upright to overturned folds plunging to the north or south. The style of deformation is the same for the Baro-Bonga and Birbir Domains. The direction and plunging of fold axes is similar with open folds and narrow hinges. However the gneissic banding in the Baro Domain was formed during an earlier period of deformation. Although the Baro and the Geba Domains share a similar structural history, major east-west fold trends in the Geba Domain are not seen in the Baro area.

4.3.6 Faults and Shear Zones

Western Ethiopia is affected by a series of lineaments, faults, and fractures, which are dominantly trending NW-SE, WNW-ESE, E-W, with few major N-S to NE-SW. These faults have an extended history, as they also affect the Tertiary volcanics. The most significant of these faults are those trending N-S, and NW-SE to WNW-ESE, as they usually form fault contacts between high and low grade rocks. These faults appear to control, cut or even truncate post-tectonic granites. Their importance over time is suggested through their control of the trend of trachytic plugs, necks and dykes in the Tertiary volcanics.

The Birbir valley is controlled by a NNE striking and westerly dipping shear zone which is about 5 km wide and over 50 km long . This shear zone separates the Baro and Birbir Domains. A second NNE trending shear zone is observed southeast of Bure and this forms the boundary between the Birbir and the Granodiorite-diorite batholiths. Each shear zone comprises numerous mylonite zones separated by less strained rocks (Moore *et al.*,1986). The abundance of mylonite in the Birbir Domain indicates a protracted period of ductile faulting and shearing.

Major NW-SE and E-W trending lineaments post-date the period of ductile faulting. The

NW-SE trending shear zones are suggested to be sinistral, while the E-W are predominantly dextrally displaced. Many of them truncate N-S trending linear topographic features, such as the Kurmuk lineaments (Berhe,1987; see section 6.6). The NW-SE fault systems show left lateral displacements of the order of several hundreds of meters (e.g. Degero shear zone) while the N-S trending Asosa - Kurmuk lineaments have experienced earlier lateral shifts, and at present shows vertical displacement as much as 1000 m above the Sudan plain. For a more detailed interpretation of the fracture pattern see section 6.6.2.

4.4 METAMORPHISM

The metamorphic complex of Western Ethiopia can be subdivided into three metamorphic zones:

i) the Geba structural domain and the Granodiorite-diorite batholiths have attained metamorphic grades into upper amphibolite facies ii) while the Yubdo-Birbir belt is lower greenschist to lower amphibolite facies and iii) the Baro-Gambela structural domain has attained the upper amphibolite facies.

The transition in metamorphic grade between the Geba and Yubdo structural domains is abrupt, while the transition is more gradational from Birbir to Baro structural domains in the west.

There is a distinct difference between the timing of metamorphic mineral growth in Geba, Yubdo and Baro Domains. In the Geba and Baro Domains the high grade metamorphism attained during D_1 has obliterated all pre-D_1 mineral assemblages except for the gneissic foliation. However the growth of the main index minerals post dates the gneissic fabric i.e the development of porphyoblasts and migmatisation. Hence it can be concluded that the Geba, and Baro Domains had previously undergone a separate tectono-metamorphic event. This is supported by the structural data available.

The Bonga belt mineral assemblages are sillimanite-microcline, sillimanite-garnet-biotite, hornblende-clinopyroxene and garnet have been observed , which are significantly of higher grade than those of the Birbir Domain.

Table 4.1 Typical Mineral Assemblages of the Metamorphic Complex of W.Ethiopia

Rock Group	Rock Type	Mineral Assemblages
	Granitoid	Quartz - biotite - hornblende - myrmekite/microcline-plagioclase - allanite - epidote, - sphene and apatite.
Geba Domain	Granitoid	Quartz - orthoclase - biotite - hornblende - epidote - allanite - apatite - zircon - sphene.
	Mafic	Hornblende - epidote - chlorite - plagioclase - secondary minerals are magnetite - titanomagnetite
Yubdo Domain		
	Ultramafic	a) Olivine - clinopyroxene - quartz - accessory minerals are chromite - magnetite.
		b) Clinopyroxenes - orthopyroxenes- secondary minerals are tremolite and chlorite.
	Pelitic	a) Quartz - muscovite-green biotite-plagioclase (albite)
		b) Quartz-garnet-brown biotite-muscovite- plagioclase-chlorite
Birbir Domain		
	Mafic	Hornblende/actinolite-biotite-epidote-chlorite-plagioclase-quartz.
	Pelitic	Quartz-biotite-muscovite-oligoclase/andesine-garnet (almandine)-sillimanite.
Bonga	Calcareous	Hornblende-diopside-grossular-labradorite-calcite± wollastonite.
	Mafic	Hornblende-diopsidic augite-garnet-andesine-phlogopite.
Gambela	Granitoid	Quartz-microcline-biotite-plagioclase. Accessory minerals are sphene - allanite-apatite.

In the Birbir Domain the common mineral assemblage is hornblende, biotite and oligoclase and the absence of chlorite indicates lower amphibolite facies metamorphism. The Birbir Domain developed a penetrative cleavage during D_1 under low to middle greenschist facies metamorphism. The main period of recrystallization and mineral growth in the Birbir rocks occurred during D_2 during which an upper greenschist to lower amphibolite grade of metamorphism was attained. The two episodes of deformation of the Birbir rocks is best illustrated by mineral assemblages in a thin section

(Plate 4.9). In this section the schistosity wraps around cordierite which suggests that metamorphism began earlier than the last episode of deformation (D_2). DeWit (1977) suggested that the metamorphic assembleges attained in Bonga area (Baro Domain) as compared to the Birbir domain (during D_1) are a result of a drier environment (low water pressure, PH2 O <P total) with the temperature/pressure gradient increasing from east to west.

The metamorphic assemblages in the mafic-ultramafic units of Yubdo-Tulu Dimtu belt reflect mainly zeolite and greenschist facies P-T conditions.

An attempt is made to outline the P-T conditions based on mineral assemblages which is presented in Table 4.1. The sequence of metamorphism is shown in Figure 4.9. The Geba Domain is the most intensely deformed zone, and has attained the highest grade of metamorphism. The fact that partial melting of quartzofeldspathic paragneisses, and granitoids occurred to form migmatites - suggests that temperatures over 600° C may have been reached. Anatexis in gneisses may take place at minimal temperature of about 600° C at 3.5 Kb and 615° C at 10 Kb depending on H_2O availability (Winkler, 1976) i.e. if H_2O pressures are larger than about 3.5 Kb. The amphibolites of the Yubdo-Birbir belt (Table 4.1) can be marked to the high temperature side of the chlorite out curve (Figure 4.10). However the presence of epidote, hornblende and/or actinolite suggests that the amphibolites have reached the transition to the epidote amphibolite facies. The occurrence of andalusite and staurolite with biotite and muscovite in the metasedimentary schists of the Birbir Domain is consistent with a low P/T regional facies with peak pressures below 3.5 kb.

In the Bonga - Baro area the presence of sillimanite rather than andalusite and the presence of cordierite and almandine, quartz and muscovite indicates that the pressure conditions were high (6 to 7 Kb, figure 4.9) (Winkler, 1976). DeWit (1977) described the presence, in the same rock, of a pressure - independent mineral like anthophyllite, together with a near temperature - independent assemblage of cordierite- almandine-sillimanite-quartz. The stability field for this assemblage is 6 to 7 kilobars and 650-750° C (Figure 4.9).

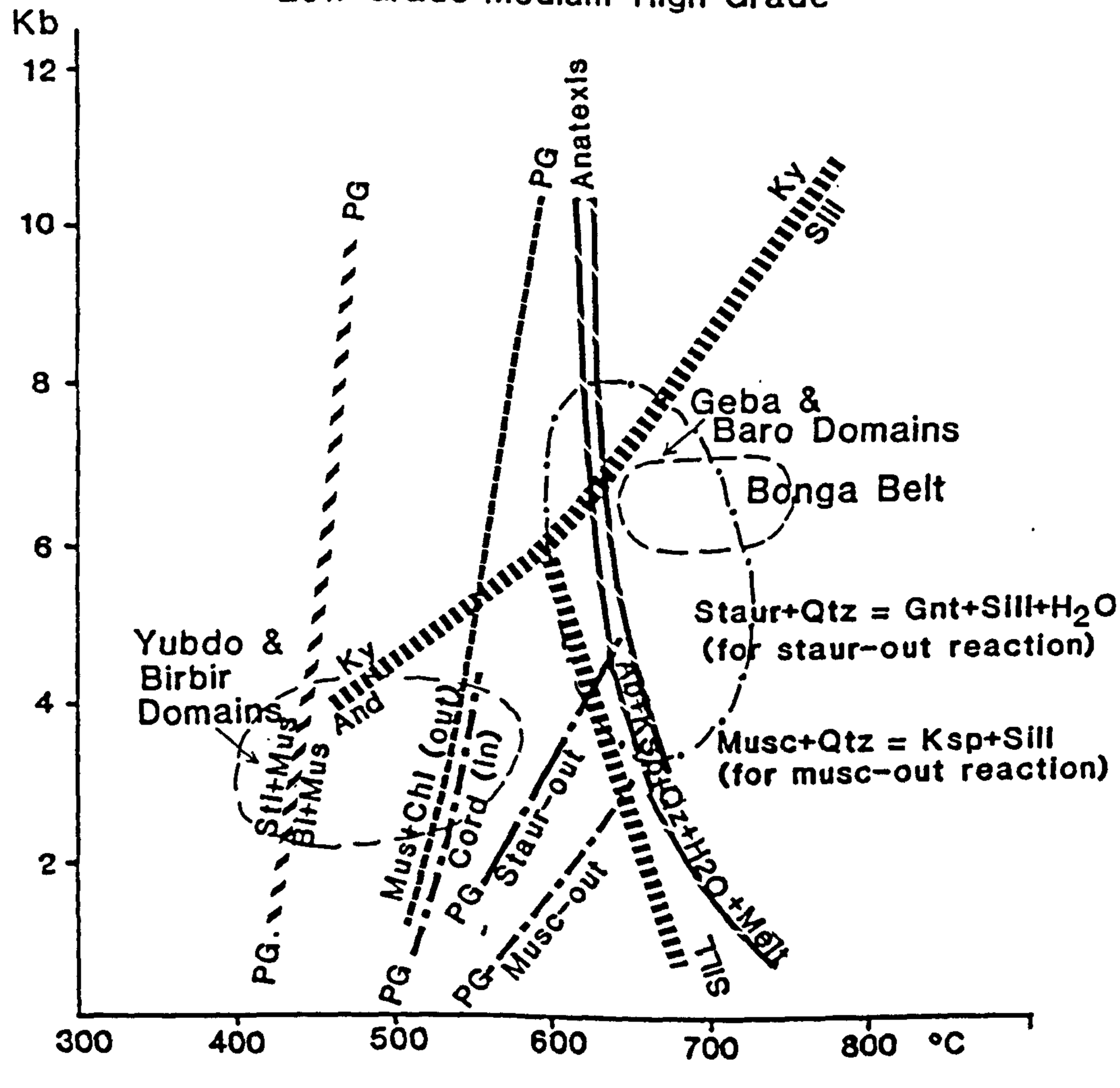

Figure 4.9 Metamorphic P-T fields of the Gore region, W Ethiopia.

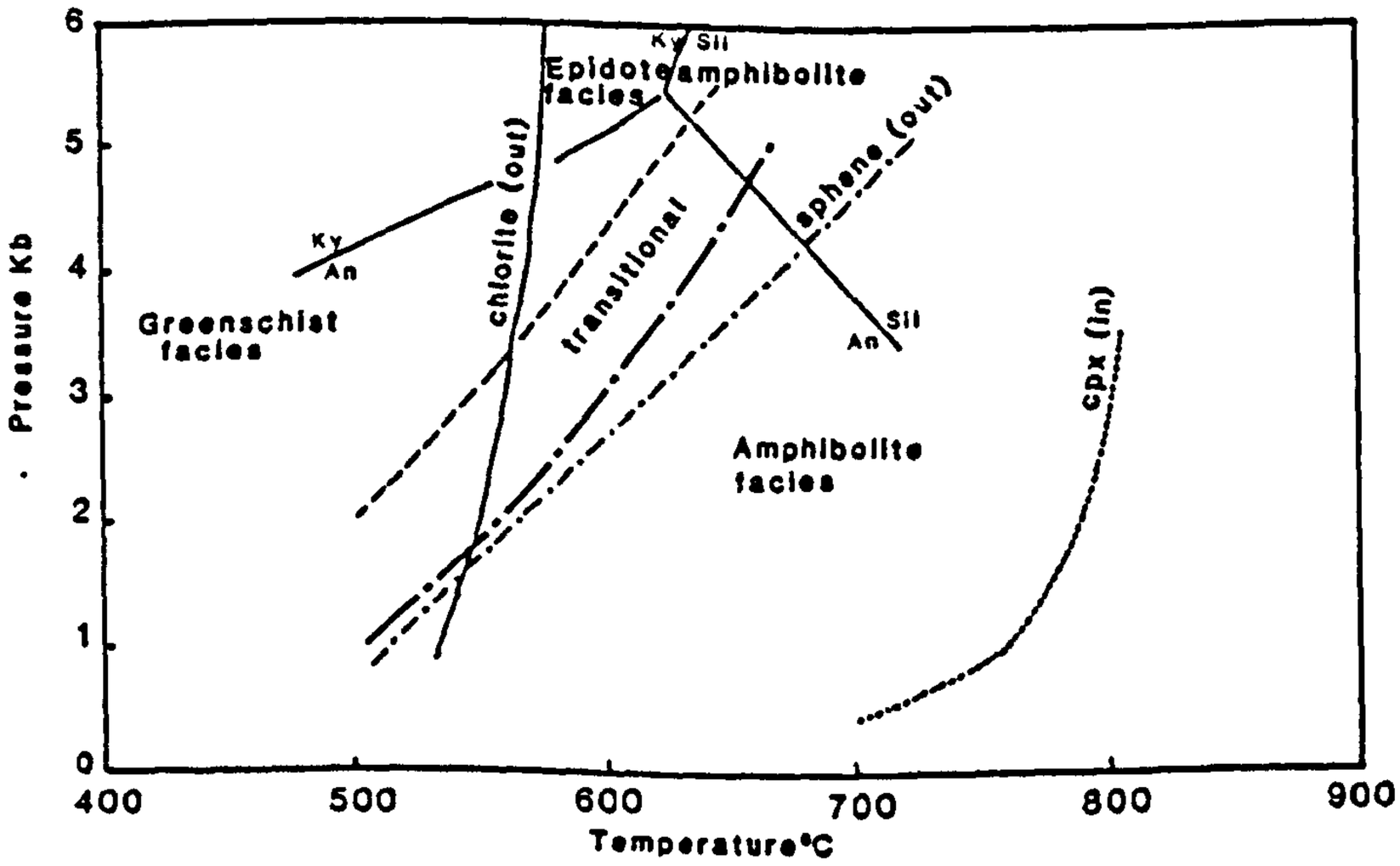

Figure 4.10 Pressure-temperature grid for regional metamorphism of Birbir amphibolites. Reaction curves from Liou et al (1974), Spear (1981). Mineral abbreviations: Ky= kyanite, An= andalusite and Sil= sillimanite.

4.5 GEOCHEMISTRY

4.5.1 Introduction

Thirty-four representative rock samples were analysed from the Gore area (see Figure 4.4) for major and trace elements. Fifteen are granitoids, seven paragneisses, five metasedimentary schists, four amphibolites, and three ultramafics. Five selected granitoids were analysed for REE. These samples are too few to provide a coherent geochemical study of the area, however in the absence of any other geochemical data they are of critical value. The purpose was to fingerprint geochemically the various lithologic domains established, and secondly to elucidate and constrain the tectonic evolution of the belt. The geochemical data are tabulated in appendix B. Sample locality maps have been included (Figure 4.4).

4.5.2 Ultramafics

All samples analysed have high CaO (11.5-13.4 wt %), Al_20_3 (11.58-16.72 wt %) and moderately high MgO (9.6-11.5 wt %) and TiO_2(0.5-1.6 wt %) as compared to mantle sequence ultramafics. Moderately high TiO_2; MgO (9.6 - 11.5 wt %) and high Y (10-20 ppm) suggests cpx as a major phase. Where CaO, and Al_2O_3 abundances are higher reflect the occurrence of relict pyroxenes, these rocks are probably wehrlites. A Cr_2O_3-NiO plot is used to separate the cumulate from the mantle sequence (Figure 4.11). It is observed that these ultramafics, contain low Ni and Cr and hence plot at the minimum level of the cumulate fields as compared to those of Baragoi area (see section 2.5.3). From this limited data no conclusion can be derived as to whether the ultramafic rocks are of oceanic or layered origin.

4.5.3 Birbir Metavolcanics

Representative metavolcanic rocks were collected from NW and SW of Bure area (Figure 4.4). The metavolcanics were plotted on TiO_2 - Ni, and TiO_2 - Al_20_3 diagrams (Figure 4.12). The metavolcanics

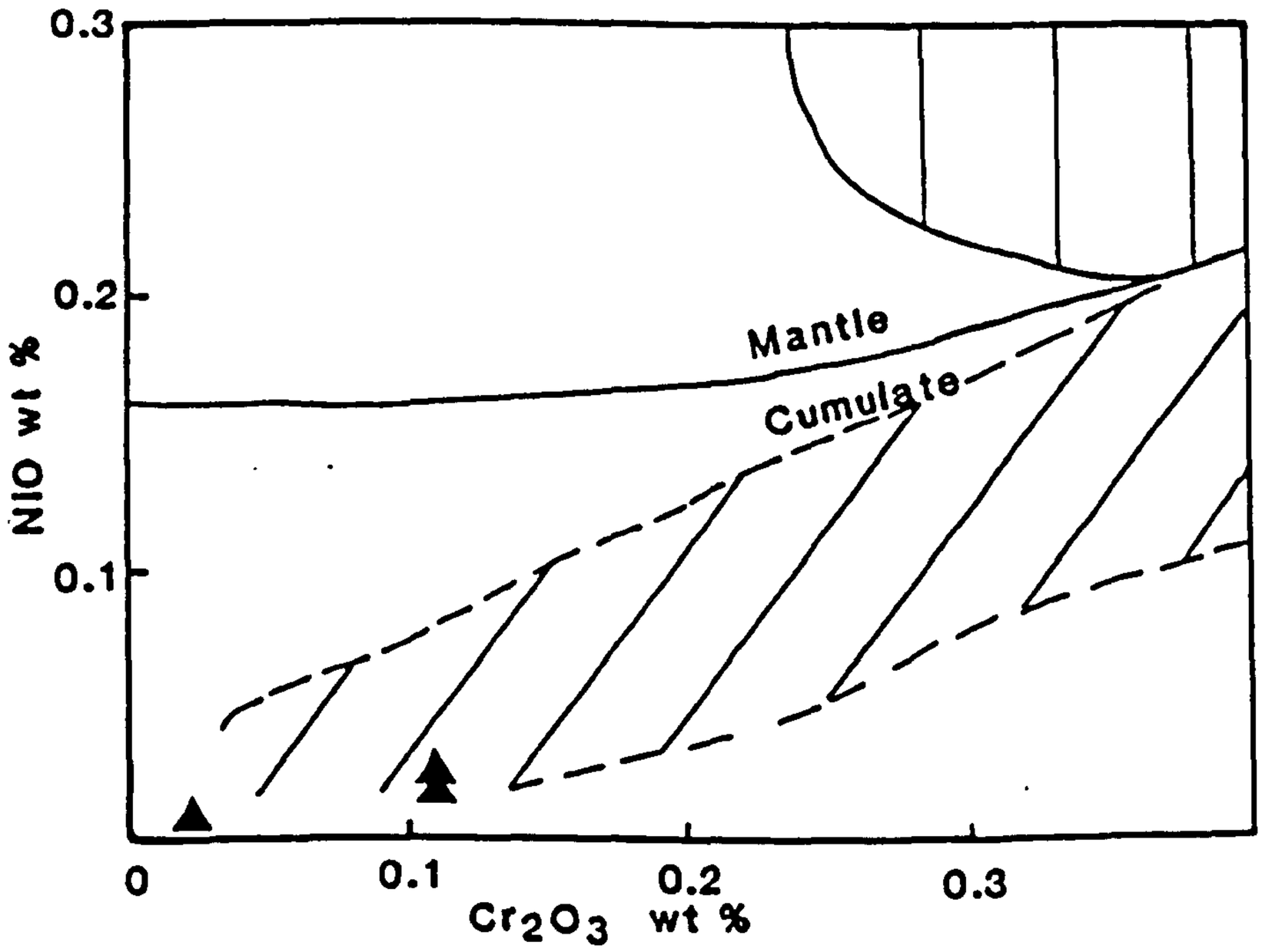

Figure 4.11 NiO- Cr_2O_3 plot for the Birbir ultramafic rocks. Shaded areas of the Bay of Islands mantle and cumulate sequences (Malpas,1978). Dividing line taken from Irvine and Findlay (1972).

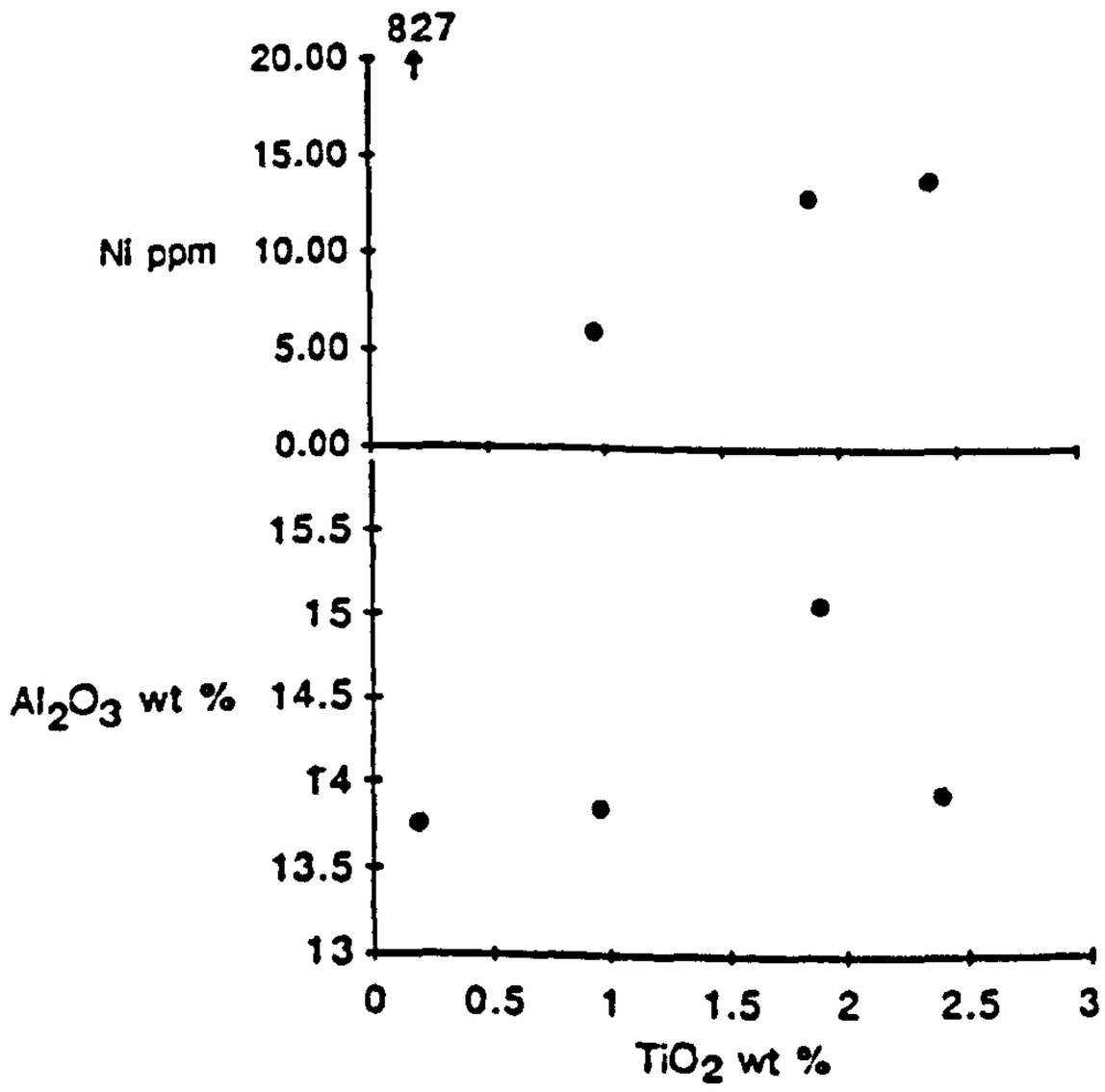

Figure 4.12 Variation of TiO_2 vs Ni and Al_2O_3 for the Birbir metavolcanic rocks.

have moderately elevated $Al_2 O_3$ (13.8 - 15.1 wt %) content, and have low Ni abundances (6-13 ppm) compared to the ultramafics except for MT107A. Sample MT 107A contains anomalous Ni (827 ppm) with no trace of Cr, while it has elevated levels of Rb (36 ppm) and anomalous Ba (1164 ppm) when compared to the other mafic rocks. This suggests that this sample is a contaminated mafic melt. The wide range in TiO_2 probably reflects fractionation of mafic phases.

Trace elements are used further to deduce their chemical affinity. On a Ti - Zr diagram (Figure 4.13a) the amphibolites (MT 107B; SB 343) plot in the MORB field and MT 107A in the arc field while SB265 plots in the within -plate field. In the Zr/Y versus Zr discriminant diagram (Figure 4.13b; Pearce and Norry, 1979) they all plot in the MORB/ IAT field except for SB265. SB 265 has been established as within -plate in both discriminant diagrams (Figure 4.13 b). This rock was sampled along the margins of the back arc basin associated with paragneisses, while the other three were sampled from the centre of the marginal basin. Zr/Nb ratios range from 14 to 37 and Ba/Zr (1.6 for MT107). These ratios are by far higher than those reported for T-type and E-type ocean ridge basalts (Saunders *et al.*,1980), but are similar to back-arc basalts. Back-arc basalts have a chemistry transitional between island-arc and ocean ridge basalts as has been suggested for some basalts from the Lau Basin (Gill, 1976), the East Scotia Sea (Saunders and Tarney, 1979), but Saunders *et al.* (1980) suggest that back-arc basins could be as diverse as those found along ocean ridges. However a lot more samples and REE data are required to verify the observations. Nevertheless in this study the tectonic setting of the metavolcanics are constrained by field observation and rock associations which indicate a back-arc origin. According to Moore *et al* . (1987) the metavolcanics and volcanoclastic rocks in the Birbir Domain are calc-alkaline and comparable to those of modern volcanic arcs.

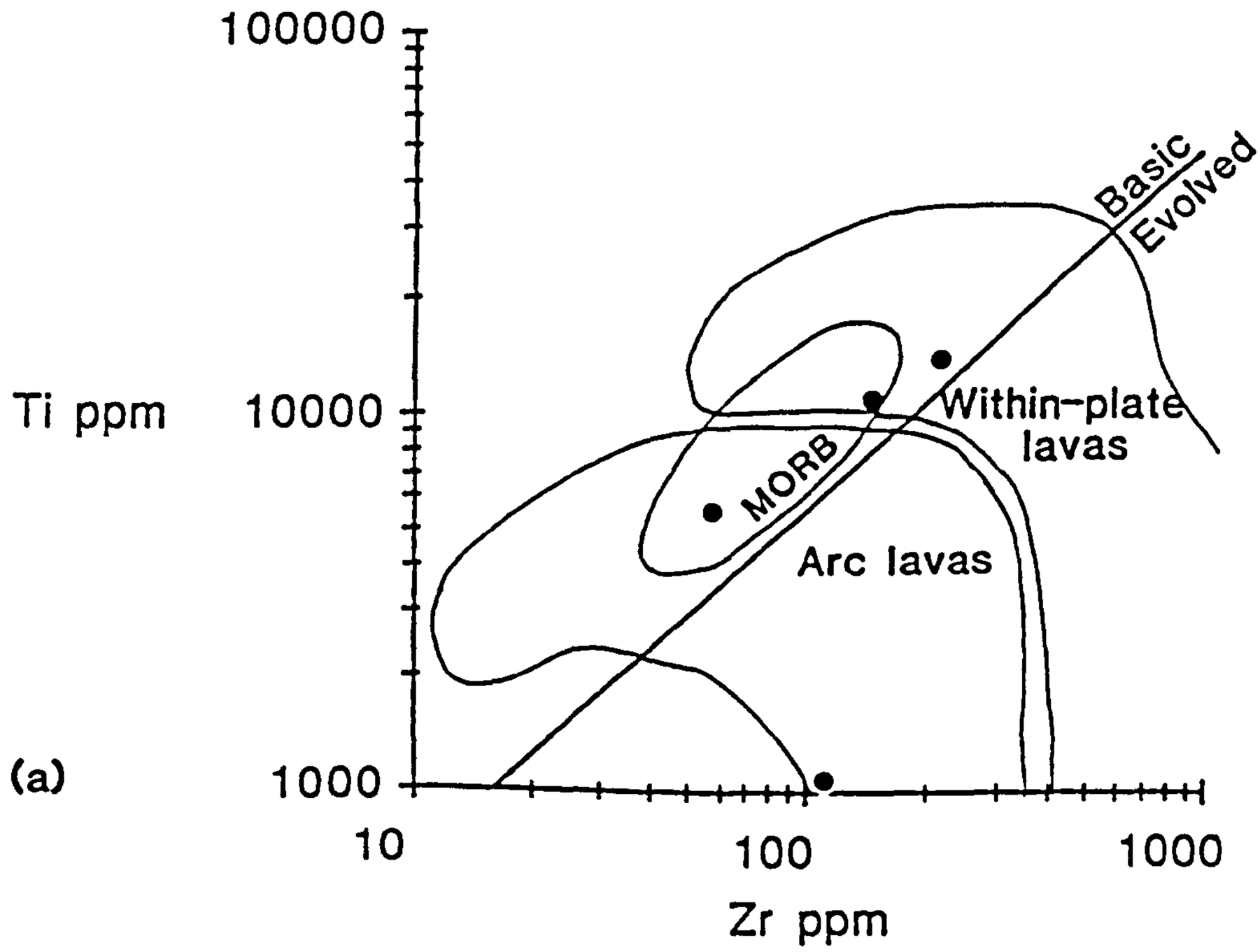

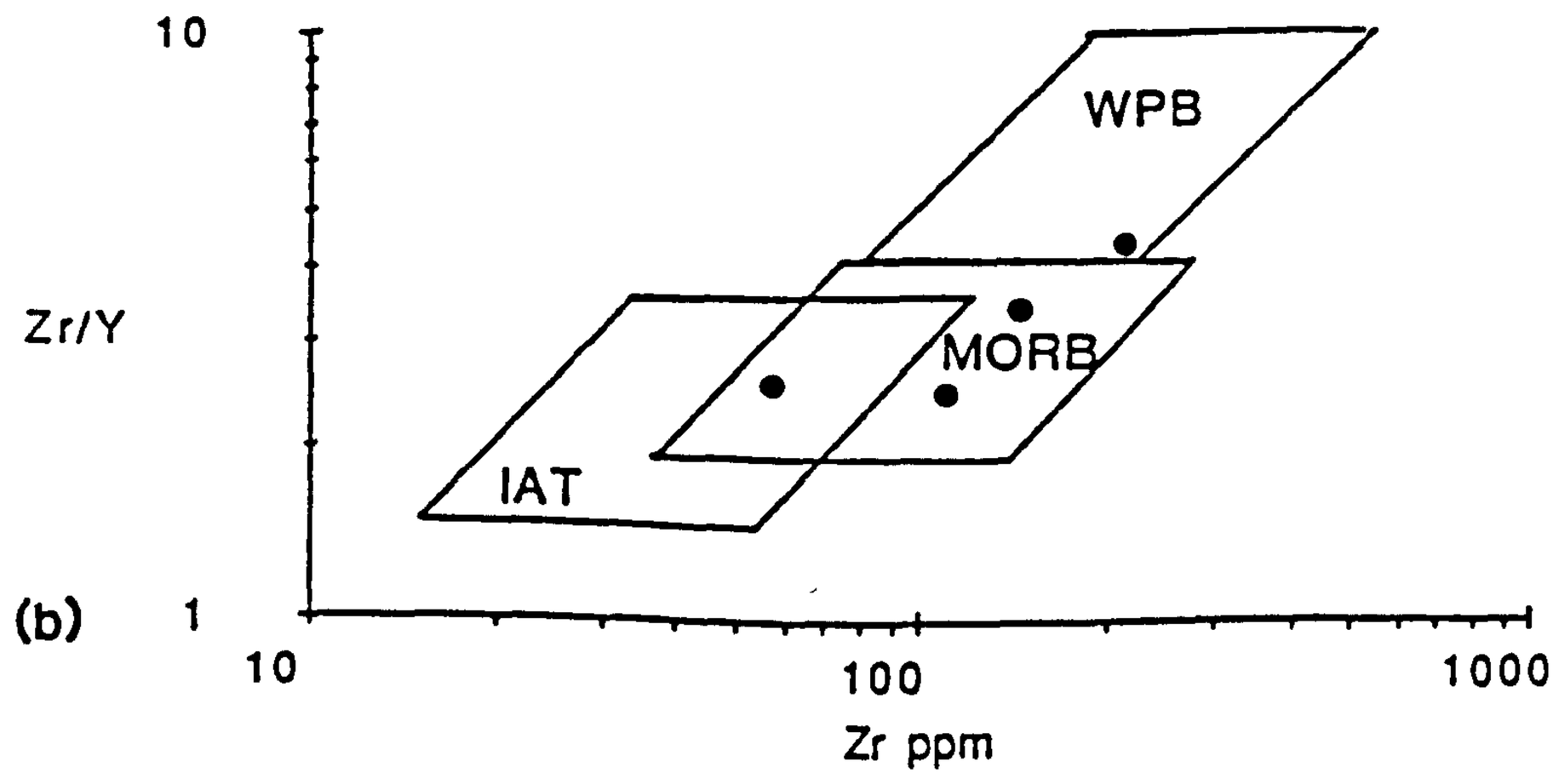

Figure 4.13 (a) Ti-Zr co-variation diagram for the Birbir metavolcanics. Fields taken from Pearce (1980). **(b)** Zr/Y-Zr discriminant diagram for the Birbir metavolcanics, and amphibolites. Fields taken from Pearce and Norry (1979).

4.6 GRANITOID GEOCHEMISTRY

4.6.1 Introduction

Major and trace element data are presented for a wide variety of granitoids from the Gore area - western Ethiopia. The granitoids studied are the Geba granitoid gneisses, the Birbir granodiorite/diorite batholith, syntectonic and post-tectonic granitoids. Although the localities of the granitoids are widespread, their relative ages has been established by field work, and they represent all the different granitoids present in the area.

This geochemical study is mainly aimed at fingerprinting the genesis, and tectonic setting of the granitoids which would elucidate the overall tectonic evolution of the belt. In general the classification of granitoids is problematical because trace element variations are a result of superimposed petrogenetic processes such as: crystal fractionation, volatile fluxing and heterogenous sources. Furthermore minor phases often control the distribution of trace elements in granitoids. These problems resulted in the publication of several classification schemes (Peacock, 1931; Shand, 1951; Streickeisen,1975; Pearce *et al.*, 1984a; Harris *et al.*, 1986). The classification schemes mentioned have been adapted in this study and combined with field data, to establish the geochemical affinty and tectonic setting of the granitoids.

4.6.2 Major Elements

The granitoids have been classified according to the Streickeisen classification scheme (Figure 4.14; Streickeisen, 1975) based on a CIPW Norm program developed by Nigel Harris for recalculation of major element analysis into minor phases. The Birbir granodiorite-diorites plot in the granodiorite field except AA54 which falls on the diorite field. Geba granitoid gneisses plot in the granite and granodiorite field, while the syntectonic granite plots in the granite field. The post-tectonic(SB205) falls in the granite field while the post-tectonic granite (MT404) plot in the alkali-feldspar granite field. This classification confirms the petrographic study carried out of the granitoids in section 4.4.

The degree of alumina saturation (i.e % $Al_2O_3/CaO+NA_2O+K_2O$) has been shown to distinguish granitoids (Shand, 1951; Chappel and White,1974) into peraluminous, metaluminous,

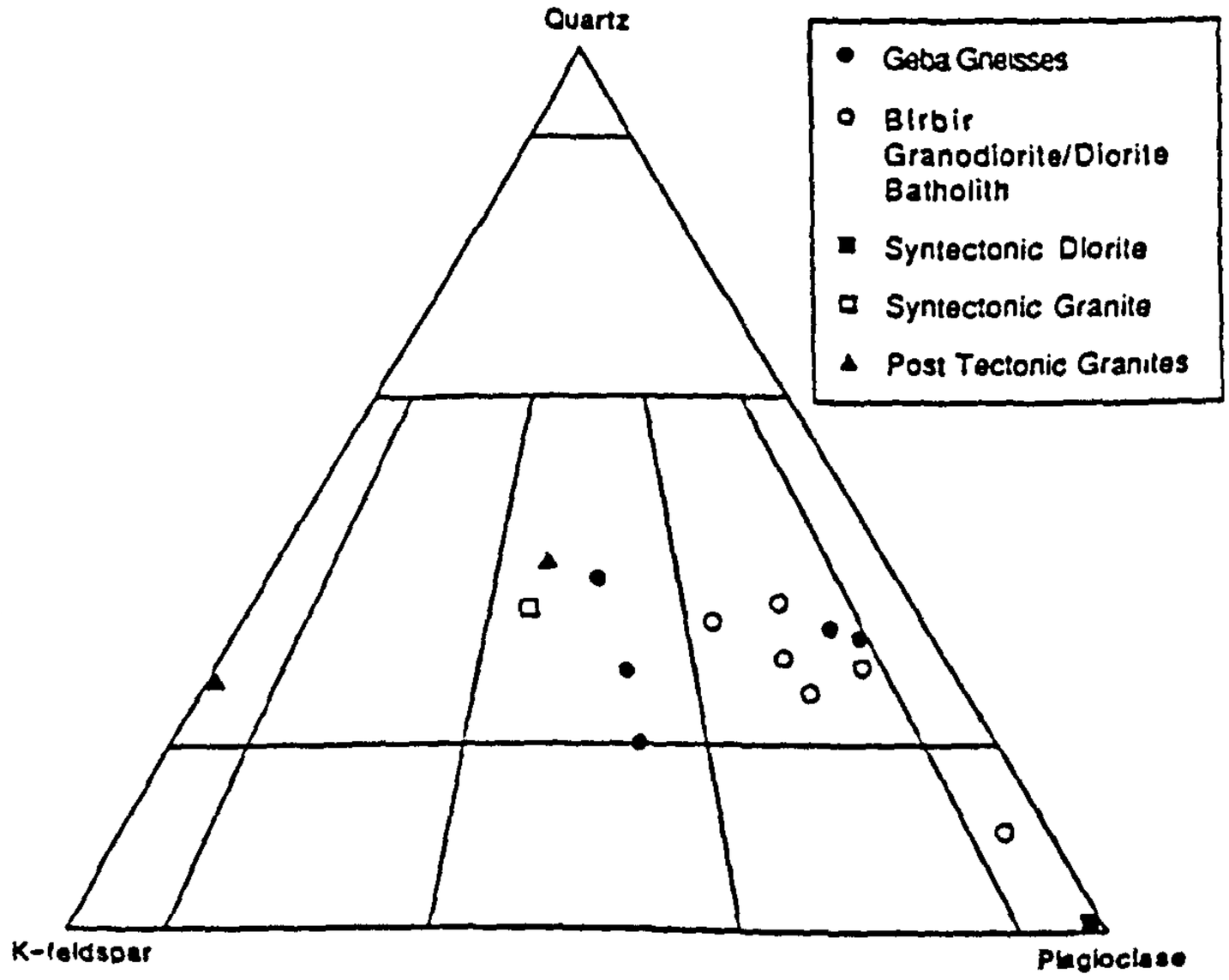

Figure 4.14 Streckeisen diagram showing representative samples from the granitoids of Gore region, W Ethiopia. Modal analyses are based on Norm program developed by Nigel Harris for recalculation of major element analysis into minor phases.

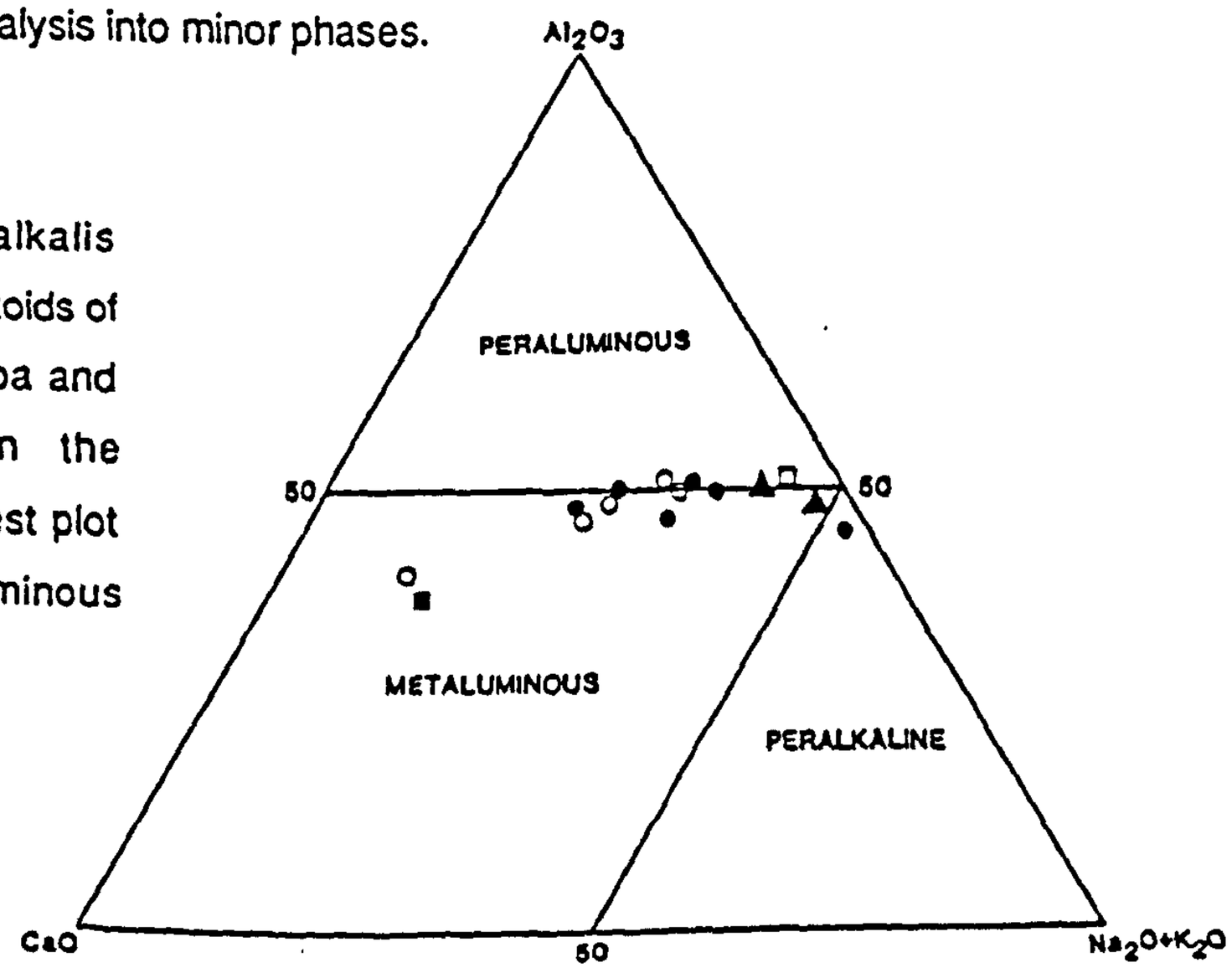

Figure 4.15 Alumina/CaO/alkalis triangular diagram showing granitoids of the Gore area, W Ethiopia. Geba and Birbir granodiorites plot in the metaluminous field, while the rest plot on the peraluminous- metaluminous line.

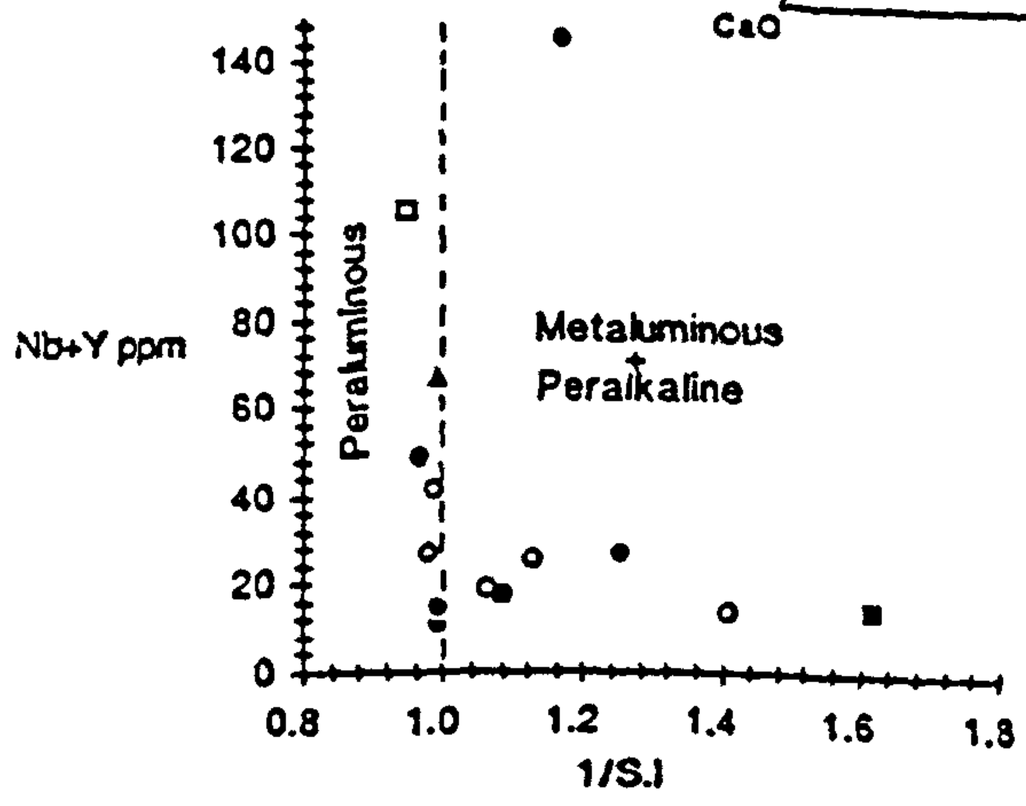

Figure 4.16 Plot of 1/Shand Index (CNK/A) vs the high field strength (HFS) elements Nb+Y for Gore area granitoids. All the granitoids except the syntectonic granite plot in the metaluminous field.

and peralkaline granites (Shand, 1951). Using this ratio variations in the molecular proportions of alumina, alkalies, and CaO have been plotted in a triangular diagram (Figure 4.15). The Geba granitoid gneisses plot in the metaluminous field, and along the borderline between metaluminous and peraluminous fields. Sample ETH D is exceptional in that it plots in the peralkaline field. The Birbir grandiorites plot in the metaluminous field, while two samples plot along the borderline of the peraluminous and metaluminous field. The post-tectonic and syntectonic granites plot in the metaluminous field. Figure 4.16 shows a plot of the Shand Index (Shand,1951) against the HFS elements Nb+Y (Pearce *et al.*,1984a). It is observed that all the granitoids except the syntectonic granite (ETH B) plot either in the calc - alkaline field or are close to 1. This is opposite to what was observed in the Adola-Moyale belt, where almost all the granitoids except the Fugugo granites plotted in the peraluminous field. (see section 3.8).

4.6.3 Trace Elements

Harker diagrams of selected trace elements for the various granioids are shown in Figure 4.17. The Birbir granodiorites are characterised by higher Sr, and lower Rb than the Geba granodiortic gneisses, while both (the Birbir and the Geba granodiorites) have elevated Sr, and lower Rb than the post-tectonic granites. Sr decreases with increasing $Si0_2$ in all the granitoid suites indicating plagioclase removal during fractionation.

The Geba and Birbir granodiorites show an increase in Rb, and Zr, while Nb and Y remain constant. The post- tectonic granites show an increase in Rb, Nb, and Y while they decrease in Zr. The syntectonic granite (ETH B) is different from the other granitoids in that it is characteristized by anomalous, Rb, Nb, and Y.

Two diorites plot separately (Figure 4.17) and indicate, low Rb, Nb, Zr, and Y, while they show elevated Sr values. Although the sample size is small plots of the three high field strength (HFS) trace elements (Nb, Y, and Zr) against SiO_2 show that the syntectonic granite, which has high Nb values to have within-plate characteristics, while the rest plot in the calc-alkaline island-arc field of Pearce and Gale (1977). In the Rb/Zr-SiO_2 plot (Figure 4.18) all the granitoids except the syntectonic

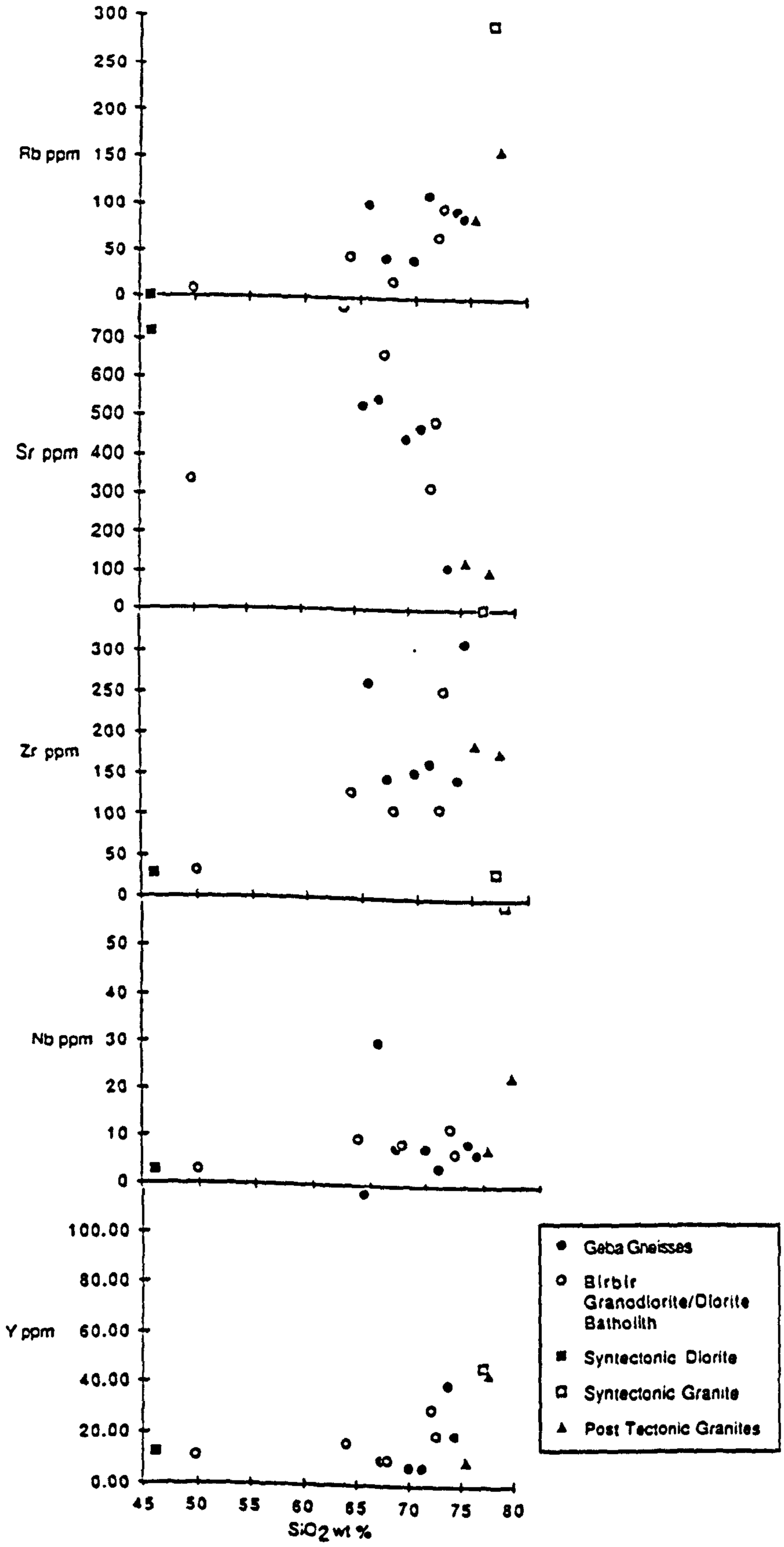

Figure 4.17 Trace element variation diagrams for W Ethiopia granitoids.

granite plot within the group III granite field of Harris *et al* . (1986) which includes post-collision and calc-alkaline intrusions.

Trace element distribution patterns for five representative suites are illustrated on a spider diagram. The trace element abundances have been normalised to the trace elements of an ocean ridge granite (ORG), (Pearce *et al.*,1984a). A comparison between the Geba and Birbir granodiorites (Figure 4.19a). shows that both are characterized by elevated K, Rb, Ba, higher Ce and Sm relative to Ta, Hf, Zr, and Yb. Such features are characteristic of volcanic arc granites (Pearce *et al.*,1984a). Geba granodiorite (ETH E) has higher Ba values when compared with the Birbir granodiorite (SB 302), however both plots are so similar that they could be genetically related.

In Figure 4.19b the trace element patterns of syntectonic and post-tectonic granitiods are compared. The post-tectonic granite (SB 205) has elevated K_2O, Rb, and Ba, and are low in high field strength elements (e.g. Ta, Nb Zr, Y) suggesting it to be volcanic arc granite. Although this granite has volcanic arc affinity it should be classified as post -collision granite because they occur as post-kinematic intrusive rocks. They are similar to the post-collision granites of the Alps (Pearce *et al.*,1984a). Whereas the syntectonic granite (ETH B) has elevated K_2O, Rb, Th, Ta, and Nb, but low Hf, Zr, Sm, Y and Yb. The high Rb, Th, Ta and Nb suggests a within-plate origin, however the syntectonic granite has exceptionally high Rb, higher Sm ,Y and Yb when compared with adjacent elements may be attributed to crustal involvement, while the negative Ba anomaly is typical of crustally derived granites.

The syntectonic diorite (ETH A) is characterized by low K_2O, Rb, Th and low HFS elements. The trace elements are low because of plagioclase accumulation which diluted the trace element values. Positive Eu anomaly indicating plagioclase accumulation is observed in Figure 4.20b. Modal % of ETH A is albite 27% and anorthite 16.7%.

4.6.4 REE Data

REE profiles for five representative samples are shown as chondrite-normalised diagrams (Figures 4.20a and 4.20b). In Figure 4.20b the Geba and Birbir granodiorites are compared. Both REE

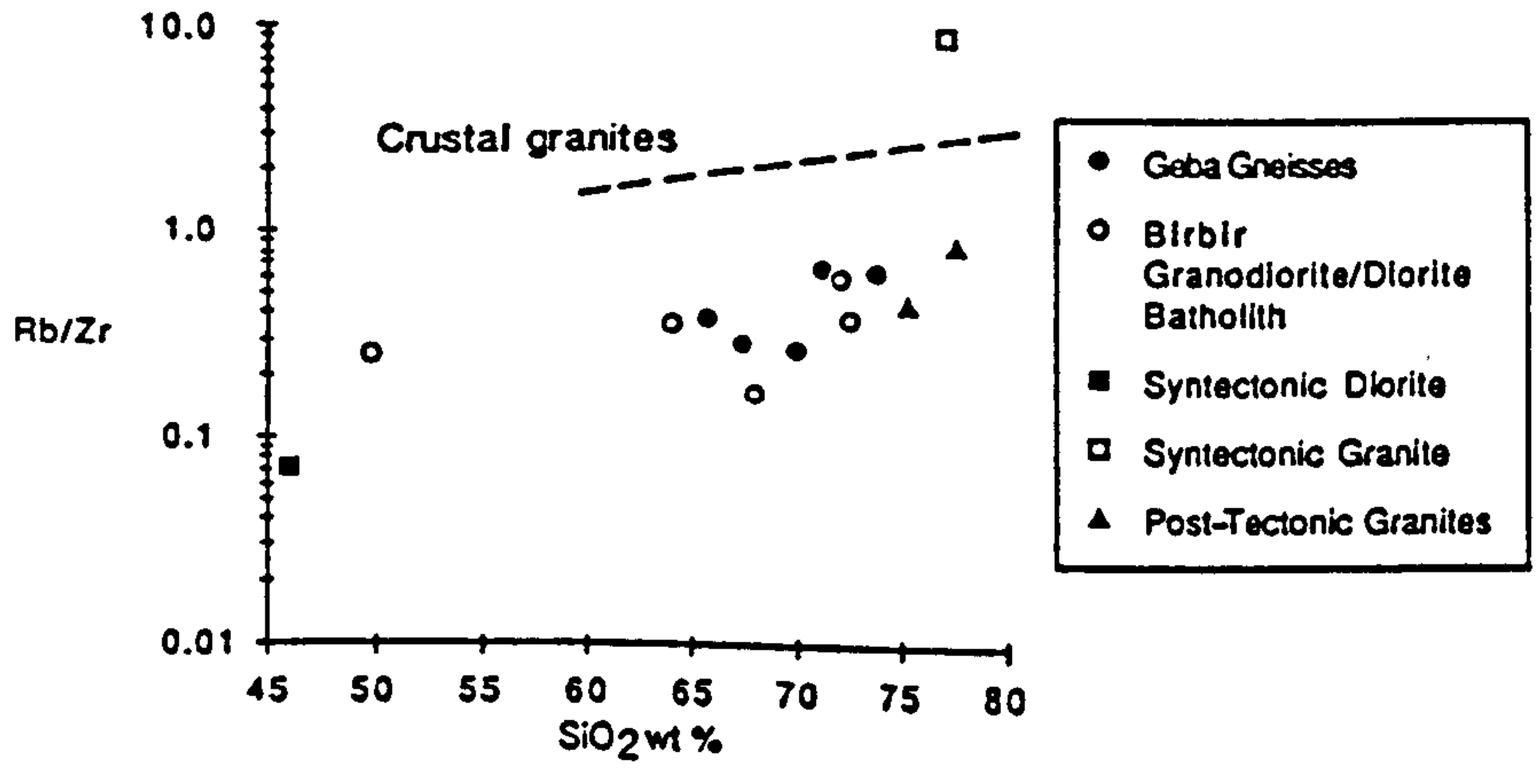

Figure 4.18 Rb/Zr vs SiO_2. The syntectonic granite have high Rb/Zr ratios and hence plot in the Group II crustal granite field of Harris et al (1986).

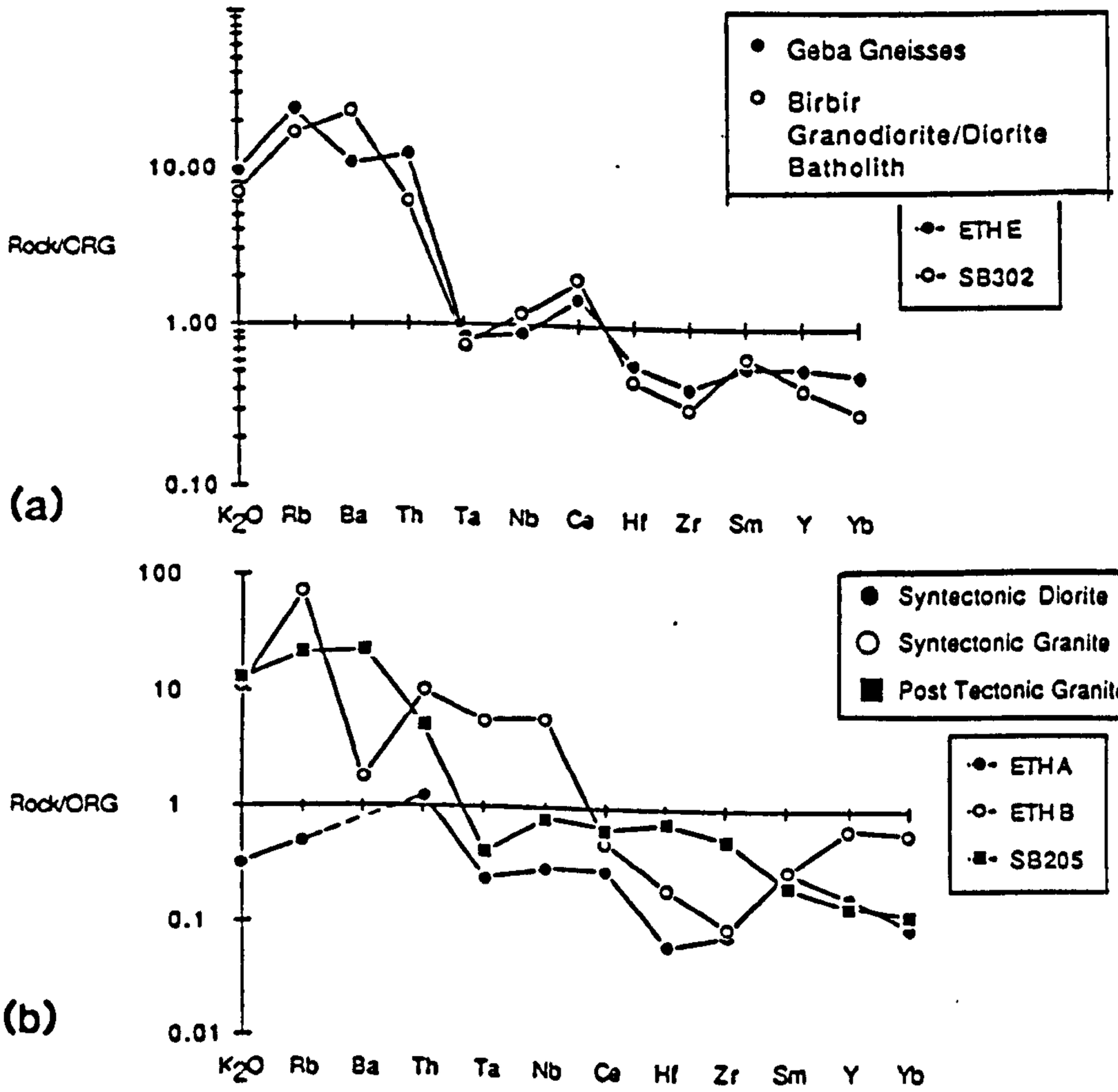

Figure 4.19 **(a)** Spider diagram for the Geba and Birbir granodiorites. Both are characterised by low Rb/Sr and low HFS elements Ta, Nb, Zr and Y. **(b)** Spider diagram for the syntectonic and post-tectonic granitoids. Syntectonic granite are characterised by high Rb, Th and high HFS elements Ta, Nb, and Y, while post-tectonic granites have moderately enriched Rb, Ba and low HFS elements.

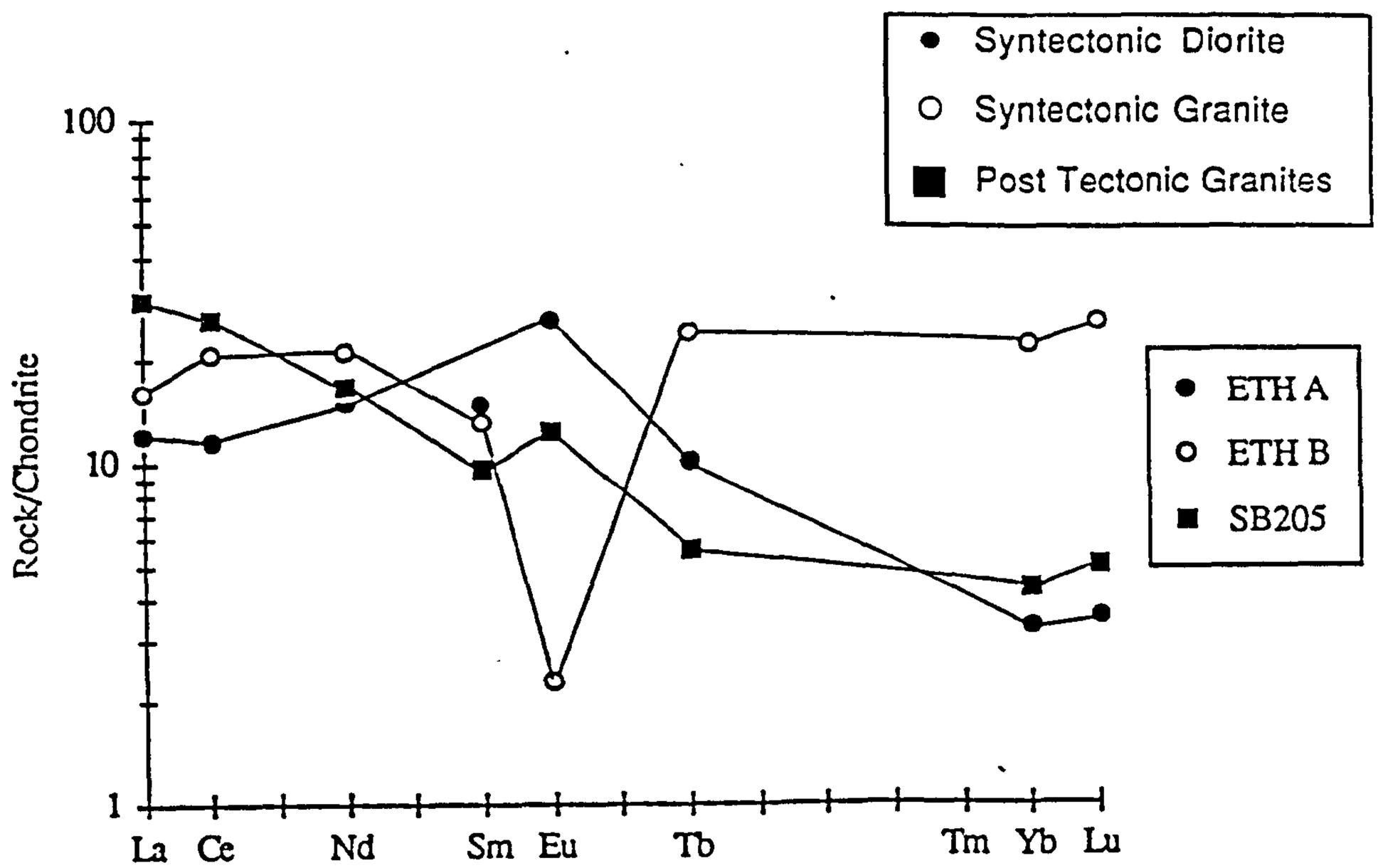

(a)

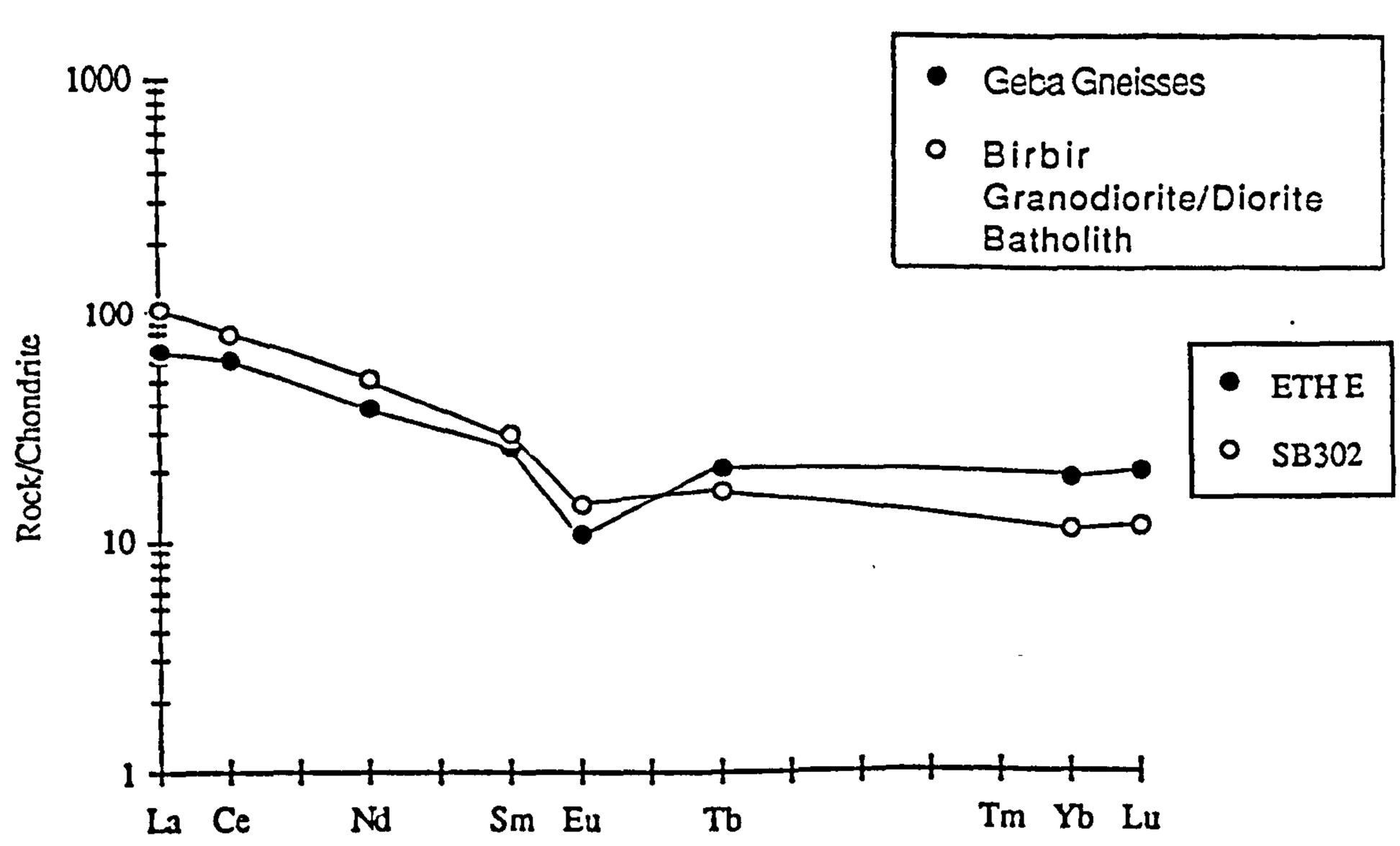

(b)

Figure 4.20 (a) Chondrite normalised REE diagram for syntectonic and post-tectonic granitoids. **(b)** Chondrite normalised REE diagram for Geba and Birbir granodiorites.

profiles show striking similarities. They show high REE abundances with steeply enriched LREE profile, which indicates a volcanic-arc affinity. The Ce/Yb ratios for the Geba granitoid (ETH E) is 12.9, while the Ce/Yb ratios are 28.6 for the Birbir granodiorite (SB302).

REE profiles were plotted for the syntectonic and post- tectonic granitoids. The syntectonic granite (ETH B) has relatively high REE abundances and large negative Eu anomaly which is typical of within-plate granitoids (Figure 4.20b). The post tectonic granite (SB 205) shows steep LREE profile with a positive Eu anomaly suggests that there was plagioclase accumulation. The Ce/Yb ratios for the syntectonic granite (ETH B) is 3.65, while for the post-tectonic granite it is 23.5. Although steeply enriched LREE profiles are typical of volcanic arc granites the relative enrichment observed in this profile is low as compared to those of Birbir volcanic-arc granitoids. The syntectonic diorite shows low REE abundances with a positive Eu anomaly, which indicates that plagioclase accumulation was a major petrogenetic process. The plagioclase accumulation was significant in lowering the trace elements and REE values. The Ce/Yb for the syntectonic diorite is 13.5.

REE are important additional constraints to the geochemical evaluation of granitoids, however the fact that REE are controlled by minor phases means that REE profiles of granitoids of the same tectonic setting could be totally different.

4.6.5 Discriminant Diagrams

Pearce *et al.* (1984a) and Harris *et al.* (1986) have established a granite classification scheme which assigns granite to four major tectonic settings. In this study all the discriminant diagrams were used to evaluate the tectonic settings in conjunction with the geochemical and field studies undertaken.

The granitoids were plotted on the Rb- (Y + Nb) discrimination diagram (Figure 4.21). The Geba and Birbir granodiorites plot in the volcanic arc/post-collision field. These rocks have firmly been established as volcanic arc granitoids based on the trace element variation diagram, and Nb/Rb against Rb/Sr diagrams (Figure 4.22). The syntectonic granite plots in the within-plate field but close to the syn-collision field, because of elevated Rb values (Figure 4.21). This granite has earlier been shown to be a crustal melt based on trace elements (Figure 4.19b). However REE data show that it could be a crustal melt with within-plate affinities.The post-tectonic granite (MT404) plots in the within

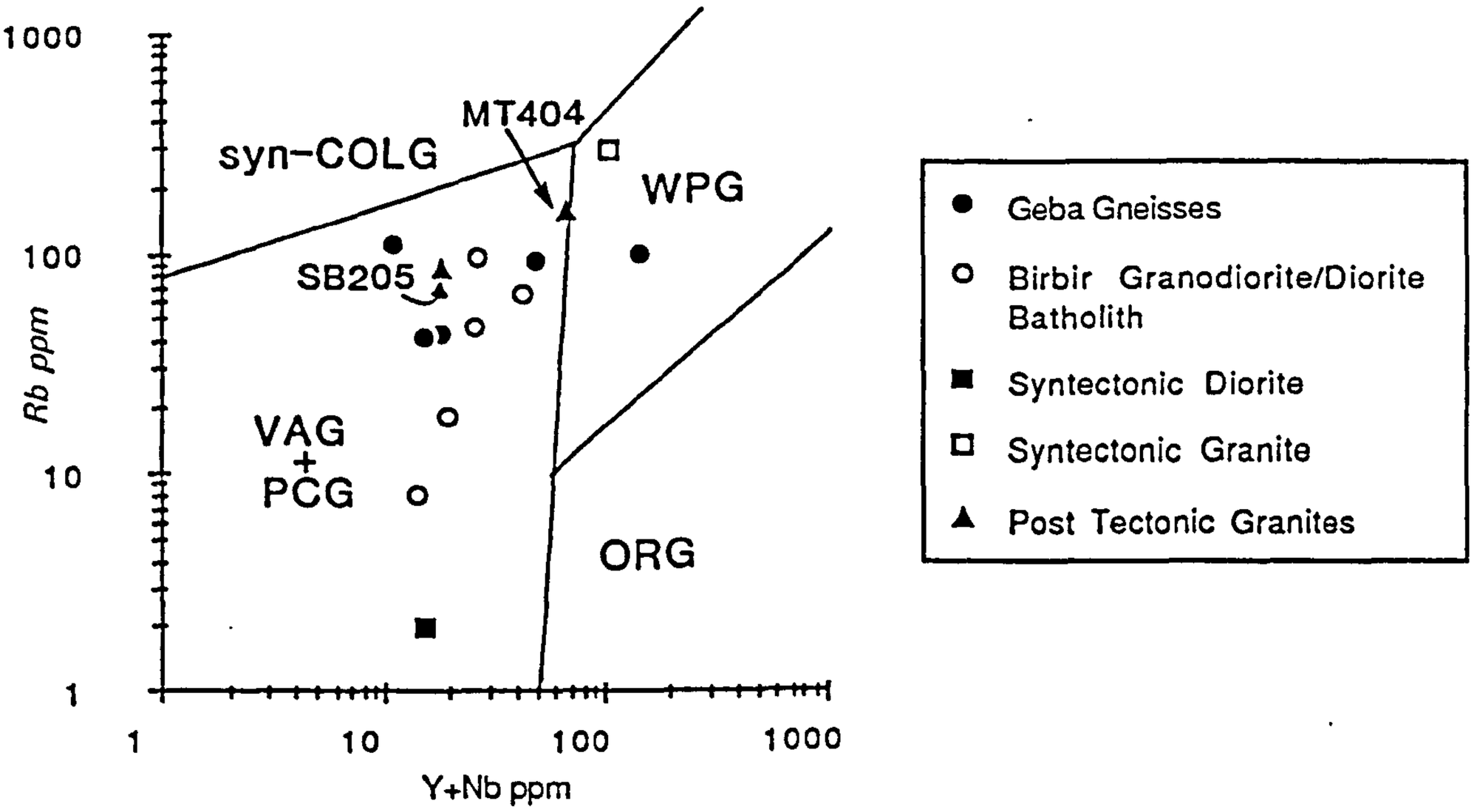

Figure 4.21 Rb vs (Nb+Y) granite discriminant diagram (after Pearce et al,1984a) for the Gore area granitoids. Syn-collision (syn-COLG), volcanic arc (VA), within-plate (WP) and ocean ridge granite (ORG).

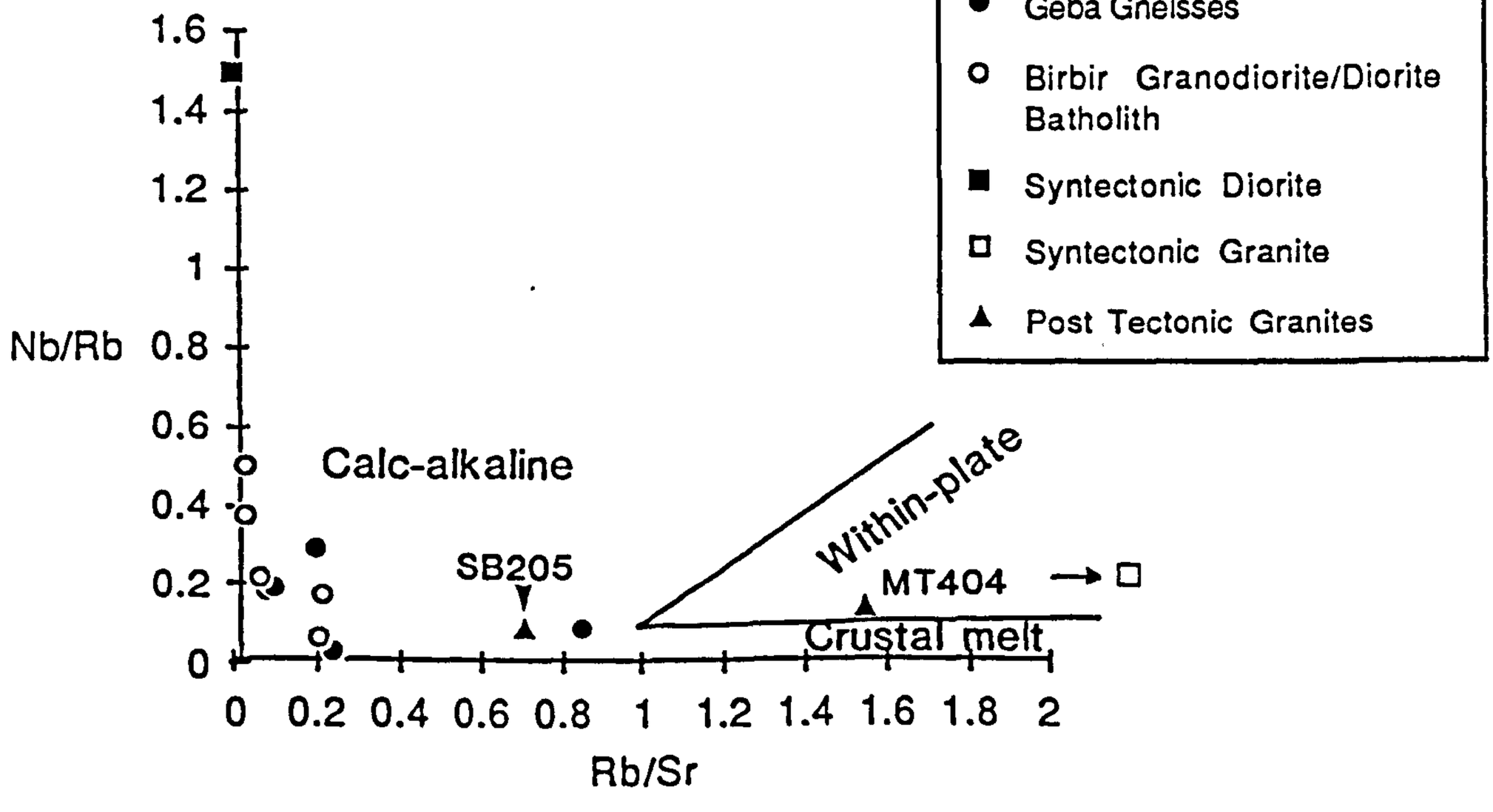

Figure 4.22 Nb/Rb vs Rb/Sr diagram for the Gore area granitoids. Within-plate granitoids have high Nb/Rb ratios, whereas crustal-melt granitoids have low Nb/Rb ratios. Crustal-melt granitoids have high Rb/Sr ratios, whereas calc-alkaline granitoids have low Rb/Sr ratios.

- plate field, while the post-tectonic granite (SB205) plots in the volcanic arc/post-collision field.

The Nb/Rb against Rb/Sr plot which has been effective in discriminating the various granitoid rocks in the Damara (McDermott, 1986) has been used to differentiate the granitoids of W. Ethiopia. Nb/Rb ratios discriminate between within plate-granitoids (Nb/Rb > 0.1) and crustal melt granitoids which have low Nb/Rb ratios (<0.1). The Geba and Birbir granodiorites and diorites are characterized by low Rb/Sr and plot in the calc-alkaline field (Figure 4.22). The syntectonic diorite has high Nb/Rb ratio (c.1.5) and Rb/Sr ratio lower than 0.2. One of the post-tectonic granites plots in the calc-alkaline field, while the second plots in the within plate field. The syntectonic granite has low Nb/Rb ratio and high Rb/Sr ratio (C. 97), and hence plot within the crustal melt field of the Damara (McDermott, 1986).

In summary three geochemically distinct granitoid types have been established in Western Ethiopia. The Geba and Birbir granodiorites, syntectonic diorite, and post tectonic granitoids (SB 205) show volcanic arc characteristics, however the post-tectonic granite (SB205) is a post-collision granite which shows calc-alkaline affinity because it is near a subduction zone or could be remobilised pre-existing volcanic arc granites. The syntectonic granite and the post-tectonic granite (MT 404) show within-plate characteristics, however the former has exceptionally high Rb and Nb which implies crustal contamination. The fact that it has large negative Ba is typical of crustally derived granitoids.

Detailed study of granitoid rocks in the Birbir Domain has enabled Teklewold *et al.* (1987) to recognise three distinct granitoid suites: i) low K gabbro-tonalites ii) medium K quartz diorites and iii) high K granitoids. Trace element data indicates that the low and medium K granitoids are of volcanic arc origin, while the high K granitoid suite represent a within-plate origin.

4.7 TECTONIC EVOLUTION

The geologic evolution of Western Ethiopia was discussed by Kazmin *et al.* (1978, 1979a, 1979b); DeWit and Chowaka (1981) and Berhe (1981). However the present interpretation is markedly different from previous studies which suggested an Upper Proterozoic basin between two cratons. In this study Western Ethiopia has been subdivided into five major tectonic domains. In order to

understand the geologic evolution of the area, the tectonic nature of the various tectonic domains have to be ascertained.

1. The Geba Domain which is represented by granitic and granodioritic gneisses, migmatites, and paragneisses could be interpreted as an older continental mass because of relict east-west structures (Kazmin *et al.*, 1979 a). At the western edge of the continental block there are strong N-S trending structures similar to those in the low grade Birbir Domain. This is a clear proof that refolding took place during collision of the Geba tectonic domain with the Birbir Domain. Generally the metamorphic grade is so high that the original composition of the metasediments can not be made. However the presence of compositionally layered paragneisses, and schists suggests that they could be metasediments of continental origin which were intruded by granitic and granodioritic rocks. The granodiorites are geochemically characterized as typical volcanic arc granites.

2. The Yubdo - Tulu Dimtu belt is composed of a succession of mafic and ultramafic rocks associated with pelitic, psammitic and graphitic schists with cherty bands suggesting that the complexes are dismembered ophiolites. Trace element data confirm the ophiolitic affinity of theTulu Dimtu mafic-ultramafic sequence which has a MORB/IAT related geochemistry (Warden *et al.*, 1982). The ophiolite belt dips mostly to the west and northwest. The ophiolites were thrust to the east and form a series of nappe sheets. The ophiolite contacts with the Geba high grade gneisses are all tectonic.

3. The granodioritic-dioritic batholiths and andesitic-dacitic volcanics most probably represent an island arc structure exposed at different erosional levels (Kazmin *et al.*,1979a). Directly against the granodioritic batholith there are thin metasedimentary units, which might be the products of erosion of the magmatic arc.The Birbir granodiorite/diorite batholith have been geochemically classified as calc-alkaline. Although the Birbir volcanic arc granitoid sequence is lithologically and geochemically similar to the Geba granitoids, it is not a fragment of an eastern continental mass that rifted and moved westwards, as suggested by Kazmin *et al.* (1979a), but forms a later subduction related volcanic arc sequence.

4. The Birbir Domain metavolcanics and metasediments which contain elongate granitic and granodioritic bodies could be interpreted as remnants of a marginal basin that was partly floored with oceanic crust (Kazmin *et al.*,1979a ,1979b). The wide distribution of metabasic rocks points to extensive submarine basaltic volcanism. These mafic rocks are geochemically similar to back-arc basin basalts.

DeWit (1977) has reported the existence of a series of parallel mafic dykes with cooling margins, in some cases on both sides, in a greenstone succession at the western periphery of the marginal basin, and these are thought to represent a metabasic sheeted dyke complex.

At the western end of the margin of the basin are extensive linear silicic volcanics. These may represent products of early silicic volcanism during back-arc extension. Early crustal extension prior to the production of oceanic crust may be preceded by extensive silicic volcanism (Sugimura and Uyeda, 1973) .

The presence of silicic volcanics, back-arc basalts and sheeted dyke complex indicates that rifting and back-arc spreading had definitely taken place. The geological evolution of the Birbir Domain is similar to the marginal basins of the SW Pacific. Erosion of the volcanic products of the adjacent island arcs, and the uplifted older crust on either side would provide the extensive clastic sediments to fill the basin. Sedimentation behind intraoceanic arcs in the SW Pacific includes the spread of pyroclastic materials over wide areas, and the construction of turbidite wedges built into deepwater from the rear of the arc structures (Karig, 1970, 1971). Plutons cut the successions in some arcs (Mitchell and Warden, 1971), similar to observations in the Birbir Domain although they vary in composition from gabbro to diorite, most plutons are dioritic or granodioritic (Mitchell and Reading, 1971). Marginal basins were probably created by crustal extension due to periodic splitting of arc systems. Karig (1971) favours the extensional mechanism to be in response to large mantle diapirs behind the active arcs.

5. The Baro high grade gneisses are equivalent to those of the Geba Domain, however the former are dominantly composed of granitoid gneisses, biotite gneisses, calc-silicate gneisses and

pegmatites. The Baro gneisses are older island arc-volcanics, which form a continental block bounding the marginal basin to the west. The Bonga belt which is part of the Birbir Domain includes calc-silicate rocks and minor outcrops of biotite gneisses, and garnet anthophyllite schists. This unit is included separately because it is lithologically different from the Baro high grade gneisses. It possibly developed on a shallow lying basin on the western margins of the marginal basin.

Table 4.2 Comparative data of the various tectonic domains of the Gore area, W. Ethiopia

Domain	Lithology	Metamorphism	Tectonic episode	Structural trend	Phasesof deformation
Geba	Plutonic rocks & gneisses predominate	Upper amphibolite facies	D_1 D_2	E-W N-S	Polyphase
Yubdo	Mafic-ultramafic rocks	Greenschist facies	D_2	N-S to NE-SW	One
Grano-diorite/ diorite belt	Granodirite, tonalite, diorite & associated volcanics	" "	D_2	" " "	One
Birbir	Intermediate to mafic intrusion & metasedimentary schists	Greenschist facies	D_2	N-S to NE-SW	One
Baro	Plutonic rocks, granitoid and calc-silicate gneisses predominate	Upper amphibolite facies	D_1 D_2	N-S	Polyphase

A comparative chart of the five tectonic domains is presented in Table 4.2. The lithologic assemblages in the Geba and Baro Domains differ from those in the Birbir and Yubdo Domains. The aluminous and calc-silcate gneisses of the Baro do not correspond to any rocks in the Birbir Domain. The mafic-ultramafic rocks of the Yubdo Domain do not exist in the Baro and Geba Domains. The

Birbir Domain is characterized by intermediate to mafic intrusions, while the granitoid rocks predominate among the plutonic rocks of the Geba and Baro Domains.

The Geba and Baro Domains have attained metamorphic grades of the upper amphibolite facies, while the Yubdo and Birbir Domains are metamorphosed from lower greenschist to lower amphibolite facies. In the latter two domains the grade of metamorphism increases westwards gradually, with no distinct or structural break. This increase in grade of metamorphism is related to the progressive continent - collision event that took place at D_2 deformation episode.

Two distinct plate tectonic models have been suggested for the geological evolution of western Ethiopia: i) Kazmin *et al*. (1978,1979a) had suggested that the Yubdo and Birbir Domains were formed in intracratonic rifts. The plate tectonic model (Kazmin *et al.*, 1979 a; Berhe, 1981) was also originally compared to that of the marginal basin of the Rocas Verdes complex of S. Chile (Tarney *et al.*,1976); ii) Moore *et al* . (1987) suggest that the Geba, Birbir and Baro Domains have been tectonically assembled by major translations, implying that their origin and age could be different. This assembly is suggested to have taken place during predominantly transcurrent movement of contrasting crustal segments in a regime of active magma generation.

Firstly it is clear that no rocks older than late Proterozoic has been found in W. Ethiopia . The Geba Domain granitoid gneisses which were originally thought to be Archaean have been found to be c. 800 Ma (unpublished data). The Geba and Baro granitoid gneisses have been geochemically established as of volcanic arc origin. Hence this domain could be older arc material which was subsequently split to form a small ocean basin which later was obducted during arc-arc or continent-continent collision. Secondly in the Birbir Domain no ophiolitic assemblage of significant extent is present. However the presence of silicic volcanics, cumulate ultramafic rocks, back-arc basin basalts, volcanogenic sediments, turbidites and marbles and possible sheeted dykes strongly suggests that the Birbir Domain is a marginal basin.

Field and Landsat study (see chapter 6, section 6.6) has shown the presence of major shear zones with dextral and sinistral sense, which have played a major role in the evolution of western Ethiopia. There was some translation movement along major ductile shear zones produced by horizontal compression across the orogen. However the displacement along shear zones has never

been observed to be more than few kilometres, which means that there could be no transcurrent faults which could be attributed to assembling contrasting crustal segments from far away places as suggested by Moore *et al.* (1987). This area lies in an area of complex suture zones (Vail,1983; Shackleton,1986; Berhe and Rothery,1986).

The tectonic evolution of Western Ethiopia can be best summarized in the following sequence; and the plate tectonic model has been presented in Figure 4.23.

1. Crustal thinning, and rifting of an early volcanic arc complex.
2. The opening of a small oceanic basin and development of oceanic crust
3. Extension and subduction with concomitant development of volcanic arc
4. Back-arc extension produces rifting followed by volcanism in the marginal basin.
5. Sediments of continental and volcanogenic origin fill the basin from adjoining volcanic arc.
6. Continental collision causes deformation of the rocks in the marginal basin, and the obduction of the ophiolites onto the eastern continental block.
7. Late stage injection of granodioritic plutons at the western edge of the back- arc basin during deformation.

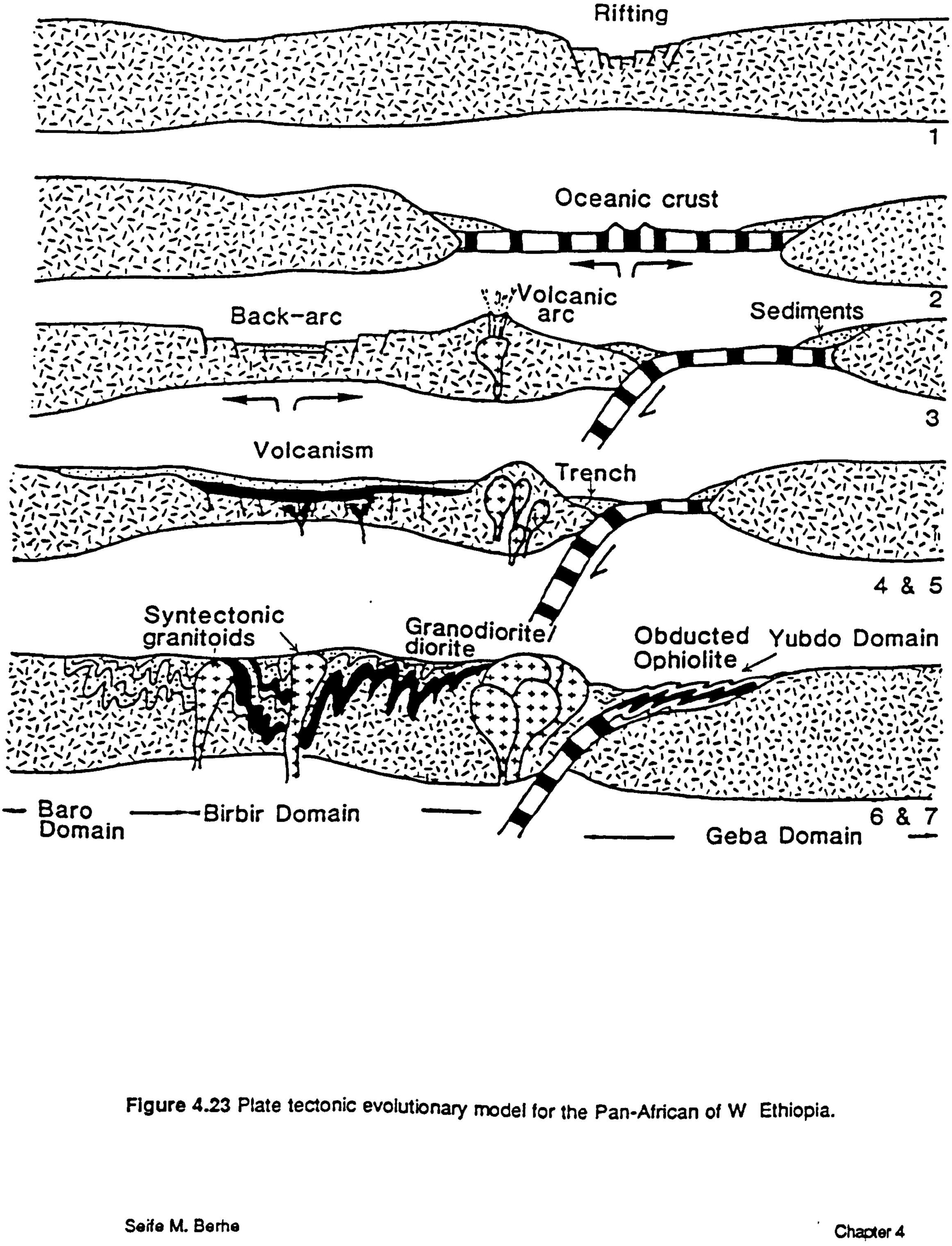

Figure 4.23 Plate tectonic evolutionary model for the Pan-African of W Ethiopia.

CHAPTER 5

LITHOLOGIC AND STRUCTURAL MAPPING USING REMOTE SENSING

5.1 INTRODUCTION

Satellite images provide synoptic views enabling large scale structures to be identified and traced over wide areas. This can expand a localized and carefully directed field programme into a regional study. East Africa is a prime candidate for such techniques as there are large areas that have not been geologically mapped.

The easiest and cheapest way to handle multispectral data is to select the most suitable spectral band and reproduce it photographically in black and white. This rendition is good for interpretation of textural features but any colour distinctions between surface types are reduced to grey tone which means that areas with different spectral responses may appear identical. Photographic FCC's (False Colour Composite) overcome this difficulty to some extent, but interactive processing of digital data enables the production of colour images which are optimised to suit the visual idiosyncrasies of the interpreter.

Preliminary interpretation was carried out using bulk processed photographic black and white MSS band 5 images covering parts of Sudan, Ethiopia and Kenya (Figure 5.1) enlarged to a scale of 1:500,000 using dry season (mostly January and February 1973) imagery. During the dry season the cloud cover of the Landsat MSS images is at its minimum. To optimise the identification of structural and lithological features, more complex image processing was carried out on selected digital images of W Ethiopia , SE Sudan and the Baragoi area, N Kenya.

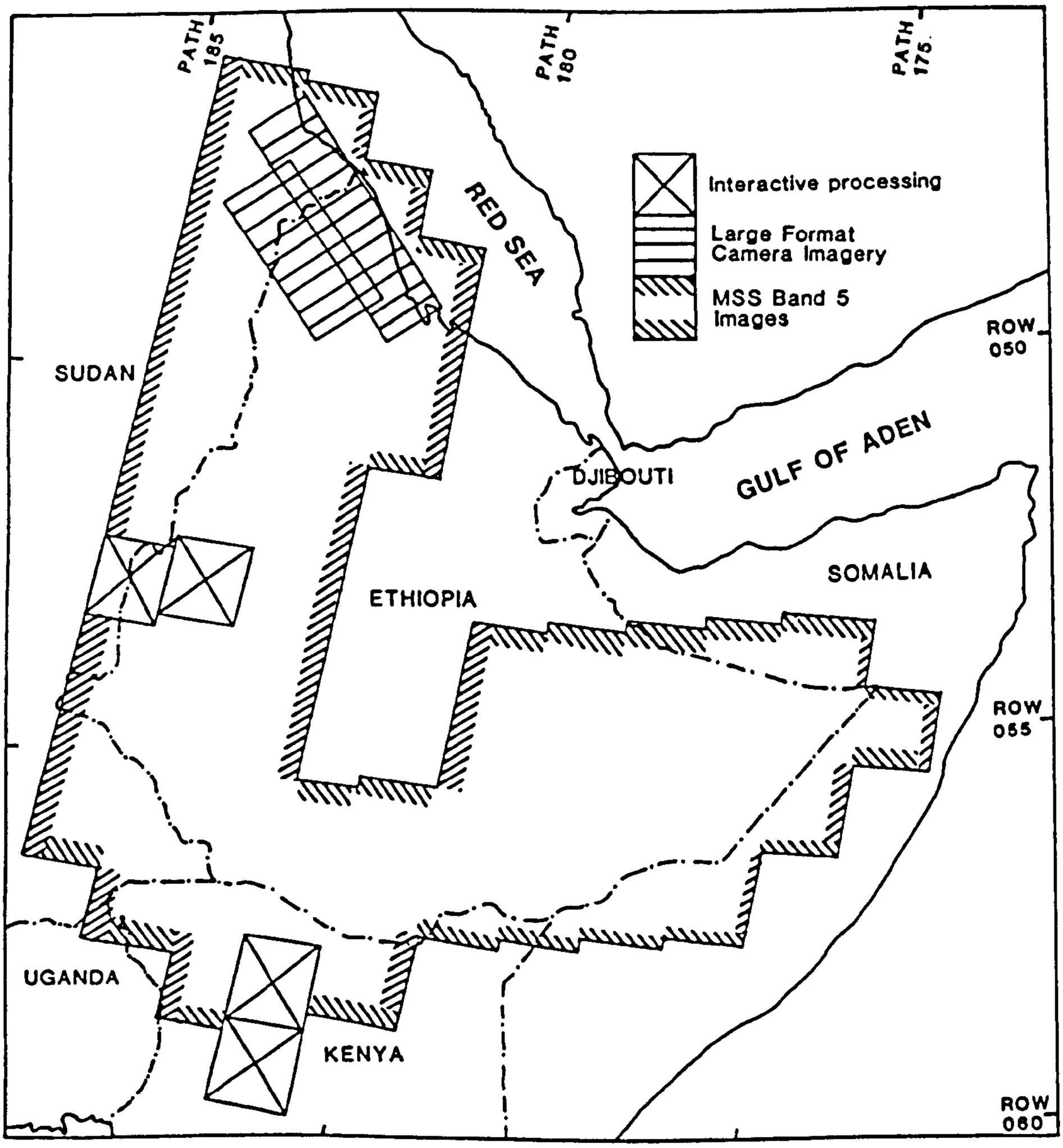

Figure 5.1 Coverage of Remote Sensing study in NE Africa.

5.2 TERRAIN CONSIDERATIONS FOR REMOTE SENSING IN NE AFRICA

Direct lithostructural mapping is possible only if the spectrally different rock types are sufficiently well exposed and distributed to render a diagnostic signature. This works best in terrains with little or no soil cover, and sparse vegetation. However ,exposure and vegetation vary considerably over NE Africa. In Eritrea and northeast Sudan (the Red Sea Hills) exposure can be as high as 80-100%. Soils are thin and stony, with only local development of savannah grassland and thorn scrub. Thick cover by Quaternary sediments and alluvium hinders interpretation in SE Sudan, SE Kenya and the western borders of Ethiopia. In most of W Ethiopia and NW Kenya lateritic soils, thick vegetation (60% cover) and agricultural burn scars made image interpretation complex, but NE Kenya is drier with limited vegetation cover and good (50-60%) exposure. In SE Kenya thick Quaternary sediments obscure the continuity of basement structure.

5.3 VISUAL INTERPRETATION OF MSS IMAGERY

Since the satellite imagery covers an enormous area at poor resolution (80m), it is not possible to see individual outcrops to the same level of detail compared with aerial photographs. However, it is possible to identify gross lithological boundaries, compositional banding and other planar fabrics, circular features (mainly intrusions), faults and shear belts. Visual interpretation of such imagery was based on published maps and aided by widely spaced field work.

Bedding, layering, folds and faults can be mapped indirectly from analysis of their morphological expression in most terrains where direct lithological observations are masked by soil or vegetation. Units were distinguished on the basis of their tone colour, texture, drainage pattern, landform and vegetation cover. Primary interpretation was confirmed and expanded after field visits.

The image interpretations were reduced to a scale of 1:1 million using aeronautical charts as a base. It was possible to produce improved geological maps for limited areas (e.g. W. Ethiopia, Figure 4.2) and regional structural maps of the NE and E African region (Figure 5.2). These maps were further improved by data acquired after detailed image processing of selected areas had been

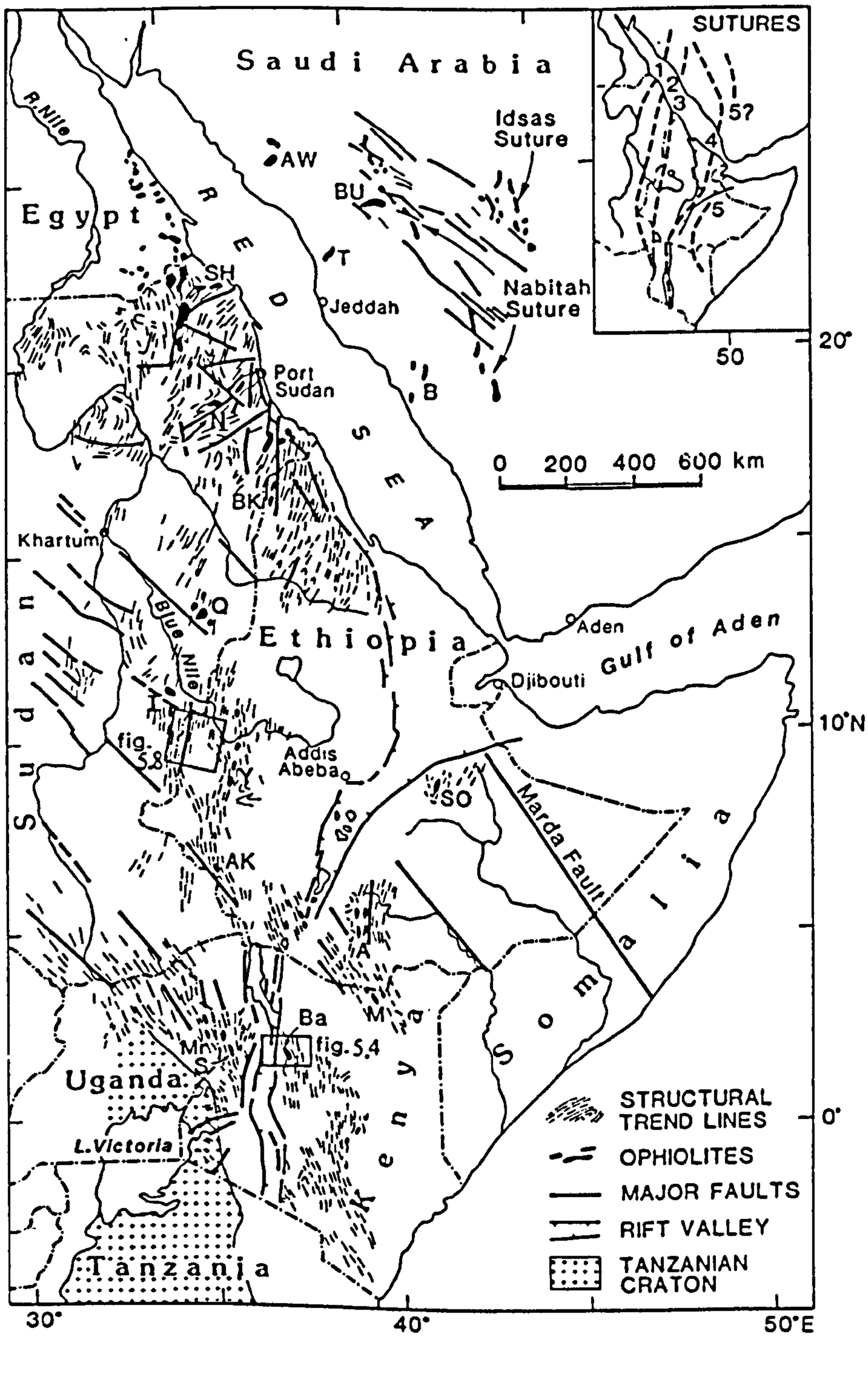

Figure 5.2 Sketchmap of the major trends of megastructural elements and ophiolite belts of the Precambrian of NE Africa, (after Berhe and Rothery,1986). Place names are : AW - Jebel al Wask; BU - Bir Umq; T - Jebel Thurwah; B - Bishah; SH - Sol Hamed; N - Nakasib; Bk - Barka; Q - Qala al Nahal; I - Ingessana; Y - Yubdo; Ak - Akobo; So - Soka; A - Adola; My - Moyale; Mr - Moroto; S - Sekerr; Ba - Baragoi.

carried out.

5.4 INTERACTIVE PROCESSING OF LANDSAT IMAGERY

5.4.1 Introduction

Interactive digital processing enables distinctions between rock units to be enhanced in a variety of ways not possible by standard photographic techniques. This is because weathering and alteration severely reduce the differences between the average spectral reflectances of various rocks on standard aerial photographiy, causing considerable overlap between the fields occupied by several rock types. Rothery (1985) has shown that black and white interactively processed MSS images are better than standard product images for mapping purposes, because of their superior resolution, and more adequate tonal range.

5.4.2 Spectral Information In Landsat MSS Images

The Landsat MSS produces simultaneous images in four spectral bands: 500-600 nm (band 4), visible green, 600-700 nm (band 5) red, 700-800 nm (band 6) and 800-1100 nm (band 7) both in the very near IR, where reflectance is at a maximum. However, these bands are far from ideal for lithological discrimination (Hunt, 1979; Seigrist and Schnetzler, 1980; Goetz and Rowan, 1981; Goetz *et al.*,1983), being more suited to the monitoring of crops and natural vegetation.

The scene recorded represents a rhombic area about 185 km across, and each image consists of a set of scan lines 79 m wide sampled into picture elements or pixels every 58 m. Data is transmitted in digital form, every pixel been assigned a digital number (DN) over the range 0-127 (7 bits) for bands 4-6, and 0-63 (6 bits) for band 7. The image can be reconstructed either in photographic form, or displayed on a television screen.

In moderately well-exposed terrains the spectral response detected by a remote sensing system is due to a mixture of surface types. A single pixel is likely to contain areas of rock (which are variably weathered), bare soil or alluvium and several types of vegetation. Landsat MSS pixels comprise radiance data averaged over an area of about 80 m by 80 m (Slater, 1979). Usually, the

intermingling of surface types is on a small enough scale that the spectral response recorded in these pixels is relatively homogeneous across a rock unit. A neighbouring rock unit may have a different spectral response due to the rock type itself, bare soil derived from the underlying rock and differences in the vegetation community related to the chemistry and moisture content of its substrate. Distinction between rock types is reduced if there is a uniform weathering of exposed surfaces (such as in a desert-varnished area), if the soil or alluvium cover is not locally derived, or if the vegetation is not related to its substrate. Vegetation anomalies due to rock type are often well expressed only while the vegetation is thriving during the wet season, whereas vegetation on dry season imagery can be drab and uniform (Grootenboer, 1973).

5.4.3 Image rectification

The MSS scenes were geometrically corrected and resampled from the original MSS data by identification of ground control points with UTM coordinates and then warping through a polynomial transform cubic convolution to 100 x 100 in square pixels. However, for more detailed investigation of limited areas such as the Baragoi, N Kenya, the original MSS data were resampled to give 50 x 50 m square pixels. The training areas selected were from known outcrops, and represent a range of rock types which are found in the MSS scene.

5.4.4 Colour image display

The conventional way to display Landsat MSS images in colour is to show band 7 in red, band 5 in green, and band 4 in blue to produce a false colour composite (FCC). Bare rocky areas usually appear fairly natural in this rendition (although red beds appear yellow), but healthy vegetation appears red because of the high near infrared (band 7) reflectance of leafy material. Suppliers of photographic format ('hard copy') MSS images usually offer FCCs as standard products, but the definition and colour balance of these are often unsatisfactory (Rothery, 1985). However, interactive processing of digital data enables the production of colour images which are optimized to suit the visual idiosyncrasies of the interpreter. The colour display techniques considered during this study are summarized in Table 5.1.

Table 5.1 Summary of the advantages and disadvantages of colour display options during interactive processing of Landsat MSS images.

Technique	Advantages	Disadvantages
False colour composite (simple contrast stretch)	Easily interpreted,consistent colours.	Poor use of colour space, not colourful. Uses data from only three out of the four spectral bands.
False colour composite (decorrelation stretch)	Easily interpreted,consistent colours. Good use of colour space,colourful.	Uses data from only three out of the four spectral bands.
Principal components image (red,green,blue display)	Colourful. Uses data from all four spectral bands.	Meaning of colours is not immediately obvious. Colours not consistent between different images. Noisy.
Principal components image (Taylor Colour Space i.e. brightness,red-greenness blue-yellowness)	Colourful. Uses data from all four spectral bands.Uses colour processing capability of human visual system effectively.	Meaning of colours is not immediately obvious. Colours not consistent between different images.

The simplest procedure is just to alter the contrast stretch for each of bands 4, 5 and 7 to give suitable colours and brightness to the parts of the image under interpretation. Because of the commonly high degree of correlation between spectral bands, contrast stretching parallel to the spectral band axes maintains the ellipsoidal distribution of data in multispectral space and leaves large volumes unoccupied near some corners of this space. If however, stretches are applied along the direction of maximum variance (the first principal component) (Figure 5.3) and also along directions orthogonal to this (second and third principal components) the image data can be made to occupy a near-spherical volume of space, with much smaller unoccupied volumes near the corners. This is known as 'decorrelation stretch' and concentrates as much colour as possible into the display whilst maintaining the colour relationships of the original FCC (Soha and Schwartz, 1978; Gillespie *et al.*, 1987).

Instead of representing three of the spectral bands in red, green and blue, we may choose to use the principal component directions themselves as display axes. This allows us to use data from all four MSS bands. The first three principal components, derived by four-dimensional principal components transformation of the image, usually contain all but about 0.1% of the total image variance. These principal components may be displayed as red, green and blue in a simple colour composite, or transformed into a more sophisticated colour space, such as Taylor Space (Taylor, 1974) in which one channel (e.g. first principal component) modulates the display brightness whereas two other channels (e.g. second and third principal components) are used to determine the colour balance (red-greenness and blue-yellowness). In both cases the display has a high colour contrast, which helps the interpreter to discriminate between areas of only slightly different spectral response, but the meaning of each colour is not obvious. A principal components transformation may be driven by the spectral signature either of the whole image or of just a critical portion of the image (canonical analysis). Examples of some of these processes are presented in figures 5.4 and 5.5.

5.4.5 Spatial image processing

Emphasizing the high spatial frequency component of the image can further enhance obscure features (Leith and Alvarez, 1985), or pick out features of interest hidden within a cluttered, highly textured, original image (Drury, 1986). This may be done by masking out part of the Fourier transform of the image (filtering in the frequency domain) or, more simply, by convolving the image with a box-car filter (filtering in the spatial domain).

A simple box-car (or 'kernel') of size n x n pixels replaces the value of each pixel by the average value of the pixels in its n x n neighbourhood. The result is a smoothed, or 'low pass' filtered, image. By subtracting a weighted proportion of the smoothed image from the original image a 'high pass' filtered image is created. If the weights are equal this is an edge detection image, which ignores relative brightness but picks out edges and linear features as bright or dark lines. In edge detection each pixel is replaced with the difference between the input pixel and the local mean which when added back to the original image produces an edge enhanced image. By giving the smoothed image

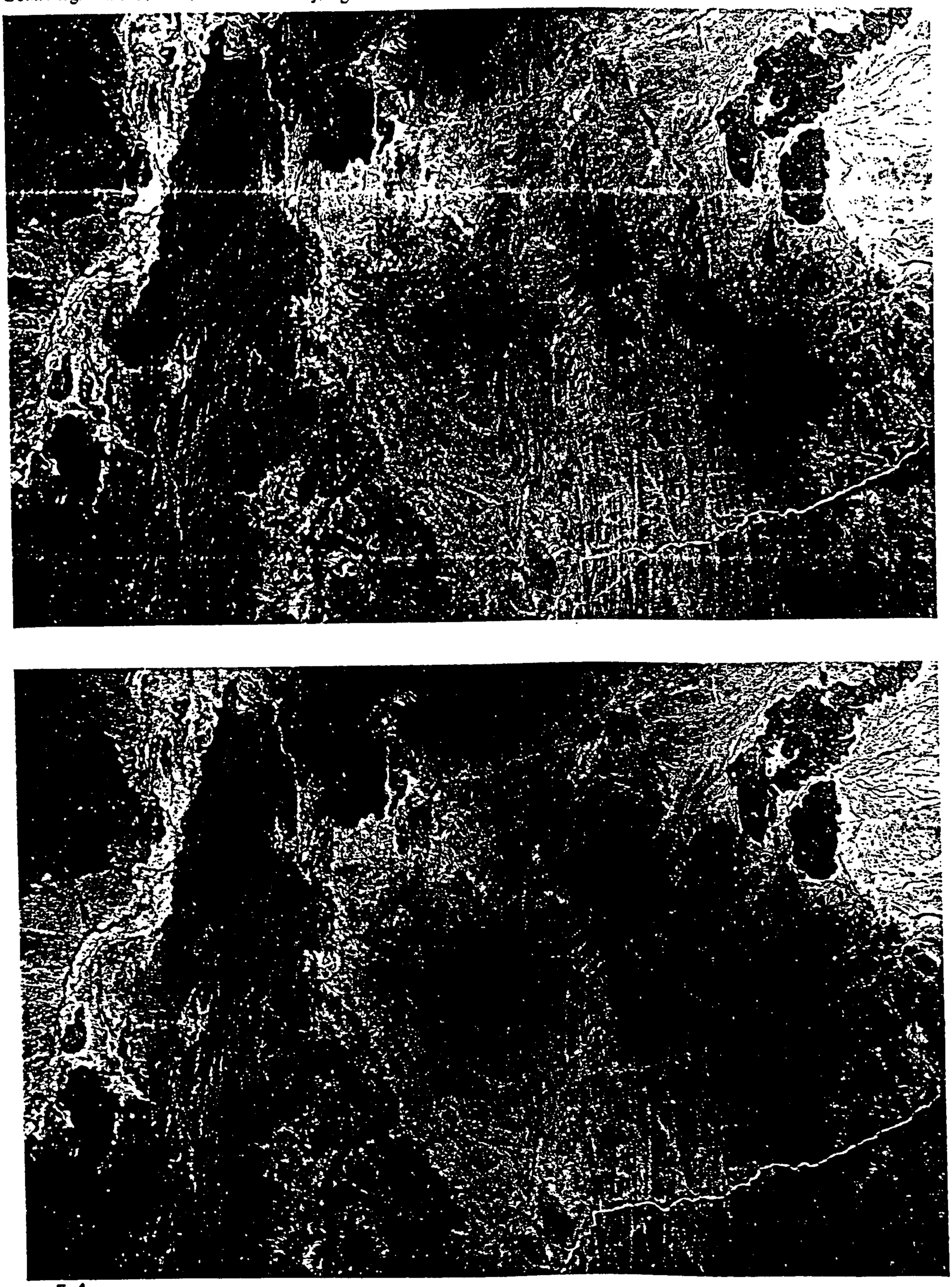

Figure 5.4. Baragoi area, 60km across (see Fig. 3). Landsat MSS imagery acquired 31st January 1973. Top: interactively processed false colour composite. Bottom: same image after application of a decorrelation stretch.

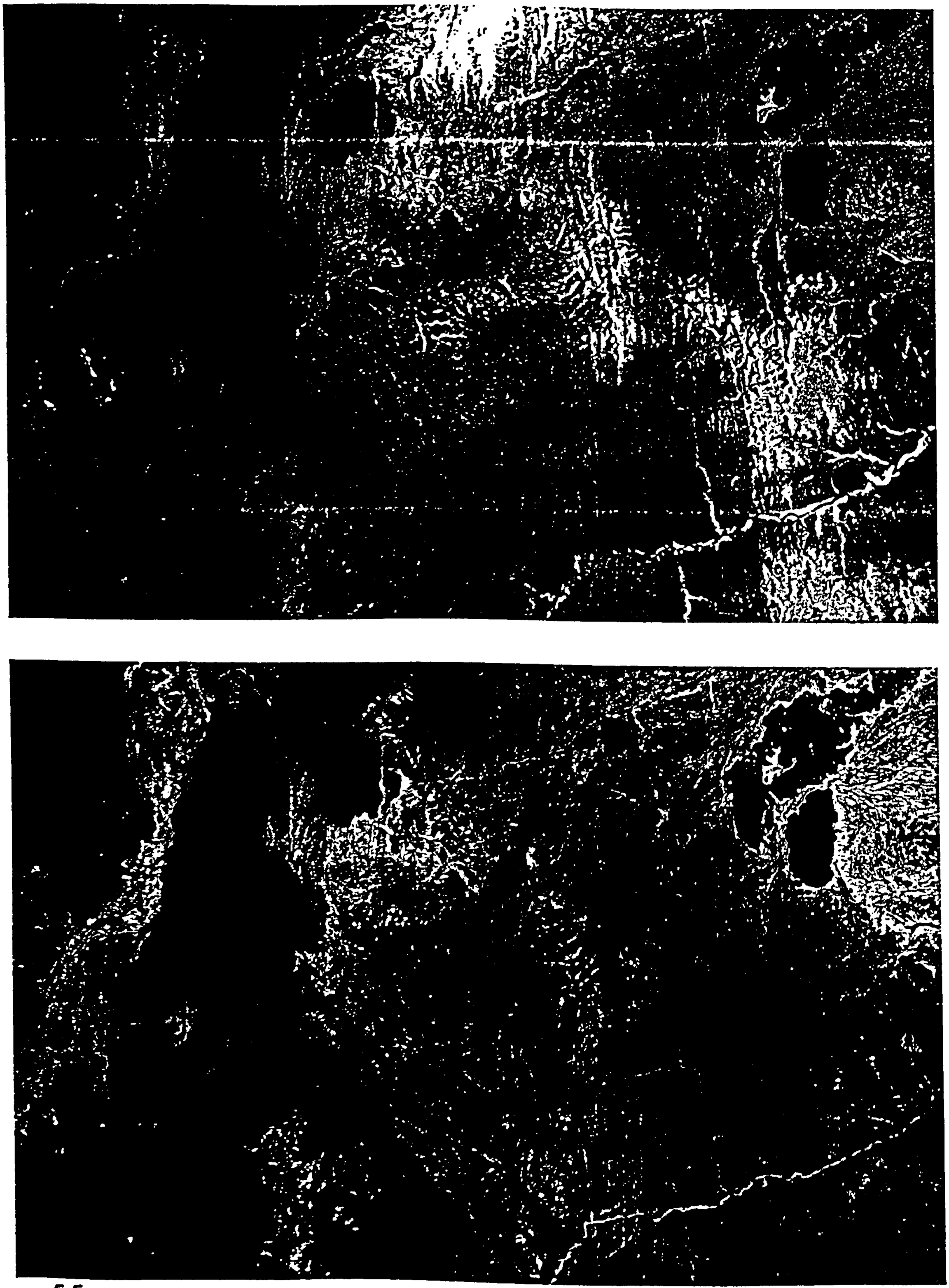

Figure 5. Baragoi area, 60km across (see Fig. 3). Canonical principal components transformation of Landsat MSS data. Top: 1st principal component in red, 2nd principal component in green, 3rd principal component in blue. Bottom: same data transformed into Taylor colour space; 1st principal component controls brightness, 2nd principal component controls red-greenness, 3rd principal component controls blue-yellowness.

a lower weighting an edge enhanced image is formed, which looks like the original image except the edges and linear features are sharper. Use of an asymmetrically weighted box-car enables features with a particular orientation to be enhanced at the expense of others (directional filtering). The optimum size of box-car depends on the degree of roughness in the image and the scale of the features which the interpreter wishes to enhance (Chavez and Bauer, 1982).

A preliminary lineament analysis using edge-enhanced MSS bands 4,5 and 7 was attempted on a Landsat scene (path 184, row 53) in W Ethiopia. Slightly different lineaments were revealed in each band. However, all these lineaments could be located on a first principal component image. The first principal highly correlated component, as well as combining highly correlated spectral information from all four bands, has minimal noise content. The lineament analysis discussed here is based on spatial frequency filtering of canonical first principal component, using terrain covered by diverse rock types as the training area.

The outcome of spatial filtering depends on box-car size and symmetry and the texture of the terrain. In this study using directional filters, a 9 x 9 box-car was found to show major lineaments but to miss what were regarded as significant smaller ones. A 3 x 3 box-car enhanced all fine structure making it hard to distinguish valid lineaments from irrelevant clutter. A 7 x 7 box-car was found to be a suitable compromise. For non-directional filtering, the comparable box-car size was 13 x 13 (Berhe and Rothery,1986).

Both edge enhanced and edge detection images were considered. Some lineaments are more clearly identified on edge enhanced images, because the preservation of distinctions between areas of different grey tone means they can be seen to be continuous, whereas on edge detection images they are reduced to fragmentary lineament segments. However, edge detection images revealed more lineaments in total. Four directional edge detection filters (N-S, NE-SW, E-W and NW-SE) were also applied. These tended to produce artefacts consisting of faint, exactly straight lines running at about 20° either side of the filter direction, which were discounted. Artefacts apart, directional filters preferentially enhance lineaments running at right angles to the filter direction, so that the four directionally filtered images revealed a total of 762 different lineaments, whereas only 487 were identified on the single, non-directional edge detection image. Rose diagrams to illustrate

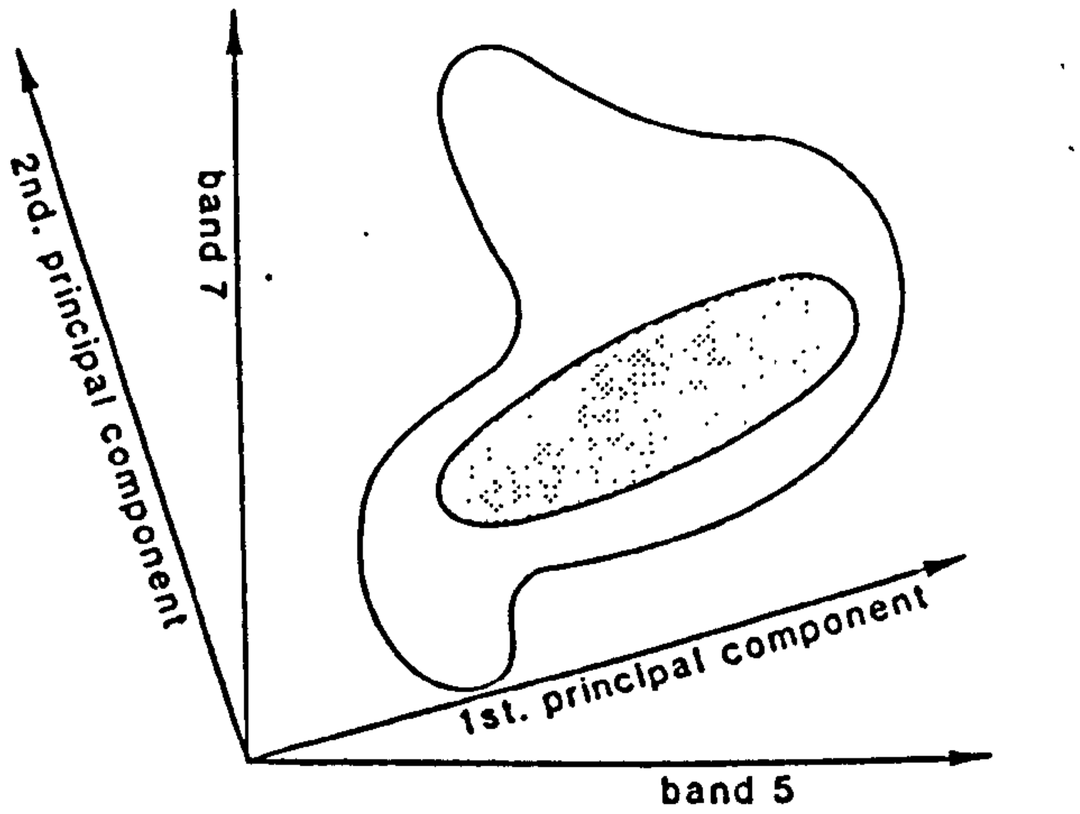

Figure 5.3 The concept of principal components. The diagram shows a plane in multidimensional data space, in this case the band 5, band 7 plane. The outline encloses the region occupied by all the data in the image. The shaded area shows the region in which falls the data from particular terrain units of interest, which might be bare rocky areas, but excluding vegetation, alluvium, water etc. In this canonical example, the first principal component direction is that along which the data from the 'training set' has maximum variance. In a four dimensional example (as for Landsat MSS) this would be at an angle to all four axes, and would not lie within a 2-band plane as in this illustration. Second and higher principal components would be orthogonal and lie in directions of successively lower variance.

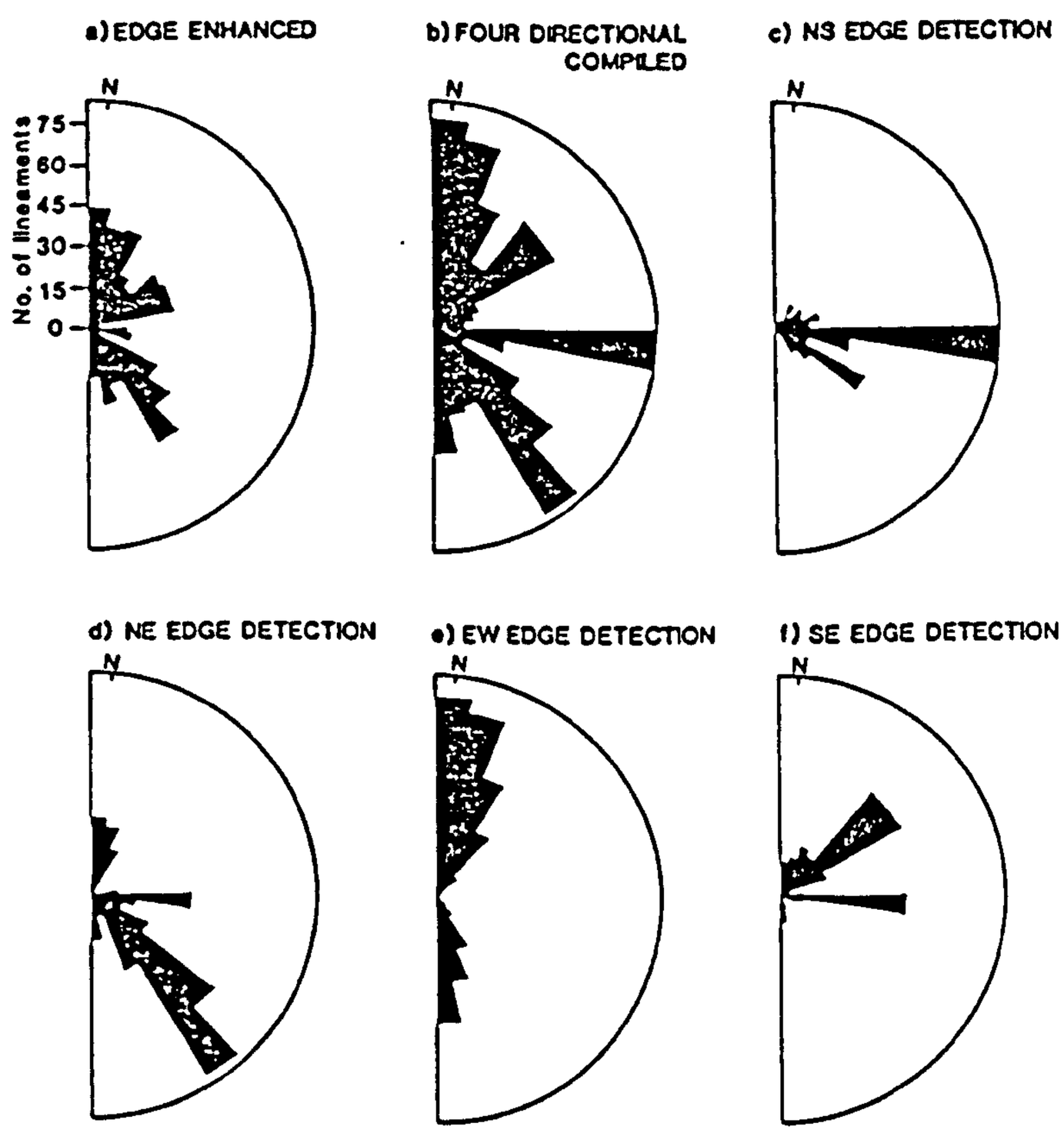

Figure 5.6 Rose diagram produced from lineament interpretation of canonical first principal component of MSS scene with different high pass filters. (a) edge enhanced; (b) all lineaments detected by four directional edge detection filters; (c) lineaments detected on north-south edge detection image; (e) lineaments detected on east-west edge detection image; (f) lineaments detected on southeast edge detection image.

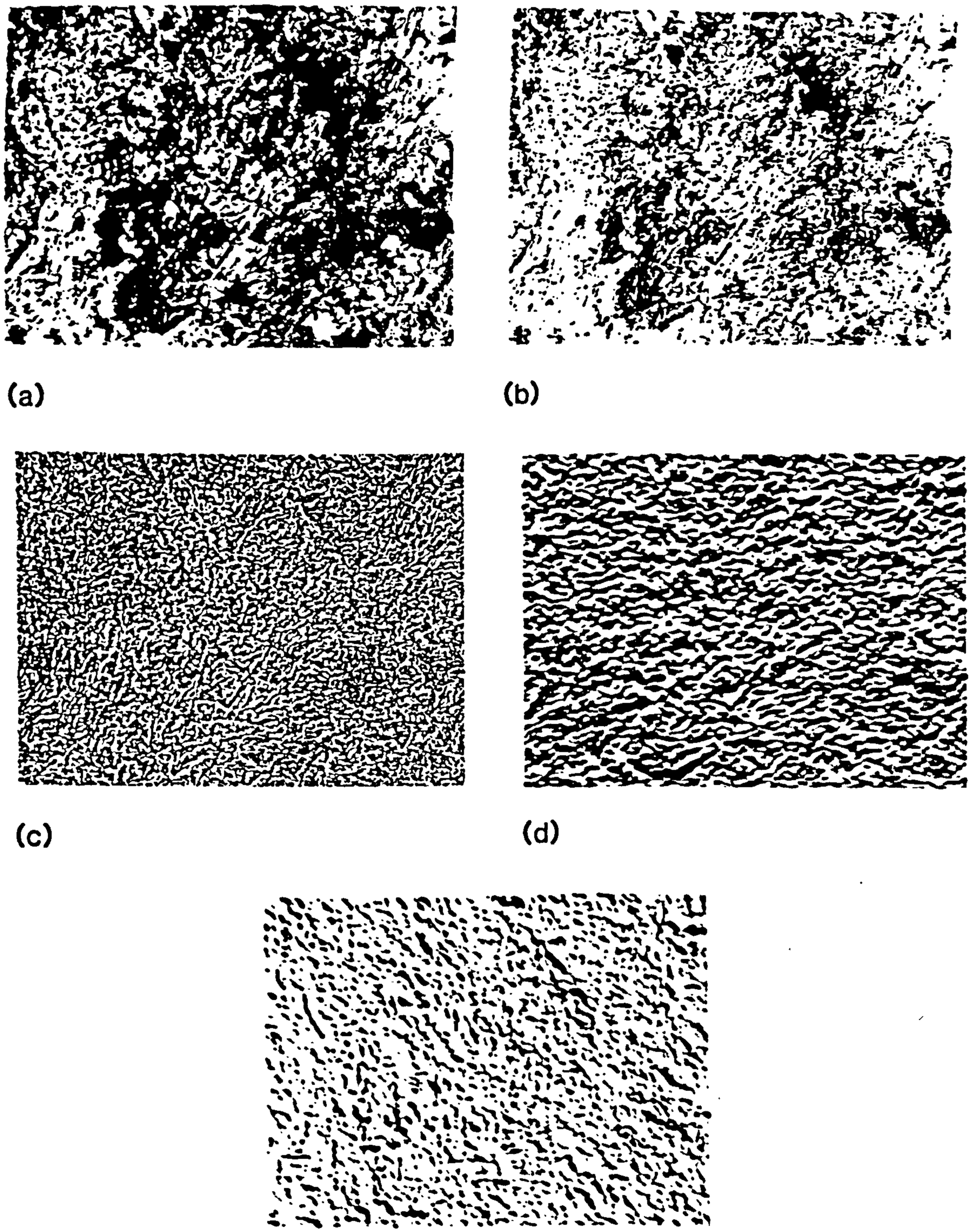

Figure 5.7 A subscene of Landsat MSS data with various spatial filters applied. Location shown in Figure 5.8. **(a)** Canonical first principal component; **(b)** same after application of a 7x7 edge enhancement; **(c)** 7x7 edge detection; **(d)** 7x7 north-south edge detection; **(e)** 7x7 northeast edge detection; **(f)** 7x7 east-west edge detection; **(g)** 7x7 southeast edge detection; **(h)** 13x13 edge enhancement; **(I)** 13x13 edge detection.

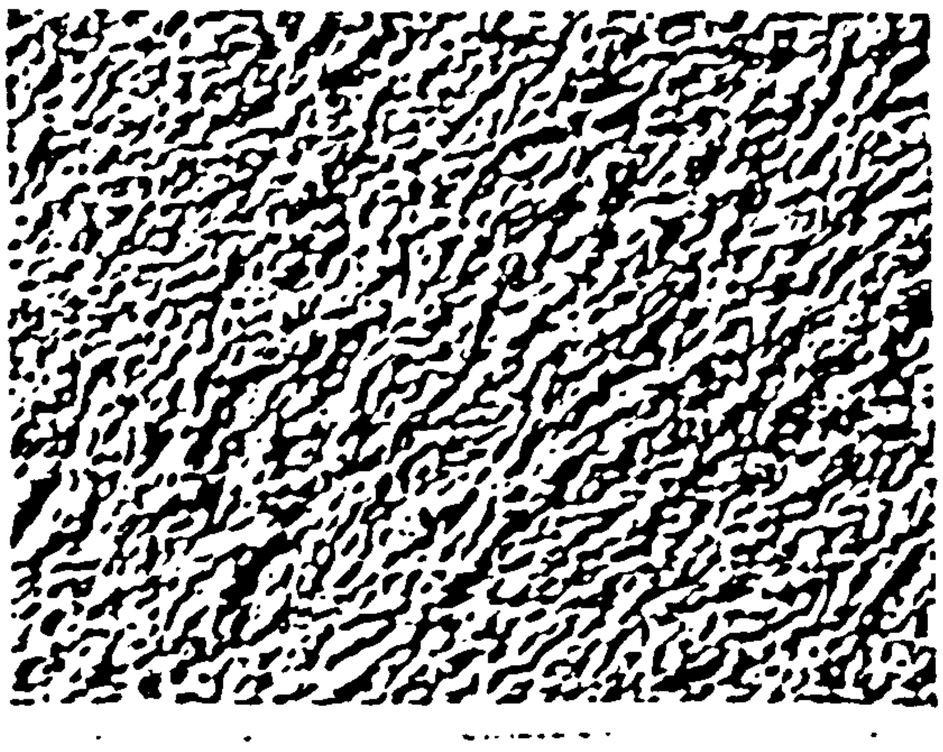

(f)

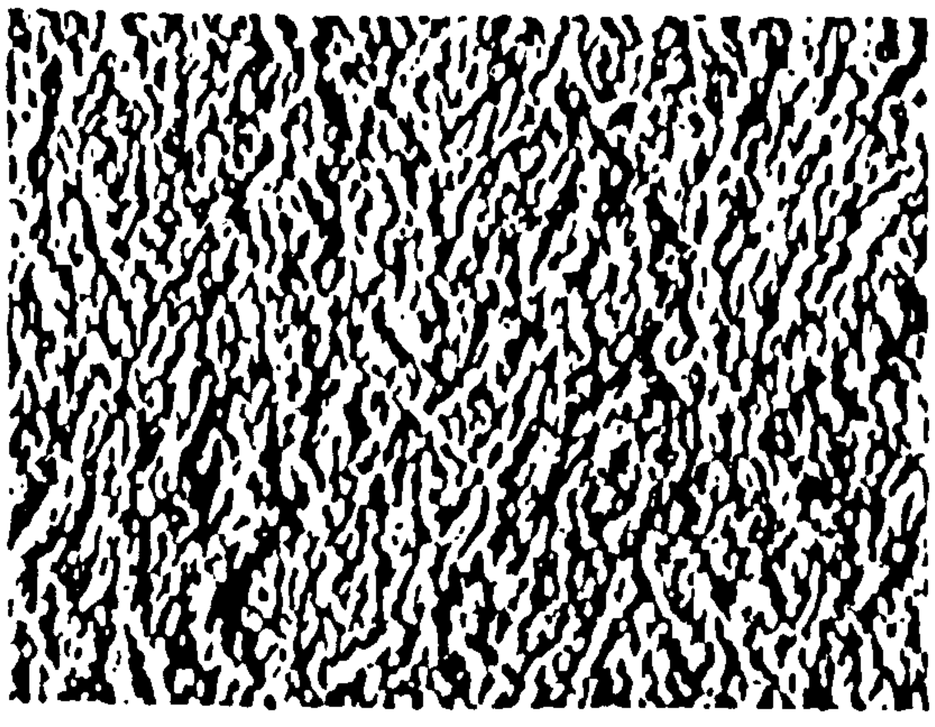

(g)

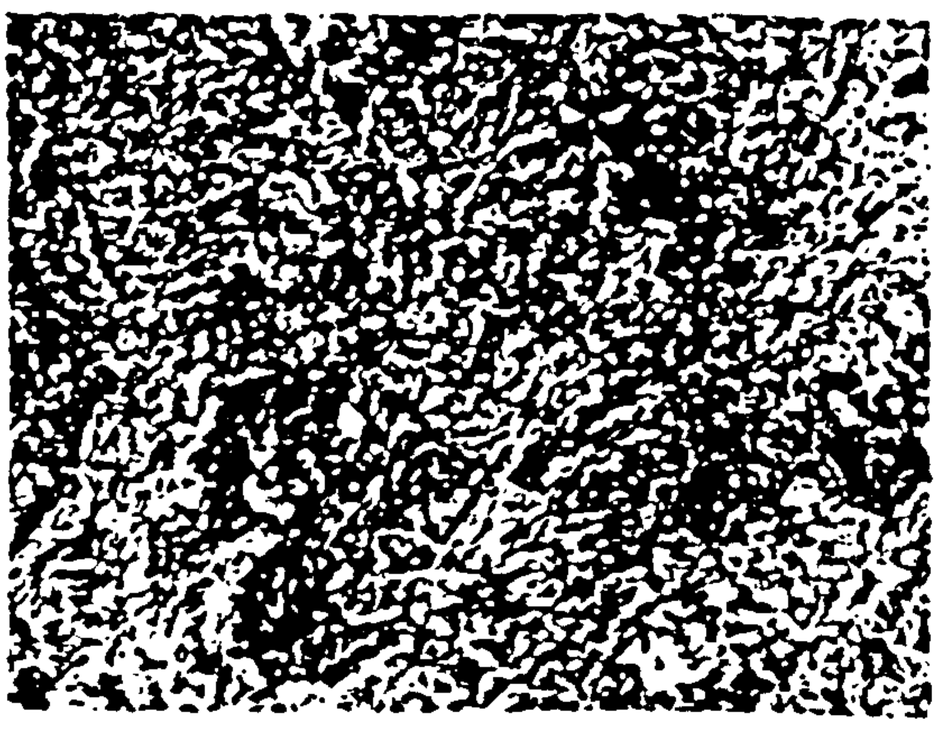

(h)

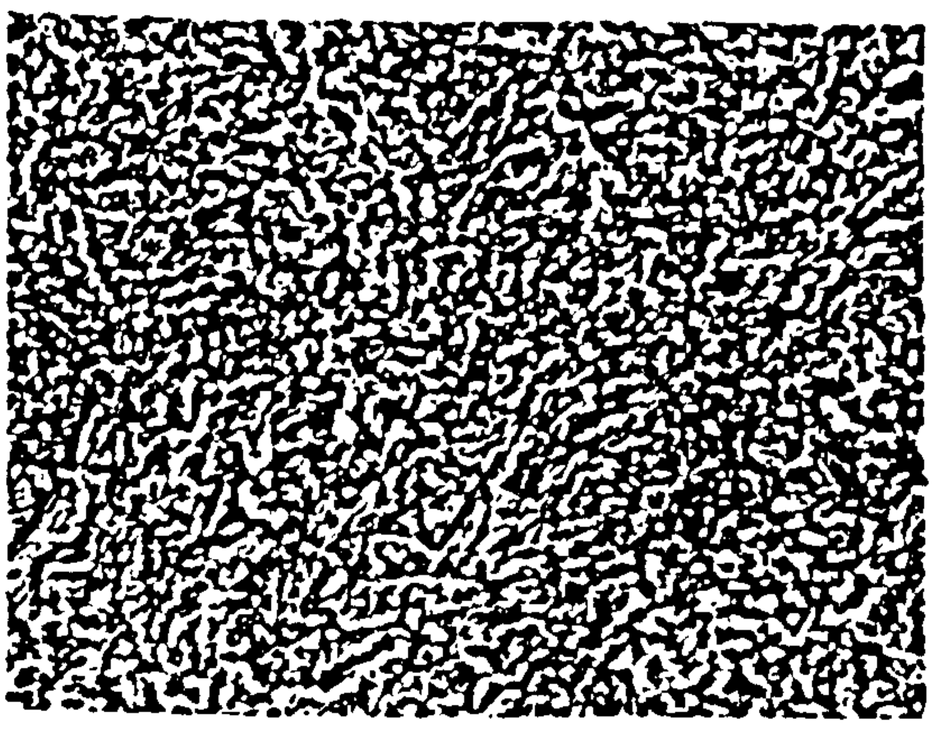

(i)

Figure 5.7 A subscene of Landsat MSS data with various spatial filters applied. Location shown in Figure 5.8. (f) 7x7 east-west edge detection; (g) 7x7 southeast edge detection; (h) 13x13 edge enhancement; (I) 13x13 edge detection.

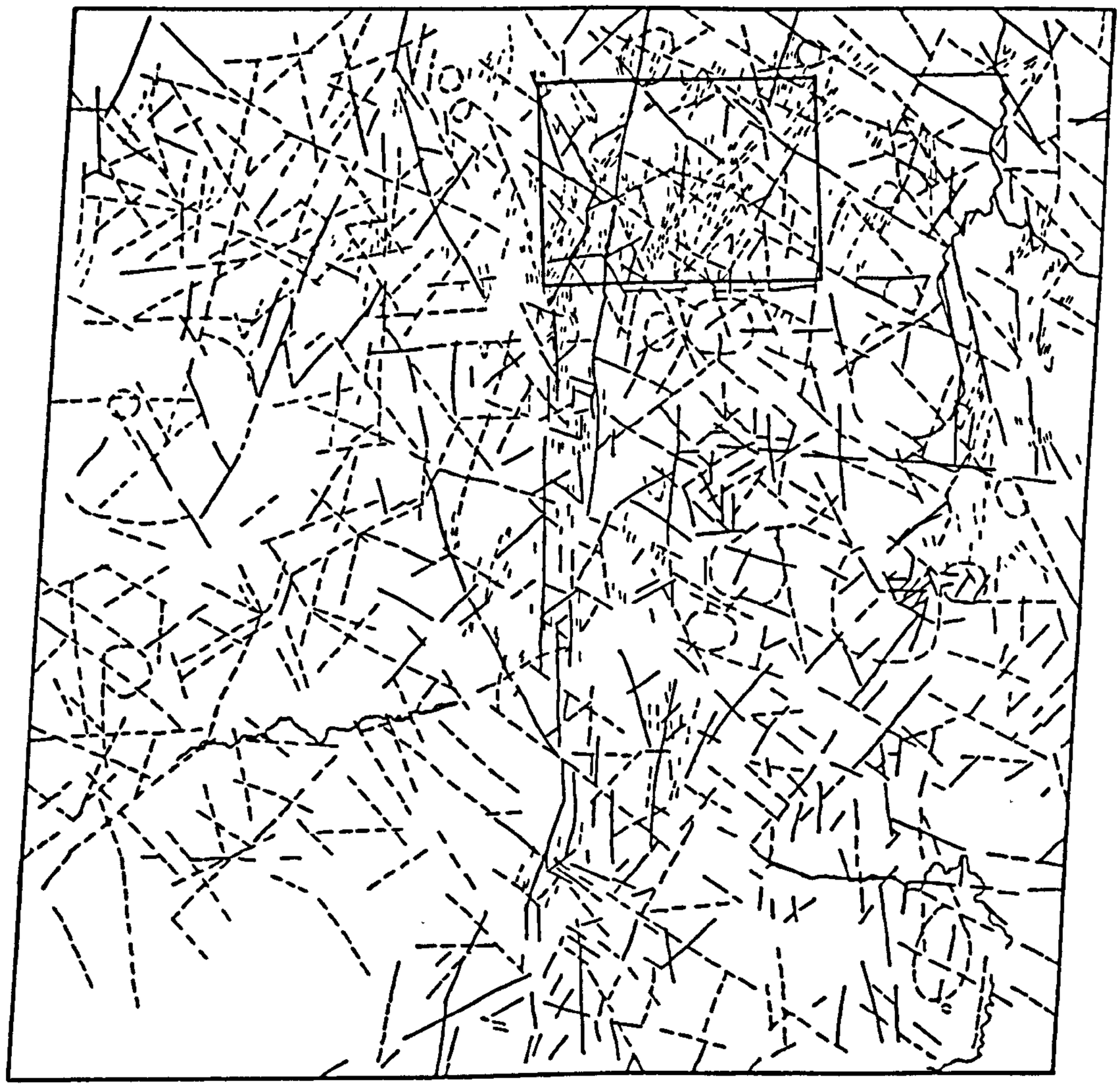

Figure 5.8 Lineament map of MSS scene path 184, row 53 (see figure 5.2 for location), showing the most convincing lineaments detected by a combination of filtering techniques (Figure 5.7). The subscene shown in Figure 5.7 is outlined.

this are given in Figure 5.6 Figure 5.7 shows a variety of filtered versions of part of the scene, and Figure 5.8 shows the resulting lineament map of the entire scene.

All the known major structures were enhanced by both the directional and non-directional filtered images. There are significantly more east west lineaments in the directionally filtered images, which were introduced especially by the north-south filter. These are mostly artefacts related to scan-lines.

In general, the author recommends that it is easiest to produce a mega-lineament map using an edge enhanced, non-directional high pass filtered image, although the confidence level of most detected lineaments is greater if results are combined from directionally filtered images. If more detailed lineament data are required, then it is suggested that directionally filtered edge detection techniques are more suitable, provided care is taken to recognize and discount artefacts.

5.5. LITHOLOGIC DISCRIMINATION AND INTERPRETATION OF ENHANCED IMAGERY

5.5.1 Introduction

There are two possible approaches to lithological discrimination using remote sensing data. One is to produce a high quality image suitable for photogeological interpretation in which the geologist makes the decision of locating lithologic boundaries. The other method is to use the image processing computer itself to divide the image into areas of different spectral response which is known as 'classification'. In this study the former approach is adopted. Classification is of little use because of variable cover over similar rock types.

Lithologic discrimination has been achieved in three ways:

1) Lithologic contact can be extended over large areas with minimum control, and identification of rock types is achieved by extrapolating from well studied areas using photogeological interpretation techniques. The characteristics adopted for lithologic discrimination are presented in Table 5.2.

2) Lithologic discrimination is achieved indirectly from structural information. If the structural trend of a well known lithologic unit is traced and extrapolated along strike, the lithologies could be considered to belong to the same structure. However, facies variations and pinch-outs should be taken into consideration.

3) Classification i.e the computer-assisted recognition of surface materials based on their spectral properties, was attempted. The computer employs the statistics of data from training areas based on field observations. This works well only in terrains with little or no soil cover and sparse vegetation. However the presence of many shadows and burn scars disrupted the process. As a result of these problems this technique was used rarely.

Table 5.2 **Characteristics adopted for lithologic discrimination in Landsat MSS band 5 and Large Format Camera Images.**

Lithology	Tone	Texture	Morphology
Alluvial cover.	Usually pale to grey white.	Flat and smooth.	Mainly confined to wadis and plains.
Tertiary volcanics.	Very dark.	Very rough and flat.	Plateau forming, unconformable on Precambrian rocks.
Post-tectonic granites.	Variable, but usually an intermediate tone.	Rugged.	Distictly circular in outline.
Syntectonic granite.	Usually pale.	Subdued.	Usually elliptical bodies.
Schist.	Intermediate.	Schistose.	Fine banding on a reginal scale.
Mafic-ultramafics.	Very dark.	Rugged and imbricated	Forms elongate lenses, and are aligned in zones.
Volcano-sedimentary rocks.	Intermediate.	Rough.	Generally form linear ridges.
Gneisses.	Dark.	Rough.	Subdued topography.

Since hard copy colour imagery is expensive to print, Landsat scene was examined on the television screen and then a series of colour slides or black and white pictures were taken after favourable structural and lithologic continuity was observed. In less complex cases, interpretation of lithology was achieved directly from the screen, and was plotted onto bulk processed black and

white imagery.

5.5.2 Mapping of mafic- ultramafic complexes

The main aim was to distinguish mafic-ultramafic rocks from adjoining, metasediments, and acidic rocks. To distinguish the different lithological units in an ophiolitic sequence analogous to that of the Oman ophiolite (Rothery,1984) would have required a far more detailed study than has been attempted here. Although mafic-ultramafic rocks are spectrally dissimilar to the metasediments, some misclassification can result due to areas receiving full or oblique illumination and also due to burn scars which affect a range of rock types, and hence appearing darker than the bulk of the pixels in the same rock type. Since there could be misclassification when using enhanced MSS colour imagery, it was found useful to interpret these together with a first principal component which enhances structural and textural information.

Serpentinites were used as marker horizons in defining an ophiolitic belt, because dunite/serpentinite bodies tend to form hills devoid of vegetation as compared to the surrounding areas. The dunite/serpentinites and the gabbros are responsible for the darkest signitures on the imagery. The ultramafic masses are often thin elongate and aligned in zones. Serpentinites are also readily distinguished from most other lithologies because of their overalll reflectance in the visible and reflected infrared and particularly their low band 7 values (Sultan *et al.*,1986).

5.5.3 Landsat Interpretation of key areas in NE Africa

5.5.3.1 NE Sudan - Eritrea

Geology

The bedrock geology of Eritrea and adjacent areas of Sudan is dominated by highly deformed crystalline Precambrian basement (Figure 5.9). This comprises an ophiolitic mafic-ultramafic suite, tectonically emplaced within a complex of anorogenic granitoids, supracrustal volcanics and sediments. (Kazmin, 1975; Embleton *et al.*,1983) This Pan-African complex has been punctured by various post-tectonic granitic bodies. (Vail and Kuron, 1978; Vail, 1985b).

GEOLOGICAL MAP OF OF NE SUDAN-ERITREA REGION

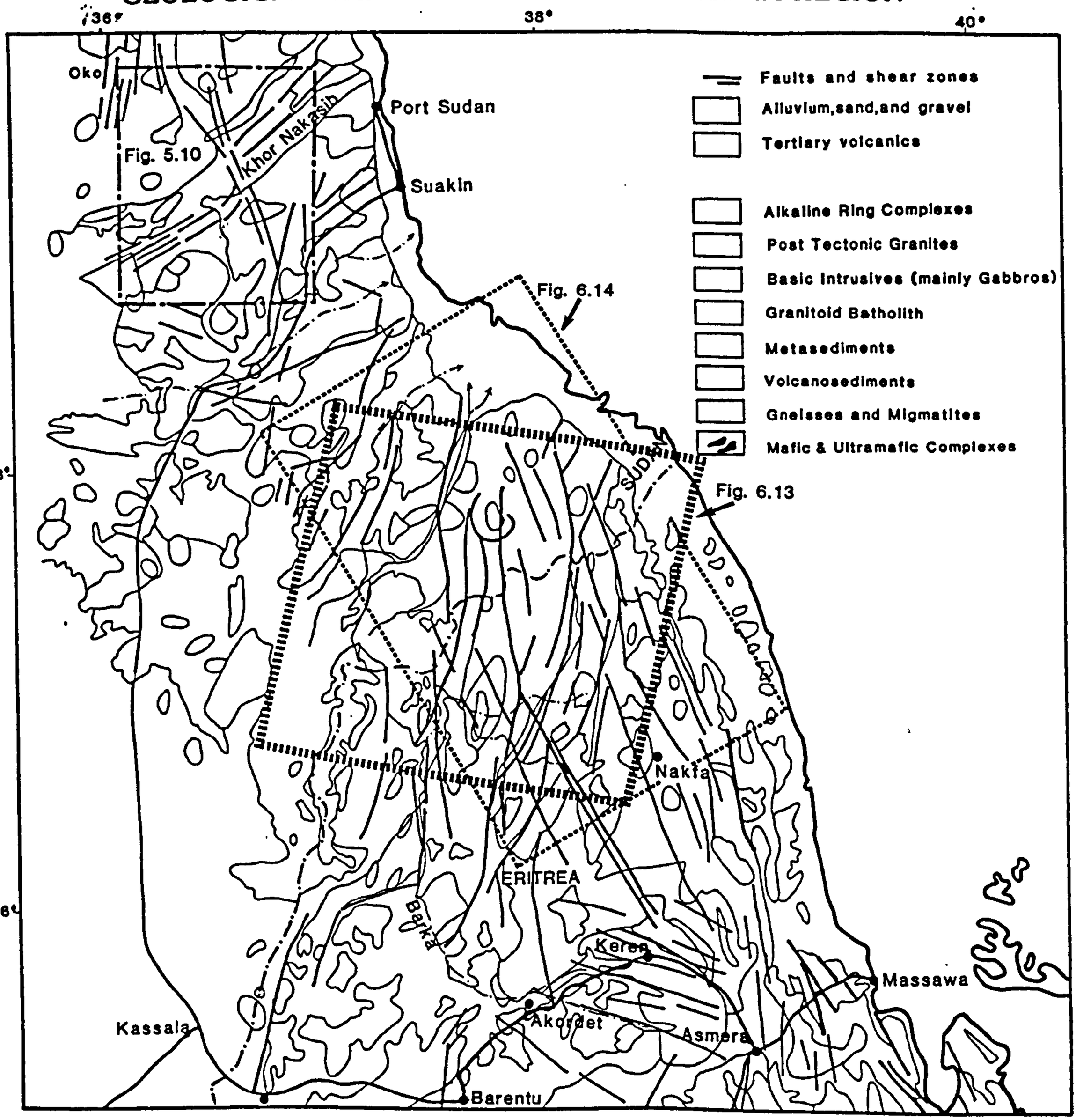

The ophiolite complexes are restricted to two main areas, southwest of Port Sudan, and in the Barka river area (NW Eritrea). They are usually found scattered along shear zones. The ultramafics are the darkest on the imagery and are often elongated and aligned in zones (Figure 5.10). The gneisses and migmatites occur in isolated outcrops along the length of the Red Sea Hills, NE Sudan and along the Red Sea escarpment of Eritrea (Figure 5.9). The high grade gneisses are distinctly darker than the light toned volcano-sedimentary sequence of the Eritrean Highlands to the west, and the pale coastal plain to the east. The areal extent of the gneisses and migmatites is small compared with the volcano-sedimentary sequences and syn-tectonic intrusive granitoids. These account for the bulk of the rocks exposed in NE Sudan and Eritrea. The Eritrean highlands comprise subparallel NNE trending synforms and antiforms represented by volcanoclastic rocks and metasediments approximately 200 km across in the south (Figure 5.9). This volcano-sedimentary sequence was metamorphosed to greenschist facies. The assemblage is composed mainly of schists, phyllites, slates, quartzites and marble in association with basaltic to andestitic lavas and pyroclastics. A common feature of the volcano-sedimentary rocks is the presence of a tectonic or fine compositional fabric.

Syntectonic granitoids (batholith) with irregular intrusive forms are widespread in the Red Sea Hills of NE Sudan and Eritrea. They are predominantly granodioritic to tonalitic in composition and are usually pale and show fabric. The largest syntectonic granite in Eritrea occupies an area of some 700 km ^{2} between Asmera and Akordet. (Kazmin, 1973).

There are many small syenite and alkali granitic intrusives that are post-tectonic. These intrusives are often characterized by well-developed ring structures. The younger granite ring complexes that characterize the Red Sea Hills of NE Sudan die out abruptly southwards near the Eritrean-Sudan border (Vail, 1978). The post-tectonic granites are easily identified on the Large Format Camera images by their characteristic ring structures. The spectral signature of the post-tectonic granites vary from pale to very dark and texturally they range from smooth to rugged (Table 5.2).

Figure 5.10 (a) Large Format Camera imagery of the Khor Nakasib area, NE Sudan. The area is outlined in figure 5.9. An interpretative sketchmap is presented in figure 5.10 (b) which shows a sinistral displacement of the Khor Nakasib ophiolite belt. Scale approximately 1:1 million.

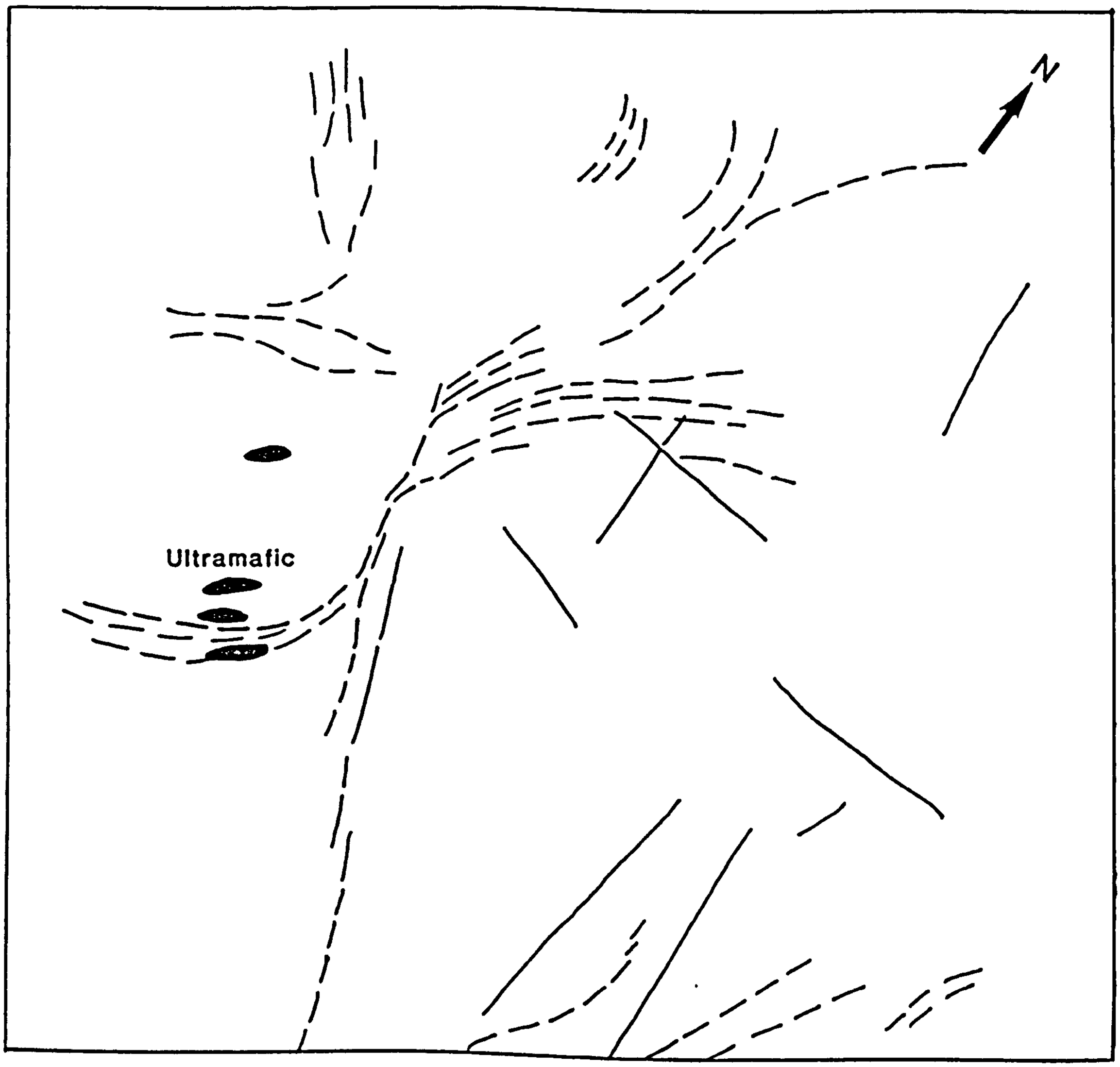

Figure 5.10 (b) An interpretative sketchmap is presented which shows a sinistral displacement of the Khor Nakasib ophiolite belt. Scale approximately 1:1 million.

5.5.4 W. Ethiopia

Part of a decorrelation stretched Landsat MSS image showing the study area is reproduced (Figure 5.11a). The ophiolitic rocks which are found in the centre of this area show strong linear fabric,and swings in an S-shape fashion (Figure 5.11b). The ophiolite belt forms imbricated slabs overthrust onto the high grade gneisses and migmatites in the east. West of the ophiolite belt is a zone of diorite-granodiorite batholiths and associated sediments. This zone is cut by syntectonic and post -tectonic granites (observed at the northern end of the sub-area) (Figure 5.11a). In the southwestern and eastern corner of the sub-area, plateau- forming Tertiary volcanic cover is observed.

The easiest lithologies to recognise from the deccorelation stretched image are the Tertiary volcanics which appear as yellow, and granites which appear as red. The red color is partly due to vegetation cover. However the gneisses are identified from their green-blue colour, the ophiolites appear green and are no different from the volcano-sedimentary rocks to the west. Hence the misclassification is a result of combination of mainly mineralogical absorption features due to soil cover and complications arising from burn scars and vegetation cover. The colours in such an image should be interpreted by considering the possible absorption features affecting the different bands, and remembering that decorrelation stretching forces an almost complete range of possible colours into the image. Since the ophiolite belt forms prominent thrust blocks, the deccorrelation stretched image is best interpreted in conjunction with first principal component image which preserves structural and textural information.

Deccorelation stretched image of the Kurmuk area (Figure 5.12a) show metasedimentary schists which are dextrally displaced. Few post-tectonic granitoids are also prominent because of their circular outcrop. Burn scars have complicated the discrimination of lithological units, however major NW trending faults are observed.

5.5.5 SE Sudan

In figure 5.13 two major N-S trending lineaments are cut or truncated by NE-SW, E-W and NW-SE lineaments. The N-S lineaments control the distribution of two major lithological units. To the west the

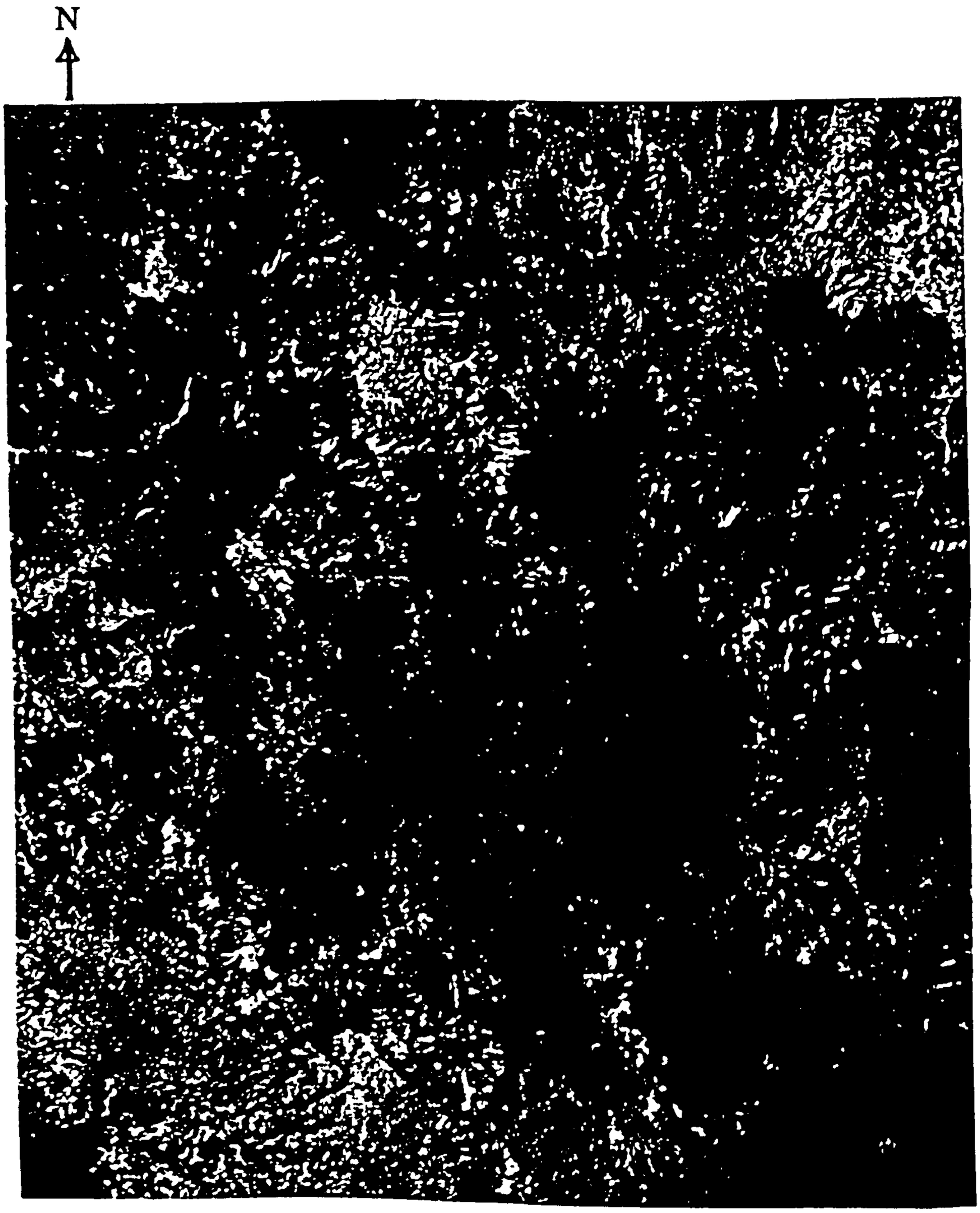

Figure 5.11 (a) Deccorelation stretched image of the Blue Nile area, W Ethiopia. Note that the S - shaped structural trend at the centre of the imagery is the Yubdo ophiolitic belt. The interpretation of this Landsat scene is presented in figures 4.3 and 5.12. Scale approximately 1:1 million.

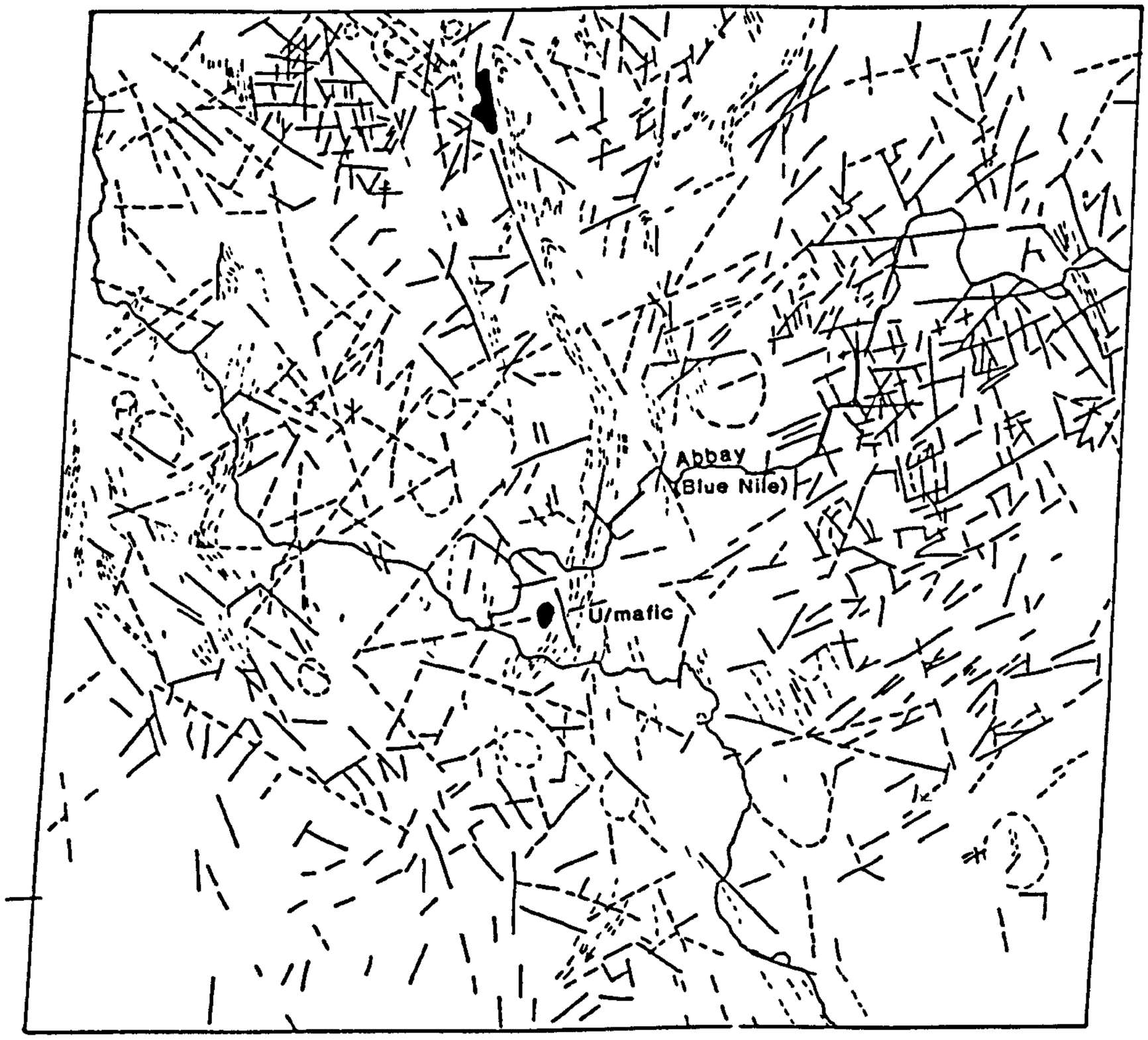

—— TOPOGRAPHIC LINEAMENTS

---- TONAL LINEAMENTS

STRUCTURAL TREND LINES

Figure 5.11 (b) Lithostructural map of Abbay (Blue Nile) area . MSS scene path 183, row 53. See figure 5.1 for location.

Figure 5.12 (a) Decorrelation stretched image of the Kurmuk area, W Ethiopia . This image shows NW trending lineaments displacing dextrally a metasedimentary unit. (b) Interpretative sketchmap of the Kurmuk area. Symbols are: Mv= metavolcanic; Ms= metasediments; A= amphibolites; Sch= schists; S.Gr= syntectonic granitoids; Gr= granodiorites and Al= alluvium. Scale approximately 1: 500,000.

bluish-green represent schists and alluvial cover, while to the east they are predominantly granitoids. Southeast of Kurmuk area there is the Ingessana mafic-ultramafic complex . Although SE Sudan is semi-arid and the vegetation cover is limited, there is a lot of alluvial cover which makes image interpretation difficult. On the MSS image the Ingessana mafic-ultramafic body appears as a dark circular body which without field control, could easily have been mistaken for a gabbroic or gabbro-dioritic intrusive body. The Ingessana ophiolite has a subcircular form (Price, 1984) that contrasts with most other ophiolitic complexes which are lenticular in shape.

North of Ingessana the Qala En Nahal mafic-ultramafic complex forms a lenticular outcrop, preserved in a synform bounded by faults (Wilcockson and Tyler, 1933). Although there is no extensive development of linear and planar fabrics to establish its direct continuity with the Ingessana, the two ophiolites are aligned along strike of the elongate Qala En Nahal complex and are considered to be related.

5.5.6 Baragoi, N. Kenya

In N Kenya two Landsat MSS images (paths 181, rows 058 and 059) were interpreted using different enhancement techniques. Hard copies were prepared for the Baragoi area, while interpretations from the Lake Turkana area were based directly on video displays and photographs of the video screen.

Figure 5.4 is a 60 km wide portion of the Baragoi Landsat scene. The area can broadly be classified into three terrains from west to east is; the Kenyan Rift characterized by downfaulted Tertiary volcanics and the Baragoi ophiolitic complex that is truncated to the east by N-S trending metasedimentary ridges. To the northeast Recent lavaflows cover the alluvial plain.

The conventional false colour composite (Figure 5.4a) using MSS bands 7, 5, and 4 in red, green and blue respectively, identifies all the major units. When a decorrelation stretch is applied to the same image, however, more subtle colour distinctions are emphasised (Figure 5.4b). The dunite bodies in particular are more effectively discriminated (see image interpretative map for comparison Figure 5.8). Figure 5.5a shows a principal component transformation of Landsat MSS data, but it is difficult to interpret colour variations or to appreciate relationships between areas with

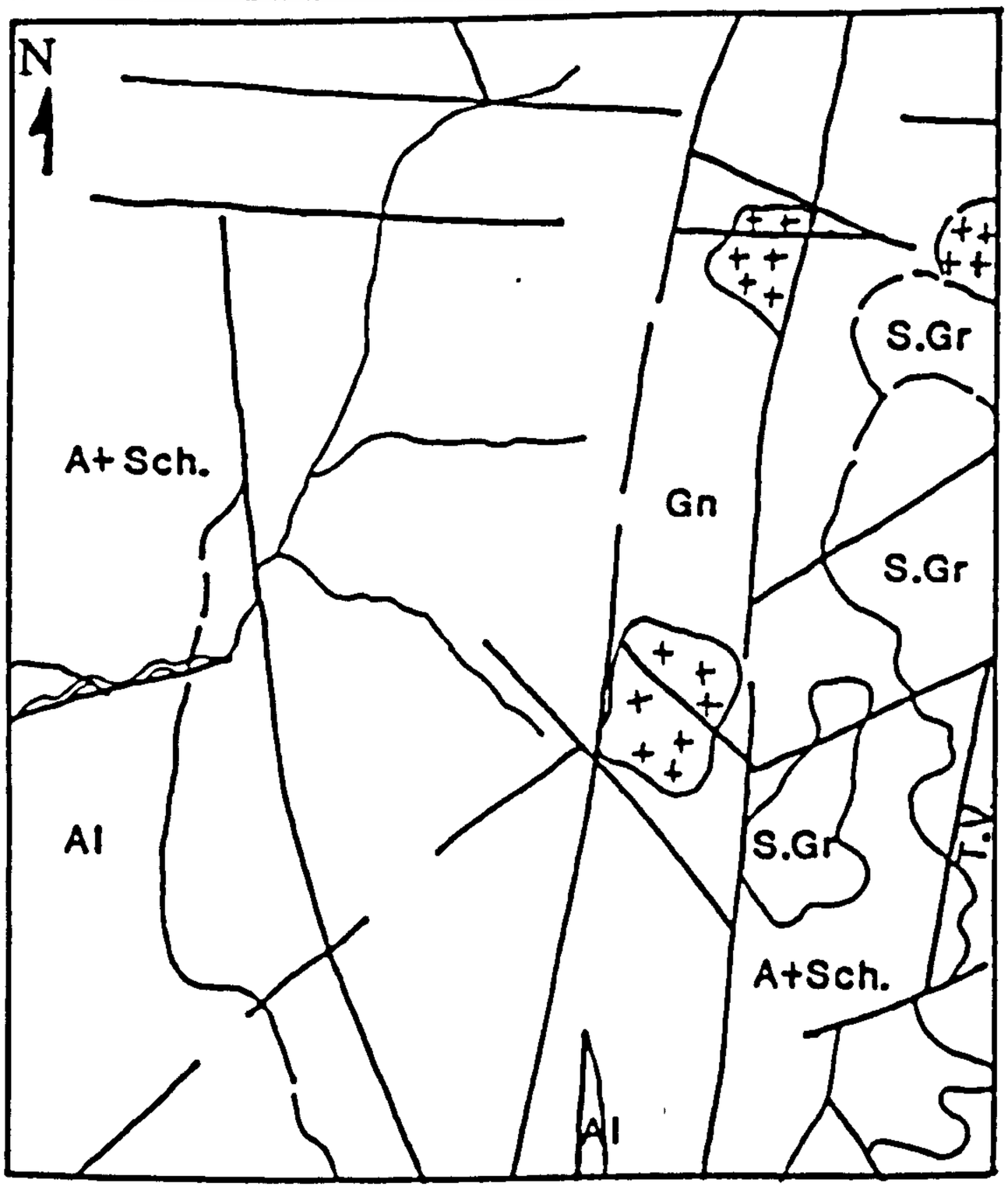

Figure 5.13 (a) Deccorelation stretched image of the Kurmuk area, W Ethiopia. (b) Schematic interpretation of the Kurmuk area. The subscenes are outlined in figure 5.2. This imagery shows a section of the Kurmuk lineaments which trend N-S for over 700 kilometres . These lineaments are often observed displaced dextrally by NW trending faults.Symbols are Mv=metavolcanic; A= amphibolites; Ms = metasediments; Sch= schists; S.Gr= syntectonic granitoids; Gr= granodiorites and Al=alluvium. Scale approximately 1: 500,000.

different colour. There is execssive saturation of colour and the new colours do not easily relate to spectral features. The image transformed by Taylor's colour space (Taylor,1974) (Figure 5.5b) preserves the structural information, but loses lithologic discriminability.

Interactive processing of Landsat MSS imagery indicates a northward continuation of the Baragoi ophiolite, and is observed to be overlapped byTertiary volcanics in the Turkana area. In the Turkana Landsat scene the Barsaloi N-S to NNW trending ridges are observed to dip below the Tertiary volcanics. These ridges seem to control faulting along the Kenya rift.

In conclusion decorrelation stretching and other enhancement techniques have been more effective in semi-arid areas such as Baragoi than in highly vegetated lateritized areas as in western Ethiopia. Nevertheless it has been possible to trace the ophiolite belt in W Ethiopia for hundreds of kilometers, without the time consuming use of such techniques.

5.6 REGIONAL DISPOSITION OF LATE-PROTEROZOIC MAFIC-ULTRAMAFIC ROCKS IN NE AND E AFRICA

Study of Landsat MSS imagery combined with field data and the published maps of other workers has been used to constrain a revised structural interpretation of the region. The mafic-ultramafic complexes are shown to lie on five narrow belts trending between north-south and northeast-southwest, outcropping discontinuously for at least 2500 km. In grouping these complexes three criteria had to be satisfied; (a) that the rocks have a convincing Penrose (1972) ophiolitic assemblage; (b) that the structural trends within the ophiolites showed them to align along strike; and (c) that there should be a contrast in the geology on either side of the proposed suture.

Based on these criteria, the five ophiolitic belts recognized (Figure 5.2) are (from west to east) the (1) Sol Hamed-Wadi Onib belt; (2) Ingessana-Port Sudan belt; (3) Sekerr-Yubdo-Barka belt; (4) Baragoi belt; and (5) Adola-Moyale belt. It is suggested that these represent sutures formed by the closure of small ocean basins between island arcs, after the model suggested by Gass (1981) for Saudi Arabia and northeast Sudan (see chapter 3 and 4). The ages of the ophiolites are not well known. The only published dates of emplacement metamorphism in the Arabian-Nubian shield are

around 740-780 Ma (Claesson *et al.*,1984).

According to Dewey (1977) the simplest kind of suture is a high-strain zone containing disrupted ophiolite remnants separating two regions usually of different pre-collisional strain history. The ophiolites of NE Africa are highly strained and linearly oriented for hundreds of kilometers and hence mark suture zones. However some ophiolites are not rooted in the related suture, but have been tectonically transported because most of the mafic-ultramafic masses are found as isolated fragments thrust from the main belt of deformation. The sutures for the Baragoi and the Adola-Moyale belts probably lie a few tens of kilometres west of these complexes, where southeastward directed (Baragoi) and eastward-directed (Adola-Moyale) thrusts are now identified. However, the other ophiolite belts are considered to lie more closely along sutures because of their continuity over hundreds of kilometres. Also crustal shortening in northeast Africa has been less extensive than that observed in the Alpine and Himalayan orogenies, and thus the ophiolite complexes are unlikely to have been subsequently displaced by more than a few tens of kilometres from their sites of emplacement. Exceptions to this are the ophiolitic occurrences in the Eastern Desert of Egypt which are in a tectonic mélange (Shackleton *et al.*, 1980; Ries *et al.*, 1983) with possibly very large horizontal displacements. The ophiolite belts swing to the southeast near the Sudan-Kenya border suggesting that the accreting fragments were compressed (with a greater degree of crustal shortening than in the north) against the Tanzanian craton to the west. Hence the present location of ophiolite belts further south-*viz.* Kenya, Tanzania and Mozambique-do not necessarily delineate the original sites of the marginal basins.

CHAPTER 6

THE TECTONIC FRAMEWORK OF NE AND E AFRICA

6.1 INTRODUCTION

The orogenic history of the Pan-African Mozambique belt is not well known. To further elucidate the tectonic history of the area structural trend lines (strike of regional foliation and bedding) have been used as a basis for correlating age sequences including the interpretation of lineaments in four critical areas: (i) NE Sudan-Eritrea, (ii) W Ethiopia, (iii) SE Ethiopia and (iv) Baragoi, N Kenya. Structural trend lines and lineaments have been interpreted from Landsat MSS and Large Format Camera images. The existence of a widespread system of shear zones within the Proterozoic rocks of NE Africa has been discussed previously (Ahmed,1983; Berhe and Rothery, 1986). It has been shown that these structures form characteristic lineament patterns. These studies provide a background to the significance, origin and age relationship of the various lineaments.

This information is used to decribe the stress distribution in NE Africa and is constrained with the background knowledge of the area. In this chapter the nature of shear zones is described and their general relationship to the tectonic evolution of the Arabian-Nubian shield is investigated. The main aim is to integrate the detailed structural observation of four key areas and try to relate these structures to microcontinental accretion models.

6.2 STRUCTURAL TRENDS IN NE AND E AFRICA

Structural trend lines have been interpreted from Landsat imagery and are presented in Figure 5.2. Since only structural trends mappable on a 1:500,000 scale have been incorporated, detailed interpretation could only be carried out using structural studies aquired on the ground.

Structural trends usually are a composite feature made up of :

1) Strike of lithological units

2) Strike of foliation

3) trend of fold axes

4) the trace of shear and thrust planes.

Structural trend lines have been used as a basis for correlation of age sequences (Holmes, 1951; Pallister 1971; Bowes and Hopgwood ,1976) and were used to construct previous configurations of continental masses. However, their uncritical use in defining age sequences can be misleading. Bowes and Hopgwood, (1976) suggest that structural elements are rarely precisely defined, in many cases they are composite and in the majority of instances their relative time of formation in polyphase deformational sequences can not be determined. Hence the use of a common structural trend as evidence of similar age in the Arabian-Nubian shield is not legitimate. However the possiblity of erroneous correlation of trends whose nature has not been specified, was avoided by splitting NE and E Africa into separate blocks. This made it easier for the corresponding structural sequences to be demonstrated. Correspondence in orientations of successively formed structural elements in extensive polyphase deformational sequences of the Adola - Moyale belt, with the Baragoi, (N.Kenya) , Yubdo (W.Ethiopia) and NE Sudan - Eritrea metamorphic belts can provide a basis for correlation in NE Africa.

6.3 TECTONIC DOMAINS

6.3.1 NE Sudan - Eritrea Sector

Structural trends are very prominent in the Eritrean Highlands, being dominated by linear ridges and long, steep-sided vallies. Four tectonic zones have been identified (Figure 6.1). In the Mareb area (zone A), the dominant structural trend is 055°, which is related to folds and linear metasedimentary beds; West of Barka (zone B) the structural trend swings to the N-S, with dips steeply to E and W, which are related to tightly compressed folds plunging 360 N. This belt generally strikes N-S to 010°N, progressively swings to 350° structural trend and bifurcates in zone C into 040° trending

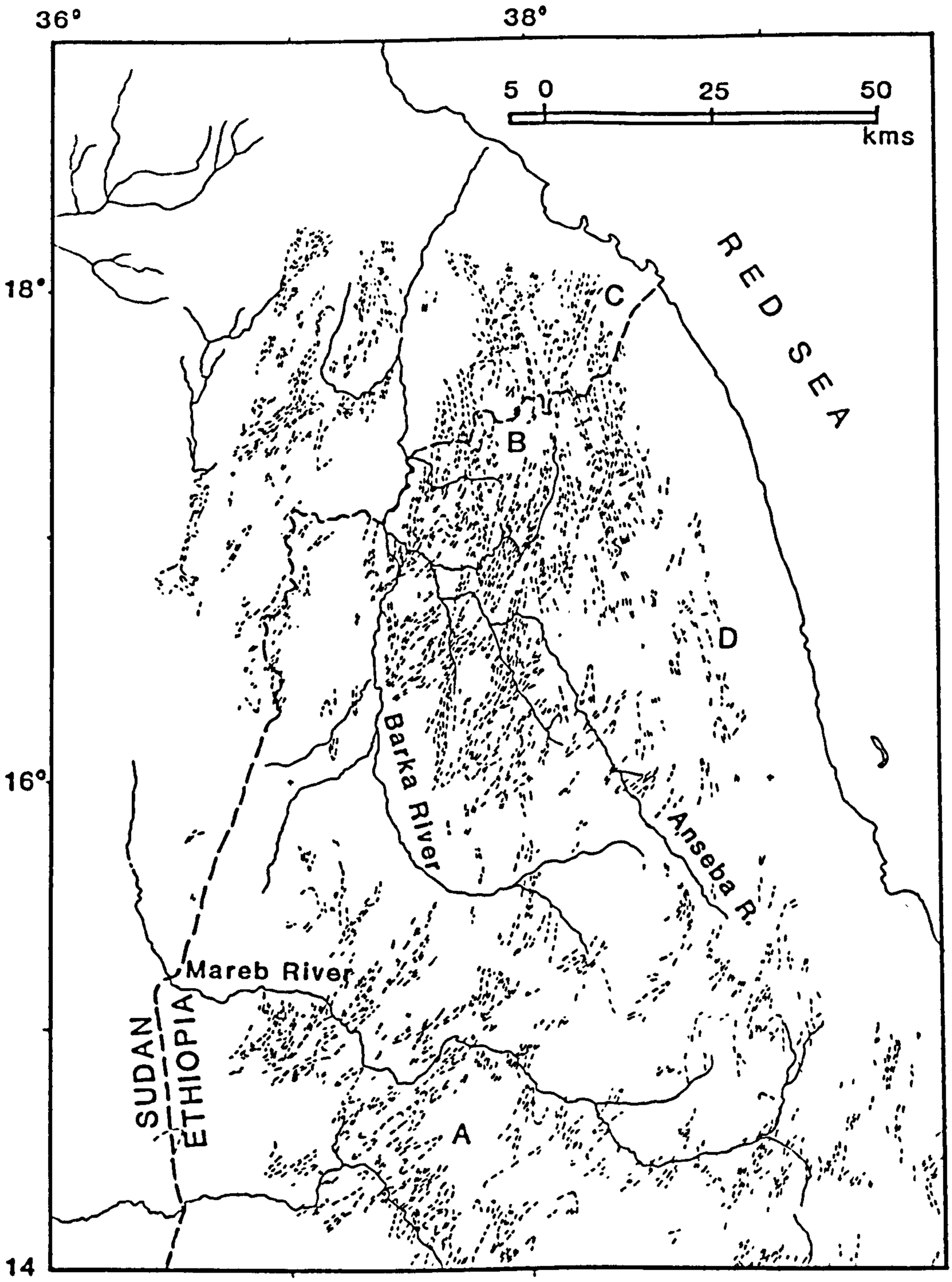

Figure 6.1 Sketchmap of the major structural trends in NE Sudan-Eritrea. Various tectonic belts indicated by symbols. A, NE-SW trending; B, N-S trending; C, NNE-SSW trending; D, NW-SE trending structures. Based on Landsat MSS band 5 and supplemented by Large Format Camera images.

structures. In contrast the main structural and lithological features of the eastern block of the Red Sea area (zone D) which is about 50 km wide, strikes 335° for at least 200 km. These NNW-SSE structures are truncated by the 040° trending structures (zone C) further north. Regionally, the foliation trends 055° in the Mareb area (zone A) but changes to N-S in the Barka area (zone B) and later bifurcates to 040° in the northeast (zone C).

The level of deformation in these areas is usually low, except along shear zones where it is intense. Extensive shearing in this area has caused local structural complexities, such as sinuous structural trends, the curving in and displacement of structural trends along shear zones. Complex structural patterns as in the NE Sudan- Eritrea (Figure 6.1) reflect the superimposition of successive fold structures and the variation of intensity of each deformational phase from place to place. A detailed structural synthesis of the area is presented in section 6.5.

6.3.2 SE Sudan - W Ethiopia Sector

Figure 6.2 is a simplified interpretation of the mosaic in this area. Three major tectonic zones have been identified: the most easterly zone (zone A) which is about 40 km wide is dominated by E-W trending banding and foliation. Large E-W isoclinal folds overturned to the south are easily identified on Landsat imagery and were confirmed by field observation (Kazmin *et al.*,1979a; Berhe,1981). These are accompanied by small amplitude (metre scale) isoclinal folds of the same trend with sharply undulating axes. Westwards into zone B, the older gneissic banding was refolded along north-south axes, as indicated by the intersection of gneissic banding by later axial planar cleavage. This N-S trending belt bifurcates into 025° and 340° trending segments, which later converge back into a N-S trending structure further north (Figure 6.2). This suggests that the structural belt is deflected either by an intrusion or by a broad antiform or dome. The intrusion can not be substantiated as there is extensive Tertiary volcanic covering the central part of the area.

To the southwest, a fold belt trending 320° truncates the N-S strike of zone B. Strong compression within this fold belt (Figure 6.2) implies considerable crustal shortening (zone B) and deformation of the margins of the gneiss-migmatite block (zone A) suggests that this shortening was

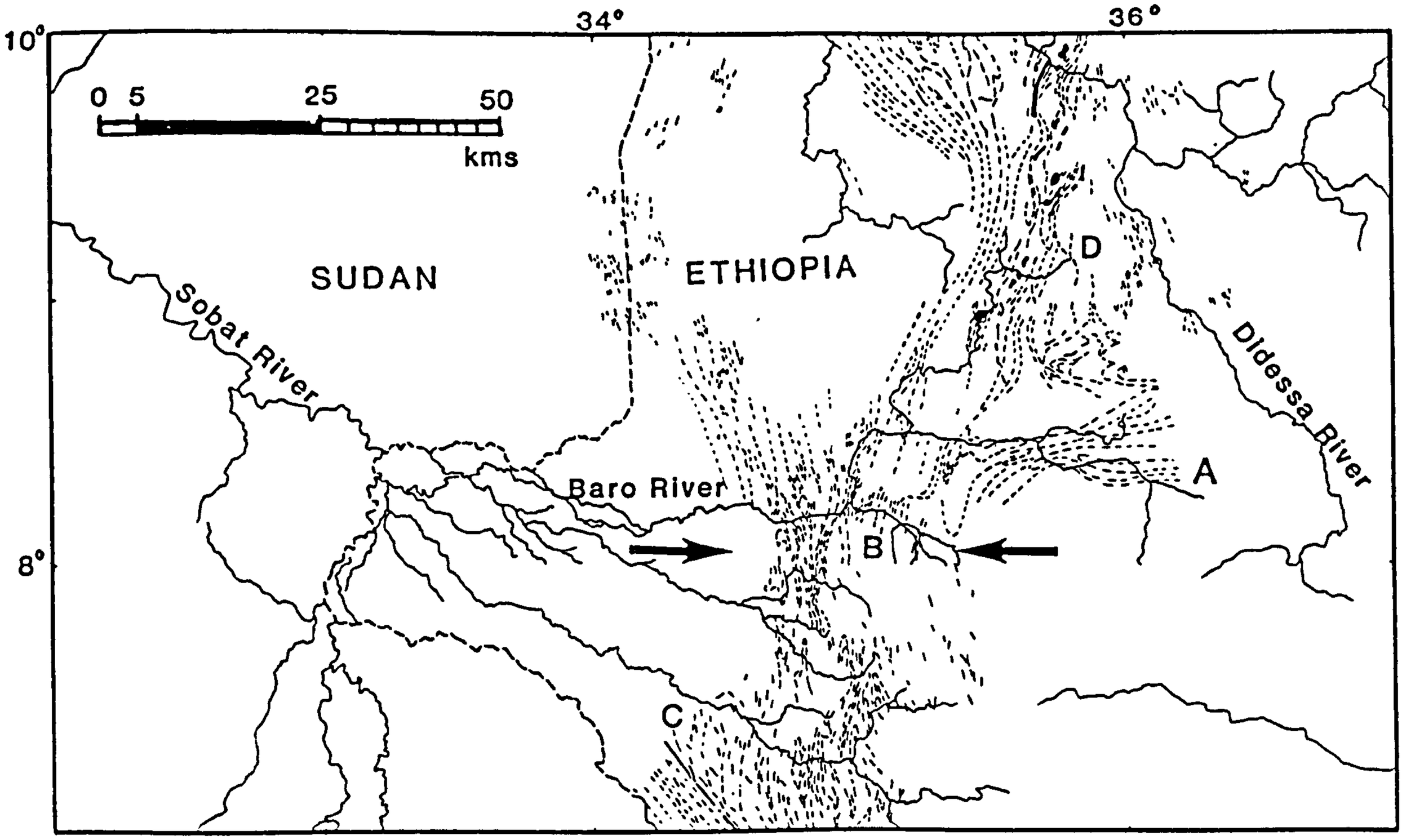

Figure 6.2 Sketchmap of the major structural trends in W Ethiopia. Various tectonic belts indicated by symbols. A, E-W trending; B, N-S trending; C, NW-SE trending; D, NE-SW trending structures. Based on interpretation of Landsat imagery and confirmed by fieldwork.

due to convergence of these blocks.

6.3.3 S.Ethiopia - NE Kenya Sector

In S Ethiopia - N Kenya the most prominent structural trend is NW-SE (Figure 5.2). However on a more detailed map (Figure 3.4) of the Adola area (S. Ethiopia) the area has been subdivided into four tectonic zones: zone 1 (western zone) is characterized by E-W trending structures; zone 2 (central zone) is characterized with structural trends varying from N-S to E-W with subvertical dips; Zone 3 (eastern zone), is dominated by major N-S trending folds, and zone 4 (SW zone) is characterized by major NW-SE trending structures. As has been discussed in section 3.4 the sequence of deformation which is based on cross-cutting relationship of folds is E-W, followed by N-S (the result of E-W compression) and then refolded by NW-SE trending strike-slip faults. (see chapter 3 and section 6.8 for detailed analysis).

The NW-SE structural trends that are dominant in S. Ethiopia, and Kenya have been explained as a consequence of shearing along NW trending faults. (Berhe and Rothery 1986). Davidson *et al.* (1976) explained these shear zones as a cataclastic domain which produced mylonite, ultramylonite, and belts of refoliated rocks.

6.3.4 Central Kenya

In the Baragoi area two major structural trends have been identified (Figure 6.3). These are the NW-SE and N-S structures which have been named the Baragoi and the Barsalol phases respectively (Charlesly *et al.*, 1984). The NW-SE structures are refolded into a N-S trending axes. The NW-SE structures are probably related to the emplacement and deformation of the Baragoi ophiolite. The dominance of northwesterly structural trends is maintained in southern Kenya. For a more detailed structural analysis see chapter 2 and section 6.7.

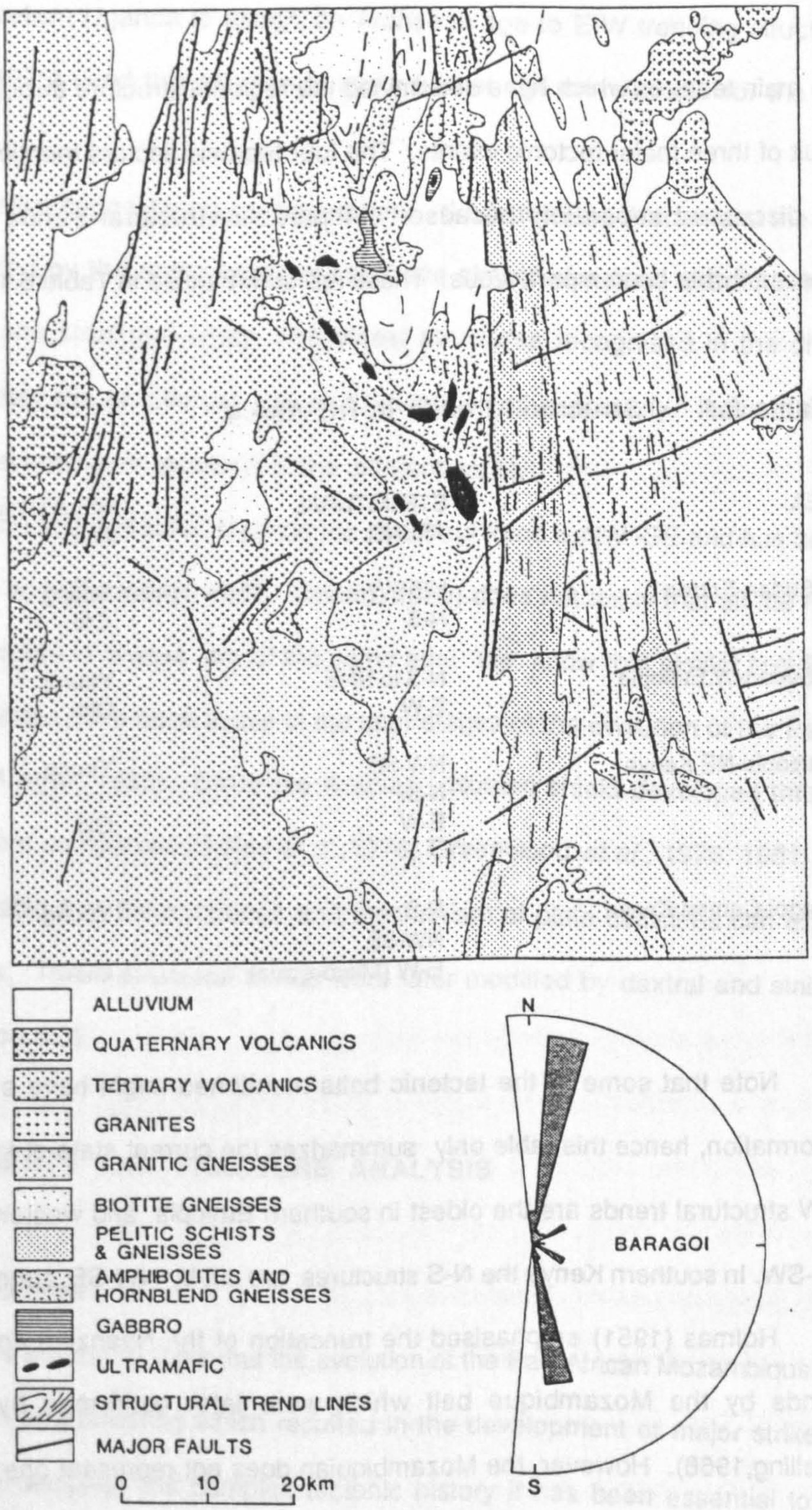

Figure 6.3 Geological map of the Baragoi area, N Kenya. Based on Landsat image interpretation aided by fieldwork.

6.4 IMPLICATIONS OF STRUCTURAL TRENDS

The main features which have determined the regional structure throughout NE and E Africa are the result of three major tectonic events. The four tectonic sectors mentioned previously (section 5.5.3) are discussed separately because comparable structural trends in different areas might not necessarily be contemporaneous. These are summarized in Table 6.1.

Table 6.1 Structural trends in NE Africa.

AREA	STRUCTURAL TREND	RELATIVE AGE	PHASES OF DEFORMATION
NE Sudan-Eritrea	NE-SW N-S	Young Old	Two
SE Sudan-W.Ethiopia	N-S to NNE E-W	Young Old	Two
S.Ethiopia-NE Kenya	NW-SE N-S E-W	Young Old	Three
Baragoi-Central Kenya	N-S NW-SE E-W (Micro-scale)	Young Old	Three

Note that some of the tectonic belts mentioned might have experienced more episodes of deformation, hence this table only summarizes the current state of knowledge. It is suggested that E-W structural trends are the oldest in southern Ethiopia, and western Ethiopia, followed by N-S to NE-SW. In southern Kenya the N-S structures are cut by NW-SE structural trends.

Holmes (1951) emphasised the truncation of the Nyanzian and Dodoman (E-W to NW-SE) trends by the Mozambique belt which were later confirmed by isotopic ages (Cahen and Snelling,1966). However, the Mozambiquian does not represent one episode of deformation, but is a sequence of deformational episodes which were co-axially folded.

In eastern Uganda, Hepworth and Macdonald (1966) and Almond (1969) recognized relict E-W structures which were referred to as the Watian and have been dated as Archaean (Leggo,

1974). Kazmin (1972) and Kazmin *et al*, (1978) used the similarities in lithology and structural alignment of Eastern Uganda to assign an Archaean age to E-W trending structures in Ethiopia. Similarly Vail (1976) used this criterion to make further age correlations for the whole NE African region.

An alternative suggestion is presented here. Since the Pan-African and the Mozambique belt are both affected by the same orogeny and have similar structural characteristics, they can be considered as one structural entity. The oldest structures recognised in the different areas are E-W,however, they are of different age and have evolved separately. Neverthless, it seems that similar tectonic events were recorded in the different areas.

Similarly the fact that in NE Uganda the structural trend is NW -SE and has been considered to be of Archaean age (Hepworth, 1967, Almond, 1969) does not imply that all the NW -SE structural trends in S Ethiopia - N Kenya are of the same age. We know that similar NW-SE trending shear belts in Saudi Arabia have been active in the later stages of the evolution of the Pan-African c.a 600 Ma (Stacey and Agar, 1985). Since the Arabian - Nubian shield developed through accretion of oceanic island-arc complexes (Bakor *et al.*,1976; Greenwood *et al.*, 1976, 1981 and Gass, 1977; 1981) it is plausible that the sequence and mechanism of plate collisions can explain the various structural trends. These structural trends were later modified by dextral and sinistral shears (this study, see section 6.5).

6.5 LINEAMENTS AND FRACTURE ANALYSIS

6.5.1 Introduction

It is the aim of this section to show that the evolution of the Pan-African Mozambique belt of NE Africa involved collision and thrusting which resulted in the development of major strike-slip faults and shear zones. To decipher this complex tectonic history it has been essential to understand the nature of the lineament patterns. Because some lineaments have often served to control geological events from the Precambrian to Recent times they can be used to evaluate the tectonic history of the area. Analysis of lineaments may also show how the basement rocks have been fragmented into

crustal blocks. This is critical in locating the most important fault zones, giving information about the orientation of stress and locating zones most likely to carry hydrothermal mineralization.

Lineaments were interpreted from bulk processed black and white Landsat MSS images at a scale of 1:500,000, covering a major portion of NE Africa (Figure 5.1.). This was followed by various image enhancement techniques to identify as many lineaments as possible in W Ethiopia and the Baragoi area, N Kenya. The length and orientation of each individual fracture is determined using Landsat MSS and Large Format Camera images of known scale. Fracture orientation is measured as a declination from true north in degrees. These results are plotted preferably as histograms on polar co-ordinates (rose diagrams) .

6.5.2 Definition,Scale and Distribution of Lineaments

Although there are various definitions of linear features in the literature, the most important criteria for interpretation of fractures on Landsat imagery are: topographic lineations, such as drainage alignments and tonal lineations such as boundaries between surface types and alignments of tonal features. A definition is presented here which highlights all the criteria for lineament identification established by various authors.

A lineament is an observable linear feature which can be identified by its physical characteristics as shown on physiographic, gravity anomaly, magnetic maps and remote sensing images. In remote sensing a lineament is a linear high spatial frequency change in contrast observed on an image. It may be simple, consisting of a single feature, or composite, combining a number of different physiological or structural features that are more or less obviously connected. It may be continuous, straight or curvilinear and sometimes greater than 100 km in length. Very long lineaments (with a magnitude of hundreds of kilometres) are often the surface manifestations of deep seated structural controls. Some lineaments can be related directly to faults, joints, fractures, alignments of intrusive plutons, linear outcrop boundaries and compositional or tectonic planar fabric. Major strike-slip faults form lineaments but this is not a necessary criterion for their definition. Although many authors have suggested that their location may relate to the presence of mineralization, this is a subsequent feature related to the passage of fluids along the lineament and not to its formation.

Lineaments show few local deflections in orientation, which indicates that they are related to a fundamental and uniform stress field. The features found on Landsat imagery can be 5 km to 500 km in length. On airphotography only features of the order of 0.5. - 5.0 km can be observed.

A major difficulty in mapping lineaments is their subjectivity i.e different interpreters can produce different lineament patterns for the same image. In any scene with lineaments of various strikes and lengths, one interpreter could view these as discontinous lineaments, but others could interpret it as probable alignments. The following procedure has been used in this study: straight linear features are picked and traced, then any significant cross-cutting linear structure at both ends of the traced segment are checked to see their relationships. This routine analysis is repeated under different viewing angles. Features that are sharp are interpreted with good confidence. Larger features that do not have sharp features may be of no significance or could be surface expression of deep seated fractures. The physical significance of a class of lineaments are confirmed if detected by another observer. These precautions should provide sufficient degree of confidence to distinguish between bedding and tectonic lineament features and to eliminate most of agricultural and other artifacts. Note that on a vertical image, steep structures show up better than low angle structures, so there is a bias towards strike-slip zones and against thrusts and low angle extensional faults (S. Drury, pers. comm.)

6.6 BASEMENT TECTONIC ANALYSIS

6.6.1 Introduction

In the course of a remote sensing study, systematic relationship between various linear trends are often observed. Some of these large structural elements, are either related to extensional or compressional settings. The question is how to recognise diagnostic elements of particular geodynamic settings in a remote sensing study.

There are two approaches in fracture analyses:

1) Digital scanning, storing, and plotting of tectonic features using software based on more or less

sophisticated algorithms of pattern recognition (Podwysocki *et al.*,1975). This approach tries to substitute geological reasoning by statistical analyses from large populations of measurements.

2) The second approach is based on geological evaluation of the lineaments through a set of comprehensive steps based on structural analysis and plate tectonic hypothesis.

Here the latter approach is adopted. Since the area is large there is no adequate field control, so the conclusions merely form the basis of a preliminary working model for further research.

Before understanding the significance of lineaments occurring in NE and E Africa, however, the evolution of stress orientations through time and the fundamentals of geological stress and its influence on rocks need to be discussed. In this section the fundamental theories of extensional and compressional tectonics are briefly described, followed by case studies of critical regions within the study area in order to relate the observed data to the theoretical models.

6.6.2 Stress and Fracturing of Rocks

When rocks fail under compression in experimental conditions, it is found that they break along two sets of planar shear surfaces which intersect in a line parallel to the intermediate principal stress axis σ_2. Moreover the acute angle between the shear fractures is bisected by the maximum principal stress σ_1. (Figure 6.4) In general one of these shear planes will fracture first and is dominant.

Theoretically the greatest shearing stress will always occur on the planes which contain the 2 axes and make an angle of 45° to the principal stresses σ_1 and σ_3 (Ramsay, 1967). The angle θ, which is between the direction of the maximum principal stress and the fracture, is a function of a material constant and is therefore variable. θ is generally less than 45 degrees, and for most rock types falls between 20° and 40°.

Figure 6.4 shows a simple threefold classification of near surface fault sets, based on three possible orientations of the stress axes (Anderson, 1951) into normal faults, thrusts, and wrench faults. This theory applies to the initiation of fractures in completely homogeneous material, and to the brittle upper crust only (< 15 km). These simple theories fail where a stress is applied to a rock

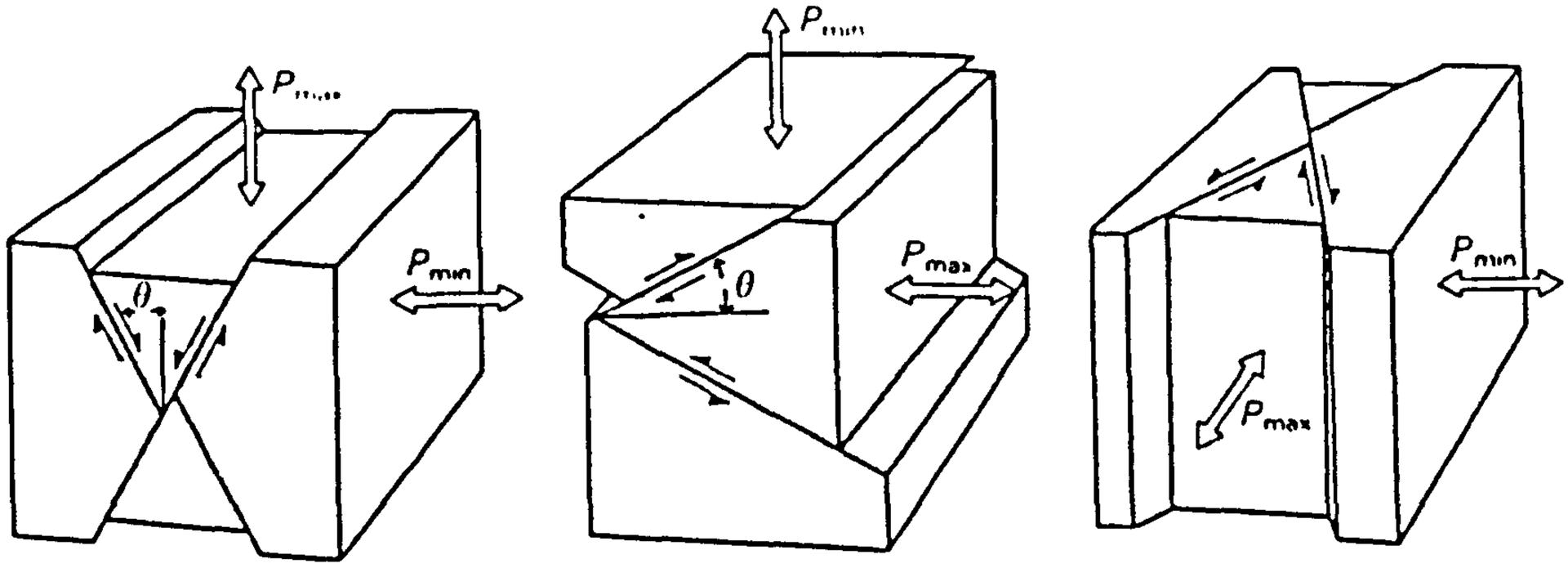

Figure 6.4 These block diagrams show the relationships between the three main classes of fault and the required arrangements of the maximum and minimum principal axes.

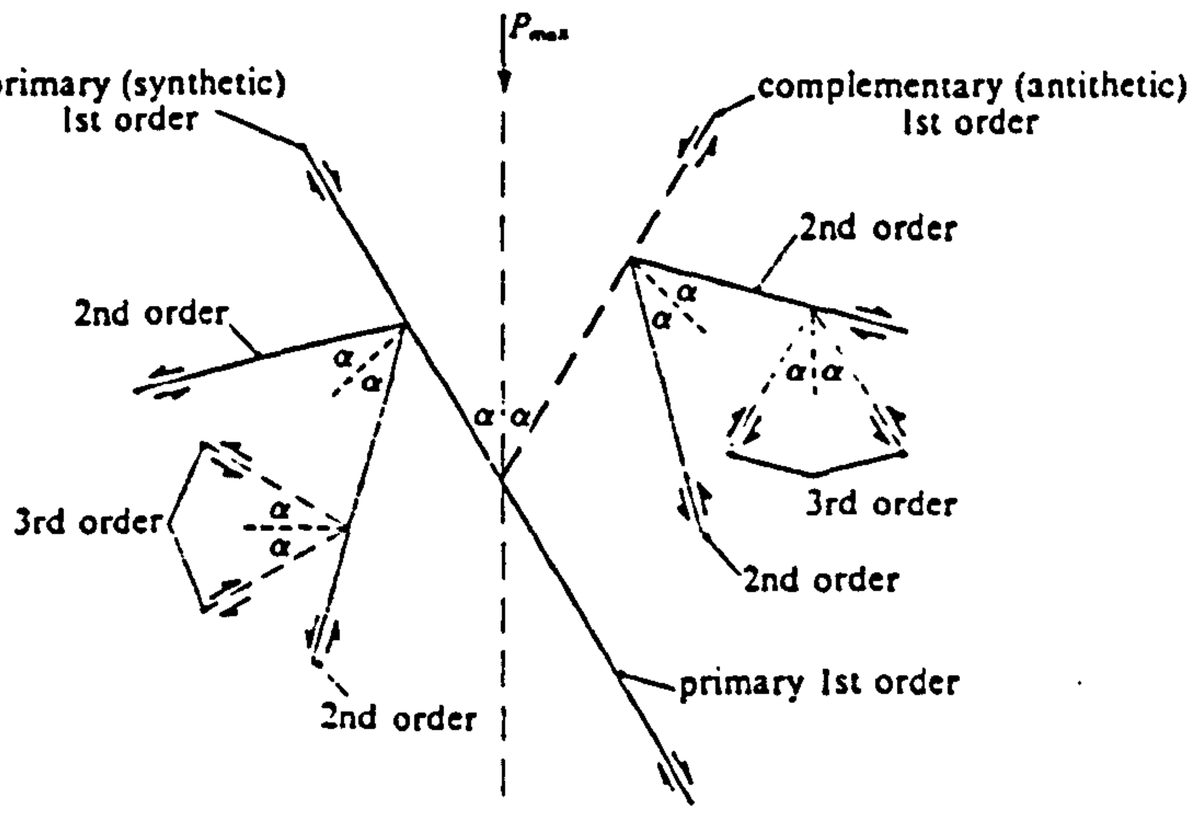

Figure 6.5 Schematic representation of the relationships of synthetic and antithetic faults of different orders under north-south simple compression. (After Moody and Hill,1956).

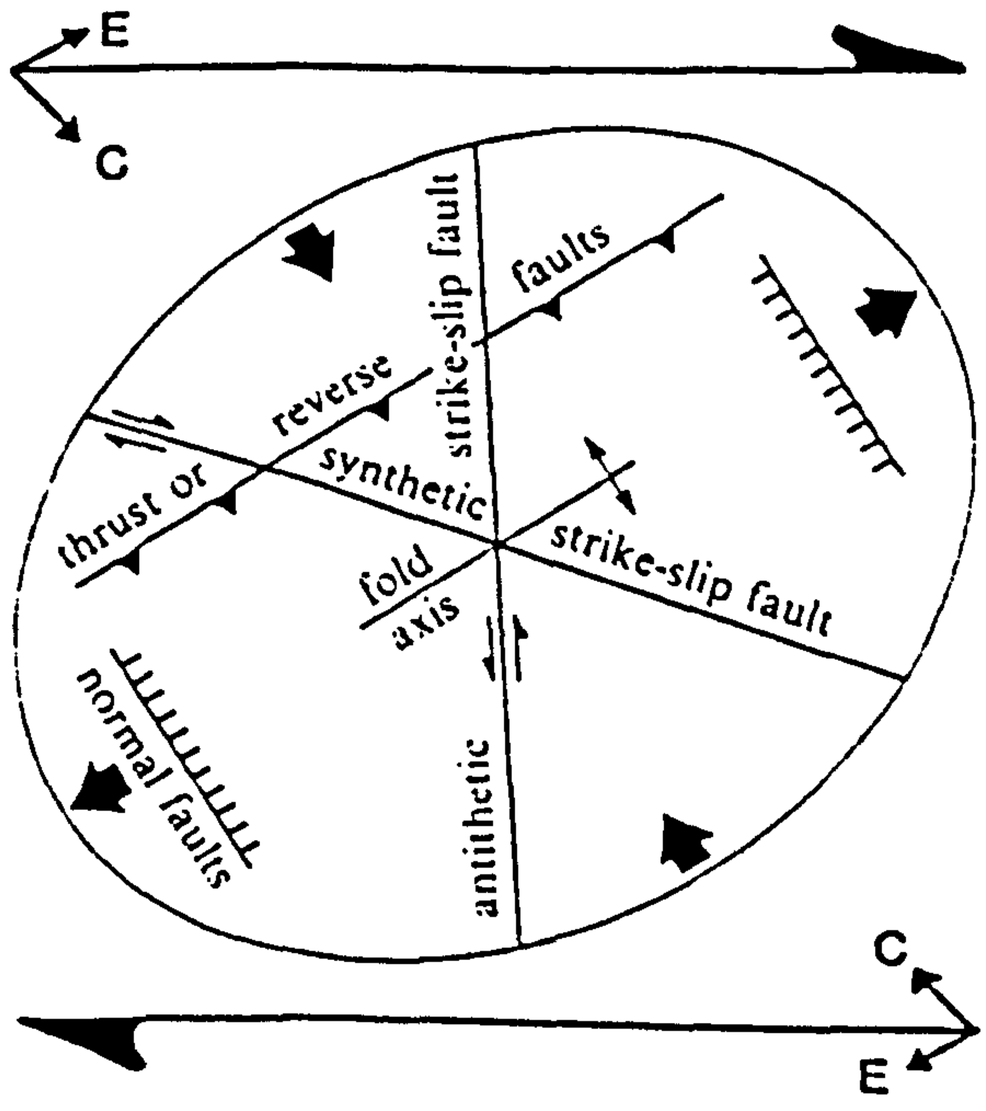

Figure 6.6 Forces and composite structures that can result in idealised collision zone combined with a wrench component shown schematically with strain ellipse. Depicts right-lateral movements; view in reverse for left - lateral. (After Harding, 1974).

C-Vector of compression

E- Vector of extension

body containing different rock types, and planar discontinuities of different orientations. During protracted tectonic movements Moody and Hill (1956) and more recently Moody (1973) concluded that for any given area upto eight directions of wrench faulting and four second order features such as folding and or thrusting would accomodate the regional structural elements (Figure 6.5). In the case of first order faults, the primary or synthetic fault dominate, the antithetic fault which is complementary to the synthetic fault has less influence in local deformation. The antithetic faults and the second order, third and higher order faults are consequences of shear on the primary or synthetic fault. The directions of the wrench faults are considered to be more or less symmetrical to the direction of the maximum principal stress. The angle α is defined as the azimuth of the maximum principal stress direction which gives rise to first - order shears, while the angle β may be 45° at the maximum. The value of the critical angle γ was considered to range between 5° and 30°, with an average value of 15°. However Wilcox *et al.* (1973) based on experiments with clay model have revealed that it is approximately 30°.

In the wrench fault model Moody and Hill (1956) assumed that the right lateral wrench fractured first and is dominant. Nevertheless Freund (1974) argues that if the magnitudes of shear strains in progressive deformation are similar, then any fault set will have an equal chance to occur. In nature failure takes place first along one of the surfaces, which is probably an earlier line of crustal weakness. It is clear, however, that whichever set forms first it continues to develop at the expense of the other. However, if fault sets are later rejuvenated, those most favourably oriented to the subsequent stress directions will preferably be utilized.

Simple shear creates compression and tension in different directions, which will result in the development of synthetic faulting (Riedel shears) and antithetic faults (Wilcox *et al.*, 1973). The result is shown in Figure 6.5. The strain ellipse shows the directions of shortening and extension so that the local orientations of principal stresses in the shear belt can be assessed (Figure 6.6).

6.6.3 Extensional tectonics

Extension may be caused by stretching and thinning in a ductile substratum, or on a larger scale by the penetrative stretching of the ductile lower crust during rifting (Figure 6.7). Important

manifestations of extensional tectonics are cross-faulting between normal faults or parallel wrench faults and all forms of block tilting. Kinematically brittle extension and thinning of a rock mass takes place by rotational planar normal faults, or the domino model of extension (Wernicke and Burchfiel, 1982). Rotation of planar normal faults in a domino model can lead both to large extensions and to low-angle normal faults. However, the domino faulting process produces empty spaces at the base of domino fault blocks. Listric normal faults function to relieve the space problems between families of planar fault blocks (Wernicke and Burchfiel, op. cit.). Listric faults are difficult to prove from field evidence alone, however, they are seen on many seismic sections. Rotational planar and listric faults can be found in close genetic relationships. It is concluded that extension in the lithosphere is probably achieved by discrete detachments extending right into the mantle (Wernicke and Burchfiel, 1982; Wernicke,1985).

6.6.4 Strike-slip tectonics

The analysis of the directions and geometry of the structural elements relies on the fundamental structural associations related to strike and oblique-slip tectonic settings and low angle thrust environments. Understanding the stress distribution inside an inhomogenous segmented crust composed of crustal blocks separated by vertical weak zones is of fundamental importance.

Folds and thrust faults have an oblique relationship with respect to the moving vertical master faults and related shear zones (Figure 6.8). Because the deformation is rotational, the orientation in plane view of the tectonic elements between shear zones varies from slightley oblique to near parallel to the shear zone (Thomas,1974). The latter situation occurs in advanced stages as simple shear coupling or results from the deformation at low, ductile crustal levels. Foliation and other structural elements are seen to curve towards the vertical shear zones where they may become folded along vertical axes.

Ramos (1977) synthesised the works of Sales (1968), Thomas (1971) and Wilcox *et al.* (1973) and suggested two deformational models depending on the presence or absence of a sedimentary cover.

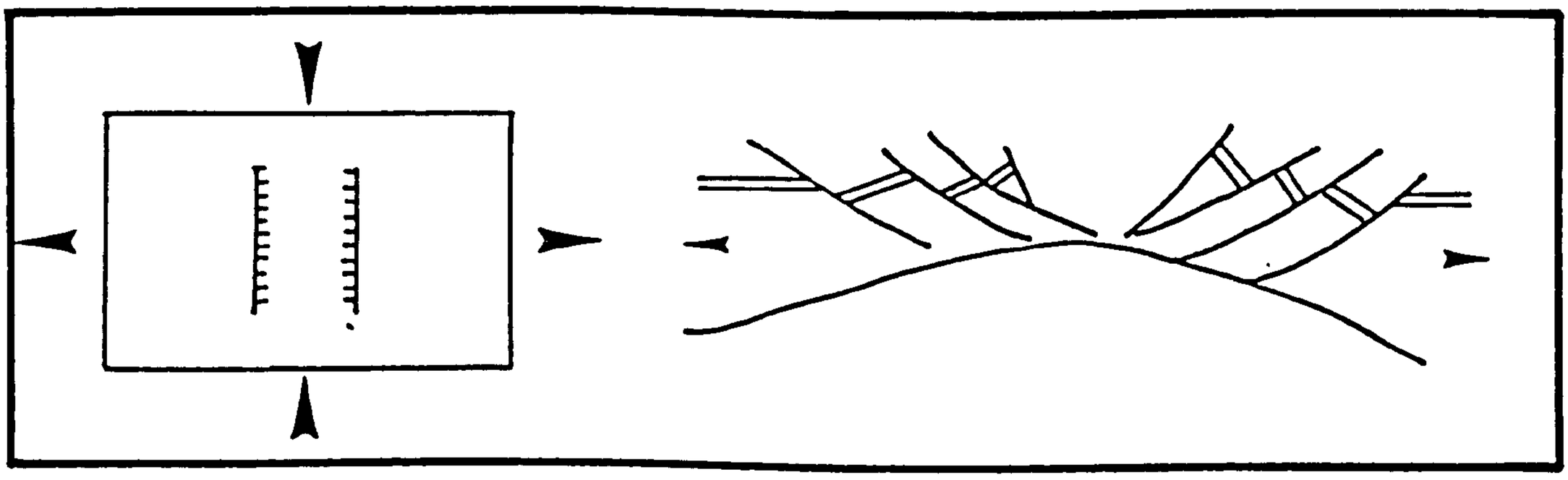

Figure 6.7 Extensional tectonics in a stress system as a result of crustal attenuation.

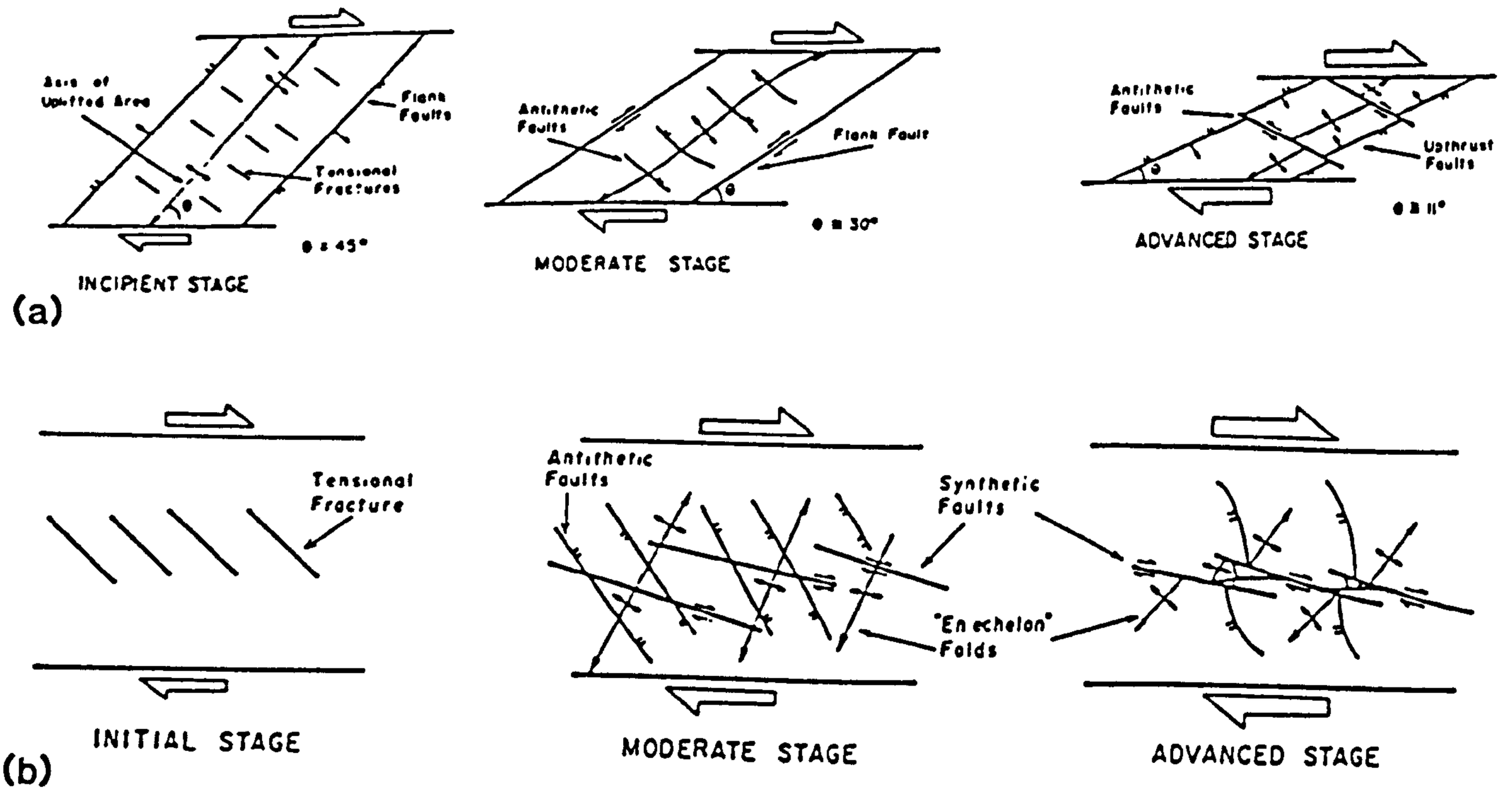

Figure 6.8 Block coupling and simple shear. **(a)** Increasing deformation stages in a rigid basement coupling. **(b)** Deformation stages in a rigid mantled basement under coupling. After Ramos, 1977.

Figure 6.9 Schematic explanation for the different shear orientations in the three experimental cases. (a) No pre-stress. (b) H max parallel to basement fault. (c) H max perpendicular to basement fault. (After Naylor et al,1986).

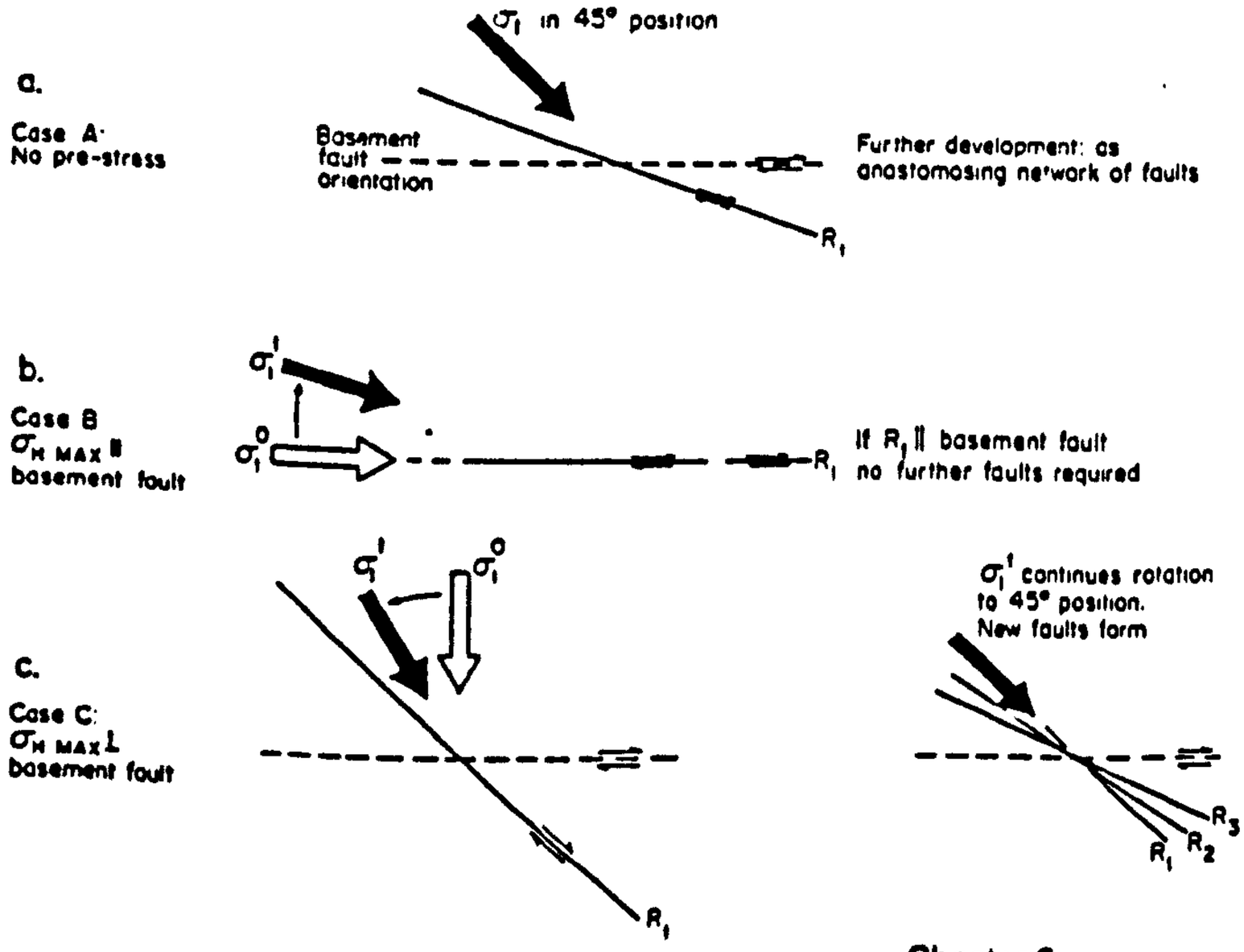

Model 1

This model is based an previous work of Sales (1968) and Thomas (1971) and is applied to high grade metamorphic and plutonic environments with negligible plastic deformation. Three stages are identified: (1) Formation of a conjugate set of faults i.e. the flank faults and tension fractures. The angle between the fold exes, and the wrench fault (known as ø angle) is 45° ; (2) As the intensity of deformation increases angle ø decreases and lateral adjustement occurs along the previously formed flank faults which coincide with the synthetic direction; (3) During extreme intensity of deformation, the flank faults become active upthrusts and angle ø decreases to 11°. (Figure 6.8a). This model is applicable so long as the orogenic forces act progressively in the same direction.

Model 2

In areas where a thick cover of undisturbed sedimentary rocks overlies the basement a dynamic model following Wilcox *et al.* (1973) is proposed (Figure 6.8b).

Stage 1. At this stage tensional joints or normal faults develop oblique to the shear. These tensional fractures soon disappear as lateral displacement increases. At stage 2, a conjugate fracture system is developed. The synthetic strike- slip faults intersects the major lineament at an angle between 10 and 30 degrees and have the same type of displacement, while antithetic faults intersect the mega shear zone at an angle between 70 - 90 degrees and have an opposite displacement. As deformation increases the synthetic faults tend to rotate toward the lineament trend. Antithetic faults tend to become perpendicular to the main lineament. En-echelon folds develop synchronously with conjugate faulting at an angle of less than 45° with the main lineament. At an advanced stage the antithetic faults are deformed to give a sigmoidal 'S' shape for left lateral adjustment or 'Z' shape for right lateral areas. The main wrench fault gradually ends as an interconnected series of earlier conjugate faults which offset the en-echelon folding (Figure 6.8b).

The previous discussion about wrench fault systems have been in an essentially dynamic context i.e. considering ideal orientations of faults, folds, and fabrics, with respect to the stresses or elastic strains within the fault zone (Tchalenko, 1970; Wilcox *et al.*, 1973). These approaches are good in areas where there is small displacement. However, the theory applies to isotropic rocks,

which makes it inappropriate to dip-slip systems whose low angle faults are more affected by the anisotropy of the sedimentary bedding (Woodcock and Fischer, 1986).

Naylor *et al.* (1986) experimented with sand-box models using different initial stress states. They show how grossly straight faults often comprise en-echelon conjugate Riedel shears (R_1 and R_2 Figure 6.9) at low displacement but these become linked together at higher displacements by further shears at a low angle to the slip vector. They suggest that each Riedel shear has a helicoidal form so that the faults may converge at depth into a single shear zone. Woodcock and Fisher (1986) illustrate the development of duplexes along strike slip systems. Strike-slip fault systems often contain zones of steep imbricate faults geometrically similar to imbricate fans and duplexes in dip-slip, thrust and normal fault systems. Woodcock and Fisher (op. cit.) conclude that strike-slip duplexes are a response to imposed boundary constraints rather than by the stress - control or bulk strain approaches usually applied to wrench tectonics. Hence it is important to identify the complexities of strike-slip fault systems, in map view before we adopt any of the models discussed above. This is because in many real cases, wrenching does not progress beyond the first set of riedel shears. For example, representations of wrench fault orientation on a strain ellipse (e.g. Wilcox *et al.*,1973) are suggested to be valid to the No pre-stress stage of Naylor *et al.* (1986) (refer to Figure 6.9).

6.6.4.1 Transpression and transtension

It is commonly observed at all scales that faults are not ideal planar surfaces but rather occur as arrays of second order en-echelon fractures which combine and anastomose. Gammond (1987) recognises two main types of en-echelon patterns, involving right-or left-stepping fractures. When the motions of the fault blocks are away from one another, they give a tensile effect, which produce a minor basin or pull-apart (Figure 6.10). The depressions are likely to develop within such tensile bridges which are wedge shaped and produce a negative flower structure (Naylor *et al.*,1986). If the motion of the fault blocks are opposed to give compression across the fault in the bridge structure is called a transpressional zone (Figure 6.10), or a restraining bend (Woodcock and Fisher, 1986) in strike-slip duplexes. In large stike-slip faults shortening in the bridge area is through the formation of pressure ridges, folds and positive flower-structure patterns (Figure 6.11).

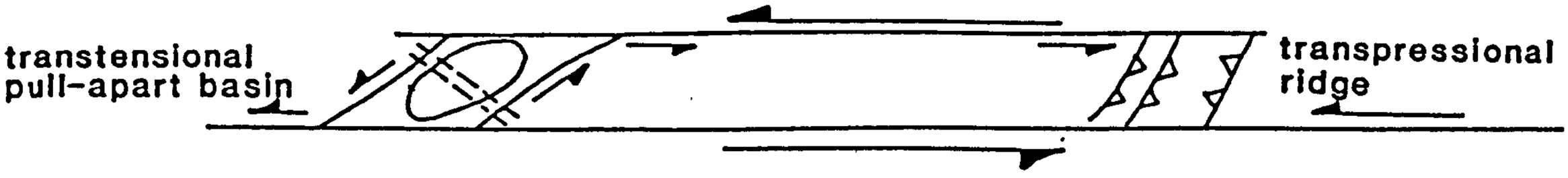

Figure 6.10 Structural elements diagnostic for simple shear tectonics in a sinistral couple. Simplified after Gammond (1987).

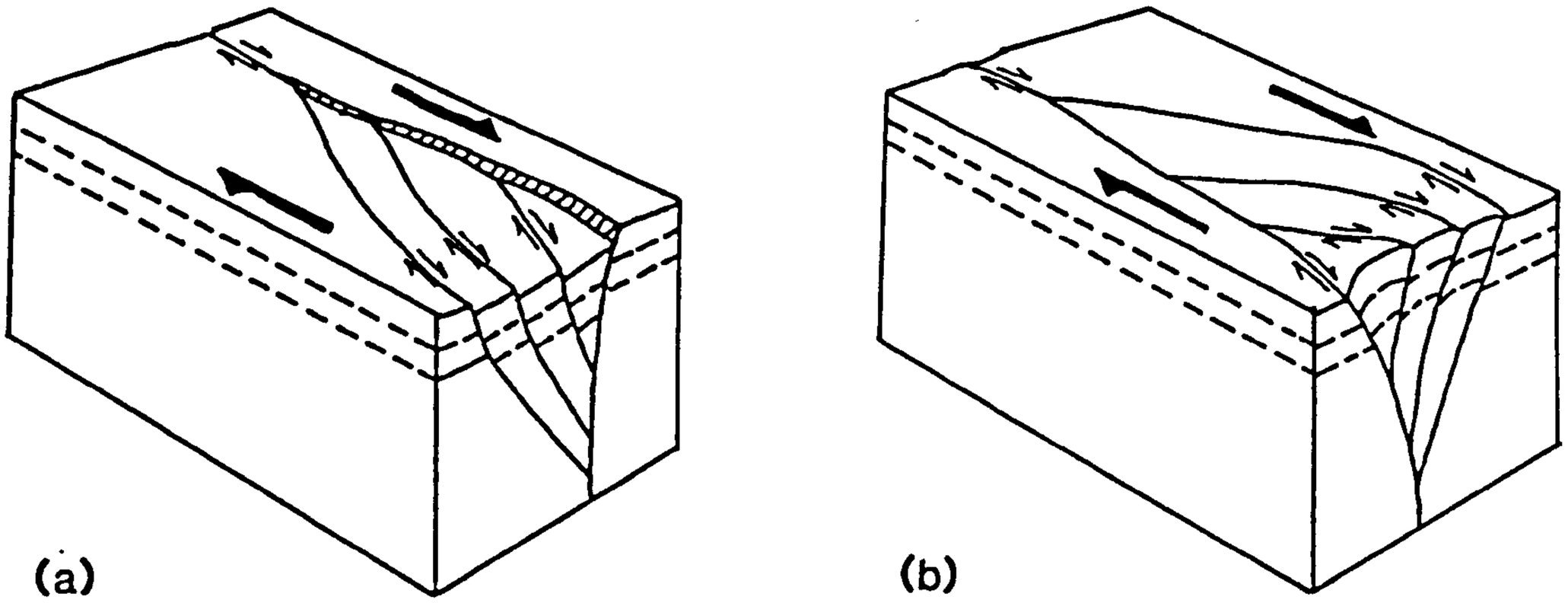

Figure 6.11 Diagram showing (a) an extensional duplex (showing a negative flower structure) and (b) a contractional duplex (showing positive flower structure). (After Woodcock and Fisher, 1986).

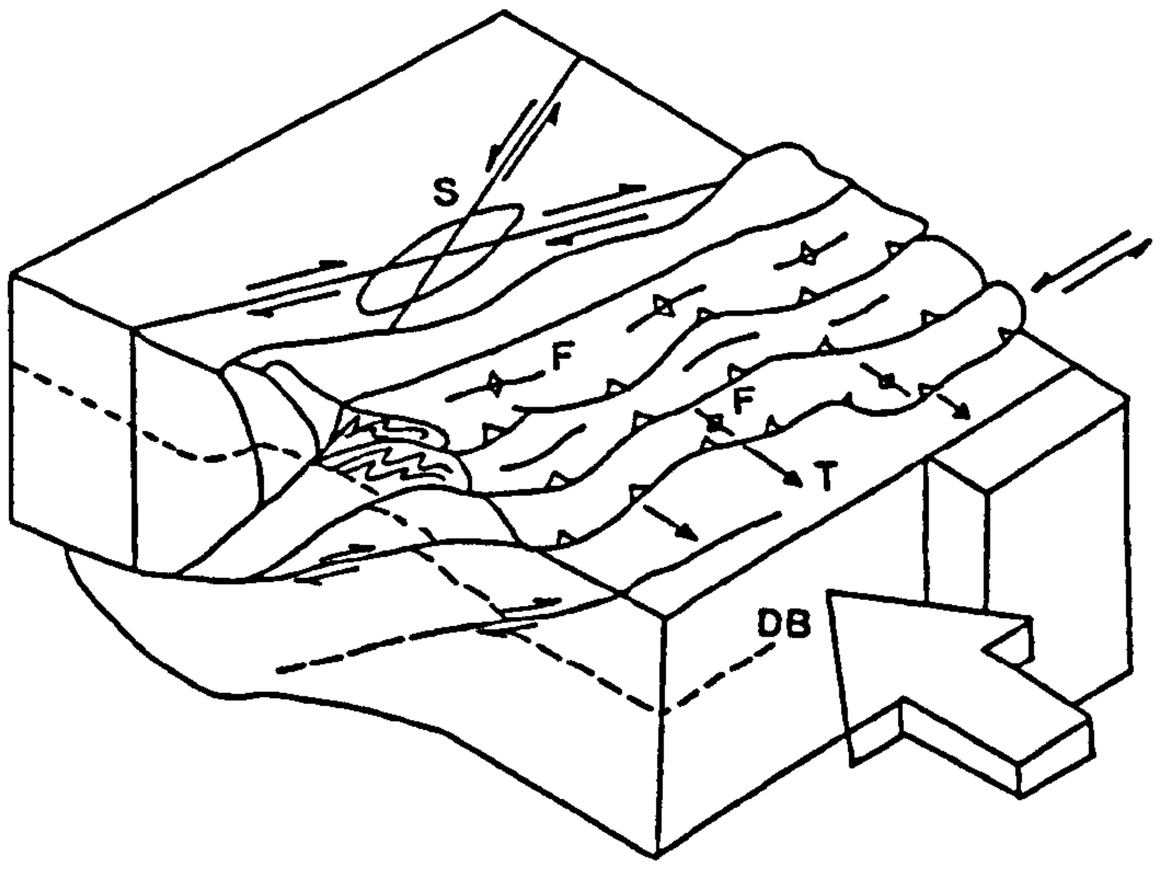

Figure 6.12 An idealised diagram of 'head-on' collision zone. Modified after Sugden (1987). S: strike-slip faults in the hinterland; F: folds; T: transport direction of foreland nappes; DB: brittle-ductile transition.

6.6.5 Thrust tectonics

Compressional deformation causes contraction in the length of the crust, and results in the thickening of the continental crust . Crustal thickening can be accomplished by a series of listric thrusts and leads to overlapping, thrust imbricates (Figure 6.12). In regional compressional belt i.e those of the continent -continent collision type we not only find reverse faults, but also normal and strike-slip motions. In many cases these have been active over extended periods of time and are reflected in complex relations between a variety of fault types. Folding during compression complicates the thrust sequences even further.

Many shear zones are undetectable by means of remote sensing unless folded and outropping in windows (Boyer and Elliot, 1982). Other lines of evidence do nevertheless reveal the particular tectonic style of low-angle thrust belts. Many belts have arc-shaped outlines and the common types of topography are parallel valleys and ridges. The tectonic vergence is prominent and only interrupted by minor backthrusting. Imbricate fans and duplexes, the roof thrust of which is eroded (Boyer and Elliot,1982; Butler,1987), are mapped as sequences of faulted anticlines with sharp crests and repetitions of beds. Synclines are far less numerous. In other cases large doubly plunging anticlines or a sequence of anticlines and synclines are situated on top of one single thrust sheet (Boyer and Elliot,1982; Hobbs *et al.*,1976). Characteristic for thrust systems are shear zones parallel to the direction of tectonic transport (Coward,1980). The shear zones may be the expression of tear faults, culmination walls and lateral ramps. They are all transverse to the fold and thrust belt. Frontal ramps with shearing contemporaneously with thrusting and which is transverse to the direction of tectonic transport are incompatible with thrust tectonics.

It is believed that a lineament study may help to differentiate between vertical basement adjustments which are intimately linked to long linear fractures as compared to thrust tectonics. It is concluded that arcuate patterns and repetition of bedding are key indicators of thrust tectonics. Therefore the study of fault systems, including establishing their relative movements be it through direct field evidence or indirectly through secondary structural elements and by comparison with theoretical and experimental work it is possible to get information about the orientation of the

principal stresses, and where tensional fractures may have occured.

6.7 MEGASTRUCTURAL ELEMENTS IN NE SUDAN - ERITREA

In the NE Sudan - Eritrea region extensive shearing occurs in a wide zone. Several linear features have been identified from Landsat imagery (Figure 6.1). The lineaments of regional extent are 015°-025°, 055°-065°, 145°-155° and 165°-175°. There are also dykes trending 090° (Figure 6.13a, and 6.13b).

The NW-SE (145°-155°) trending lineaments are prominent to the southeast in Eritrea, while they decrease further north in Port Sudan area. In the Port Sudan area the Nakasib ophiolite belt has been sinistrally offset by a NW trending shear zone (Figure 5.9). These same shear zones have been reactivated in the Cenozoic faulting of the Red Sea escarpment area.

The most prominent NNE (020°) trending shear zones are the Oko shear zone, NE Sudan (Almond *et al.*, 1984; Almond and Ahmed, 1987) (Figure 5.9), and the Barka and Adobaha in Eritrea (Mohr, 1979; present study) (Figure 6.13b). In the western Red Sea hills extending from the Nile to Abu Hamed, the dominant structural trend is N-S with steep dips to E or W. (Almond and Ahmed, 1987). In contrast in the eastern block of the Red Sea the main structural trend is northeasterly (Figure 6.1). The N-S (± 020°) and NE (050°) trending shear zones are partially aligned by mafic-ultramafic rocks and appear to mark the location of possible sutures (Figure 5.9). The Nakasib shear belt is believed to mark an island arc suture (Vail, 1985a; Embleton *et al.*, 1983; Almond and Ahmed ,1987).

A Landsat scene (path 183 row 48) was chosen for more detailed structural analyses of the area . All interpretations are presented in figures 6.13a and 6.13b. Although Landsat MSS band 5 was found satisfactory, additional data was acquired from Large Format Camera images which have a significantly superior resolution (Figure 6.14).

The chosen area can be subdivided into four tectonic domains (Figures 6.13a and 6.13b). To the west of the Barka is zone A which is delimited by the 165-175° trending Barka lineament, forming a boundary between regions of contrasting fault patterns. Zone A is dominated by a conjugate set of

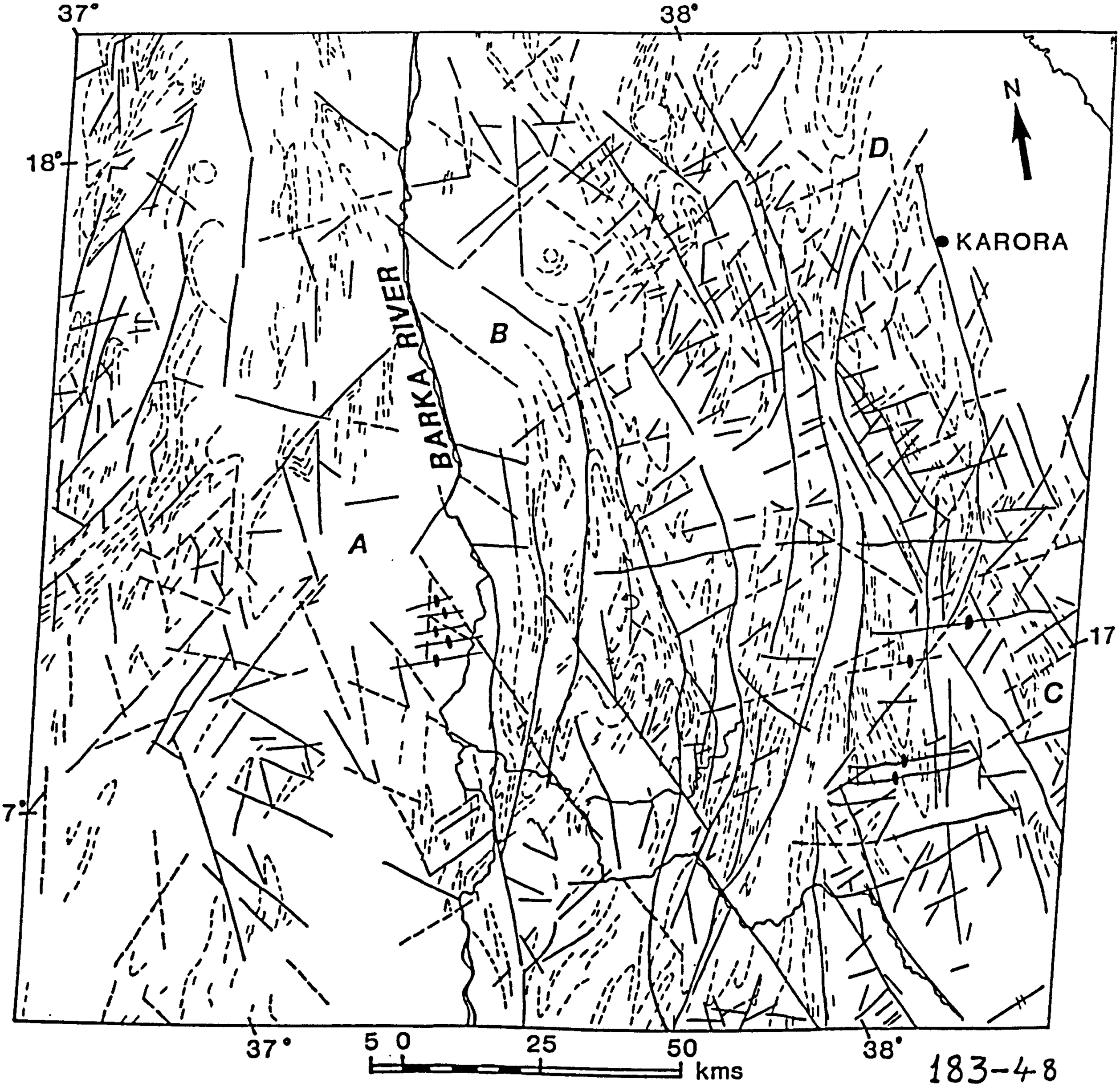

—— TOPOGRAPHIC LINEAMENTS

---- TONAL LINEAMENTS

STRUCTURAL TREND LINES

DYKES

Figure 6. 13 (a) Lineaments and structural trends in NE Sudan and Eritrea. Interpretation based on Landsat MSS band 5 and Large Format Camera images. The outline of this Landsat scene (path 183 and row 48) is shown in figure 5.9.

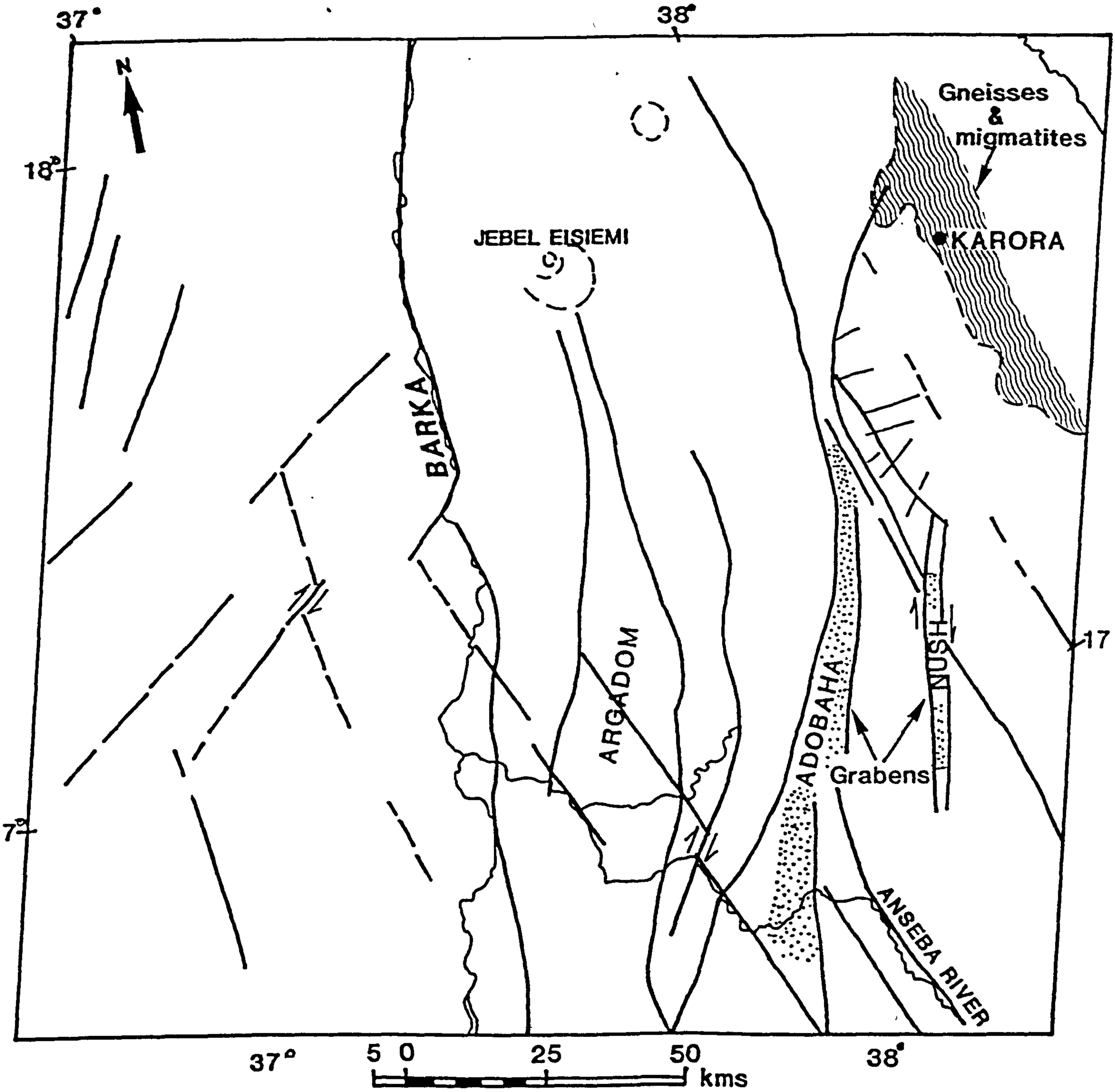

Figure 6. 13 (b) Simplified lineament map of the NE Sudan-Eritrea region.

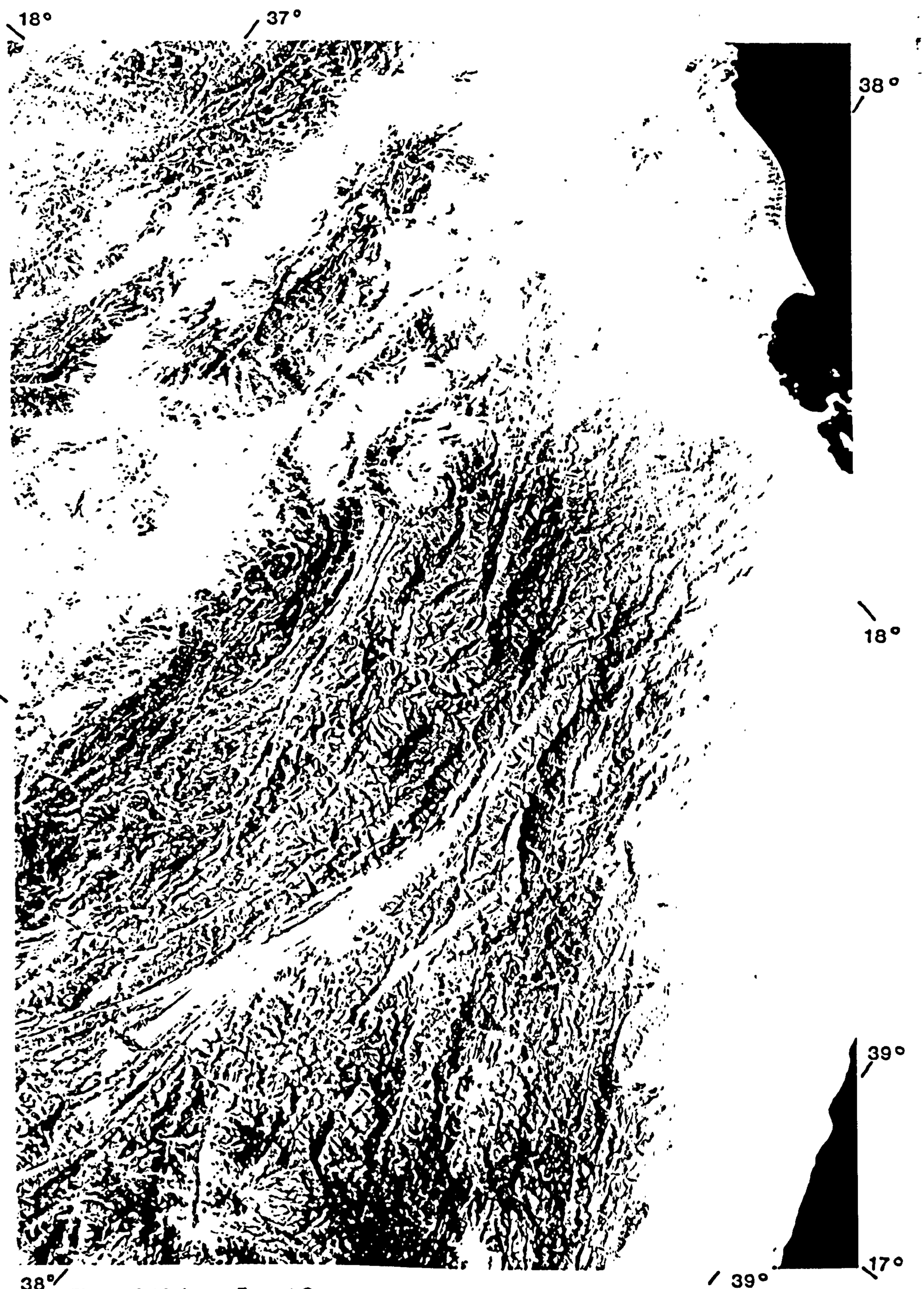

Figure 6.14 Large Format Camera Photography of NE Sudan-Eritrea region. Scale 1:1 million. The area is outlined in figure 5.9.

fractures trending 165°-175° and 055° respectively. Zone B comprises an area of subparallel NNE-SSW trending synforms, antiforms and lineaments which form a curvilinear belt. Mohr (1979) named two tectonic zones; the Adoboha and Argadom zones. Although this domain has been separated into two zones, in this study they are considered as forming one megastructure. The limits of the domain is the Adobaha zone. Zone C is dominated by NNW-SSE (165-175°) trending lineaments, while those trending between 255-270° being dykes. In zone D the structural trend is N-S, although major lineaments trend NNW-SSE (165-175°) and 070°N. The area looks like an hour glass structure which is bound by the Adobaha shear belt and a NE-SW trending lineament.

6.7.1 The major faults

The Barka lineament

The Barka lineament is partially aligned with mafic-ultramafic (ophiolite) complexes, forms a tectonic break separating zones of different lithological assemblages and has been interpreted as a suture. Although the tectonic zones C and D (Figure 6.13b) show different styles of deformation from zone B, there are no mafic-ultramafic (ophiolite) rocks (Alem Kibreab, pers. comm. 1986) between the two belts as suggested by Mohr (1979). The belts are therefore considered as a coherent structural unit. The implications of this will be discussed in greater detail in the following section.

The Adobaha belt

The Adobaha belt looks like an hour glass structure (Figure 6.13b), being widest in the south (c. 30 kms) and narrowest (c. 8 - 10 kms) in the centre. This width is maintained for about 100 kms. Further north it bifurcates into a funnel shape. On Landsat imagery, the belt is marked by a light toned formation which persists along its entire length (Figure 6.14). This formation consists of talc-sericite, talc-chlorite and graphitic schists, interbedded with crystalline linestones (Alem Kibreab, pers. comm.1986). The Adobaha belt lies at present in a graben (Kibreab, pers. comm.) although it definitely originated as a shear belt which later experienced a component of dip slip.

The Argadom belt

The Argadom belt (Mohr, 1979) (Figure 6.13b) extends for about 140 kms due south of the Jebel Eisiemi (J.E) post- tectonic granitic body. This belt widens from 5 - 7 km in the north to about 25 kms in the south. Although Mohr (1979) suggests that the Argadom belt cuts the Adobaha belt in the south, in fact the Aragadom and the Adobaha merge with the Barka lineament which is considered to be the master fault. The curvature of the Adobaha and the Argadom lineaments makes it difficult to analyse their structure statistically.

The Nush (Adobaha Nush) graben

The Nush graben is about 50 kms long and 4 kms wide (Figure 6.13b). The graben is floored by talc sericite, talc chlorite and graphite schists, interbedded with crystalline limestones (Alem Kibreab, pers. comm.) which was subsequently filled by Quaternary sediments. The rocks preserved in the floor of the graben must have structurally overlain the volcanosediments on either side of the graben.

6.7.2 Secondary structures

South of latitude 17° /19°N the Adobaha belt dextrally displaces two prominent NW (150-160°) trending lineaments which control the course of the Anseba River (Figure 6.13a and 6.13b). The NW-SE trending lineaments have been reactivated during the Tertiary to form normal faults along the coastal areas of the Red Sea.

In the Adobaha belt, closely spaced E-W to ESE-WNW trending structures were observed by Mohr (1979) and which have been confirmed by this study. These ESE-WNW to E-W trending secondary structures cut the Adobaha belt and are closely associated with dykes emplaced along the same trend. These dykes are exposed strongly in the Central Highlands of Eritrea. Similar dykes in NE Sudan range in composition from dolerite to andesite microgabbro, microdiorite, microgranite, rhyolite and trachyte (Nour ,1981). South of Massawa more ESE-WNW trending pegmatites and dykes are observed. These dykes are thought to be of Tertiary age (Mohr, 1979), however some of the dykes have been found to be older than the younger granites and are therefore not considered to be related to the opening of the Red Sea. Another group of dykes in this area is clearly related to a

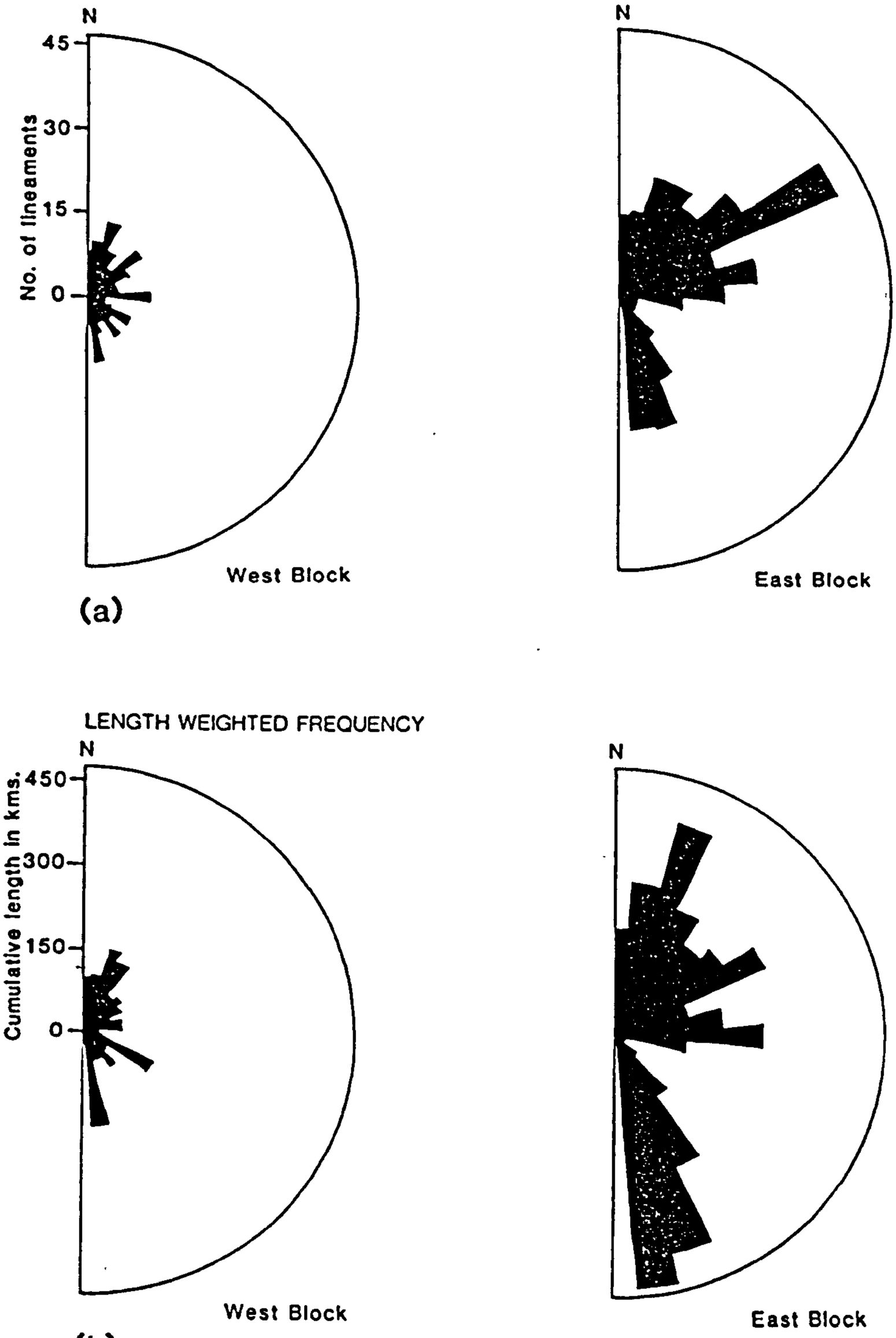

Figure 6.15 Rose diagrams produced from lineament interpretation of Landsat scene (path and row), NE Sudan-Eritrea. (a) Directional frequency rose diagrams. (b) Length-weighted rose diagrams.

N-S alignment of syenite complexes and post-Mesozoic faults (Nour, 1981).

6.7.3 Nature and timing of shear zones and associated stress patterns.

Landsat scene (path 183 row 48) covering parts of NE Sudan-Eritrea has been divided into two blocks. For ease of statistical interpretation directional frequency and length-weighted frequency rose diagrams have been plotted. In Figure 6.15a it can be seen that the 055-060° lineaments are the most numerous, followed by NNW (165-175°) trending lineaments. However in terms of length - weighted frequency of linear features (Figure 6.15b) 015-025° trending lineaments have a total length of 273 km, while 055-065° trending lineaments have 288 km cumulative length and the 005-015° lineaments have a total fault length of 456 kms. In the western block the most prominent are the 015-025° and the 005-015 ° trending faults. Although these are similar to the eastern block, the lineaments are smaller in scale and less numerous. This area shows different deformational history compared to the eastern block as block segmentation is more apparent.

Hence from the rose diagrams it is clear that the NE-SW and NW-SE trending lineaments are by far the longest and it is reasonable to assume that the longer the horizontal extent, the deeper it penetrates into the earth's crust (Gilluly,1976). Thus the Barka lineament which forms a boundary between regions of contrasting fault patterns (block geometry) is considered a master fault. This lineament terminates in an array of curved splays trending NE to N-S. i.e. the Adobaha and Argadom fault belts. Chinnery (1966) had suggested that anomalous stress concentrations at the tip of a master fault could be dissipated by propagation of the master fault along divergent splay faults or by creation of arrays of secondary fractures. I suggest that both mechanisms have operated in the area.

The helicoidal model (Figure 6.11) of Naylor *et al.* (1986) and Woodcock and Fisher (1986) which suggests that every riedel shear would unite to form a single step fault zone is applicable to this area. The Adobaha and Argadom belts curve and merge with the Barka lineaments and it is plausible that these faults merge at depth during compression.

Several folds are observed whose axial traces are parallel and sometimes transverse to the major faults. The 165-175° trending master faults and the secondary faults which trend NE-SW (055-065°) are observed to displace dextrally the NW (145°) trending faults. The NW-SE faults may

have been reactivated to form riedel (or synthetic) shears (Wilcox *et al.*, 1973).

The compressional regions are complemented by extension on the opposite side of the master fault. The presence of two dyke swarms, one trending NE-SW parallel to the Adobaha belt (Kibreab, pers. comm.) and E-W trending dykes observed on the satellite imagery (Figure 6.14) indicate that there were two episodes of extension: i) during the opening of the Adobaha and Nush grabens, extension was along a NW-SE axis, while ii) a N-S extension resulted in the emplacement of E-W dykes. Vail (1978) and Nour (1981) indicate that there are three generations of dyke emplacement in NE Sudan, a dominant N-S set, and E-W and NNE-SSW trending dykes.

6.7.4 Tectonic Modelling of Fracture Behaviour

The pattern of fractures discussed previously could be modelled to predict the likely motion of a particular fracture during deformation. Stress theory predicts (Moody and Hill, 1956; Wilcox *et al.*, 1973) that the maximum principal stress bisects the acute angle of a conjugate set of fractures. Hence a principal compressive stress oriented at about 155° could generate the N-S trending Barka fault and the 145° trending faults as a conjugate set. During this stage of deformation the anomalou stress concentrations along the Barka lineament propagated along divergent splay faults which are dextral. The Adobaha and Nush grabens are bounded between the NW-SE (150°) trending lineaments (i.e Anseba) (Figure 6.13b). These two grabens may have developed as pull aparts in order to accomodate the northward relative motion of a continental fragment along strike-slip faults during convergence, analogues to movement along the Anatolian fault in Turkey (Sengor and Yilmaz, 1981). Although the Adobaha and Nush grabens are formed by the same tectonic process they are not necessarily of the same age. A reorientation of the principal compressive stress oriented along an E-W axis would cause regional folds trending N-S to NE-SW, which with increasing deformation, would result in N-S extension and emplacement of E-W trending dyke swarms.

The curvilinear fault west of Karora gives the impression of an indenter because there is a series of NE trending ridges which are observed in the imagery (Figures 6.14) and minor E-W to ESE-WNW structures are observed fanning outwardly (Figures 6.13b). Thus the change in strike of

the Adobaha in the NE could be due to the bending effect of a rigid indentor. The rigid indenter could be the high grade gneisses and migmatites, which are considered to represent a micro-continent (Gibson,1986) caught up in the accretion process. Although such microcontinents can exist, it is also possible that such severely deformed crust as the migmatites in Eritrea, would resist further deformation and therefore cause tighter folding and rotation of the Adobaha belt during collision. Similar conclusions were reached for the Colorado Plateau in the USA (Sales ,1968). The rigid indenter suggested for NE Saudi Arabia (Davies,1984) has a similar orientation to that suggested for this area. Another possible explanation for the development of the Adobaha hour glass structure (Figure 6.13b) is E-W crustal shortening, is accomodated by crust being squeezed out northwards and southward, similar to observations in the Tibetan Plateau (Molnar and Tapponnier, 1975; Tapponnier and Molnar, 1976; Rothery and Drury, 1986)

This deformational history is much more complex than the two or more episodes of simple E-W compression suggested for the area (Mohr, 1979). The limiting factor in this analysis however is deducing the sense of shear because, as Wheeler (1987) suggested, the feature may either be a foliation produced during the deformation, associated with shearing or could be a planar or linear feature whose origin predates the shearing. Although bending in the sense of pre-existing planar or linear features and the relative frequencies of one fault set terminating against another were used to determine their relative ages, (for example see Cohen,1985), this does not mean that faults did not experience a different sense of shear at different times as was found for the Najd fault of Saudi Arabia (Agar, 1987). Additional fieldwork is required to establish a deformation model for the area.

6.8 WESTERN ETHIOPIA

6.8.1 Introduction

Six bulk processed Landsat MSS band 5 images at 1:500,000 of W Ethiopia were analysed. Various image enhancement techniques were used to highlight as many lineaments as possible on a geometrically corrected digital Landsat scene (path 184, row 53). The most satisfactory techniques developed (see section 5.4.5) were applied to another Landsat scene (path 183 row 53).

6.8.2 Structural Interpretation

Lineament analysis with rose diagrams are presented for six Landsat scenes in figure 6.16. These rose diagrams show that Western Ethiopia is affected by major lineaments and faults which have a dominantly trimodal distribution trending 010±10°, 065±10°, 135±10°,although a small number also trend 090°. Although the directional frequency of the N-S (010±10°) faults is not limited (Figure 6.16) their cumulative length is very large. These major faults have significantly affected the geology and mineralisation of the area (Berhe,1987).

The most significant fault belts are the NNE (010°) trending Asosa - Kurmuk, the N-S Mole-Belcore lineaments; and the NW (140°) trending Degero shear belt (Figure 6.16). The Kurmuk lineaments are about 300 kms long in Ethiopia but they extend upto 700 km to the Sudan where they are known as the Odib Fault Zone (Razvlayev and Shakov, 1976). These authors suggest that the N-S trending Odib Fault Zone is associated with narrow sedimentary basins, and dates from 470 - 450 Ma (based on K-Ar dates of granitic intrusive bodies which are controlled by this fault system). The Kurmuk lineament has a complex history from late Precambrian to Mesozoic times.

The Mole -Belcore lineaments (6.16) form a graben 165 km long and 15 km wide (Berhe, 1981). It is expressed by alkaline stocks, plugs, and dykes and covered by Tertiary volcanics. The graben floor is covered by younger rocks but could be rejuvenated late Precambrian lineaments, as they control basement geology and mineralisation of the area.

Northwesterly trending lineaments are well developed in the central area of western Ethiopia. The Degero shear belt (Figure 6.16) has sinistrally offset the Kurmuk lineaments, the Yubdo ophiolite belt and the Birbir dioritic - granodioritic batholith (Figure 6.17). The swing of the strike of the Yubdo ophiolite belt, and Birbir batholith was noted north of the Nejo area by Kazmin *et al* (1979a) . However, it is only since this regional remote sensing study that the change in structural trend was clearly related to a major strike-slip movement.

The map of lineament trends (Figure 6.16) shows several distinctive patterns in the different areas. Western Ethiopia has been subdivided into three; the southern (A), central (B) and northern (C) sectors. In the southeastern corner of W Ethiopia (see zone A' on figure 6.16) E-W lineaments

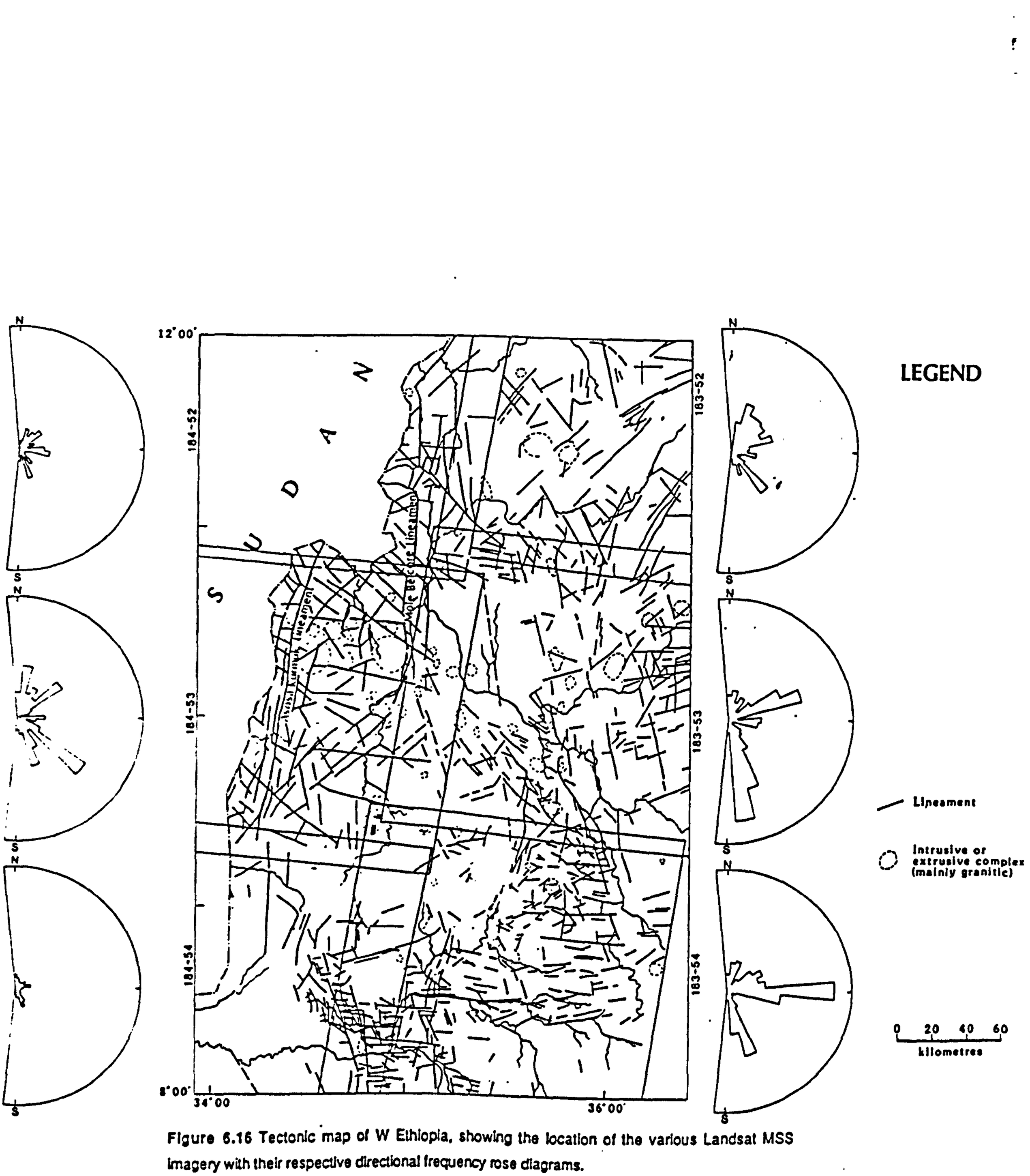

Figure 6.16 Tectonic map of W Ethiopia, showing the location of the various Landsat MSS imagery with their respective directional frequency rose diagrams.

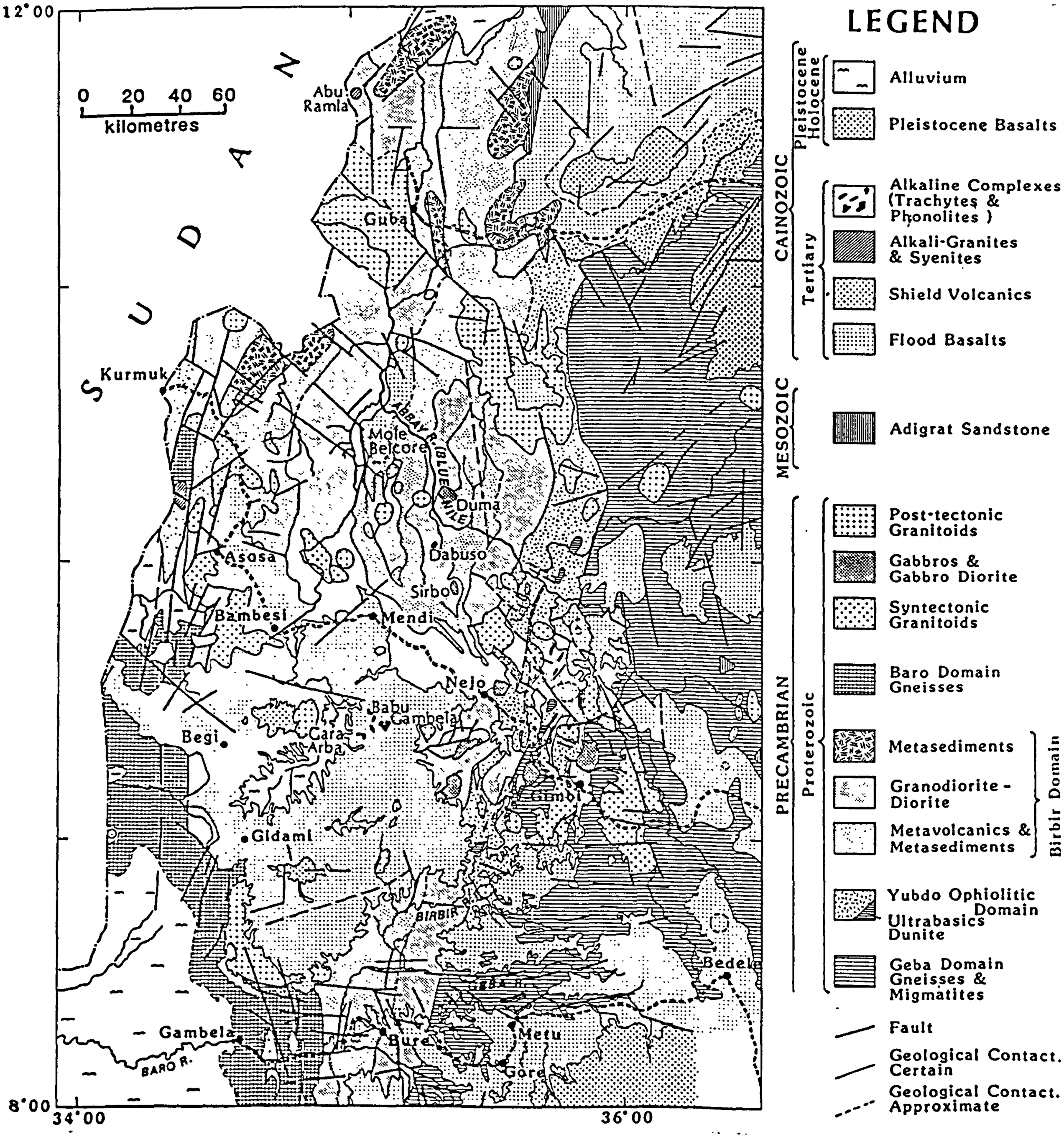

Figure 6.17 Geological map of W Ethiopia. Based on Ethiopian Institute of Geological Survey maps, aided by Landsat interpretation and fieldwork.

dominate. In the southwest (A) an additional set of N-S to NE lineaments also occurs giving the area the appearance of block segmentation. This type of block segmentation can only be explained if the primary stress does not coincide with the bisectrix of a pre-existing conjugate set. It is extremely rare that the primary stress bisects pre-existing conjugate fractures to produce an equal development of both systems (Ramos, 1977) but if that situation occured, as in W Ethiopia, then it would produce a lateral adjustment in both systems, one as a sinistral shear, and the other as a dextral shear. The dominance of E-W trending structures in the southeastern part of W Ethiopia partly reflects the existence of E-W folds (Figure 6.2). In the central sector of Western Ethiopia the lineaments have a trimodal distribution; a dominant set trending 135± 10° and two sub-dominant sets striking 010 ±10° and 065 ±10°. Berhe (1981) has shown using field evidence that numerous 065° and 135° trending faults are also present in this area.

In the northern sector the dominant lineaments trend N-S, 040° and 135°. The 135° lineaments are observed truncating the N-S Mole-Belcore lineaments. This area is structurally similar to the central sector.

The relative movement of the Kurmuk lineaments is dextral as deduced from the swing of structures in the proximity of the lineaments. These lineaments are sinistrally displaced by later NW trending faults.The 065° lineaments in turn truncate NNE lineaments in a few places. The relative frequencies of one fault set terminating against another was used to determine their relative ages, for example see Cohen (1985). Comparison with theoretical work and with experimental data (Moody and Hill, 1956; Price, 1968; Moody, 1973; Wilcox *et al.*, 1973) it is suggested that the 010 ° trending Asosa-Kurmuk and the 135° trending faults are a conjugate set. This may have resulted from a compressive stress oriented at about 165°, which correlates with the D_1 episode of deformation. A change of stress regime with the onset of the D_2 east-west compression caused the 135° trending wrench faults (Berhe and Rothery, 1986).

Overall the area between the Kurmuk and Mole- Belcore lineaments formed different basement blocks during block coupling and simple shear which resulted in a conjugate set of fractures, the 140±10° antithetic faults, and the NE (060°) synthetic faults. A tensional behaviour for the northwesterly trend was inferred from transverse grabens that exist in central Sudan along the

same strike (Browne *et al.*, 1984).

6.9 BARAGOI, NORTHERN KENYA

The Baragoi area of N. Kenya has experienced three deformation events the oldest of which (D_1) is characterised by E-W isoclinal folds (Samburu phase). Subsequently these were refolded to northwesterly trending folds by the D_1 Baragoi phase. A third phase (D_3) of deformation overprinted the earlier structures by refolding them into gently plunging folds trending north to northeast. (Barsaloi phase) . See chapter 2 for detailed structural synthesis.

A lithostructural map of the Baragoi area is presented (Figure 6.3). Lineament trajectories are represented by a rose diagram . The directional frequency diagram shows that there are four sets of lineaments trending 010°, 060°, 120° and 160°. The 010° and 160° are numerically the most significant, while the 120° trending linear features are very rare. Since the NNE (010°) faults are related to the Tertiary Kenya Rift, they have been avoided in the analyses, although further north the rift uses the NNW basement grain. The N-S lineaments separate the Baragoi mafic-ultramafic rocks from the Barsaloi metasediments and are considered of major significance (Figure 6.3). The earliest compressive stress oriented at about 170° based on mechanical analysis (Moody and Hill, 1956; Wilcox *et al.*, 1973) forms conjugate fractures trending N-S and 160°. The reorientation of the primary compressive stress to 065° caused the northwesterly trending folds to be refolded into north to northeast and caused the development of the 060° trending fractures. The 060° trending fractures may have been reactivated as transfer faults during extension of the Kenyan Rift.

6.10 ADOLA - MOYALE BELT, S ETHIOPIA / NE KENYA

The regional geology and structure of the Adola - Moyale area has been discussed in chapter 3 and in section 6.3.3. In this section discussion is restricted to the role of lineaments in the structural evolution of the area. In figure 6.18 the dominant lineaments trend N-S and 135±5°° The 135° trending lineaments are occasionally observed sinistrally offseting the N-S lineaments and the

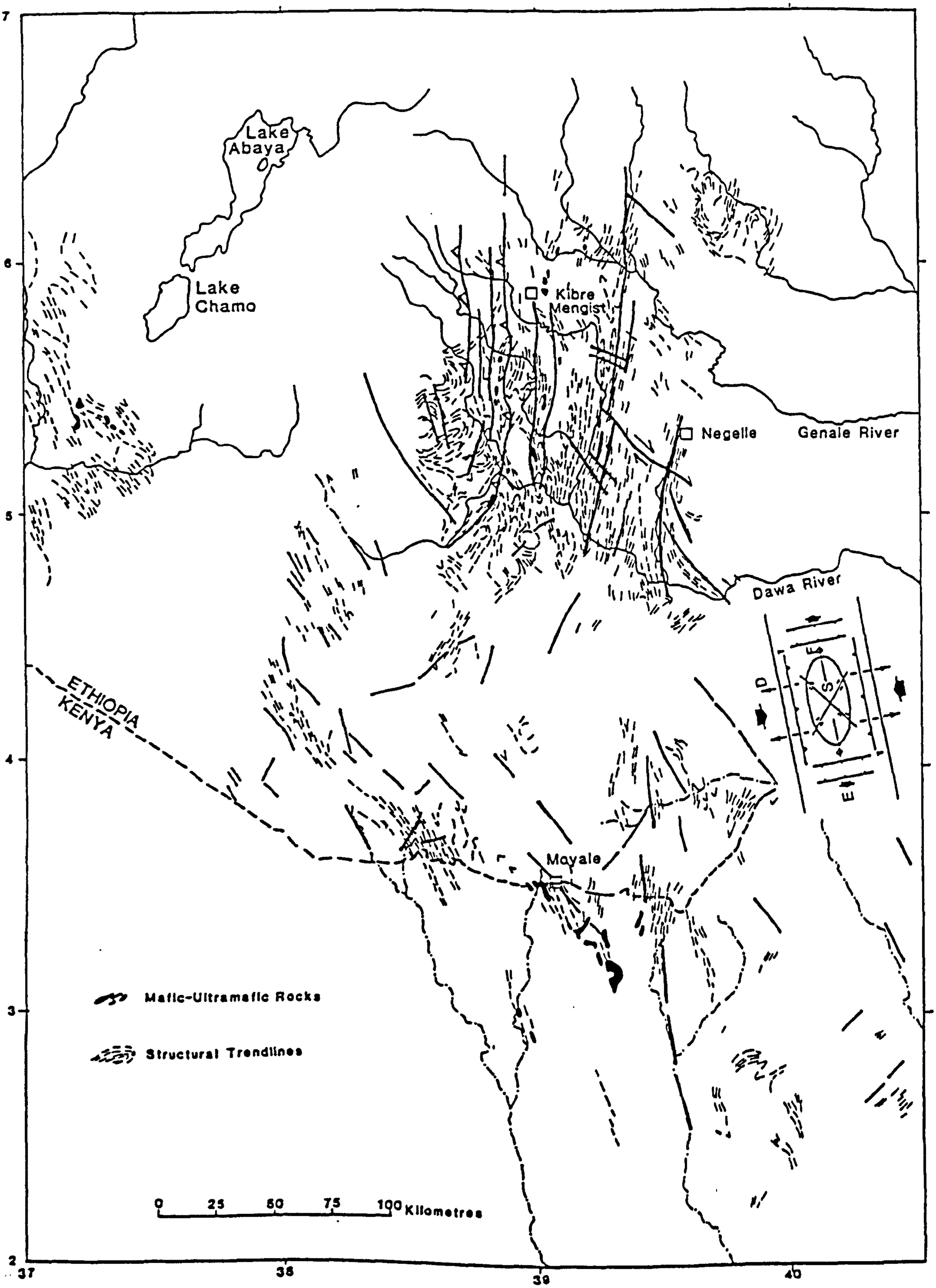

Figure 6.18 Lineaments and structural trends in S Ethiopia-NE Kenya. Based on Landsat interpretation aided by unpublished maps and fieldwork. A diagram is inset to illustrate attitudes of principal structures in the area. E: extension; D: direction of thrusting and napping; S: conjugate pair of strike-slip faults; F: fold axes.

ophiolite belt. The strain ellipse presented (Figure 6.18) shows the direction of shortening and extension so that the local orientations of principal stresses can be assesed. It is suggested that an E-W directed compressive stress caused the N-S trending thrusts and the 135° trending strike-slip faults. The 135° trending faults were reactivated during oblique collision of the Mozambique belt, causing sinistral displacement of the N-S trending ophiolite belt.

6.11 THE SIGNIFICANCE OF NORTHWESTERLY TRENDING FAULTS IN NE AND E AFRICA

6.11.1 Introduction

Northwest trending faults are widespread throughout the whole of the NE Africa - Arabia region (Brown, 1970; Davidson *et al.*,1976; Moore, 1979; Vail 1983; Browne *et al.*,1984; Berhe, 1986) (Figures 5.2 and 6.19). In Africa, these are most strongly developed in NE Sudan - Eritrea, and S Sudan - S Ethiopia - and W Kenya. Berhe (1986) and Berhe and Rothery (1986) however have shown that northwest trending lineaments are even more widespread than has so far been recognised. In this section, the role of these lineaments from the late Precambrian to the Tertiary will be discussed, primarily because their origin and tectonic implications can only be understood if their Recent history is included, however, emphasis is put on the earlier history of these faults.

6.11.2 The Marda Fault Belt - (SE Ethiopia - Somalia)

A map has been prepared showing the major structural and tectonic features of SE Ethiopia, using bulk processed Landsat MSS images at a scale of 1:500,000 (Figures 6.19 and 6.20), supported by fieldwork (Berhe,1982,1986) and which has been constrained by geological studies carried out by Black *et al*, (1974) and Purcell, (1976). Figure 6.20 and 6.21 shows an array of NW-SE (140°) trending lineaments, which continue for approximately 700 km. The northwesterly trending lineaments are discontinous further south in the Ogaden where they are dextrally offset by NE trending lineaments.

Structures associated with these faults occur on many scales. Small faults are traceable up to

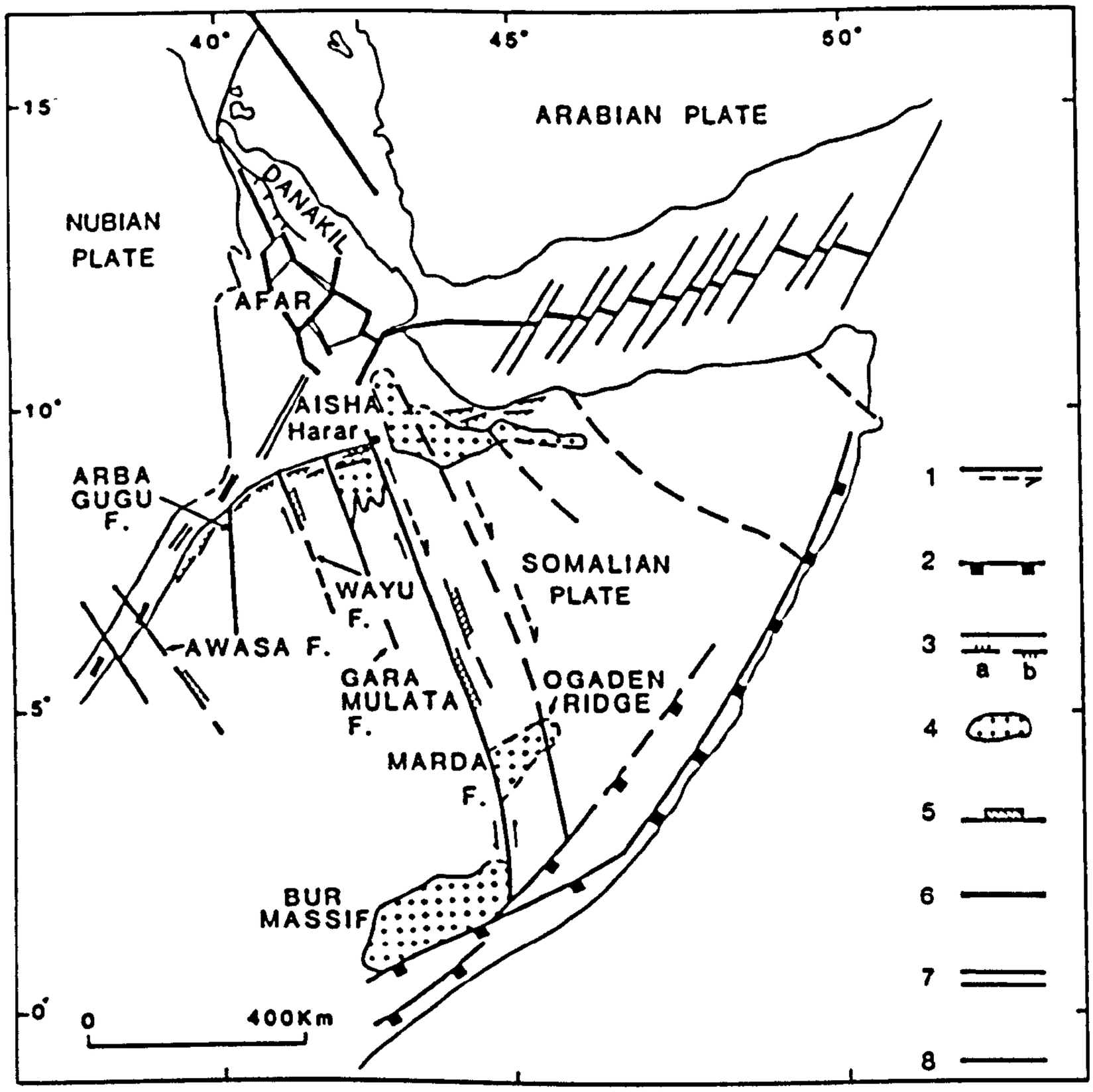

Figure 6.19 Simplified structural map of the Horn of Africa (after Berhe,1986). Modified from Barberi and Varet(1977), Courtillot(1982) and Kazmin and Berhe (in press). Northwesterly faults(broken where inferred). Solid arrows direction of late Precambrian motion. Broken arrows direction of late Tertiary-Quaternary motion. (2) Major normal faults of Somalia coast (Late Palaeozoic-Early Mesozoic). (3) Types of rift escarpments: (a) with predominant synthetic faults; (b) with predominant antithetic faults. (4) Basement blocks along the Marda Fault. (5) Late Palaeozoic grabens. (6) Main oceanic spreading axes. (7) Attenuated continental crustal zones. (8) Transform faults.

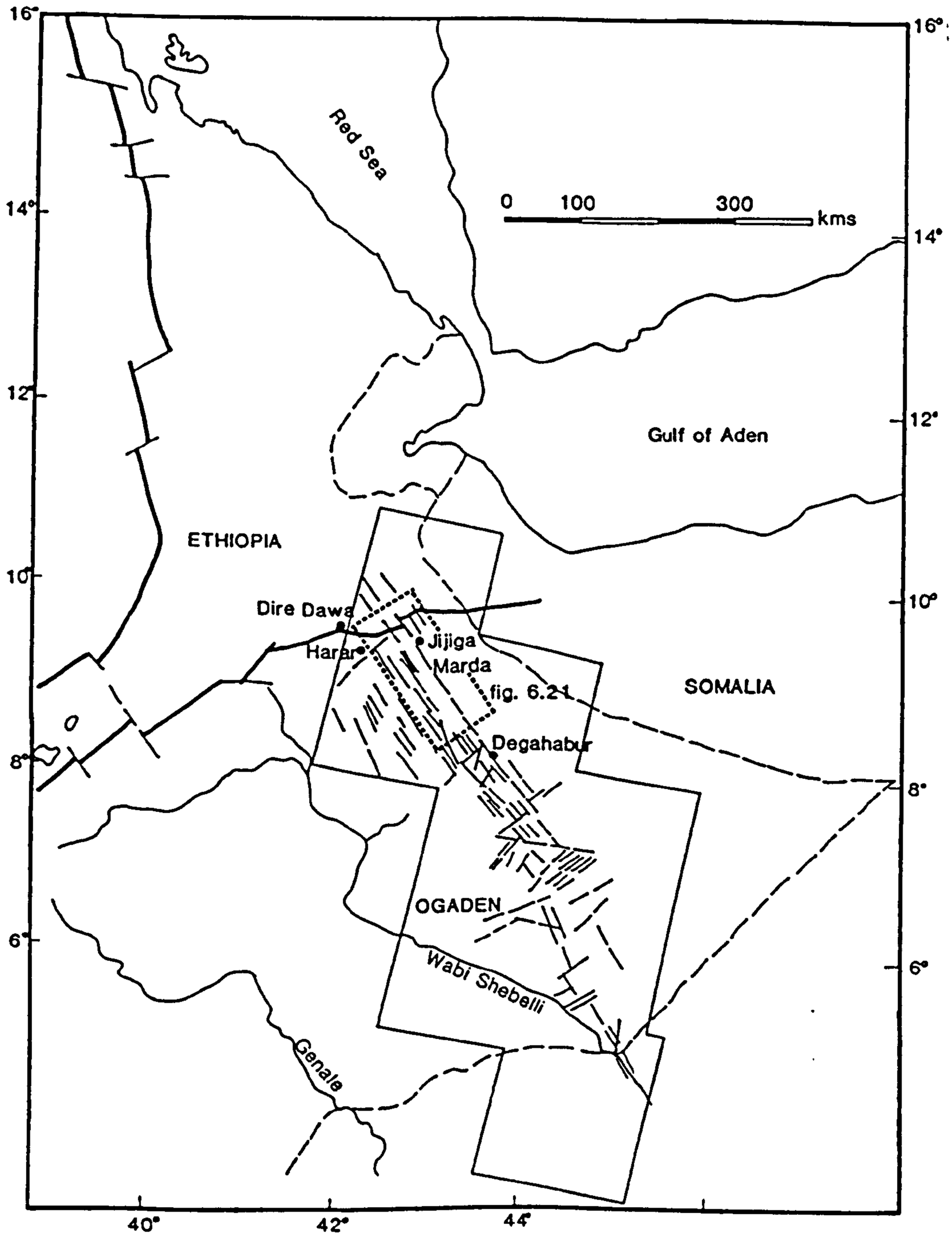

Figure 6.20 The Marda Fault Zone and related structures. Based on interpretation of Landsat MSS band 5 and Large Format Camera images. These fault zones have been confirmed by various workers (Purcell,1976; Black et al,1974; Berhe,1986).

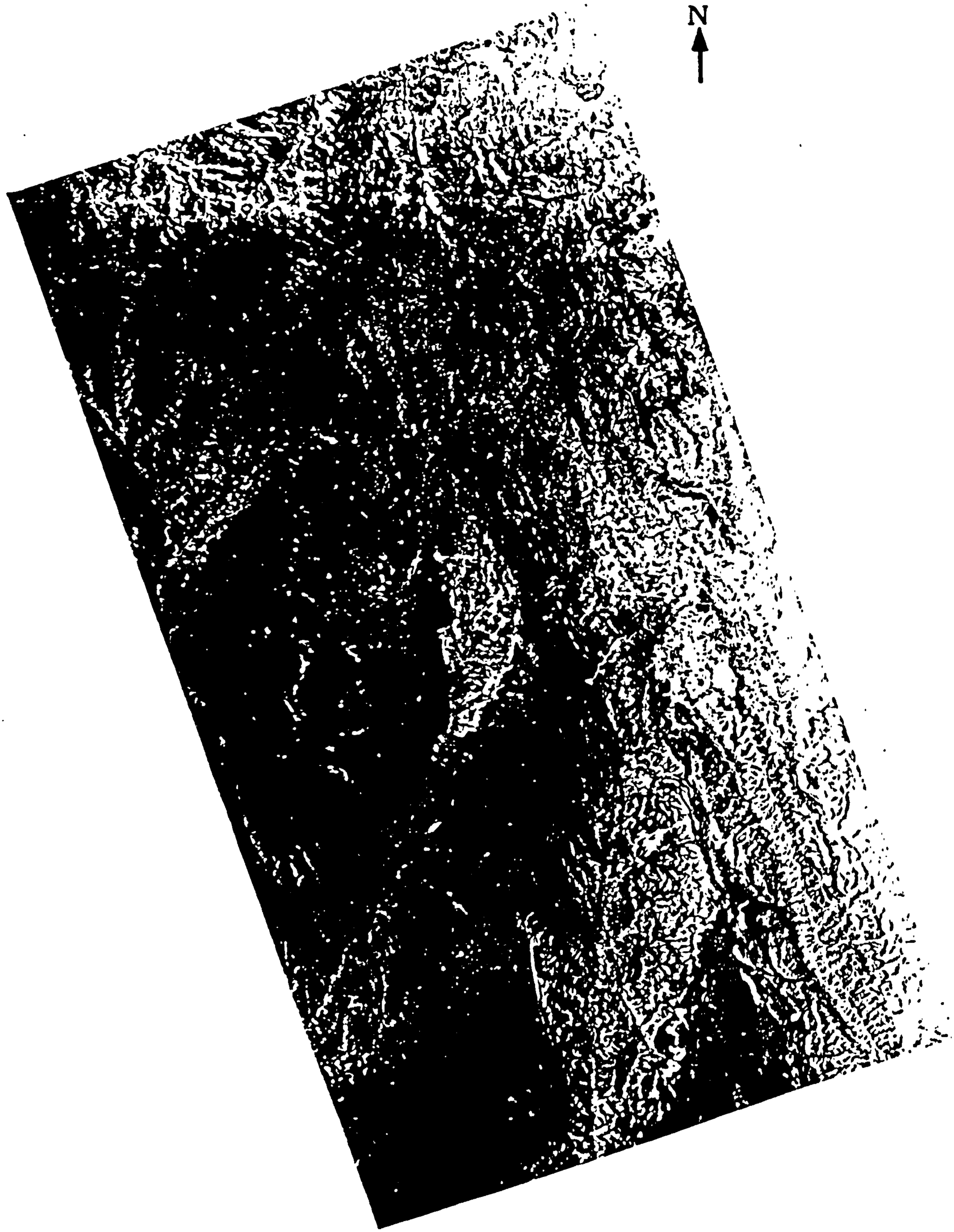

Figure 6.21 Large Format Camera imagery of the Marda Fault Zone,SE Ethiopia. Note how the Marda faults have been cut by Afar Rift faults. Approximate scale 1:500,000.

the rift margins (Figure6.19) where they offset the escarpment and continue to Central Afar where northwesterly fault zones have displaced the south-eastern escarpment by 10-15 km, in the Dire Dawa area (Figure 6.19). Similarly the Marda Fault has sinistrally displaced the Aisha block by about 110 km.The northwesterly trending fault zones in the Dire - Dawa area are parallel to the Marda Fault zone, which is a major structural element in the Horn of Africa (Black *et al.*, 1974; Purcell, 1976). A post-Lower Miocene dextral displacement of 110 km along the Marda Fault Zone was suggested by Wood (1979) to eliminate the Aisha block from the Afar and to allow complete closure of the Red Sea and the Gulf of Aden as advocated by Girdler and Styles (1978). Similarly Black *et al.* (1974) suggested large-scale Tertiary dextral transcurrent motion along the Marda Fault Zone, related to the plate separation of the Gulf of Aden. Later Purcell (1976) revealed that there was a consistent swing to the right of structures in the proximity of the Marda Fault Zone consistent, with dextral displacement.

However, if there was a large displacement in either sense it must have predated the Tertiary since neither the continental margin in the Afar nor along the Sinai or Indian Ocean have been offset. If there was a large scale sinistral displacement in the Tertiary, the effect would have either closed the Gulf of Aden or opened the south-western Afar and offsetting the escarpment, for which there is no evidence.

Purcell (1981) and Berhe (1986) have provided more satisfactory solutions to the history of the dominant North-westerly Fault Zones in the Horn of Africa. They suggest that two stages of transcurrent movement occurred along the Marda Fault Zone, both prior to deposition of the Mesozoic sedimentary cover. Extensive Precambrian sinistral transcurrent movement was inferred along the Gara Mulata Fault Zone (Figures 6.19 and 6.20). Drag folds with nearly vertical axes are developed in the Precambrian gneisses along this fault, consistent with sinistral movement. Renewed strike-slip movement in the late Palaeozoic is evident from narrow grabens filled with the Wayu clastics of Carboniferous age (Beauchamp and Lemoigne,1974). Most of the sinistral displacement probably occurred in the Late Precambrian to Palaeozoic, because the Marda Fault Zone is cut by NNE-trending coastal faults (Bruni and Fazzuoli ,1980) which delimit Triassic-Jurassic sedimentary basins. Kozerenko and Lartsev (1976) suggested that such movement occurred along

the Marda Fault on the basis of geophysical data. These workers noted that east of the Marda Fault Zone the subsurface of the Bur Massif is sinistrally offset from the Ogaden Ridge by about 170 km (Figure 6.19). Purcell (1981) also suggested a similar early tectonic history for the Marda Fault. Since the end of the Mesozoic the block west of Marda Fault Zone has been uplifted acting as a barrier to Cenozoic marine transgressions. Late in the Tertiary renewed activity along some north-westerly faults apparently controlled basaltic eruptions. (Berhe, 1986).

Kazmin (1976) suggested the possibility that the Red Sea and Gulf of Aden were sited along zones of pre-existing crustal weakness. The hypothesis that the Red Sea may have developed along a pre-existing Pan-African suture was put forward by DeWit and Chewaka (1981) and Harris and Gass (1981). The latter suggested that the compositional differences of plutons on either side of the Arabian-Nubian shield could be explained by an easterly dipping subduction along the Red Sea. Although part of the Red Sea may follow a suture zone, a shear movement only along north-westerly trending fault zones may have been responsible for locating the initial rift of the Red Sea which would have synchronously caused rifting of the Gulf of Aden along ENE trending faults consistent with the suggestion that the Gulf of Aden rift may have propagated along ENE faults (Berhe,1986).

6.11.3 Northwesterly Faults In S. Sudan - SW Ethiopia and Kenya

Many NW trending lineaments have been traced from W Ethiopia to S Sudan. These lineaments have sinistrally offset N-S lineaments, and late Precambrian rocks (see section 6.2). In S Sudan the NW-SE lineaments form deep-seated basins (Browne *et al.*,1984) and have been collectively called the Southern Sudan Rift. The oldest sediments in the rifted basin of southern and central Sudan are lower Cretaceous. (Browne *et al.*, 1984). It is clear that these faults extend via SW Ethiopia (Davidson *et al.*, 1976) to L. Turkana area, N. Kenya (see Figure 5.2). The northern end of the Southern Sudan Rift terminates along a major NE-SW trending lineament, with a dextral sense of motion (Browne *et al.*, 1984). Similarly the NE-SW trending lineaments are observed cutting NW-SE trending lineaments in W. Ethiopia and NE Sudan - Eritrea (see sections 6.7 and 6.8.2).

6.11.4 Origin of the Northwesterly Fault Zones

The northwesterly faults have had an extended history from the late Proterozoic to Tertiary. The Najd Fault formed in the interval 630- 560 Ma (Fleck *et al.*, 1976; Stacey and Agar, 1985). The Marda Fault Belt extend into the late Precambrian, however the earliest date so far available is Palaeozoic, based on age of sediments (Beauchamp and Lemoigne, 1974). Even though some of these faults in the Sudan have been dated as Lower Cretaceous, it is clear that they were formed much earlier. Most workers have concluded that the Najd Faulting is related to a major Late Precambrian collision event. This collision was considered to be between the Arabian shield and a rigid indenter, east of the Idsas suture (Figure 6.22) (Schmidt *et al.*, 1979; Fleck *et al.*,1980; Davies, 1984). However Stern (1985) suggests that they represent a set of transform faults developed in response to a major episode of extension, in northernmost Afro-Arabia. His objections to the continent-continent collision is 1) the absence of much older continental crust east of the Idsas suture. 2) orientation of Najd faults 3) the asynchrony of Najd Faulting and collision suturing events and 4) lack of evidence for major uplift accompanying faulting. These objections are discussed in light of new data acquired in East Africa and the implications for these observations examined, and a new model is presented. Discussion about the Najd faulting is important because it has implications for the NW trending faults in the Horn of Africa, and more important the Najd is the only one where detailed work and time constraints are available.

Recently the presence of early Proterozoic continental crust east of the Nabitah and Al Amar sutures, separating the Afif and Ar Rayn terranes has been ascertained (Stacey and Stoesser, 1983; Stacy and Hedge, 1984; White, 1985; Stacey and Agar, 1985). The presence of significantly older crust is suggested by 2000 Ma old zircons from a trondhjemite that forms the western margin of the Ar Rayn terrane (Calvez *et al.*,1983).

Since the Najd Faults consists of parallel array of faults which do not resemble a conjugate set of strike-slip faulting as in Tibet, Stern (1985) concluded that it could not have been caused by continent-continent collision. However field observations and Landsat data suggest the presence of numerous conjugate sets of fractures in NE and E Africa. In NE Sudan-Eritrea there are major

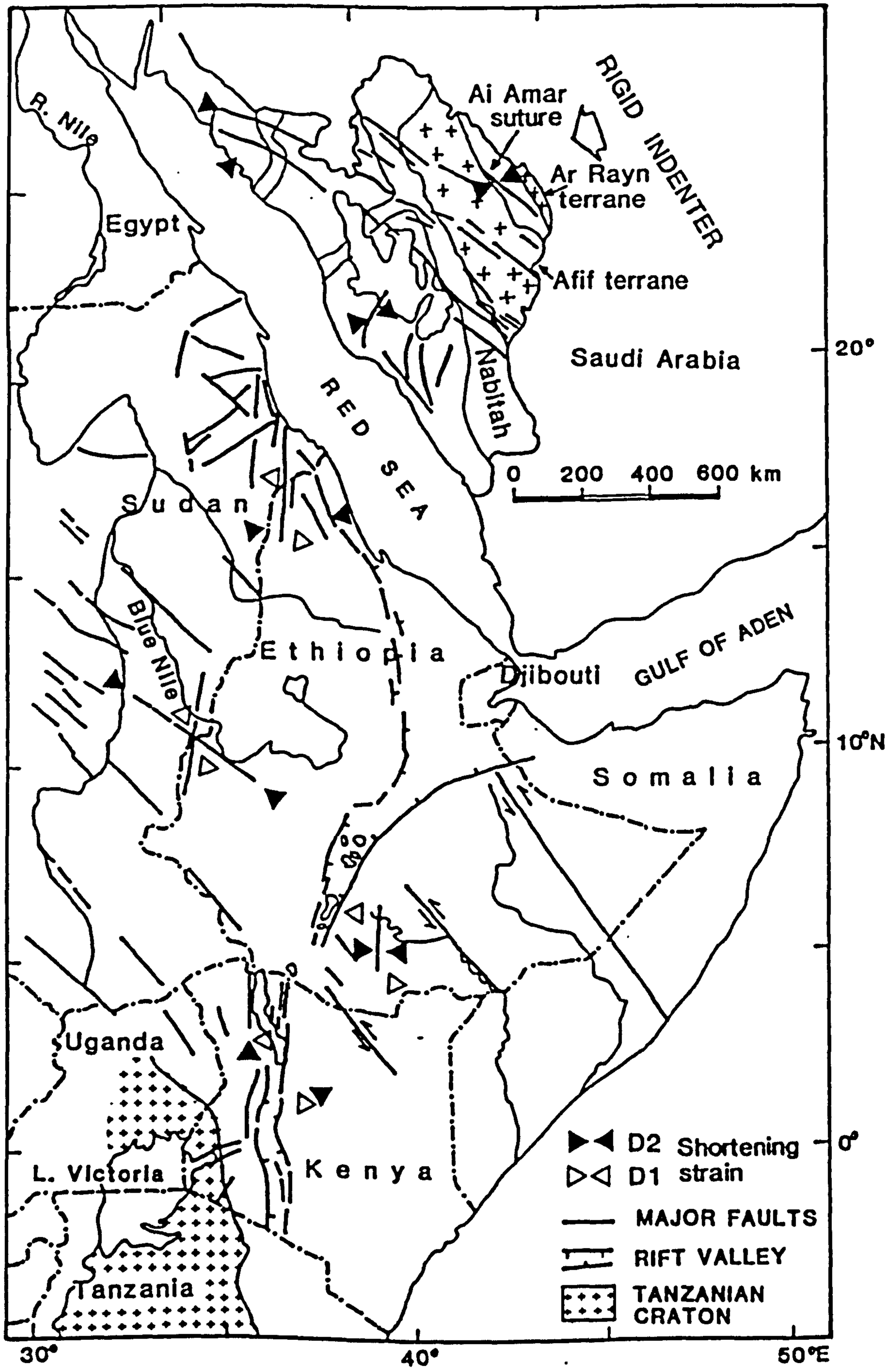

Figure 6.22 Megatectonic structures in the Pan-African/Mozambique belt. With orientation of principal shortening direction indicated. Source of data for Saudi Arabia: Davies (1984); Stoesser and Camp, (1985).

NE-SW trending faults cutting the northwesterly faults. In SE Sudan-Ethiopia, major N-S faults as long as 700 km and NE trending shear delimits the Southern Sudan Rifts (Browne *et al.*,1984). The faults in Saudi Arabia might not be as long as those on the Nubian Shield, but they do exist because Davies (1984) has suggested that N-S and NE-SW trending faults in Southern Arabia represent a contemporaneous conjugate set of faults. Slip line theory also explains that when a conjugate set is formed, whichever set forms first continues to develop at the expense of the other. However a fault set will be rejuvenated if it is oriented favourably to a subsequent stress. It is suggested that the northwesterly fault zones were oriented favourably to the D_2 stress discussed in the next section.

The third objection to the collision model is that the suture events were over by 640 Ma, before Najd Faulting and hence could not be related. It is important to note that the Northwesterly Fault Zones are collision-related but are later strike-slip adjustments during the deceleration of the Pan-African event. Finally it is not surprising that there was no uplift comparable to that observed in Tibet, because collision was mild causing less crustal shortening in NE Africa.

6.12 TECTONIC EVOLUTION

Analyses of structural trendlines in NE and E Africa indicate three major tectonic trends. Cross cutting relationships show that the E-W trending are the oldest which are refolded into N-S to NE-SW and later sheared and rotated into NW-SE trends. Extensive shearing in localised areas has caused structural complexities, however regional synthesis can be made. Similarities in structural trends do not necessarily mean that similar ages can be assigned to them, however the sequence of events from E-W to N-S and NW-SE have been confirmed in the different areas. Fieldwork has also confirmed that folds of similar orientation are present in the studied areas. The present analysis demonstrate that major crustal shortening occurred across the wrench fault zones and was particularly intense in NE Sudan - Eritrea, and S Ethiopia as compared to W and N Kenya. It is suggested that the sequence and mechanism of plate collisions can explain the various structural trends.

The non-ductile layer of the lithosphere in E Africa is segmented in blocks limited by the N-S,

influence of thrusting and nappe formation was dominant. Collision with a wider indenting mass is prefered than a rigid narrow indentor because the ophiolites are parallel and straight.

Strike-slip tectonics has developed on smaller scale as compared to the Tibetan Plateau which means no large volume of crust has been squeezed out. This could be due to physical constraints because there was no space for large crust to escape.

If the presence of two rigid indentors is accepted then collision may have happened at different times. A plausible scenario suggested would be earlier collision from the east (NE Saudi Arabia) followed by oblique collision from the southeast causing stacking of crustal blocks along NW trending faults.

CHAPTER 7

DISCUSSION AND CONCLUSION

7.1 INTRODUCTION

This study has sought to combine field, remote sensing and geochemical data in order to understand the geological evolution of the Pan-African/Mozambique belt. In this chapter an attempt is made to integrate all lines of evidence by summarising the geology and geochemistry of ophiolite complexes and the geochemical variations of granitoid rocks in E Africa. This includes a synthesis of available geochronological data. Finally a plate tectonic model is presented which encapsulates all the observed geologic and geochronological data. This model provides constraints for continental breakup and crustal accretion processes and has implications for plate reconstructions of Gondwanaland.

7.2 OPHIOLITE BELTS IN NORTHEAST AND EAST AFRICA AND THEIR IMPLICATION

7.2.1 Introduction

The presence of ophiolite complexes has been documented in the Eastern Desert of Egypt (Bakor *et al.*, 1976; Garson and Shalaby, 1976; Dixon, 1979; Shackleton *et al.*, 1980; Ries *et al.*, 1983), in Ethiopia (Kazmin, 1976; DeWit and Aguma, 1977; Kazmin *et al.*, 1978, 1979 a, 1979b; Berhe, 1981; Warden *et al.*, 1982), in Sudan (Hussein, 1977; Fitches *et al.*, 1983; Abdel Rahman, 1983; Embleton *et al.*, 1983; Vail, 1983) and Kenya (Shackleton, 1979; Vearncombe,1983b; Price, 1984). The recognition of such complexes led to attempts at integrating their presence into models for the evolution of the Arabian-Nubian Shield (Gass,1977; Shackleton,1979,1986; Vail,1983; Camp,1984; Stoesser and Camp,1985). However in these models the structural link between the ophiolites was incompletely documented. This prompted Berhe and Rothery (1986) to use Remote Sensing techniques to address this problem. This study supplemented by fieldwork and geochemical investigation has helped constrain the evolutionary model of the Pan-African/Mozambique belt.

7.2.2 Ophiolite Belts

Study of Landsat MSS imagery combined with new field data and published data of other workers has been used to constrain a revised structural interpretation of the region (Berhe and Rothery,1986). The mafic-ultramafic complexes (Figure 7.1) to lie on narrow belts trending between north-south and northeast-southwest, outcropping discontinously for at least 4500 km. In grouping these complexes three criteria had to be satisfied: (a) the presence of convincing Penrose (1972) ophiolitic assemblages; (b) that the structural trends within the ophiolites showed them to align along strike; (c) that there should be a contrast in the geology on either side of the proposed suture. Based on these criteria the ophiolite belts recognised (Figure 7.1; Table 7.1) are (from west to east) the (1) Sol Hamed-Wadi Onib belt; (2) Ingessana-Port Sudan belt; (3) Sekerr-Yubdo-Barka belt; (4) Baragoi belt; and (5) Adola-Moyale belt. It is suggested that these represent sutures formed by the closure of small ocean basins between island arcs, after the model suggested by Gass (1977) for Saudi Arabia and northeast Sudan. The ophiolite belts are discussed separately from west to east.

1. Sol Hamed - Wadi Onib

The geology of the Sol Hamed area has been reviewed by Vail (1978). Detailed studies have shown that the Sol Hamed mafic-ultramafic rocks are ophiolitic (Hussein,1977; Fitches *et al.*, 1983; Price, 1984). Similarly the Onib complex (Hussein *et al.* 1984; Kroner, 1985) which is a probable continuation of the Sol Hamed ophiolite complex contains interlayered ultramafic rocks with podiform chromite lenses and gabbros. Geochemical data of the sheeted dykes and pillow lavas display a marked enrichment in incompatible elements. The presence of podiform chromites and Ti depletion in cumulate pyroxenites is considered to be typical of supra-subduction ophiolites (Kroner *et al.* 1987). The Sol Hamed and Wadi Onib complexes were considered to mark a major Pan-African suture (Fitches *et al.*, 1983; Hussein *et al.*, 1984), and Fitches *et al.* (1983) suggested that the Benioff zone dipped southeastwards because the ophiolite faces southeast.

The Sol Hamed and Wadi Onib mafic-ultramafics could be extrapolated because of relatively good exposure and direct alignment along strike but further south its extension is unclear, because of Quaternary sedimentary cover. However structural alignment suggests that this belt could

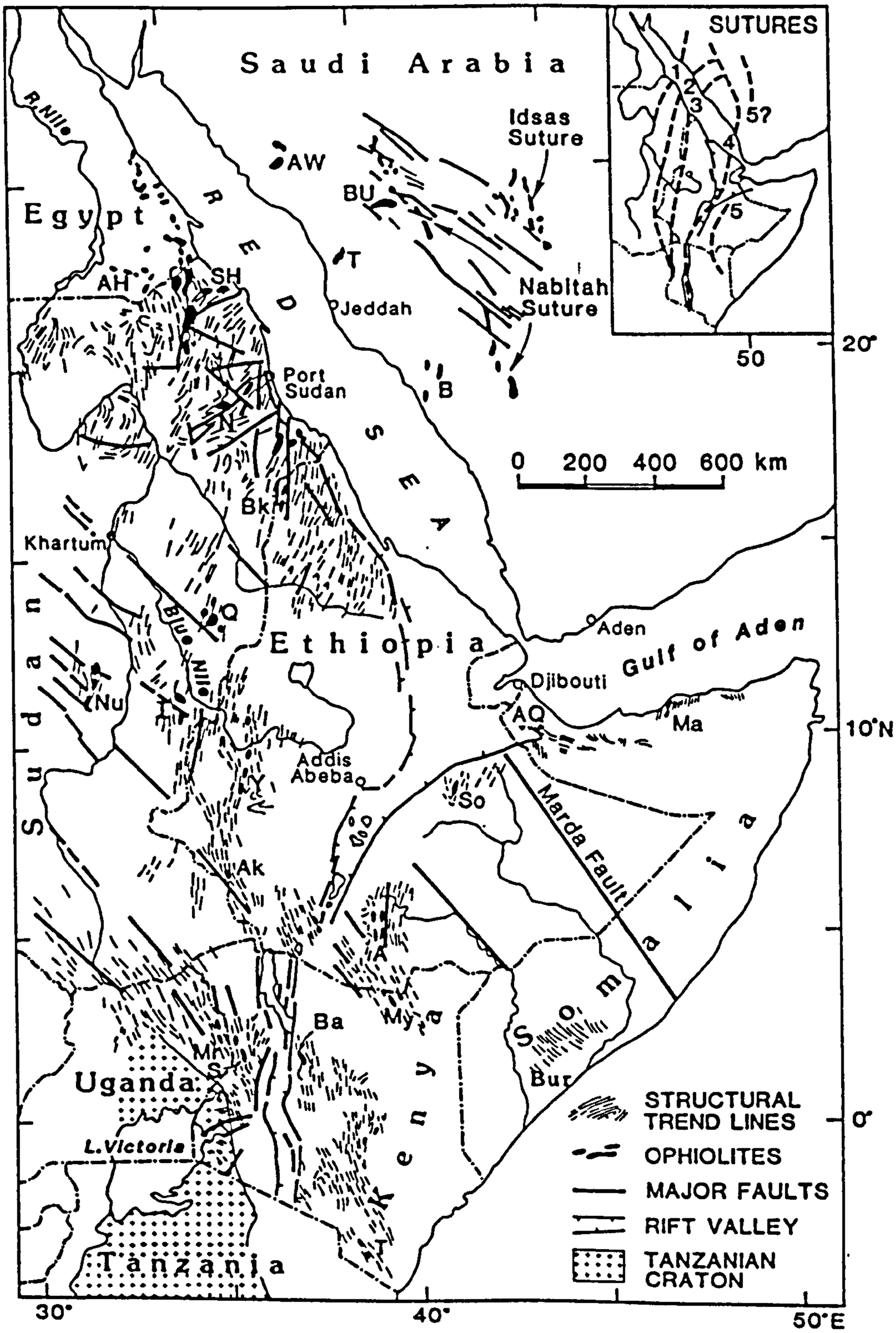

Figure 7.1 Ophiolite belts of NE Africa . (modified after Berhe and Rothery,1986). Place names are : AW - Jebel al Wask; BU - Bir Umq; T - Jebel Thurwah; B - Bishah; SH - Sol Hamed; AH - All aqi - Heini B.; N - Nakasib; Bk - Barka; Q - Qala al Nahal; Nu - Nuba; I - Ingessana; Y - Yubdo; Ak Akobo; So - Soka; A - Adola; My - Moyale; AQ - Abdul Qadr; Ma - Mait; Mr - Moroto; S - Sekerr; Ba - Baragoi; T - Taita Hills. Suture zones : (1) Sol Hamid - Wadi Onib (Africa) , Jebel al Wask (Arabia) ; (2) Ingessana - Port Sudan (Africa), Jebel Thurwah (Arabia) ; (3) Sekerr - Yubdo - Barka (Africa) ; (4) Baragoi (Turkana) - Nabitah (Arabia) ; (5) Adola - Moyale (Africa) , Idsas (Arabia).

possibly extend to the Bayuda area were ultramafics and island arc volcanics have been idenified between Abu Hamed (Dawoud,1980; Ries *et al.*1985; Hirdes and Brinkmann,1985) and Atbara west of the Nile (El Rabaa,1976). Ries *et al.* (1985) considered this tectonic boundary separating higher grade metasediments from low-grade metavolcanics as a possible suture. Further south they may extend upto the Nuba ophiolite complex (Figure 7.1) (Steiner,1987) and then further south merge with the Ingessana - Port Sudan ophiolite belt.

2. Ingessana - Port Sudan belt.

The first major work on the Ingessena region was by Kabesh (1961). He concluded that the serpentinites were intrusive into the surrounding metasediments. However detailed work by Abdel Rahaman (1983) and Price, (1984) established that the Ingessana complex represents a disrupted ophiolite. The attitude of the major thrusts suggests a SE-NW movement direction and tectonic transport of the ophiolite from the southeast (Abdel Rahaman. op. cit). Since a plutonic - volcanic complex outcrops along the eastern part of the complex which has continental margin-island arc affinity (Abdel Rahaman, 1983) it is plausible to assume that subduction is southeasterly.

Extrapolation over wider areas in SE Sudan is fraught with problems, because of extensive young sedimentary cover. Nevertheless the tracing of structural trends shows that the Ingessana could form part of the Qala En Nahl mafic-ultramafic complex along strike, where serpentinites and gabbros together with associated chromite and asbestos deposites were reported Wilcockson and Tyler (1933). The structural trend of these two mafic-ultramafics complexes shows an alignment with the Khor Nakasib complex in the Port Sudan region. These have been defined as the Khor-Nakasib ophiolite (Embleton *et al.*, 1983). The alignement of the Khor Nakasib to Saudi Arabia is well documented and is known as the Bir Umq-Port Sudan suture zone (Camp, 1984). The southernmost extensions of the Ingessana ophiolites could be the mafic-ultramafics of the Moroto area - Karamoja, NE Uganda where amphibolites, talc, chlorite schists and chromitiferous serpentinites similar to those of Ingessana and Sekerr have been described (Fleuty, 1961,1963).

3. Sekerr - Yubdo - Barka belt

Linear bodies of highly sheared ultramafic material where the maximum deformation is concentrated in a narrow (4 to 5 kilometre) zone continue from Yubdo area into Tulu Dimtu (W Ethiopia) (Figure 6.2) have been regarded as the site of a major suture (Kazmin, 1978; DeWit and Aguma, 1977; Berhe, 1981). Structural trendlines, and lithologic discrimination by Landsat had indicated a northward extension into the Barka area (Eritrea, and NE Sudan) and southwards into the Omo River Valley, SW Ethiopia (Davidson *et al.*, 1973) and further south to Sekerr, NW Kenya.

The dismembered Sekerr ophiolite was considered as a probable suture (Vearncombe, 1983b) and since sutures like plate margins must have considerable strike lengths (Shackleton *et al.*, 1980) extensions northwards into the Karasuk area, where Walsh (1966) described the presence of hornblende schists, biotite schists, talc schists, crystalline limestone, quartzites and pillow lavas can be expected.

Subduction in the Yubdo region, (W. Ethiopia) was westerly (Kazmin *et al.*, 1979a , 1979b; Berhe, 1981) while in the Sekerr area it was to the east (Vearncombe, 1983a,1983b). It is suggested that there were changes in subduction direction along the same suture zone, and this change in direction could have taken place along the NW trending Akobo Shear zone (Figure5.2).

The ophiolitic nature of the Tulu Dimtu (Warden *et al.*, 1982) and Sekerr complexes (Price, 1984) has been confirmed geochemically. The presence of mafic -ultramafic rocks in the Barka area has been established (Francaviglia, 1939; Kazmin, 1973; Kibreab, pers. comm. 1987).

4. The Baragoi belt

The northward extension of the Baragoi ophiolite is observed to be overlapped by Tertiary volcanics in the Turkana area, and has been considered to have been thrust to the southeast from the Turkana Rift (see chapter 2). Hence its northward extension can only be traced below the Main Ethiopian Rift and Afar Depression. Norhtheast of Lake Turkana there are high grade mafic and ultramafic rocks (peridotite, dunite, pyoxenite, gabbro-norite and diorites) in the Konso area (Davidson *et al.*,1973). It is possible that these mafic-ultramafic rocks which may represent a highly metamorphosed ophiolitic assemblage, could be related to the Baragoi ophiolite.

GEOLOGICAL SKETCHMAP OF THE METAMORPHIC COMPLEX
OF CHERCHER - DIRE DAWA REGION

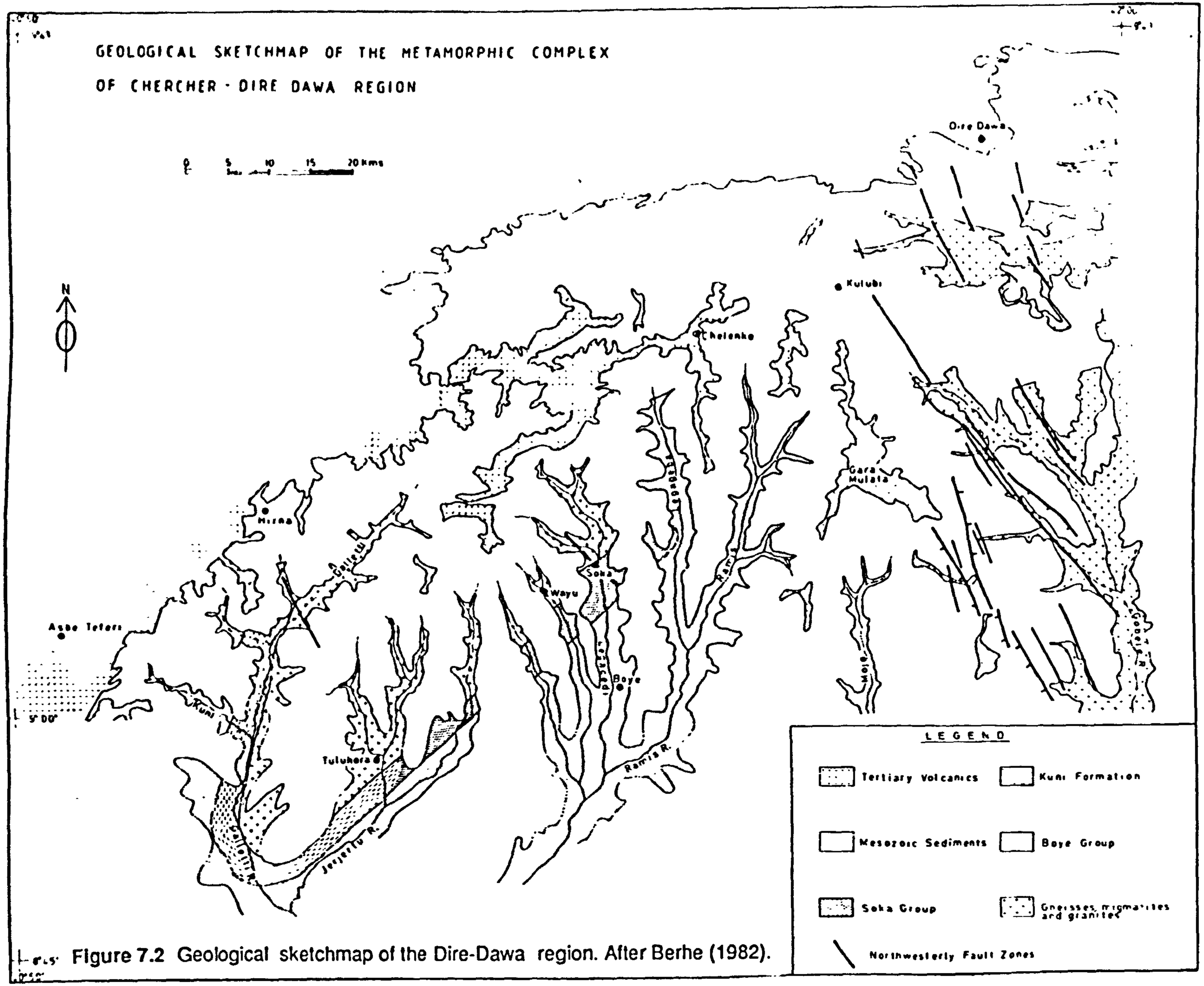

Figure 7.2 Geological sketchmap of the Dire-Dawa region. After Berhe (1982).

DeWit and Chewaka (1981) suggested that the main Ethiopian Rift could have been formed along a Pre-cambrian suture zone. They also suggested that the Red Sea could have been controlled by a Pan-African suture zone, however unlike DeWit and Chewaka (op. cit.) I suggest that the ophiolitic suture zones cut across the Red Sea Rift and do not follow the Red Sea trend. The Baragoi ophiolite can only be extrapolated into the Nabitah suture because the other ophiolitic sutures in Saudi Arabia, can confidently be traced to the other ophiolite belts established in NE Africa.

5. The Adola - Moyale - Soka belt

Three mafic -ultramafic belts have been reported in Southern Ethiopia (Kazmin, 1976; Gilboy,1970; Chater, 1971; Kazmin *et al.*, 1978). These belts have been considered to be imbricated ophiolites which are overthrust upon each other in an easterly direction (Kazmin *et al.*, 1978; see chapter 3). The Adola belt ophiolites extend south as far as Moyale (NE Kenya) which have been confirmed as ophiolitic (this study). Northwards it may possibly extend to the Soka area, SE Ethiopia (Figure 7.2), where metavolcanics, gabbros, serpentinised ultramafics and sedimentary schists have been described (Berhe, 1982). Unlike the other belts where reliable alignment of structural trendlines are observed, the area between the Adola-Moyale belt and Soka is covered by Mesozoic sediments.

In conclusion, the geometry of ophiolites in NE Africa suggests that the Sol-Hamed - Wadi Onib suture continues into Jebel Al Wask, while the Ingessana - Port Sudan suture could be aligned to Jebel Turwah- Bir Umq (Camp, 1984). The possible extension of the Seker- Yubdo - Barka suture is the Bishah mafic-ultramafic assemblage although Camp (1984) considers the Bidah - Bishah volcanics as an area of inter-arc volcanism. The Baragoi suture follows the Ethiopian rift system and its trajectory could be aligned with the Nabitah suture, while the Adola-Moyale belt can be extrapolated to the Al Amar suture (Stoesser and Camp,1985) of Saudi Arabia.

7.2.3 Geochemistry

A variety of tectonic settings have been suggested on geochemical grounds as viable sites to generate the ophiolites, which include mid-oceanic ridges,small marginal basins,back-arc basins and

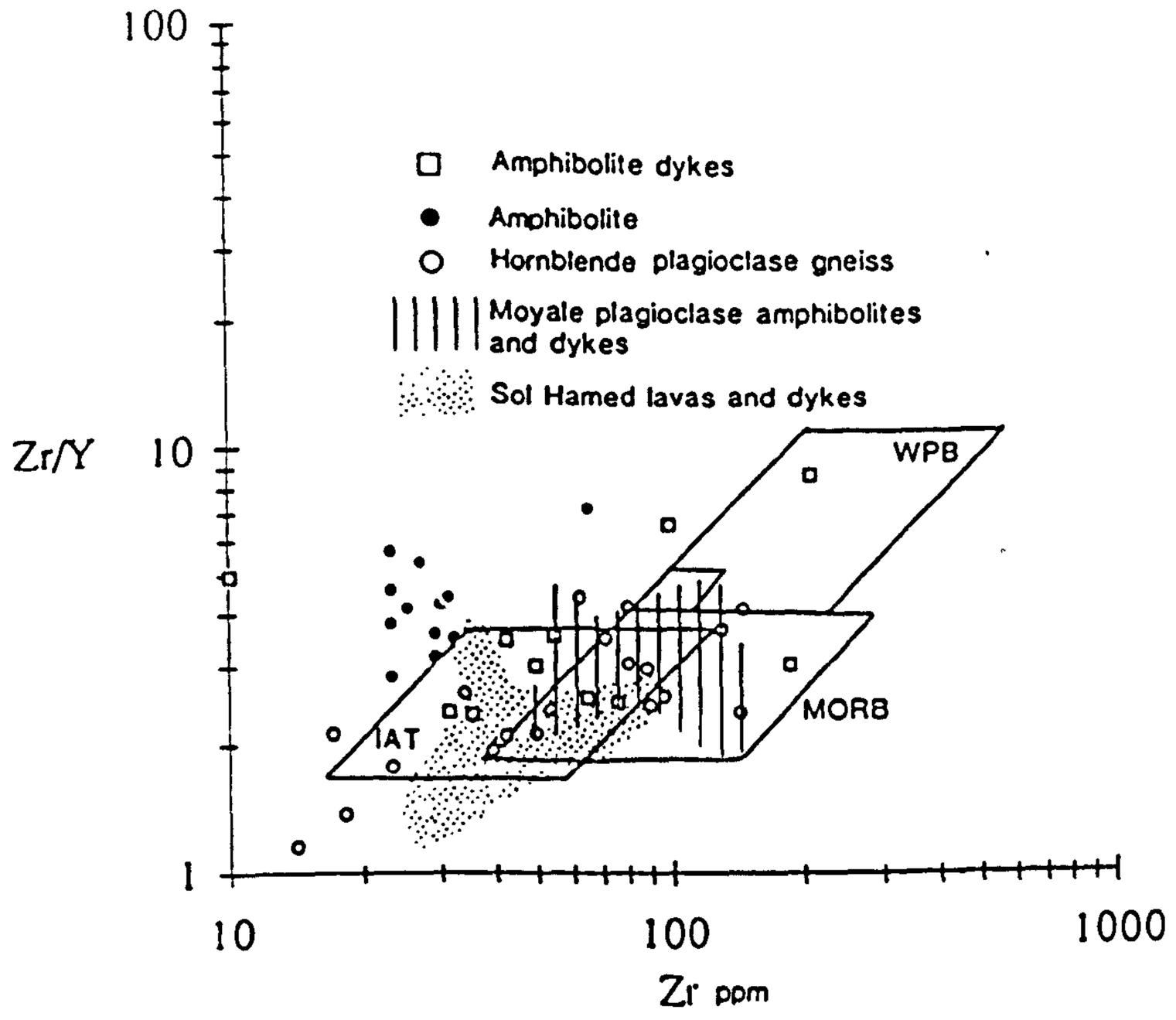

Figure 7.3 *Zr/Y* vs *Zr* discriminant diagram for basic rocks of Baragoi , Moyale, and Sol Hamed ophiolite zones . The Sol Hamed field from Price (1984). Discriminant fields taken from Pearce and Norry (1979).

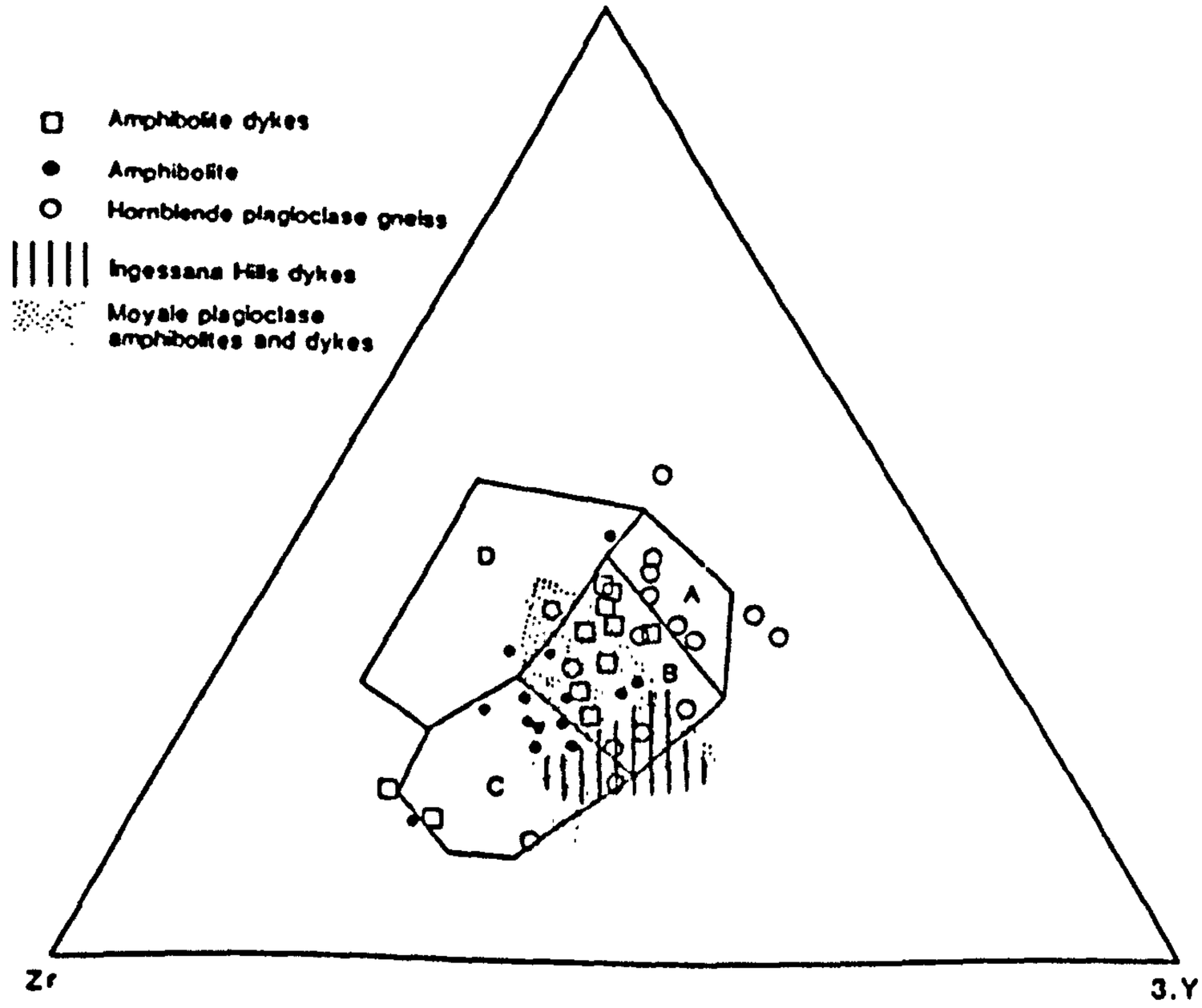

Figure 7.4 Ti - Zr - Y discriminant diagram for basic rocks from Baragoi, Moyale and Ingessana ophiolitic belts. The Ingessana field taken from Price (1984). Discriminant fields taken from Pearce and Cann (1973). Ocean island or continental basalts plot in field D; ocean- floor basalts in field B; low -potassium tholeiites in fields A and B; calc-alkali basalts in fields C and B.

island arcs (Miyashiro,1973; Pearce,1975,1980; Beccaluva *et al.*,1979).

Trace element data were used to classify the various ophiolite complexes. Data compiled from Price (1984) and this study show that most of the mafic-ultramafic complexes have a distinctive subduction related signature. The Ingessana and the Baragoi ophiolites developed in a supra-subduction setting. Trace element data indicate an island arc tholeiitic (I.A.T) tectonic affinity for the former, while the Baragoi complex shows a transitional MORB to IAT affinity (Figures 7. 3 and 7.4; table7.1). Both indicate derivation from a depleted mantle source. The Adola-Moyale belt indicate an island arc and MORB geochemistry, which developed in a back-arc tectonic setting. Trace element data of the Sol Hamed,Yubdo-Tulu Dimtu, and Sekerr ophiolite complexes suggest development in back-arc basins. Similarly Stern (1981) showed that the lavas in the Eastern Desert of Egypt plot in the fields of MORB and island-arc volcanics and concluded that they formed in a small oceanic rift or back-arc basin.

Discriminant diagrams such as Zr/Y-Zr (Pearce and Norry,1979) (Figure 7.3) and Ti-Zr-Y plots (Figure 7.4) show the data overlapping the fields of mid-ocean ridge basalt (MORB) and island-arc tholeiites (IAT) defined by Pearce and Cann (1973) and Pearce (1980). Modern analogues of these volcanics are situated near destructive plate margins above subduction zones (Pearce, 1980) in an island-arc setting. This interpretation is supported in the case of the Baragoi complex by the MORB normalised geochemical diagram (Figure 7.5). The amphibolites (which are of boninitic affinity) are richer in Ni, Cr but are poorer in high field strength elements (Y,Hf,Nb and TiO_2) and REE. The lavas have enriched P_2O_5 and depleted Nb, and Ta compared to MORB. This is consistent with generation from depleted mantle source. The amphibolites have a LILE enrichment similar to that of IAT. Geochemical patterns for the hornblende plagioclase gneisses are similar to oceanic calc-alkaline basalts and Sol Hamed lavas (Price,1984). The metamorphic process has not altered the HFSE and REE, hence the geochemical data of the immobile elements reflects the original geochemistry of the rock, while the LILE enrichment by hydrothermal processes are post formation phenomena. The selective enrichment in LILE, may reflect hydrothermal processes and/or mobilisation of aqueous fluids off a subducted slab into the overlying mantle (Ringwood,1974). These patterns are transitional between MORB and IAT.

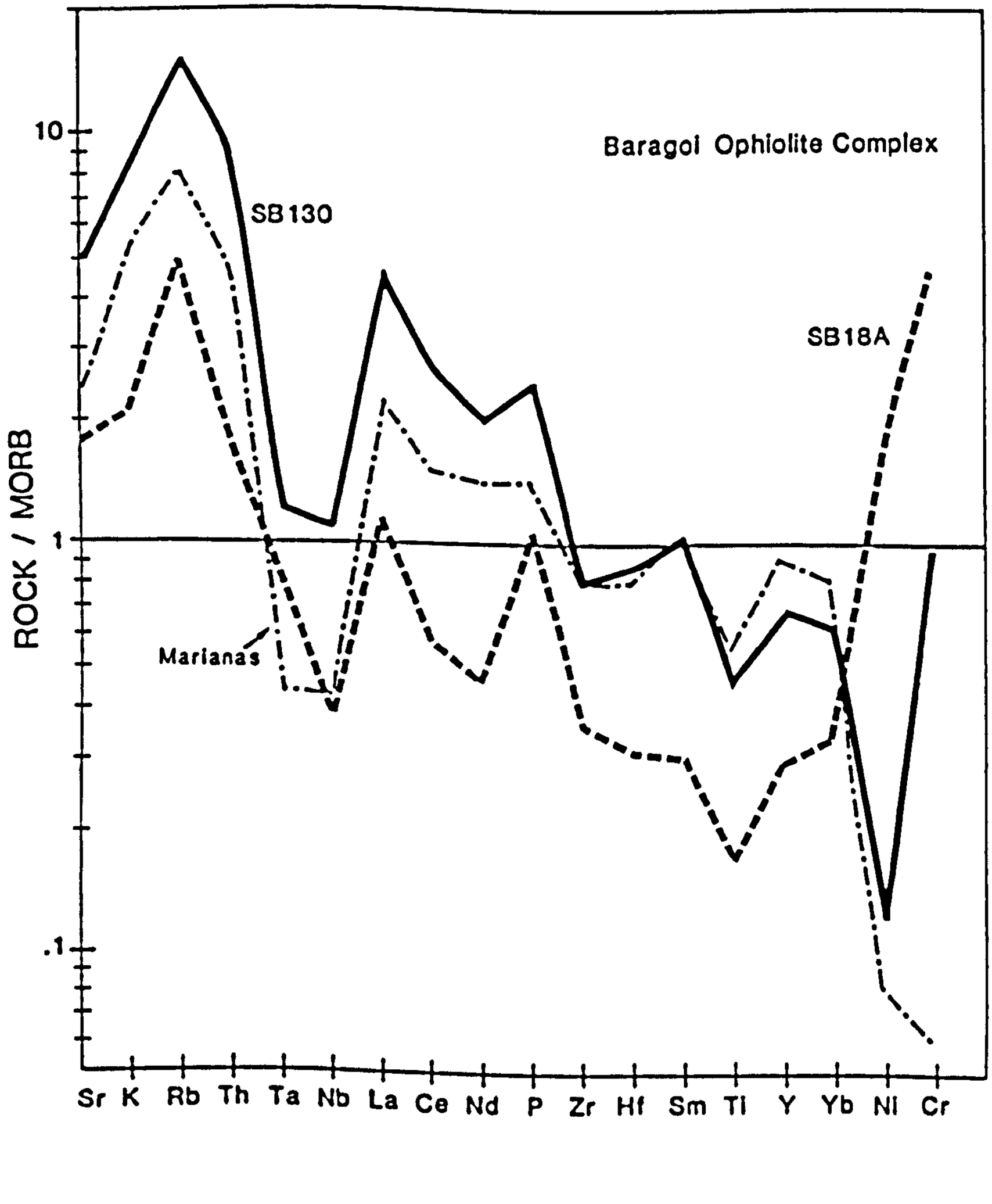

Figure 7.5 Representative geochemical patterns for the Baragoi lavas . Hornblende plagioclase gneiss (SB 130); amphibolites (SB 18A). Normalising values taken from Pearce (1980). The Baragoi lavas are compared with an average Marianas island arc lava (Hole et al,1984).

The association of the complexes with immature volcanoclastic sediments similar to present day island arcs (Mitchell and Reading,1971) and the limited extent of sheeted dyke complexes suggest that oceans or marginal basins did not develop to any appreciable size.

Table 7.1. Comparative data for ophiolite complexes in NE and E Africa.

MORB (Mid Ocean Ridge Basalts); IAT (Island Arc Tholietes); C.A (Calc-alkalin Basalts).

Geochemical data for Sol Hamed, Ingessana and Sekerr from Price(1984); data for Tulu Dimtu from Warden *et al.* (1982) and for Yubdo, Moyale and Baragoi areas, this study.

Name	Associated Sediments	Accretion to Continents	Tectonites	Cumulates	Sheeted Dykes	Volcanics	Metamorphism
Sol Hamed	Immature volcanoclastics turbidites, limestones and pelagics.	Arc-Arc collision emplaced onto volcanoclastic sequence.	Harzburgite	Dunites werhlites pyroxenite gabbro.	50 %	MORB IAT C.A	Greenschist facies
Ingessana	Shales, limestones quartzites.	Emplaced onto continental margin.	"	Dunites gabbros.	70 %	"	"
Sekerr	Psammites,semi-pelites,calc-silicates, and limestones.	Passive continental margin.	Absent	Pyroxenites gabbros	20-50 %	MORB IAT C.A	Epidote amphibolite facies.
Yubdo-Tulu Dimtu	Deepwater metasediments: volcanoclastics, quartzites, marbles graphitic schists.	Arc-Arc	Harzburgite	Dunite, pyroxenite	Rare	MORB IAT	Greenschist facies.
Baragoi	Psammites and semi- pelites.		Mantle dunite	Wehrlites gabbros.	20 %	MORB IAT Boninite	Upper amphibolite facies.
Moyale	Continental shelf sediments.	Emplaced onto continental margin shelf sediments.	Harzburgite (serpentinised)	Gabbros	Rare	MORB IAT	Upper greenschist facies.

Major element data of ultramafics from Baragoi show that they are rich in MgO and low in Al_2O_3, TiO_2 and CaO. All the dunites of Baragoi and Tulu Dimtu are rich in Mg, Cr and Ni reflecting the high modal abundance of olivine. Geochemical data suggest that the harzburgites and dunite pods of Baragoi

(this study) and Tulu Dimtu (Warden *et al.*,1982) form part of an ophiolite mantle sequence. In the Cr_2O_3-TiO_2 plot (Figure 2.10) the Baragoi mantle sequence, has Cr values ranging from 2200-2800 ppm and TiO_2(0.01 %) which are consistent with a supra-subduction ophiolitic field of Pearce *et al.* (1984b). The chromites of Baragoi and Moyale have relatively high Cr_2O_3 which follow an ophiolitic trend (see Figure 3.8).

In summary all available geochemical data indicates that the ophiolites in NE and E Africa are of back-arc or supra-subduction origin. There is, as yet, no evidence of an ophiolite complex with a true MORB trace element signature.

7.2.4 Structure

All of the ophiolite complexes in NE and E Africa are highly imbricated and are in no way stratigraphically coherent. Some ophiolites are not rooted in the related suture but have been tectonically transported. The Sol Hamed and Yubdo complexes (which are in the north) are considered to be more or less in situ, because they are not in a tectonic melange and extend linearly for hundreds of kilometers, while the southerly ophiolites, Ingessana,Sekerr, Baragoi and Adola-Moyale (Figure 7.1) have been tectonically transported as far as 100 kms.This is mainly because there is severe crustal shortening in S. Sudan, Kenya and SE Ethiopia as compared to the north. Crustal shortening in northeast Africa was less extensive than that observed in the Alpine and Himalayan orogenie, and the ophiolite complexes are unlikely to have been subsequently displaced by more than a few tens of kilometers from their sites of emplacement. Exceptions to this are the ophiolitic melange in the Eastern Desert of Egypt (Shackleton *et al*,1980) with possibly very large horizontal displacements. Crustal shortening in Kenya and Tanzania is reflected by an increase of metamorphism of the dismembered ophiolites.

The major strike - slip fault systems are, the Najd of Saudi Arabia which has a cumulative displacement of about 300 km , the Marda Fault Belt (Berhe,1986), the Akobo shear zone in SW Ethiopia (Davidson *et al.* 1976), the Aswa shear zone and the Tanganyka-Rukwa-Malawi lineament (TRM) (Chorowicz *et al.* 1987) and the Zambesi Belt (Figure 7.7)). The Aswa lineament is about 1200 km long and 60 km wide and in the western part is underlain by mylonites of Pan-African age

(Cahen,1970). The TRM is 1000 km long by 200 km wide (Chorowicz *et al.* 1987), is underlain by blastomylonites. This lineament was affected by the Ubendian orogeny c. 2000 Ma (Dodson *et al.* 1975) and is bound by a series of major shear zones. All the lineaments had a sinistral movement during the Precambrian while the TRM and the Zambezi faults had a dextral movement during the Tertiary (Chorowicz *et al.* 1987). The Adola ophiolite complex has been displaced sinistrally by about 50 kms from the Moyale ophiolite, whereas the Baragoi complex is suggested to have been thrust from the north or northwest from the Turkana area for approximately 50 km (Charlesley *et al.* 1984; this study). The displacement of the TRM was approximately 40 kms in the Tertiary (Chorowicz *et al.* 1987). The reactivation of these strike-slip faults during the Tertiary makes it difficult to estimate total displacement. It is however not impossible to make a microplate reassembly. One of the methods used in the microplate reconstruction is to establish the occurrences of ophiolites or mafic-ultramafic rocks between the major stike-slip faults and then try to allign the mafic-ultramafic complexes within the different crustal blocks. The integrity of the ophiolite belts along strike in each block suggests that offsets across individual northwesterly fault zones can be no more than a few tens of kilometers. However, the cumulative displacement of the ophiolite belts in the entire Pan African-Mozambique belt may be several hundred km .

The age sequence and dip direction of the ophiolitic sutures is still not certain. Ries *et al.* (1983) proposed SE subduction to explain the geological evolution of Central Eastern Desert of Egypt. However El Ramly *et al.* (1984) and Kroner *et al.* (1987) suggest that thrust direction and nappe transport were towards the SW. Further south Fitches *et al.* (1983) in their study of the Sol Hamed ophiolite of NE Sudan, suggested that the ophiolite occurs on a suture in which the original subduction zone dipped to the southeast. According to Camp (1984) and Stoesser and Camp (1985) the Yanbu and the Bir Umq suture zones are considered to represent a southeast dipping subduction zone while Embleton *et al.* (1983) suggest that the Sol Hamed and Nakasib ophiolites which lie along strike to the Yanbu and Bir Umq ophiolite occur on a suture which dips to the NW. An easterly dip is indicated for the Ingessana and Sekerr (Price,1984) while a westerly dip is suggested for the Yubdo,Baragoi and Adola-Moyale ophiolites.In Mozambique-Malawi area Andreolli (1984) suggests an early episode of eastward dipping subduction, which eventually flipped into a westerly

dipping subduction during island arc-continent collision. This means that along some of the postulated sutures for example the Ingessana-Port Sudan-Bir Umq suture the dip is reported to be either to the southeast in Saudi Arabia, to the southwest in NE Sudan and then to the southeast in Ingessana area. This is unacceptable, although changes in dip of subduction may happen along a major transform fault and possibly during continent collision, the different interpretations are mainly due to lack of adequate structural data. However there seems to be overwhelming evidence for westerly to southwesterly dips in the Nubian Shield ,since the inferred southwesterly dips of subduction in the Red Sea Hills, NE Sudan (Embleton *et al.*, 1983; Kroner *et al.*,1987) agrees well with our observations in Ethiopia and Kenya. Major obduction and nappe movement direction is to the east in the Yubdo, Adola-Moyale and Baragoi areas, and calc-alkaline volcanics are observed to lie west of the postulated suture in the Yubdo area (Figure 7.1). The westerly dips suggested for the Baragoi and the Adola-Moyale ophiolite belts is supported by the southwesterly dips indicated for the Nabitah and the Idsas sutures (Stoesser and Camp,1985) which are considered to form the same belt, as well as the fact that in Mozambique Saachi *et al.* (1984) have indicated major thrusting and nappes from the WNW .

7.2.5 Age relationships of the ophiolite belts

The problem of dating ophiolite complexes has been discussed by Desmons (1982). Generally the ophiolite rocks in the Shield are so dismembered and affected by low to Upper amphibolite facies metamorphism that it is difficult to find primary igneous minerals for reliable age dating unless zircons can be separated from trondhjemites. Hence, all radiometric ages with the possible exception of those obtained from Sm/Nd systematics represent metamorphic cooling ages dating the emplacement of the ophiolite. However, age constraints can be established if the ages of the associated volcanics are available. In this reconstruction a review of all available dates relevant to ophiolite emplacement in the Arabo-Nubian shield is carried out.

If it is accepted that the NE and E African ophiolite belts are continous with those of Saudi Arabia the age sequences established there could be used for correlation of the ophiolite belts in NE Africa. The only reliable age of an ophiolite is a U-Pb age of 822±12 Ma (Kemp *et al.*,1980) on zircon

from a cogenetic plagiogranite from Jabel al Wask, Saudi Arabia. More recently Claeson *et al.* (1984) give Sm/Nd isochron ages of 743±24 initial ratio ($^{143}Nd/^{144}Nd$=0.512069±31 and MSWD=0.58) and 782±38 Ma initial ratio ($^{143}Nd/^{144}Nd$ = 0.51168±0.26 and MSWD=2.44) for gabbros from the Jabel al Wask and Jebel Ess ophiolite complexes. These ages are not dramatically different however the U/Pb dating could be more reliable as the isotope systematics could preserve the original ages.The oldest Rb/Sr age of a calc-alkaline tonalite intruding the Baish and the Bahah Groups from western Saudi Arabia is 901 ±37 Ma (based on 9 points, R_i=0.70246±14 and MSWD=2.86) (Marzouki *et al.*,1982). This is a reliable estimate of the commencement of subduction in the area.

In NE Sudan the Naferdieb volcanics yield Rb/Sr age of 712±58 Ma with R_i=0.70234±1 and MSWD=4.9 (Fitches *et al.*,1983), while the Kadaweib and Awat island-arc volcanics gave Rb/Sr age of 723±6 Ma , R_i=0.7027±12 and MSWD=1.1 (Klemenic,1985) which could be considered the upper age limit of the Sol Hamed and Nakasib ophiolites. Rb/Sr ages of 673±33 Ma (R_i=0.7030±25 and MSWD =7.45), were determined for the earliest granitoids in the Red Sea Hills area (Cavanagh,1979). This confirms an upper age limit for the evolution of the mafic-ultramafic rocks of the Red Sea Hills area. Similarly in Western Ethiopia the Geba gneisses which are considered to be older than the Yubdo - Tulu Dimtu ophiolites are dated c. 800-820 Ma using Rb/Sr systematics (Berhe,in prep). This could be the maximum age limit for the ophiolites.

In S Ethiopia the upper age limit of the Adola -Moyale ophiolite belt (Figure 7.1) is 680±30 Ma, (initial ratio of 0.7082±24) based on Rb/Sr age of syntectonic granites (Gilboy,1970) while in Kenya the Sekerr marginal basin must have opened prior to 1000 Ma based on the oldest age of the Marich volcanic series (Ries, in prep.) while the younger age limit could be about 600 Ma based on Rb/Sr data of the Marich granite (Harris *et al.*, 1984). There is some complication in dating rocks adjoining an Archaean craton,as Harris *et al.* (1984) have found that the Marich peraluminous granites contain significant contributions from pre Pan-African crust. In the Baragoi area , Central Kenya two separate suites of gabbroic rocks give preliminary model Nd ages of around 796 and 609 Ma (Berhe and Davies, in prep). In Mozambique a quartzite unit from the Morrua ophiolitic complex gave a whole rock Rb/Sr isochron of 950±40 Ma ($^{87}Sr/^{86}Sr$= 0.7091), (Sacchi *et al.*, 1984).

Although the ages are limited, and while it is difficult to compare ages obtained by different techniques (Rb/Sr,Sm/Nd and U/Pb), some correlations can be made based on younger and older age limits for the ophiolitic sequences. It is apparent that the ophiolite emplacement took place between 900-700 Ma. Putting the relative ages into perspective there seems to be younging in age eastwards in the Red Sea Hills, NE Sudan (Embleton *et al.*,1983). Similarly in Kenya, the Sekerr ophiolite belt is considered to have opened earlier than the Baragoi and the Adola-Moyale ophiolite belt suggesting an eastward younging . This eastward younging is broadly similar to that suggested for Saudi Arabia (Schmidt and Brown, 1982; Darbyshire *et al.*,1983; Roobol *et al.*, 1983; Camp,1984). Nevertheless the fact that there is little agreement on the direction of plate convergence, or the age and paleogeographic position of each collision event, suggests that the Arabian-Nubian shield did not simply accrete sequentially as a series of accretionary arcs where southeast convergence played a major role.

7.3 PLATE RECONSTRUCTION OF THE PAN- AFRICAN / MOZAMBIQUE BELT

Since the recognition of ophiolites in Saudi Arabia and Egypt attempts have been made to define their possible extension further south. Further south, ophiolites have been recognised in Ethiopia (Kazmin,1976) and their probable wider extent has been indicated (Shackleton,1979, this study). If the continuity of these ophiolitic sutures is established for NE Africa (Vail,1983; Berhe and Rothery,1986) then sutures like plate margins, cannot suddenly stop (Shackleton *et al.*,1980) hence these ophiolite belts which have been interpreted as forming sutures must continue further south. In this section all mafic and ultramafic occurrences in East Africa , and Madagascar are evaluated in the light of experience gained in the study of ophiolites in NE and N Africa. Published and unpublished material are used and these have been critically reviewed and re-interpreted in this study. The same criteria that were used for the study of ophiolites in NE Africa (Berhe and Rothery,1986) were applied for these areas. As we found in Kenya the mafic-ultramafic bodies in Tanzania were originally mapped as intrusives. Although some of these may be intrusives, a large proportion of the mafic-ultramafic rocks contain convincing ophiolite pseudo-stratigraphy. All these

mafic-ultramafic assemblages require remapping.

Two maps are presented (Figures 7.1 and 7.6) which are compiled from various sources: NE Africa (Berhe and Rothery,1986); Somalia (Warden and Horkel,1984); Tanzania (Geological map of Tanganyika,1959); Mozambique (Geological map of Mozambique, 1968; Saachi *et al.*,1984); Madagascar (Hottin, 1972). The reconstruction of Madagascar is adopted from Reeves *et al.* (1987).This reconstruction suggests that the Sol Hamed - Wadi Onib belt could be extended further south to the Nuba ophiolite complex (Steiner,1987) while the Sekerr-Yubdo-Barka ophiolite belt continues further south into the Itiso mafic-ultramafic complex of Tanzania, where pillow lavas are found associated with the ultramafic complex (Shackleton,1986). The Baragoi ophiolite which has been suggested to follow below the Kenyan Rift could be related to the dismembered mafic-ultramafic rocks of the Mpwapwa area of Southern Tanzania (Figure 7.6). In the Mpwapwa area a succession of pyroxenites,plagioclase amphibolites and metabasalts have been observed (Temperley,1938; King,1952).The Uluguru ultramafic complex of Tanzania (Sampson and Wright,1964) which is to the east of the Mpwapwa complex is a meta-anorthositic intrusive body, however several bodies of metapyroxenites and gabbros occur within or near the boundaries of this complex (Sampson and Wright,1964). Few peridotites are found southeast and west of the complex.

The Adola-Moyale belt could be related to the Mtito-Andei (Taita Hills) ophiolites of SE Kenya (Frisch and Pohl,1986). This can be extrapolated to the dismembered mafic ultramafic rocks of the Pare Mts. (Bagnall,1960) and further south to the Morrola mafic-ultramafic rocks where ultrabasics,gabbros and dolerites are reported (Geological map of Mozambique,1968). Prochaska and Pohl (1983) dispute the presence of ophiolitic rocks in the Pare Mts. of Northern Tanzania, however their analysis is based on few samples and secondly their trace element patterns seem to be obtained from cumulate rocks (because they show high Cr values). Cumulate rocks are ineffective for discriminating the presence or absence of ophiolites, and moreover intrusive ultramafic bodies can exist in an ophiolitic complex, which means that the presence of ophiolitic rocks can not be ruled out. A careful study of the geological map of the Pare Mts (Bagnall, 1960) indicates the presence of a sequence of dismembered serpentinites, metapyroxenites (websterite, hypersthenite), metagabbros and amphibolites. The mafic-ultramafics are highly dismembered and scattered making

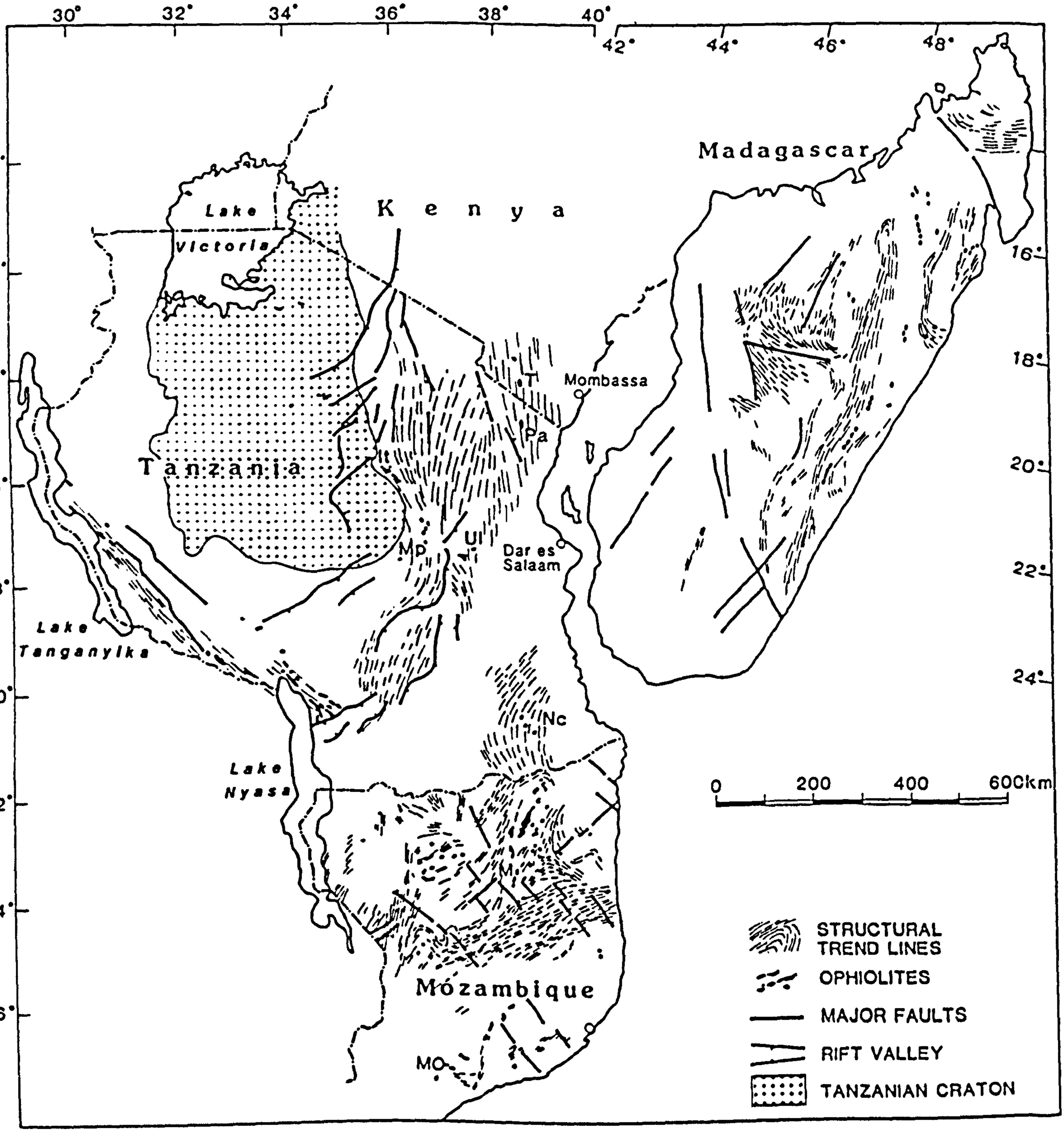

Figure 7.6 Ophiolitic belts of E Africa. Place names are: It - Itiso; Mp - Mpwapwa; Ul - Uluguru; Pa - Pare ; Nc - Nachingwea ; M - Morrola; Mo - Mocuba.

it difficult to carryout an effective geochemical study unless representative samples are collected from a large area. Also the further south one goes the harder it is to differentiate mafic-ultramafic bodies (Andreoli,1984), because there is severe crustal shortening causing complex deformation and thrusting.

In Mozambique, thrusting has been so extensive that it is difficult to use structural trendlines to align the ophiolite belts. However the Mocuba ophiolite (Sacchi *et al.*, 1984) could form part of the Morrola mafic-ultramafic rocks (Figure 7. 6), but may have been thrust from WNW, because Sacchi *et al.* (1984) suggest extensive nappes of granulitic rocks which are rooted 200 km to the WNW.

The Precambrian of Madagascar is dominantly made up of of strongly tectonised and metamorphosed Archaean rocks (Hottin,1972; Vachette,1979). A belt of mafic-ultramafic rocks has been mapped in the NE part of Madagascar trending approximately N-S (Hottin, 1972). The mafic-ultramafic rocks are localised in a zone 5 to 20 km wide which extends for 150 kms in a NW direction and comprise of dunites, harzburgites associated with nickel and chromite deposits, gabbros and amphibolites (Giraud, 1954; Jourde, 1967). This belt is probably ophiolitic as typical ophiolitic assemblages are present and has already been recognised as possibly of ophiolitic origin (Jourde,1967) , although Giraud (1960) considered them as intrusive complexes which included imbricated lenses of amphibolites, ultramafics and basic sills and dykes. The mafic-ultramafic rocks of Andriamena are found particularly associated with the crystalline schists of Vohibory , and there is a preferential development of granitoids which are parallel to the Vohibory and their ages spread from 550 to1500 Ma (Jourde, 1971; Hottin, 1976). If these are indeed ophiolites then they possibly form a suture between two Archaean blocks.

Plate reconstruction of Madagascar into the Lamu embayment in SE Kenya (Reeves *et al.*, 1987) and structural trends indicate that it belongs to the Mozambique belt of Kenya and Somalia. When Madagascar is refitted to the Horn of Africa, these mafic-ultramafic belts could only extend east of the Bur massif of Somalia (Figures 7.1 and 7.6) below the Mesozoic sediments as no mafic-ultramafic rocks have been reported from the Bur region. Northwards it could extend to the the Mait greenstone belt (Figure 7. 1) (Mason and Warden, 1956; Warden and Horkel,1984) where basaltic pillow lavas,tuff and agglomerate are found associated with diorite and overlain by phyllite or

the Abdul Qadr volcanic series of Northern Somalia (Warden and Daniels,1983) where metabasalts,calc alkaline volcanics with immature clastics and ophiolite slices are present. Warden and Daniels (1983) suggest that these mafic-ultramafic rocks were formed by closure of a small island-arc basin.

7.4 SUMMARY AND CONCLUSIONS

A simplified sketchmap showing ophiolite belts and recognisable Archaean rocks of the Precambrian of NE and E Africa are presented (Figure 7.7). The present work shows five major ophiolitic sutures in NE Africa, while plate reconstruction of Africa and Madagascar indicates six ophiolite belts. The ophiolites represent remnants of back-arc basin, supra-subduction zone and a possible suture between two Archaean blocks. The terrain delimited by the Ingessana - Port Sudan suture and the Adola - Moyale ophiolite belts defined in this study (Figure 7.1) represents an area where the crust was accreted from oceanic and island arc material (Berhe and Rothery,1986). Relative age reconstruction across the Shield broadly indicates eastward younging of the ophiolite belts, except for the Egyptian ophiolites which show younger ages.

Crustal shortening in Sudan and Ethiopia is less extensive and hence the ophiolite complexes except the ophiolitic mélange in in the Eastern Desert of Egypt (Shackleton *et al.*,1980), are unlikely to have been displaced by more than a few tens of kilometres from their sites of emplacement and are considered to form sutures. The ophiolite belts swing to the southeast near the Sudan- Kenya border suggesting that the accreting fragments were compressed (with a greater degree of crustal shortening than in the north) against the Tanzanian craton to the west. In central Kenya, Tanzania and Mozambique the sutures of the ophiolite belts should be found west of their present position as extensive east directed napping and thrusting has been observed in central Kenya (this study) and in Mozambique (Saachi *et al.*, 1984).

The geometry of the ophiolite belts can be used to roughly estimate the extent of crustal shortening. Measurements of the extent of ophiolite belts (from 1 to 5, Figure 7.7) across Sudan,

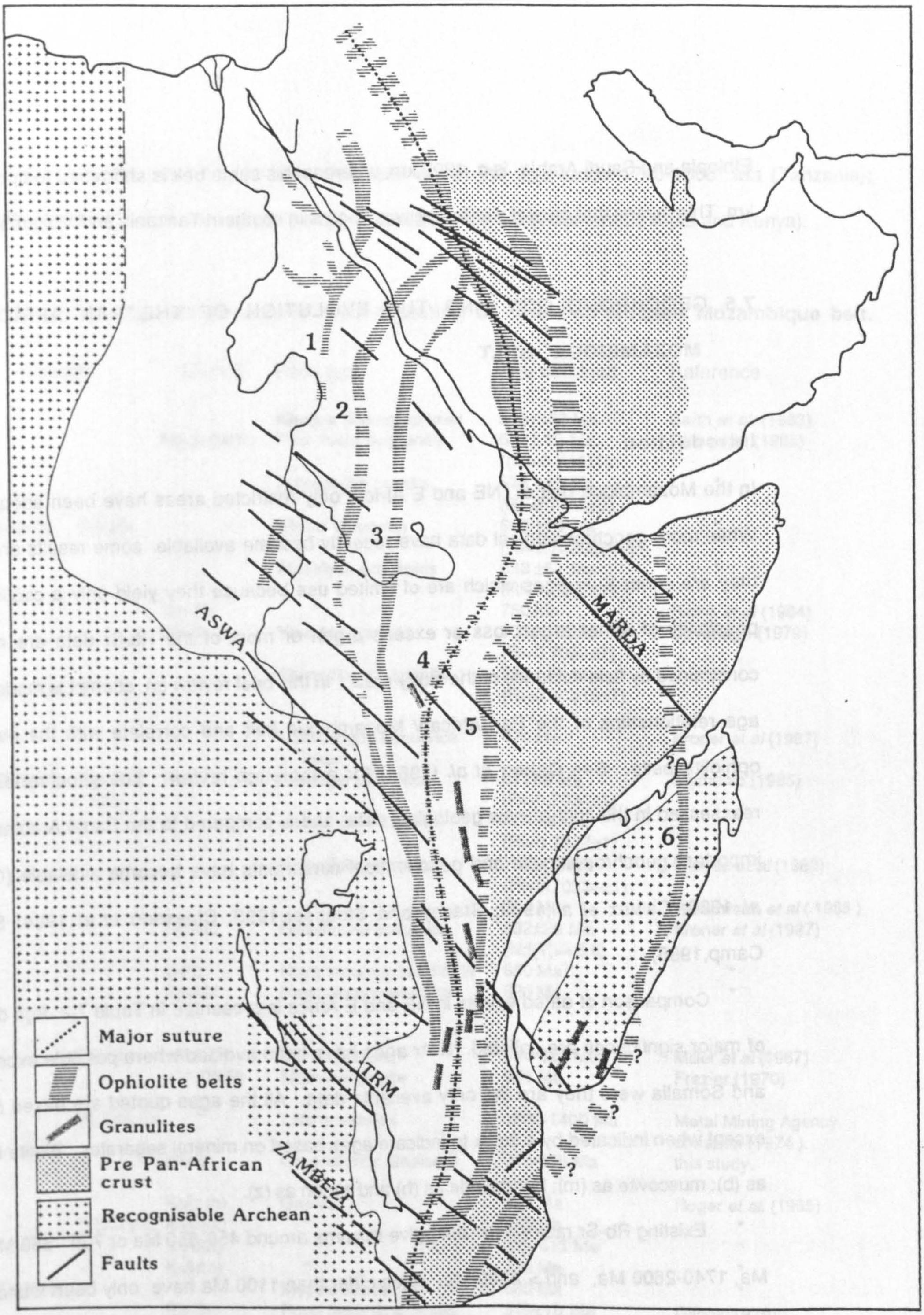

Figure 7.7 Ophiolite Belts in NE and E Africa . Saudi Arabia and Madagascar in pre - drift reconstruction. (1) Sol Hamed Wadi Onib - Nuba (Africa), Jebel al Wask (Arabia); (2) Port Sudan - Qala al Nahal - Ingessana - Moroto (Africa) , Jebel Thurwah (Arabia) ; (3) Barka - Yubdo - Sekerr - Itiso (Africa) ; (4) Baragoi(Turkana) - Mpwapwa (Africa) , Nabitah (Arabia) ; (5) Adola - Moyale - Taita - Pare -? Nachingwea - Morrola (Africa), Idsas (Arabia); (6) Madagascar - ? Mait (Africa).

Ethiopia and Saudi Arabia is c. 1200 km, whereas this same belt is shortened to approximately 500 km. This means that crustal shortening was c. 40% in southern Tanzania and Mozambique.

7.5 GEOCHRONOLOGY AND THE EVOLUTION OF THE PAN AFRICAN-MOZAMBIQUE BELT

Introduction

In the Mozambique belt of NE and E Africa, only restricted areas have been adequately studied. While more geochronological data have recently become available some results are unreliable as they are either K-Ar ages which are of limited use because they yield only a cooling age or the possibility of either argon loss or excess argon or most of the Rb/Sr data are not adequately constrained by field evidence of the study area . In this brief review an attempt is made to discuss the age relationships of the Pan-African/ Mozambique belt and correlate with the evolution of the ophiolite belts. See Cahen *et al.* (1984) for a thorough review. The geochronological data is reassessed in the light of new geological data, and is compared to the Saudi Arabian shield where important geochronological and geochemical constraints have become available (Greenwood *et al.*,1980; Calvez *et al.*,1983; Stacey and Stoesser,1983; Claesson *et al.*,1984; Stoesser and Camp,1985).

Comparison of dated events in NE and E Africa is presented in Table 7.2. Age determinations of major signficance are collated. K-Ar ages have been avoided where possible except in Ethiopia and Somalia were they are the only available data. All the ages quoted are based on whole rock except when indicated by a suffix to indicate ages based on mineral separates. Biotite is represented as (b); muscovite as (m); hornblende as (h) and zircon as (z).

Existing Rb-Sr radiometric data give maxima around 450-650 Ma or 700 - 850 Ma, 950 - 1100 Ma, 1740-2600 Ma, and > 2800 Ma. Ages older than 1100 Ma have only been found in Tanzania, Mozambique and Madagascar (Table 7.2). If the ages are grouped by rock types (excluding Madagascar) the post-tectonic granitoids and alkaline ring complexes fall between 660-480 Ma, syntectonic granitoids c. 725-580 Ma, arc-related batholith and plutons 900-800 Ma, whereas arc

related volcanics are 800-670 Ma. Gneisses are in the age range 1740-2600 Ma (Tanzania); 830-740 Ma (Ethiopia, Kenya and Tanzania) and 680-600 Ma (Southern Ethiopia and Kenya).

Table 7.2 Age constraints in the evolution of the Pan African- Mozambique belt.

Country		Method	Rock type	Age obtained	Reference
			Alkaline ring complexes	573 -157 Ma	Barth *et al.* (1983)
		Rb-Sr (W.R)	Post- tectonic granite	549 ±12 Ma *(Ri=0.704±1)	Ries *et al.* (1985)
			Syntectonic granite	678 ±43 Ma (Ri=0.7028±1)	"
SUDAN	Bayuda		Elkoro Volcanics	800 ±83 Ma (Ri=0.70299±62)	"
			Abu Harik granitoids	898 ±51 Ma (Ri=0.7025±1)	"
		Sm-Nd	" "	750 Ma	Harris *et al* (1984)
		Rb-Sr	Younger granites	633 ±19 Ma (Ri=0.7032±7)	Cavanagh (1979)
			Granodiorites, granite	686 ±18 Ma (Ri=0.70315±7)	"
			Volcanic-arc sequence in Tokar	670 Ma	Kroner *et al* (1987)
SUDAN	Red Sea Hills	Rb-Sr	Homogar volcanics	671±8 Ma (Ri=0.7034±1)	Klemenic (1985)
			Kadaweb volcanics	723 ±6 Ma (Ri=0.7027±1)	"
			Naferdieb volcanics	712±58 Ma (Ri=0.70234±1)	Fitches *et al* (1983)
		"	"	714 Ma	Reischman *et al* (1985)
		Sm-Nd	Gebeitmine volcanics	832±26 Ma (Nd(T)=+6.8)	Kroner *et al* (1987)
		U-Pb	Haya terrain granodiorite	850 Ma	"
		Sm-Nd	Haya terrain volcanics	920 Ma	"
Eritrea		K-Ar(b)	Mareb granite	690-627 Ma	Miller *et al* (1967)
		" (W.R)	Massawa granite	988 Ma	Frazier (1970)
W. Ethiopia		"	Late granitoids	1380-1400 Ma	Metal Mining Agency of Japan (1974).
		Rb-Sr	Granodioritic Gneisses	816-806 Ma	this study.
		K-Ar (b)	Gneiss	505 Ma	Roger *et al.* (1965)
S.Ethiopia		K-Ar(m)	"	490 Ma	"
		K-Ar(h)	"	625-615 Ma	"
		K-Ar(b)	"	739 Ma	"
ETHIOPIA		"	Moyale diorite	680 Ma	"
		Rb-Sr	Post- tectonic granites	515±10 Ma (Ri=0.7062±91)	Gilboy(1970)
				480±50 Ma (Ri=0.708±1)	Chater(1971)
		"	Syntectonic granite	680±30 Ma (Ri=0.7082±24)	Gilboy (1970)

S.Ethiopia		"	Gneiss	630 ±50 Ma (Ri=0.7049±5)	"
		"	"	680±30 Ma (Ri=0.703±2)	Chater (1971)
		"	Phyllite	620 ±20 Ma (Ri=0.7065±3)	"
		"	"	1030 ±40 Ma (Ri=0.703±1)	"
		Rb-Sr(b)	Migmatite (Bur area)	495-485 Ma	Borsi (1965)
		Rb-Sr(W.R)	"	604 ±21 Ma	"
SOMALIA		K-Ar(b)	Post- tectonic granite	500 Ma	D'Amico *et al* (1981)
		"	Gneiss	600 Ma	"
		"	Gneiss	740 Ma	"
		Rb-Sr	Arc-related volcanics	663 ±49 Ma (Ri=0.7035±1)	Ries *et al* (in prep)
		"	Metasediments	584 ±25 Ma (Ri=0.7042±2)	"
		Sm-Nd	"	1150-1100 Ma	Harris *et al* (1984)
	NW	Rb-Sr	Syntectonic plutons	593 ±50 Ma (Ri=0.7072)	Ries *et al* (in prep)
		Sm-Nd	"	1950 Ma	Harries *et al* (1984)
KENYA		Rb-Sr	Amphibolite	982±40 Ma (Ri=0.7029±2)	Ries *et al* (in prep)
		Sm-Nd	"	1000 Ma	Harris *et al* (1984)
	Central	Rb-Sr	Granitic gneiss	766 ±29 Ma (Ri=0.7041±11)	Shibata & Suwa (1979)
	SE	"	Gneisses	827±55 Ma (Ri=0.7047±6)	Shibata (1975)
		Rb-Sr	Granulites	908±38 Ma (Ri=0.7056±7)	Spooner *et al* (1970)
		U-Pb (z)	Furua granulite	652 ±10 Ma	Coolen *et al* (1982)
		"	Wami granulites	715 Ma	Maboko *et al* (1985)
TANZANIA		Rb-Sr	Usagaran gneisses	1920 Ma	Wendt *et al* (1972) Gabert &Wendt (1974)
		"	Usagaran gneiss	589 ±70 Ma (Ri=0.7194	Priem *et al* (1979)
		"	Usagaran granites	1747 ±145 Ma (Ri=0.704±3)	"
		U-Pb(z)	Usagaran gneiss	2566±9 Ma	Maboko *et al* (1985)
		Rb-Sr	Post- tectonic granite	500 Ma (Ri=0.707-.712)	Saachi *et al* (1984)
		"	Syntectonic granite	1100 Ma (Ri=0.7027)	"
		"	Granulite	1200 Ma (Ri=0.706)	"
MOZAMBIQUE		"	"	827±45 Ma (Ri=0.7150±32)	Araujo (1976)
		"	Quartzite(assoc. with ophiolite).	950 ±40 Ma (Ri=0.709)	Saachi *et al* (1984)

	"	Paragneisses	1000 Ma (Ri= 0.713)	"
	"	Gneiss-migmatite	1050-1000 Ma (Ri=0.7028)	"
	"	Gneiss	1391±88 Ma (Ri=0.7070±12)	Araujo (1976)
		"	1080±53 Ma (Ri=0.7072±16)	"
Rb-Sr		Post- tectonic granitoids	706±22 Ma (Ri=0.7048±5)	Hottin (1976)
		"	546±13 Ma (Ri=0.7116±5)	Vachette (1979)
MADAGASCAR	"	Schists and gneisses	1367±111 Ma (Ri=0.7011±4)	Vachette (1979)
		"	740 Ma	"
	"	Gneisses	2882±170 Ma	"
	"	"	2505 ±56 Ma (Ri=0.7145±5)	Vachette(1979)
	"	Granitoids	3190 ±244 Ma (Ri=0.7009±25)	Hottin (1976)

* R_i, indicates initial ratios $^{87}Sr/^{86}Sr$.

The oldest Rb-Sr ages so far obtained in Sudan are the Abu Hariik granitoids 898±51 Ma (Ries *et al.*, 1985), and in Ethiopia a Rb-Sr age of 1030±40 Ma was obtained for phyllites within the upper part of the Precambrian of southern Ethiopia (Chater, 1971). K-Ar ages of 1380-1400 Ma for late tectonic granitoids intruding the western volcanic Belt of Ethiopia (Metal Mining Agency of Japan, 1974) are the oldest ages so far obtained. However the K-Ar age of 1380-1400 Ma of a granitoid in W Ethiopia is based on one sample, and this age does not correspond to any ages of post- tectonic granitoids in NE Africa whereas the age of the phyllites may be reliable as these are weakly metamorphosed rocks, and the isochron which is based on 11 samples shows a good fit.

The only reliable Rb Sr whole rock isochron in central Kenya is 766 ±29Ma (Shibata and Suwa, 1979) with a low initial ratio (0.7041), while further south Spooner *et al.* (1970) obtained two Rb/Sr whole rock ages of 936 ±63 Ma and 731±8 Ma with low initial ratios of 0.7056-0.7064. These preliminary isochrons either reflect the main Mozambiquian metamorphism or represent mixed ages due to the influence of this metamorphism on pre-Mozambiquian rocks (Spooner *et al.*,1970). The slightly elevated $^{87}Sr/^{86}Sr$ initial ratios may imply a mantle source with a crustal component. U-Pb zircon age on the Furua granulite complex in S Tanzania gives a lower intercept of 650 Ma and an upper intercept of 2-3 Ga (Coolen *et al.*, 1982) which indicates evidence for older crustal material.

Recent work in the Furua granulite complex (S. Tanzania) and Wami River granulites, SE Tanzania (Andriessen *et al*,, 1985; Maboko *et al.*, 1985) shows that the former has an age of 652 Ma, and the latter 715 Ma. Hence contrary to the prevailing opinion that the granulitic complexes in the Mozambique belt are relicts of older (possibly Archaean) metamorphism, this age relates the granulite facies metamorphism to the Pan-African thermo-tectonic episode. In Malawi, Mozambique and Madagascar a period of metamorphism and migmatisation has been dated at about 750 ±50 Ma (Cahen *et al.*, 1984) which might be related to the phase of granulite-facies metamorphism in the Furua and Wami River.

This conclusion is not unequivocal as zircon ages can be reset during granulite facies metamorphism (P. Van Calsteren, pers. comm). However three of the granulites contain minor amounts of an inherited older zircon component which is > 1600 Ma (Maboko *et al.*, 1985). In SE Tanzania the Mozambique belt consists predominantly of the Usagaran gneisses which has been dated c .1950 (Wendt *et al.*, 1972; Priem *et al.*, 1979) and U/Pb zircon age of biotite gneisses gives 2566 Ma (Maboko *et al.*, 1985). In Mozambique, older gneisses are found c. 1391-1080 Ma (Araujo, 1976) while Saachi *et al.* (1984) dated paragneisses c. 1000 Ma with relatively high intial ratios (0.713) and all the dated post-tectonic granitoids have high intial ratios (see Table 7.2). The high $^{87}Sr/^{86}Sr$ initial ratios imply remelting of older continental crust. Araujo (1976) stated that the rocks in N Mozambique are older than those linked to the Mozambique orogeny further north, which is charaterised by Rb/Sr and K/Ar ages in the 650-485 Ma range (Cahen *et al.*, 1984).

In summary, the Mozambique belt yields younger ages in Ethiopia, Kenya, and N Tanzania, while older ages are present in SE Tanzania and N Mozambique. However rocks of Pan-African ages have been described in Kenya, Tanzania, and Madagascar. An orogenic event c.845 Ma is considered as the most important tectono-thermal event in the Mozambique belt (Cahen *et al.*,1984) while Rb-Sr and K-Ar biotite ages extending from 650-450 Ma are very widespread in NE and E Africa. The "Pan African" Orogeny (Kennedy,1964) is a tectono-metamorphic event supposedly dated at 550-650 Ma, but these are now known to be cooling ages. The range of the thermal event is now controversial. Recent workers (Kroner, 1979a,1979b ; Gass, 1981,1982; Delfour,1980) have proposed that the term Pan-African should be expanded to include the period from 1100 to 500 Ma.

However since there are other belts, with different sequences and similar time spans across Africa which were affected by this thermotectonic event, various authors (Almond,1983; Warden and Horkel,1984; Price,1984) argue that the Pan-African episode should be restricted to the original defintion of orogeny which is c. 500 600 Ma (Kennedy, 1964). In this study the term Pan-African is extended to include 1100 to 500 Ma , however the c. 500 Ma orogeny is considered as the cooling age related to the Pan-African episode of metamorphism and deformation. The term Pan-African / Mozambique belt is used because since at least 1100 Ma both belts have experienced a similar tectonic history.

The evidence so far available is inadequate to disprove the existence of older basement flanking the ophiolite belts in Kenya and Tanzania. Firstly, no adequate geochronological data is available in NE and E Africa and secondly, age determinations for Saudi Arabia, Ethiopia and Somalia according to rock type has shown that granites are the most sampled while gneisses and mafic-ultramafic rocks have recieved low priority (Warden,1981). Metavolcanic rocks are completely unrepresented, while metasedimentary rocks and paragneisses are under- represented. It is suggested that some of these rocks may yield older ages. Also the techniques employed have not included Sm Nd, U-Pb and Pb-Pb determinations, which could yield maximum ages.

At the Western margin of the Mozambique belt of Kenya the Mozambiquian shelf facies sediments (c. 1100 Ma old quartzites - limestones and pelites) are thought to unconformably overlie Archaean greenstone belts intruded by granodiorites (Sanders, 1965). These sediments appear to be the same as the Konse,Tanzania which according to Wendt *et al.* (1972) and Gabert and Wendt (1974) is >1850Ma. Sediments of similar facies continue right across the Mozambique belt, which is assumed to be underlain by older rocks (possibly Archaean ,Shackleton, 1986). However no one has yet demonstrated complete stratigraphic continuity in East Africa across the Pan-African belt from craton to craton.

The east-west Nyanzian and Kavirondian folds are truncated by the north-south Mozambique front in Tanzania and Western Kenya (Sanders, 1965). Shackleton (1976) suggests that the structures truncated must have continued because in many cases younger fold belts have been superimposed on older ones. However it is clear that the whole Mozambique belt is not simply

comprised of deformed and metamorphosed Nyanzian and Kavirondian rocks.

Most authors (Clifford,1968; Wendt *et al.*,1972; Kazmin *et al.*,1978; Cahen *et al.*,1984) consider that the available ages of the Mozambique belt have been reset by the Pan -African thermotectonic event. It is considered that in Southern Tanzania the young ages of the Mozambique gneisses reflects a metamorphic imprint of the Usagaran - Ubendian assemblage dated at c.1950 Ma (Wendt *et al.*, 1972) near the margin of the Tanzanian shield but has been reset to give ages of about 500 Ma. The fact that the Rb-Sr ages of gneisses in Taita Hills (SE Kenya) give a whole rock age of 827 ±55 Ma (Shibata, 1975), and the K-Ar ages of biotite and hornblende give 498 Ma and 519 Ma respectively indicates slow cooling with minerals defining closure temperatures at about 500 Ma. The fact that the Rb-Sr data do not define a unique isochron is further evidence that there occurred some disturbance in the Rb-Sr whole rock system at a later date. However the 827 Ma old rocks have low intial ratios of 0.7047, suggesting a mantle origin and not remobilised older crust. It is possible, that during complete rehomogenisation the $^{87}Sr/^{86}Sr$ would also be affected. The same orogenic events that affected the Mozambique belt in Kenya, has also affected the Usagaran in SE Tanzania and Mozambique, but older ages of c.1300-2000 Ma have been obtained in SE Tanzania and Mozambique. Thus, either older rocks similar to those of SE Tanzania and Mozambique have not been found because of inadequate geochronological data, or the gneisses of the Mozambique belt in S Ethiopia, Kenya and N Tanzania could indicate primary emplacement and or age of metamorphism.

7.6 THE GRANITE EVIDENCE

Granitoid rocks are unevenly distributed in the Pan-African / Mozambique belt. Granitoids form about 60 percent of the crystalline basement in the Arabian shield, NE Sudan, and NE Ethiopia, decreasing to about 30 percent in W. Ethiopia, however in S Ethiopia and Kenya the percentage decreases from 20 to about 10 percent of the basement outcrop. Since understanding the geochemistry of granitoids can constrain the sources of the voluminous intrusions in NE Africa and their tectonic setting, several granitoid rocks of W and S Ethiopia, central and NE Kenya were investigated.

Combining major, and trace element data three geochemically distinct granitoid types have been identified. Three granitoid types, distinguished are crustal melt granitoids, calc - alkaline granitoids and within-plate granitoids. The principal characteristics of each granitoid types by area are summarised in table 7. 3.

Table 7.3 Summary of the geochemical characteristics of granitoids from Ethiopia and Kenya.

AREA	ROCK NAME	MAJOR ELEMENTS	TRACE ELEMENTS	Rb/Sr	Nb/Rb	POSSIBLE SOURCE ORIGIN
Geba	Granodiorite /Adamellite	Metaluminous	low Rb/Sr low HFS	0.08- 1.50	0.04- 0.30	Volcanic arc
Birbir	Granodiorite	"	Low Rb/Sr low HFS	0.02- 0.21	0.07- 0.5	Volcanic arc
	Syntectonic granite	"	High Rb,Th,Ta,Nb low Hf,Zr,Sm,Y,Yb	97.67*	0.2	Within-plate
	Syntectonic quartz-diorite	Metaluminous	low Rb,Th low HFS	0.003*	1.5	Volcanic arc
	Post- tectonic granite (SB205)	"	Elevated Rb,Ba low HFS	0.71*	0.1	"
	Post- tectonic granite(MT404)	Peraluminous	High Rb High HFS	1.54*	0.15	Within-plate
Gariboro	Gneissose granite	"	High Y low Ta,Nb,Zr,Hf low REE	0.07- 3.53	0.08- 0.17	Crustal melt
Godoloka	Granite	Metaluminous	High HFS High REE	0.90- 1.48	0.29- 0.39	Within- plate
Kufole	Granite	Peraluminous	High Rb,TH,Ta,Nb low Sr,Hf,Zr,Sm REE enriched	2.50- 3.59	0.15- 0.46	Within-plate
Fugugo	Monzonite	Metaluminous	Moderately elevated Rb,Ba low HFS	0.07- 0.12	0.16- 0.27	Volcanic arc
Moyale	Granodiorite	Peraluminous	low Rb/Sr low HFS	0.08- 0.30	0.08- 0.11	Volcanic arc

Adadi Jolle	Granitic gneiss	"	High Nb,Zr,Hf,Y High REE	1.17- 6.52	0.19- 0.76	Within- plate
Luwamara	Granite	"	High Rb/Sr low HFS	0.10- 1.09	0.08- 0.03	Crustal melt
Sartim	Granite	"	High Rb low HFS	0.05- 0.09	0.10- 0.04	Volcanic arc
Ol'Doinyo Wassin	Granodiorite	"	Low Rb/Sr low HFS	0.01- 0.05	0.05- 0.10	Volcanic arc
Sabatchi	Granitic gneiss(I)	Metaluminous	Low Zr,Y,Nb	0.02- 0.07	0.16- 0.83	Volcanic arc
Sabatchi	Granitic gneiss(II)	Peraluminous	Elevated Rb low Nb,Y,Zr	0.07- 0.34	0.0763- 0.108	Crustal melt

The asterisk (*) indicates values obtained from one sample.

Major element study indicates that the western Ethiopian granitoids are dominantly metaluminous, while in S Ethiopia, NE Kenya and Central Kenya granitoids are dominantly peraluminous. Crustal melt granitoids are characterized by high alumina contents, and low HFS element abundances while calc-alkaline granitoids also have low HFS element abundances and are LREE enriched. Within-plate granitoids are characterised by elevated HFS elements, low CaO and relatively low alumina contents. Although the primary aim of this study is to establish the tectonic setting of the granitoids, it is difficult to differentiate the post-collision and volcanic arc granites which can only be distinguished on the basis of initial $^{87}Sr/Sr^{86}$ ratio (Pearce *et al.*, 1984a) which is unavailable at present.

All the granitoids studied either plot in the volcanic arc/post-collision field or the within -plate field, the only exception being the Luwamara granite (Figure 2.31) and the syntectonic granitoid which overlap into the syn-collision field (Figures 4.18). Pearce *et al.* (1984a) state that the lower boundary for the syn-collision field is arbitrary, and that only granites which have been subjected to Rb-rich volatile fluxing will plot in this field and that if the source is low in Rb or volatiles are not present then syn-collision granites may plot below the line. Hence the Luwamara granites may actually be syn-collision granites as trace element ratio (Nb/Rb=0.08-0.03) indicate that it could be a crustal melt.

Rb/Sr, and Nb/Rb ratios for all the granitoids are shown in Table 7.3. The within-plate granitoids

which are effectively discriminated by the discrimant diagrams of Pearce *et al* (1984a), show Rb/Sr ratios greater than about 1 and Nb/Rb ratios greater than about 0.15 (Figure 3.29) while McDermott (1986) has used Nb/Rb > 0.1 for discriminating within-plate granitoids in the Damara belt of Namibia.

It is difficult to constrain the possible source of within-plate granitoids, while the possible source of calc-alkaline and crustal melt granitoids can be ascertained more easily using geological constraints. In this study calc-alkaline granitoids (Figure 3.23a) have Rb/Sr ratios lower than 0.2 (Figure 3.29), while the crustal-melt granitoids have low Nb/Rb ratios (< 0.15). In NE Kenya the Kufole granite, and the Adadi Jolle granitic gneiss plot in the within-plate field, however Rb/Zr, Rb/Sr and Nb/Rb ratios suggest that the Kufole could be a crustaly derived granitoid (Figure 3.28) or could possibly be of mixed source (mixed mantle and crust), while the Fugugo and Moyale show calc-alkaline affinity.

The granitoids which are believed to be crustal melts i.e. the Gariboro granitic gneisses (S Ethiopia) and the Luwamara granites (N Kenya) do not fall on the crustal melt field as defined by Pearce *et al.*, (1984a) (Figure 3.32a and 3.32b), because the protoliths of these rocks may have had low Rb values and hence after remelting the Rb values could still be low so that it plots in the volcanic arc field. However combining the Nb/Sr against Rb/Sr plot (Figure 3.29) and trace element diagram (Figure 3.26c) it was possible to suggest its crustal melt characteristic. Calc-alkaline rocks predominate in W.Ethiopia, whereas the proportion of crustal melts appear to increase going further south in S. Ethiopia/NE Kenya and central Kenya. Although it is difficult to ascertain the volumetric proportions of the granitoids at this stage, diorites form about 10 percent of Precambrian outcrop in NE Sudan (see Figure 5.9) while further south diorites are almost insignificant. Only in NE Sudan, W.Ethiopia and S. Arabia do diorites feature prominently.

Having demonstrated the presence of volcanic arc and within-plate granites in the Pan-African/ Mozambique belt, independent constraints are required on the timing of melt extraction from the mantle (e.g. Nd model ages), otherwise the tectonic setting information may relate to previous orogenies. Tectonic discrimination diagrams have severe shortcomings due to trace element variations as a result of fractional crystallisation, volatile fluxing and heterogenous sources. Further more minor phases can control trace element variations in granitoids which would cause

misclassification in discriminant diagrams.

The rarity of granite plutons in Kenya and Tanzania when compared with Egypt, Sudan and Ethiopia is considered to indicate that the former represents deeper levels of the crust, where high-temperature metamorphic assemblages and gneisses are prevalent (Shackleton, 1976). However the lack of extensive calc-alkaline volcanic rocks, could simply reflect relatively narrow oceans and insufficient subduction of oceanic or perhaps lower continental crust to produce large quantities of calc-alkaline melts.

The widespread occurrence of migmatite-gneiss complexes, granulites (Figure 7.7) and the greater amount of crustal melt granitoids suggest a continent-continent collision model (Shackleton, 1986; Maboko, *et al.*,1985), which would cause crustal thickening, increase of geoisotherms which would cause melting of crustal material.

7.7 STRUCTURAL EVIDENCE

The study of structural trends in NE and E Africa shows that the general trend is N-S to NE-SW in Sudan, N-S, to E-W in W Ethiopia while in S Sudan, SW Ethiopia and Kenya it is generally NW-SE. The NW structural trends were explained as a consequence of shearing along northwesterly trending faults. (Berhe and Rothery, 1986; Berhe,1987). The structural trends swing to the southeast near the Sudan-Kenya border suggesting that the accreting island-arcs were compressed against the Tanzanian craton to the west. This tectonism caused recumbent folds and major thrusts similar to those observed in the Sabatchi Hills area, Central Kenya (Plate 7.1). However, regional variations in the orientation of the compressional regimes producing the different fold and structural trends may be explained in terms of a sequence of plate collisions. The sequence of deformation events are E-W which were subsequently refolded into gently plunging folds trending north to northeast. A third phase (D_3) of deformation overprinted the earlier structures by refolding them into northwesterly trending folds. This is based on the cross-cutting relationships of the folds. The oldest deformation phase is characterised by E-W trending isoclinal folds. This phase has been recognised in W Ethiopia (Kazmin *et al.*,1979a; Berhe,1981), in S Ethiopia (Chater,1971) and in the Baragoi area, N Kenya

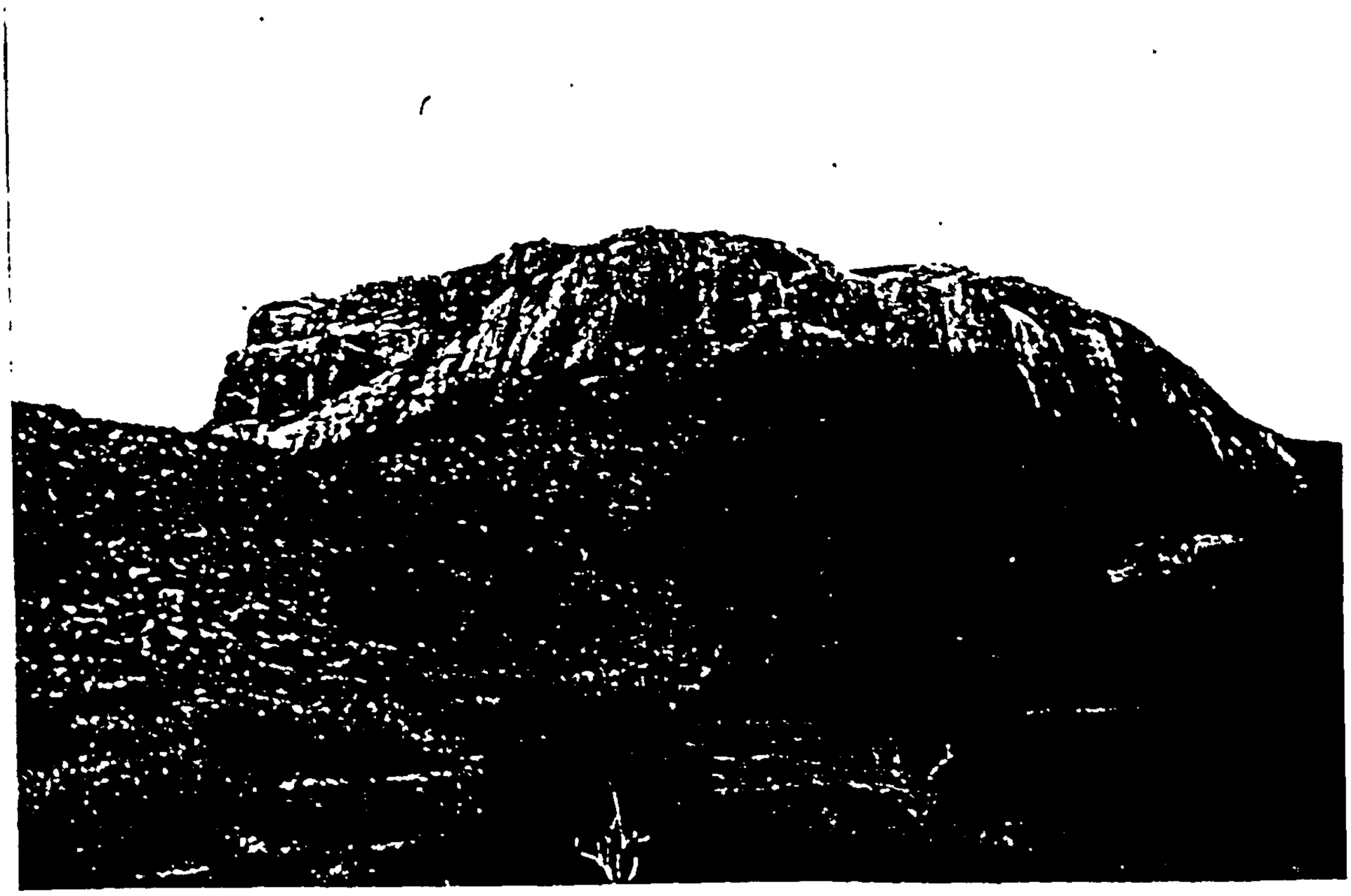

Plate 7.1 Thrust sheets in the Sabatchi Hills, Central Kenya.

(Charlesly *et al.*,1984). The E-W trending structures however are not of Archaean age as suggested by Kazmin *et al.* (1978) and Vail (1976), but are of late Proterozoic age, and appear to have evolved separately. Nevertheless it seems that the sequence of deformation has followed a similar pattern in the different areas.

Major crustal lineaments identified in NE and E Africa are N-S, NE-SW, and NW-SE. Since most fault intersections show offsets their relative ages can be deciphered.

An interpretation of NE Sudan-Eritrea data reveals faults trending 015-025°, 055-065°, 145-155° and 165-175°. There are also dykes trending 090°. The 165-175° trending Barka lineament which forms a boundary between regions of contrasting fault patterns is by far the longest and has been considered a master fault. The 165-175° trending master fault and the secondary faults which trend 055-065° are observed to displace dextrally the 145° trending faults. The 145° trending lineaments are major late Proterozoic features that were reactivated during the early stages of rifting in the Red Sea. A principal compressive stress oriented at about 155° would generate the 175° trending Barka fault and the 145° trending faults. During this deformation the anomalous stress concentrations along the Barka lineament propagated along divergent splay faults trending NE-SW to N-S. A reorientation of the principal compressive stress oriented along E-W would cause regional folds trending N-S to NE-SW. Increasing deformation causes N-S extension and dyke emplacement along E-W axis (see section 6.7).

In W Ethiopia edge enhancement filtering, both non-directional and directional helped detect many subtle structural features. An interpretation of these data reveals: a dominant set of faults trending 135±10° and two subsidiary sets striking 010± 10° and 065±10°. The 135° and 010° faults are a conjugate set resulting from a horizontal compressive stress oriented at about 165°, correlated with D_1 episode of deformation. A change of stress regime with the onset of the D_2 phase east-west compression caused the 135° faults to be reactivted concomitantly with the generation of the 065° first order wrench faults (Berhe and Rothery,1986). Although the directional frequency of the 010° faults is limited their cumulative length is very significant.

In SE Ethiopia three major fault trends are recognised : NE (045°), E-W (090°) and NW-SE (150°). The NE-SW and the E-W faults form the escarpments of the Ethiopian rift while the NW-SE

trending fault zones cause offsets of the rift margins and continue for hundreds of kilometres to Somalia. The northwesterly faults have long histories dating back at least from the Palaeozoic-Jurassic to the Tertiary.The northwesterly shear zones are sinistral and played a major role in the late stage evolution of the Pan-African, and are thought to have controlled the initiation of the Red Sea (Berhe,1986).

Hence it is suggested that there are three kinematic regimes in NE and E Africa: (i) NE Sudan-Eritrea, (ii) E Sudan - W Ethiopia, and (iii) S Ethiopia - Kenya. Since the overall pattern of deformation for each regime is intrinsically different, local deviations from regional kinematic trends will tend to develop at the boundaries between regimes as deformation progresses.The three kinematic regimes are a regional - scale phenomena that cannot be attributed to unique local rotations.

In conclusion this study shows that the major lineaments identified in the Horn of Africa are 010 ± 10° , 055-065° and 145-165°. Two major deformation mechanisms most likely controlled the growth of the wrench faults. It also indicates that the major folds were developed contemporaneously with shearing deformation. The earliest conjugate fractures trend N-S and NW-SE trending while the later deformation reactivated NW-SE trending lineaments, and caused NE-SW lineaments. These lineaments have extended histories from the late Proterozoic to the Tertiary.

The present study supports an oblique collision of the accreting arc terranes as suggested by Shackleton and Ries (1984). The D_1 compressive stress was oriented NNW-SSE while the D_2 compressive stress changes from WNW in W. Ethiopia, to E-W in NE Sudan-Eritrea area (Figure 6.7). The present analysis demonstrated that major crustal shortening occurred across the wrench fault zones and was particularly intense in NE Sudan-Eritrea, and S Ethiopia. It is suggested that there was oblique collision from the southeast causing stacking of crustal blocks along NW trending faults. The origin of these transcurrent shear zones could have been the oblique collision of the accreting arc terranes against the rigid African craton. In the southeast this would have been by westward movement of Madagascar (this study) and in the east by westward movement by the Ar Rayn microcontinent of the eastern Arabian Shield (Stoesser *et al.*,1984).

7.8 A MODEL FOR THE PAN AFRICAN - MOZAMBIQUE BELT

A simplified model is proposed which takes into account the following key observations:-

1. Presence of ophiolites and ophiolitic sutures.
2. The lithological differences between the Mozambique Belt and the Arabian-Nubian Shield.
3. The presence of voluminous arkosic - clastic - quartzite sequences within the Mozambique belt. Such sediments suggest the proximity of continental source rocks.
4. The contrast in type of magmatism I.e the extensive development of granitoid plutons in Saudi Arabia, Egypt, Sudan and Ethiopia, and their rarity in Kenya, and Tanzania.
5. The increase in the proportion of crustal melt granitoids in the southern part of the Mozambique belt.
6. The existence of significant low $^{87}Sr/^{86}Sr$ initial ratios in Sudan, Ethiopia and Kenya, increasing of initial ratios in SE Tanzania (Priem *et al.*, 1979) and Mozambique (Araujo,1976; Saachi *et al.*,1984).
7. The increase of metamorphic grade further south, which is represented by the existence of migmatite - gneiss complexes and the presence of mafic-ultramafic rocks which have reached the upper amphibolite facies grade (this study).
8. The existence of relict E-W structures in the gneisses of W and S Ethiopia, that have been reworked (Kazmin *et al.*,1979a; Berhe,1981).
9. The existence of northwest trending shear zones in Saudi Arabia, Sudan, S Ethiopia, Kenya and Uganda, where extensive mylonitisation and substantial transcurrent dislocation has occurred. A regional pattern of such lineaments is recognised.
10. Palaeomagnetic constraints which preclude the existence of an oceanic basin with a width in excess of 1000 km (Piper *et al.*, 1973). Later work demonstrates wide oceans between E and W Gondwanaland (McWilliams,1980).
11. The presence of Archaean crust in Madagascar (Hottin,1976; Vachette,1979).

Three stages are distinguished in the evolution of the Pan-African /Mozambique belt : an early stage

of rifting followed by a phase of subduction and island arc accretion, followed by continent-continent collision. The early rifting stage is critical to the model for the following reasons: 1) to account for early development and deposition of passive margin shelf sediments in the Mozambique belt. 2) To account for the early Proterozoic to Archaean rocks in eastern part of the Saudi Arabian Shield and Madagascar. The subduction - island - arc accretion stage explains the existence of the ophiolite belts while continent - continent - collision stage is critical in explaining the nappe- types fold and thrusts that occur on a regional scale in the Mozambique belt (Kazmin *et al.*, 1978; Maboko *et al*,. 1985; Shackleton, 1986; Saachi *et al.*,1986; this study) and the increase of crustal melt granitoids from Ethiopia to the Mozambique belt of southern Kenya.

A simplified sketch map showing ophiolite belts and Archaean cratons and a simplified cross sectional model of the Precambrian of NE and E Africa are presented (Figures 7.7 and 7.8). The model proposed is different from the model proposed by Kazmin (1976) which suggests a transition from a wide zone with oceanic crust to a series of narrower rifts with attenuated continental crust in the south, but involves total separation of the continental fragments by oceanic crust . However the ocean is considered to have been narrower further south in Tanzania and Mozambique. This model is constrained further by palaeomagnetic evidence (McWilliams,1980) which indicates a large misfit betwwen East and West Gondwana and shows that there must have been at least one large ocean between them.

The recognition of older crustal terrains (Afif terrain) (Camp. 1984; Stoesser and Camp, 1985) and the implausiby high juvenile crust - generation rates implied by the simple accretion models (Reymer and Schubert, 1984) and the lack of modern analogues where subparallel arc-arc plate boundaries are an average of <200 km apart, led Stoesser and Camp (1985) to consider the Arabian Afif terrain as a detached fragment of the African continent. They infer a period of rifting c. 1200-950 Ma.

Widespread rifting accompanied the break up of the Gondwana super continent 1200 - 1000 Ma ago (Windley, 1979). The opening of this rift could be dated c.1165 Ma, the age obtained for metabasalts in Saudi Arabia (Fleck *et al.*, 1979), which are the oldest recorded so far. DeWit and Chewaka (1981) had earlier suggested that rifting had taken place c.1200, and compared the

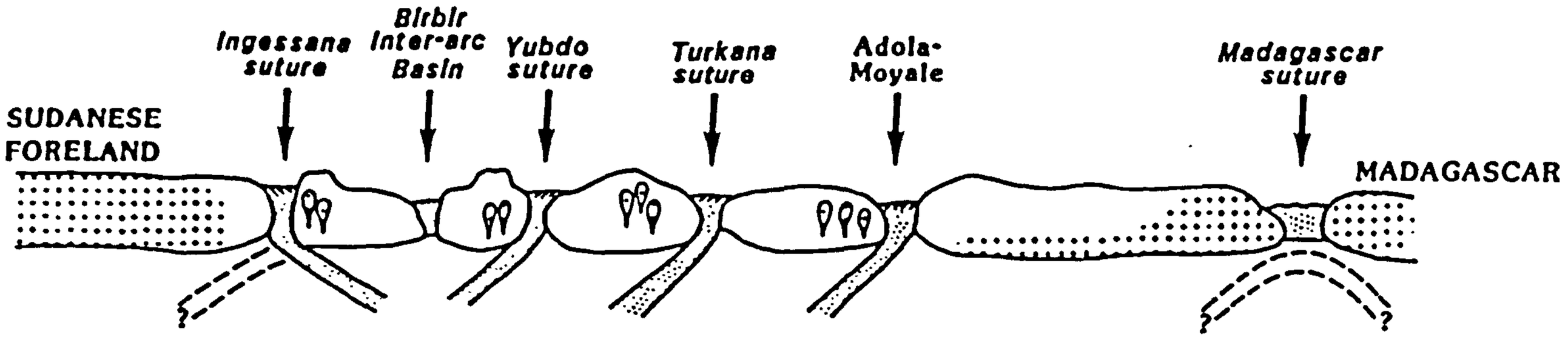

Figure 7.8 Cross sectional evolution of the Pan-African/Mozambique Belt.

evolution of the Pan-African with that of the Caribbean region which contains four island arcs and fragments of Mesozoic and Precambrian(?) craton (Kesler,1978). According to Key (1987) the Mozambique Belt of central Kenya is floored by Kibaran (c.1200 Ma) migmatites overlain by metasediments. This could probably indicate the earliest age of deposition of passive margin shelf sediments.

An intraoceanic island arc development is postulated between the Afif microplate and the African continental margin (Sudanese foreland) for the period 950 to 715 Ma while the main island-arc microplate accretion and collision events took place between 715-640 Ma ago (Stoesser and Camp, 1985; Agar, 1985; Kroner *et al.*, 1987). It is at present not possible to confidently indicate the timing of collision in the Mozambique Belt, however if Madagascar is considered to be the rigid continental block which collided with the accreted island-arcs, then it is plausible that collision happened much earlier in Kenya and Tanzania than in the north (e.g Egypt, Sudan and Saudi Arabia).

New palaeomagnetic data (McWilliams, 1980) suggest that the proto - Gondwana supercontinent only came into existence at about 550 - 600 Ma through collision of East Gondwana (Antarctica, India, Australia) with West Gondwana (Africa, S. America possibly N. America). However Bond *et al.* (1984) suggest that the supercontinent breakup took place between 625-555 Ma, based on constructing tectonic subsidence curves. The ancillary effects of a widespread episode of continental rifting and breakup at the end of the Proterozoic could account for widespread marine transgression on most of the continents in the Cambrian. The shelf sediments of Mozambique Belt were probably deposited during the Gondwana rifting (c. 1200-1000 Ma) and possibly between 625-555 Ma. Basinal closure by westward movement of the Madagascar craton accompanied by westward dipping subduction zones is envisaged.

The collision event created the dominantly NE-SW shear zones and NW-SE left lateral wrench faults. These transcurrent movements could have been caused by the oblique collision of the accreting arc - terranes. The collision also resulted in crustal thickening in the south and a thicker crust with attendant higher grades of metamorphism compared to lower topography and lower grades of metamorphism in the north.

Throughout this Afro-Arabian region, the collision event was followed by alkaline, to peralkaline

granitic intrusions, usually recognisable through their spectacular ring complex features (e.g NE Sudan), including post- tectonic granitic and gabbroic plutons are to be found. Locally they constitute over 30% of the crust.

SE Asia probably affords the most compelling analogy to the Pan-African/Mozambique Belt. In SE Asia a sequence of marginal basins floored by oceanic crust opened sequentially and were consumed over a period of 300 Ma by suduction beneath an adjacent continental crust. Their development was accompanied by the formation of volcanic arcs, probably both within continental margins and oceanic crust (Mitchell,1977). However the widespread thermal event and associated crustal deformation during continent-continent collision is comparable to that of the Tibetan tectono-magmatic terrain, which formed in response to the collision of India with Eurasia (Chengfa *et al.*,1986).

7.9 CONCLUDING REMARKS

Landsat and geochemical studies have placed constraints on the evolution of the Pan-African/ Mozambique belt. The following are put in chronological order.

1. The present work shows five major ophiolitic sutures in NE Africa, while plate reconstruction of Africa and Madagascar indicates six ophiolite belts. On geochemical grounds the ophiolites represent remnants of back-arc basin formed in a supra-subduction zone environment. The terrain delimited by the Ingessana - Port Sudan suture and the Adola - Moyale ophiolite belts defined in this study (Figure 7.1) represents an area where the crust was accreted from oceanic and island arc material (Berhe and Rothery,1986). Relative age reconstruction across the Shield broadly indicates eastward younging of the ophiolite belts. The exception are the Egyptian ophiolites which show younger ages. Structural and metamorphic evidence suggests that crustal shortening was severe in S Sudan, Kenya and SE Ethiopia as compared to Saudi Arabia, NE Sudan and N and W Ethiopia due to oblique collision from the southeast.

2. Combining major and trace element data, three geochemically distinct granitoid types have been identified; volcanic arc granitoids, crustal melt granitoids and within-plate granitoids. Calc-alkaline

rocks predominate in W Ethiopia, whereas the proportion of crustal melts appear to increase going further south in S Ethiopia/ NE Kenya and central Kenya. Although it is difficult to ascertain the volumetric proportions of the granitoids at this stage, diorites form about 10 percent of Precambrian outcrop in NE Sudan (see Figure 5.9) while further south diorites are almost insignificant. Only in NE Sudan, W Ethiopia and S audi Arabia do diorites feature prominently. However the lack of extensive calc-alkaline volcanic rocks, could simply reflect relatively narrow oceans and insufficient subduction of oceanic crust to produce large quantities of calc-alkaline melts, while the increase in the proportion of crustal melt granitoids in the southern part of the Mozambique belt indicates crustal thickening due to continent-continent collision.

3. This study shows that the major lineaments identified in the Horn of Africa are 010 ± 10°, 055-065° and 145-165°. Two major deformation mechanisms are thought to have controlled the growth of the wrench faults. It also indicates that the major folds were developed contemporaneously with shearing deformation. The earliest conjugate fractures trend N-S and NW-SE trending while the later deformation reactivated NW-SE trending lineaments, and caused NE-SW lineaments. The NW trending megashears are related to large scale crustal deformation during final welding in response to oblique collision.

In conclusion the Pan-African/Mozambique Belt is a rifted orogenic belt which evolved by successive collisions of arc-arc and arc-continent plate boundaries. Although the Mozambique Belt may be older than the Pan- African both have undergone a common structural evolution and evolved coevally at least since 1000 Ma. Regional geologic, tectonic and geochemical studies suggest rifting c.1200 Ma which led to deposition of passive margin shelf sediments followed by the development of intraoceanic arcs and associated marginal basins in the north and narrow basins within sialic basement gneisses further south in Kenya and Tanzania. This model suggests rapid crustal growth in Sudan and Ethiopia by a process of horizontal crustal accretion as has been suggested for Saudi Arabia , however crustal growth further south is less extensive simply because sufficiently wide oceanic crust did not develop. This was followed by continent-continent collision which led to accretion of island arcs by mild collision from the northeast in Saudi Arabia and severe crustal shortening in S Sudan, Kenya and SE Ethiopia as compared to Saudi Arabia, NE Sudan and N and W Ethiopia due to oblique

collision from the southeast.

It is at present not possible to outline a detailed chronological sequence of events and to describe the mechanisms involved, which will have to await future geochronological, geochemical and structural studies.

7.10 TESTS FOR THE MODEL

Problems that need to be addressed in the study of continental accretion history of NE and E Africa can be grouped into three: A) the need for age constraints , B) understanding the nature of the crust and C) structural constraints.

A) Age constraints

1. There is a debate regarding the age of the Mozambique Belt. The geochronological data from this region are consistent with a Late Proterozoic age, but they are at present too few and ambiguous to allow meaningful correlations. In addition the Mozambique belt is claimed to be the result of continent- continent collision. Undoubtedly some constraint is required on the timing of post-collision uplift. Determination of cooling ages across the Pan-African/Mozambique belt would shed considerable light on the uplift history of the area .

2. In order to determine the direction and sequence of accretion of the Pan- African Mozambique belt the relative age sequences of the ophiolite belts across the Shield has to be ascertained. It is envisaged that Nd model ages would help constrain relative ages of ophiolites.

B) Nature of the crust

1. What is the style of crustal evolution during the Pan-African event? Did crustal growth take place in Kenya and Tanzania during the Pan-African event, or did magmatism result in remobilisation of pre-existing crustal material?

2. Study of granitoid rocks suggests that there is less evidence of calc-alkaline activity further south (in the Mozambique Belt) than in the Arabian-Nubian Shield. Is the spatial variation of granitoid types due to different evolutionary processes?

3.What lies beneath the shelf facies metasediments of Kenya and Tanzania?

C) Structural constraints

1. There is gross oversimplification on the direction of subduction. The Saudi Arabian studies favour easterly dipping subduction zones while in NE Africa westerly dipping subductions are suggested. There is clearly a need for detailed structural studies to establish transport direction of the ophiolites.

2. Did collision take place oblique or perpendicular to the ophiolite belts?

3. In addition, seismic reflection profiling in Kenya or Tanzania would help to place further constraints on the nature of the crust at depth and for tectonic modelling.

4. In order to establish whether there are allochtonous terrains and to help in plate reconstruction purposes palaeomagnetic studies would be of crucial importance.

REFERENCES

Abbey, G. 1980 Studies in "standard samples" for use in the general analysis of silicate rocks and minerals. Geostandards Newsletter, Geol. Surv. Canada 4, 163-190.

Abdel Rahman, E.M. 1983, The geology of mafic-ultramafic masses and adjacent rocks southof the Ingessana igneous complex, Blue Nile Province, E. Sudan. Unpublished M. Phil. thesis:, Portsmouth Polytechnic, Portsmouth, England 210 p.

Agar, R.A. 1985 Stratigraphy and palaeogeography of the Siham group: direct evidence for a late Proterozoic continental microplate and active continental margin in the Saudi Arabian Shield. J. Geol. Soc. Lond. 142, 1205-1220.

Agar, R.A. 1987 The Nadj fault system revisited: a two way strike-slip orogen in the Saudi Arabian Shield. J. Struct. Geol. 9, No. 1, 41-48.

Ahmed, F. 1983. ' Relationships of mineral deposits and lineament analysis of the Red Sea region, *northeastern Sudan*', Adv. Space Res., 3, 71-79.

Allegre, C.J., Treuil, M., Minster, J.F., Minster, B. and Albarede, F. 1977. Systematic use of trace elements in igneous processes. Part 1 : Fractional crystallisation processes in volcanic suites. Contrib. Mineral. Petrol. 60, 57-75.

Allen C.R. 1975 The petrology of a portion of the Troodos plutonic complex, Cyprus. Unpubl. Ph.D thesis, University of Cambridge 161 pp.

Almohandis, A.A. 1983 Occurence and the compositional variations of chromite in the Kapalagulu intrusion, Western Tanzania. Bull. Fac. Earth Sci. King Abdulaziz Univ. 6, 619-632.

Almond, D.C., 1969. Structure and metamorphism of the basement complex of NE Uganda. Overseas Geol. Miner. Res. 10, 146-163.

Almond, D.C., 1983. The concepts of the " Pan-African Episode" and " Mozambique Belt " in relation to the geology of east and north-east Africa, King Abdulaziz University, Jeddah, Fac. Earth Sci. Bull., 6, 71-78.

Almond, D.C., Ahmed, F. and Dawoud, A.S. 1984. Tectonic, metamorphic and magmatic styles in the northern Red Sea Hills of Sudan. Fac. Earth Sci. Bull., King Abdulaziz Univ., Jeddah, 6, 450-458.

Almond , D.C. and Ahmed. F. 1987 Ductile shear zones in the northern Red Sea Hills of Sudan and their implications for crustal collision. African Geol. Rev. (eds. P. Bowden and J.A Kinnaird). Wiley.

Al-Shanti A.M. and Gass I.G. 1983 The Upper Proterozoic ophiolite melange zones of the easternmost Arabian Shield. J. Geol. Soc. Lond. 140 , 867-876.

Anderson, E.M., 1951. The dynamics of faulting and dyke formation, with applications to Britain. 2nd. Ed.: Edinburgh, Oliver and Boyd, 206 p.

Andreoli, M. A. G. 1984 Petrochemistry, tectonic evolution and metasomatic mineralisations of Mozambique Belt gmulites from S Malawi and Tete (Mozambique). Prec. Res., 25, 162-186.

Andriessen, P. A. M., Coolen, J.J.M.M.M., and Hebeda, E. H. 1985. K-Ar hornblende dating of Late Pan- African metamorphism in the Furua granulite complex of Southern Tanzania. Prec. Res., 30, 351-360.

Araujo, J. R., 1976. Mozambique Belt : uma interpretacao geocronologica. Memorias e Noticias Mus. Lab. Min. Geol. Univ. Coimbra. 81, 85-102.

Arth, J.G. and Hanson, G.N. 1975 Geochemistry and origin of the early Pre-cambrian crust of northeastern Minnesota. Geochim. Cosmochim. Acta. 39, 325-362.

Augustithis, S.S. 1965 Mineralogical and geological studies of the platiniferous dunite-birbirite pyroxenite complex of Yubdo/Birbir, Western Ethiopia. Chem. de Erde 24, 159-196.

Bagnall, P.S. 1960 , Geological map of the North Pare area. Published by the Geol. Surv. Div., Dodoma,Tanganyka: Scale 1: 125,000.

Baker B.H. 1963 Geology of the Baragoi area. Report 53 Geol. Surv. Kenya ,74pp.

Bakor, A.R., Gass, I.G and Neary, C.R. 1976. Jabal al Wask, northwest Saudi Arabia, an Eocambrian back-arc ophiolite. Earth . Planet .Sci. Lett. 30, 1-9.

Barth, H., Besang, C., Lenz, H., Meinhold, K.D. 1983. Results of petrological investigations and Rb/Sr age determinations on the non-orogenic igneous ring-complexes in the Bayuda Desert, Sudan. Geol. Jahrbuch. B 51, 3-34.

Beauchamp, P. and Lemoigne, Y. 1974. Sur la presence de terrains Palaeozoiques en Ethiopie. C.R. Acad. Sci., Paris 278, Ser. D, 29-32.

Beccaluva, L, Di Girolamo, P., Macciotta, G., and Morra ,V. 1983 Magma affinities and fractionation trends in ophiolites. Ofioliti 8(3), 307-324.

Beccaluva, L., Ohnenstetter, D. and Ohnenstetter, M. 1979. Geochemical discrimination between ocean floor and island arc tholeiites - applications to some ophiolites. Can. J. Earth Sci. 16, 1874-1881.

Beeson, M.H. and Jackson, E.D. 1969 Chemical composition of altered chromite from the Stillwater complex, Montana. Am. Mineral. 54,1084-1100.

Berberian, M. and King, G.C.P. 1981. Towards a palaeogeography and tectonic evolution of Iran. Can. J. Earth Sci. 18, 210-265.

Berhe, S.M. 1981. Application of Remote Sensing in tectonic and metallogenic studies, Western Ethiopia. Unpublished M.Sc thesis. Leicester University. Leicester.

Berhe, S.M. 1982 The geology of the Dire Dawa area (explanatory notes for Dire Dawa mapsheet, NC 37-12). Eth. Inst. Geol. Sur. Mem.

Berhe, S.M. 1986. Geologic and geochronologic constraints on the evolution of the Red Sea-Gulf of Aden and Afar Depression. J. African Earth Sci. 5, No. 2, 101-117.

Berhe, S.M. 1987 Application of Remote Sensing to tectonic and metallogenic studies in NE Africa. Symp. Proc. "Remote Sensing for Exploration". Reno, Nevada. 1, 383-391.

Berhe, S.M. and Rothery, D.A. 1986. Interactive processing of satellite images for structural and lithological mapping in northeast Africa. Geol. Mag. 123 (4), 393-403.

Besairie, H., 1970. Description geologique du massif ancien de Madagascar. LeSud. Doc. Bur. Geol. No. 177e, Tananarive, 163 pp.

Black, R., Morton, W.J. and Tsegaye Hailu. 1974. Early structures around the Afar triple junction. Nature 248, 496-497.

Bond, G.C., Nickeson, P.A., and Kominz, M.C. 1984 Breakup of a supercontinent between 625 Ma and 555 Ma: new evidence and implications for continental histories. Earth Planet Sci. Lett. 70, 325-345.

Borsi, S. 1965. Determinazione di eta con il metodo Rb/Sr di alcune rocce della " Regione dei Bur" in Somalia. Atti. Soc. Tosc. Sc. Nat.,A, 72, . 3-6, Pisa.

Boudier, F. Boucher ,J.L, Nicolas, A., Cannat, M., Geuleneer, G., Misseri, M. and Montigny, R. 1985. Kinematics of oceanic thrusting in the Oman ophiolite: model for plate convergence. Earth, Planet. Sci Lett. 75, 215-222.

Boyer, S.E. and Elliot, D. 1982. Thrust systems. Am. Ass. Petr. Geol. Bull., 66, 1196-1230.

Bowes, D.R. and Hopgood, 1976 Significance of structural trend in Pre-cambrian terrain. Acta Geol. Polonica, 26, No. 1, 57-82.

Brown, G.C. 1979. The changing pattern of batholith emplacement during earth history. In Origin of granite batholiths-geochemical evidence. M.P. Atherton and J. Tarney (eds.). Shiva Publishing Ltd.

Brown, G.F. 1970. Eastern margin of the Red Sea and coastal structures in Saudi Arabia. Phil. Trans.R. Soc. Lond. A267, 75-87.

Brown, M.A. 1982 Chromite deposits and their ultramafic host rocks in the Oman ophiolite. Unpubl. PhD thesis, The Open University, 263 pp.

Browne, S.E., Fairhead, J.D., and Mohammed , I.I. 1984 Gravity study of the White Nile Rift, Sudan, and its regional tectonic setting. Tectonophysics 113, 123-137.

Browning, P. 1982 The petrology, geochemistry and structure of the plutonic rocks of the Oman ophiolite. Unpubl. PhD thesis, The Open University 404 pp

Bruni, P. and Fazzuoli, M. 1980. Mesozoic structural evolution of the Somali coast on the Gulf of Aden. In: Geodynamic Evolution of the Afro-Arabian Rift System, Acc. Naz. dei Lincei, 47, 193-207.

Burke, K., and Dewey, J.F. 1972. An outline of Precambrian plate development. In: Implications of continental drift to the earth sciences (ed. D.H. Tarling and S.K. Runcorn), Vol. 2, pp. 1035-46. Academic Press, New York.

Burke, K. and Dewey, J.F. 1973. Plume generated triple junctions: Key indicators in applying plate tectonics to old rocks. J. Geol. 81, 406-433.

Burke, K. and Sengor, C. 1985 Tectonic escape in the evolution of the continental crust. In "Deep structure of the Earth's Crust." Geophys. Monogr. Ser., edited by L. Brown and M. Barazangi, AGU Washington D.C.

Butler, R.W.H. 1987. Thrust sequences. J. Geol. Soc. 144, 619-634.

Calvez, J.Y., Alsac. C., Delfour, J., Kemp, J. and Pellaton, C. 1983. Geologic evolution of western , central and eastern parts of the northern Precambrian Shield, Kingdom of Saudi Arabia. Unpublished Rept Saudi Arabian Deputy Ministry of Mineral Resources. Open - File Report BRGM-OF-03-17, 57p.

Cahen, L. 1961. Review of geochronological knowledge in Middle and Northern Africa. In: Geochronology of Rock Systems. Ann. New York Acad. Sci. 91, 535-66.

Cahen, L. 1970. Igneous activity and mineralisation episodes in the evolution of the Kibaride and Katangide Orogenic belts of Central Africa. In: CLIFFORD, T.N. & GASS, I. (eds) African Magmatism and Tectonics. Oliver and Boyd, Edinburgh, 97-118.

Cahen, L. and Snelling, N. J. 1966. The Geochronology of Equatorial Africa. North-Holland Publ. Co. pp 195.

Cahen, L., Snelling, N. J., Delhal, J. and Vail, J. R. 1984. The geochronology and evolution of Africa, Clarendon Press, Oxford.

Cameron, E.N. 1975 Post cumulus and subsolidus equilibration of chromite and co-existing silicates in the eastern Bushveld complex. Geochim. Cosmochim. Acta. 39, 1021-1033.

Cameron, W.E. 1985. Petrology and origin of primitive lavas from the Troodos ophiolite, Cyprus. Contrib. Mineral. Petrol., 89, 1-17.

Cameron, W.E., McCulloch, M.T. and Walker, D.A. 1983. Boninite petrogenesis chemical and Nd-Sr isotopic constraints. Earth Planet. Sci. Letts., 65, 75-89.

Camp, V. E. 1984.' Island arcs and their role in the evolution of the western Arabian Shield'. Geol. Soc. Amer. Bull. 95, 913-921.

Cann J.R. 1971 Metamorphic rocks from Palmer ridge. Phil. Trans. R. Soc. Lond., 268 , 605-617.

Carmichael, I.S.E., Turner, P.J. and Verhoogen, J. 1974. Igneous petrology. McGraw Hill, 739pp.

Cavanagh, B.J. 1979 .Rb-Sr geochronology of some pre-Nubian igneous complexes of central and northeastern Sudan., Unpubl. Ph.D thesis, 239pp.

Chappel, B.W. and White, A.J.R. 1974 Two contrasting granite types. Pacific Geology 8, 173-174.

Charlesley, T.J., Hackman, B.D., Jall, M., Kagasi, J., Key, R. M., Muturi, H., Siambi, W.S. and Wilkinson, A.F. 1984. The Samburu-Marsabit geological mapping and mineral exploration project - a preliminary statement. Brit. Geol. Surv. Report 16 (10), 18-19.

Chater A.M. 1971 The geology of the Megado region of southern Ethiopia. Unpubl. PhD thesis University of Leeds, 193pp.

Chavez, P.S. and Bauer, B. 1982. An automatic optimal kernel-size selection technique for edge enhancement. Rem. Sen. Envir. 12, 23-38.

Chengfa, C. et al. 1986. Preliminary conclusions of the Royal Society and Academia Sinica 1985 geotraverse of Tibet. Nature, 323, No. 6088, 501-507.

Chernosky J. V. 1976 Stability of anthophyllite - a re-evaluation based on new experimental data. Am. Mineral. 61. 1145-1155.

Chinnery, M.A. 1966. Secondary faulting. 1. Theoretical aspects, 2. Geological aspects. Can. J. Earth Sci. 3, 163-190.

Chorowicz, J., Le Fournier, J. and Vidal, G. 1987. A model for rift development in Eastern Africa. Geol. Mag. 22, 495-513.

Claesson, S., Pallister, J.S.and Tatsumoto, M. 1984. Samarium-neodymium data on the late Proterozoic ophiolites of Saudi Arabia and implications for crustal and mantle evolution. Contrib. Mineral.Petrol. 85, 244-52.

Clark, A.M.S. 1978. Chemical and mineralogical development of the Sidamo nickeliferous serpentinites, Ethiopia. Mineral. Deposita (Berl) 13, 221-234.

Clifford, T.N. 1968. Radiometric dating and the pre-Silurian geology of Africa. In: Radiometric dating for geologists (ed. E. I. Hamilton and R.M. Farquhar), pp. 299-416. Interscience, London, New York, Sydney.

Clifford, T.N. 1970 The structural framework of Africa. In: African magmatism and tectonics (eds Clifford and Gass). Oliver & Boyd, Edinburgh. pp 1-26.

Cloos, H. 1939. Hebury-Spelting vulcanismus. Geol. Rund. 30, 405.

Cohen, C.R. 1985. Role of fault rejuvenation in hydrocarbon accumulation and structural evolution of the Reconcavo Basin, Northeastern Brazil. AAPG, 69, No. 1, 65-76.

Colsh R.A. 1977. Ocean floor metamorphism in the Betts Cove ophiolite New foundland. Contribs. Mineral. Petrol. 60 , 255-270.

Colsh, R.A, Hickey, R., and Frey, F.A. 1982 Rare earth element geochemistry of the Betts Cove ophiolite, Newfoundland: complexities in ophiolite formation .Geochim. Cosmochim. Acta. 46, 2117-2134.

Coleman R.G. 1977 "Ophiolites" - Ancient Oceanic Lithosphere? Springer-Verlag, Berlin, Heidelberg, New York.

Coleman R.G. 1980 Tectonic inclusions in serpentinites. Archives des Sci. Geneva 33, 89-102.

Coolen, J.J.M.M.M., Priem, H.N.A., Verdurmen, E.A. Th. and Verschure, R. H., 1982. Possible zircon U-Pb evidence for Pan- African granulite facies metamorphism in the Mozambique belt of southern Tanzania. Prec. Res. , 17, 31-40.

Cooper, J.A., Stacey, J.S., Stoeser ,D.G. and Fleck, R.J.1979, An evaluation of the zircon method of isotopic dating in the southern Arabian craton. Contrib. Mineral. Petrol. 68,429-439.

Coward, M.P. 1980. Shear zones in the Precambrian crust of Southern Africa. J. Struct. Geol., 2, 19-27.

Crawford. A.J., Beccaluva L., and Serri, G. 1981 Tectono-magmatic evolution of the West philippine Mariana region and the origin of Boninites. Earth Planet. Sci Lett. 54, 346-356.

Dalwitz, W.B. 1968. Chemical composition of clino enstatie-bearing volcanic rocks from Cape Vogel area, Papua: a discussion. In: Proc 23rd Int. Congr. 2, 229-245.

Dalwitz, W.B., Green, D.H. and Thompson J.E. 1966. Clinoenstatite in a volcanic rock from Cape Vogel, Papua : a discussion. Proc. 23rd Int. Geol. Cong. Prague. 2, 229-242.

D'Amico, C., Ibrahim, H.A.,Sassi., F.P. 1981. Outline of the Somalian Basement. Geol. Rund. 70, No. 3, 882-896.

Darbyshire, D.P.F., Jackson, N.J., Ramsay, C.R. and Roobol, M.J. 1983 Rb-Sr isotope study of latest Proterozoic volcano-sedimentary belt in the Central Arabain Shield. J. Geol. Soc. Lond. 140, 203-213.

Davidson, A., Moore, J.M., Davies, J.C., Gebreleul, E., Shifferaw, A., Degeffu, A.,Guyassa, A., WoldeRufael, A. and Gelatta, M. 1973. Preliminary report on the geology and geochemistry of parts of Sidamo, Gemu Gofa, and Kefa Provinces, Ethiopia. Omo River Project Report No. 1. Ministry of Mines and Power.21pp.

Davidson, A., Moore, J.M., Davies, J.C., Shifferaw, A., Degeffu, A., Guassa, A.M., Wolderufael, A., Gelatta, M. and Hintsa, N. 1976. Preliminary report on the geology and geochemistry of parts of Gemu Gofa, Kefa and Ilubabor Provinces, Ethiopia, Omo River project Report no. 2. Ministry of Mines and Power, Ethiopia. 28 pp.

Davidson, A. 1983 Reconnaissance geology and geochemistry of parts of Illubabor, Kefa, Gemu-Gofa, and Sidamo Ethiopia. Ministry of Mines and Energy, Eth. Inst. Geol. Surv. Bul. No. 2.

Davies, B.F. 1984 Strain analysis of wrench faults and collision tectonics of the Arabian Shield. J. Geol. 82, 37-53.

Dawoud, A.S., 1980. Structural and metamorphic evolution of the area southwest of Abu Hamed, Nile Province, Sudan. Unpublished Ph.D thesis, University of Khartoum.

Delfour, J. 1980. Geologic, tectonic and metallogenic evolution of the northern part of the Precambrian Arabian shield (Kingdom of Saudi Arabia). Bull. Bur. Rec. Geol. Min. 11, 1-20, Orleans.

Deslo, A. 1938 Sulla presenza di molibdeniti nelle pegmatiti dell Vallega (A.O.I.): Materie Prime D'Italia e dell'Impero. 5. No. 8, 305-308 ,Rome.

Deslo, A. 1940 Prime notizie sullamineralizzazione aurifera dell Vollega e del Beni Sclangul (A.O.I.) Boll. Soc. Geol. Ital. 59, Rome.

Desmons, J. 1982 Radiometric dating of Late Proterozoic ophiloites: meaning, correlations and problems. Prec. Res. 16, pA15.

Desmons, J. 1980. Iran: correlation of the phases of deformation, metamorphism and magmatism. In 26th Int. Geol. Congr. Geology of the Alpine chains born of the Tethys. BRGM No. 115, p. 308.

Dewey, J. F 1977 Suture zone complexities: a review. Tectonophysics. 40, 53 - 67.

DeWit, M.J. 1977 Notes on the geology of part of sheet NC - 36-16 (Gore). Eth. Inst. Geol. Surv. Rept No. 51.

DeWit , M.J. and Abera Aguma 1977 Geology of the ultramafic and associated rocks of Tulu Dimtu, Welega. Eth. Inst. Geol. Surv. Report No. No. 57.

DeWit, M.J., Berg, R., Balcha, B., Guyessa, A., and Bekele, T. 1978 Geology of the Kata area, Welega. Eth. Inst. Geol. Surv. Report . No. 65.

DeWit, M.J. and Chewaka, S. 1981. Plate tectonic evolution of Ethiopia and the origin of its mineral deposits: an overview. In Plate Tectonics and Metallogenesis: Some Guidelines to Ethiopian Mineral Deposits (ed. S. Chewaka and M.J. de Wit), Inst. Geol. Surv. Bull. No. 2, 115-29.

Dick, H.J.B. and Bullin, T .1984 Chromian spinel as a petrogenetic indicator in abyssal and alpine -type peridotites and spatially associated lava. Contrib. Mineral. Petrol. 86, 54-76.

Dickey, J.S. 1975 A hypothesis of origin for podiform chromite deposits. Geochim. Cosmochim. Acta 74, 1061-1074.

Dickinson, W.R. 1970 Relations of andesites, granites, and derivative sandstones to arc -trench tectonics. Rev. Geophys.Space Physics. 8, 813-860.

Dietrich, V., Emmermann, R. and Puchelt, H. 1978. Geochemistry of basaltic and gabbroic rocks from the west Mariana Basin and the Mariana Trench. Earth Planet Sci. Lett. 39, 127-144.

Dixon, T.H. 1979 .The evolution of continental crust in the Late Precambrian Egyptian Shield. Unpubl. PhD thesis University of California, San Diego 232 pp.

Dodson, M.H., Cavanagh, B.J., Thatcher, E.C and Aftalion, M. 1975. Age limits for the Ubendian metamorphic episode in Northern Malawi. Geol. Mag. 112, 403-410.

Drury, S.D 1986. Remote sensing of geological structure in Europian agricultural terrains. Geol .Mag. 123, 113-21.

Duncan R.A. and Green D.H. 1980 Role of multistage melting in the formation of oceanic crust. Geology. 8 , 22-26

Duyverman, H.J. 1981 Late Precambrian volcanic rocks of the Arabian shield, Saudi Arabia. Unpubl. PhD thesis. The Open University. 192 pp.

El Rabaa, S.M. 1976. Structural and metamorphic evolution of west Berber District, Sudan with special reference to the structural control of mica bearing pegmatites. In: TSEGAYE, H. (editor) Proceedings 2nd Conference on African Geology. Addis Ababa. Geological Society of Africa. 81-96.

El Ramly, M.F., Grelling, R., Kroner, A., and Rashwan, A.A. 1984 On the tectonic evolution of the a Wadi Hafafit area and environs, Eastern Desert of Egypt, Fac. Earth Sci., Univ. Jeddah, Bull., 6, 113-126.

Elliot, D. 1976 The motion of thrust sheets. J. Geophys. Res. 81, 949-63.

Embleton, J. C. B., Hughes, D.J., Klemenic, P.M., Poole, S. and Vail, J. R. 1983. A new approach to the stratigraphy and tectonic evolution of the Red Sea Hills, Sudan Bull.Fac.Earth.Sci., King Abdul Aziz University, Jeddah, Kingdom of Saudi Arabia 6, 101-12.

Engin, T. and Aucott J.W. 1971 A microprobe study of chromites from the Andizhk-Zimparalik area, south west Turkey. Min. Mag. 38, 76-82.

Evans, B.W., Johannes ,W., Oterdoom, H. and Trommsdorff, V. 1976 Stability of chrysotile and antigorite in the serpentinite multisystem. Schweiz. Mineral.Petrogr. Mitt. 56, 79-93.

Evans, B.W. and Trommsdorf, V. 1970 Schweiz. Mineral Petrog. Mitt. 50, 481-492.

Fairhead, J.D. and Girdler, R. W. 1970. The seismicity of the Red Sea, Gulf of Aden and Afar triangle. Phil. Trans. R. Soc. Lond. A267, 49-74.

Fielder G. 1976 Lineament patterns of the Moon, Mars and Mercury In the :2nd Inter. Proc. Bas. Geol. Univ. of Utah. R.A. Hogson et al. Editors. 379-389.

Fisher, R.A. 1953. Dispersion on a sphere. Proc. R. Soc. Lond, A217, 295-305.

Fitches, W.R., Graham, R.H., Hussein, I.M., Ries, A.C., Shackleton, R.M. and Price, R.C. 1983 The late Proterozoic ophiolite of Sol Hamid, NE Sudan. Prec.Res. 19 , 385-411.

Fleck, R.J. , Coleman, R.G., Cornwall, H.R., Greenwood, H.R., Hadley, D.G. Schmidt, D.L., Prinz, W.C. and Ratte, J.C. 1976. Geochronology of the Arabian Shield, Western Saudi Arabia: K/Ar results. Geol. Soc. Am. Bull., 87, 9-21.

Fleck R.J., Greenwood, W.R., Hadley, D.G., Anderson, R.E., and Schmidt, D.L. 1979. Rubidium-strontium geochronology and plate tectonic evolution of the southern part of the Arabian Shield. U.S. Geol. Surv. Saudi Arabian Project Rept. 245,105p.

Fleck, R.J., Greenwood, W.R., Hadley, D.G., Anderson, R.E. and Schmidt, D.L. 1980. Age and evolution of the southern part of the Arabian Shield. Inst. Appl. Geol. Bull.3 Vol. 3, 1-19.

Fleuty, M.J. 1961. The geology of the Nakiloro Chromite area,Karamoja Geol. Surv. Uganda. Records for 1957-1958, 19-36.

Fleuty, M.J. 1963. Explanation of the geology of sheet 27 (Moroto). Rep. Geol. Surv. Uganda.

Fourcadre, S. and Allegre, C.J. 1981 Trace elements behaviour in granite genesis : a case study. The calc-alkaline plutonic association from the Querigot complex (Pyrenees, France).Contrib. Mineral. Petrol. 76, 177-195.

Francaviglia, T.I. 1939. Note sulla constituzione geologica della zona del Basso Barca. Giornale di Geol. (Bologna). Ser. 2 (a), 13, 23-27.

Frazier, S.B. 1970. Adjacent structures of Ethiopia: that portion of the Red Sea coast including Dahlak Kebir Island and the Gulf of Zula. Phil. Trans. R.Soc. Lond. A267, 131-41.

Freund, R.1971 The Hope Fault, a strike slip fault in New Zealand. N.Z. Geol. Surv. Bull.86, 49pp.

Freund, R. 1974 Kinematics of Transform and transcurrent faults. Tectonophysics 21, 93-134.

Frisch, W. and Al-Shanti, A. 1977 Ophiolite belts and the collision of island arcs in the Arabian shield. Tectonophysics. 43, 293-306.

Frisch, W. and Pohl, W. 1986. Petrochemistry of some mafic and ultramafic rocks from the Mozambique Belt, SE Kenya. Mitt. Osterr. Geol. Ges. 78, 97-114.

Gabert, G. and Wendt, I. 1974. Dateirung von granitscher Gesteinen im Dodoman- und Usagaran- System und in der Ndembera - Serie (Tanzania). Geol. Jahrb. Hannover B 11 , 3-55.

Gammond, J. F. 1987. Bridge structures as sense of displacement criteria in brittle fault zones. J. Struct. Geol., 9, No. 5/6, 609-620.

Garcia, M.O. 1978. Criteria for the identification of ancient volcanic arcs. Earth Sci. Rev., 14, 147-65.

Garson, M.S. and Shalaby, I.M. 1976. Precambrian-Lower Proterozoic plate tectonics and metallogenesis in the Red Sea region. Spec. Pub. Geol. Assoc. Can. 14, 573-96.

Gass, I.G. 1977. The evolution of the Pan African crystalline basement in NE Africa and Saudi Arabia. J. Geol. Soc. Lond.134, 129-38.

Gass, I.G. 1981. Pan African (Upper Proterozoic) plate tectonics of the Arabian-Nubian Shield. In: Precambrian Plate Tectonics (ed. A. Kroner). pp. 387-405. Amsterdam: Elsevier.

Gass I.G. 1982 Upper Proterozoic (Pan-African) calc-alkaline magmatism in north eastern Africa and Arabia. In: Andesites (ed.)R.S. Thorpe pp 591-609.

Gass, I.G. and Smewing, J.D. 1973. Intrusion, extrusion and metamorphism at constructive ridge margins: evidence from the Troodos massif, Cyprus. Nature, 242, 26-29.

Geological Map of Ethiopia, 1973 Compiled by V. Kazmin. Geol.Surv. Ethiopia, Ministry of Mines. Scale 1:2,000,000.

Geological map of Mozambique, 1968 Compiled by W.F Oberholzer. Published by Direccao Provincial Dos Servicos De Geologia E. Minas. Scale 1:2,000,000.

Geological map of Tanganyka, 1959 Published by the Geological Survey of Tanganyika. Scale 1:2,000,000.

Ghidey W. Gabriel 1981 - Minor report on the geology of the Yubdo area. Unpublished report. pp 8.

Gibson, P. J. 1986 Remote sensing techniques applied to Pan-African terrain in NE Africa. Unpubl. M. Phil. thesis, The Open University.

Gilboy, C.F,. 1970 The geology of the Gariboro region of Southern Ethiopia. Unpubl. Ph.D thesis University of Leeds 176 pp.

Gill J.B. 1976 Composition and age of Lau basin and ridge volcanic rocks: implications for evolution of an interarc basin and remnant arc. Geol. Soc. Am. Bull. 87 . 1384-1396.

Gillespie, A.R. 1980. Digital techniques of image enhancement, in Remote Sensing in Geology, edited by B.S. Seigal and A.R. Gillespie, New York, John Wiley, 139.

Gillespie, A.R., Kahle, A.B. and Walker, R.E. 1986. Color enhancement of highly correlated images. I. Decorrelation and HSI contrast stretches. Remote Sensing of Environment. 20, 209-235.

Gilluly , J. 1976 Lineaments - Ineffective Guides to Ore Deposition. Econ. Geol. 71, p. 1507.

Giraud, P. 1954. Les roches basiques de la region d' Andriamena et leur mineralisation chromifere. Thése Cleremont- Ferrand. Annale s Géologique de Madagascar . Fascicule no. XXVII.

Giraud, P. 1960. Les roches basiques de la region D'Andriamena a Madagascar et leur mineralisation chromifere. Annales Géologiques de Madagascar, Fascicule No XXVII Tananarive. p. 95.

Girdler, R.W. and Hall, S.A. 1972. An aeromagnetic survey of the Afar triangle of Ethiopia. Tectonophysics 15,52.

Girdler, R.W. and Styles, P. 1978. Seafloor spreading in the western Gulf of Aden. Nature 271, 615-617.

Goetz, A.F.H. and Rowan, L.C. 1981. Geologic remote sensing. Science 211, 781-91.

Goetz, A.F.H., Rock, B.N. and Rowan, L.C. 1983. Remote sensing for exploration : An overview. Econ. Geol. 78, 573-90.

Golding, H.G. and Bayliss, P. 1968 Altered chrome ores from the Coolac serpentine belt New South Wales, Australia. Am. Mineral. 53,162-183.

Greenwood, W.R., Anderson, R.E., Fleck. R.J. and Roberts, R.J. 1980. Precambrian geologic history and plate tectonic evolution of the Arabian shield. Bull. Saudi Arabian Dir. Gen. Mineral Res.24, 35 pp.

Greenwood, W.R., Hadley, D.G., Anderson, R.E., Fleck, R.L. and Schmidt, D.L. 1976. LateProterozoic cratonisation in southwestern Saudi Arabia. Phil.Trans. R. Soc.Lond. A280, 517-27.

Grootenboer, J. 1973. The influence of seasonal factors on the recognition of surface lithologies from ERTS imagery of the western Transvaal. Proc. 3rd ERTS Symp. 643-55.

Halligan, R. 1962. The Proterozoic rocks of Western Tanganyika. Geol. Surv. Tanganyika. Bull. No. 34, 33 pp.

Hamilton, D.K. 1951 Debel chromite prospect .Geol. Surv. Kenya .Unpublished Rept.

Hanson, G.N. 1978. The application of trace elements to the petrogenesis of igneous rocks of granitic composition. Earth Planet. Sci. Lett. 38, 26-43.

Harpum, J. R. 1958. The geology of the Kipengere area. Geol. Surv. Tanganyika. Quarter Degree Sheet. 79 NW.

Harris, N.B. W. and Gass, I.G. 1981. Significance of contrasting magmatism in North East Africa and Saudi Arabia. Nature 289,No. 5796, 395-396.

Harris, N.B.W., Hawkesworth, C.J. and Ries, A.C. 1984. Crustal evolution in northeast and east Africa from model Nd ages. Nature 309, 773-76.

Harris, N.B.W., Pearce, J.A. and Tindle, A.G 1986 Geochemical characteristics of collision - zone magmatism.In: Coward, M.P & Ries. A.C (eds) Collision Tectonics Geol. Soc. Spec. Publ. No. 19, pp 67-81

Hart, R.A. 1973 A model for chemical exchange in the basalt-seawater system of oceanic layer II. Can. J. Earth Sci.

Hawkesworth, C.J. 1982 Isotope characteristics of magmas erupted along destructive plate margins. In : Andesites. Thorpe, R.S. (ed) chichester: Wiley, 549-71.

Hawkesworth, C.J., O' Nions, R.K., Pankhurst, R.J., Hamilton, P.J. and Evensen, N.M. 1977 A geochemical study of island arc and back-arc tholeites from the Scottia Sea. Earth Planet. Sci. Letters 36, 253-262.

Hawkins, J.W. Jr, Bloomer S., Evans, C and Melchair, J. 1979. Mariana arc-trench system: Petrology of inner trench wall. EOS Trans. Am. Geophys Un. 60. 968p.

Hepworth, J.V. 1967 The photogeological recognition of ancient orgenic belts in Africa Quart. J. Geol. Soc. Lond 123, 253-292.

Hepworth, J.V. 1979. Does the Mozambique orogenic belt continue into Saudi Arabia? In: Evolution and Mineralisation of the Arabian-Nubian Shield, vol 1, 39-52. Pergamon Press. (Inst. Appl. Geol. Bull. 3, 29-52.)

Hepworth, J.V., and Macdonald, R., 1966. Orogenic belts of the northern Uganda basement. Nature 210, 726-727.

Hickey, R.L. and Frey, F.A. 1982. Geochemical characteristics of boninite series volcanics: implications for their source. Geochim. Cosmochim. Acta. 46, 2099-2115.

Hirdes, W. and Brinkmann, K. 1985. The Kabus and Balula serpentinite and metagabbro complexes - a dismembered Proterozoic ophiolite in the north-eastern Nuba Mountains, Sudan. Geol. Jahrbuch. B58, 3-43.

Holmes, A. 1951. The sequence of Precambrian orogenic belts in south and central Africa. Proc. 18th Inter. Geol. Congr. Lond. 254-69.

Holubec, J. 1976 The arucuate structure of the Earths crust with tectonic map of the World . Praha Academica.

Hottin, G. 1970. Geochronologie et stratigraphie Malgaches-essai d'interpretation. Serv. Geol. Malgasy.Docum. Bur. Geol. Mad. 182, 21 pp.

Hottin G. 1972. Geological map of Madagascar. Published by Bur.Rech. Geol. Min. Scale,1:2,000,000.

Hottin, G. 1976. Presentation et essai d'Interpretation du Precambrien de Madagascar. Bull. Bur. Rech. Geol. Min. Paris, 2e Serie, 4, No. 2, 17-53.

Hunt, G.R. 1979. Near-infrared (1.3-2.4 μm) Spectra of alteration minerals - potential for use in remote sensing. Geophysics 44, 1974-86.

Hunt, J. A. 1960. Geology of the Diamoleh area, Berbera and Burao District. Somalia. Prot. Geol. Surv. Rept. No. 4,pp 27.

Huntings 1969. Photogeological and mineral Surveys of two selected areas of Ethiopia. Hunting Geology and Geophysics Rept.

Hussein, I.M. 1977. Geology of the Halaib area of the northern Red Sea Hills, Sudan, with special reference to the Sol Hamed basic complex. Unpublished M. Phil. Thesis. Portsmouth Polytechnic, 175 pp.

Hussein, I.M., Kroner, A. and Durr, St. 1984. Wadi Onib- A dismembered Pan-African ophiolite in the Red Sea Hills of Sudan, King Abdulaziz Univ., Jeddah. Fac. Earth Sci. Bull., 6, 320-327.

Irvine, T.N. 1965 Chromian spinel as a petrogenetic indicator. Part 1 theory. Can. J. Earth Sci. 2, 648-672.

Irvine, T.N. 1967 Chromian spinel as a petrogenetic indicator. Part 2 Petrologic applications. Can. J. Earth Sci. 4, 71-108.

Irvine,T.N. and Baragar, 1971 A guide to the chemical classification of the common volcanic rocks. Can. J. Earth Sci. 8,523-548.

Irvine, T.N. and Findlay, T.C. 1972. Alpine type peridotite with particular reference to the Bay of Islands igneous complex. Publication of Earth Physics Branch , Department of Energy, Mines and Research, Canada, 42, 27-128.

Jagoutz, E., Palme, H., Hildegard Baddenhausen, Blum, K., Cendales, m., Gerlind, D., Spettel, B, Lorenz, V. and Wanke, H. 1979. The abundances of major, minor and trace elements in the Earth's mantle as derived from primitive ultramafic nodules. Proc. 10th Lunar. Planet. Sci. Conf., 2031-2030.

Jakes, P. and Gill, J. 1970. Rare earth elements and the island arc tholeiitic series. Earth Planet. Sci. Lett., 9, 17-28.

Jelenc, D.A . 1966 Mineral occurences of Ethiopia .Ministry of Mines, Addis Ababa.

Jenner, G.A. 1981 Geochemistry of high Mg andesites from Cape Vogel, Papua New Guinea. Chem. Geol. 33, 307-332.

Jenning, D.J. 1967. Geology of the Archer's Post area. Ministry of Nat. Res. Geol. Surv. Kenya. Rept No. 77.

Johnson, R.L. 1968. Structural history of the western front of the Mozambique Belt in northeast Southern Rhodesia. Geol. Soc. Am. Bull. 79, 513-26.

Jourde, G. 1967. Essai d' interpretation stratigraphic, tectonique et palaeogeographique du socle a la latitude d' Andriamena. Centre Nord de Madagascar. Comptes Rendue Societe Geologique de France. 43-48.

Jourde, G. 1971. Essai de synthese structurale et stratigraphique du Précambrian Malgache. Comptes Rendue Societe Géologique de France. 59-70.

Kabesh, M.L. 1961 The geology and economic minerals and rocks of the Ingessana Hills. Geol. Surv. Sudan Bull. 11, 61 pp.

Kampschur, W. and Press, N. 1976 Iberian Tectonics from Landsat. Unpublished Tectosat Report.

Karig, D.E. 1970. Ridges and basins of the Tonga-Kermadec island arc system. J. Geophys. Res. 75, 239-254.

Karig, D.E. 1971 Origin and development of marginal basins in the Western Pacific J. Geophys. Res. 76, 2542-2561.

Kazmin, V. 1971 Pre-cambrian of Ethiopia Nature. Phys. Sci. 230, 176-177.

Kazmin, V. 1972. The Geology of Ethiopia. Ministry of Mines, Addis Ababa (Unpublished).

Kazmin, V. 1973 Geological map of Ethiopia. Ministry of Mines. Scale 1:2,000,000.

Kazmin ,V. 1975 The Pre-cambrian of Ethiopia and some aspects of thegeology of the Mozambique Belt . Bull. Geophys. Obs. Addis Ababa, 15. 27-43.

Kazmin ,V. 1976 Ophiolites in the Ethiopian basement. Eth. Inst. Geol. Surv Note 35. 16 pp.

Kazmin, V. 1978 Geology of the Tulu Dimtu area Welega Eth. Inst. Geol. Surv. Report No. 90.

Kazmin, V., Shifferaw ,A.,and Balcha, T. 1978 The Ethiopian Basement : stratigraphy and possible manner of evolution. Geol. Rund. 67, 531-546.

Kazmin, V., Berhe, S.M. and Teffera, M. 1979 a. Basement structure of western Ethiopia and its bearing on the pre-Upper Proterozoic tectonic plan in East Africa. Sinet (Eth. J. Sci.) 2, (2), 129-36.

Kazmin, V., Shifferaw, A., Teffera, M., Berhe, S.M. and Chowaka, S. 1979 b. Precambrian structure of western Ethiopia. Proc. 5th Conf. African Geol. Annals Geol.Surv. Egypt. Cairo. vol. 9, pp. 1-8.

Kemp, J., Pellaton, C. and Calvez, J.Y. 1980. Geochronological investigations and geological history in the Precambrian of northwestern Saudi Arabia. Bur. Rec. Geol. Min., Open File Report 01-1, 120 pp.

Kennedy, W.Q. 1964 The structural differentiation of Africa in the Pan-African±500my) tectonic episode. Univ. Leeds Res. Inst. Afr. Geol. Dep. Earth Sci.Ann. Rept. 8, 48-49.

Kesler, S.E. 1978. Metallogenesis of the Caribbean region. J. Geol. Soc. 135, 429-441.

Key, R. 1987. Superimposed Upper Proterozoic collision-controlled orogenesis in the Mozambique orogenic belt of Kenya (Abstracts). 14th Coll. African Geology- Berlin, pp 209.

King, A.J.1953, Geological map of the Mpwapwa area. South B37/11: Publ. Geol.Surv. Dept. Dodoma, Tanganyka.

Klemenic, P. 1985. New geochronological data on volcanic rocks from the Sudan and their implication for crustal evolution, Prec. Rec., 30, 263-276.

Kozerenko, V.N. and Lartzev, V.S. 1976. Geology and mineral resources of Somalia Democratic Republic. In: Problems of Geology and Metallogeny of East Africa, Proc. Polytech. Inst. 101, 6-117 (in Russian).

Kroner, A. 1979a Pan-African mobile belts as evidence for a transitional tectonic regime from intraplate orogeny to plate margin orogeny. Inst. Appl. Geol. Bull. No. 3 1, 21-37.

Kroner, A. 1979b Pan-African plate tectonics and its repercussion on the crust of northeast Africa. Geol. Rund. 68 , 565-583.

Kröner, A. 1985. Ophiolites and the evolution of tectonic boundaries in the late Proterozoic Arabian-Nubian shield of northeast Africa and Arabia. Prec. Res. 27, 277-300.

Kroner, A., Greiling, R., Reischman, T., Hussein, I.M., Stern, R.J., Durr, S., Kruger, J and Zimmer, M. 1987. Pan-African crustal evolution in the Nubian segment of Northeast Africa. In " Proterozoic Lithospheric Evolution "(ed). A. Kroner, Geodynamics SeriesVolume 17. International Lithosphere Program Contribution. Am. Geophys.Union. Washington, D.C. pp, 235-257.

Laird, J. and Albee, A.L. 1981. Pressure, temperature and time indicators in mafic schist : their application to reconstructing the polymetamorphic history of Vermont. Am. J. Sci. 281, 127-175.

Leggo, P.J. 1974. A geochronological study of the basement complex of Uganda. J. Geol. Soc. Lond., 130, 263-278.

Leith, W .and Alvarez, W. 1985. Structure of the Vakhsh fold and thrust belt, Tadjik SSR: Geologic mapping on a Landsat image base. Geol. Soc. Am. Bull. 96, 875-85.

Liou, J.G., Kuniyoshi ,S. and Ito, K. 1974 Experimental studies of the phase relations between greenschist and amphibolite in a basaltic system. Am. J. Sci. 274, 613-632.

Maboko, M.A.H., Boelrijk, N.A.I.M., Priem, H.N.A., and Verdurmen, E.A.Th. 1985. Zircon U-Pb and biotite Rb-Sr dating of the Wami River granulites, eastern granulites, Tanzania: evidence for approximately 715 Ma old granulite facies metamorphism and final Pan- African cooling approximately 475 Ma ago. Prec. Res. 30, 361-378.

Marzouki, F.M.H., Jackson, N.J., Ramsay, C.R. and Darbyshire, D.P.F. 1982 Composition, age and origin of two Proterozoic diorite-tonalite complexes in the Arabian Shield. Prec. Res. 19,31-50.

Mason, J. E. and Warden, A. J., 1956. Geology of the Heis- Mait- Waqdeira area, Erigavo District. Somalia. Prot. Geol. Surv. Rept. No. 1, pp23.

McCarthy, T.S. and Hasty, R.A. 1976. Trace element distribution patterns and their relationship to the crystallisation of granitic melts. Geochim. Cosmochim. Acta 4, 1351-1358.

McDermott, F. 1986. Granite petrogenesis and crustal evolution studies in the Damara Pan-African orogenic belt, Namibia. Unpubl. Ph.D thesis, The Open University, 404 pp.

McWilllams, O. 1981. Palaeomagnetic and Precambrian tectonic evolution of Gondwana. In: Kroner,A. (ed) Developments in Precambrian Geology:Precambrian Plate Tectonics,pp. 649-87. Elsevier, Amsterdam, New York.

Meljer, A. 1980. Primitive arc volcanism and a boninite series: examples from the western Pacific island arcs. In The Tectonic and Geologic Evolution of Southeast Asian Seas and Islands. D.E. Haynes (ed) Am. Geophys. Un. Mem. N° 23 269-282.

Meljer, A., Anthony, E. and Reagan, M. 1981. Petrology of volcanic rocks from the fore-arc sites. Initial Reports DSDP ,60 ,709-730

Menzies, M. 1975 Spinel compositional variation in the crustal and mantle lithologies of the Othris ophiolite. Contribs. Mineral. Petrol. 51,303-309.

Menzies, M. and Allen, C. 1974 Plagioclase 1herzolite- residual mantle relationships within two eastern Mediterranean ophiolites. Contribs. Mineral. Petrol. 45 , 197-213.

Menzies, M., Blanchard, D. and Xenophontos, C. 1980. Genesis of the Smartville arc-ophiolite, Sierra Nevada Foothills, California. Am. J. Sci .280-A, 329-344.

Miller, C.F. 1985. Are strongly peraluminous magmas derived from pelitic sedimentary sources. J. Geol. 93, 673-689.

Miller, J.A., Mohr, P.A and Rogers, A.S 1967. Some new K/Ar age determinations of basement rocks from Eritrea. Bull. Geophs. Obs. Addis Ababa, 10, 53-57.

Mitchell, A.H.G. and Reading, H.G. 1971 Evolution of island arcs. J. Geol. 79, 253-284.

Mitchell, A. H.G. and Warden, A.J. 1971. Geological evolution of the New Hebrides Island arc. J. Geol. Soc. 127, 501-529.

Miyashiro, A. 1973. The Troodos ophiolitic complex was probably formed in an island arc. Earth Planet. Sci. Lett. 19, 218-224.

Mohr, P. 1979 Lithology and structure of the Precambian rocks of Eritrea. In : Evolution and Mineralisation of the Arabian - Nubian Shield .A.M.S Al-Shanti (Convenor) Pergamon Press, Oxford, 7-15.

Molnar, P. and Tapponier, P. 1975 Cenozoic tectonics of Asia. Science 189, 419-426.

Moody, J.D. 1973. Petroleum exploration aspects of wrench-fault tectonics. AAPG 57, 449-476.

Moody, J.D. and Hill, M.J. 1956. Wrench fault tectonics. Geol. Soc. Am. Bull. 67, 1207-46.

Moody, J.B., Meyer, D. and Jenkins, J.E. 1983 Experimental characterisation of the greenschist/ amphibolite boundary in mafic systems. Am. J. Sci. 283 , 48-92.

Moore, J.M. 1979. Tectonics of the Najd Transcurrent Fault system Saudi Arabia. Geol. Soc. Lond. 136, 441-454.

Moore, J.M., Morgan, J., Teffera, M., and Teklay, M. 1987. Geology of the Gore-Gambela geotraverse, Western Ethiopia. In 'Current research in African earth sciences, Matheis & Schandelmeier (eds). Balkema, Rotterdam, 109-112.

Muhlen, Von L. 1936 Die grundzuge des geologishen baues des hochlandes Von Wollega und der dabussteppe in West Obessinien. Zs. Deutsch. Geol. Ceo. 88, Heft 1, 1936.

Muhlen ,Von L., and Hellmers, J. 1936 Die petrographie der eruptirgesteine der dabussteppe und des hochlandes von Wollega in West Abessinien. V. Jahrbuch J. Mineral et. Beil. Bd. 71 AC1. A.

Mullen, E.D. 1983. $MnO/TiO_2/P_2O_5$: a minor element discriminant for basaltic rocks of oceanic environments and its implications for petrogenesis. Earth Planet. Sci. Lett. 62, 53-62.

Murton, B.J. 1986 The tectonic evolution of the Western Limassol Forest Complex, Cyprus. Unpublished Ph. D. thesis, the Open University, Milton Keynes, pp 331.

Naylor, M.A., Mandl, G., and Sijpelteijn, C.H.K. 1986. Fault geometries in basement-induced wrench faulting under different initial stress states. J. Struc. Geol. 8, No. 7, 737-752.

Neary, C.R. and Brown, M.A. 1979. Chromites from Al Ayes complex, Saudi Arabia and the Semail Complex, Oman. In: Evolution and Mineralisation of the Arabian Shield, (ed) Al-Shanti, A.M.S. Inst. Appl.Geol. Bull., 2, 193-205.

Nour, J.M. 1981 Geological relationships of some dyke swarms in NE Sudan. Abstracts 11th colloquium of African Geology. The Open University, Milton Keynes.

Pallister, J.W. 1971 The tectonics of East Africa. Tectonics of Africa (Earth Sciences 6) UNESCO.

Parkinson, J. 1920. Report on the geology and geography of the northern part of the East African Protectorate. Colon. Rep. Misc. Ser. 91.

Peacock, M.A. 1931.Classification of igneous rock series. J.Geol. 39, 65-67.

Pearce, J.A. 1975. Basalt geochemistry used to investigate post tectonic environments on Cyprus. Tectonophysics, 25,41-67.

Pearce, J.A. 1980 Geochemical evidence for the genesis and eruptive setting of lavas from Tethyan ophiolites. Proc. Int. Ophiolite Symp. Cyprus, 261-272.

Pearce, J.A. 1982 Trace element characteristics of lavas from destructive plate boundaries. In: Andesites, ed R.S. Thorpe (Wiley & Sons)., 525-548.

Pearce, J.A. 1987. An expert system for the tectonic characterisation of ancient volcanic rocks. J. Vol. Geoth. Res.

Pearce, J.A., Alabaster, T., ,Shelton, A.W. and Searle, M.P. 1981 The Oman ophiolite as a Cretaceous arc-basin complex: evidence and implications. Phil. Trans. R. Soc Lond. A300, 299-317.

Pearce, J.A. and Cann, J.R. 1973 Tectonic setting of basic volcanic rocks determined using trace element analysis. Earth Planet. Sci. Lett. 19 , 290-300.

Pearce, J.A. and Gale, G.M. 1977 Identification of ore deposition environment from trace element geochemistry of associated igneous host rocks. in:Volcanic processes in ore genesis, Geol. Soc. Lond. Spec. Publ. 7,14-24.

Pearce, T.H., Gorman, B.E. and Birkett, T.C. 1977. The relationship between major element chemistry and tectonic environment of basic and intermediate volcanic rocks. Earth Planet. Sci. Lett., 36, 121-32.

Pearce, J.A., Harris, N.B.W, and Tindle, A.G. 1984a Trace element discrimination diagrams for the tectonic interpretation of granitic rocks. J. Petrol. 25, 956-983.

Pearce, J.A., Lippard ,S.J. and Roberts, S. 1984b Characteristics and tectonic significance of supra-subduction zone ophiolites. In :Marginal Basin Geology. (eds Kokelaar and Howells) Spec. Publ. Geol. Soc. Lond. 16 , 77-94.

Pearce, J.A. and Norry, M.J. 1979 Petrogenetic implications of Ti, Zr, Y and Nb variations in volcanic rocks. Contribs. Mineral. Petrol. 69 , 33-47.

Penrose, 1972, Penrose field conference on ophiolites. Geotimes 17, 24-5.

Piper, J.D.A., Briden, J.C. and Lomax, K. 1973 Precambrian Africa and South America as a single continent. Nature 245, 244-248.

Potts, P.J., Thorpe, O.W. and Watson, J.S. 1981 Determination of the rare-earth element abundances in 29 international rock standards by instrumental neutron activation analysis: a critical appraisal of calibration errors. Chem. Geol. 34, 331-352.

Potts, P.J., Tindle, A. and Isaacs, M.C. 1983. On the precision of electron microprobe data : a new test for the homogeneity of mineral standards. Am. Mineral. 68,1237-1242.

Potts, P.J., Webb, P.C. and Watson, J.S. 1984. Energy dispersive X-ray fluoresence analysis of silicate rocks for major and trace elements. X-ray spectrometry, 13, 2-15.

Powdwysockl, M.H., Molk, J.G. and Shonp, W.C. 1975 Quantification of geologic lineaments by manual and machine processing techniques. Proc. NASA Earth Res. Surv. Symp. Houston, Texas. Nasa TMX-58168, 1 885-903.

Price, N.J. 1968. Fault and joint development in brittle and semi-brittle rock, Oxford: Pergamon Press, 176 pp.

Price, R.C. 1984 Late Pre-cambrian mafic-ultramafic complexes in Northeast Africa.Unpublished PhD thesis, the Open University, Milton Keynes, pp 325.

Priem, H.N.A., Boelrijk, N.A.I.M., Hebeda, E.H., Verdurmen, E. A. Th., Verschure, R.H., Oen, I.S. and Westra, L., 1979. Isotopic age determinations on granitic and gneissic rocks from the Ubendian- Usagaran System in southern Tanzania. Prec.Res. ,9, 227-239.

Prochaska, W. and Pohl, W. 1983. Petrochemistry of some mafic and ultramafic rocks from the Mozambique Belt, northern Tanzania. J. African. Earth. Sci. 1, No. 3/4, 183-191.

Purcell, P.G. 1976. The Marda Fault Zone Ethiopia. Nature 261, 569-571.

Purcell, P.G. 1981. Phanerozoic sedimentary history and petroleum potential. In: Plate Tectonics and Metallogenesis: Some Guidelines to Ethiopian Mineral Deposits (edited by Chewaka, S. and deWit, M.) Eth. Inst. Geol. Surv. Bull. No. 2, pp. 97-114.

Ramos, V. A. 1977. Basement tectonics from Landsat imagery in mining exploration. Geol. Mijnbouw, 567 (3), 243-252.

Ramsay, J.G. 1967. Folding and fracturing of rocks. McGraw-Hill, Inc., 568 pp.

Razvalayev, A.V and Shakov, G.P. 1976 New data on ring intrusions of the Red Sea Rift Zone. Doklady Akad. Nauk SSSR, 229, 114-116.

Reeves, C. V., Karanja, F. M., Macleod, I. N. 1987. Geophysical evidence for a failed Jurassic rift and triple junction in Kenya. Earth. Planet. Sci. Lett. 81, 299-311.

Relschmann, T., Kroner, A. and Hofmann, A.W. 1985. Isotope geochemistry of Pan-African volcanic rocks from the Red Sea Hills, Sudan (abstract), Terra Cognita, 5, 288,

Reymer, A. and Schubert, G. 1984. Phanerozoic addition rates to the continental crust and crustal growth, Tectonics, 3, 63-78.

Rles, A.C., Shackleton, R. M., and Dawoud, A.S. 1985. Geochronology, geochemistry,and tectonics of the NE Bayuda Desert, N. Sudan : implications for the Western margin of the Late Proterozoic fold belt of NE Africa. Prec. Res., 30, 43-62.

Rles, A.C., Shackleton, R.M., Graham, R.H. and Fitches, W.R. 1983. Pan African structures, ophiolites and melange in the Eastern Desert of Egypt: a traverse at 26° N. J. Geol. Soc.Lond. 140, 75-95.

Rles, A.C., Shackleton, R. M. and Dawoud, A.S. 1985. Geochronology, geochemistry,and tectonics of the NE Bayuda Desert, N. Sudan : implications for the Western margin of the Late Proterozoic fold belt of NE Africa Prec. Res. 30, 43-62.

Rles, A.C., Vearncombe, J.R., Price, R.C. and Shackleton, R.M. (in prep) The geology, geochronology and geochemistry of rocks associated with an ophiolite at Sekerr, NW Kenya.

Ringwood A.E. 1974 The petrological evolution of island arc systems. J. Geol. Soc. Lond. 130 , 183-204.

Ringwood, A.E. 1977. Petrogenesis in island arc systems. In: Island arcs, deep sea trenches and back-arc basins. M. Talwani & W.C. Pitman (Eds.). Am. Geophys. Union, 311-24.

Rix, P. 1973. Geology of the Kauro-Merille area. Ministry Nat. Res. Mines and Geol. Dept. Rept No. 92, 29 pp.

Rogers, A.S., Miller, J.A and Mohr, P.A 1965. Age determinations on some Ethiopian basement rocks. Nature. 206, No 4988, 1021-1023.

Roobol, M.J., Ramsay, C.R., Jackson, N.J. and Darbyshire, D.P.F. 1983 Late Proterozoic lavas of the Central Arabian shield: evolution of an ancient volcanic system. J. Geol. Soc. Lond. 140, 185-202.

Rothery, D.A. 1984 Reflectances of ophiolite rocks in the Landsat MSS bands : relevance to lithological mapping by remote sensing. J. Geol. Soc. Lond. 141, 933-939.

Rothery, D.A. 1985. Interactive processing of satellite images for geological interpretation - a case study. Geol. Mag. 122, 57-63.

Rothery, D.A. 1987. Decorrelation stretching and related techniques as an aid to image interpretation in geology. In: Advances in digital image processing. The Remote Sensing Society, 194-203.

Rothery, D.A. and Drury, S.A. 1984 The neotectonics of the Tibetan Plateau. Tectonics 3, No. 1, 19-26.

Rowan, L.C., Wetlaufer, P.H., Goetz, A.F.H., Billingsley, F.C. and Stewart, J.H. 1974. Discrimination of rock types and detection of hydrothermally altered areas in South -central Nevada by the use of computer enhanced ERTS images. U.S. Geol. Surv. Prof. Paper 883.

Sabins, F.F. 1978 Remote Sensing : principles and interpretation. San Francisco: W.H. Freeman.

Sacchi, R., Marques., Costa, M. and Casati, C. 1984. Kibaran events in the southernmost Mozambique Belt. Prec. Res., 25, 141-159.

Sales, J. 1968. Crustal mechanics of Cordilleran foreland deformation: a regional and a scale model approach. A A P G. 52, 2016-2044.

Sampson, D. N. and Wright, A. E. 1964. The geology of the Uluguru Mts. Geol. Surv. Tanzania. Bull. No. 37, 69 pp.

Sanders, L.D. 1965. Geology of the contact between the Nyanza Shield and the Mozambique belt in western Kenya. Bull. Geol. Surv. Kenya. 45pp

Saunders, A.D and Tarney, J. 1979 The geochemistry of basalts from a back - arc spreading centre in the East Scotia Sea. Geochim. Cosmochim. Acta 43, 555-572.

Saunders, A.D., Tarney, J., Stern, C.R. and Dalziel, .W.D. 1979 Geochemistry of Mesozoic marginal basin igneous rocks from southern Chile. Geol. Soc. Am. Bull. 90, 237-258.

Saunders, A.D., Tarney, J., Marsh, N.G. and Wood, D.A. 1980 Ophiolites as oceanic crust or marginal basin: A geochemical approach. Proc. Int. ophiolite Symp. Cyprus. 193-204.

Schmidt, D.L. and Brown, G.F. 1984. Major-element chemical evolution of t6he late Proterozoic shield of Saudi Arabia, Fac. Earth Sci. Univ. Jeddah, 6, 1-21.

Schmidt, D.L., Hadley, D.G. and Stoesser, D.B. 1979. Late Proterozoic crustal history of the Arabian Shield, Southern Najd province, Kingdom of Saudi Arabia. Inst. Appl. Geol. Bull. 3, Vol. 2, 41-58.

Selgrist, A.W.and Schnetzler, C.C. 1980. Optimum spectral bands for rock discrimination. Photo. Eng.Rem. Sen. 46, 1207-15.

Sengor, A.M. C. and Kidd, W.S.F. 1979. Post collisional tectonics of the Turkish-Iranian plateau and a comparison with Tibet. Tectonophysics 55, 361-376.

Sengor, A.M.C. and Yilmaz, Y. 1981 Tethyan evolution of Turkey : a plate tectonic approach. Tectonophysics ,75, 181-241.

Serri, G. 1981 The petrochemistry of ophiolite gabbroic complexes; A key for the classification of ophiolites into low Ti and high Ti types. Earth Planet. Sci. Lett. 52 , 203-212.

Shackleton, R.M. 1946. Geology of the country between Nanyuki and Maralal. Geol. Surv. Kenya. Rept No. 11, pp 54.

Shackleton, R.M. 1976 Pan-African structures. Phil. Trans. R. Soc. Lond. A280,491-497.

Shackleton, R.M. 1979. Precambrian tectonics of northeast Africa. In :Evolution and Mineralisation of the Arabian-Nubian shield. vol 2, pp. 1-6. Pergamon Press. (Inst. Appl.Geol. Bull. 3, 1-6.)

Shackleton, R.M. 1986. Precambrian collision tectonics in Africa . From Coward ,M.P. & Ries, A.C. (eds) Collision Tectonics, Geol. Soc. Spec. Pub. No.19, 329-349.

Shackleton, R.M., Ries, A.C., Graham, R.M. and Fitches, W.R. 1980. Late Precambrian ophiolitic melanges in the eastern desert of Egypt. Nature 285, 472-74.

Shackleton, R.M. and Ries, A.C. 1984 The relation between regionally consistent stretching lineations and plate motions. J. Struct. Geol. 6,111-117.

Shand, S.J. 1951. Eruptive rocks. J. Wiley (Publisher) N. York.

Sharaskin, A.Y., Dobretsu, N.L. 1980. Marianites: the clinoenstatite bearing pillow lavas associated with ophiolites of the Marianas Island Arc. In:' Ophiolites' Ed. Panayiotu, A., Proc. Int. Symp. Ophio., Cyprus, 1979, 166-175.

Shibata, K. 1975. Preliminary geochronological study on metamorphic rocks from Taita Hills, Southern Kenya. 1st Prelim. Rept. on African Studies. Dept. Earth Sci., Nagoya Univ., Japan, pp. 72-5.

Shibata, K. and Suwa, K. 1979 A geochronological study on granitoid gneisses from Mbooni Hills, Machakos area, Kenya. 4th Prelim. Rep. Afr. Studies Nagoya Univ. 163-167.

Slater, P.N. 1979. A re-examination of the Landsat MSS. Photo.Eng.Rem. Sen. 42, 1479-85.

Soha, J.M. and Schwartz, A.A. 1978. Multispectral histogram normalisation and contrast enhancement. Proc. 5th Can. Symp. Rem. Sen. Victoria, B.C., 86-93.

Soukhoroukov, Y., Bekele, W., Mohammed, A., Kidane, A. and Hagos, M. 1980 a Geology and geochemical prospection for gold and copper and zinc in the Mole - Belcore Area, Western Welega province. Eth. Inst. Geol. Surv. Report.

Soukhoroukov, Y., Bekele, W., Ebba ,H., Demoz, W., Bekele, T., Tezara, B., and Biset, A. 1980b Geology and geochemical prospection for copper, zinc and gold and the Abo-Kami-Kata Area, Western Welega Province. Eth. Inst. Geol.Surv. Report.

Spear, F.S. 1980 NaSi=CaAl exchange equilibrium between plagioclase and amphibole : an empirical model. Contribs. Mineral. Petrol. 72,33-41.

Spear, F.S. 1981 An experimental study of hornblende stability and compositional variability in amphibolite. Am. J. Sci. 2812 , 697-734.

Spooner, C.M., Hepworth, J.V., and Fairbairn, H.W. 1970. Whole rock Rb-Sr isotopic investigation of some East African granulites. Geol. Mag. 107, 511-21.

Stacey, J.S. and Agar, R.A. 1985. U-Pb isotopic evidence for the accretion of a continental microplate in the zalm region of the Saudi Arabian Shield. J. Geol. Soc. Lond .142, 1189-1203.

Stacey, J.S., and Hedge, C.E. 1984. Geochronologic and isotopic evidence for early Proterozoic crust in the eastern Arabian Shield. Geology,. 12, 310-313.

Stacey, J.S., and Stoeser, D.B. 1983. Distribution of oceanic and continental leads in the Arabian- Nubian Shield: Contrib. Mineral. Petrol,. 84,. 91-105.

Starkey, J. 1977. The contouring of orientation data represented in spherical projection. Can. Jour. Earth Sci. 14, 268-272.

Steiner, L. 1987. The Nuba ophiolite and its geological setting : In Current research in African earth sciences, Matheis & Schandelmeier (eds). Balkema, Rotherdam,101-104.

Stevens, R.E. 1944 Composition of some chromites of the western hemisphere. Am. Mineral. 29,134.

Stern, R.J. 1979 Late Precambrian ensimatic volcanism in the Central Eastern Desert of Egypt. Unpubl. PhD thesis, University of California, San Diego. 210 pp.

Stern, R.J. 1985. The Najd fault system, Saudi-Arabia and Egypt: A late Precambrian rift-related transform system. Tectonics, 4, 497-511.

Stoesser, D.B. and Camp, V.E. 1985 Pan-African micro-plate accretion of the Arabian Shield. Geol. Soc. Am. Bull. 96, 817-26.

Stoesser, D.B., Stacey, J.S., Greenwood, W.R. and Fisher, L.B. 1984. U/Pb zircon geochronology of the southern portion of the Nabitah mobile belt and Pan-African continental collision in the Saudi Arabian Shield. Ministry of Petr. Min. Res., Jiddah, Technical Record USGS-Tr-04-5, 88pp.

Streickeisen, A. 1975. Classification and nomenclature of volcanic rocks, lamprophyres, carbonatites and melilitic rocks: Recommendations and suggestions of the IUGS Subcommission on the systematics of igneous rocks. Geology, 7, 331-5.

Sugimura , A. and Uyeda, S. 1973 Island arcs Japan, and its environs. Elsevier Amsterdam, 247 pp.

Sultan, M., Arridson, R.E, and Sturchio, N.C. 1986 Mapping of Serpentinites in the Eastern Desert of Egypt by using Landsat thematic mapper data. Geology 14, 995-999.

Sun, S. and Nesbitt, R.W. 1978 Geochemical regularities and genetic significance of ophiolitic basalts. Geology 6, 689-693.

Suwa, K., Nureki, T., Inoue, H., Biyajima, K., and Miyakawa, K. 1979. Geology and Petrology of the Machakos area, Kenya. 4th Prelim. Rept. on African Studies, Dept., Earth Sci. Nagoya Univ., Japan, pp. 3-20.

Tapponier, P. and Molnar, P. 1976. Slip-line theory and large scale continental tectonics. Nature, 264, 319-324.

Tarney, J., Dalziel, I.W.D., and DeWit, M.J. 1976 Marginal Basin "Rocas Verdes" Complex from S. Chile : A Model for Archean Greenstone Belt Formation . In B.F. Windley (Ed.) the Early History of the Earth. Wiley London 131-146.

Tarney, J., Saunders, A.D., Mattey, D.P., Wood, D.A. and Marsh, N.G. 1981 Geochemical aspects of back-arc spreading in the Scotia Sea and Western Pacific. Phil. Trans. R. Soc. Lond. A300, 263-285.

Taylor, M.M. 1974. Principal components colour display of ERTS imagery. Proc. 3rd ERTS-1 Symp. NASA Sp-351, 1877-97.

Tchalenko, J.S. 1970 Similarities between shear zones of different magnitudes. Geol. Soc. Am. Bull. 81, No. 6, 1625-1640.

Teffera, M. and Berhe, S.M. (in press) Geological map of the Gore area. Sheet NC36-16. 1:250,000 scale. Eth. Inst. Geol. Surv.

Teklewold, A., Bell, K. and Moore, J.M. 1987. Magmatic arc intrusive complexes in the Birbir Domain, Western Ethiopia. In Current research in African earth sciences, Matheis & Schandelmeier (eds). Balkema, Rotterdam, 113-115.

Temperly, B. N. 1938. The geology of the country around Mpwapwa. Tanganyika Territory. Dept. Land & Mines, Geol. Div. Short Paper No. 19,

Thomas, G.E. 1971 Continental plate tectonics: Southwest Wyoming; Wyoming Geol. Assoc. 23rd. Field Conf. Guide Book. 103-123.

Thomas, G.E. 1974. Lineament-block tectonics : Willston Blood Creek Basin. Am. Ass. Petr. Geol. Bull., 58, 1305-1322.

Tindle, A.G. and Pearce, J.A. 1981. Petrogenetic modelling of in-situ fractional crystallisation in the zoned Loch Doon pluton, Scotland. Contrib. Mineral. Petrol. 78, 198-207.

Treuil, M. and Varet, J. 1973 Criteres volcanologiques, petrologiques et geochemiques de la geneses et de la differentation des magmas basaltiques : exemples de l'Afar. Bull. Soc. Geol. France. 15. 401-644.

UNDP 1972 Mineral Survey in two Selected Areas Vol. I, II. Ethiopia.

Vachette, M. 1979. Radiochronologie du Precambrien de Madagascar. 10 Colloq. de Geol. Africaine. Montpellier. 25-27 Avril 1979, Resumes, pp. 20-1.

Vail, J.R. 1976. Outline of the geochronology and tectonic units of the basement complex of northeast Africa. Proc. R. Soc. Lond. A350, 127-41.

Vail, J.R. 1978 Outline of the geology and mineral deposits of the Democratic Republic of the Sudan and adjacent areas. Overseas Geol. Miner. Res. 49 ,68 pp.

Vail, J.R. 1979 Outline of geology and mineralisation of the Nubian shield east of the Nile valley, Sudan. In: Evolution and mineralisation of the Arabian-Nubian shield. Vol 1, 97-107.

Vail, J.R. 1983. Pan-African crustal accretion in north-east Africa. J. African Earth Sci. 1, 285-94.

Vail, J.R. 1985a Pan-African (Late Precambrian) tectonic terrains and the reconstruction of the Arabian-Nubian Shield. Geology 13, 839-842.

Vail, J.R. 1985b. Alkaline ring complexes in Sudan . J. African. Earth Sci. 3, No. 1/2, 51-59.

Vail, J.R. and Kuron, J.L. 1978 High level igneous emplacements in the Red Sea Hills, Sudan. Geol. Rund. 67, No. 2, 521-530.

Vearncombe, J.R. 1983a A proposed continental margin in the Precambrian of Western Kenya. Geol. Rund.72, 663-670.

Vearncombe, J.R. 1983b A dismembered ophiolite from the Mozambique Belt, West Pokot, Kenya. J. African Earth Sci. 1, 133-43.

Walsh, J. 1966 Geology of the Karasuk area. Geol. Sur. Kenya. Report No. 72.

Walsh J. 1972 Geology of the Moyale area. Geol. Surv. Kenya . Rept. No.89, 33 pp.

Warden, A.J. 1974. Catalogue of geological formations of Ethiopia. Eth. Inst. Geol. Surv. Addis Ababa (unpubl. Rept).

Warden, A.J. 1975. Catalogue of geological formations of Ethiopia. Eth. Inst. Geol. Surv. Addis Ababa (unpubl. Rept).

Warden, A.J. 1981 Correlation and Evolution of the Pre-cambrian of the Horn of Africa and Southwestern Arabia - Unpublished Ph.D thesis. Mining University. Loeben. 348pp.1

Warden, A. J. and Daniels, J.L. 1983. Evolution of the Precambrian of Northern Somalia. Bull. Fac. Earth. Sci., King Abdulaziz Univ., 6, 145-164.

Warden , A.J. and Horkel, A.D. 1984 The Geological evolution of the NE branch of the Mozambique belt (Kenya, Somalia, Ethiopia). Mitt. Osterr. Geol. Ges. 77, 161-184.

Warden, A.J., Kazmin, V, Kiesel, W., and Pohl, W. 1982 Some geochemical data of the mafic-ultramafic complex at Tulu Dimtri, Ethiopia and their genetic significance, Smn 191-5,111-131.

Watson, G.S. 1965. Equatorial distributions on a sphere. Biometrika, 52, 193-201.

Watson, G.S. 1966. The statistics of orientation data. J. Geol. 74, 786-797.

Wendt, I., Besang, C., Harre, W., Kreuzer, H., Lenz, H., and Muller, P. 1972 . Age determinations of granitic intrusions and metamorphic events in the Early Precambrian of Tanzania. 24 Int. Geol. Congr. Montreal. Section 1, p. 314.

Wernicke, B. 1985 Uniform-sense normal simple shear of the continental lithosphere. Can. J. Earth Sci. 22, 108-125.

Wernicke, B. and Burchfiel, B.C. 1982 Modes of extensional tectonics. J. Struct. Geol. 4, No. 2, 105-115.

Wheeler, J. 1987 The determination of true shear senses from the deflection of passive markers in shear zones. J. Geol. Soc. Lond.144, 73-77.

White, D.L 1985 The significance of continental derivation of the Proterozoic Mahanid Formation, Southeastern Arabian Shield. J. Geol. Soc. Lond.142, 1235-1238.

White, A.J.R., Clemens, J.D., Holloway, J.R., Silver, L.T., Chappell, B.W. and Wall, V.J. 1986. S-type granites and their probable absence in s. western North America. Geology 14, 115-118.

Wilcockson ,W. H. and Tyler, W.H. 1933 On an area of ultrabasic rocks in the Kassala province of the Anglo- Egyptian Sudan. Geol. Mag. 70 ,305-320.

Wilcox, R. E., Harding, T.P. and Seely, D.R. 1973. Basic wrench tectonics. AAPG, 57, 74-96.

Williams, H. and Smyth, W.R. 1973 Metamorphic aureoles beneath ophiolite suites and Alpine peridotites Tectonic implications with West Newfoundland examples. Am. J. Sci 273, 594-621.

Windley, B.F. 1977. The evolving continents. Wiley, London and New York.

Winkler, H.G.F 1976 Petrogenesis of metamorphic rocks, 4th edition, Springer, Berlin-Heidelberg.

Wood, A.C. 1979. Were the Aisha hills emplaced by movement along the Marda Fault Zone? In: Geodynamic Evolution of the Afro-Arabian Rift System. 104-107. Int. Symp. Abstracts, Roma.

Woodcock, N.H. 1977 . Specification of fabric shapes using an eigen value method. Bull. Geol. Soc. Am., 88, 1231-1236.

Woodcock, N.H. and Fischer, M. 1985 Strike-slip duplexes J. Struc. Geol. 8, No.7, 725-735.

Appendix A

Analytical techniques

A1.1 Sample preparation

For whole rock geochemical analysis 1-3 kg samples were collected. Samples were first split using a hydraulic splitter down to a 3cm cube size. During this stage any remaining weathered patches were removed. A piece was retained for thin section and future reference. The samples were then washed and dried to remove any contamination that may have been present at the splitting stage. Following this each rock was crushed in a jaw crusher to produce small 5mm long chips. The samples were coned and quartered, one quarter placed in an agate tema. Depending on the hardness of the rock, samples were gound for 10-15 minutes to produce about 100g of powder. The powder was then available for use in XRF and INAA analysis. Powdered samples previously prepared for geochronological studies by Gilboy (1970) were also used for geochemical investigations.

A 1.2 XRF sample preparation

Trace elements were determined on pressed powder pellets while major elements were analysed on glass beads. For pressed pellets about 8 kg of rock powder was mixed with Moviol binder and pressed into a 3 cm diameter pellet using a hydraulic press. Pellets were dried and hardened overnight in an oven at 110° C. When dry, each pellet was labelled on it's edge and stored in a pill-box for analysis.

Glass beads were prepared by mixing a 4:1 lithium metaborate: tetraborate mixture (Spectraflux 100B) with pre-dried rock powder in the ratio 6:1 and fusing the mixture in a platinum-gold alloy crucible in a muffle furnace at 1100º C for 20 minutes. A flux loss correction was applied to each batch of eight samples. Loss on ignition data were obtained by heating about 2.5g of rock powder in a silica crucible at 1000º C for twenty minutes and calculating the percentage weight loss.

A1.3 X-ray fluorescence (XRF) analysis

A1.3.1 Data aquired by energy dispersive XRF

Major element analyses were aquired from the Open University's energy dispersive Link system Mecca 20 XRF. The EDXRF method of x-ray fluoresecence is not commonly used for the analysis of silicate materials. Under this system samples are excited by low-power (49W) x-ray tube and the fluorescent x-rays produced are detected by a Si(Li) detector. Unlike wavelength systems where one element is analysed at a time. The excited sample produces a series of electronic pulses that are processed using a multi-channel analyser to give an output of the spectra. Peak stripping and mass absorption co-efficients are used to convert the spectra to oxide concentrations.

Major element data are obtained from fused glass beads made following the method described by Potts *et al.* (1984). In addition to the major elements the counting energy of 10keV allows Cr, Ni, Ba and V to be picked up on the spectrum. International standards were analysed along with the unknowns during each run and compared with the values given in Abbey (1980) as a check on the accuracy of the data. It was found that the calibration commonly used produced low totals particularly for low silica rocks rich in Fe and Ca. This was corrected by using a calibration over a smaller Si range and counting the heavy elements once only. A full description of the operating conditions, count rates, precision and limits of determination are given in Potts *et al.* (1984).

A1.4 Instrumental neutron activation analysis (INAA)

This technique is used for the routine analysis of the rare earth elements at the Open University. In addition to these elements Hf, Th, Ta, Sc, Co and Fe_2O_3 spectra are also detected and their concentrations determined. The Open University system utilises two detectors i) a lithium drifted germanium detector for La and Co of low energy, 20-200keV (LEPS) and ii) a hyperpure germanium detector for the remaining elements at higher energy gamma radiation 500-2000keV (co-axial). The work of Potts *et al.* (1981) reports a precision of <7% and an accuracy better than 5% during routine analysis.

The experimental technique is that of Potts *et al.* (1981) with samples irradiated at the university of London reactor centre, Ascot for one day of reactor time spread over a working week. Each batch of samples contained 8 unknowns, an international standard and the in-house standard ACOURS, a microgranite from Ailsa Craig.

A1.5 Electron microprobe analysis

Mineral chemistry data were obtained routinely on the Open University's wavelength dispersive Cambridge Instruments Microscan 9 electron microprobe. This system is fully computerised providing automatic control of spectrometer angle, count times, diffracting crystal selection, movement of samples and ZAF corrections. Routine analysis of minerals were performed at an accelerating potential of 20kv, a specimen current of 30nA and a spot size of 8-15u. Typical analysis times for common minerals are olivine 11 mins, plagioclase 9mins, and chromite 14mins. The instrument was calibrated using natural and synthetic mineral standard, the details of which are given in Potts *et al.* (1983). A full calibration is performed daily and checked against the internal standards ABG; a basaltic glass and ABX; a chromite before commencing analysis of unknown. Potts *et al.* (1983) reported homogeneity within single grains of ABG. Following the work of Browning (1982) that found heterogeneity in ABX a new chromite standard ABY was introduced. Mean analyses of these secondary standards, aquired over a period of several months during routine analysis, are presented in table A1.1.

APPENDIX B

	Cpx Cumulate									
	SB7	SB12	SB10C	SB10D	SB10E	SB15G	SB24	SB27	SB30	SB31
SiO2	47.05	51.00	55.05	55.11	54.53	52.47	48.92	49.28	48.62	49.17
TiO2	0.11	0.51	0.19	0.21	0.28	0.49	0.95	0.97	0.63	0.69
Al2O3	7.51	5.66	3.41	3.00	3.50	2.95	8.34	8.43	7.31	7.71
Fe2O3	8.91	8.71	8.35	8.18	8.35	6.78	8.09	8.52	8.87	9.35
MnO	0.13	0.17	0.23	0.22	0.19	0.16	0.14	0.16	0.17	0.17
MgO	23.03	14.07	20.87	20.61	20.10	23.34	12.43	13.61	17.05	17.14
CaO	9.52	17.73	10.60	10.93	11.62	11.08	17.29	16.70	13.13	12.56
Na2O	0.46	0.79	0.46	0.46	0.52	0.46	1.16	0.55	0.81	1.54
K2O	0.06	0.31	0.04	0.04	0.05	0.05	0.17	0.20	0.13	0.14
P2O5	0.10	0.17	0.08	0.06	0.07	0.07	0.12	0.18	0.07	0.05
L.O.I	4.44	1.09	1.89	1.84	1.85	2.58	2.59	1.93	2.60	2.00
Total	101.32	100.21	101.17	100.66	101.06	100.43	100.20	100.53	99.39	100.52
Zr	9	25	14	14	18	28	65	69	33	39
Y	1	8	5	4	6	7	18	20	15	15
Nb	1	3	2	2	2	5	2	4	3	2
Rb	1	4	2	2	2	2	3	3	4	3
Sr	26	149	46	48	46	18	401	348	87	93
Ba	226	301	245	247	265	287	375	387	337	338
Cr	2864	899	2083	2165	2700	1522	1105	755	1615	1598
Ni	931	105	675	674	584	1039	225	142	394	305
Zn	58	42	65	59	57	27	46	53	49	48

	Cpx Cumulate				Peridotites				
	SB32	SB33	SB95	SB51	SB57	SB59	SB61	SB15B	SB15c
SiO2	48.96	50.00	44.35	53.51	34.65	28.70	30.58	40.54	37.58
TiO2	0.64	0.68	0.55	0.08	0.01	2.01	2.56	0.01	0.01
Al2O3	8.33	8.54	4.75	4.06	0.71	17.44	16.03	2.04	1.06
Fe2O3	8.62	8.67	7.67	7.01	8.28	12.93	8.96	8.84	6.89
MnO	0.17	0.17	0.13	0.19	0.11	0.15	0.06	0.11	0.10
MgO	16.44	16.88	21.84	22.69	37.58	28.01	31.15	43.07	37.10
CaO	12.67	13.12	12.44	10.48	0.66	0.25	0.31	0.18	1.20
Na2O	1.22	0.96	0.45	0.48	0.41	0.42	0.42	0.43	0.41
K2O	0.21	0.16	0.07	0.14	0.04	0.04	0.05	0.04	0.05
P2O5	0.12	0.11	0.10	0.05	0.02	0.20	0.27	0.04	0.05
L.O.I	1.96	1.93	7.75	2.55	18.67	10.96	11.51	5.75	16.80
Total	99.34	101.22	100.10	101.24	101.14	101.11	101.90	101.05	101.25
Zr	36	37	38	9	4	114	98	5	4
Y	13	16	10	10	1	11	5	1	1
Nb	2	2	2	2	1	10	15	1	1
Rb	4	3	2	2	1	2	1	1	2
Sr	195	151	461	30	5	5	13	7	18
Ba	1859	321	794	215	155	279	289	148	160
Cr	1750	951	2266	3125	2526	506	246	2789	2276
Ni	318	247	472	829	2172	485	755	2160	1875
Zn	46	46	47	45	31	92	44	35	30

	Peridotites	Baragoi Gabbro I					Baragoi Gabbroll	
	SB15F	SB29	SB26	SB94	SB96A	SB96B	SB2	SB3
SIO2	38.07	49.20	48.72	49.10	48.67	47.23	57.03	52.72
TIO2	0.01	0.72	0.64	0.69	0.68	0.78	1.11	1.55
AI2O3	0.70	8.05	15.95	19.02	14.20	11.50	15.15	17.64
Fe2O3	7.58	9.68	5.94	5.59	8.36	9.56	4.94	6.58
MnO	0.11	0.17	0.11	0.08	0.14	0.15	0.11	0.11
MgO	37.40	16.38	8.38	5.62	11.98	14.26	4.57	3.81
CaO	0.24	13.24	16.32	14.24	13.09	13.60	7.00	10.16
Na2O	0.41	1.12	1.79	3.30	1.68	1.50	3.44	4.97
K2O	0.04	0.25	0.25	0.52	0.70	0.47	5.18	0.52
P2O5	0.02	0.15	0.13	0.17	0.04	0.05	1.02	0.19
L.O.I	16.51	1.77	1.58	1.53	1.76	1.66	1.03	2.75
Total	101.09	100.73	99.81	99.86	101.30	100.76	100.58	101.00
Zr	1	44	45	71	45	40	362	99
Y	1	16	14	11	15	12	31	22
Nb	1	3	2	5	1	2	26	9
Rb	1	4	4	7	7	17	96	9
Sr	4	145	1219	1796	1150	1496	4310	1132
Ba	151	338	337	788	495	738	5272	459
Cr	2203	1246	424	417	398	409	84	276
NI	2126	265	134	75	112	96	10	39
Zn	30	59	38	51	59	45	96	58

	Baragoi Gabbroll	Koitokol Gabbro					Headstream Baragoi Gabbro	
	SB142	SB11A	SB11E	SB13	SB90B	SB15E	SB113	SB115
SIO2	53.30	45.50	47.68	50.15	51.04	46.63	53.70	54.22
TIO2	1.58	0.22	0.34	0.41	0.59	0.29	0.37	0.74
AI2O3	19.41	24.69	23.40	17.58	17.22	19.13	20.88	23.82
Fe2O3	7.44	4.98	4.62	6.06	7.40	4.61	3.52	2.98
MnO	0.11	0.06	0.11	0.12	0.16	0.13	0.07	0.05
MgO	3.92	6.64	6.00	8.02	7.68	9.36	2.96	2.08
CaO	8.40	16.07	15.31	14.46	12.41	17.55	12.31	9.98
Na2O	4.37	1.43	1.93	2.17	1.95	0.72	4.79	5.40
K2O	0.86	0.12	0.09	0.17	0.20	0.12	0.59	0.66
P2O5	0.33	0.05	0.10	0.10	0.26	0.03	1.05	0.12
L.O.I	0.64	0.83	0.89	1.45	1.14	0.42	0.41	0.52
Total	100.36	100.59	100.47	100.69	100.05	98.99	100.65	100.57
Zr	72	14	18	22	23	41	51	47
Y	17	4	8	8	11	8	21	7
Nb	8	2	2	2	2	3	3	4
Rb	11	2	2	2	2	2	11	6
Sr	1538	1098	1452	827	1133	6792	1345	1793
Ba	703	265	469	359	537	287	520	363
Cr	187	799	443	850	342	279	184	110
NI	47	79	41	67	44	108	12	21
Zn	68	22	35	38	63	34	27	28

	SB126	SB128
SIO2	55.80	57.49
TiO2	0.51	0.61
Al2O3	22.91	22.22
Fe2O3	3.94	3.07
MnO	0.05	0.06
MgO	1.67	1.00
CaO	8.79	8.89
Na2O	5.68	4.95
K2O	0.36	1.41
P2O5	0.37	0.47
L.O.I	0.54	0.67
Total	100.62	100.84
Zr	51	84
Y	13	20
Nb	3	6
Rb	4	11
Sr	1611	1441
Ba	477	1304
Cr	67	102
Ni	15	11
Zn	43	27

	Amphibolites						
	SB17	SB18A	SB18B	SB20	SB21	SB23A	SB23B
	51.94	52.88	52.97	50.69	52.84	56.49	54.94
	0.23	0.26	0.25	0.27	0.27	0.22	0.20
	9.70	11.41	11.61	9.41	10.78	9.21	9.13
	10.44	9.26	9.44	9.95	9.26	9.43	9.77
	0.19	0.29	0.35	0.26	0.16	0.19	0.18
	10.85	9.46	8.98	13.75	9.56	9.54	10.06
	13.56	13.85	13.20	13.11	15.28	11.92	11.88
	0.91	1.28	1.24	1.95	1.05	1.48	1.48
	0.33	0.32	0.31	0.61	0.19	0.42	0.62
	0.10	0.13	0.10	0.09	0.14	0.09	0.11
	0.70	0.78	0.85	0.94	0.91	0.78	0.78
	98.95	99.92	99.30	101.03	100.44	99.77	99.15
	23	32	30	23	31	23	23
	5	9	7	6	7	4	6
	1	2	2	3	3	2	2
	6	10	8	12	8	13	28
	173	217	208	259	351	329	243
	266	271	269	264	276	331	260
	1526	1153	1151	1555	1145	1118	1085
	302	217	216	193	243	83	78
	87	72	78	65	70	60	73

	Amphibolites					
	SB42	SB43	SB44	SB81	SB84	SB87
SIO2	47.50	47.42	57.52	51.07	53.60	56.27
TiO2	0.34	0.33	0.25	0.29	0.32	0.32
Al2O3	11.08	8.41	8.08	16.73	16.97	15.46
Fe2O3	7.82	8.90	6.23	8.43	6.53	9.26
MnO	0.13	0.15	0.20	0.15	0.12	0.14
MgO	14.02	16.45	11.66	8.42	7.53	5.85
CaO	15.71	15.15	12.26	12.40	11.99	9.95
Na2O	0.92	0.59	1.47	1.90	1.88	1.85
K2O	0.53	0.35	1.51	0.31	0.35	0.80
P2O5	0.10	0.09	0.16	0.11	0.21	0.12
L.O.I	0.84	1.51	0.94	1.10	1.00	0.95
Total	98.99	99.35	100.28	100.91	100.50	100.97
Zr	27	25	65	29	23	29
Y	5	6	9	8	8	9
Nb	2	3	4	2	2	3
Rb	10	8	36	3	2	12
Sr	666	380	371	224	304	442
Ba	292	279	484	509	267	363
Cr	1021	1320	1312	325	546	398
Ni	321	345	250	75	89	68
Zn	47	53	85	53	45	71

	Hornblende Plagioclase Gneisses		
	SB86	SB88	SB19A
	56.15	53.30	62.61
	0.61	0.31	0.64
	13.16	15.95	15.13
	9.24	6.30	6.93
	0.14	0.15	0.12
	6.66	7.51	1.82
	9.26	14.51	7.58
	2.29	1.30	3.48
	0.76	0.34	1.45
	0.22	0.16	0.26
	0.98	1.27	0.50
	99.47	101.10	100.52
	41	80	86
	20	19	29
	3	3	4
	11	6	28
	250	375	745
	308	370	881
	833	407	166
	117	80	9
	84	50	79

	Hornblende Plagioclase Gneisses									
	SB19B	SB119	SB120	SB121	SB127	SB118	SB103	SB106	SB104	SB112
SIO2	57.83	53.16	40.85	58.27	44.50	46.69	49.72	53.70	47.27	48.79
TIO2	0.80	0.64	1.08	0.86	1.44	1.65	0.92	0.82	0.57	1.77
Al2O3	15.00	11.54	16.28	15.09	16.88	15.27	15.50	15.05	17.81	15.70
Fe2O3	8.89	10.46	17.17	9.95	11.04	11.63	10.24	9.43	10.82	11.49
MnO	0.16	0.19	0.17	0.08	0.17	0.20	0.19	0.17	0.18	0.18
MgO	2.91	9.62	7.33	3.54	10.15	6.56	7.53	6.01	6.25	5.93
CaO	8.99	10.33	12.91	7.42	13.40	13.21	10.91	10.11	11.83	11.23
Na2O	3.29	1.96	1.19	4.18	1.73	2.05	2.72	2.66	2.81	3.12
K2O	1.01	0.49	0.56	0.35	0.50	0.72	0.57	0.53	0.84	0.59
P2O5	0.35	0.21	0.10	0.36	0.08	0.23	0.10	0.17	0.19	0.43
L.O.I	0.61	1.23	1.83	0.57	1.17	1.59	0.91	0.89	0.74	0.75
Total	99.84	99.83	99.47	100.67	101.06	99.80	99.31	99.54	99.31	99.98
Zr	80	62	17	39	53	88				130
Y	26	14	8	20	22	29				35
Nb	3	6	2	3	4	6				6
Rb	15	5	8	1	7	15				5
Sr	711	326	332	386	369	320				442
Ba	550	315	1297	315	609	636				409
Cr	112	793	99	69	249	403				341
NI	15	73	14	11	100	15				13
Zn	92	86	104	31	76	76				95

	Hornblende Plagioclase Gneisses									
	SB136	SB130	SB133	SB78	SB79	SB1	SB40	SB49	SB117	SB123
SIO2	48.21	57.65	48.27	46.05	54.95	58.12	48.97	59.07	44.09	50.15
TIO2	1.09	0.70	0.55	1.11	0.50	0.40	1.83	0.38	2.53	1.93
Al2O3	15.33	16.34	17.49	13.66	15.17	13.03	14.47	15.95	13.54	15.07
Fe2O3	10.85	8.24	11.45	12.27	13.00	10.28	13.51	10.34	17.57	11.96
MnO	0.17	0.16	0.24	0.19	0.20	0.17	0.23	0.22	0.28	0.18
MgO	7.98	3.76	6.98	8.12	3.96	6.16	5.96	3.15	6.78	5.48
CaO	13.06	8.80	12.42	13.17	10.04	8.63	10.39	8.23	11.20	10.66
Na2O	2.28	2.87	2.36	2.03	1.19	1.66	2.88	2.33	1.93	2.66
K2O	0.51	1.24	0.66	0.79	0.42	0.41	0.58	0.35	0.68	0.60
P2O5	0.16	0.29	0.19	0.45	0.11	0.15	0.29	0.12	0.25	0.08
L.O.I	1.12	1.03	0.95	1.43	0.52	1.41	0.29	0.42	0.77	0.76
Total	100.76	101.08	101.56	99.27	100.06	100.42	99.40	100.56	99.62	99.53
Zr	49	71	18	71	23	34	96	14	146	
Y	23	20	13	20	13	13	37	12	35	
Nb	2	4	3	11	1	3	4	3	7	
Rb	4	27	5	6	4	5	5	9	9	
Sr	271	586	418	563	231	268	234	237	477	
Ba	374	725	409	610	293	380	414	286	1452	
Cr	370	244	142	480	148	488	212	164	107	
NI	42	16	17	37	12	41	28	10	24	
Zn	89	71	110	94	97	85	116	76	157	

	SB124	SB125	SB129	Hornblende Plagioclase Biotite Gneisses SB69	SB76A	SB76B	SB77B	SB107
SiO2	39.04	44.68	45.21	59.15	53.69	50.34	68.50	67.70
TiO2	5.62	2.07	1.79	0.61	0.79	0.65	0.55	0.25
Al2O3	7.70	15.09	14.80	17.26	15.21	20.03	16.46	16.86
Fe2O3	20.04	13.23	12.56	6.25	8.10	7.27	3.72	3.36
MnO	0.24	0.21	0.19	0.13	0.13	0.15	0.11	0.16
MgO	9.72	9.17	10.21	3.31	7.86	4.84	0.75	0.85
CaO	12.24	11.72	13.15	6.68	8.55	8.87	2.10	6.36
Na2O	2.16	2.10	1.04	4.53	3.87	4.21	5.68	4.07
K2O	0.19	0.32	0.31	1.49	1.46	2.30	2.30	0.24
P2O5	2.24	0.24	0.10	0.34	0.37	0.20	0.15	0.16
L.O.I	0.38	1.07	1.13	0.67	0.84	1.64	0.42	0.51
Total	99.57	99.90	100.49	100.42	100.87	100.50	100.74	100.52
Zr	142	89	42	139	111	101	343	30
Y	60	36	20	13	17	16	38	6
Nb	15	6	4	11	11	8	18	2
Rb	3	7	3	26	24	60	44	2
Sr	177	332	192	1336	579	940	440	876
Ba	573	593	1390	1395	965	1492	1476	231
Cr	147	312	530	124	578	188	62	62
Ni	66	79	137	19	147	41	7	7
Zn	192	92	86	70	77	101	47	50

	Amphibolite Dykes SB50	SB53	SB56	SB62	SB4B	SB100	SB101	SB102	SB110A	SB110B
SiO2	46.57	46.25	45.34	56.47	54.79	45.80	54.19	49.85	51.44	51.36
TiO2	0.15	1.47	1.24	0.70	1.02	4.05	1.00	0.40	0.52	0.55
Al2O3	16.32	14.78	16.72	15.63	14.58	5.70	13.83	8.61	16.74	17.08
Fe2O3	6.48	12.50	10.91	11.27	9.03	16.73	8.59	9.76	10.74	10.90
MnO	0.12	0.20	0.17	0.21	0.22	0.28	0.21	0.30	0.22	0.20
MgO	11.29	8.21	7.79	4.02	4.62	13.35	5.10	16.08	5.43	5.10
CaO	15.48	10.83	13.41	8.17	8.28	11.55	9.24	13.04	9.50	9.40
Na2O	0.93	3.30	2.71	2.80	2.26	0.77	2.40	0.85	3.48	4.33
K2O	0.35	0.51	0.34	0.68	3.44	0.29	2.73	0.55	1.74	1.09
P2O5	0.04	0.15	0.11	0.25	0.68	0.11	1.10	0.11	0.19	0.21
L.O.I	2.20	0.96	1.04	0.53	0.60	1.21	0.62	1.66	0.79	0.68
Total	99.93	99.16	99.78	100.73	99.52	99.84	99.01	101.21	100.79	100.90
Zr	10	75	64	49	210	186		99	31	35
Y	2	30	25	16	24	60		15	13	15
Nb	1	4	2	5	8	14		2	2	2
Rb	10	8	6	10	35	4		2	22	11
Sr	199	411	240	320	3454	125		106	487	743
Ba	252	385	379	327	3658	513		283	565	307
Cr	681	361	507	129	84	626		246	132	74
Ni	117	101	70	12	31	149		109	19	12
Zn	30	94	76	115	128	137		150	95	86

	Baragoi						Western Ethiopia.			
	Amphibolite Dykes			Felsic Dykes			Birbir Metavolcanics			
	SB110C	SB111	SB135	SB97	SB114	SB116	MT107A	MT107B	SB265	SB343
SiO2	51.61	53.41	49.86	63.93	57.95	60.30	74.13	56.28	50.78	54.31
TiO2	0.54	0.49	0.68	1.01	0.90	1.03	0.18	0.95	2.39	1.88
Al2O3	16.61	14.91	14.69	15.58	15.23	15.60	13.77	13.86	13.95	15.07
Fe2O3	10.65	10.30	8.70	5.13	6.51	5.80	2.13	13.17	13.38	11.24
MnO	0.22	0.19	0.19	0.07	0.13	0.12	0.05	0.18	0.23	0.37
MgO	4.94	6.62	8.86	2.38	3.39	2.97	0.71	4.04	4.84	5.50
CaO	9.70	9.82	12.46	3.55	6.64	7.70	1.66	6.67	8.98	6.31
Na2O	3.20	2.28	1.42	3.74	2.68	3.95	4.84	3.98	3.10	4.30
K2O	1.30	0.97	0.81	4.28	4.86	1.50	1.88	0.14	0.41	0.04
P2O5	0.19	0.21	0.21	0.63	0.89	0.66	0.02	0.21	0.41	0.25
LOI	0.86	0.88	2.00	0.79	0.67	0.65	1.00	0.35	0.69	0.71
Total	99.82	100.08	99.88	101.09	99.85	100.28	100.37	99.83	99.16	99.98
Zr		42	54	365	295	269	110	57	215	146
Y		12	15	16	37	20	44	22	48	42
Nb		4	3	9	7	9	5	4	12	4
Rb		16	18	89	48	8	36	2	5	7
Sr		444	444	1417	3467	1936	84	272	356	136
Ba		471	377	2158	4260	2166	1164	90	0	0
Cr		235	307	70	77	73	0	68	68	0
Ni		40	10	30	25	44	827	6	14	13
Zn		82	92	84	98	83	33	122	115	104

Baragoi REE data.

	SB18A	SB62	SB102	SB121	SB130	SB3	SB11E
La	3.49	7.95	4.45	8.38	13.08	16.90	4.00
Ce	5.76	17.21	12.17	17.41	26.57	39.10	8.70
Nd	n/d	11.36	10.34	11.66	15.32	25.40	7.20
Sm	1.03	2.45	2.52	3.01	3.37	4.93	1.69
Eu	0.36	0.91	0.51	1.19	1.08	2.32	1.18
Tb	0.28	0.50	0.51	0.60	0.56	0.79	0.28
Tm	n/d	n/d	n/d	n/d	0.23	n/d	n/d
Yb	1.15	2.05	1.38	2.08	2.09	2.26	0.58
Lu	0.18	0.32	0.23	0.34	0.34	0.35	0.10
Th	0.35	1.02	0.28	0.84	1.87	0.58	n/d
U	n/d	n/d	n/d	n/d	n/d	0.40	n/d
Ta	n/d	0.19	0.20	n/d	0.22	0.58	n/d
Hf	0.76	1.24	2.07	1.29	1.84	2.45	0.41

Pyroxene analyses from the Moyale Chromites

	SiO2	TiO2	Al2O3	Cr2O3	FeO*	MnO	MgO	CaO	Na2O	Total
M64A SMRRK C	53.79	0.08	1.49	0.00	0.97	0.08	17.42	24.83	0.27	98.93
M64A SMRRL C	53.75	0.10	1.49	0.00	1.14	0.06	17.30	24.90	0.20	98.94
M64B CXTTG C	53.84	0.08	1.65	0.00	1.24	0.08	17.18	24.42	0.49	98.98
M64B CXTTH C	53.79	0.08	1.84	0.00	2.03	0.09	17.21	23.36	0.60	99.00
M64B CXTTL C	54.27	0.06	1.30	0.00	1.36	0.06	17.33	24.31	0.41	99.10
M64B1CXTTM C	53.61	0.08	2.11	0.00	2.09	0.09	17.28	22.82	0.61	98.69
M64B1CXTTN C	53.96	0.09	2.05	0.00	2.68	0.09	21.45	18.17	0.38	98.87
M64B1CXTTO C	53.60	0.10	2.01	0.00	1.28	0.08	16.99	24.31	0.44	98.81
M64D CXYYG C	54.13	0.08	1.78	1.35	1.75	0.09	17.10	23.37	0.54	100.19
M64D CXYYH C	54.01	0.09	2.01	1.42	2.02	0.06	17.17	23.01	0.60	100.39
M64D CXYYI C	54.01	0.08	1.89	1.30	1.16	0.06	17.08	24.10	0.46	100.14
M64D CXYYJ C	54.45	0.08	1.39	1.00	1.34	0.08	17.26	24.18	0.37	100.15
M64D CXYYL C	54.28	0.08	1.67	1.11	1.13	0.06	17.27	24.49	0.35	100.44
M64E CXSSI C	53.84	0.11	1.81	1.00	1.14	0.08	17.34	24.33	0.41	100.06
M64E CXSSJ C	53.95	0.10	1.71	1.13	1.24	0.08	17.08	24.37	0.43	100.09
M64E CXSSM C	53.61	0.13	2.14	1.13	1.23	0.06	17.34	23.99	0.34	99.97
M64F CXXXH C	53.78	0.10	1.65	1.30	1.26	0.08	17.19	24.28	0.35	99.99
M64F CXXXI C	54.23	0.08	1.43	1.30	1.20	0.06	17.27	24.19	0.34	100.10
M64F CXXXK C	54.33	0.08	1.89	1.25	1.34	0.06	17.00	23.98	0.44	100.37
M64F CXXXL C	53.92	0.08	2.08	1.30	2.02	0.09	16.94	22.86	0.60	99.89

	Moyale Granitoids. Kufole					Fugugo								Moyale			
	SM4A	SM4B	SM4C	SM4D	SM4E	SM5	SM6	SM7	SM8	SM9	SM10	SM11	SM12	SM13	SM14	SM15	SM16
SiO2	73.83	74.90	74.60	73.60	73.57	60.27	60.12	59.94	64.78	61.14	62.25	62.68	61.24	70.39	70.64	66.11	71.97
TiO2	0.14	0.16	0.14	0.19	0.18	1.44	1.39	1.33	0.80	1.39	1.05	1.03	1.14	0.35	0.36	0.39	0.21
Al2O3	14.00	13.78	13.69	13.67	13.68	16.33	16.02	15.95	16.47	16.17	16.97	16.50	16.68	16.10	15.64	17.85	14.66
Fe2O3	1.65	1.64	1.77	1.89	1.80	6.49	6.15	6.06	4.13	6.41	5.14	4.99	5.72	2.45	2.53	2.68	1.46
MnO	0.04	0.05	0.05	0.05	0.05	0.08	0.08	0.08	0.04	0.08	0.06	0.06	0.08	0.04	0.03	0.05	0.03
MgO	0.23	0.15	0.20	0.19	0.14	2.20	2.01	1.98	1.26	2.02	1.72	1.77	2.05	0.84	0.99	1.23	0.48
CaO	0.73	0.74	0.59	0.73	0.66	3.70	3.39	3.51	2.09	3.76	3.28	3.13	3.18	3.36	3.43	4.38	0.72
Na2O	3.96	4.14	3.86	4.01	3.90	4.47	4.43	4.31	4.25	4.53	4.73	4.66	4.64	4.56	4.34	4.91	4.81
K2O	5.20	4.87	5.09	5.19	5.23	4.18	4.10	4.14	6.09	4.04	4.35	4.15	4.25	1.82	1.92	1.67	4.65
P2O5	0.07	0.07	0.03	0.03	0.04	0.88	0.78	0.77	0.29	0.85	0.50	0.45	0.56	0.11	0.12	0.17	0.09
Total	99.85	100.50	100.02	99.55	99.25	100.04	98.47	98.07	100.20	100.39	100.05	99.42	99.54	100.02	100.00	99.44	99.08
Rb	244	267	280	253	255	97	94	93	110	95	98	108	129	53	56	51	115
Sr	87	88	78	101	98	1393	1367	1413	1133	1335	1158	1035	1082	545	530	646	438
Ba	314	346	303	470	434	2717	2664	2845	4082	2718	2589	2469	2592	995	1027	812	1150
Zr	170	163	157	201	202	452	521	488	264	468	548	511	590	136	145	131	143
Hf		5.51				11.46								3.98			
Nb	49.0	39.5	127.4	38.6	39.0	24.8	25.6	24.7	17.5	25.3	18.5	23.9	21.3	4.6	5.3	4.8	10.2
Ta		5.15				1.47								0.27			
Y	46	37	52	38	39	16	16	16	11	16	14	17	15	5	4	6	9
Th	42	39	51	43	45	6	5	5	9	6	5	10	7	5	5	2	11
U	10	6	14	5	5	4	4	4	4	4	4	4	4	3	3	3	3
La		45.9				122								24.2			
Ce		85.5				223								42.8			
Nd		33.3				80.3								15.3			
Sm		6.35				12.6								2.42			
Eu		0.71				3.06								0.75			
Tb		0.97				0.86								0.29			
Tm		0.00				0.00								0.00			
Yb		3.59				1.20								0.42			
Lu		0.60				0.18								0.09			
Ni	10	6	7	7	7	9	11	19	8	13	14	17	18	7	7	7	6
Cu	5	5	5	5	5	27	20	24	10	17	18	23	19	5	5	7	13

	Moyale				Adadi Jolle						Adola Granitoids. Garlboro						
	SM18	SM19	SM20	SM21	SM41	SM42	SM43	SM44	SM45	SM46	D4	D5	D6	D8	D9	D10	D11
SiO2	73.79	71.63	67.08	66.70	77.55	76.50	72.63	73.74	76.06	73.03	76.94	75.46	73.03	75.83	77.11	71.52	75.36
TiO2	0.18	0.24	0.39	0.36	0.04	0.05	0.31	0.24	0.04	0.32	0.18	0.20	0.20	0.24	0.15	0.26	0.20
Al2O3	14.32	14.87	17.28	17.92	12.44	13.11	13.47	13.42	12.15	13.61	13.06	13.61	14.68	13.36	12.81	15.43	12.49
Fe2O3	1.24	1.51	2.81	2.76	1.19	1.01	3.06	2.75	1.97	2.80	1.44	1.82	1.23	1.99	1.15	1.42	2.10
MnO	0.03	0.04	0.04	0.05	0.03	0.02	0.03	0.03	0.02	0.06	0.03	0.04	0.02	0.02	0.03	0.03	0.04
MgO	0.14	0.58	1.02	1.20	0.15	0.24	0.15	0.20	0.17	0.27	0.20	0.23	0.45	0.29	0.11	0.62	0.11
CaO	0.82	1.02	3.65	4.20	0.34	0.47	0.92	0.61	0.65	0.87	0.53	0.93	1.30	0.48	0.91	1.58	0.40
Na2O	4.73	4.82	4.58	5.18	3.86	3.88	3.27	3.72	3.50	3.29	3.77	3.32	2.92	4.03	3.52	4.65	2.77
K2O	4.47	4.77	2.33	1.65	4.36	4.57	5.32	5.11	4.81	5.21	4.84	4.95	5.65	4.02	4.27	4.23	5.07
P2O5	0.06	0.14	0.15	0.12	0.03	0.04	0.08	0.05	0.03	0.08	0.07	0.12	0.06	0.07	0.03	0.09	0.06
Total	99.78	99.62	99.33	100.14	99.99	99.89	99.24	99.87	99.40	99.54	101.06	100.68	99.54	100.33	100.09	99.83	98.60
Rb	121	127	68	57	115	118	130	128	137	127	135	182	129	128	90	149	166
Sr	404	532	607	628	28	29	76	63	21	109	66	65	38	53	67	423	47
Ba	942	1243	1075	751	162	172	668	588	114	784							
Zr	129	152	127	148	154	165	340	294	151	355	187	174	394	145	141	137	320
Hf					11.94										4.61		
Nb	9.9	10.8	6.2	6.3	87.9	85.3	35.4	45.2	95.9	23.9	13.8	14.2	22.5	5.3	5.5	9.2	26.5
Ta					5.08										0.48		
Y	8	8	4	7	119	128	93	100	134	66	60	43	60	27	25	7	73
Th	12	12	2	2	4	5	14	10	6	13	11	18	9	9	10	15	10
U	5	3	3	3	2	2	3	3	5	3	0	0	0	0	0		
La					12.3										11.7		
Ce					31.2										28.3		
Nd					21.9										12.5		
Sm					8.99										2.68		
Eu					0.14										0.28		
Tb					2.40										0.57		
Tm					2.23										0.31		
Yb					15.0										2.99		
Lu					2.27										0.52		
Ni	6	7	8	7	6	6	12	7	9	7	1660	891	454	1011	1779	646	1777
Cu	4	9	5	5	4	4	5	5	5	5	2	41	10	6	14	13	17

	Garlboro	Godoloka			Adola Gneisses. Biotite Gneiss (Lower Group)			Quartzofeldspathic Gneiss			Baragoi Granitoids. Louwamara Granite		Sartim Granite		Central Kenyan Ol'Doinyo Wass Granodiorites	
	D12	D1	D2	D3	D13	D14	D15	E25	E26	E36	SB82A	SB82B	SB9A	SB9B	SA1	SA2
SiO2	76.06	69.66	71.74	69.92	65.01	60.55	73.31	58.05	72.04	62.44	72.79	73.55	68.26	72.19	65.56	66.2
TiO2	0.08	0.34	0.27	0.36	0.63	0.66	0.21	0.44	0.26	0.40	0.17	0.01	0.51	0.24	0.53	0.28
Al2O3	13.47	14.33	13.85	14.10	16.17	15.49	15.23	19.73	13.56	13.03	15.28	15.28	16.67	15.86	16.82	19.12
Fe2O3	1.17	3.66	3.01	4.16	4.84	8.05	0.95	7.78	2.36	6.13	1.16	0.58	2.48	1.3	4.9	1.54
MnO	0.04	0.09	0.06	0.08	0.12	0.20	0.01	0.14	0.05	0.21	0.02	0.08	0.04	0.02	0.12	0.01
MgO	0.00	0.06	0.13	0.29	2.25	3.49	0.26	1.33	0.96	1.03	0.5	0.15	1.05	0.44	1.36	1.06
CaO	0.96	1.18	0.84	1.26	3.57	4.97	2.35	2.74	1.77	2.15	1.68	1.4	2.69	1.88	3.67	1.74
Na2O	3.67	3.58	3.98	4.35	5.10	3.97	3.88	7.05	2.89	2.04	4.76	5.33	5.23	5.07	5.32	6.01
K2O	4.29	5.73	5.39	4.86	1.94	1.93	3.48	3.31	4.81	4.02	3.37	3.66	2.86	3.57	2	4.18
P2O5	0.04	0.08	0.07	0.15	0.21	0.16	0.11	0.20	0.06	0.21	0.07	0.04	0.19	0.06	0.3	0.22
Total	99.78	98.71	99.34	99.53	99.84	99.47	99.79	100.77	98.76	91.66	99.8	100.08	99.98	100.63	100.58	100.36
Rb	109	95	105	155	115	117	63	86	171	97	56	111	54	63	45	62
Sr	85	105	89	104	449	374	585	393	103	197	566	102	1144	690	1033	1149
Ba											589	224	1151	1199	3216	4867
Zr	115	614	5021	470	159	74	96	265	105	170	87	74	138	104	154	172
Hf				14.06		2.08										4.94
Nb	4.1	37.4	30.7	46.7	18.0	23.3	2.7	6.3	4.1	9.3	4.5	2.9	5.3	2.3	2.9	3.3
Ta				3.33		2.78										
Y	37	50	40	74	31	55	4	23	14	36	3	2	8	5	6	11
Th	11	5	10	15	11	14	2	8	17	11	2	2	5	3	2	2
U				0	0	0	0	0	0	0	3	3	3	3	3	3
La				72.6		13.0										6.28
Ce				170		32.5										9.2
Nd				70.5		19.4										9.94
Sm				12.9		5.21										1.25
Eu				1.82		1.16										0.7
Tb				2.01		1.28										0.27
Tm				1.20		1.02										0.17
Yb				7.50		6.24										1.04
Lu				1.20		0.97										0.19
Ni	48	1520	1122	771	1382	861	684	529	716	943	6	6	12	5	12	21
Cu	7	3	3	6	12	36	7	5	5	102	36	9	4	4	5	15

	Granitoids. Ol'Doinyo Wassin Granodiorites							Sabatchi Gneisses I			Sabatchi Gneisses II					
	SA3	SA4	SA5	SA6	SA7	SA8	SA9	SA10	SA11	SA12	SA13	SA14	SA15	SA17	SA18	SA19
SiO2	71.97	70.21	70.66	68.26	70.37	70.61	70.25	73.42	64.41	60.24	74.49	74.31	73.69	74.28	64.48	71.07
TiO2	0.51	0.12	0.22	0.17	0.13	0.16	0.19	0.17	0.89	1.26	0.2	0.2	0.29	0.24	0.53	0.39
Al2O3	10.67	18.13	16.86	18.22	17.04	17.54	17.34	15.41	14.47	15.04	13.57	13.98	14.38	13.04	16.6	15.14
Fe2O3	8.92	0.59	0.92	0.92	0.73	0.84	1.07	1.73	5.49	8.49	1.9	2.07	2.54	2.39	4.92	2.87
MnO	0.15	0.01	0.02	0.01	0.01	0.02	0.02	0.05	0.11	0.38	0.08	0.07	0.06	0.08	0.13	0.07
MgO	0.14	0.32	0.54	0.63	0.67	0.73	0.97	0.33	1.81	1.44	0.24	0.34	0.45	0.46	1.36	0.7
CaO	1.06	2.2	2.05	2.01	1.56	1.69	1.72	2.4	6.53	8.05	1.19	1.01	1.83	1.42	3.72	2.02
Na2O	2.89	7.12	6.55	6.72	6.37	6.21	6.59	5.18	5.08	3.26	4.56	4.5	4.66	4.9	5.46	5.12
K2O	3.44	1.91	1.97	2.94	2.88	2.63	2.32	1.58	0.73	0.61	3.39	3.69	2.68	2.95	2.03	2.34
P2O5	0.05	0.11	0.13	0.24	0.12	0.11	0.08	0.07	0.28	0.43	0.06	0.08	0.1	0.07	0.29	0.18
Total	99.8	100.72	99.92	100.12	99.88	100.54	100.55	100.34	99.8	99.2	99.68	100.25	100.68	99.83	99.52	99.9
Rb	31	21	28	42	39	40	42	26	10	9	59	62	52	50	40	50
Sr	209	1521	1338	1051	917	1013	1049	390	473	139	216	180	282	171	562	367
Ba	599	2743	2459	3159	3037	2594	2273	504	311	534	1132	987	763	1136	692	1062
Zr	1953	211	159	135	104	159	185	61	166	165	149	157	187	183	142	183
Hf																
Nb	30.8	2.1	1.8	3.1	2.3	2.3	3.8	4.2	5.8	7.5	4.5	4.9	4.8	4	3.9	5.4
Ta																
Y	96	5	4	11	3	6	7	6	29	42	23	23	18	26	20	17
Th	9	2	2	2	2	2	2	2	4	2	5	5	6	6	2	4
U	3	3	3	3	3	3	3	2	2	2	3	3	3	2	3	3
La																
Ce																
Nd																
Sm																
Eu																
Tb																
Tm																
Yb																
Lu																
Ni	10	6	9	10	8	8	12	10	13	13	6	6	7	7	8	7
Cu	7	22	16	4	4	5	5	4	5	6	5	5	5	5	5	5

	Western Ethiopian Granitoids. Geba Gneisses						Birbir Granodiorite--Diorite Batholith					Syntectonic Diorite	Syntectonic Granite	Post-tectonic Granites	
	SB1	ETH C	ETH E	SB317	SB320	ETH D	SB260	SB302	MT 235	SB329	AA 545	ETH A	ETH B	SB205	MT404
SiO2	71.11	67.26	73.67	65.7	69.85	74.34	72.51	72.05	63.99	67.88	49.86	46.02	77.01	75.31	77.58
TiO2	0.32	0.59	0.37	0.82	0.3	0.14	0.28	0.41	0.52	0.38	0.35	2.89	0.04	0.22	0.18
Al2O3	15.44	15.28	13.53	15.42	15.94	12.19	14.62	14.77	16	16.08	17.74	17.04	13.58	13.17	12
Fe2O3	2.19	4.85	2.8	4.4	2.25	1.67	2.36	2.72	4.77	3.54	8.25	10.98	0.35	1.13	1.82
MnO	0.04	0.09	0.07	0.13	0.03	0.01	0.04	0.08	0.08	0.08	0.18	0.14	0.06	0.02	0.05
MgO	0.95	1.74	0.63	1.7	0.92	0.4	0.8	0.85	2.23	1.46	7.35	6.55	0.37	0.37	0
CaO	2.42	4.78	2.02	3.54	3.75	0.27	2.74	2.53	5.04	4.34	11.04	11.55	0.75	0.64	1.08
Na2O	3.92	3.9	3.15	4.7	4.68	5.34	4.4	4.21	4.17	4.9	2.77	3.9	4.01	4.48	3.49
K2O	4.12	1.32	3.85	3.49	1.2	5.52	1.9	2.81	1.78	1.03	0.31	0.13	4.51	5.23	3.86
P2O5	0.08	0.2	0.07	0.33	0.1	0.02	0.1	0.14	0.26	0.12	0.06	0.55	0	0	0
Total	101.29	100.77	100.54	100.89	99.92	100.12	100.33	100.97	99.86	100.36	100.04	100.57	101.1	100.97	100.62
Rb	111	43	94	101	42	88	98	67	46	18	8	2	293	88	159
Sr	469	545	111	526	445	59	484	320	783	658	336	719	3	125	103
Ba	1433	896	537	985	448	627	2329	1164	985	1612	358	0	90	1164	358
Zr	165	146	146	263	154	310	253	110	128	108	31	28	31	188	179
Hf			5.20					4.17				0.58	1.83	6.82	
Nb	4	8	9	30	8	7	7	12	10	9	3	3	59	8	23
Ta			0.59					0.53				0.17	4.85	0.29	
Y	7	10	40	116	7	20	20	30	16	10	11	12	47	10	44
Th	16	2	10	17	6	4	16	5	3	2	1	1	8	4	27
U			1.89										46.96	0.62	
La			22.45					33.24				3.94	5.23	9.82	
Ce			52.9					69.25				9.96	17.76	22.64	
Nd			23.9					31.68				9.39	13.18	10.49	
Sm			5.22					5.97				2.6	2.63	1.95	
Eu			0.82					1.1				2.02	0.18	0.94	
Tb			1.06					0.86				0.52	1.25	0.29	
Tm			0.42					0.26				0	0	0	
Yb			4.1					2.42				0.74	4.86	0.96	
Lu			0.67					0.39				0.12	0.87	0.17	
Ni	1	12	3	17	10	2	5	5	25	2	32	50	1	1	2
Cu	7	11	7	18	19	6	16	8	20	11	41	55	7	7	8

Baragol Chromites.

		SiO2	TiO2	Al2O3	Cr2O3	FeO*	MnO	NiO	MgO	CaO	Total	M	C	F	Al	Cr	Fe3+	Mg	Fe2+
S63A SPRRA	C	0.13	0.16	7.88	56.25	23.22	0.34	0.10	10.64	0.01	98.73	53.30	82.70	9.30	2.49	11.90	1.48	4.24	3.72
S63A SPRRB	C	0.08	0.12	8.13	55.41	23.16	0.38	0.11	10.83	0.01	98.23	54.60	82.00	10.00	2.57	11.75	1.59	4.33	3.60
S63A SPRRC	C	0.05	0.12	7.02	57.46	22.84	0.37	0.10	10.43	0.01	98.40	52.90	84.60	9.00	2.23	12.26	1.43	4.20	3.73
S63A SPRRD	C	0.08	0.15	7.43	57.22	22.54	0.34	0.09	10.80	0.01	98.66	54.30	83.80	8.90	2.35	12.13	1.42	4.32	3.64
S63A SPRRE	C	0.05	0.13	7.99	56.53	23.60	0.37	0.10	10.80	0.03	99.60	53.80	82.60	9.90	2.50	11.85	1.58	4.27	3.66
S63H SPKKD	C	0.05	0.16	7.43	59.35	20.69	0.42	0.09	10.87	0.01	99.07	54.60	84.30	6.50	2.34	12.54	1.03	4.33	3.60
S63H SPKKE	C	0.05	0.20	8.10	59.66	19.68	0.42	0.10	11.20	0.01	99.42	55.80	83.20	5.40	2.53	12.51	0.86	4.43	3.51
S63H SPKKF	R	0.03	0.13	6.86	59.88	21.21	0.42	0.04	10.74	0.03	99.34	54.10	85.40	6.90	2.16	12.66	1.11	4.28	3.64
S63H SPYYB	C	0.05	0.22	8.50	58.73	19.07	0.41	0.06	11.47	0.01	98.52	57.30	82.20	5.40	2.67	12.37	0.85	4.55	3.40
S63H SPYYC	C	0.05	0.21	7.88	58.94	19.49	0.40	0.07	11.38	0.01	98.43	57.10	83.40	6.00	2.48	12.46	0.95	4.53	3.41
S64B SPBBB	C	0.08	0.13	8.71	61.68	14.48	0.32	0.10	13.63	0.01	99.14	66.60	82.60	3.20	2.68	12.72	0.51	5.30	2.65
S64B SPBBC	C	0.10	0.13	8.82	61.77	14.18	0.32	0.13	13.57	0.01	99.03	66.40	82.40	2.70	2.72	12.57	0.43	5.28	2.67
S64B SPBBD	C	0.05	0.13	9.09	61.44	14.33	0.33	0.07	13.78	0.01	99.23	67.20	81.90	3.20	2.79	12.63	0.51	5.34	2.61
S64B SPBBE	C	0.08	0.13	8.85	61.21	14.47	0.35	0.09	13.75	0.01	98.94	67.30	82.30	3.50	2.72	12.63	0.56	5.35	2.60
S64D SPSSA	C	0.05	0.10	7.88	60.04	18.74	0.43	0.07	11.57	0.01	98.89	57.90	83.60	5.30	2.47	12.63	0.84	4.59	3.33
S64D SPSSD	C	0.10	0.16	8.80	60.04	17.83	0.42	0.09	11.86	0.01	99.31	58.60	82.10	4.10	2.73	12.51	0.64	4.66	3.29
S64D SPSSE	C	0.08	0.10	7.50	59.97	19.06	0.42	0.10	11.41	0.01	98.65	57.40	84.30	5.50	2.36	12.67	0.88	4.54	3.38
S64D SPSSF	C	0.05	0.15	8.94	61.02	17.50	0.40	0.07	11.86	0.01	100.00	58.30	82.10	3.30	2.76	12.63	0.52	4.63	3.31
S64D SPSSH	C	0.08	0.15	8.63	60.52	16.99	0.42	0.06	11.96	0.01	98.82	59.40	82.50	3.40	2.69	12.67	0.54	4.72	3.22
S64D SPSSK	C	0.08	0.13	8.95	60.01	17.42	0.41	0.09	11.60	0.03	98.72	57.80	81.80	3.30	2.80	12.58	0.52	4.59	3.34
S64D SPSSL	C	0.08	0.16	8.99	59.88	17.71	0.39	0.09	11.73	0.01	99.04	58.10	81.70	3.70	2.80	12.51	0.59	4.62	3.33
S64D SPSSM	C	0.08	0.10	7.97	59.69	19.01	0.40	0.06	11.41	0.01	98.73	57.10	83.40	5.20	2.50	12.58	0.84	4.53	3.40
S64E SPKKC	C	0.08	0.13	7.16	58.14	24.17	0.54	0.04	8.50	0.01	98.77	43.70	84.50	6.70	2.30	12.54	1.06	3.46	4.46
S64E SPEEA	C	0.08	0.13	9.47	58.95	18.03	0.48	0.09	11.80	0.01	99.04	58.50	80.70	4.30	2.94	12.28	0.69	4.63	3.28
S64E SPEEB	C	0.10	0.13	8.97	59.08	18.65	0.46	0.07	11.71	0.01	99.18	58.00	81.50	4.90	2.79	12.32	0.79	4.60	3.33
S64E SPEEC	C	0.10	0.13	9.04	59.37	18.14	0.52	0.07	11.68	0.01	99.06	58.10	81.50	4.30	2.81	12.40	0.69	4.60	3.32
S64E SPEEE	C	0.13	0.13	9.11	58.91	18.72	0.45	0.06	11.54	0.03	99.08	57.20	81.30	4.70	2.84	12.30	0.74	4.54	3.39
S64E SPEEG	R	0.08	0.13	8.88	59.03	18.78	0.49	0.07	11.53	0.01	99.00	57.40	81.70	4.90	2.77	12.35	0.79	4.55	3.37
S65B SPMMA	C	0.05	0.16	8.88	58.79	18.69	0.51	0.12	11.74	0.03	98.97	58.60	81.60	5.40	2.77	12.28	0.86	4.62	3.27

			SiO2	TiO2	Al2O3	Cr2O3	FeO*	MnO	NiO	MgO	CaO	Total	M	C	F	Al	Cr	Fe3+	Mg	Fe2+
S65B	SPMMB	C	0.08	0.15	8.27	58.91	19.17	0.52	0.11	11.63	0.03	98.87	58.20	82.70	6.00	2.59	12.36	0.95	4.60	3.30
S65B	SPMMD		0.08	0.15	9.30	58.15	18.07	0.49	0.10	12.02	0.01	98.37	59.90	80.70	5.20	2.90	12.17	0.83	4.74	3.18
S65B	SPMME		0.08	0.18	9.53	57.88	19.15	0.46	0.12	11.13	0.01	98.54	55.60	80.30	4.70	2.99	12.16	0.74	4.41	3.52
S65B	SPMMF		0.05	0.15	8.29	58.34	20.19	0.49	0.11	11.14	0.01	98.77	56.00	82.50	6.40	2.60	12.29	1.02	4.42	3.48
S65B	SPMMG		0.08	0.15	7.96	58.39	20.54	0.56	0.07	11.03	0.01	98.79	55.50	83.10	6.70	2.51	12.32	1.07	4.39	3.52
S65D	SPLLA	C	0.08	0.18	7.84	56.33	22.27	0.46	0.10	11.15	0.01	98.42	56.10	82.80	9.40	2.47	11.91	1.50	4.45	3.48
S65D	SPLLB	C	0.08	0.15	8.26	56.72	21.70	0.46	0.11	11.25	0.01	98.74	56.30	82.20	8.60	2.59	11.93	1.37	4.46	3.46
S65D	SPLLC	C	0.08	0.16	7.45	58.01	21.43	0.48	0.10	11.11	0.03	98.85	55.90	83.90	8.20	2.35	12.25	1.30	4.42	3.49
S65D	SPLLD	C	1.09	0.16	7.34	57.11	20.48	0.44	0.12	11.78	0.03	98.55	57.00	83.90	6.80	2.30	12.01	1.04	4.67	3.52
S65D	SPLLE	C	0.08	0.18	7.66	57.91	21.45	0.47	0.07	11.13	0.01	98.96	55.70	83.50	8.00	2.41	12.21	1.27	4.42	3.51
S65D	SPLLF	R	0.08	0.18	7.13	56.47	23.46	0.46	0.13	10.84	0.01	98.76	54.70	84.20	10.50	2.25	11.96	1.67	4.33	3.59
S65E	SPPPA	C	0.08	0.12	8.29	58.99	18.94	0.49	0.10	11.58	0.01	98.60	58.10	82.70	5.60	2.60	12.41	0.90	4.59	3.32
S65E	SPPPD	C	0.05	0.10	8.34	59.71	18.63	0.49	0.10	11.78	0.01	99.21	58.70	82.80	5.40	2.60	12.48	0.86	4.64	3.26
S65E	SPSSA	C	0.08	0.12	8.73	58.86	22.09	0.46	0.06	8.84	0.03	99.27	44.80	81.90	3.80	2.77	12.53	0.61	3.55	4.37
S65E	SPSSC	C	0.08	0.12	8.81	58.82	22.15	0.50	0.04	8.99	0.01	99.52	45.40	81.70	4.10	2.79	12.48	0.65	3.59	4.32
S65E	SPSSD	C	0.10	0.12	8.11	59.75	21.94	0.53	0.03	8.82	0.01	99.41	44.80	83.20	3.60	2.58	12.74	0.58	3.55	4.37
S65E	SPSSE	C	0.10	0.12	8.88	57.80	22.67	0.48	0.04	8.82	0.01	98.92	44.70	81.40	4.60	2.83	12.34	0.74	3.55	4.38
S65G	SPXXA	C	0.05	0.10	8.19	59.18	18.37	0.43	0.10	11.95	0.03	98.40	59.90	82.90	5.80	2.57	12.45	0.92	4.74	3.17
S65G	SPXXB	C	0.08	0.13	8.96	59.85	17.31	0.43	0.12	11.92	0.01	98.81	59.30	81.70	3.80	2.79	12.51	0.60	4.70	3.22
S65G	SPXXC	C	0.08	0.13	8.54	59.87	17.54	0.43	0.09	12.10	0.01	98.79	60.20	82.50	4.50	2.66	12.52	0.72	4.77	3.16
S65G	SPXXD	C	0.08	0.13	8.59	60.25	16.74	0.41	0.09	12.34	0.01	98.64	61.30	82.50	4.00	2.68	12.60	0.63	4.86	3.07
S65G	SPXXF	C	0.05	0.12	8.84	59.42	17.38	0.42	0.10	11.98	0.01	98.32	59.90	81.80	4.30	2.77	12.47	0.68	4.74	3.18

Moyale Chromites.

			SiO2	TiO2	Al2O3	Cr2O3	FeO*	MnO	NiO	MgO	CaO	Total	M	C	F	Al	Cr	Fe3+	Mg	Fe2+
M64A	SPFFB	C	0.08	0.18	19.20	49.26	17.29	0.13	0.12	13.07	0.03	99.36	60.90	63.20	3.10	5.66	9.74	0.49	4.87	3.12
M64A	SPRRA	C	0.08	0.17	21.74	48.13	15.26	0.13	0.16	14.53	0.01	100.21	66.00	59.80	2.50	6.24	9.27	0.39	5.27	2.72
M64A	SPRRB	C	0.11	0.15	21.29	48.37	15.40	0.13	0.15	14.50	0.01	100.11	66.00	60.40	2.70	6.13	9.34	0.43	5.28	2.72
M64A	SPRRC	C	0.08	0.18	20.77	48.41	15.53	0.16	0.16	14.49	0.03	99.81	66.40	61.00	3.20	6.01	9.39	0.50	5.30	2.68
M64A	SPRRD	C	0.08	0.17	22.30	46.78	15.79	0.16	0.17	14.40	0.01	99.86	65.60	58.40	3.00	6.41	9.02	0.47	5.23	2.75
M64A	SPRRE	C	0.05	0.18	22.14	47.74	15.45	0.16	0.15	14.64	0.01	100.52	66.30	59.10	2.80	6.33	9.15	0.44	5.29	2.69
M64A	SPRRF	C	0.11	0.17	21.69	48.09	15.49	0.13	0.15	14.64	0.01	100.48	66.20	59.80	2.80	6.21	9.23	0.44	5.30	2.70

	SiO2	TiO2	Al2O3	Cr2O3	FeO*	MnO	NiO	MgO	CaO	Total	M	C	F	Al	Cr	Fe3+	Mg	Fe2+
M64A SPRRG R	0.11	0.15	21.10	48.18	15.80	0.16	0.13	14.27	0.08	99.98	65.30	60.50	3.00	6.09	9.33	0.47	5.21	2.77
M64B SPTTA C	0.11	0.20	21.06	48.06	16.74	0.16	0.13	13.78	0.03	100.27	63.00	60.50	3.00	6.09	9.32	0.47	5.04	2.96
M64B SPTTB C	0.05	0.23	20.59	48.25	16.95	0.17	0.12	13.33	0.01	99.70	61.50	61.10	2.70	6.01	9.44	0.44	4.92	3.07
M64B SPTTC C	0.08	0.23	23.61	44.48	19.86	0.24	0.12	11.53	0.03	100.18	53.10	55.80	2.20	6.86	8.67	0.35	4.24	3.74
M64B SPTTD C	0.11	0.20	20.87	48.22	16.89	0.16	0.14	13.49	0.03	100.11	61.90	60.80	2.70	6.06	9.38	0.43	4.95	3.05
M64B SPTTE C	0.08	0.20	19.94	49.37	16.81	0.16	0.12	13.65	0.03	100.36	62.70	62.40	3.00	5.79	9.61	0.48	5.01	2.98
M64B SPTTF R	0.08	0.18	20.29	49.17	16.78	0.16	0.12	13.50	0.01	100.29	62.00	61.90	2.70	5.89	9.58	0.42	4.96	3.04
M64D SPYYA C	0.14	0.18	22.31	47.18	15.61	0.13	0.16	14.57	0.03	100.31	65.90	58.60	2.70	6.38	9.05	0.44	5.27	2.73
M64D SPYYB C	0.05	0.17	23.02	46.31	15.71	0.10	0.16	14.74	0.01	100.27	66.50	57.40	3.10	6.56	8.85	0.50	5.31	2.68
M64D SPYYC C	0.08	0.18	22.33	47.56	15.61	0.13	0.16	14.69	0.01	100.75	66.20	58.80	2.80	6.36	9.08	0.45	5.29	2.70
M64D SPYYD C	0.08	0.20	23.23	45.94	15.79	0.16	0.15	14.58	0.03	100.16	65.90	57.00	3.00	6.63	8.79	0.47	5.26	2.73
M64D SPYYE C	0.08	0.19	23.70	45.27	15.98	0.14	0.16	14.61	0.01	100.14	65.80	56.20	3.10	6.75	8.65	0.50	5.26	2.73
M64D SPYYF R	0.11	0.22	23.51	45.77	16.29	0.13	0.12	14.28	0.03	100.46	64.20	56.60	2.70	6.70	8.74	0.43	5.14	2.87
M64E SPSSA C.0	0.08	0.22	23.82	45.00	16.69	0.16	0.13	14.07	0.01	100.18	63.50	55.90	2.90	6.80	8.62	0.46	5.08	2.92
M64E SPSSB C	0.08	0.19	23.10	46.15	16.48	0.13	0.15	14.22	0.03	100.53	64.20	57.30	3.00	6.59	8.83	0.47	5.13	2.86
M64E SPSSC C	0.08	0.22	25.48	43.20	16.56	0.18	0.16	14.41	0.03	100.32	64.50	53.20	3.10	7.20	8.19	0.49	5.15	2.83
M64E SPSSD C	0.06	0.23	25.99	43.11	15.99	0.12	0.16	14.94	0.01	100.61	66.30	52.70	3.00	7.29	8.11	0.48	5.30	2.70
M64E SPSSE R	0.06	0.22	26.53	42.29	16.13	0.17	0.16	14.84	0.01	100.41	65.90	51.70	3.10	7.44	7.96	0.49	5.26	2.72
M64E SPSSF C	0.05	0.18	22.15	47.05	16.24	0.13	0.12	14.18	0.03	100.13	64.50	58.80	3.00	6.37	9.07	0.48	5.15	2.83
M64E SPSSG R	0.08	0.19	23.22	45.96	16.31	0.16	0.17	13.86	0.04	99.99	63.10	57.00	2.40	6.67	8.85	0.38	5.03	2.95
M64F SPXXA C	0.05	0.16	21.60	47.63	16.20	0.15	0.16	14.31	0.01	100.27	65.20	59.70	3.30	6.21	9.18	0.53	5.20	2.78
M64F SPXXB C	0.08	0.17	22.01	46.88	16.59	0.16	0.15	13.93	0.01	99.98	63.60	58.80	3.10	6.35	9.06	0.49	5.08	2.91
M64F SPXXC C	0.05	0.17	22.47	46.49	16.08	0.16	0.16	14.40	0.01	99.99	65.50	58.10	3.30	6.45	6.95	0.52	5.22	2.75
M64F SPXXD C	0.14	0.17	24.68	44.44	15.59	0.14	0.17	15.11	0.04	100.48	67.40	54.70	3.20	6.96	8.40	0.51	5.39	2.61
M64F SPXXE C	0.08	0.17	23.60	45.37	15.73	0.11	0.19	14.85	0.01	100.11	66.90	56.30	3.30	6.72	8.66	0.53	5.34	2.65
M64F SPXXF R	0.05	0.20	23.50	45.21	16.73	0.13	0.15	14.22	0.01	100.20	64.30	56.30	3.40	6.71	6.66	0.53	5.13	2.86

Pyroxene analyses from the Moyale Chromites

	SiO2	TiO2	Al2O3	Cr2O3	FeO*	MnO	MgO	CaO	Na2O	Total
M64A SMRRK C	53.79	0.08	1.49	0.00	0.97	0.08	17.42	24.83	0.27	98.93
M64A SMRRL C	53.75	0.10	1.49	0.00	1.14	0.06	17.30	24.90	0.20	98.94
M64B CXTTG C	53.84	0.08	1.65	0.00	1.24	0.08	17.18	24.42	0.49	98.98
M64B CXTTH C	53.79	0.08	1.84	0.00	2.03	0.09	17.21	23.36	0.60	99.00
M64B CXTTL C	54.27	0.06	1.30	0.00	1.36	0.06	17.33	24.31	0.41	99.10
M64B1CXTTM C	53.61	0.08	2.11	0.00	2.09	0.09	17.28	22.82	0.61	98.69
M64B1CXTTN C	53.96	0.09	2.05	0.00	2.68	0.09	21.45	18.17	0.38	98.87
M64B1CXTTO C	53.60	0.10	2.01	0.00	1.28	0.08	16.99	24.31	0.44	98.81
M64D CXYYG C	54.13	0.08	1.78	1.35	1.75	0.09	17.10	23.37	0.54	100.19
M64D CXYYH C	54.01	0.09	2.01	1.42	2.02	0.06	17.17	23.01	0.60	100.39
M64D CXYYI C	54.01	0.08	1.89	1.30	1.16	0.06	17.08	24.10	0.46	100.14
M64D CXYYJ C	54.45	0.08	1.39	1.00	1.34	0.08	17.26	24.18	0.37	100.15
M64D CXYYL C	54.28	0.08	1.67	1.11	1.13	0.06	17.27	24.49	0.35	100.44
M64E CXSSI C	53.84	0.11	1.81	1.00	1.14	0.08	17.34	24.33	0.41	100.06
M64E CXSSJ C	53.95	0.10	1.71	1.13	1.24	0.08	17.08	24.37	0.43	100.09
M64E CXSSM C	53.61	0.13	2.14	1.13	1.23	0.06	17.34	23.99	0.34	99.97
M64F CXXXH C	53.78	0.10	1.65	1.30	1.26	0.08	17.19	24.28	0.35	99.99
M64F CXXXI C	54.23	0.08	1.43	1.30	1.20	0.06	17.27	24.19	0.34	100.10
M64F CXXXK C	54.33	0.08	1.89	1.25	1.34	0.06	17.00	23.98	0.44	100.37
M64F CXXXL C	53.92	0.08	2.08	1.30	2.02	0.09	16.94	22.86	0.60	99.89

NORM RESULTS

	vol%	NE	QTZ	ORTH	ALB	ANOR	RIEB	AEG	AUG	HBL	BIOT	MSC	MAG	HAEM	ILM	AP
NE Kenya																
Kufole																
SM4B	.0	30.5	27.9	35.2	3.1	.0	.0	.0	.0	.7	1.6	.0	.8	.1	.1	
SM4C	.0	31.4	28.4	33.0	2.6	.0	.0	.0	.0	.9	2.7	.0	.9	.1	.1	
SM4D	.0	29.0	30.9	34.4	3.3	.0	.0	.0	.0	.8	.4	.0	.9	.2	.1	
SM4E	.0	29.7	30.5	33.5	2.9	.0	.0	.0	.0	.7	1.6	.0	.9	.2	.1	
Fugugo																
SM5	.0	13.2	21.0	39.3	11.8	.0	.0	.0	.8	7.7	.0	.0	3.1	1.2	1.7	
SM6	.0	14.2	20.6	39.6	11.7	.0	.0	.0	.0	8.0	.0	.0	3.0	1.2	1.6	
SM7	.0	14.3	21.7	38.6	11.9	.0	.0	.0	.8	7.0	.0	.0	3.0	1.2	1.6	
SM8	.0	13.1	35.1	36.6	7.4	.0	.0	.0	1.1	3.6	.0	.0	2.0	.7	.6	
SM9	.0	13.9	21.7	39.6	11.2	.0	.0	.0	2.3	5.4	.0	.0	3.1	1.2	1.7	
SM10	.0	12.6	23.7	41.2	11.7	.0	.0	.0	1.4	5.1	.0	.0	2.5	.9	1.0	
SM11	.0	14.5	22.4	40.8	11.4	.0	.0	.0	1.3	5.4	.0	.0	2.4	.9	.9	
SM12	.0	13.2	21.2	40.9	12.0	.0	.0	.0	.0	8.0	.0	.0	2.7	.9	1.1	
Moyale																
SM13	.0	30.5	7.9	39.7	15.6	.0	.0	.0	.0	3.3	1.6	.0	1.2	.2	.2	
SM14	.0	31.6	9.2	37.8	15.9	.0	.0	.0	.0	3.8	.2	.1	1.2	.2	.2	
SM15	.0	22.8	7.1	43.1	20.3	.0	.0	.0	.0	4.8	.0	.2	1.1	.2	.3	
SM16	.0	25.1	26.2	41.5	2.9	.0	.0	.0	.0	1.9	1.5	.0	.7	.1	.2	
SM18	.0	27.5	26.1	40.4	3.5	.0	.0	.0	.0	.6	1.1	.0	.6	.2	.1	
SM19	.0	23.6	27.7	41.3	4.0	.0	.0	.0	.0	2.2	0.0	.0	.7	.2	.3	
SM20	.0	24.7	10.4	40.2	16.9	.0	.0	.0	.0	4.0	1.9	.0	1.3	.2	.3	
SM21	.0	22.0	7.0	45.0	19.6	.0	.0	.0	.0	4.6	.0	.2	1.1	.2	.2	
Adadi Jolle																
SM41	.0	37.6	24.0	32.9	1.4	.0	.0	.0	.0	.6	2.8	.0	.6	0.0	.1	
SM42	.0	35.4	24.7	33.1	2.0	.0	.0	.0	.0	.9	3.4	.0	.5	0.0	.1	
SM43	.0	31.7	30.2	28.3	3.9	.0	.0	.0	.0	1.0	2.9	.0	1.6	.3	.2	
SM44	.0	31.4	28.9	32.0	2.6	.0	.0	.0	.0	.8	2.6	.0	1.4	.2	.1	
SM45	.0	36.1	29.1	30.1	2.9	.0	.0	.0	.0	.7	0.0	0.0	1.0	0.0	.1	
SM46	.0	32.5	28.4	28.4	3.7	.0	.0	.0	.0	1.2	3.9	.0	1.4	.3	.2	
Central Kenya																
Ol'Doinyo Wassin																
SA1	.0	20.3	8.9	46.4	15.7	.0	.0	.0	.2	5.1	.0	.1	2.3	.3	.6	
SA2	.0	12.0	18.3	51.6	6.9	.0	.0	.0	.0	4.0	6.0	0.0	.7	.1	.4	
SA3	.0	41.5	20.5	25.8	4.9	.0	.0	.0	.0	.9	1.1	.0	4.7	.5	.1	
SA4	.0	16.9	9.4	60.5	9.7	.0	.0	.0	.0	1.2	1.7	.0	.3	.1	.2	
SA5	.0	21.0	9.8	56.2	9.0	.0	.0	.0	.0	2.1	1.1	.0	.4	.1	.3	
SA6	.0	14.2	14.6	57.5	8.1	.0	.0	.0	.0	2.4	2.3	0.0	.4	.1	.5	
SA7	.0	19.3	14.2	54.6	6.7	.0	.0	.0	.0	2.5	2.2	.1	.2	0.0	.2	
SA8	.0	21.0	10.3	53.0	7.3	.0	.0	.0	.0	2.7	5.0	0.0	.3	0.0	.2	
SA9	.0	19.5	9.9	56.3	7.7	.0	.0	.0	.0	3.6	2.3	.2	.3	0.0	.2	
Sabatchi Gneisses I																
SA10	.0	32.4	6.4	44.6	11.1	.0	.0	.0	.0	1.3	3.1	.0	.8	.1	.1	
SA11	.0	18.0	4.6	43.2	10.3	.0	.0	7.1	13.4	.0	.0	.0	2.3	.7	.6	
SA12	.0	21.5	3.9	26.5	19.4	.0	.0	.0	23.3	.0	.0	.0	3.4	1.0	.9	
Sabatchi Gneisses II																
SA13	.0	32.8	19.4	39.3	5.3	.0	.0	.0	.0	1.1	1.0	.0	.9	.2	.1	
SA14	.0	32.1	19.4	38.6	4.3	.0	.0	.0	.0	1.4	2.9	.0	1.0	.2	.2	
SA15	.0	32.7	13.7	40.0	8.1	.0	.0	.0	.0	1.8	1.9	.0	1.2	.2	.2	

SA17	.0	31.5	18.1	41.8	4.0	.0	.0	.0	3.1	.0	.0	.0	1.1	.2	.1
SA18	.0	18.1	11.6	47.9	14.0	.0	.0	.0	3.3	1.8	.0	0.0	2.4	.4	.6
SA19	.0	28.9	10.8	44.5	8.6	.0	.0	.0	.0	2.8	2.4	.0	1.4	.3	.4
S Ethiopia															
Gariboro															
D4	.0	35.0	26.6	31.8	2.1	.0	.0	.0	.0	.8	2.7	.0	.7	.2	.1
D5	.0	35.2	25.9	28.3	3.7	.0	.0	.0	.0	.9	4.7	.0	.9	.2	.2
D6	.0	31.8	29.7	25.1	5.8	.0	.0	.0	.0	1.7	5.0	.0	.6	.1	.1
D8	.0	36.0	19.4	34.5	1.8	.0	.0	.0	.0	1.1	5.7	.0	1.0	.2	.1
D9	.0	38.2	23.6	30.0	4.1	.0	.0	.0	.0	.5	2.8	.0	.6	.1	.1
D10	.0	25.2	23.5	39.9	7.0	.0	.0	.0	.0	2.4	1.0	.0	.7	.2	.2
D11	.0	39.6	26.0	24.1	1.6	.0	.0	.0	.0	.6	6.8	.0	1.1	.2	.1
D12	.0	36.2	23.0	31.4	4.3	.0	.0	.0	.0	.1	4.2	.0	.6	.1	.1
Godoloka															
D1	.0	25.1	34.8	31.2	5.2	.0	.0	.0	.0	.4	.9	.0	1.9	.4	.2
D2	.0	26.5	32.6	34.3	3.6	.0	.0	.0	.0	.9	.2	.0	1.5	.3	.1
D3	.0	24.0	30.2	37.7	4.2	.0	.0	.0	1.2	.0	.0	.0	2.1	.4	.3
W Ethiopia															
Geba Gneisses															
SB1	.0	27.6	22.7	33.6	11.0	.0	.0	.0	.0	3.6	.0	.1	.9	.2	.2
ETH C	.0	30.4	6.6	34.1	19.3	.0	.0	.0	3.9	2.5	.0	.1	2.2	.5	.4
ETH E	.0	36.8	20.9	27.2	9.3	.0	.0	.0	.0	2.5	1.5	.0	1.4	.3	.1
SB317	.0	17.8	21.8	40.0	8.5	.0	.0	.0	8.6	.0	.0	.0	1.9	.7	.6
SB320	.0	31.1	5.1	41.1	17.7	.0	.0	.0	.0	3.6	.0	.1	1.0	.2	.2
ETH D	.0	25.6	32.6	33.1	.0	1.8	5.0	.4	.0	.0	.0	1.4	.0	.1	0.0
Birbir Granodiorite-Diorite															
SB260	.0	34.6	9.0	38.3	12.6	.0	.0	.0	.0	3.1	.9	0.0	1.1	.2	.2
SB302	.0	32.0	14.6	36.3	11.3	.0	.0	.0	.0	3.4	.6	.0	1.3	.3	.3
MT 235	.0	23.2	10.6	36.6	18.3	.0	.0	.0	6.8	1.2	.0	.5	1.9	.4	.5
SB329	.0	26.8	5.2	42.7	17.8	.0	.0	.0	3.5	1.8	.0	.3	1.4	.3	.2
AA 545	.0	6.1	2.1	21.8	28.6	.0	.0	.0	38.4	.0	.0	.0	2.9	.0	.1
Syntectonic Diorite															
ETH A	5.9	.0	.5	27.0	16.7	.0	.0	.0	43.4	.0	.0	.0	3.4	2.1	1.0
Syntectonic Granite															
ETH B	.0	34.3	21.6	33.9	3.5	.0	.0	.0	.0	1.5	2.1	.1	.1	.0	.0
Post-tectonic Granites															
SB205	.0	27.3	31.5	37.6	.0	.0	.0	1.3	1.6	.0	.0	.0	.5	.2	.0
MT 404	.0	40.2	23.2	29.9	5.1	.0	.0	.0	.0	.1	.4	.0	.9	.2	.0
Baragoi N Kenya															
Luwamara Granite															
SB82A	.0	28.9	17.4	40.9	7.6	.0	.0	.0	.0	1.9	2.6	.0	.5	.1	.1
SB82B	.0	25.5	21.7	45.3	6.4	.0	.0	.0	.0	.7	.1	.1	.2	.0	.1
Sartim Granite															
SB9A	.0	22.0	14.7	45.3	11.8	.0	.0	.0	.0	4.1	.3	.0	1.2	.4	.4
SB9B	.0	25.0	20.0	43.2	8.5	.0	.0	.0	.0	1.7	.7	.0	.6	.2	.1

vol%	Neph	Qtz	AFspar	Plag	An(wt%)	
Granitoi	.0	-5.9	105.9	.0	.0	Palk
SM4B	.0	31.5	42.4	26.1	12.7	Palm
SM4C	.0	32.8	43.9	23.3	12.3	Palm
SM4D	.0	29.6	46.2	24.2	14.5	Palm
SM4E	.0	30.6	46.2	23.2	13.5	Palm
SM5	.0	15.4	33.6	51.0	28.2	Malm
SM6	.0	16.5	32.7	50.8	27.8	Malm
SM7	.0	16.5	34.1	49.4	28.8	Malm
SM8	.0	14.2	52.6	33.2	25.1	Malm
SM9	.0	16.0	34.4	49.6	27.1	Malm
SM10	.0	14.1	36.3	49.6	27.4	Malm
SM11	.0	16.3	34.4	49.3	26.9	Malm
SM12	.0	15.1	33.2	51.7	27.5	Malm
SM13	.0	32.5	11.3	56.1	30.7	Palm
SM14	.0	33.4	13.0	53.6	32.5	Palm
SM15	.0	24.4	10.2	65.4	34.4	Palm
SM16	.0	26.1	41.0	32.9	9.6	Palm
SM18	.0	28.1	39.6	32.3	11.7	Palm
SM19	.0	24.3	42.1	33.5	12.8	Malm
SM20	.0	26.8	15.1	58.1	32.6	Palm
SM21	.0	23.4	10.1	66.5	32.5	Malm
SM41	.0	39.0	38.0	23.0	6.8	Palm
SM42	.0	37.0	38.9	24.1	9.0	Palm
SM43	.0	33.6	45.4	21.0	20.6	Palm
SM44	.0	33.0	44.7	22.3	12.8	Palm
SM45	.0	36.7	43.0	20.3	15.2	Palm
SM46	.0	34.8	43.5	21.6	19.0	Palm
SA1	.0	22.2	13.3	64.4	27.7	Malm
SA2	.0	13.5	30.1	56.4	14.4	Palm
SA3	.0	44.7	30.9	24.4	22.7	Palm
SA4	.0	17.5	14.2	68.3	15.4	Palm
SA5	.0	21.9	14.8	63.3	15.4	Palm
SA6	.0	15.1	22.5	62.4	14.3	Palm
SA7	.0	20.3	22.0	57.7	12.8	Palm
SA8	.0	22.8	16.5	60.7	13.8	Palm
SA9	.0	20.9	15.5	63.7	13.5	Palm
SA10	.0	34.3	9.6	56.2	21.7	Palm
SA11	.0	23.7	8.5	67.8	20.7	Malm
SA12	.0	30.1	6.9	62.9	44.5	Malm
SA13	.0	33.8	29.1	37.1	15.5	Palm
SA14	.0	33.9	30.2	35.9	13.3	Palm
SA15	.0	34.6	20.6	44.8	19.9	Palm
SA17	.0	32.9	28.2	38.9	11.3	Malm
SA18	.0	19.7	17.5	62.8	25.2	Malm
SA19	.0	31.1	16.6	52.3	18.5	Palm
D4	.0	36.5	41.5	22.0	10.2	Palm
D5	.0	37.8	39.8	22.5	18.2	Palm
D6	.0	34.3	43.5	22.2	29.5	Palm
D8	.0	39.1	32.1	28.8	7.3	Palm
D9	.0	39.7	35.2	25.1	17.9	Palm
D10	.0	26.3	35.0	38.7	19.6	Palm
D11	.0	43.3	42.0	14.7	12.1	Palm
D12	.0	38.1	34.8	27.2	17.4	Palm
D1	.0	25.9	50.3	23.8	23.6	Palm
D2	.0	27.2	48.7	24.1	15.9	Malm
D3	.0	24.9	45.6	29.6	15.5	Malm

SB1	.0	29.0	32.2	38.8	31.0	Palm
ETH C	.0	33.7	9.5	56.8	38.7	Palm
ETH E	.0	39.0	29.7	31.3	32.5	Palm
SB317	.0	20.2	34.7	45.2	22.2	Palm
SB320	.0	32.7	7.1	60.1	32.1	Palm
ETH D	.0	27.9	72.1	.0	.0	Palk
SB260	.0	36.6	13.0	50.4	27.5	Palm
SB302	.0	34.0	21.1	44.9	27.6	Palm
MT 235	.0	26.2	15.6	58.2	36.6	Palm
SB329	.0	29.0	7.6	63.4	31.4	Palm
AA 545	.0	10.4	4.3	85.4	58.4	Palm
ETH A	11.8	.0	1.2	87.0	39.6	Palm
ETH B	.0	35.5	37.4	27.1	14.1	Palm
SB205	.0	28.0	72.0	.0	.0	Palm
MT 404	.0	40.7	33.3	26.0	20.9	Palm
SB82A	.0	30.4	26.2	43.5	19.2	Palm
SB82B	.0	25.7	31.8	42.5	15.8	Palm
SB9A	.0	23.4	21.8	54.8	23.8	Palm
SB9B	.0	25.8	29.3	44.9	20.4	Palm

APPENDIX C

DIGITAL IMAGE PROCESSING

1. Introduction to image processing

A digital image is a numerical representation of a sampled field. Typically the field represented is the radiance of a scene viewed in some region of the electromagnetic spectrum. The digital image is generated by sampling and measuring the local field strength of a number of points that are usually arranged in a rectilinear pattern. The field strength measured at each of these points is encoded as an integer. Thus the digital image is actually an array of numbers, which can be stored om magnetic tape or disc. The information stored on a computer compatible tape (CCT) is not in a form in which it can be exploited to its full advantage, thus the tape is digitally processed so as to present the data in the best possible manner. The optimum presentation depends on the particular interest in a scene, consequently a number of different enhancement procedures are available.

2. Image correction or cosmetic processing

This is performed on the data before image enhancement is carried out and involves rectification, or compensation for geometric anfd radiometric distortions introduced by the imaging instrument and elimination of systematic or coherent noise. The parameters considered are atmospheric and geometric corrections, scan line offsets, line dropouts and sixth line banding.

2.1 Atmospheric correction

In theory, areas not in direct sunlight should have DN values of zero. However, because of backscattering within the atmosphere these shadows can be illuminated indirectly. Band 7 is essentially unaffected by this scattering thus on a band 7 image DN's of 0 or 1 are assigned to shadows. The atmospheric effect for the other bands can be corrected by assuming the lower cut-offs in the relevant DN histograms are due to scattering and offsetting the histograms so the

lowest DN is allocated a value of zero. The histograms are shifted by different amounts because scattering is inversely proportional to wavelength (Hunt, 1980). Sabins (1978) reported typical offsets of 3, 6 and 11 for bands 6,5 and 4 respectively.

2.2 Geometric corrections

Geometric corrections have to be applied to the CCT to prevent scale distortions. Non-systemtic distortions cannot be predicted and vary from image to image. They are due to changes in velocity, altitude, roll, pitch or yaw of the satellite. The correction needed is deduced from orbital parameters (as determined by tracking data) or by comparing gound control points - whose positions are accurately known - with their observed location on an image. (It is extremely difficult to find such control points in poorly known featureless terain).

Distortion in the scan line direction occurs because the Earth rotates in the finite time (28 seconds) it takes to record a scene. This is compensated for by offsetting successive groups of 6 scan lines which results in the images having a parallelogram shape.

Systematic distortions are caused by parameters whose effects are constant and known e.g. scan skew, mirror velocity variations and scanner distortions. Up to about 1979 geometric corrections were applied when the data were used to produce the "archival images" but not to the CCT's. Since then a correction to account for the Earth's rotation has been applied to most tapes.

2.3 Scan lines

Some scan lines are offset relative to adjacent lines. At large scales this effect degrades the image. Corrections are applied by accurately aligning the start of every scan line.

2.4. Dropout lines and sixth line banding

Serious degradation can occur if some scan lines are represented by a DN value of zero due to a defect in the system. A correction is applied in which a DN value is assigned to every pixel in this line by taking the average of the DN's of adjacent pixels in lines above and below. Although the six sensors per band in the MSS were initially calibrated and matched, drift in some sensors response

has produced sixth line banding i.e. every sixth line has anomalously high (or low) DN's compared to the other lines. The data within this line are correct but does not match the overall image. This can be corrected by a program that recognized periodic deviations and applies a correction factor, or by equalizing the DN histograms of all six sensors to the best of the six.

3. Image enhancement

Five main types of enhancement are considered; contrast stretching, spatial -frequency filtering, ratioing of bands, principal component analysis (PCA) and decorrelation stretching.

3.1 Contrast stretching

It is a term commonly used in computer enhancement where the density values in a scene are literally pulled apart (i.e. expanded over a greater range). The effect is to increase the visual contrast between the two areas of different uniform densities. This enables one to discriminate easily between areas initially having a small difference in density. Usually the DN values for any particular band do not fully utilize the range of available digital numbers, 0- 255, and are often clustered within a relatively short range. An image produced using such pixel values has a low contrast and visual interpretation is difficult. If a FCC is produced from these DN's the full colour range available will not be exploited and the colour image produced will not be optimized .

The stretching techniques are best described in terms of DN histogram transformations. The simplest one - a linear contrast stretch - is when the lowest DN is assigned a value of 0 and the highest 255, the intervening values being correspondently stretched, Figure C1. This stretching increases the contrast throughout the entire scene. Alternatively a low DN can be set to black (0) and a high one saturated to maximum intensity (255 - white) which increases the contrast throughout most of the scene at the expense of a loss of contrast at the extremities. Varous more sophisticated non-linear stretches can be applied, e.g. a uniform distribution or Gaussian stretch which increases the contrast within the most populated range of DN's or in the tails of the histogram respectively. The optimum stretch depends on the nature of the scene and the particular feature which is of interest.

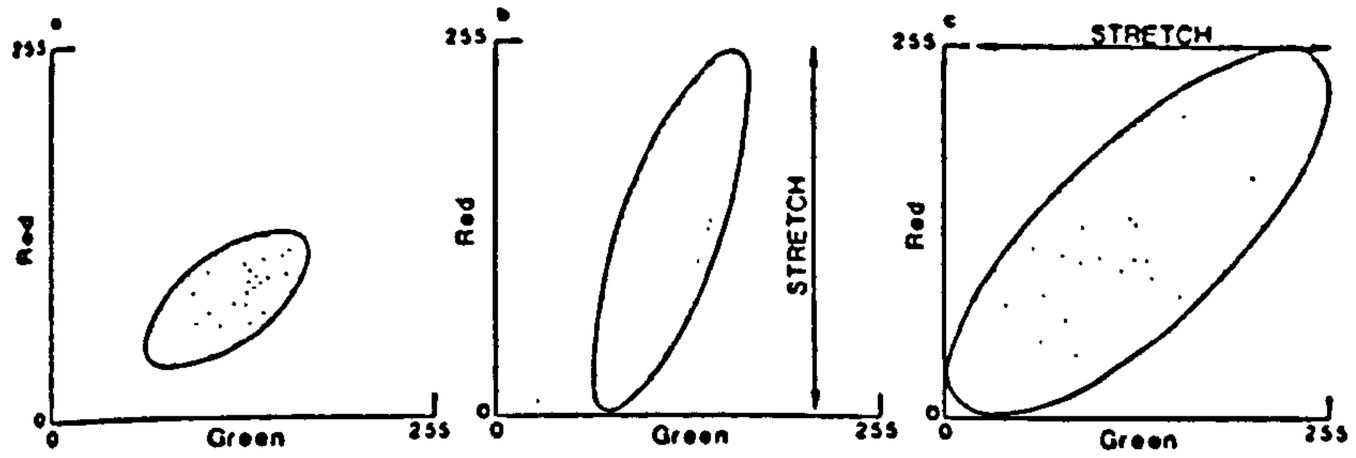

Figure C1 Conventional contrast stretching (a-c) and deccorelation stretching (d-F) of multispectral data, shown in the red-green plane of display space. (a) Raw data typically have a restricted DN range, and is also correlated. (b,c) Conventional contrast stretching is performed parallel to the input bands, which yields an image with a full range of DN in each channel, but the bands are still correlated. The corners of the display space are unoccupied. (d-f) In decorrelation stretching the data distribution is stretched parallel to the principal component axes to produce a spheroidal data distribution, with much fuller use of display colour space.

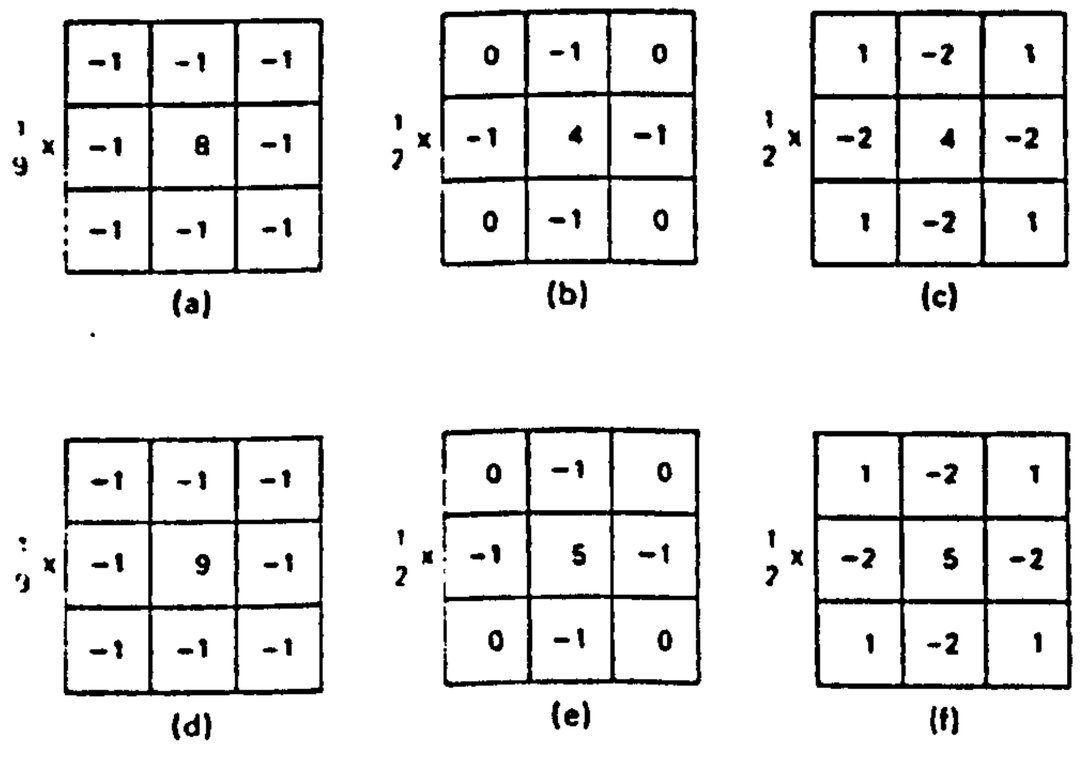

Figure C2 Convolution matrices for edge detection or high- pass filtering can be achieved by subtracting the results of a low-pass convolution from the original image (a), or by devising matrices based on more -complex algorithms (b) and (c) . Edge-enhancement matrices result from adding the edge detector to the original image (d) - (f).

3.2. Spatial-frequency filtering

Emphasizing the high spatial frequency component of the image can further enhance obscure features (Leith and Alvarez, 1985), or pick out features of interest hidden within a cluttered, highly textured, original image (Drury, 1986). This may be done by masking out part of the Fourier transform of the image (filtering in the frequency domain) or, more simply, by convolving the image with a box-car filter (filtering in the spatial domain).

A simple box-car (or 'kernel') of size n x n pixels replaces the value of each pixel by the average value of the pixels in its n x n neighbourhood (Figure C2). The result is a smoothed, or 'low pass' filtered, image. By subtracting a weighted proportion of the smoothed image from the original image a 'high pass' filtered image is created. If the weights are equal this is an edge detection image, which ignores relative brightness but picks out edges and linear features as bright or dark lines. In edge detection each pixel is replaced with the difference between the input pixel and the local mean which when added back to the original image produces an edge enhanced image. By giving the smoothed image a lower weighting an edge enhanced image is formed, which looks like the original image except the edges and linear features are sharper. Use of an asymmetrically weighted box-car enables features with a particular orientation to be enhanced at the expense of others (directional filtering). The optimum size of box-car depends on the degree of roughness in the image and the scale of the features which the interpreter wishes to enhance (Chavez and Bauer, 1982).

The outcome of spatial filtering depends on box-car size and symmetry and the texture of the terrain. With increasing scale the frequency of a particular kind of feature will tend to become higher. As resolution coarsens, the highest frquency features disappear altogether because they are smaller than an individual pixel. In geology high frequency filters are important because they emphasis edges. An edge is a sharp change in the DN value of adjacent pixels -shown on an image as an abrupt tonal change - and provides information on structures e.g. faults, fractures, joints.

3.3. Band ratioing

Using the four spectral bands available from Landsat, images can be produced in which new digital

numbers are obtained by dividing the DN value of a pixel in one band by the corresponding value of the same pixel in another band. Typically, ratioing of the pixels produces values from 0.3 - 3 which are stretched to 0 - 255. Ratioing results in variations in albedo due to the topographic effect being suppressed, thus a lithology should have the same signature whether it is in sunlight or in shadow. Ratio images indicate the gradient change of spectral reflectivity curves between the rationed bands which can be an important discriminator between different lithologies. A disadvantage is that units with very different albedos on single band imagery can be inseparable on ratio image because their spectral reflectivity slopes are similar.

Three ratios can be combined to form a colour ratio image which is commonly used for lithological discrimination or in the search for mineral deposits (Rowan et al., 1974). The ratios and their projection colours used to produce the colour ration image are dependent on the scene, particular area of interest and the operator's experience. A hybrid colour ratio composite can be formed using two ratios and single band which restores the topographic information.

3.4 Principal component analysis (PCA)

A method of improving the spread of data is to redistribute them about another set of axes in multidimensional space, which maximises the separation of differences in the data. A correlation often exists between the DN values for the four Landsat bands, thus if data for two bands are plotted a scatter diagram such as Figure 5.3 is produced. This correlation between bands means the axes are not statistically independent. Principal component analysis is a technique which results in the production of new images whose probability density function has orthogonal axes (Gillespie, 1980).

Whereas for a single variable the spread about its mean is statistically calculated from its variance, the joint variation of two variable about their respective means is give by the covariance. The covariance matrix for several bands defines a set of concentric ellipsoids about the mean. By a translation and rotation it is possible to produce a new axis along which the spread is greater than along either of the two original axes, Figure 5.3. This new axis, which is a veighted average of the inputs, is the first principal component (PC1). The second principal component (PC2) is approximately the difference between the bands. For the four Landsat bands, four principal

components can be generated.

3.5 Decorrelation stretching

As Figure C1 (Rothery,1987) shows, simple contrast stretching is useful for spreading the DN in each channel over the full range, but cannot force data towards the corners of the feature space. Therefore the image remains bland, with no pure colours. If however, stretches are applied along the direction of maximum variance (the first principal component and also along directions orthogonal to this (second and third principal components) the image data can be made to occupy a near -spherical volume of space, with much smaller unoccupied volumes near the corners. This is known as 'decorrelation stretch' and concentrates as much colour as possible into the display whilst maintaining the colour relationships of the original FCC (Soha and Schwartz, 1978; Gillespie et al, 1987).